



ALMA MATER STUDIORUM
UNIVERSITÀ DI BOLOGNA

DOTTORATO DI RICERCA IN SCIENZE VETERINARIE

Ciclo XXXVII

Settore Concorsuale: 07/H1- ANATOMIA E FISIOLOGIA VETERINARIA

Settore Scientifico Disciplinare: MVET-01/A– ANATOMIA VETERINARIA

EXPLORING THE NERVOUS SYSTEM AND SOME EFFECTOR ORGANS IN
VETERINARY SPECIES WITH A FOCUS ON CALCIUM-BINDING PROTEINS,
SEROTONERGIC, ENDOCANNABINOID AND PEPTIDERGIC SYSTEMS

Presentata da: *Dott.ssa Giulia Salamanca*

Coordinatore Dottorato

Prof.ssa Carolina Castagnetti

Supervisore

Prof. Cristiano Bombardi

Co-Supervisore

Prof. Roberto Chiocchetti

Esame finale anno 2025

A Cristiano Bombardi, maestro di laboratorio e di vita.

*"Pure science is like a blanket of beautiful golden and scarlet clouds
that spreads wonderful hues and beams of light to the west.
It is not an illusion, but the splendour and beauty of truth.
When the clouds are blown by the wind, they move over the fields
and their rain preparing them for future harvests."*

Santiago Ramón y Cajal, Advice for a young investigator, 1897.

INDEX

ABSTRACT	1
A. INTRODUCTION	2
Chapter 1: A Focus on the Investigated Biological Systems	3
1.1 Calcium-binding proteins (CaBPs)	3
1.1.1 Structure and properties	3
1.1.2 One focus on the CaBPs under investigation: distribution and roles.....	4
1.1.2.1 Parvalbumin (PV)	4
1.1.2.2 Calbindin D-28k (CB)	5
1.1.2.3 Calretinin (CR)	6
1.1.3 Studies on the neuroanatomical distribution of the CaBPs in the Bottlenose Dolphin (<i>Tursiops truncatus</i>)	8
1.2 Serotonergic System	10
1.2.1 Historical aspects	10
1.2.2 Neuroanatomical distribution: Mammals vs Honeybee, (<i>Apis mellifera</i>)	11
1.2.3 Biochemistry and biology	13
1.2.4 Physiology: roles in the CNS and behavioural effects	15
1.3 Endocannabinoid System (ECS).....	17
1.3.1 The history behind the ECS	17
1.3.2 ECS constituents	17
1.3.3 One focus on the receptors under investigation: distribution and roles.....	20
1.3.3.1 Cannabinoid receptor type 1 (CB ₁).....	20
1.3.3.2 Cannabinoid receptor type 2 (CB ₂).....	22
1.3.3.3 Transient receptor potential cation channel V1 (TRPV1) and A1 (TRPA1).....	26
1.3.3.4 Orphan G-protein coupled receptors 55 (GPR55)	27
1.3.3.5 Peroxisome proliferator activated receptor α (PPAR α) and γ (PPAR γ)	29
1.4 Peptidergic System.....	30
1.4.1 Definition, history and constituents	30
1.4.2 Biosynthesis and general functions.....	31
1.4.3 One focus on the peptides under investigations: distribution and roles.....	35
1.4.3.1 Substance P (SP)	35
1.4.3.2 Vasoactive intestinal peptide (VIP)	37
Chapter 2: Studied Areas of the Central Nervous System in Veterinary Species	40
2.1 Entorhinal Cortex in the Bottlenose Dolphin (<i>Tursiops truncatus</i>)	40
2.1.1 Definition, history, cytoarchitecture and functions with a focus on the Bottlenose Dolphin (<i>Tursiops truncatus</i>)	40
2.2 Amygdaloid Complex	44
2.2.1 Definition, history and functions	44
2.2.2 Anatomy, cytoarchitecture and connectivity with a focus on Rat (<i>Rattus norvegicus</i>) and Sheep (<i>Ovis aries</i>)	47
2.3 Optic Lobe of the Honeybee (<i>Apis mellifera</i>)	51

Chapter 3: Studied Areas of the Peripheral Nervous System in Veterinary Species	54
3.1 Trigeminal Ganglion of the Horse (<i>Equus ferus caballus</i>) and its involvement in the headshaking pathology	54
3.2 The Enteric Nervous System of the Bottlenose Dolphin (<i>Tursiops truncatus</i>)	58
Chapter 4: Studied Effector Organs in Veterinary Species.....	64
4.1 Skin of the Dog (<i>Canis lupus familiaris</i>) with a focus on canine atopic dermatitis	64
4.2 Synovial Membrane of the Horse (<i>Equus ferus caballus</i>) and Dog (<i>Canis lupus familiaris</i>) with a focus on joint diseases.....	68
B. THESIS OBJECTIVES: Exploring the Nervous System and Some Effector Organs in Veterinary Species Targeting Different Biological Systems	72
C. PUBLISHED PAPERS	74
Chapter 1: Distribution of calcium-binding proteins immunoreactivity in the bottlenose dolphin entorhinal cortex	75
Chapter 2: Distribution of vasoactive intestinal peptide (VIP) immunoreactivity in the rat pallial and subpallial amygdala and colocalization with γ-aminobutyric acid (GABA)	92
Chapter 3: Connections of the sheep basolateral amygdala: A diffusion tensor imaging study	114
Chapter 4: Immunohistochemical Distribution of Serotonin Transporter (SERT) in the Optic Lobe of the Honeybee, <i>Apis mellifera</i>	120
Chapter 5: Expression of Cannabinoid Receptors in the Trigeminal Ganglion of the Horse	129
Chapter 6: Nitrergic and Substance P Immunoreactive Neurons in the Enteric Nervous System of the Bottlenose Dolphin (<i>Tursiops truncatus</i>)	148
Chapter 7: Cannabinoid receptors in the inflammatory cells of canine atopic dermatitis.....	161
Chapter 8: Expression of cannabinoid (CB1 and CB2) and cannabinoid-related receptors (TRPV1, GPR55, and PPARα) in the synovial membrane of the horse metacarpophalangeal joint.....	184
Chapter 9: Endocannabinoid System Receptors at the Hip and Stifle Joints of Middle-Aged Dogs: A Novel Target for the Therapeutic Use of Cannabis sativa Extract in Canine Arthropathies	205
D. DISCUSSION AND CONCLUSIONS	225
LIST OF ABBREVIATIONS	228
REFERENCES.....	231

Abstract

This work aims to highlight and enrich the scientific literature on a basic veterinary science such as anatomy, considering different parts of the central nervous system (CNS), the peripheral nervous system (PNS) and some effector organs in various veterinary species, targeting different biological systems. With regard to the CNS, the areas studied were: 1) the dolphin entorhinal cortex (EC), where immunoperoxidase was used to study the distribution, cytoarchitecture and morphology of three calcium-binding proteins (calretinin, calbindin D-28K and parvalbumin); 2) the amygdaloid complex (AC) of the rat, and 3) of the sheep. For the rat, studies were carried out on the distribution, cytoarchitecture and morphology of the vasoactive intestinal peptide (a component of the peptidergic system) and its co-localization with the GABAergic system using immunoperoxidase and immunofluorescence. For the sheep, we focused on the connections within the AC with the rest of the brain, using the new non-invasive technique of diffusion tensor imaging; 4) the optic lobe (OL) of the honeybee, in which the distribution and quantification of the serotonergic system, choosing immunofluorescence against the serotonin transporter (SERT), and its correlation with the aggressive behaviour of the bees were carried out. With regard to the PNS, we focused on: 1) the trigeminal ganglion (TG) of the horse, studying the distribution of cannabinoid receptors (belonging to the endocannabinoid system) on different cellular elements using immunofluorescence and immunoperoxidase; 2) the enteric nervous system (ENS) of the dolphin, with substance P (SP) (a component of the peptidergic system) and neuronal nitric oxide synthase (nNOS) selected as target molecules for immunofluorescence to identify excitatory and inhibitory neurons, respectively. Finally, the effector organs studied included: 1) the skin of dogs with atopic dermatitis (AD); 2) the synovial membrane of the metacarpophalangeal joint in horses, and 3) the hip and stifle joints in dogs. In these tissues, we investigated the distribution of various cannabinoid receptors using immunofluorescence, given their role in pain and inflammatory conditions associated with pathological states. The work will first provide an overview of the existing literature and then present the published scientific articles on the topics under investigation. To the best of the author's knowledge, each of these scientific papers fills an existing gap in the literature and provides the fundamental anatomical basis for further investigation in these areas.

A. INTRODUCTION

Chapter 1: A Focus on the Investigated Biological Systems

1.1 Calcium-binding proteins (CaBPs)

1.1.1 Structure and properties

The category of CaBPs comprises a very large number of proteins (about 240) which, as their name suggests, are characterised by their ability to bind the calcium ion (Ca^{2+}) in different types of cells throughout the organism (1–3). They can be located both extracellularly and intracellularly and can act to regulate Ca^{2+} concentration, transport or decode signals. Although much research has been carried out in the last century to understand their role in normal physiological processes or diseases (4), they can also be useful in characterising the neurochemical properties of neurons in many areas of the nervous system. The most commonly used in this sense are *parvalbumin* (PV), *calretinin* (CR) and *calbindin D-28K* (CB) (1,5,6) which have been used as target protein for part of this work (see Section C, Chapter 1) . PV, CR and CB belong to the superfamily of EF-hand proteins that share a common structure consisting of two alpha helices (E and F), perpendicular to each other, which can embrace a Ca^{2+} ion (Fig. 1)(1,4).

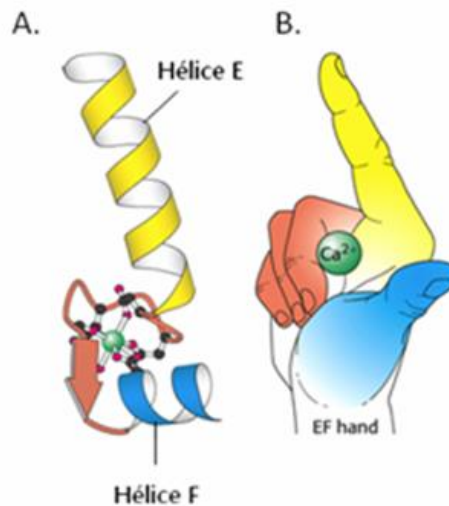


Fig.1: A: Schematic representation of an EF-motif embracing a calcium ion; B: symbolic representation of an EF-motif whose appearance is closed to a hand moving its forefinger and thumb upwards (From *Grisar et al., 2012* (7)).

1.1.2 One focus on the CaBPs under investigation: distribution and roles

1.1.2.1 *Parvalbumin (PV)*

PV is a cytosolic protein, it owes its name to its solubility similar to albumin (3). It is present in almost all vertebrate animals, acting both in excitable cells such as muscle cells, cardiac cells and neurons but also in non-excitable cells like kidney cells or the ones in endocrine glands, testis and bones (4,8–10). It has different roles in each organ and most of them are still poorly understood. For example in skeletal muscle fibres it seems to act as a relaxation accelerator and a protector against reactive oxygen species, in bones it helps the growth process, and in the testis it is involved in the production of testosterone (8,11). For what it concerns the nervous tissue, PV is virtually present only in GABAergic interneurons (Fig.2), where it regulates the excitation-inhibition balance and the short-term synaptic plasticity, controlling the amplitude and time course of the Ca^{2+} passing through the neuron terminal. If these physiological functions of the PV are altered, it has been shown to be involved in central nervous system(CNS)-related disorders such as epilepsy, anxiety, schizophrenia, bipolar syndrome, autism and depression (4,8,11,12).

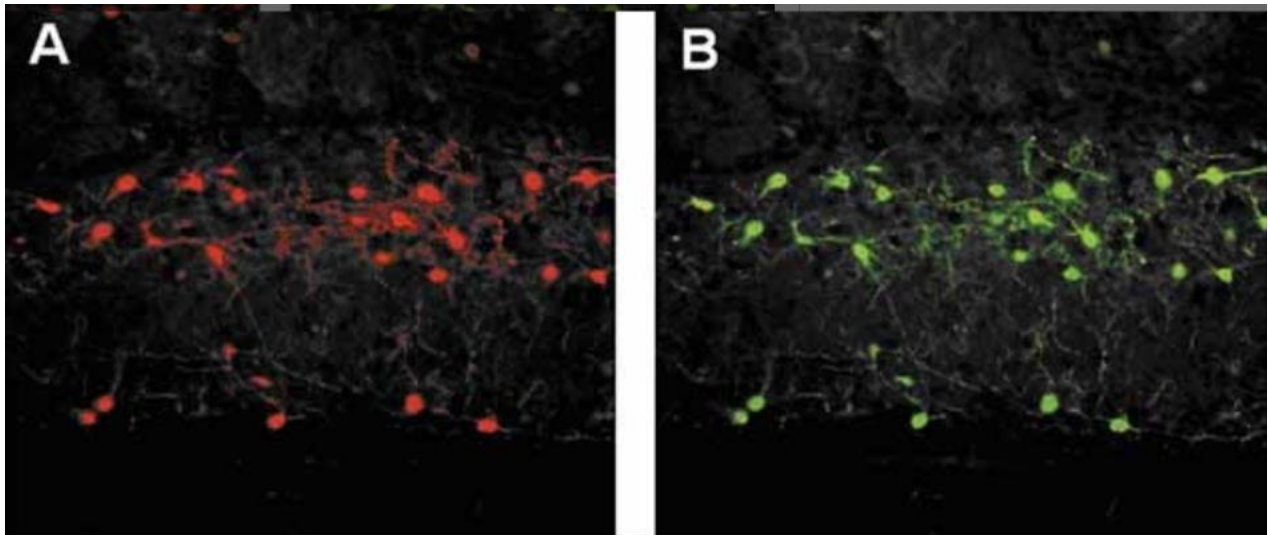


Fig.2: Two photomicrographs of the rat nervous tissue showing in A neurons immunolabeled for PV and in B neurons immunolabeled for GABA. Notice the strict correspondence of double fluorescence for each neuron. (From Arif, 2009).

1.1.2.2 Calbindin D-28K (CB)

CB is a cytosolic or nuclear protein with a molecular weight of 28,000 kDa, the first to be discovered to have an affinity for vitamin D and binding calcium, hence its name. It's well conserved throughout evolution and has been identified in many tissues and species (Table 1). Among the many functions in which it is involved are the absorption of Ca^{2+} in the gut, its role as a modulator of Ca^{2+} influx in the kidney, and in the maturation of bone and cartilage tissues (2).

Table 1 Distribution of calbindin-D_{28K}

Avian intestine
Avian, reptilian, amphibian, and mammalian kidney
Hen egg-shell gland (uterus)
Mouse reproductive tissues (uterus, oviduct, ovary)
Avian and mammalian beta cells of the pancreas
Alpha cells of the rat pancreas
Rat and chick growth cartilage
Ameloblasts and osteoblasts of rodent teeth; mouse osteoblasts
Brain (avian, reptilian, amphibian, molluskan, fish, and mammalian brain)

Table 1: List of organs and species where CB has been localized (From *Mady, 2013*).

Regarding its presence in nervous tissue, unlike the distribution of PV, CB is present in both inhibitory and excitatory neurons (Fig. 3-4) (6,13–15). Its role has been proposed to control intracellular Ca^{2+} influx and homeostasis, modulate synaptic transmission and protect against neurotoxicity. Disruption of these processes can lead to dysregulation of circadian cycles, neurodegeneration and apoptotic events (2,16).



Fig.3: Photomicrograph of a CB-positive pyramidal neuron in the human entorhinal cortex (From *Mikkonen et al., 1997*).

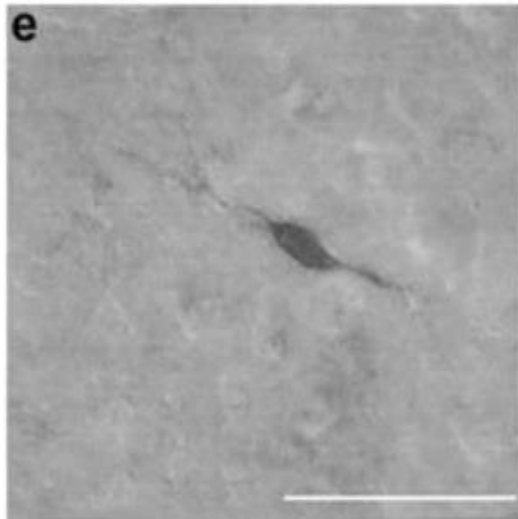


Fig.4: Photomicrograph of a CB-positive non pyramidal neuron in the sheep amygdaloid complex (From *Bombardi et.al, 2006*).

1.1.2.3 *Calretinin (CR)*

CR was named because it was first discovered in retinal cells (3). Unlike PV and CB, which are distributed in many cell types, most studies on CR confirm its major presence in neuronal cells, while it is less studied in other tissues, limited to the epithelial cells of the inner ear and ovary, the testicular cells, the adrenal glands and the thymus. On the contrary, it's well studied as a neoplastic marker in some specific neoplasia (3,16–19). As well as CB, CR is present in both excitatory and inhibitory neurons (Fig. 5-6) (6,15). To cite just a few of its roles, CR appears to have a protective function against glutamate and β -amyloid toxicity, and is involved in motor coordination and in the modulation of neuronal excitability (3,20).

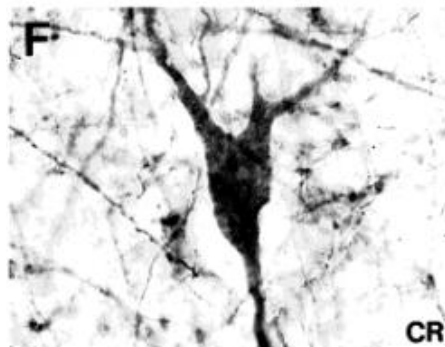


Fig.5: Photomicrograph of a CR-positive pyramidal neuron in the human entorhinal cortex (From *Mikkonen et al., 1997*).

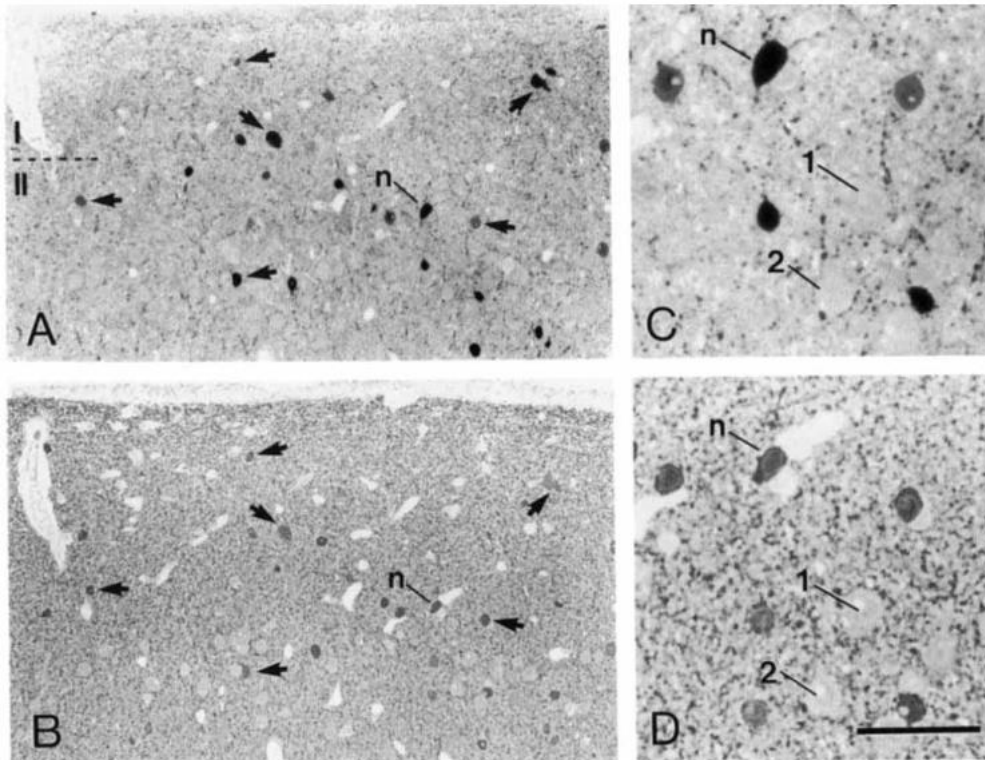


Fig.6: Photomicrographs of CR-positive non pyramidal neurons (A,C) and GABA-positive non pyramidal neurons (B,D) in the human temporal cortex; Black arrows and *n* show co-localization in different neurons; 1 and 2 indicate two non-immunoreactive cells (From *Del Rio and DeFelipe, 1996*).

1.1.3 Studies on the neuroanatomical distribution of the CaBPs in the Bottlenose Dolphin (*Tursiops truncatus*)

PV, CB and CR, among the large family of CaBPs, are useful to conduct neuroanatomical studies due to their abundance and specificity in distribution throughout the nervous system; furthermore their high solubility and presence in the cytosol allow the characterization of neuronal shape and connectivity (4). Many studies on their distribution in the nervous system have been conducted during the twentieth century in mammals (e.g. rat, human, monkey, cat, dog, pig, sheep, cetaceans) and non-mammals animals such as avian, reptile and amphibian species. These studies described the CaBPs localization in various areas including the cerebral and the cerebellar cortex, retina, hippocampus, AC, basal ganglia, mesencephalon, diencephalon, pons, medulla oblongata and spinal cord (1,21–28).

Focusing on the bottlenose dolphin (*Tursiops truncatus*), target of part of this thesis, a considerable number of studies on the distribution of CaBPs in the nervous system have been conducted in this species, as well in cetaceans more broadly. Data are available on the neocortex (Fig.7) (27,29), specifically on the primary visual cortex (30), the cerebellar cortex (Fig.8) (26), the auditory and visual systems (31), the sleep-related neural system (32) and the AC (33).

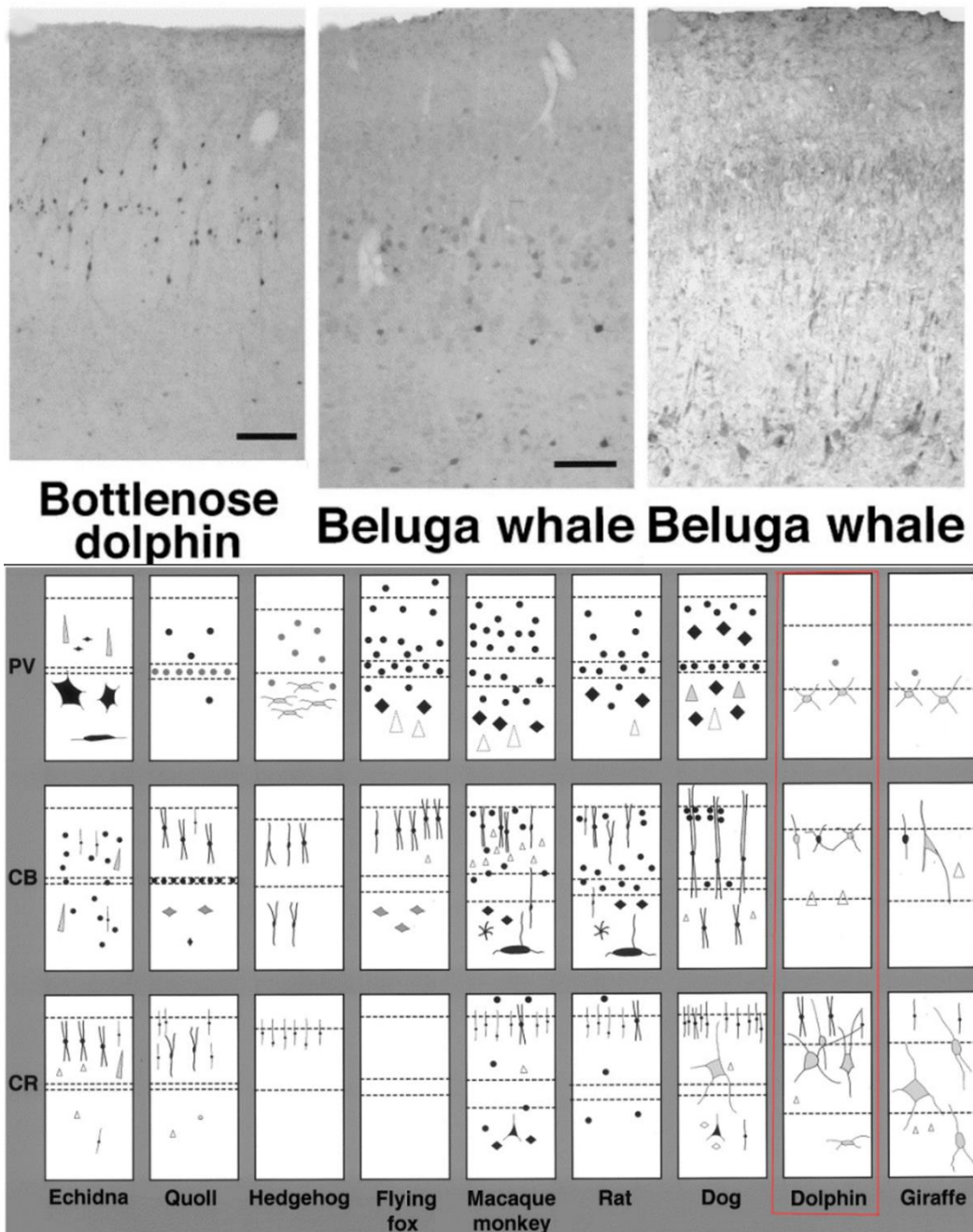


Fig.7: On the top three photomicrographs of the cetaceans neocortex with immunoreactive neurons for CR (on the left), PV (in the middle), CB (on the right). On the bottom a schematic representation of the CaBPs distribution differences in several animal species (modified from *Hof et al., 1999*).

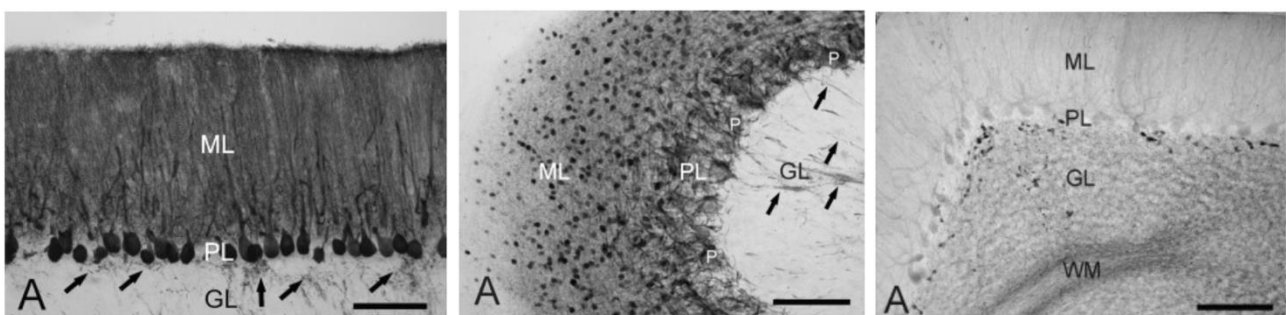


Fig.8: Three photomicrographs of the dolphin cerebellar cortex with immunoreactive neurons for CB (on the left), PV (in the middle), CR (on the right). ML, molecular layer; PL, Purkinje cell layer; GL, granular layer; WM, white matter; P, Purkinje cell (modified from *Kalinichenko et al., 2008*).

1.2 Serotonergic System

1.2.1 Historical aspects

The serotonergic system is a diffuse projecting system of the brain and, from a phylogenetical point of view, is one of the oldest (34,35). The characterizing neurotransmitter is the biogenic amine named “serotonin”, also known as 5-hydroxytryptamine (5-HT) (Fig.9) (36,37).

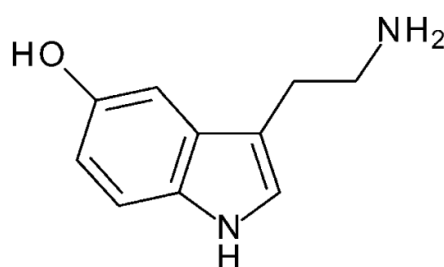


Fig.9: Chemical structure of the serotonin molecule (From *Naeem et al., 2022*).

The discovery of this molecule dates back to the middle of the twentieth century, and it occurred in two independent laboratories and at different times. In 1937 the Italian scientist Vittorio Erspamer extracted it from intestinal enterochromaffin cells and named it "enteramine". Later, in 1948, Maurice Rapport and colleagues isolated it from bovine blood serum and called it "sero-tonin" due to its presence in serum and its vasoactive properties. It was the same Erspamer who showed in 1952 that enteramine and serotonin were the same molecule (35,36,38–40).

Despite the distribution of the serotonergic system in different organs of the body (e.g. cardiovascular, pulmonary, gastrointestinal, and genitourinary systems) where it exerts different roles (41), for the purposes of this thesis we will concentrate on its presence in the CNS.

The first to find a significant amount of 5-HT in extracts of mammalian brains were Twarog and Page in 1953 (42), but we have to wait until the last years of the twentieth century, with the advent of new immunohistochemical techniques for the first studies on the neuroanatomical distribution of the serotonergic system in rats (34,43). It's curious to point out that it was already Santiago Ramon y Cajal who, in 1911, observed the presence of large multipolar neurons in the central or midline (raphe) of the brainstem (44); later, Dahlström and Fuxe (1964) enriched his description, characterising the majority of these cells as clusters of 5-HT-containing neurons extending their axons in different areas of the CNS (36,43,44).

1.2.2 Neuroanatomical distribution: Mammals vs Honeybee (*Apis mellifera*)

The subsequent numerous neuroanatomical studies conducted during the 20th century agree on the fact that in mammals the bodies of 5-HT-containing neurons are found mainly in the central or midline (raphe) of the brainstem and that they can be divided into a *rostral group* located in the mesencephalon and the rostral pons and a *caudal group* located in the caudal part of the pons and the medulla oblongata (further nuclear divisions make up these groups, but the description is beyond the scope of this thesis). The rostral group sends projections to many structures in the forebrain and plays a role in cognitive, affective and neuroendocrine mechanisms, whereas the caudal group sends projections to the spinal cord and is involved in pain perception, visceral regulation and motor control (Fig.10) (34,43,45,46).

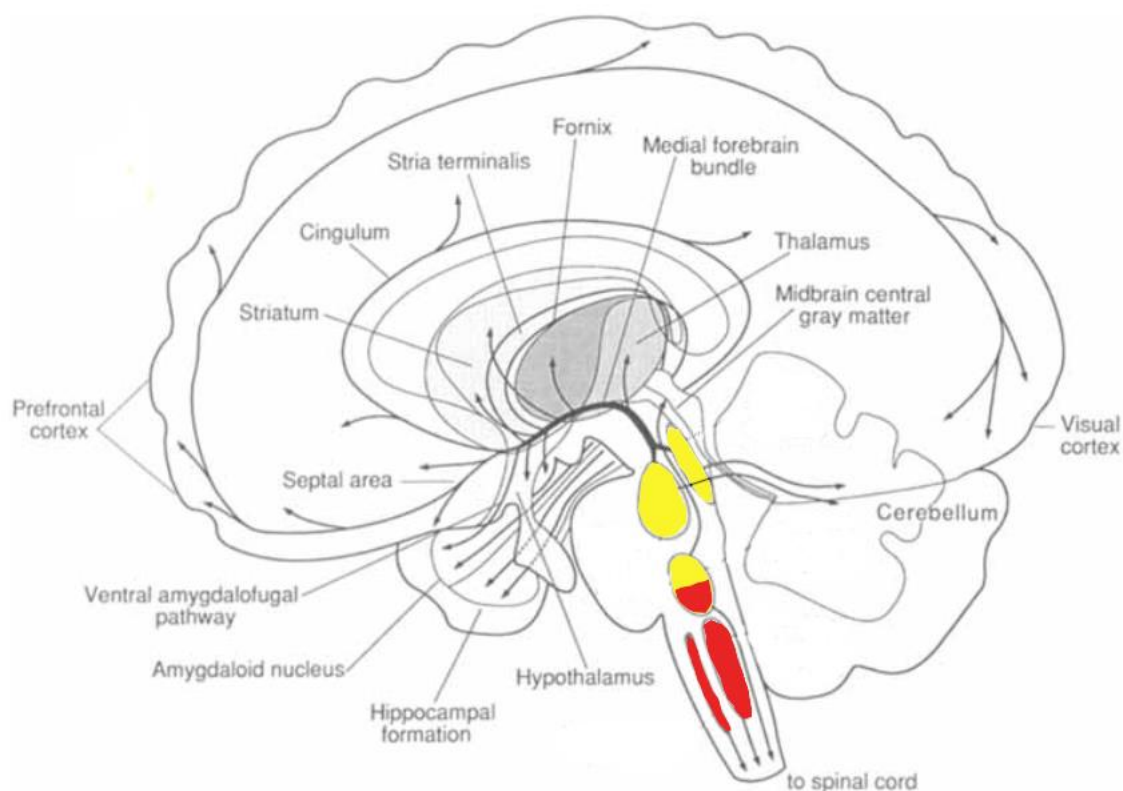


Fig.10: Schematic representation of the central serotonergic system distribution in human brain. In yellow the location of the *rostral group*, in red the location of the *caudal group* (modified from Törk, 1990).

A plethora of studies have been carried out on the presence and distribution of the serotonergic system also in invertebrates (47), including the honeybee (*Apis mellifera*) (48–50), which is a protagonist of part of this thesis. In this species, according to Schürmann and Klemm (49), the somata of the neurons are concentrated in the following six main paired clusters

(Fig.11) (for more details on the anatomy of the honeybee nervous system, the reader is referred to the Section A, Chapter 2.3):

- Group 1: near the lobula and the medulla of the optic lobe;
- Group 2: near the lateral calyx of the corpora pedunculata;
- Group 3: near the lateral mushroom body calyx;
- Group 4: near the medial calyx of the *corpora pedunculata*;
- Group 5: near the border of the central body;
- Group 6: in the suboesophageal ganglion;

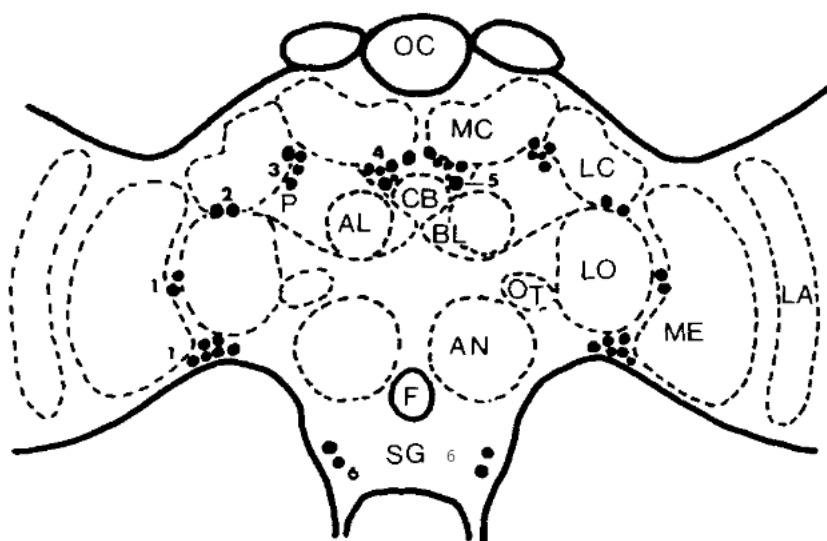


Fig.11: Schematic representation of the honeybee central nervous system in a frontal view, somata clusters of serotonergic neurons are presented with black dots (groups numbered from 1 to 6). AL, alpha-lobe; BL, beta-lobe; LC, lateral calyx; MC, medial calyx; P, pedunculus of the mushroom bodies; OC, ocellus; CB, central body; optic lobe: LA, lamina; ME, medulla; LO, lobula; OT, anterior optic tubercle; AN, antennal lobe, F, foramen oesophageal; SG, suboesophageal ganglion (modified from Schürmann and Klemm, 1989).

The immunoreactive fibres originating from this somata are widespread in almost all areas of the brain (especially in the deutocerebrum and in the protocerebrum) with different appearance and morphological organization (49,50).

1.2.3 Biochemistry and biology

The biological effects of the serotonergic system depend on the action of many other players in addition to 5-HT. Starting with its synthesis, a series of biochemical reactions take place in which various enzymes and cofactors act to produce 5-HT from the essential amino acid tryptophan (Fig.12).

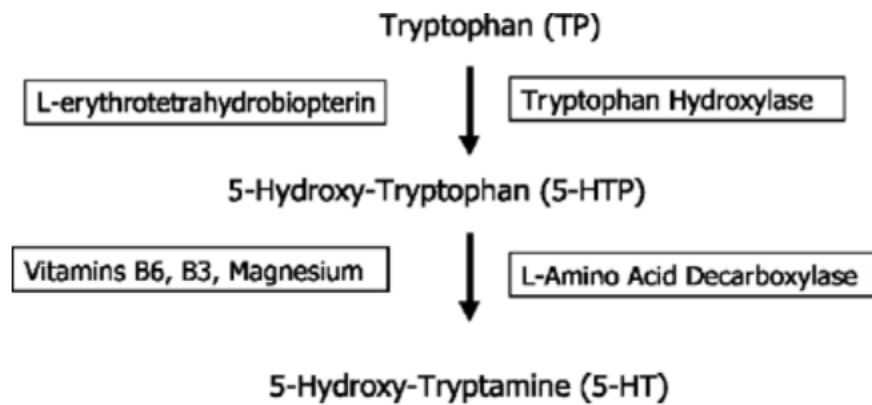


Fig.12: Metabolic pathway from Tryptophan to Serotonin, on the left are the cofactors and on the right the enzymes (modified from Graeff, 1997).

The 5-HT produced is then stored in secretory vesicles and released into the synaptic space when an electrical signal occurs; it can act on both postsynaptic and presynaptic receptors. About that it's important to know that at least seven families of 5-HT receptors (5-HT_r 1-7) have been identified, most of which are characterised by different subtypes, are widespread and act differently in many physiological systems. Going back to the biochemistry, after its action at the receptors level, 5-HT is removed from the synaptic space by the transporter (5HTT or SERT) located on the membrane of serotonergic axon terminals (Fig.13). Finally, it is catabolized within the neuron by monoamine oxidase (MAO), and the remaining 5-hydroxyindoleacetic acid (5-HIAA) is transported to the periphery and excreted in the urine (39,46).

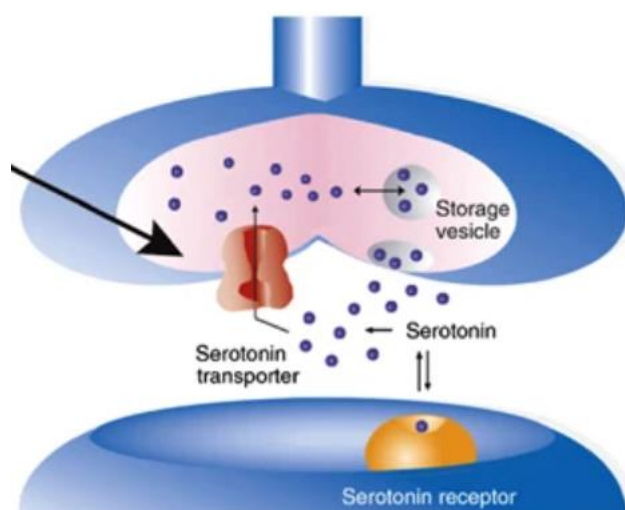


Fig.13: Schematic view of the flow of Serotonin in the neurons, highlighted by an arrow the serotonin transporter (SERT or 5HTT) (modified from *De Neve., 2011* (51)).

For the purpose of this work it is important to highlight that although the visualisation of serotonergic neurons using immunohistochemical technique can be achieved by employing antibodies directed against different markers (e.g. 5HT, 5HT_r or SERT), the use of antibodies against SERT is a better choice due to its less sensitiveness to metabolism (52); furthermore, it is important to point out that SERT (like the whole serotonergic system) is well conserved between vertebrates and invertebrates (53–55).

1.2.4 Physiology: roles in the CNS and behavioural effects

The serotonergic system is implicated in numerous physiological mechanisms ranging from the CNS to the periphery. It has been demonstrated to play a role in platelet aggregation, control of vascular tone and blood pressure, in gastrointestinal motility and secretion (36), glucose and bone metabolism and other functions outside the CNS which have been reviewed in detail by Berger and colleagues and summarized in Fig.14 (39).

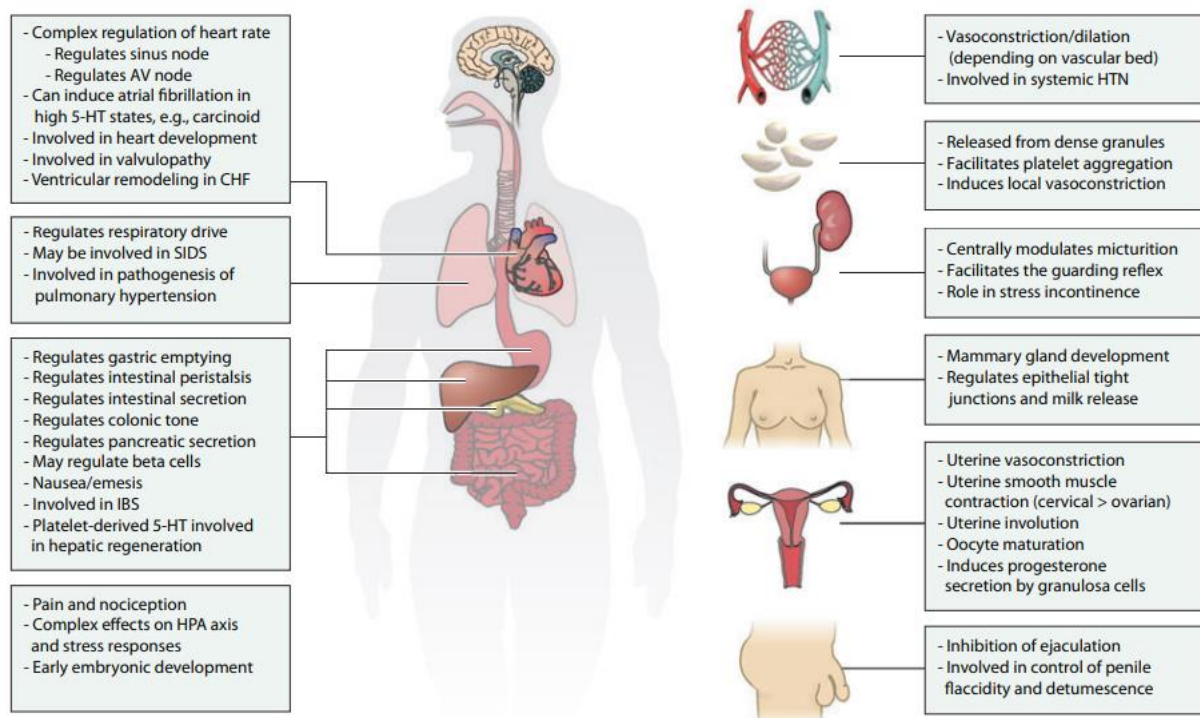


Fig.14: Roles of the serotonergic system outside the CNS (from *Berger et al., 2009*).

For what it concerns the CNS, the serotonergic system is implicated both in physiological processes driven by the central control such as emesis, pain, regulation of the body temperature, sleep cycles and motor movements, and in psychopathological conditions like depression, obsessive–compulsive, anxiety and eating disorders and in behavioural related mechanisms such as stress, memory, sexuality, attention and aggressiveness among others (35,36,39,41,56). In honey bees (*Apis mellifera*), changes in 5-HT activity are also associated with various behavioural aspects (57). The latter is the focus of part of this work, which attempts to relate the involvement of the serotonergic system in the aggressive behaviour of this species. The role of 5-HT in this tendency has been demonstrated in pharmacological studies in fish, birds and mammals, and it has been explored the possibility that genes encoding key proteins in 5-HT biology (including SERT) and some 5-HT receptors are involved in its determination (Fig.15) (58).

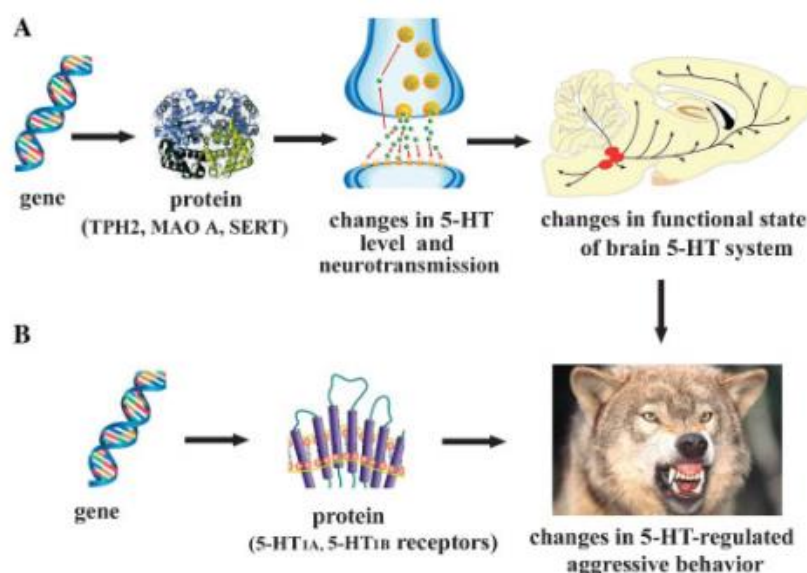


Fig.15: Schematic representation of two possible pathways (A: key proteins responsible for 5-HT synthesis, degradation and transport; B: 5-HT receptors) responsible for aggressive behaviour (from Popova, 2006).

1.3 Endocannabinoid System (ECS)

1.3.1 The history behind the ECS

Although the plant *Cannabis sativa* (better known as “marijuana”) has been used since the ancient Chinese era, around 5000 years ago, for relieve cramps and pain (59), if nowadays we can talk about the ECS, it is thanks to the Israeli chemist and biologist Raphael Mechoulam, who, after isolating and characterising the psychoactive compound THC from the cannabis plant in 1964, began to test the effects of its administration on humans and monkeys, and he found out different types of reactions in the body, this discovery gave the input to search for a new receptors system: the ECS (60). Afterwards, in the nineties, Devane et al. (1988) discovered the first cannabinoid receptor (CB₁) in the rat and human brain, as well as the first endocannabinoid compound capable of binding to the receptor: arachidonylethanolamide (AEA), also known as anandamide (61,62).

1.3.2 ECS constituents

A large number of studies have been conducted in this field over the last century, leading to the knowledge that the ECS consists of three groups of elements (Fig.16) (63,64):

- Endocannabinoids
- Metabolic enzymes and transporters
- Cannabinoid receptors

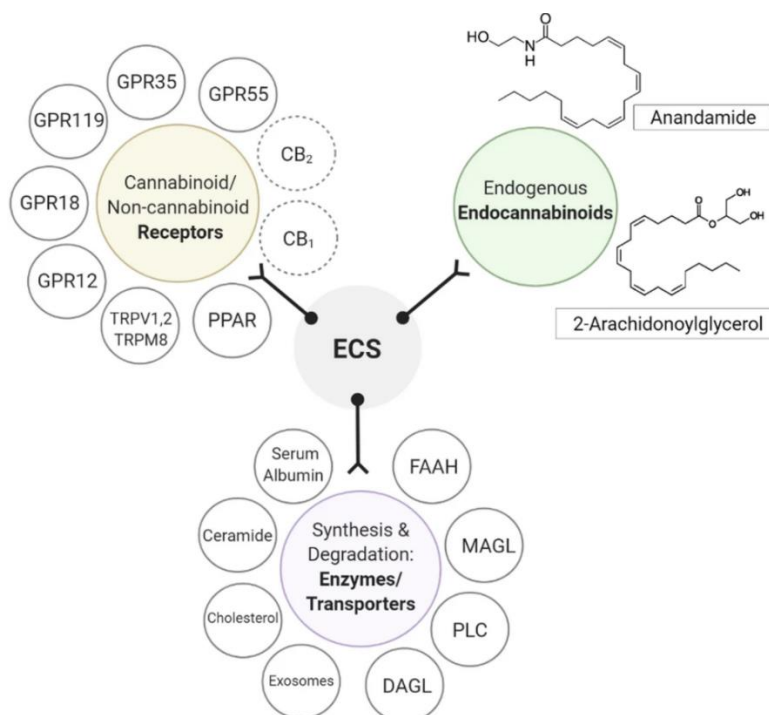


Fig.16: Schematic representation of the ECS components. Diacylglycerol lipase (DAGL), phospholipase C (PLC), monoacylglycerol lipase (MAGL), fatty acid amide hydrolase (FAAH) (from Mangal et al., 2021).

The endocannabinoids (eCBs) are a group of endogenous lipidic ligands able to bind cannabinoid receptors and produced on demand by cells from arachidonic acid present in the membrane, the first discovered and most studied are 2-arachidonoyl-glycerol (2-AG) and AEA or anandamide (65–67). It is important to point out that other molecules, the so-called "non-CB lipid mediators", share with the classical eCBs the ability to bind cannabinoid receptors and/or to mimic the effects of eCBs signalling and/or to enhance ECS activity by exerting an entourage effect. These include for example N-palmitoylethanolamine (PEA), N-oleoylethanolamide (OEA), commendamide, virodhamine (O-AEA), N-arachidonoyl serine (ARA-S), 2-arachidonoyl glycerol ether (2-AGE) and N-arachidonoyl dopamine (NADA) (63,68).

Among the metabolic enzymes and transporters responsible for the management of eCBs, it is possible to mention the ones interacting with AEA and 2-AG, which are characterized by two distinct metabolic pathways (Fig.17). For what it concerns the AEA, several routes of synthesis have been proposed, among which the best characterized are the ones involving the N-arachidonoyl phosphatidyl ethanol-preferring phospholipase D (NAPE-PLD) and the NAPE-phospholipase C (PLC). On the other hand, 2-AG is mainly synthesised by diacylglycerol lipase, which exists in two isoforms, α and β (DAGL α - β). Once synthesised, due to their polar nature, it is supposed the existence of a transporter, called eCBs membrane transporter (EMT), which is responsible for the transport of eCBs outside and inside the cell membrane. The half-life of eCBs is very short, and after exerting their action by binding cannabinoid receptors (CB₁), they are quickly transported back inside the cells and catabolized, the 2-AG is hydrolysed by the monoacylglycerol lipase (MAGL), while the AEA by the fatty acid amino hydrolase (FAAH) (59,67,69–71).

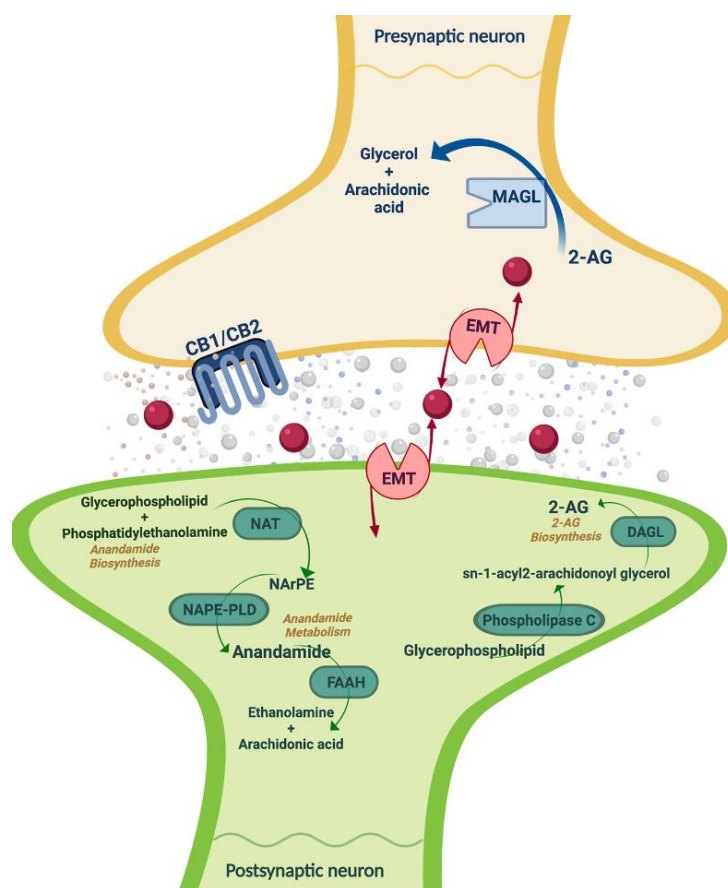


Fig.17: Schematic representation of the ECS metabolic enzymes and transporters. CB1/CB2, cannabinoid receptors 1 and 2; 2-AG, 2-arachidonoylglycerol; FAAH, fatty acid amide hydrolase; MAGL, monoacylglycerol lipase; DAGL, diacylglycerol lipase; EMT, endocannabinoid membrane transporter; NAT, N-acyl transferase; NArPE, N-arachidonoyl phosphatidylethanolamine; NAPE-PLD, N-acylphosphatidylethanolamine specific phospholipase D (from Navarrete *et al.*, 2020).

Regarding the cannabinoid receptors, the firsts to be discovered were cannabinoid receptor-1 (CB₁) and cannabinoid receptor-2 (CB₂), which have been found in neuronal cells and macrophages respectively and belong to the family of G protein-coupled receptors (GPCr). Later, the fact that cannabimimetic effects were also observed in CB₁ KO mutants led to the idea that there must be other receptors that interact with eCBs. Indeed, it is now possible to include in the ECS the so-called "non-classical cannabinoid receptors", such as the transient receptor potential cation channel (TRP) group, comprising subfamily Vanilloid member 1 (TRPV1) and member 2 (TRPV2), subfamily M member 8 (TRPM8) and subfamily Ankyrin member 1 (TRPA1); the orphan G-protein coupled receptors (GPR) group, comprising GPR55, GPR18 and GPR119, and the peroxisome proliferator activated receptors (PPAR) group, comprising PPAR α and PPAR γ . All these receptors have different affinities and functions, but they all bind eCBs, phytocannabinoids (cannabinoids produced by plants, e.g. THC, CBD, CBG etc.) and/or synthetic cannabinoids (produced by pharmaceutical companies) (Fig.18) (63,64,66,68,72–74).

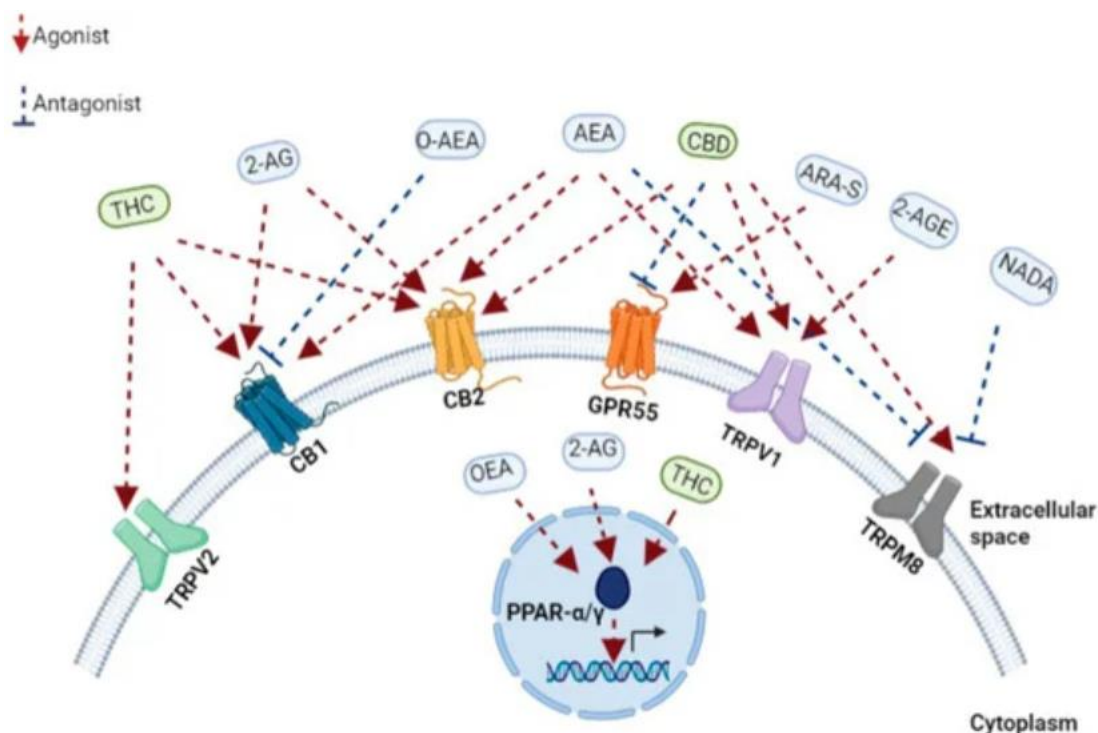


Fig.18: Schematic representation of the classical and non-classical cannabinoid receptors and their affinity with some eCBs and phytocannabinoids. THC, tetrahydrocannabinol; CBD, cannabidiol; 2-AG, 2-arachidonoylglycerol; O-AEA, virodhamine; AEA, anandamide; ARA-S, N-arachidonoyl serine; 2-AGE, 2-arachidonoyl glycerol ether; NADA, N-arachidonoyl dopamine; TRPV2, transient receptor potential cation channel subfamily V member 2; CB1, cannabinoid receptor 1; CB2, cannabinoid receptor 2; GPR55, G protein-coupled receptor 55; TRPV1, transient receptor potential cation channel subfamily V member 1; TRPM8, transient receptor potential cation channel melastatin 8; PPAR- α , peroxisome proliferator-activated receptor-alpha; PPAR- γ , peroxisome proliferator-activated receptor-gamma (from *Khoury et al., 2022*).

1.3.3 One focus on the receptors under investigation: distribution and roles

Each receptor under investigation will be described, with particular emphasis on the current literature regarding their distribution and role in the selected targets: TG, inflammatory cells and synovial membrane.

Starting with the classical cannabinoid receptors (CB₁ and CB₂), it was initially assumed that CB₁ was primarily distributed in the central nervous tissue, while CB₂ was found mainly in the cells of immune and hematopoietic tissues. Further research revealed that these receptors are distributed throughout the bodies of both mammals and non-mammalian animals with a homology varying among species between the 97-99% (75).

1.3.3.1 Cannabinoid receptor type 1 (CB₁)

The CB₁ in the central nervous system is present in cortical and subcortical regions, such as the basal ganglia, substantia nigra, globus pallidus, cerebellum, hippocampus, nucleus accumbens, amygdala, hypothalamus and also in the brainstem and in the dorsal horn of the spinal cord (69,75). It is present presynaptically and postsynaptically in both GABAergic and glutamatergic neurons and it is also present, but at lower levels, in astrocytes, oligodendrocytes and microglia (59,70,75). CB₁ can also be found in peripheral nervous tissue, specifically in nerve terminals of the sympathetic

system, in the dorsal root ganglion and in nerve endings of primary sensory neurons of the skin. Apart from the nervous system, this receptor is distributed in the gastrointestinal tract (both in neural and non-neural cells), in the liver, in the cardiovascular system, in the adipose tissue, in skeletal muscle, lung, thymus, bone, skin, eye, reproductive system, and in several types of cancer cells. Some of the major roles studied are illustrated in Fig.19 (59,69,76–80).

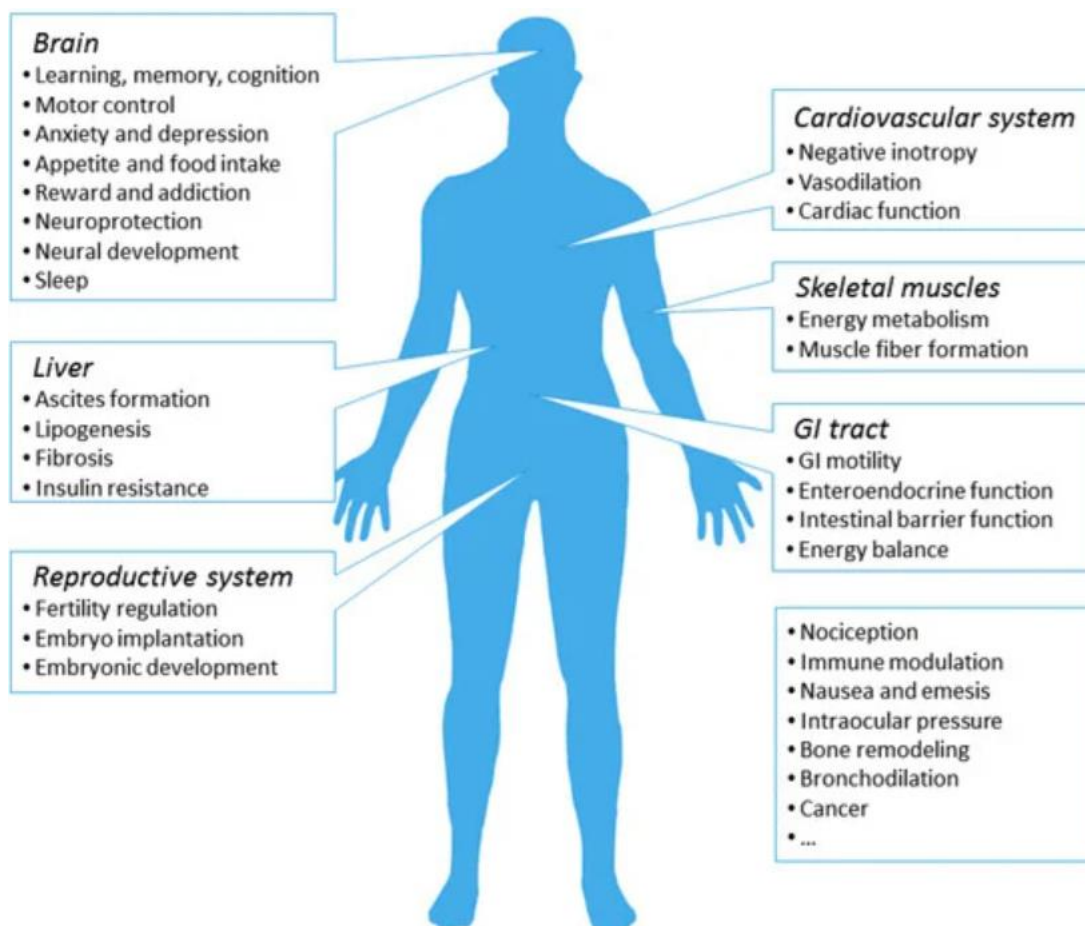


Fig.19: Schematic representation of the CB₁ receptor major roles throughout the body. (from Zou and Kumar, 2018)

For the purpose of this thesis it is important to highlight the presence and roles of CB₁ in the trigeminal ganglion, which have been studied especially on rats, where it was found mostly on myelinated neurons (Fig.20) (81) and it has been demonstrated that in this context, eCBs may inhibit the release of neuropeptides controlling nociceptive inputs through a CB₁-dependent mechanism (82).

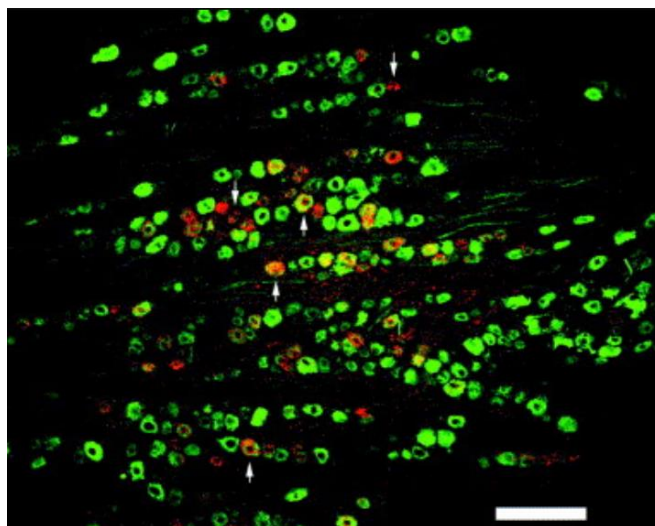


Fig.20: CB₁ colocalization (red) with N52 (a marker for myelinated neurons, green), upward arrows indicate co-labeled cells, downward arrows CB₁ labeled cells (modified from *Price et al., 2003*).

It is also important to describe its presence and roles in the synovial membrane, which has been demonstrated in humans, mice and horses (Fig.21) (in the latter without differentiating between the type of synoviocytes); however, no studies have been conducted in dogs. It appears that CB₁ mediates arthritic diseases by exerting an anti-inflammatory effect (83–86).

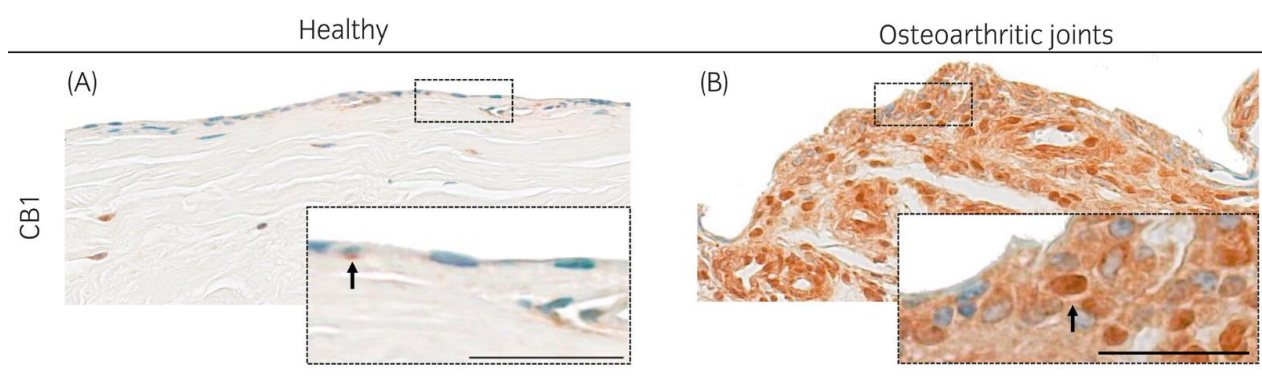


Fig.21: CB₁ distribution in the synovial membrane of a healthy horse (left) compared to that of an osteoarthritic horse (right) (modified from *Miagkoff et al., 2022*).

1.3.3.2 Cannabinoid receptor type 2 (CB₂)

Previously considered to be a peripheral cannabinoid receptor distributed mainly in immune cells, CB₂ is now recognised to be also present in the CNS, mainly in microglial cells and vascular elements and in certain pathological conditions, where it plays a neuroprotective role (67,75,87). Some studies describe its presence also in healthy nervous tissue, in area such as the frontal cortex, the striatum, the basal ganglia, the AC, the hippocampus and the ventral tegmental area, both in microglia and in neurons (Fig.22) (69,88). Moderate expression can be found also in peripheral tissues, including the cardiovascular system, the gastrointestinal tract, the adipose tissue, the liver, bone, and reproductive system. It seems to play among others a role in neurological activities, such

as nociception, drug addiction, neuroinflammation, mood disorders but also in stroke and traumatic brain injury (Fig.23) (59,71,76–78).

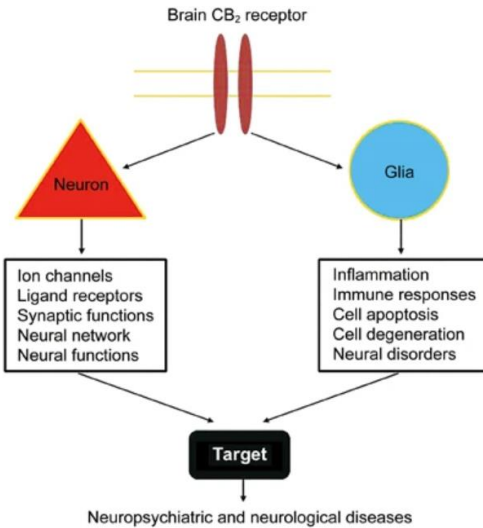


Fig.22: CB₂ schematic distribution and function in the brain (modified from *Chen et al., 2017*).

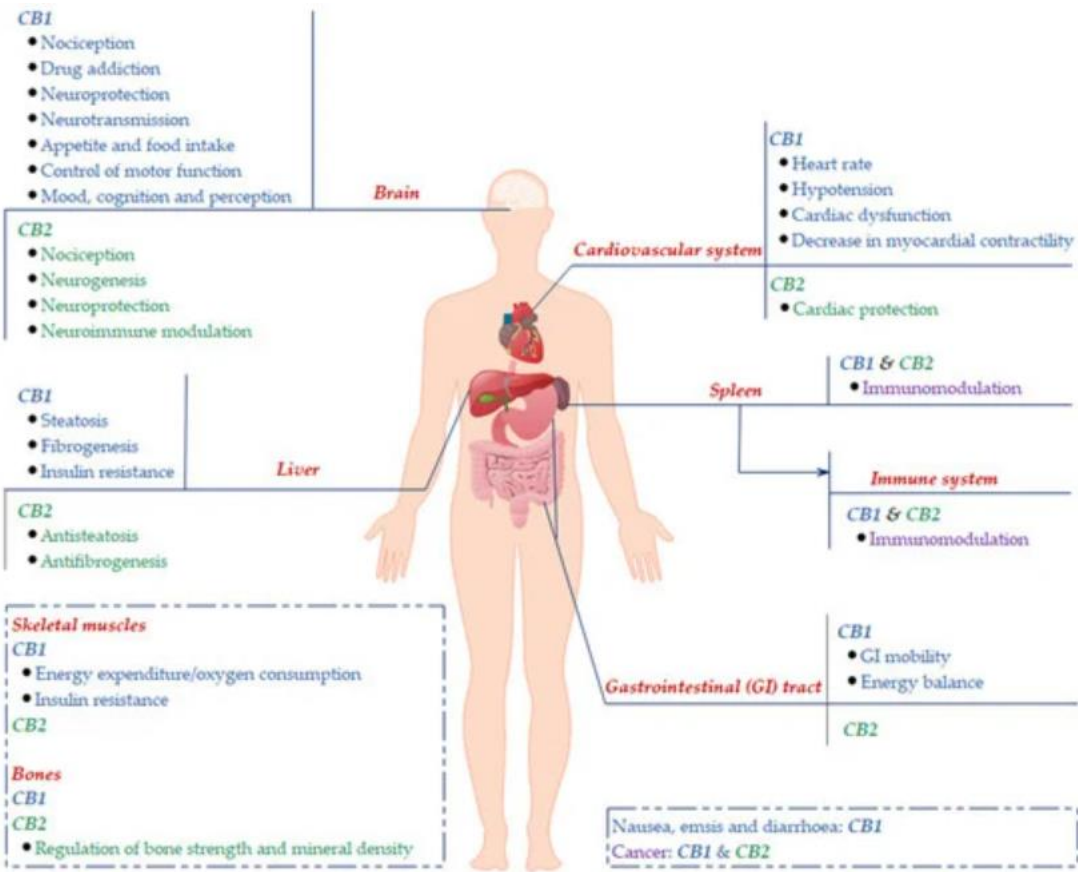


Fig.23: CB₁ and CB₂ schematic distribution and functions throughout the body [from *An et al., 2020* (89)].

Focusing on the CB₂ distribution and roles in immune cells, as one aim of this thesis is to investigate them in canine AD skin, this receptor has been found in lymphocytes, monocytes and derived macrophages and dendritic cells (DCs), neutrophils and mast cells (MCs) (Fig.24), where it is actively involved in their function in various ways (68,71,90–92). In MCs it appears

to modulate degranulation and suppress the proinflammatory response by reducing the release of nociceptor mediators (93), in macrophages it controls their action in response to chemoattractants (94), in DCs it reduces cytokine release (95), in neutrophils it is involved in modulating their recruitment and cytokine production (91), in B lymphocytes it increases the proliferation whereas in T lymphocytes it decreases it (92).

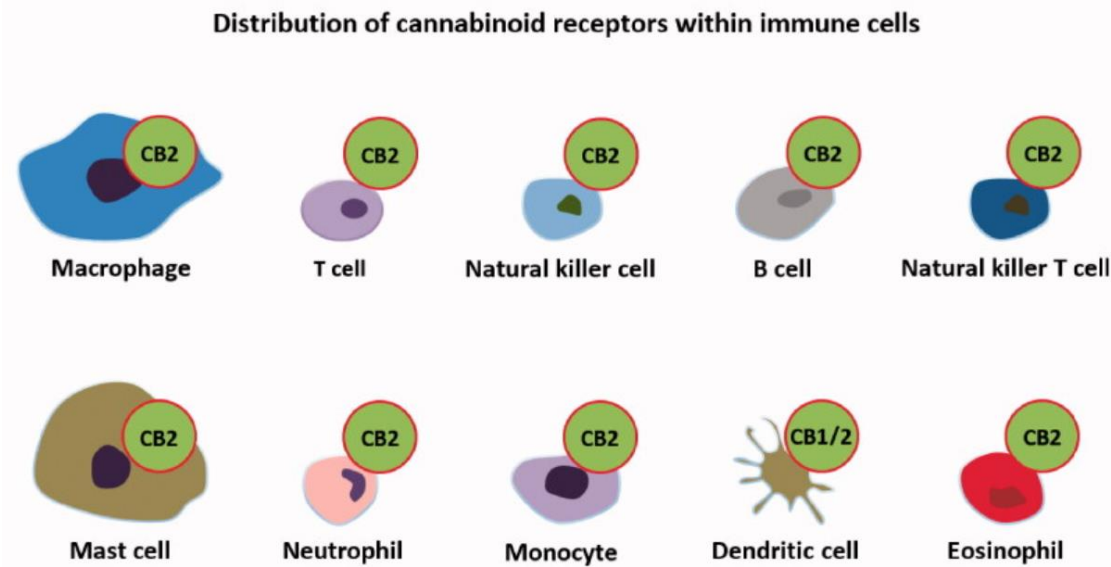


Fig.24: Schematic CB₂ distribution in immune cells (from *Lucaciu et al., 2021* (96)).

CB₂ has also been found to be expressed in peripheral sensory neurons of the rat TG (97) and in the dorsal root ganglion (DRG) of humans, dogs, mice, guinea pigs, rats (98,99) and horses (Fig.25) (100) where it may be involved in the modulation of nociception and neuropathic pain (101–103).

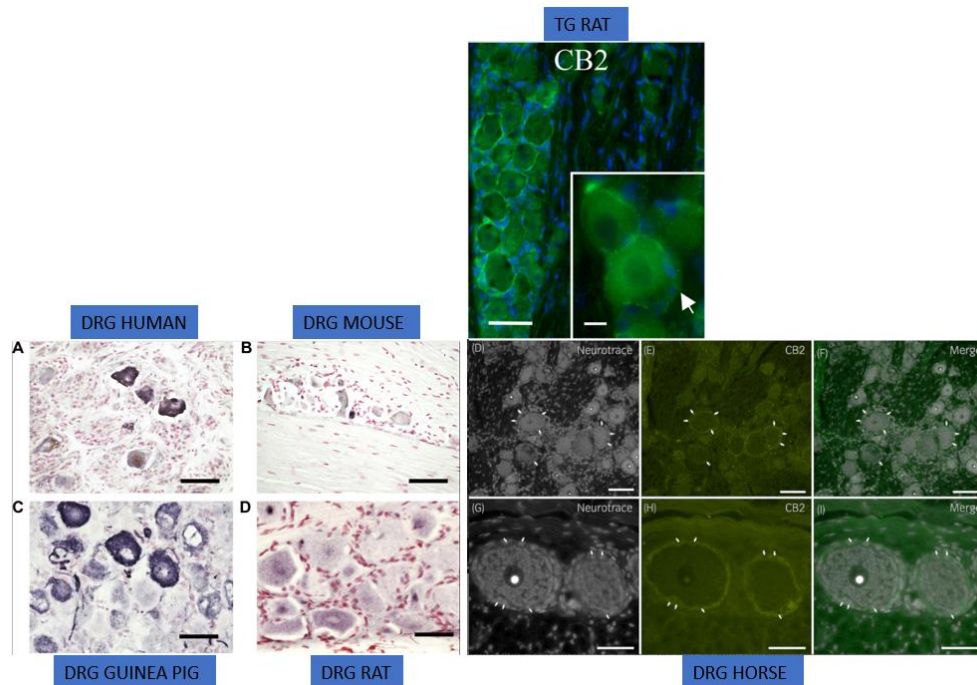


Fig.25: Micrographs of different species and tissues showing CB₂ distribution in sensory neurons. Dorsal root ganglion (DRG); Trigeminal ganglion (TG) (modified from *Christiansens et al., 2022; Anand et al., 2008; Chiocchetti et al., 2020*).

Furthermore, it is important to report that CB₂ has been identified in synovium cells of mice, rats (Fig.26) and humans (104–106), and it seems to have a protective role in the progression of joint diseases (105,107,108).

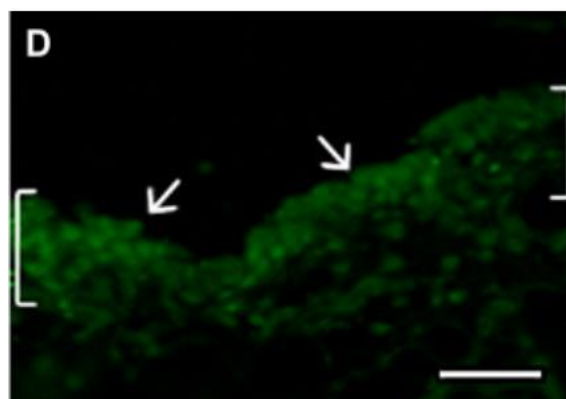


Fig.26: Micrograph showing CB₂ distribution in the rat synovial membrane (modified from *Schuelert et al., 2010*).

The following sections will take into consideration the distribution and roles of the “non-classical” CBr.

1.3.3.3 Transient receptor potential cation channel V1 (TRPV1) and A1 (TRPA1)

Both TRPV1 and TRPA1 belong to the group of TRP (transient receptor potential) membrane channel proteins, which regulate ions entry and mediate neuronal signalling processes such as temperature, sensation, smell, taste, vision, pressure or pain perception. Furthermore, by controlling the influx of calcium these channels are involved in immune and epithelial cells inflammatory processes. It was also discovered that they can be activated in various ways by eCBs, phytocannabinoids and sintetic cannabinoids (68,75,109,110).

TRPV1 and TRPA1 are primarily expressed in the peripheral nervous system, particularly in primary sensory neurons, located in trigeminal ganglion and dorsal root ganglia (Fig.27), but they are also found in various region of the central nervous system. In non-neuronal cells TRPV1 has been found in bronchial epithelial cells, uroepithelial cells and keratinocytes; on the other hand TRPA1 is also expressed in heart, small intestine, lung, skeletal muscle, and pancreas (100,109,111–114).

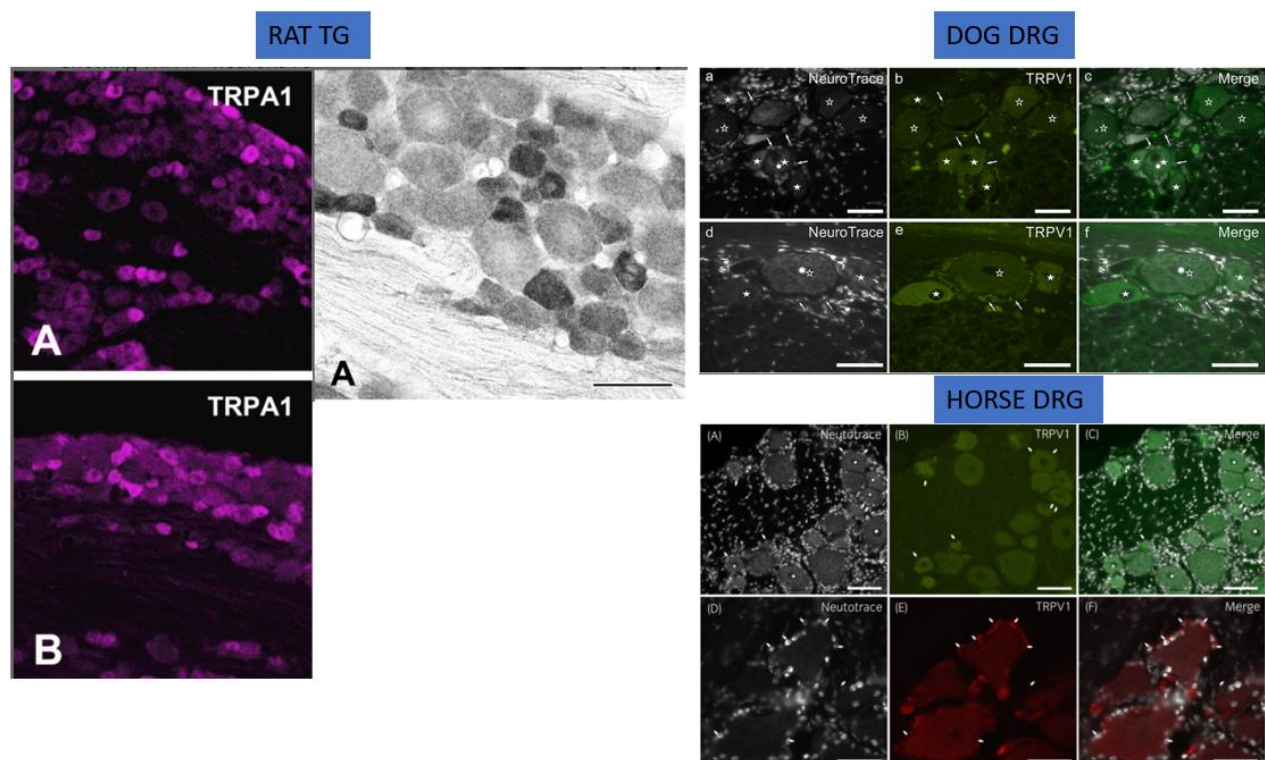


Fig.27: Micrograph showing TRPA1 and TRPV1 distribution in the trigeminal ganglion (TG) of rat and in dorsal root ganglia (DRG) of dog and horse (modified from Kim *et al.*, 2010; Chiocchetti *et al.*, 2019; Galiazzo *et al.*, 2022).

For the purposes of this thesis, it is important to note that both proteins are involved in the function of inflammatory cells. They have been characterised in rodents MCs (115,116), and it seems that the antagonism of the two proteins leads to the blockage of their degranulation and helps to alleviate the itching symptoms in condition such as AD (117,118). For what it concerns the macrophages, these receptors have been characterized in canine mononuclear cells and human macrophages (119,120), and their blockade reduces the infiltration of macrophages and suppresses the inflammatory response (121,122). Their presence has also been demonstrated in human DCs, and although the role of TRPA1 has not yet been investigated, it appears that TRPV1 agonists stimulate their maturation and migration in the skin (123,124). The presence of both TRPV1 and TRPA1 has also been demonstrated in rodent and human T lymphocytes, where they are involved in their activation during inflammatory processes (125–127). In neutrophils, there is very little evidence for the presence of the two receptors in these cells, with some authors reporting the absence of TRPA1 and very low levels of TRPV1 (124,128,129).

For what it concerns the presence of TRPV1 in sensory neurons of the TG, it has been demonstrated its presence in the ones of rat (130), where it seems that its deactivation leads to analgesic effects, making it a good target for neuropathic pain (131).

The distribution of TRPV1 in synoviocytes has been demonstrated in humans, rats and mice (132–134) and in horses, changes in protein and mRNA levels have been shown between healthy and osteoarthritic joints (135). Other studies in models of osteoarthritis and rheumatoid arthritis or in pathological tissues have demonstrated its involvement in the progression of symptoms (132,136,137).

1.3.3.4 Orphan G-protein coupled receptors 55 (GPR55)

GPR55 was first identified as an orphan GPCR enriched in the central nervous system especially in the caudate putamen, hippocampus, thalamus and midbrain but also in other tissues such as the spleen, the gastrointestinal tract, the adipose tissue, the testis, the tonsil and the myometrium (75,77,78,138). It has also been identified in sensory neurons of dogs, rats and horses (Fig. 28) (99,114). Little is known on the role of this receptor, some studies suggest its involvement in the neuronal excitation and in pathology characterised by glutamate toxicity such as epilepsy (73,139), some others claim to regulate cell proliferation and migration, angiogenesis and wound healing through eCBs (68).

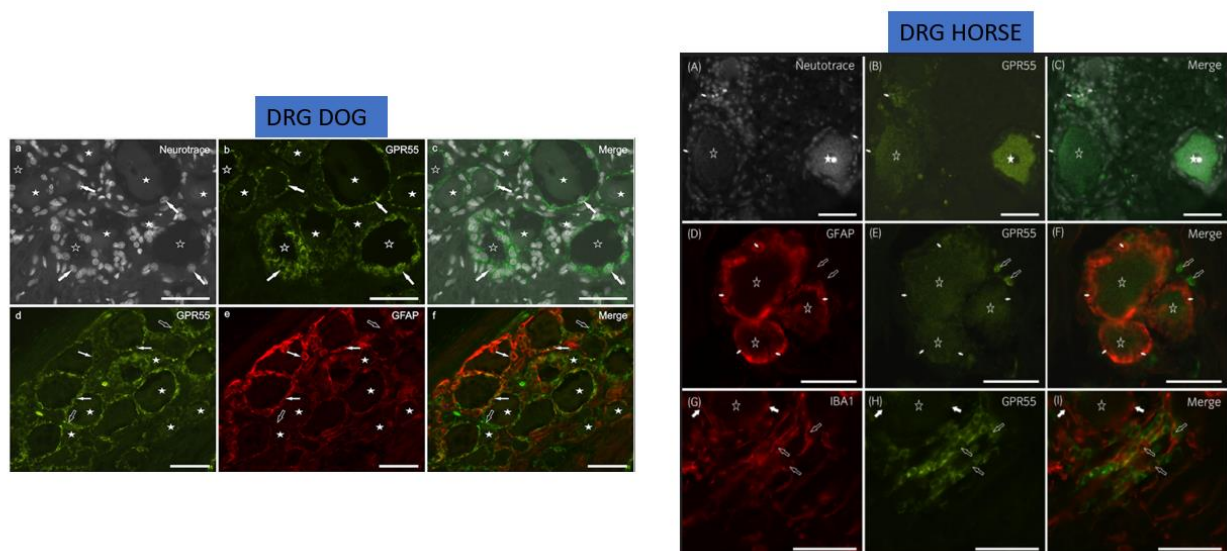


Fig.28: Micrographs showing GPR55 distribution in dorsal root ganglia (DRG) of dog and horse (modified from *Chiocchetti et al.,2019; Galiazzo et al.,2022*).

As far as the TG is concerned, to the best of the author's knowledge, no studies have been carried out to determine the distribution of GPR55 in this nervous structure. However, in terms of neuropathic pathology that can involve also the trigeminal ganglion, it can be said to play a role in neuropathic nociception, since GPR55-knockout mice showed the reduction of mechanical hyperalgesia (140), although these results are controversial (141).

Regarding inflammatory cells, it has been shown that several types of leukocytes express GPR55, including neutrophils, monocytes, lymphocytes and macrophages (142). In MCs, it appears to have an anti-inflammatory role by reducing the release of nerve growth factor, which normally induces angiogenesis (143), and it has been found in canine GI MCs (77). It has been shown to be present in human and rodent macrophages (144,145) and to have a pro-inflammatory role in monocytes in general (146). To the best of the author's knowledge, the role of GPR55 in DCs it is poorly investigated, but it was already been found in the ones of humans and mice (147,148). Little is known about its role in lymphocytes, but one study demonstrated its presence in the ones of mice intestine where it seems to negatively regulates their proliferation (149). Finally, a study demonstrated its presence in human neutrophils, where it appears to increase migration and to reduce degranulation and reactive oxygen species production (150).

Despite the presence of GPR55 has been investigated in human chondrocytes, osteoclasts and osteoblasts (151,152) and it appears to play a role in bone remodelling and resorption (153,154), to the best of the author's knowledge there are no studies investigating its presence in synoviocytes, although one study demonstrated its role in reducing nociception in joint inflammation (155).

1.3.3.5 Peroxisome proliferator activated receptor α (PPAR α) and γ (PPAR γ)

These two receptors belong to the PPARs family, a group of nuclear receptors, first discovered to induce the proliferation of peroxisomes (hence their name), which are involved in the regulation of gene transcription associated with inflammation and metabolism (68,156). When bound by cannabinoids they act in neuroprotective, anti-inflammatory, antinociceptive, antiproliferative and metabolic mechanisms. PPAR α is mainly distributed in liver, kidney, heart, muscle and adipose tissue, however it has also been found in horse ileum and sensory neurons (Fig.29) (76,109,157). PPAR γ is mainly found in heart, muscle, colon, kidney, pancreas, and spleen, but it has also been localised in brain tissue and horse sensory neurons (Fig.29) (109,114,156).

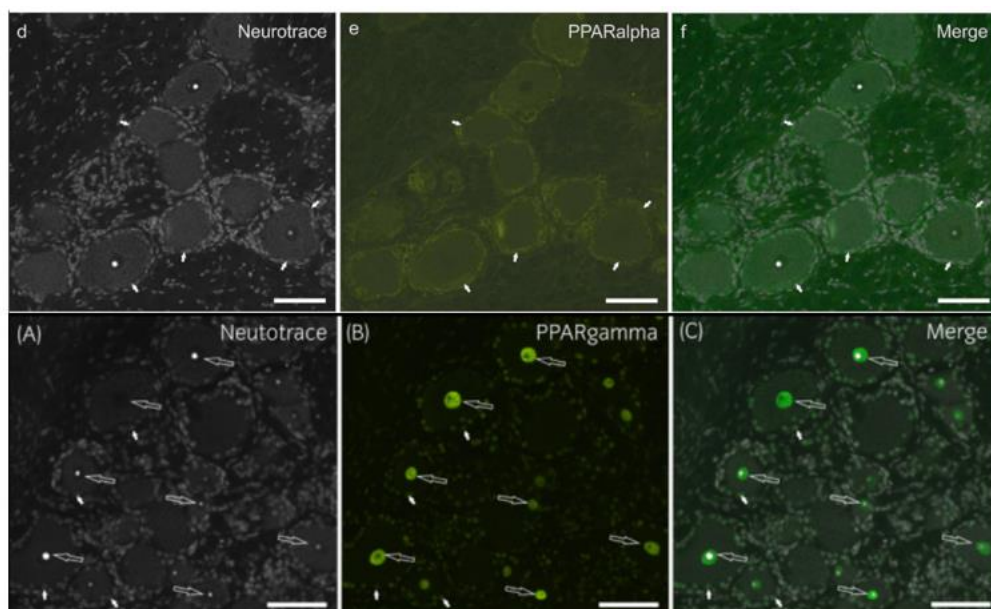


Fig.29: Micrographs showing PPAR α and PPAR γ distribution in dorsal root ganglia (DRG) of horse (modified from Chiocchetti *et al.*, 2020; Galiazzo *et al.*, 2022).

The PPAR γ has been found in satellite glial cells of the mouse TG (158), and its role in the inflammatory compression of the trigeminal nerve was demonstrated by Lyons *et al.*, 2017 in mice (159) where PPAR γ agonists reduced allodynia and pain sensitivity.

To the best of the author's knowledge no studies have investigated the distribution of PPAR α in synoviocytes, however some studies have demonstrated its involvement in joint disease, for example PPAR α agonists have reduced inflammation in rheumatoid arthritis (160) by decreasing the production of cytokines (161) and in osteoarthritis by lowering various inflammatory factors (162).

1.4 Peptidergic System

1.4.1 Definition, history and constituents

A peptidergic system is a functional complex that includes a cell producing the peptide, a cell that reacts and changes after binding the peptide itself, and a space in which the peptide is transported. Even if it can include both neuronal and non-neuronal cells (e.g. insulin producing cells) distributed throughout the body, most of endogenous peptides are neuronal in nature, for this reason are called “neuropeptides” that can act as neurohormones, neurotransmitters and neuromodulators (163,164).

The first studies on peptidergic communication were carried out in 1902 on peptide hormones secreted by endocrine glands, but it was later discovered that neurons could also produce peptides, initially limited to those produced at the level of the hypothalamus (in 1952, oxytocin and vasopressin), and then discovered to be present in other regions of the brain (165,166). They have been studied in a wide range of species, leading to the concept that they have played a role in the function of the nervous system "from the very beginning", in fact they are abundant in primitive animals such as cnidarians (hydra, jellyfish, corals and sea anemones) (166,167).

Nowadays it is possible to recognize more than fifty neuropeptides in the mammalian nervous system and some efforts have been made also to classify them (166,168). According to Hökfelt et al, 2000, they can be classified as follows:

- ❖ Hypothalamic hormones: e.g. oxytocin, vasopressin;
- ❖ Hypothalamic releasing and inhibiting hormones: e.g. corticotropin releasing hormone (CRH), growth hormone releasing hormone (GHRH);
- ❖ Tachykinins: e.g. Neurokinin α (NKA), Neurokinin β , Neuropeptide K and Substance P (SP);
- ❖ Opioid peptides: e.g. β -endorphin, Dynorphin, Met- and leu-enkephalin;
- ❖ NPY and related peptides: e.g. Neuropeptide tyrosine (NPY), Pancreatic polypeptide (PP) and Peptide tyrosine-tyrosine (PYY);
- ❖ VIP-glucagon family: e.g. Glucagon-like peptide-1 (GLP-1), Peptide histidine isoleucine (PHI), Pituitary adenylate cyclase activating peptide (PACAP), Vasoactive intestinal polypeptide (VIP);
- ❖ Other neuropeptides: e.g. Calcitonin gene-related peptide (CGRP) (α - and β -form) and Cholecystokinin (CCK);
- ❖ “Novel” neuropeptides: e.g. Corticostatin, Secretoneurin and Urocortin;

The above list is not exhaustive, for completeness see Hökfelt et al, 2000 (166). The neuropeptides of interest for this thesis are underlined.

1.4.2 Biosynthesis and general functions

Neuropeptides are encoded directly from the genome and are first produced as large molecules called preprohormones, after this, before entering the endoplasmic reticulum, through a first cleavage leading to the removal of the amino-terminal signal peptide, the prohormone is formed. Within the Golgi apparatus, it is then further cleaved at mono- or dibasic sites by endopeptidases and excreted via secretory granules. In addition, further post-translational modifications (e.g. C-terminal amidation, glycosylation, acetylation, sulphation or phosphorylation) occur for biological activity and stability (Fig. 30) (164,166).

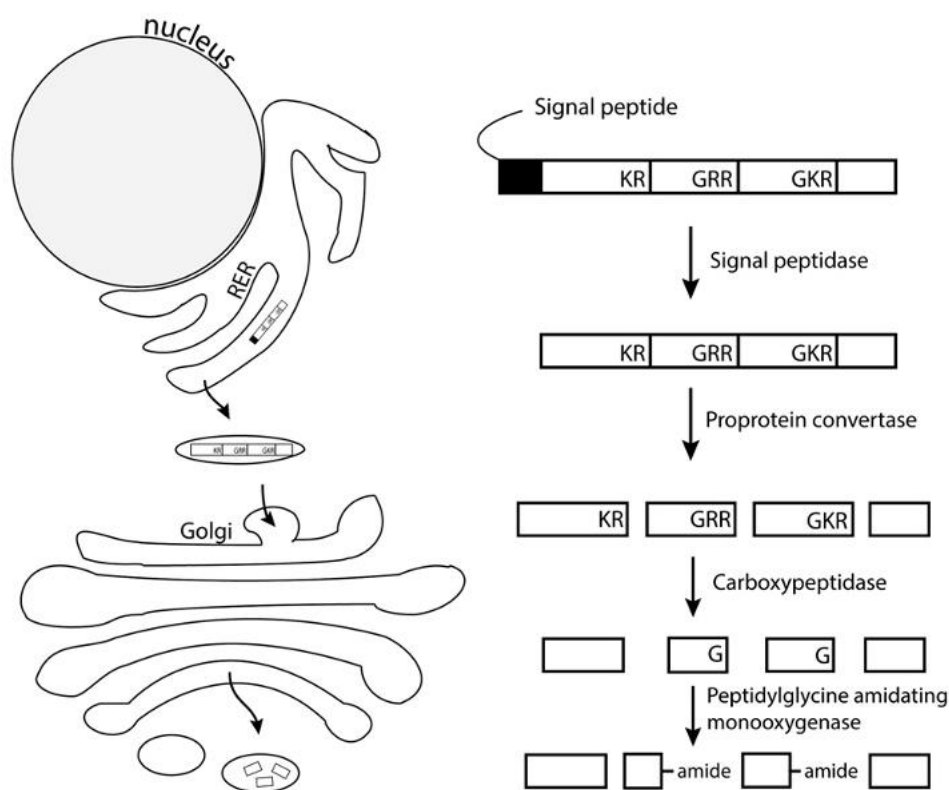
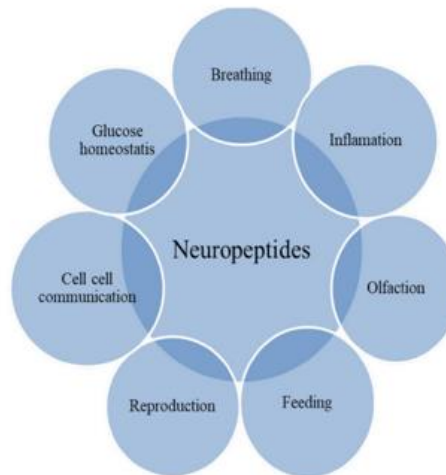


Fig.30: Schematic representation of the neuropeptide biosynthesis process (from De Haes et al.,2014).

Regarding the general functions of neuropeptides, it is important to note that establishing a complete list of their exact roles in nervous system functions is challenging, especially for those released at nerve endings to act in the central or peripheral nervous system. Nonetheless, neuropeptides are involved in both physiological and pathological mechanisms (166,169).

Among the physiological processes it is possible to mention the regulation of blood pressure by bradykinin and neuropeptide Y, sodium intake by angiotensin II, pain perception by tachykinins and opioid peptides acting on neurokinin receptors that transmit nociceptive signals, glucose

homeostasis and growth processes, as well as feeding, social, sexual and reproductive behaviour. A comprehensive list of roles is provided and schematised below (Fig. 31) (169).



S. No	Peptide	Function/role
1	Angiotensin	Regulate blood pressure via vasoconstriction
2	Neuropeptide Y	Regulation of arousal and anxiety
3	Oxytocin	Play a role in mammalian behavior and health
4	Brain opioid peptides	Play a vital role in attachment, emotion, motivation, stress, pain, and feeding behavior
5	Bradykinin	Regulate blood pressure via vasodilation
6	Ghrelin	Regulation of appetite and energy
7	Galanin	Regulation of sleep, cognition, feeding, blood pressure, and mood
8	Kisspeptin (Kp)	Regulation of reproductive functions
9	Somatostatin	Regulation of growth in vertebrates
10	Neurokinin B	Pregnancy in females and maturation in young adults
11	Hemokinin	Regulation of respiratory, endocrine, inflammatory, and immune system
12	Ghrelin	Anticonvulsant activity
13	Neuropeptide Y	Regulation of itching
14	Neuropeptide W	Regulation of energy homeostasis
15	Vasopressin	Central Autonomic Control and Blood Pressure Regulation
16	Galanin, spexin and kisspeptin	Regulation of metabolism, mood and behaviour

Fig.31: Schematic representation of the neuropeptide physiological functions (modified from *Sharma et al.,2022*).

Among the pathological conditions in which neuropeptides seems to have a role it is possible to mention the healing process of wounds during diabetes, headache and migraine, the balance process between excitation and inhibition that occurs during seizures and epilepsy, depression and neurodegenerative disorders such as Parkinson's disease and Alzheimer where some of them can have a neuroprotective role (Fig.32) (169).

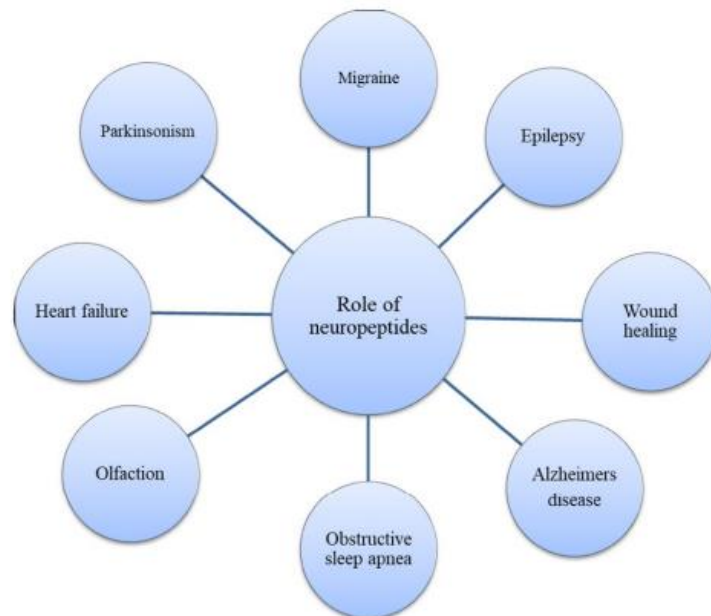


Fig.32: Role of neuropeptides in pathological conditions (from *Sharma et al.,2022*).

A fascinating mini-review by Waite and colleagues (2014), describes neuropeptides as biological system integrators, using as an example the role of oxytocin they point out how a neuropeptide can cover a range of functions, starting with those produced in the brain and released into the blood as neurohormones, for example oxytocin which cause the ejection of milk acting on muscle-like cells of the mammary ducts, going to those produced in a paracrine manner as neurotransmitter in the brain, and ending to those produced in non-neuronal tissues such as endocrine and exocrine glands. These can influence various hormonal pathways that lead to specific body responses and behaviours, for example oxytocin orchestrates a range of effects in the breastfeeding mother: protecting against stress, helping to heal wounds, supporting attachment between child and mother. Curiously, oxytocin and oxytocin receptors are present in all humans, not just mothers, and regulate social behaviour, physical affection and sexual arousal. From this point of view, it is possible to say that neuropeptides integrate body, behaviour and mind (Fig.33) (170).

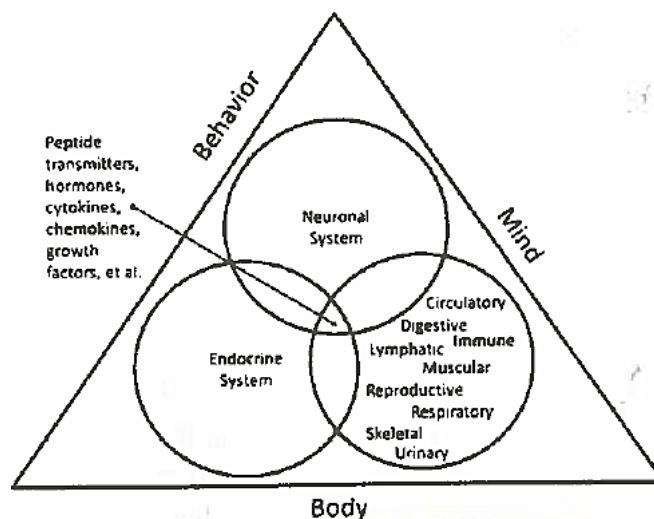


Fig.33: Neuropeptides as biological system integrators (from *Waite et al., 2014*).

1.4.3 One focus on the peptides under investigations: distribution and roles

1.4.3.1 *Substance P (SP)*

SP is an 11 amino acid neuropeptide belonging to the tachykinins family (166,171). It was the first neuropeptide to be discovered and has been described as the “pioneering neuropeptide”. It was isolated from extracts of equine brain and gut, then purified and dried in a powder form (hence its name) (172,173). It is produced from a polyprotein precursor derived from the preprotachykinin A gene (171) and binds with decreasing affinity to tachykinins receptors [neurokinin receptors (NKR) 1,2,3], which are GPCR: NK₁R>NK₂R>NK₃R (172).

SP is distributed in the central and peripheral nervous system, as well as in immune cells (173,174). In the nervous system, it acts as a neuromodulator and a neurotransmitter and is primarily involved in nociception, however it also has other functions including effects on mood, anxiety, stress, reinforcement, neurogenesis and neurotoxicity (171). Neuroimmune communication is one of the more recently recognised aspects of SP, controlling immune responses at multiple levels from recruitment, proliferation and activation (173,175).

Among the functions in which SP is involved, for the purposes of this thesis, it is important to highlight those in the gastrointestinal tract and in the enteric nervous system (ENS). In ENS, SP is an excitatory neurotransmitter which is found in excitatory muscular motor neurons of the myenteric plexus, in intrinsic primary afferent neurons of both the submucosal and myenteric plexus and in extrinsic sensory fibres and enteroendocrine cells (for a description of the ENS see Section A, Chapter 3.2) (176,177). SP is considered a cholinergic co-mediator (177,178) and is involved in the control of motility and secretion, autonomic reflexes (e.g. vomiting and swallowing), as well as inflammatory and immunomodulatory effects (Fig.34) (172,175,179,180). The role of SP in the gut has been demonstrated in several conditions, including inflammatory bowel disease and gastrointestinal infections (175).

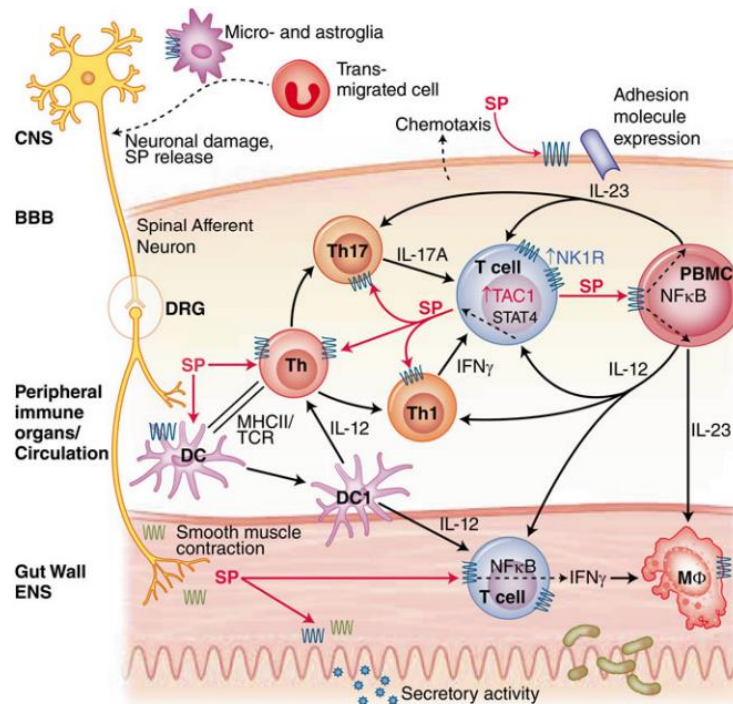


Fig.34: Schematic representation of SP neuroimmune interactions. In blue NK1R, in green NK2R; SP effects are shown in red. Abb: CNS (Central nervous system); BBB (Blood brain barrier); ENS (Enteric nervous system); DRG (Dorsal root ganglion); DC (dendritic cell); M Φ (macrophage); PBMC (peripheral blood mononuclear cell); MHCII (major histocompatibility complex II); TCR (T-cell receptor); Th (T helper cell) (from Vilisar and Arsenescu, 2016).

Although various immunohistochemical studies on SP distribution in the gastrointestinal tract have been carried out in veterinary species such as pigs, dogs, horses and sheep (Fig.35) (181–185), in cetaceans this has only been done in one study in striped dolphins (*Stenella coeruleoalba*) by Domeneghini et al., in 1997, with some shortcomings in the quantification analysis (186).

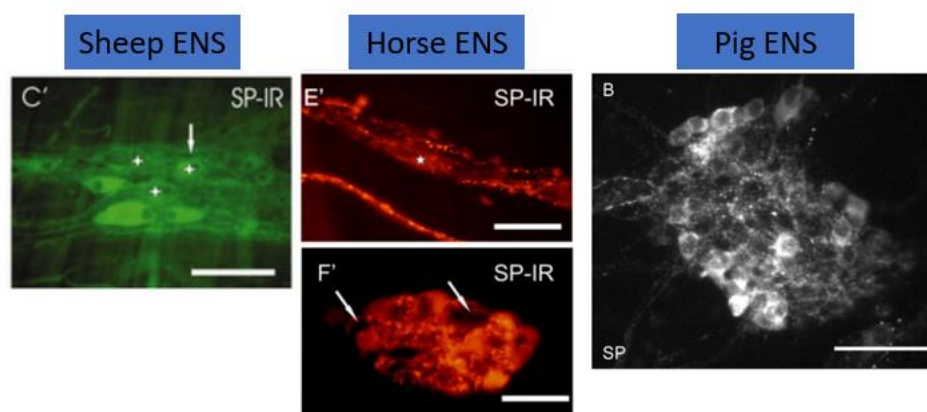


Fig.35: Photomicrographs of SP-IR neurons in the sheep, horse and pig enteric nervous system (ENS) (modified from Mazzuoli et al., 2007; Chiocchetti et al., 2009; Petto et al., 2015).

For the sake of logical consistency, it is important at this point to introduce the second marker chosen in this thesis to study the neuronal population in the dolphin ENS: nNOS. Although it is not part of the peptidergic system, nNOS was useful for distinguishing excitatory neurons from inhibitory ones, as it synthesizes nitric oxide (NO), the primary inhibitory neurotransmitter in the gastrointestinal tract, which induces relaxation of the muscles and sphincters (187,188).

1.4.3.2 Vasoactive Intestinal peptide (VIP)

VIP is a 28-amino-acid peptide first discovered in porcine duodenum in 1970 and described as a molecule capable of inducing vasodilation in blood vessels (hence its name) (189,190). It belongs to the VIP-glucagon family (166) and it is produced by proteolytic cleavage from a 170-amino-acid precursor preproVIP localized on chromosome 6 (191). The aminoacidic sequence is identical in mammals (human, cow, pig, goat, dog and rat, with the exception of guinea pig), suggesting that it has been conserved throughout evolution; in non-mammals it differs from the human sequence by only four or five positions, but the bioactive site is well conserved in these animals (192,193). VIP exerts its roles acting on three GPCR with different affinity (PAC₁, VIP₁ and VIP₂; VIP₁ and VIP₂ > PAC₁) (194).

Although VIP is widely distributed throughout the body in different tissues such as heart, lungs, intestine, thyroid, kidney as well as in immune and endocrine cells, where it acts as a vasodilator, bronchodilator, anti-inflammatory, immunosuppressor and smooth muscle relaxant (189,191), for the purposes of this work it is important to point out its distribution and roles in the nervous system.

VIP is widely distributed in both the CNS and the PNS (193). Centrally, it can be found in the cerebral cortex, in the hypothalamus, in the amygdala, in the hippocampus, in the corpus striatum and in the medulla oblongata (191). VIP acts as a non-adrenergic, non-cholinergic neurotransmitter and neuromodulator (191,195); in some brain regions, VIP-IR neurons have been shown to target other GABAergic interneurons, causing disinhibition of principal excitatory cells (196,197). Among the roles in the CNS, we can mention the enhancement of neuronal cell survival through a neuroprotective role, mainly mediated by glial cells through the production of neurotrophic factors and the inhibition of pro-inflammatory mediators (Fig.36) (189,198) as well as cognitive, behavioural, emotional and endocrine activities (199–203).

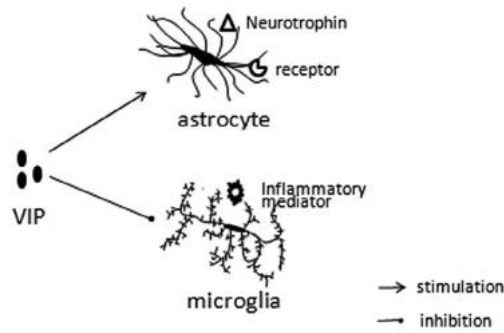


Fig.36: Schematic representation of VIP neuroprotective roles through the control of glial cells (*Deng and Jin, 2017*).

With regard to the AC, a brain region under investigation in this thesis, it is important to highlight the presence of other studies in the literature that have investigated the distribution of VIP in this structure, especially in rat and mouse, focusing only on the central and basolateral nuclei (Fig.37), where it has been found that VIP-IR neurons were GABAergic neurons with different morphologies (small bipolar, bitufted, basket cells and multipolar) (196,204–207).

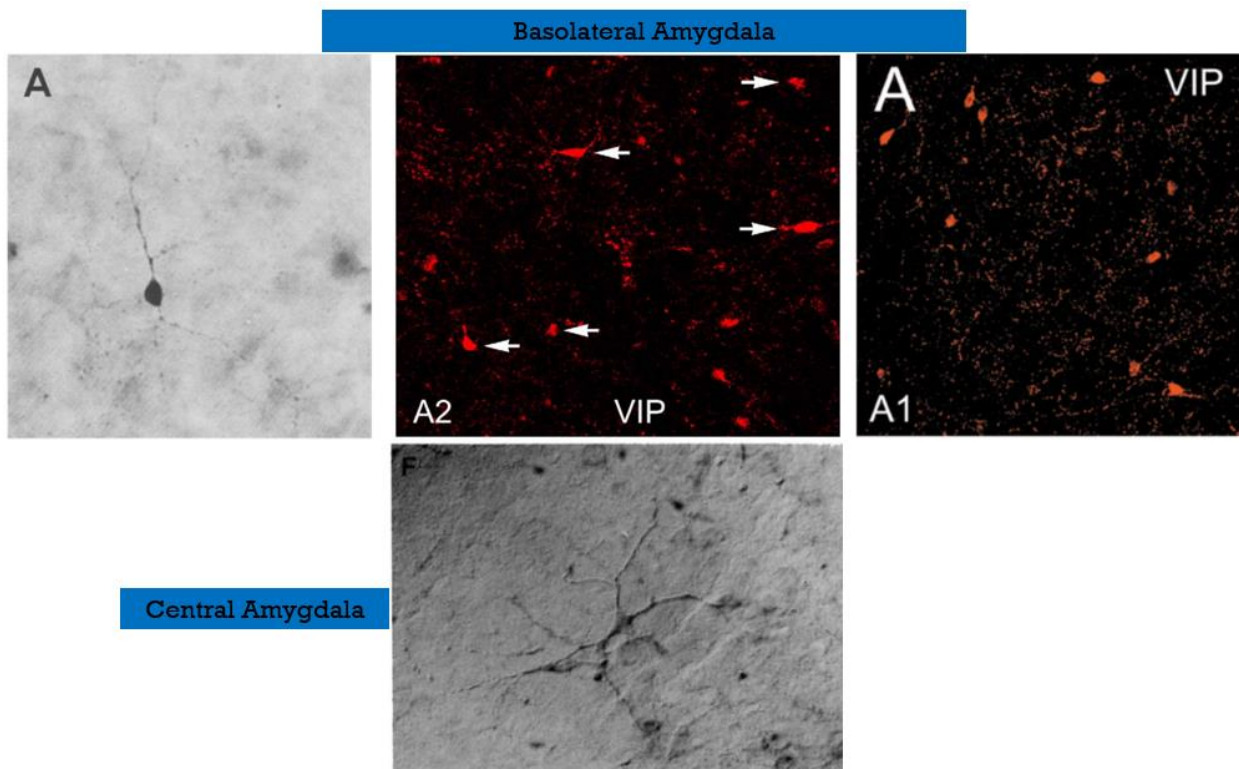


Fig.37: Photomicrographs showing VIP-IR neurons in the basolateral and central amygdala (modified from *Mascagni & McDonald, 2003; McDonald, 1985; Muller et al., 2003; Cassell & Gray, 1989*).

Few studies have been conducted addressing the specific roles of VIP in the amygdaloid complex, among which it is possible to mention its role in the modulation of pain (208), it was found out that plasma levels were negatively correlated with anxiety and depression symptoms, and positively associated with amygdala volume and functional connectivity (209), and that injection of VIP into the amygdala was associated with REM sleep improvement parameters (210).

Chapter 2: Studied Areas of the Central Nervous System in Veterinary Species

2.1 Entorhinal Cortex

2.1.1 Definition, history, cytoarchitecture and functions with a focus on the Bottlenose Dolphin (*Tursiops truncatus*)

The entorhinal cortex (EC) is a brain structure located in the medial temporal lobe, named for its proximity to the rhinal sulcus (Fig.38). The first person to take an interest in the EC was Santiago Ramón y Cajal in the 20th century, who described it as a part of the temporal cortex, closely connected to the hippocampus by what he called the "temporo-ammonic tract" (211–213).

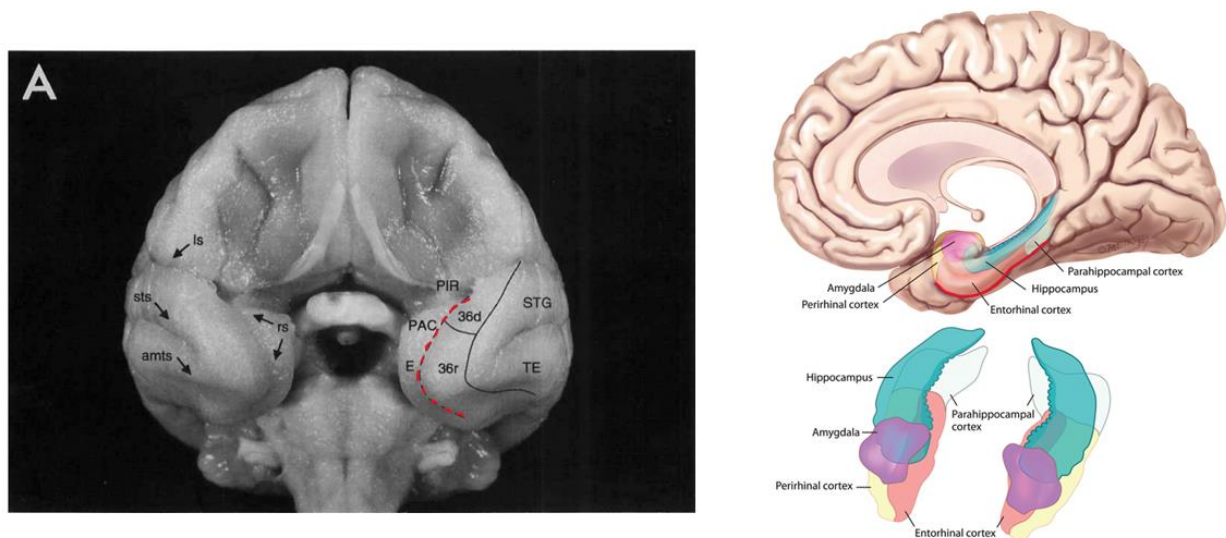


Fig.38: On the left a ventral view of a *Macaca fascicularis* brain showing the entorhinal cortex (E) near the rhinal sulcus (red dashed line), on the right a schematic view of a human brain showing the components of the medial temporal lobe which comprises the entorhinal cortex, in red line the rhinal sulcus (modified from *Raslau et al., 2015; Suzuki and Amaral, 1994*).

In dolphins, although they have a large brain (Fig.39) due to the selective pressure imposed by the aquatic environment on motor, sensory and social abilities, the EC (Fig.40) is relatively reduced (214,215).

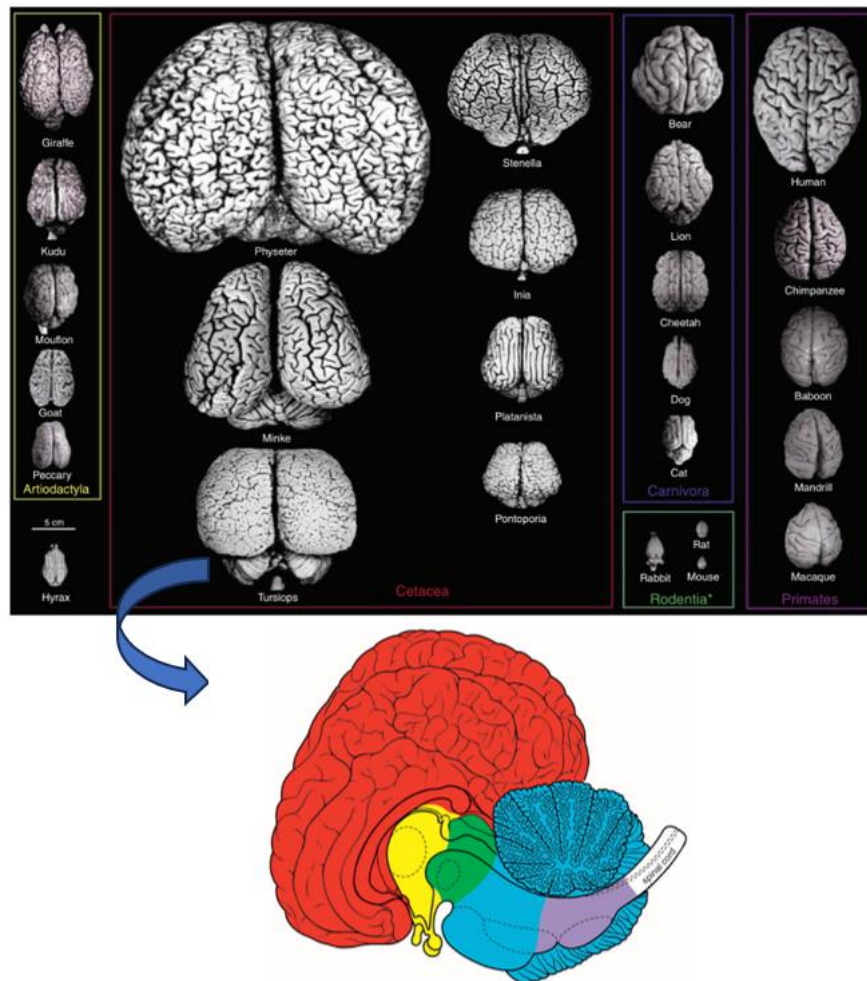


Fig.39: Photographs showing various mammalian brains highlighting the comparative size. On the bottom a schematised *Tursiops truncatus* brain with parts in different colours: telencephalon in red, diencephalon in yellow, mesencephalon in green, metencephalon (cerebellum/pons) in blue, myelencephalon in lilac (modified from Cozzi *et al.*, 2017).

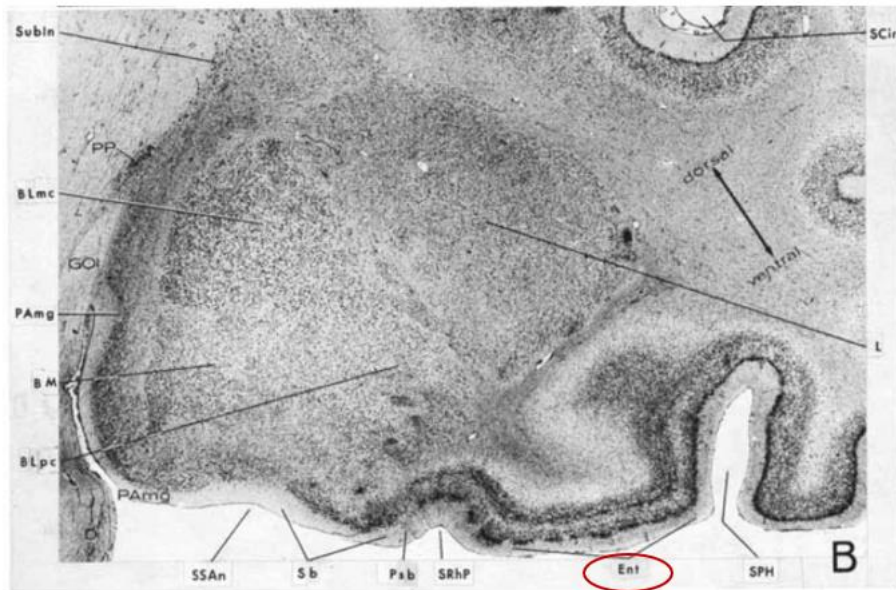


Fig.40: Photomicrographs of a transverse section at the level of the entorhinal cortex (Ent) highlighted in red of a *Tursiops truncatus* (modified from Jacobs *et al.*, 1971 (216)).

Various subdivisions have been proposed for the EC, this work will refer to the ones that divide it in the lateral entorhinal area or cortex (LEA/LEC) and the medial entorhinal area or cortex (MEA/MEC) (Fig.41) (212,217).

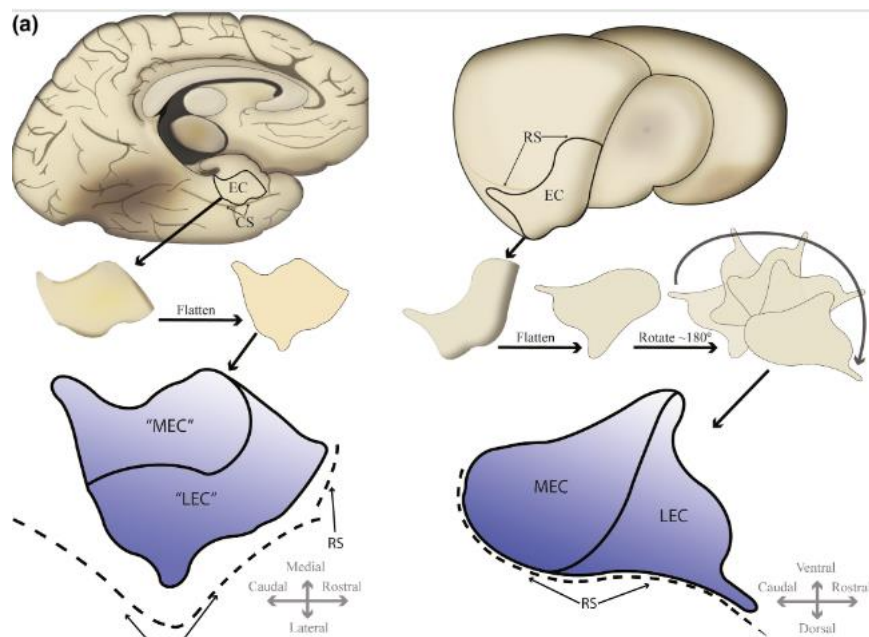


Fig.41: Schematic representation of the EC subdivisions (LEC= lateral entorhinal cortex; MEC=medial entorhinal cortex) in a human brain on the left and in a rat brain on the right (modified from Kibro-Flatmoen *et al.*, 2019).

Each subdivision can be further partitioned in six layers (I-VI), where MEC is characterised by a very regular structure with an homogeneous distribution of neurons whereas LEC is less regular (Fig.42) (212).

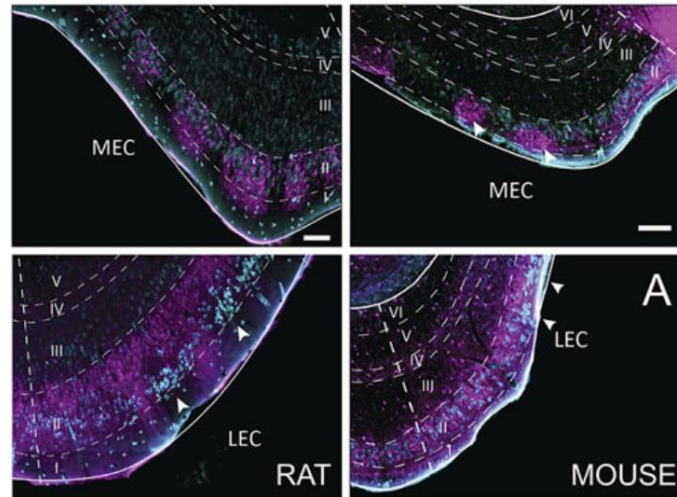


Fig.42: Photomicrographs of rat and mouse entorhinal cortex showing the six layers (I-VI) (modified from Witter *et al.*, 2017).

Only one study from Jacobs *et al.*, 1979 (218) describes the six layered division of EC in dolphins as well with a IV layer almost acellular, similar to other mammals, that can be referred as *lamina dissecans*. To the best of the author knowledge no studies have been conducted showing the cytoarchitecture and the cytoidentity of the bottlenose dolphin EC.

In terrestrial mammals the EC is involved in high-cognitive functions, serving as the main entry point for the information processed by the hippocampal formation, the limbic complex originating from the amygdala and the olfactory bulb. It is also a relay point to send information to the neocortex (212,219). Several populations of neurons responsible for spatial orientation and navigation, which control locomotion by taking into account parameters such as location, head position, speed, distance and time, have been found in the EC (215).

2.2 Amygdaloid Complex

2.2.1 Definition, history and functions

What is nowadays called the ‘Amygdaloid Complex’ or ‘Amygdala’ or ‘Amygdalar Complex’ represents a set of numerous equilateral structures located deep in the cranial and medial area of the temporal lobe (Fig.43) (220–222).

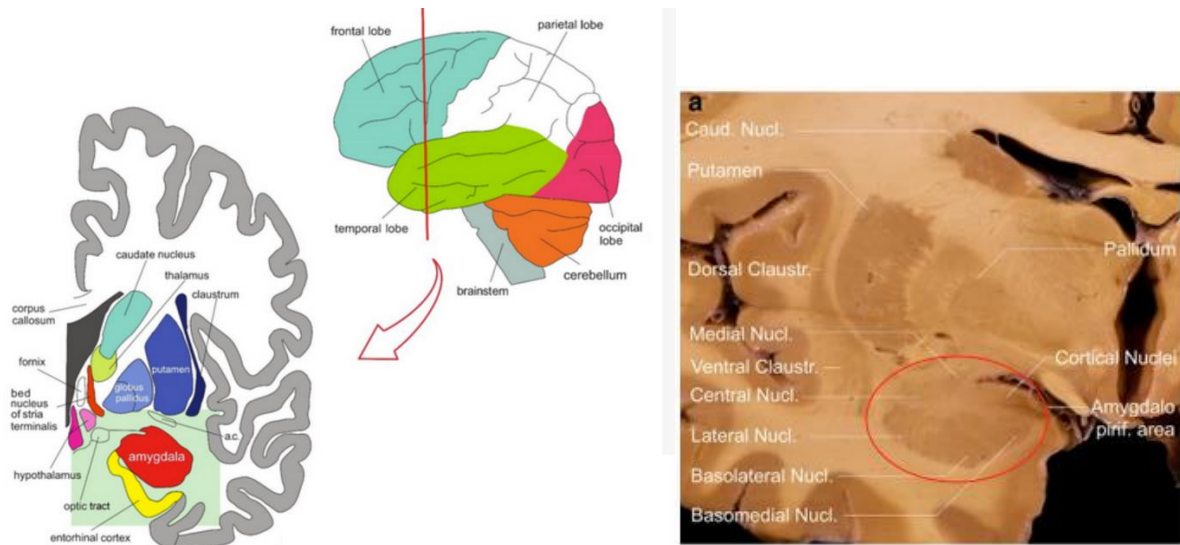


Fig.43 Left: top drawing of male encephalon (temporal lobe in green); bottom drawing of coronal section made at the level of the cranial portion of the left temporal lobe (red line), note in red the amygdaloid complex (AC) in frontal view positioned in the medial part of the temporal lobe. Right: coronal section of human encephalon taken at the level of the anterior commissure, circled in red the area of the AC (modified from Šimić *et al.*, 2021; Weiss *et al.*, 2021 (223)).

The characterisation of the totality of these structures took place in stages, decade after decade, mainly due to the development of histological techniques since the end of the 19th century (224). The first description and illustration of the amygdala dates back to 1822 and is attributed to the German Karl Friedrich Burdach (225) who, while making coronal cuts in the cerebral hemispheres of man (221), noticed an area of grey matter in the anterior part of the temporal lobes to which he gave the name “Mandelkern” (*Amygdalar nucleus*) precisely because of its almond-nut shape (Fig.44) (226,227).

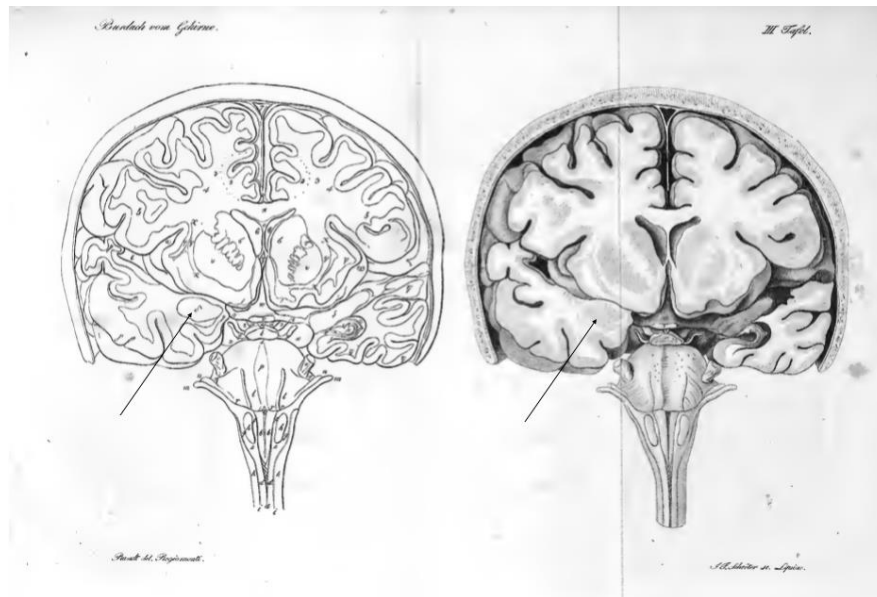


Fig.44: First stylised representation of the human amygdala (indicated by the arrow) according to K.F. Burdach. In both images there is an anterior coronal section on the left (at the level of the amygdala) and a posterior coronal section on the right that makes the hippocampus visible (modified from *Burdach, 1822*).

After Burdach, many other scientists have been worked trying to characterised morphologically and cytoarchitectonically the AC with the aim of defining a complete and comprehensive subdivision of the component parts, this has led to the emergence of different nomenclatures and terminologies which are still a cause of confusion when interpreting and systematising data obtained in the laboratory, making the AC one of the most discussed structures of the brain (226,228,229).

The AC has been poetically considered the ‘sensory gateway to emotions’ by Aggleton and Mishkin (1986) (230), a structure that acts as a ‘filter’ for the constant barrage of input from both the external and internal worlds, which modulates these signals and sends responses to the remaining brain structures that subsequently translate into specific adaptive behaviours and physiological responses of the organism (231). The AC is essentially the structure that interconnects the regions of the brain responsible for processing sensitive information (such as the cerebral cortex) with the regions responsible for emotional and motivational reactions (such as the

hypothalamus, brainstem and striatum) (232). Not by chance the AC has been included in the limbic system, an ensemble of brain structure which are considered the anatomical basis for the emotions (233,234). The AC is activated when a negative emotion is involved, while it is inhibited when a positive emotion is involved (222). Among the most extensively investigated AC emotions is undoubtedly fear (228) the oldest and strongest of the emotions, which plays a fundamental role in vertebrate evolution (222). The AC plays an important role in preparing the organism for the ‘fight or flight’ mechanism (235). In this sense, numerous studies have been carried out to investigate which areas of the AC are involved through the creation of the so-called ‘Pavlovian conditioning’ (named after its creator Ivan Pavlov). These studies have confirmed that conditioning causes synaptic plasticity in the lateral nucleus of the amygdala, which is then ‘trained’ to reactivate upon the second presentation of the conditioned stimulus. When this happens, the signal is sent from the lateral nucleus to the other amygdaloid nuclei and finally to the central nucleus, the latter's efferences then recruiting the brain areas deputed to fear responses (such as freezing or related endocrine and autonomic physiological changes) (Fig.45) (228,236).

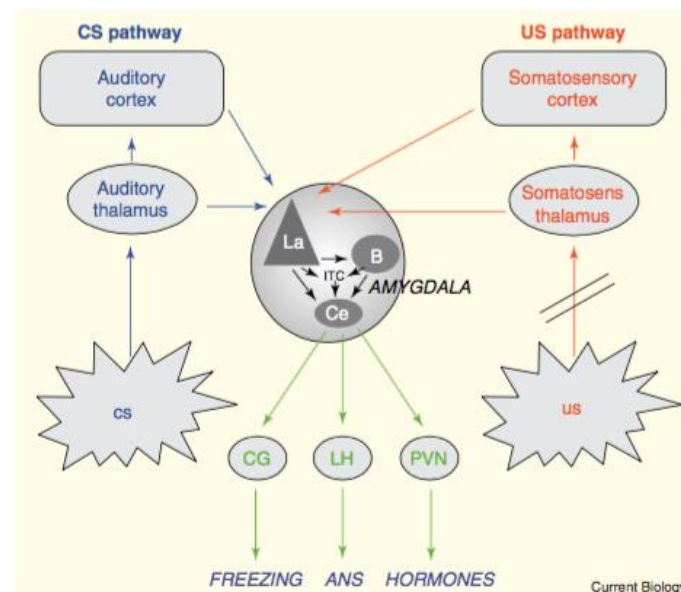


Fig.45: Summary diagram of the mechanisms involving the AC during ‘Pavlovian conditioning’. CS= Conditioned stimulus (e.g., a sound); US= Unconditioned stimulus (e.g., an electric shock); La= Lateral nucleus; B= Basal nuclei; Ce= Central nucleus; ITC= Intercalated nuclei; CG= Central or periaqueductal grey; LH= Lateral hypothalamus; ANS= Autonomic nervous system; PVN= Paraventricular nucleus of the hypothalamus (from *LeDoux, 2007*).

Other emotions in which AC is functionally involved include: aggression (both impulsive and premeditated) (222). A study conducted on dogs that underwent temporal lobe ablation showed an increase in their ease of training (237), behaviours associated with the sexual and reproductive sphere, including related neuroendocrine responses such as reactions induced by chemical stimuli such as pheromones (238) and eating behaviour. AC plays a pivotal role in reward processes to reinforce a certain type of behaviour, learning or motivation as well as substance addiction

(228,238–240); it also plays a key role in the consolidation of memories associated with an emotional experience (241) as well as in other cognitive functions such as attention and perception (228). Moreover, the amygdala is implicated in behavioural disorders such as anxiety, depression, bipolarism, panic attack , social phobias, post-traumatic stress disorder and autism spectrum disorders (222,242,243), in addition to neurodegenerative diseases (Alzheimer's disease, Lewy body dementia and Parkinson's disease (244) and the pain circuit, playing a role in conscious awareness and cognitive assessment of pain and its modulation (245).

2.2.2 Anatomy, cytoarchitecture and connectivity with a focus on Rat (*Rattus norvegicus*) and Sheep (*Ovis aries*)

The nomenclature used in this work for the subdivision of nuclei contained within the AC is derived from Pitkänen and Kemppainen, 2002 (246) with appropriate modifications to take into account contributions from other authors based mainly on data from humans, rats, monkeys and cats. The AC is composed of different cortical and subcortical nuclei that are distinguished by embryogenic developmental, cytoarchitectural and immunohistochemical features. From an embryogenic point of view, the AC can be divided into pallial, for those nuclei originating from the neuroepithelium of the embryonic pallium and ganglionic eminences, which comprise deep and superficial nuclei and subpallial, for those nuclei originating from the telencephalic subpallium, which comprises the remaining nuclei also called “extended amygdala”. The lists of nuclei and subdivisions of nuclei are given in Fig.46 and a schematic view of the rat amygdala is given in Fig.47 (221,224,246–255).

PALLIAL AMYGDALA					SUBPALLIAL AMYGDALA				
DEEP NUCLEI					SUPERFICIAL NUCLEI				
Lateral Nucleus					N. of the Lateral Olfactory Tract				
Human	Rat	Monkey	Cat	NS	Human	Rat	Monkey	Cat	NS
lateral	dorsolateral	dorsal	NS		NS	NS	NS	NS	
medial	ventrolateral	interm. dorsal			Interstitial N. of the Accessory Olfactory Tract				
	medial	interm. ventral			Human	Rat	Monkey	Cat	NS
		ventral			NS	NS	NS	NS	
Basal Nucleus					Anterior Cortical Nucleus				
Human	Rat	Monkey	Cat		Human	Rat	Monkey	Cat	NS
magnocellular			magnocellular		NS	NS	NS	NS	
parvocellular			parvocellular		Posterior Cortical Nucleus				
intermedial					Human	Rat	Monkey	Cat	NS
Accessory Basal Nucleus					NS	NS	NS	NS	
Human	Monkey	Rat	Cat		Periamygdaloid Cortex (PAC)				
magnocellular		magnocellular			Human	Rat	Monkey	Cat	
parvocellular		parvocellular			oral PAC	PAC	oral PAC	NS	
ventromedial					PAC 1	medial PAC	PAC 1		
Anterior Amigdaloid Area					PAC 3	sulcale PAC	PAC 2		
Human	Rat	Monkey	Cat		sulcale PAC		PAC 3		
NS	NS	NS	NS				Sulcale PAC		
Amigdalohippocampal Area					Bed N. of the Stria Terminalis				
Human	Rat	Monkey	Cat		Human	Rat	Monkey	Cat	
lateral	medial	dorsal	NS		NS	NS	NS	NS	
medial		ventral							
Paralaminar Nucleus					Intercalated Nuclei				
Human	Rat	Monkey	Cat		Human	Rat	Monkey	Cat	
lateral	A	NS	NS		NS	NS	NS	NS	
medial									

Fig.46: List of AC nuclei and nuclei subdivisions in human, monkey, rat and cat. A=absent; NS=no subdivision; colours are given accordingly to the next figure (modified from Pitkänen and Kemppainen, 2002).

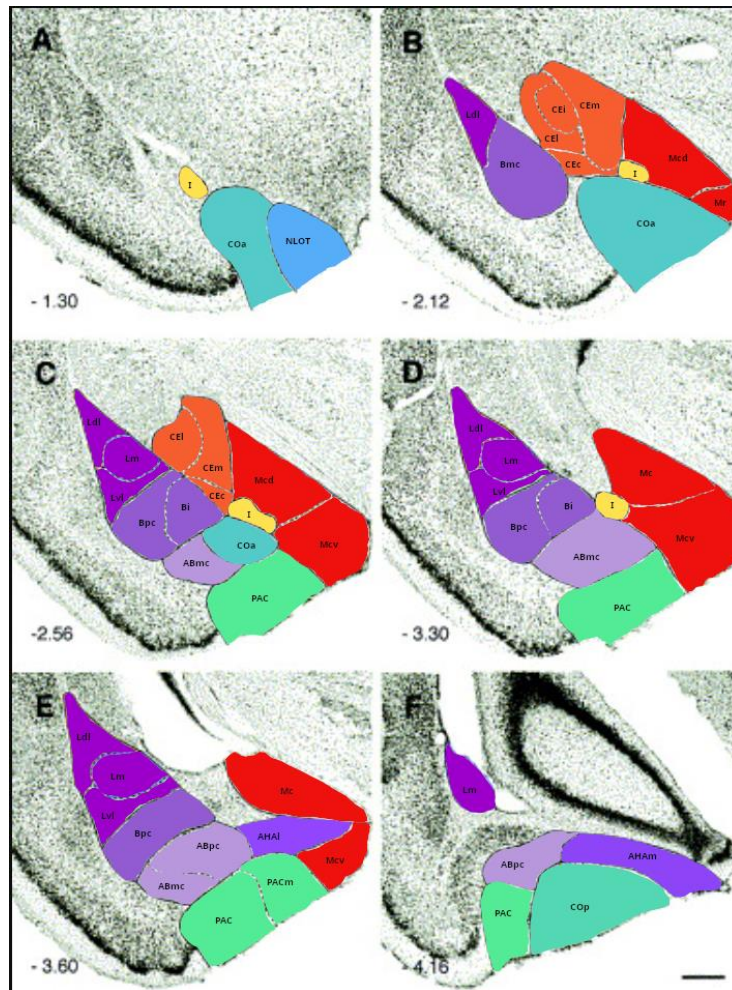


Fig.47: Schematic representation of AC nuclei and nuclei subdivisions in rat. Colours have been superimposed on rostro (A) caudal (F) amygdala sections. Ldl= lateral nucleus dorsolateral subdivision (sub.); Lm= lateral nucleus medial sub.; Lvl= lateral nucleus ventrolateral sub.; Bi= basal nucleus intermediate sub.; Bmc= basal nucleus magnocellular sub.; Bpc= basal nucleus parvocellular sub.; NLOT= nucleus of the lateral olfactory tract; COa= Anterior cortical nucleus; COp= Posterior cortical nucleus; Mr= Medial nucleus rostral sub.; Mcd= Medial nucleus central sub. dorsal part; Mcv= Medial nucleus central sub. ventral part; Mc= Medial nucleus caudal sub.; PAC= Periamygdaloid cortex proper; PACm= Periamygdaloid cortex medial sub.; PACs= Periamygdaloid cortex sub. sulcale; CEC= Central nucleus capsular sub.; CEI= central nucleus lateral sub.; CEi= central nucleus intermediate sub.; CEm= central nucleus edial sub.; AHAl= amygdaloippocampal area lateral sub.; AHAm= amygdaloippocampal area medial sub.; I= Intercalated nuclei (modified from *Pitkänen and Kemppainen, 2002*).

For sheep, there are limited data in the literature on an exhaustive subdivision of the nuclei, only one study focusing on the comparison of fear conditioning in sheep and goats gives a brief anatomical description of the nuclei, subdividing them into: the deep group or basolateral complex, which includes the basal, lateral and accessory basal nuclei; the superficial group, which includes the cortical nuclei; and the anterior group, which includes the central nuclei (Fig.48) (256).

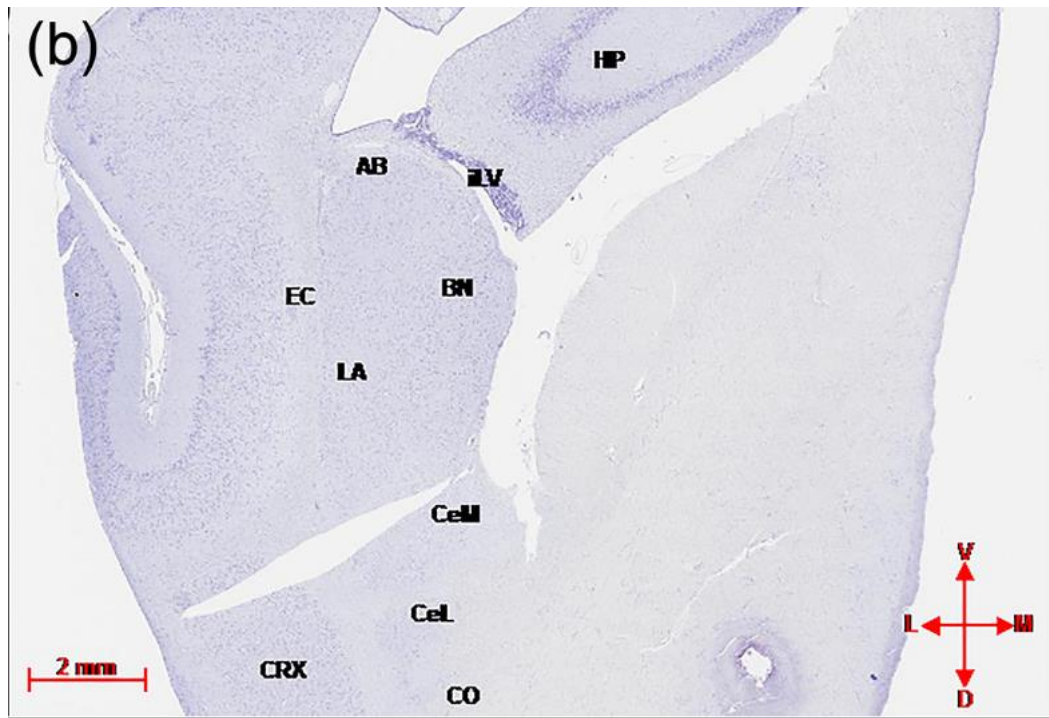


Fig.48: Photomicrographs of a coronal section of the sheep amygdala illustrating the nuclei and the surrounding structures. AB= Accessory basal, BN= basal nuclei, LA= lateral nuclei, CeM= central medial nuclei, CeL= central lateral nuclei, CO=cortical nuclei, iLV= inferior horn of lateral ventricle, HP=hippocampus, CRX=cortex, EC=external capsule; D=dorsal, V=ventral, L=lateral, M=medial (modified from *George et al., 2021*).

Morphological studies based mainly on rodents describes how the superficial and deep nuclei are characterised by a cortical-like structure, in which approximately 85% of the neurons are glutamatergic pyramidal or pyramidal-like neurons with spiny dendrites, and the other 15% are mainly GABAergic non-pyramidal neurons with spine-sparse dendrites, which can be characterised by their protein content (e.g. PV, somatostatin (SOM), VIP, CCK). In contrast, the remaining nuclei or extended amygdalar nuclei contain predominantly GABAergic spiny projection neurons, like the striatum (257).

With regard to AC connections, there is an extensive literature, based mainly on the use of anterograde and retrograde tracers in rats, monkeys and cats, which leads to the knowledge that they can be divided into three different groups:

- *extramygdaloid*: these include afferences and efferences connecting the amygdala with cortical and subcortical areas;
- *intramygdaloid*: connecting circuits within the amygdala itself. These can be further subdivided into intra-divisional, inter-divisional and internuclear;
- *interamygdaloid*: connecting the amygdalae to each other;

Among the extramygdaloid connections, three bundles of fibres seem to be the most important, especially for the connections within the basolateral group of nuclei, which represents the main input area of the CA: the ventral amygdalofugal pathway, the stria terminalis, which are mainly the subcortical fibre system, and the external capsule, which is mainly the cortical fibre system (220,226,228,232,257–263).

Little data exist specifically on the connectivity of the sheep AC, only one study examined the afferent and efferent connections, using anterograde and retrograde tracers, within the medial and cortical nuclei and the rest of the brain, anyway no data exist on the connectivity within the basolateral group (264).

2.3 Optic Lobe of the Honeybee (*Apis mellifera*)

Firstly, a general description of the CNS of such an unconventional animal species as the honeybee is essential to help the reader understand a specific area of its nervous system: the optic lobe. The CNS of the honeybee comprises three connected parts: the brain, the subesophageal ganglion (SOG) or gnatocerebrum, which are located in the head, and the ventral ganglion chain which starts from the SOG and runs through the thorax and the abdomen along the median ventral line (Fig.49) (265,266).

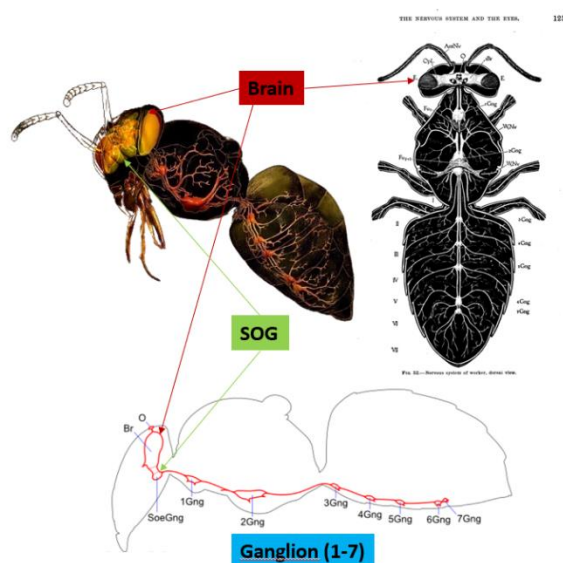


Fig.49: Schematised view of the honeybee SNC composed by brain, subesophageal ganglion (SOG) and ganglion (1-7) [modified from Snodgrass, 1996 and websites sources (267,268)].

The brain, the part of the CNS that contains the optic lobes, is approximately 1 mm² in volume and contains nearly 1 million neurons. Despite the small size, bees demonstrate very complex cognitive abilities, making them an important animal model for ethology and neurobiology (269,270). Its main function is to assimilate sensitive information, process it, elaborate appropriate responses and send them to the periphery (271). The brain can be subdivided in three parts: the protocerebrum, the deutocerebrum and the tritocerebrum. The protocerebrum is the most rostral and dorsal segment and it comprises the optic lobe (OL), the central complex and the mushrooms bodies. The deutocerebrum comprises the antennal lobes. The tritocerebrum is the smallest component and comprises two bilateral lobes in the ventral part of the brain connected each other through a commissure passing caudally the oesophagus (Fig.50) (57,269,271–274).

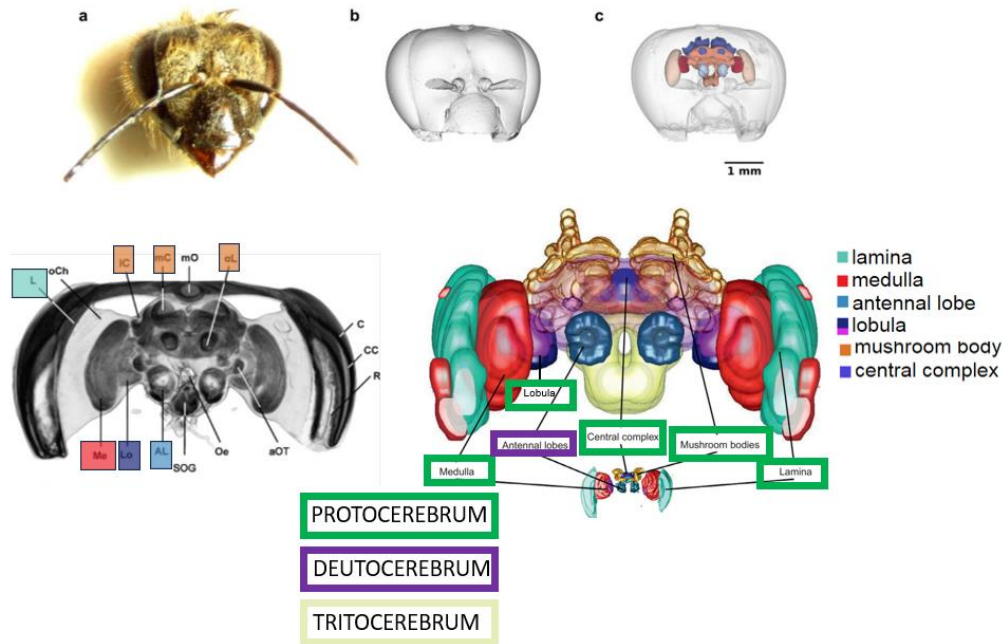


Fig.50: Different perspective of the honeybee brain composed by the protocerebrum in green [composing parts: Optic Lobes, divided in Lamina (L), medulla (Me), Lobula (Lo), the central complex and the mushroom bodies divided in lateral calyx (lC), medial calyx (mC), alpha e beta lobe (α - β L)], the deutocerebrum in purple, comprising the antennal lobes (AL), and the tritocerebrum in yellow (modified from Lösel *et al.*, 2022, Ribi *et al.*, 2008 and Søvik *et al.*, 2015).

The OLs are lateral extensions of the protocerebrum, each consisting of three neuropil layers from distal to medial: lamina, medulla and lobula (Fig.51) (269,275,276), with some authors including also the lobular plate, especially in *Drosophila* (277,278). The lamina and the medulla can be divided in an inner and outer subregion, the medulla has a thin layer between the inner and outer subregions called the serpentinite layer (276). Between the layers there are also groups of fibres that connect them: the first or outer optic chiasm, which connects the lamina and the medulla, and the second or inner optic chiasm, which connects the medulla and the lobula. In each layer, the neuropil is organised into columns, each corresponding to an ommatidium in the retina, in fact the OL is responsible for transmitting visual information received from the compound eyes to the centre of the brain, where visual inputs are processed and integrated with information from other sensory modalities. Neurons projecting from the optic lobes to the mushroom bodies are sensitive to color and motion, providing specific visual features to higher-order brain structures (57,275,277,279). In addition it has been demonstrated that the OL is involved in attention-like processes and behaviour (280).

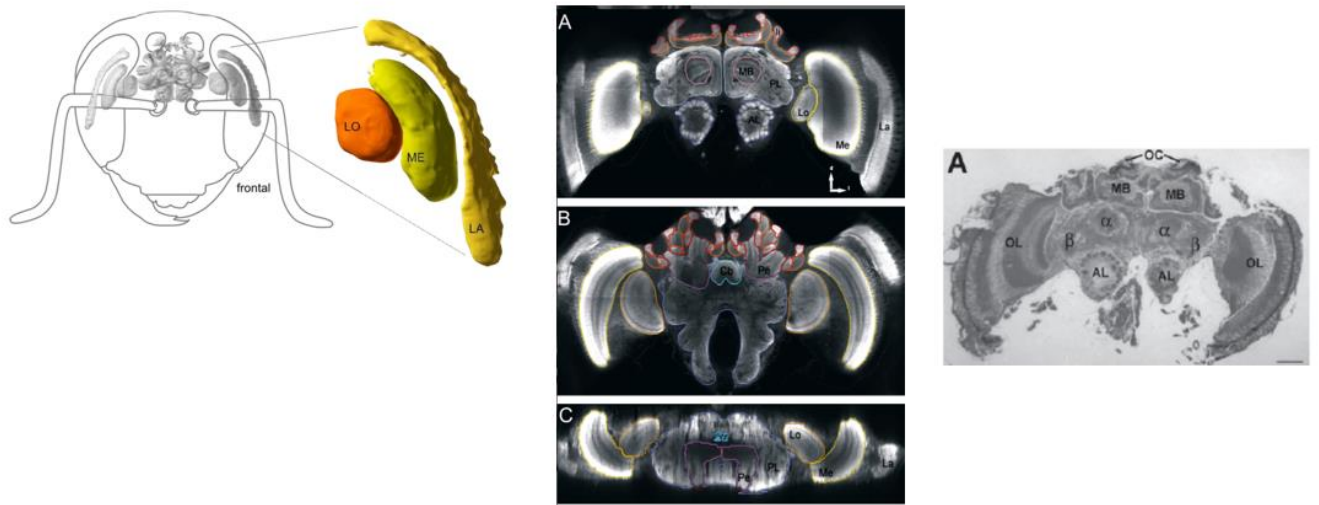


Fig.51: Representation of the constituent parts of the Optic lobe (OL): Lobula (Lo), Medulla (Me) and Lamina (La) [modified from *Honkanen et al., 2023*, *Ribi et al., 2008*; *Brandt et al., 2005*; *Calábria et al., 2010* (281)].

Chapter 3: Studied Areas of the Peripheral Nervous System in Veterinary Species

3.1 Trigeminal Ganglion of the Horse (*Equus ferus caballus*) and its involvement in the headshaking pathology

The TG, also known as “Gasser's ganglion” or “semilunar ganglion”, is one of the components of the trigeminal nerve, fifth cranial nerve and the largest of the twelve, emerging near the caudal edge of the pons and located in the trigeminal cave. It is the part conferring the major sensitivity (a small part is conferred also from the nucleus of the mesencephalic tract) to all three sensory nerves composing the trigeminal nerve (hence its name): the ophthalmic, the maxillary and the mandibular, this latter has also motor function deriving from motor fibre originating from the motor nucleus located in the pons (Fig.52).

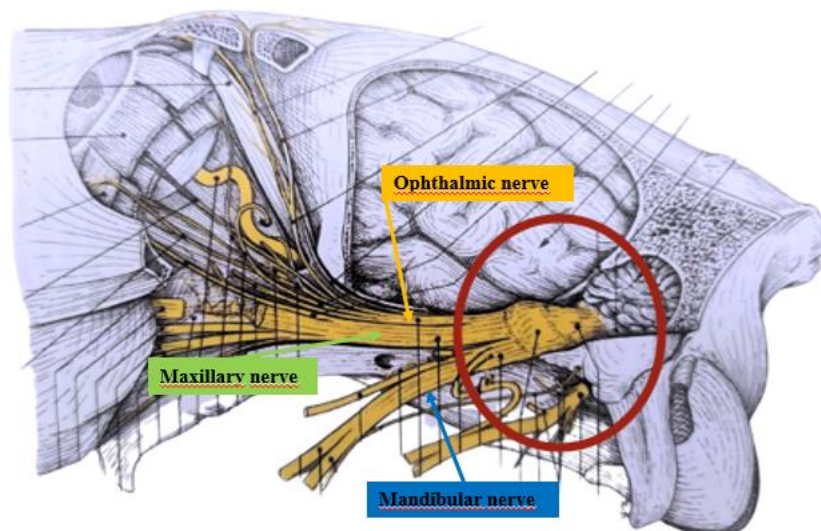


Fig.52: Drawing of a horse head lacking some part of the bones to make visible the trigeminal ganglion (red circle) and the three branches of the trigeminal nerve (maxillary, ophthalmic and mandibular) (modified from Barone and Simoens, 2012).

The TG which contains sensory neuron bodies for pain and temperature modalities gives rise to the three peripheral nerves which innervate and confer the sensitivity almost to the entire corresponding half of the head, in fact the ophthalmic branch innervates the frontorbital plane, the maxillary branch the nasomaxillary one and the mandibular branch the mandibolingual one (Fig.53). The motor part of the mandibular nerve, on the other hand, is distributed only to the masticatory muscles and, via small branches, to the digastric and mylohyoid muscles.

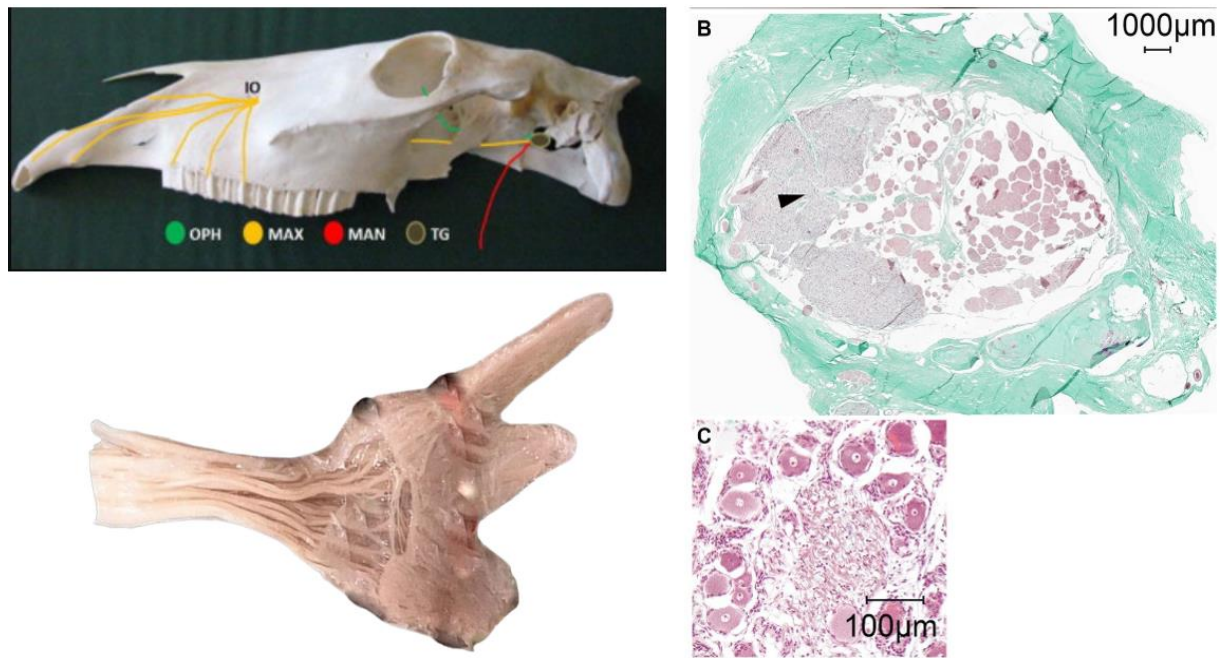


Fig.53: On the left top a schematic representation of the directions of the three nerve branches (oph: ophthalmic, max: maxillary, man: mandibular); on the left bottom a trigeminal ganglion (TG) deriving from an human cadaver; on the right two photomicrographs showing the TG (black arrowhead) and the same part at higher magnification showing the large bodies of sensitive neurons coloured by hematoxylin and eosin [modified from *Pickles et al., 2014; Becker et al., 2024; Zhang et al., 2024* (282)].

In addition to the bundles of peripheral fibres that enter into the constitution of the three branches of the trigeminal nerve, central fibre bundles also originate from the trigeminal ganglion which penetrate the pons and on the one hand with ascending bundles terminate in the pontine nucleus of the trigeminal nerve, and on the other hand with descending bundles form the trigeminal tubercle that heads into the brainstem, reach the spinal cord and terminate in the nucleus of the spinal tract of the trigeminal nerve, which extends to the second cervical vertebra (Fig.54) (283–285).

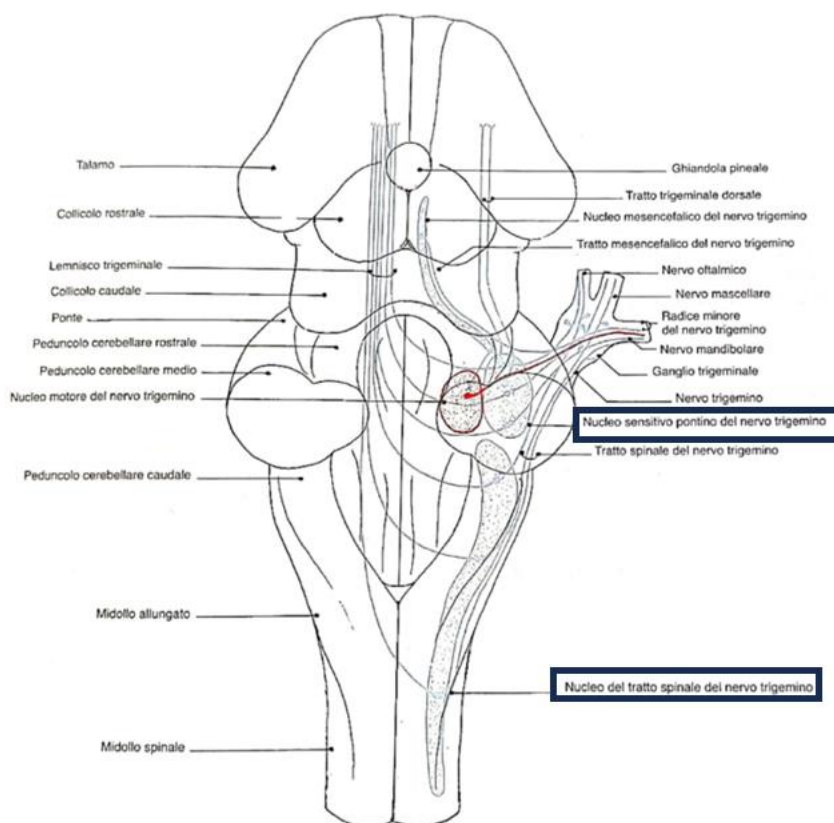


Fig.54: Drawing of a brainstem tract showing the fibres originating from the trigeminal ganglion, highlighted in blue the central branches going to the nucleus of the spinal tract and the pontine nucleus of the trigeminal nerve (modified from *Barone and Simoens, 2012*).

TG is implicated in a clinical syndrome affecting the horse called headshaking (HSK). This is characterized by repeated, uncontrollable, predominantly vertical movements of the head and neck, often accompanied by nasal irritation, with severe discomfort to the horse, which may traumatize itself and others (286). Although this pathology has been recognised in horses more than 100 years ago and the involvement of the trigeminal nerve has always been suspected, it was confirmed in 2013 by a study performed by Aleman and colleagues using the sensory nerve conduction evaluation on HSK-affected and control horses with a somatosensory evoked potential technique, in which they found out that the activation threshold of the infraorbital nerve (a branch of the maxillary division) of the trigeminal nerve was abnormally lower in HSK-affected horses than in controls (284,287). Until this time, the most commonly used term was idiopathic headshaking, because when other causes of facial pain responsible for uncontrollable movements, including guttural pouch disease, dental pathology and sinus disease, were excluded, the only appropriate cause seemed to be neuropathic facial pain without a precise aetiology (286). Nowadays, with the understanding of the TG involvement, it is more correct to speak of TG mediated HSK, which affects approximately 1% of the equine population (284,288,289).

Despite the fact that some pathogenetic evidence in humans differs from that in horses, such as the demyelination of the trigeminal nerve root or the involvement of a herpes virus in some cases, the similarities in clinical signs make equine TG-mediated HSK a condition comparable to human trigeminal neuralgia and therefore a suitable model for translational research (289). Further studies are needed to understand the exact cause of the abnormal trigeminal hypersensitivity in horses, as the pathogenesis of TG-mediated HSK remains insidious (284).

Although various treatments have been proposed and tested to handle the disease in horses, ranging from surgery to unconventional techniques such as neuromodulation and electroacupuncture, to drug therapies such as anticonvulsants gabapentin or carbamazepine, among others (for a complete review see Roberts, 2019), an effective and definitive treatment with low side effects is still lacking, and for this reason research in this field is still useful (289). In this sense, and for the purposes of this work, it is important to highlight that no studies have been carried out on the use of cannabinoids as a treatment for TG-mediated HSK in horses, but promising results can be found in the treatment of neuropathic pain and trigeminal neuralgia in humans (290,291).

3.2 The Enteric Nervous System of the Bottlenose Dolphin (*Tursiops truncatus*)

The digestive system of cetaceans is radically different from that of other land mammals, though it is curious that little is known about their ENS in particular. Among the main differences in the digestive system of the dolphin, caused by the adaptation of life under water, we can mention, first of all, those of the teeth, the shape of the mouth and the development of the masticatory muscle, due to the necessity to swallow the prey (usually fish or cephalopods), limiting the ingestion of water, dolphins have a wide oral rim to allow the mouth to be opened to a large vertical angle, teeth that are almost identical with no clear distinction between the crown, neck and root because chewing is not required, as well as limited development of the masseter muscle, which is responsible for the repetitive grinding of food. The tongue has no conventional papillae and taste buds but only anterolateral papillae, with some authors suggesting to have a role in creating a seal between the tongue and the oral cavity (Fig.55) (215).

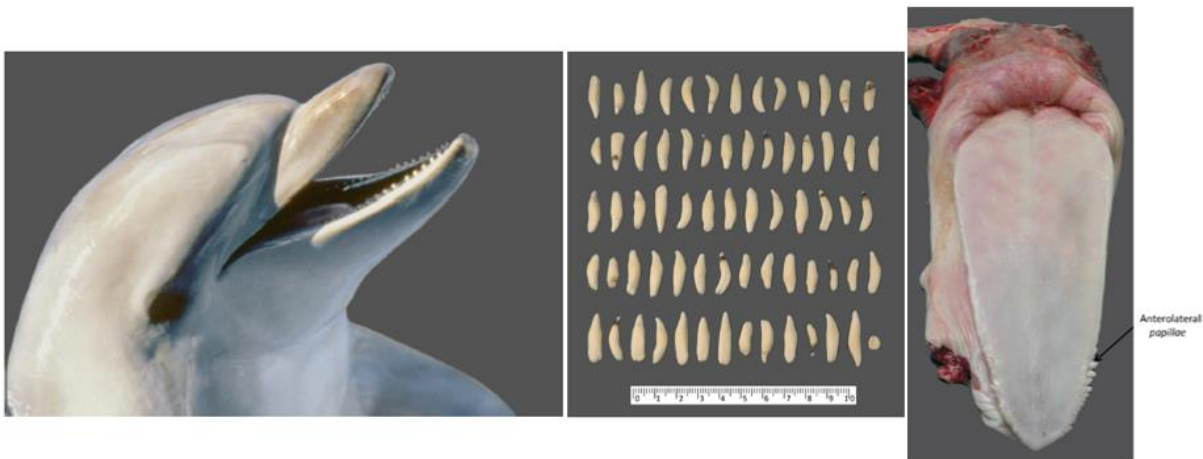


Fig.55: Mouth, teeth and tongue of an adult *Tursiops truncatus* (modified from Cozzi *et al.*, 2016).

At the end of the mouth the faucal isthmus allows the passage of the food and limits the quantity of water entering the pharynx, which consists of two dorsally connected canals that wrap around the larynx and then join the oesophagus and pass dorsally to the trachea. The larynx can be voluntarily pushed aside to allow the passage of food (Fig.56) (215,292).

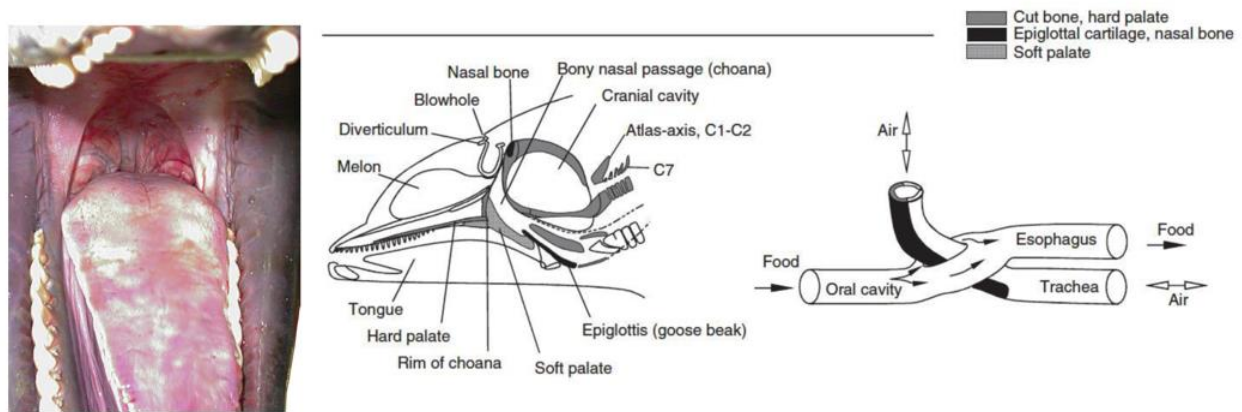


Fig.56: On the right the faucal isthmus, on the left a schematic representation of pharynx and larynx of a *Tursiops truncatus* [modified from Cozzi *et al.*, 2016 and from website source (293)].

Dolphins have a multi-chambered stomach to compensate for the lack of chewing, made up of: the first (the forestomach), which acts as a grinding and compressing chamber, the second (the true stomach), which produces the gastric juice, and the third (the pyloric stomach), which is continuous in the duodenal ampulla, an initial enlargement of the duodenum (Fig.57) (215,294).

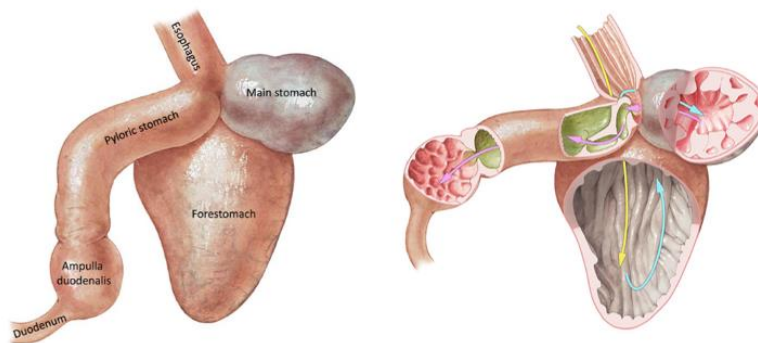


Fig.57: Schematic representation of the multi-chambered stomach and its chambers connections of a *Tursiops truncatus* (modified from Cozzi *et al.*, 2016).

The peculiar feature of the dolphin's intestine is the lack of external subdivision of the various tracts, so much so that it is considered the analogue of the human small intestine, also because of the similarities within the mucosa (Fig.58). It also lacks a caecum or vermiform appendix and a gallbladder. These differences are probably due to their diet, which is mainly protein-based (215,294).

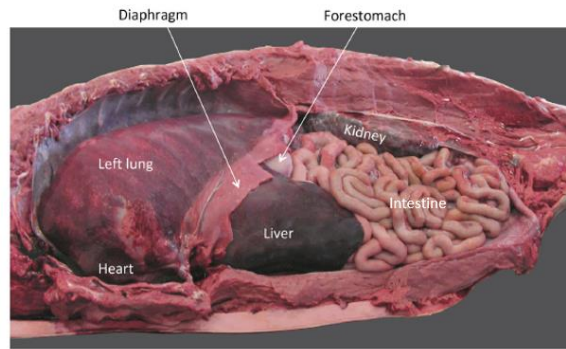


Fig.58: General appearance of the thorax and abdomen cavities of a *Tursiops truncatus* in which it can be visible the intestine (modified from Cozzi *et al.*, 2016).

As far as the microscopic characteristics of the intestinal layers are concerned, no differences have been found with respect to land mammals, which are characterised by an inner mucosa with villi and microvilli, the *lamina propria*, the *muscularis mucosae* and the subsequent layers, the submucosa, the muscularis externa and the serosa. Within the layers of the muscularis externa and on its inner surface, the so-called ENS can be found (215).

As noted above, little is known specifically about the characteristics of the cetacean ENS, with studies investigating the orexin system, leptin-like peptide, other neuropeptides and biogenic amine distribution (186,295,296). The ENS comprises a large amount of neural tissue (approximately 1000-15000 cell bodies/cm², roughly the same number as in the spinal cord) embedded in the wall of the gastrointestinal (GI) tract from the upper oesophagus to the internal anal sphincter of the rectum. It also appears to be present in the biliary system and in the pancreas (as these structures arise from parts of the intestine during embryogenesis) and in the walls of the trachea and bronchi, where fibres appear to be sent from bodies in the oesophagus (177).

Because of its autonomy, it is considered part of the autonomic nervous system, along with the sympathetic and parasympathetic systems (Fig. 59), and because of its complexity, it has been called "the brain in the gut" or "the second brain", with some authors arguing that it is the "first brain" because it has appeared before and independently of the brain throughout evolution and is present in species without a developed CNS (297,298).

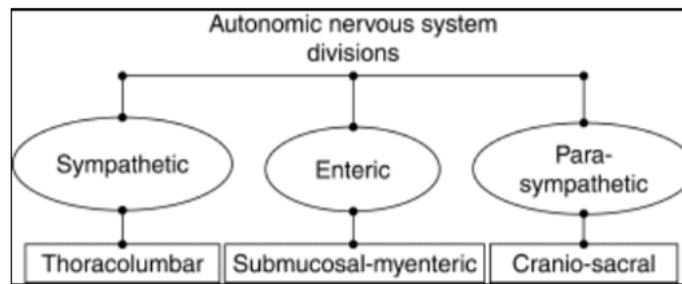


Fig.59: Divisions of the autonomic nervous system comprising the ENS (modified from *Wood, 2009*).

It is organised into neurons and supporting glial cells, grouped in small clusters (enteric ganglia) which are connected by bundles of nerve fibres. There are two main divisions in the distribution of neurons, which differ depending on the GI tract considered: the myenteric plexus (MP) or Auerbach's plexus and the submucosal plexus (SMP) or Meissner's plexus. The MP is located between the internal circular muscle layer and the external longitudinal muscle layer of the muscularis externa and is distributed continuously along the GI tract, whereas the SMP is located between the circular muscle layer and the mucosa and its distribution is most pronounced from the first part of the duodenum, whereas in the oesophagus and stomach there are sparse neurons that do not form ganglia. It consists of a single layer in common laboratory species (i.e. mouse, rat and guinea pig), but in larger mammals and humans it consists of two layers of ganglia called the inner and outer submucosal plexus (Fig.60) (177,298–300).

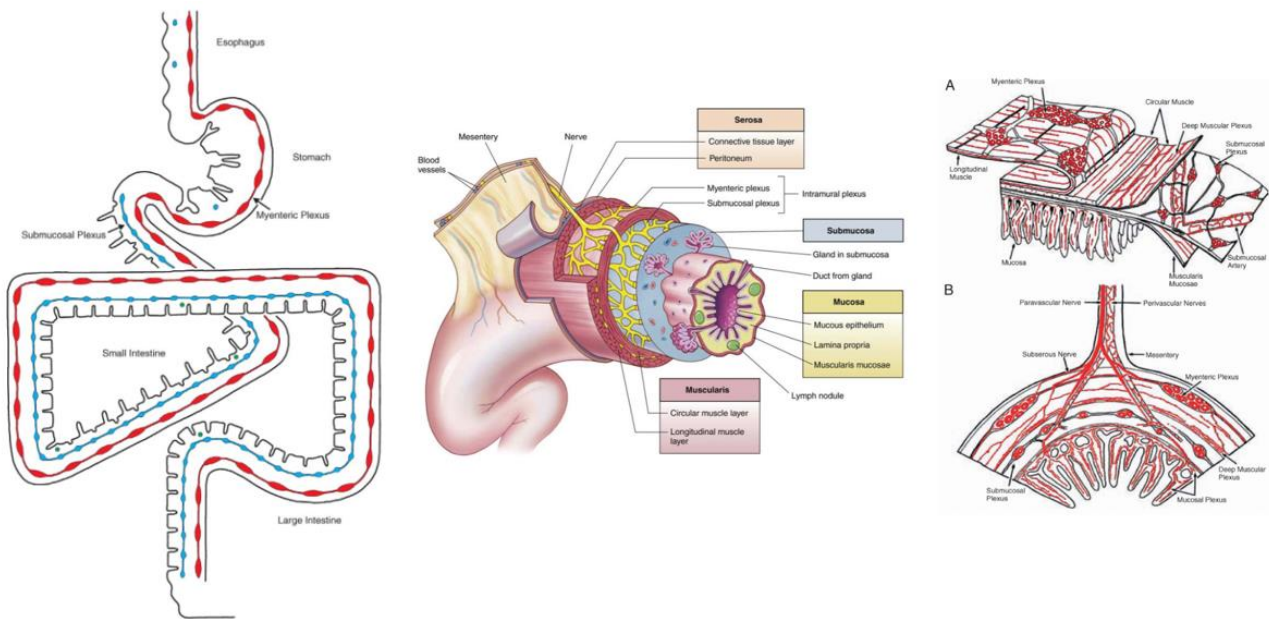


Fig.60: Schematic representation of the ENS distribution, on the right in blue the SMP in red the MP, in the centre the different layers of gut, notice the location of the two plexuses, on the top left a wholemount of intestine, on the bottom a transverse section of intestine [modified from *Furness, 2008* and website source (301)].

The ENS controls the vast majority of digestive functions and activities, such as motility, absorption, secretion and blood flow, with effects on immune, humoral and metabolic homeostasis, through its connections with the longitudinal and circular muscles, muscularis mucosa and mucosa, submucosal arteries and gut-associated lymphoid tissues. In this sense, the continuous communication between the CNS and the ENS (the so-called gut-brain axis) integrates the digestive and defensive functions of the gut with those of other organs to maintain homeostasis (298,300,302). The neurons of the ENS can be grouped into four different functional classes based on the expression of different neurochemical features, shape, electrophysiological properties and projections: intrinsic primary afferent neurons (IPANs) or Dogiel type II, excitatory motoneurons, inhibitory motoneurons and interneurons (both Dogiel type I), although in recent years it has become clear that each type of neuron can be multifunctional in nature (Fig.61) (298).

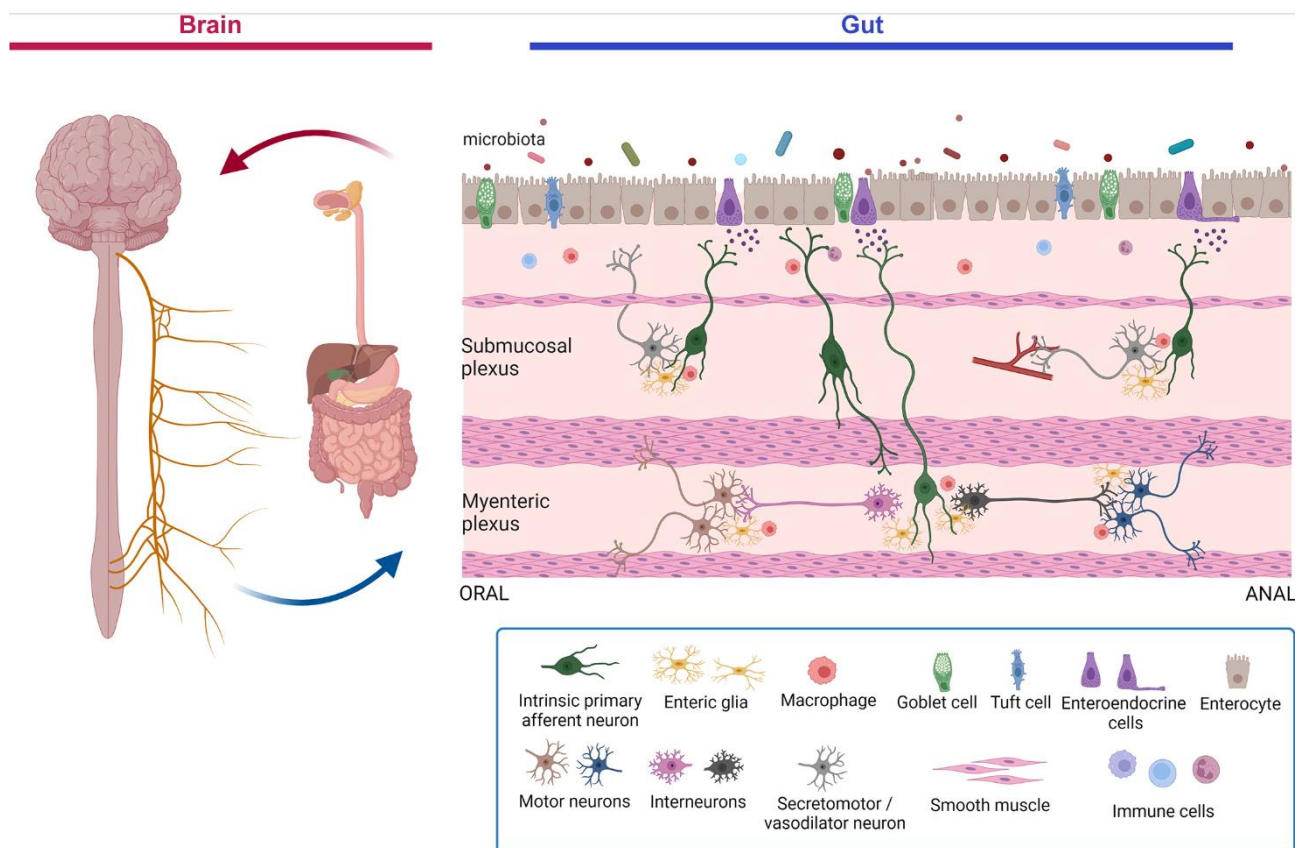


Fig.61: Schematic representation of the brain-gut axis on the right and populations distribution of ENS neurons and other cells in a putative GI tract (from *Sharkey and Mawe, 2023*).

Chapter 4: Studied Effector Organs in Veterinary Species

4.1 Skin of the Dog (*Canis lupus familiaris*) with a focus on canine atopic dermatitis

The skin, the largest organ in the body (accounting for 12% of total body weight in the adult dog), forms part of the integumentary system together with the hypodermis, hair, nails and associated glands (303,304). In addition to fulfilling the very important role of acting as a protective barrier for the body, the skin can be considered an effector organ because it is involved in the response to various external and internal stimuli, controlling thermoregulation, the immune response, secretion and possessing sensory properties (305–308). It is normally subdivided in three major layers: the epidermis, the derma and the subcutaneous fat tissue (Fig.62). The epidermis, which is a stratified squamous epithelium, can be further subdivided into five sublayers or strata (from the outermost to the innermost): corneum, lucidum, granulosum, spinosum and basal. In general, the epidermis is thicker in areas without a dense coat and thinner in areas with dense hair growth. In dogs, the thickest epidermis is found on the nose and digital pads. It is a constantly renewing layer, in fact the basal cells of the epidermis (keratinocytes) undergo cycles of proliferation that ensure the replacement of the outer epidermis (s.corneum), which is made up of corneocytes (terminally differentiated keratinocytes), they prevent water from leaving the body and toxic substances from entering. Other cell types found in the epidermis include: melanocytes, which protect the skin from UV rays and give it colour; Langerhans cells, which present potential pathogens to the immune system; and Merkel cells, which are type I mechanoreceptors located in areas of high tactile sensitivity. Furthermore, the epidermis gives rise to derivative structures, such as pilosebaceous apparatuses, nails, and sweat glands, which are accommodate in the dermis. This latter lies underneath and provides support and elasticity to the skin thanks to the elastin and collagen produced by the fibroblasts within it. It also contains immune cells such as lymphocytes, eosinophils, MCs, neutrophils, DCs and macrophages, which defend the skin against pathogens and toxic substances, as well as capillaries and various types of nerve endings (C-fibres, Ruffini, Pacinian and Meissner corpuscles), which serve to give the skin sensations of itching, pain, pleasure and warmth. The last layer, the subcutaneous fat, is made up of adipocytes and fibrocytes, and serves as an energy store and endocrine organ, important for lipid and glucose metabolism, connecting the dermis to muscle and bone and controlling body temperature (304,305,307,309).

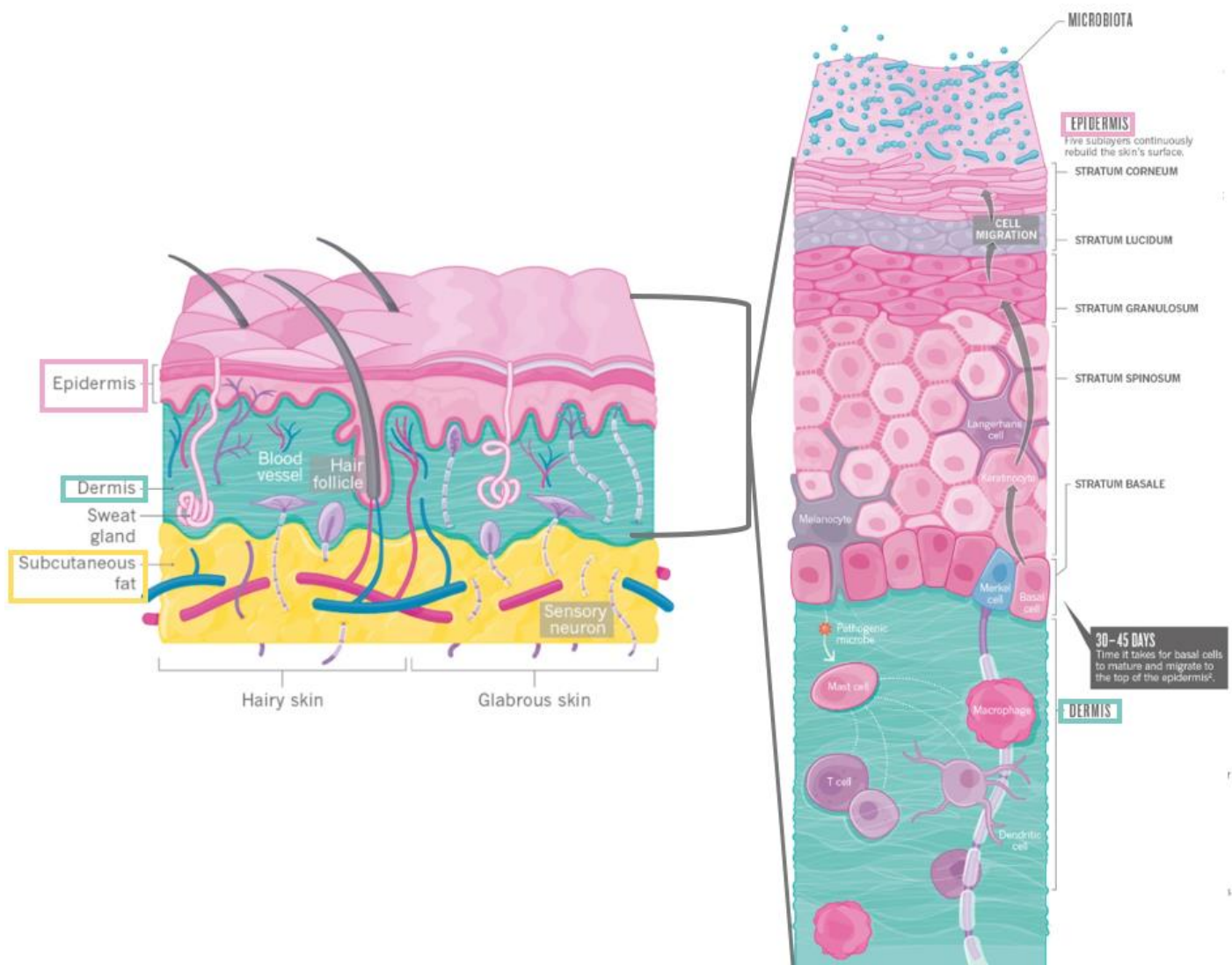


Fig.62: Schematic representation of the skin with its layers on the left and sub-layers on the right. In purple, on the left, different types of sensory neurons, on the right different types of cells within it (modified from Gould, 2018).

Among the diseases that can affect canine skin in the three different layers, including inflammatory, dysplastic, degenerative and neoplastic, AD is one of the most common with an incidence of 27%. It is classified as a perivascular inflammatory disease of the dermis because perivascular infiltration of inflammatory cells is the main and predominant pattern (310,311). Clinical signs include: generalised pruritus with skin lesions such as erythema, papules, pustules, crusts and excoriations, usually on the head, paws, abdomen, perineum and ventral tail (Fig.63). It is a pruritic and inflammatory disease caused by a genetic predisposition to produce abnormal immunoglobulin (Ig) E to environmental allergens, which penetrate the skin barrier and interact with IgE to induce degranulation of MCs, which can release a variety of proinflammatory, vasoactive and nociceptive mediators (e.g. histamine). However, the pathogenesis is not fully understood, in fact there is activation of both type IV and type I hypersensitivity, the latter particularly with chronicity of the disease. Although there is a disruption of the skin barrier, it is not

clear whether this is a primary or secondary defect, dietary habits and various cutaneous infections (e.g. *Malassezia*, *Staphylococcus*) may also lead to disease progression (310,312,313).



Fig.63: Pictures of a Dalmatian affected by atopic dermatitis with areas of erythema throughout the body (modified from *Gross et al., 2005*).

Other skin cells involved in AD include keratinocytes, activated T cells, macrophages, DCs, Langerhans cells, basophils and eosinophils (314,315). The production of inflammatory mediators and neurotrophins exacerbates the pruritus and hyperinnervation of AD lesions, which results from a complex interface between skin cells, cutaneous nerve fibres and the peripheral and central nervous systems (Fig.64) (316–319).

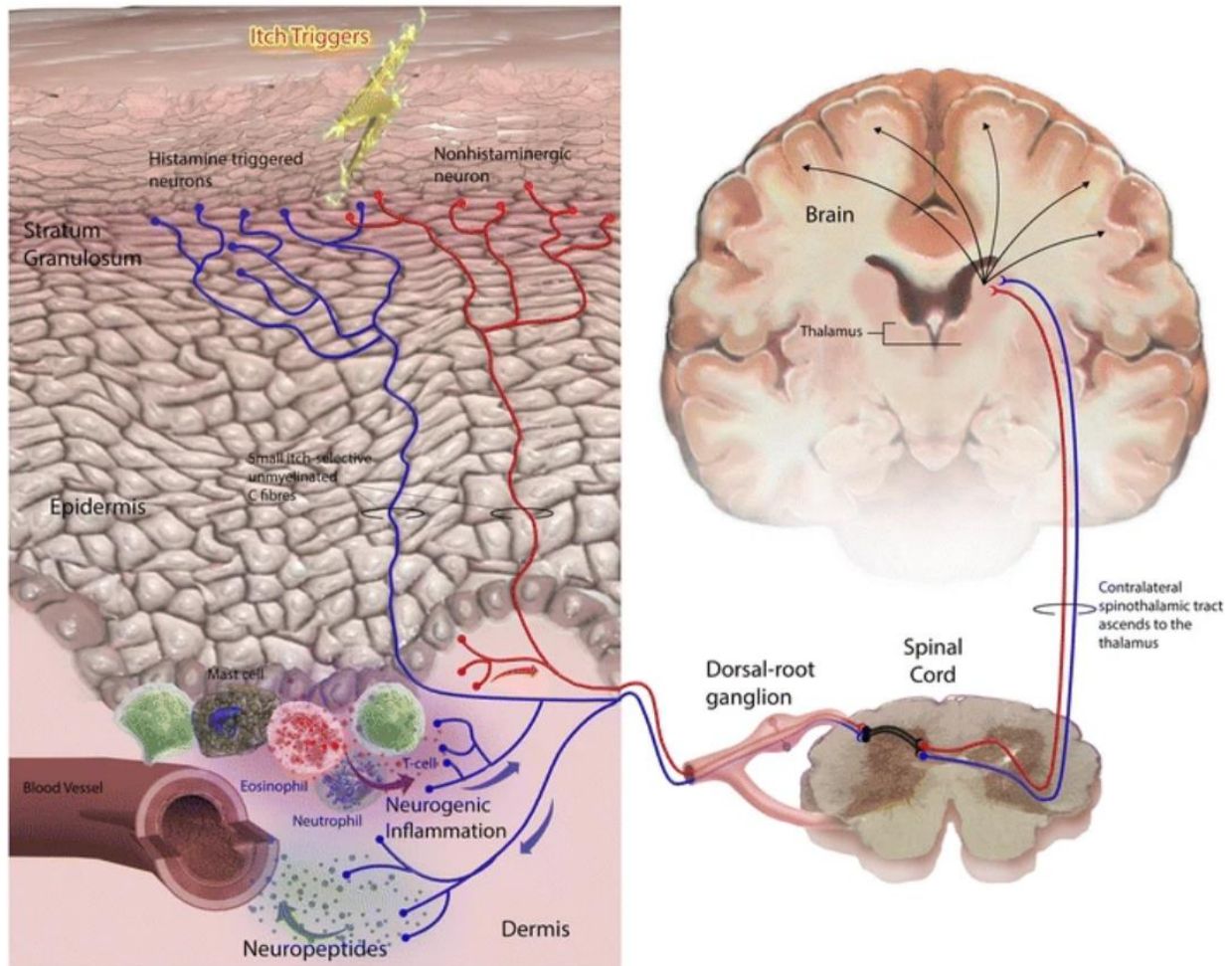


Fig.64: Schematic representation of the complex inter-talk between skin cells, cutaneous nerve fibres and nervous system after an itch trigger during AD (modified from Mollanazar *et al.*, 2016).

In terms of treatment options, the first step is to rule out the presence of pathogens such as fungi or bacteria, which would require specific therapy. For AD itself, there are several options, ranging from topical to systemic therapies. Topical therapies are aimed at reducing pruritus and the inflammatory response and repairing the skin barrier using, for example, moisturisers, glucocorticoids, calcineurin inhibitors as well as antihistamines, local anaesthetics, topical fatty acids, ceramides and essential fatty acids. Among the systemic therapies aimed at reducing the inflammatory response and pruritus, we can mention the classical glucocorticoids and cyclosporine, as well as novel drugs such as oclacitinib and lokivetmab, which seem to be safe alternatives compared to the classical ones, which on the other hand have some side effects. In recent years, there has been an increased interest in alternative therapies, more natural compounds with fewer side effects (312), among which it is possible to mention cannabinoids, such as cannabidiol, which have been studied in numerous preclinical studies on animal models, as well as in AD dogs and an *in vitro* canine model, giving promising results and justifying the need for further investigations in this field (311,320–323).

4.2 Synovial Membrane of the Horse (*Equus ferus caballus*) and Dog (*Canis lupus familiaris*) with a focus on joint diseases

The synovial membrane is a structure located in the joint, the place where two skeletal elements come together. More precisely, it is part of the synovial or diarthrodial/diarthroses joints. In fact, joints can be classified according to the type of movement they allow: immovable joints (synarthroses), slightly movable joints (amphiarthroses) and movable joints (diarthroses). If, on the other hand, we consider the connective tissue between the two skeletal elements, they can be classified as follows: syndesmoses or synchondroses, also known as solid joints, in which the connective tissue is a fibrous or cartilaginous membrane (usually comprising the immovable or slightly movable joints) and synovial or diarthrodial joints (where we find the movable ones), in which the two bony structures are covered by hyaline cartilage but are also completely surrounded by an articular cavity lined by the synovial membrane (Fig.65) (324,325).

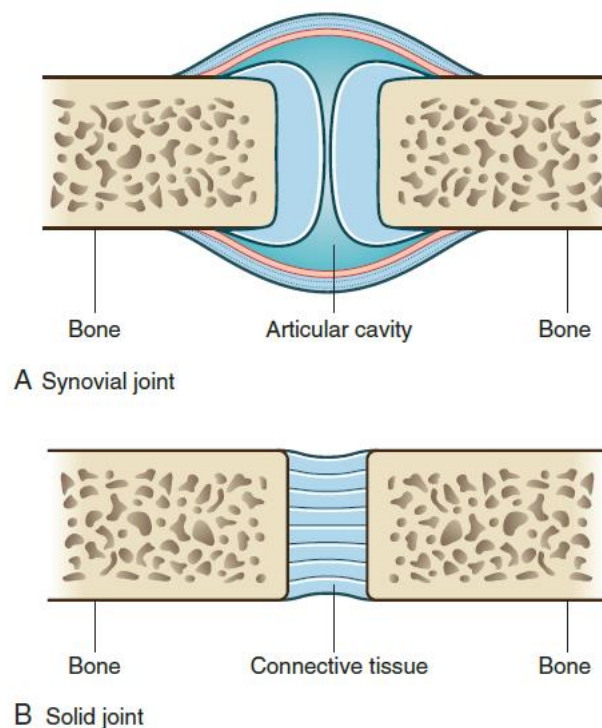


Fig.65: Schematic representation of the two types of joints: synovial or diarthrodial/diarthroses joints and solid joints or syndesmoses/synchondroses (comprising the synarthroses and amphiarthroses joints) (from Drake *et al.*, 2019).

Synarthroses are generally found in the skull; amphiarthroses are found between the vertebrae, the distal tibiofibular joint, the pubic symphysis and the upper two-thirds of the sacroiliac joint; and diarthroses are mostly found in the extremities (e.g. metacarpophalangeal, hip and stifle joints)(325).

The synovial membrane (Fig.66) is one of the two layers (the innermost and thinnest) that, together with the fibrous membrane (the outermost and thickest), form the wall of the joint capsule that encloses the joint cavity (324).

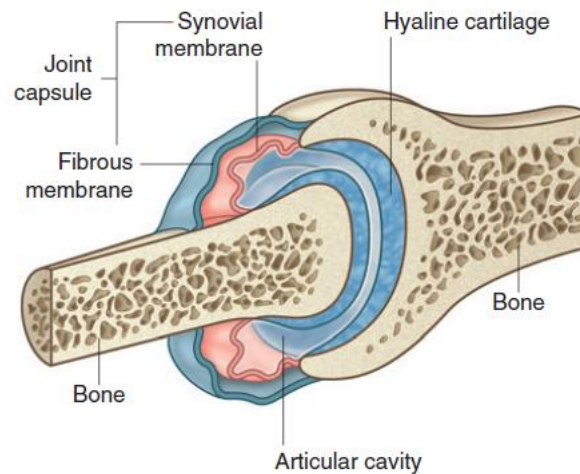


Fig.66: Schematic representation of structures composing the joint, notice the synovial membrane, the inner layer of the joint capsule (from *Drake et al., 2019*).

It has been shown in both humans and animals that the synovial membrane is composed of two types of synoviocytes: macrophage-like (MLS), also known as type A synoviocytes, and fibroblast-like (FLS) or type B synoviocytes, which are the most abundant. These cells are embedded in a thin layer of connective tissue rich in fenestrated capillaries and their main physiological role is to produce and control synovial fluid. FLS produce lubricating synovial substances (e.g. hyaluronic acid), matrix components (e.g. collagens and proteoglycans) and degradative enzymes (e.g. metalloproteinases), whereas MLS serve as resident macrophages with a role in phagocytosis of cell debris and waste in the synovial fluid and antigen-presenting ability (326–332). They are also both involved in pathological inflammatory conditions [e.g. osteoarthritis (OA) and rheumatoid arthritis] where they produce cytokines that can lead to overproduction of degradative enzymes and consequent cartilage destruction (Fig.67). In this sense, it can be said that the synovial membrane in pathological conditions is an effector organ that interacts with the surrounding environment to generate a response, moreover during inflammation nociceptors start to innervate the synovium and subchondral bone (Fig.68). In contrast, under physiological conditions, cartilage is an avascular and aneural tissue (333,334).

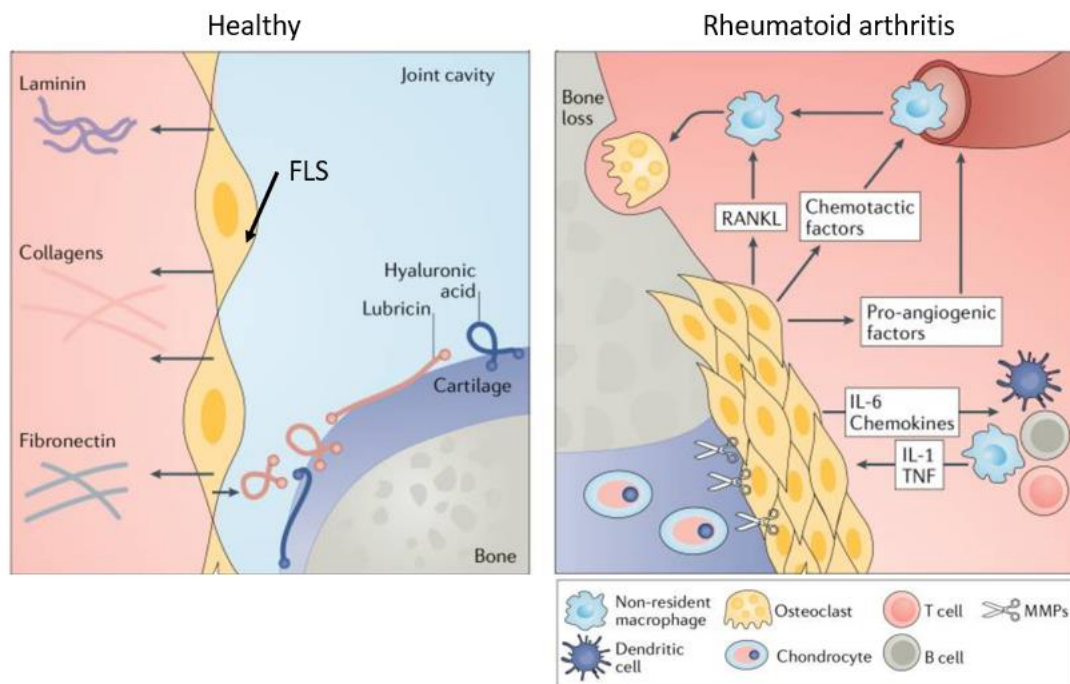


Fig.67: Schematic representation of the roles of synoviocytes (e.g. FLS) in the physiology (healthy, on the left) and in pathology (rheumatoid arthritis, on the right); MLS not shown (from Drake *et al.*, 2019).

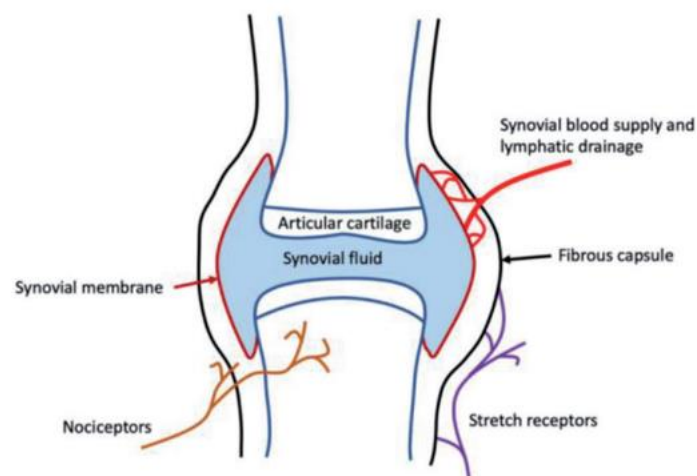


Fig.68: Schematic representation of a synovial joint during inflammation: nociceptors innervating the synovium and subchondral bone are responsible for arthritic pain (from Biddle and Sofat, 2020).

Regarding joint pathologies in horses, OA (Fig.69) is the most commonly reported cause of lameness with an incidence of 14% (335). It is a disease process that occurs in the synovial joints where there is destruction of articular cartilage, subchondral bone sclerosis, osteophyte formation, joint effusion and synovitis. One of the most commonly affected joints is the metacarpophalangeal, as it is a highly mobile joint that is subjected to high loads during racing. The most common causes are acute or chronic trauma or microtrauma, which induce an inflammatory response that drives cartilage damage and remodelling of the surrounding bone. There is a plethora of studied treatments

for equine OA, used as symptomatic drugs to reduce pain and inflammation [e.g. non-steroidal anti-inflammatory drugs (NSAIDs) in combination with intra-articular corticosteroids], but none of these are expected to act on the causes of the pathology and various side effects are reported, prompting further studies into the pathogenesis of OA and new target drugs for its resolution (135,336,337). Among newly explored and promising field, especially conducted on humans and animal models, we can find the involvement of the eCB system and its target cannabinoid compound. Indeed, it appears to play a crucial role for maintaining joint health and bone metabolism by regulating the activity of immune cells and reducing inflammation within both tissues, with evidence suggesting that it may control bone formation and resorption (85,134,338–344).

As in horses, OA is the most common form of arthritis in dogs, with an incidence of 2.5-20% (345) of the dog population. It is characterised by a gradual loss of cartilage, leading to the development of bony bumps and cysts at the edges of the joints and associated pain. Unlike horses, the most common sites and causes are the elbow or hip affected by dysplasia or osteochondrosis, or the knee affected by cranial cruciate ligament injury, as well as excessive running or exercise, injury and/or genetic predisposition. As in horses, NSAIDs are also the first choice in dogs to relieve pain and slow progression, with various side effects, especially on the GI tract and kidneys, for this reason targeting the ECS is a new and safer target to investigate also in this species, with some promising studies already conducted (345–349).

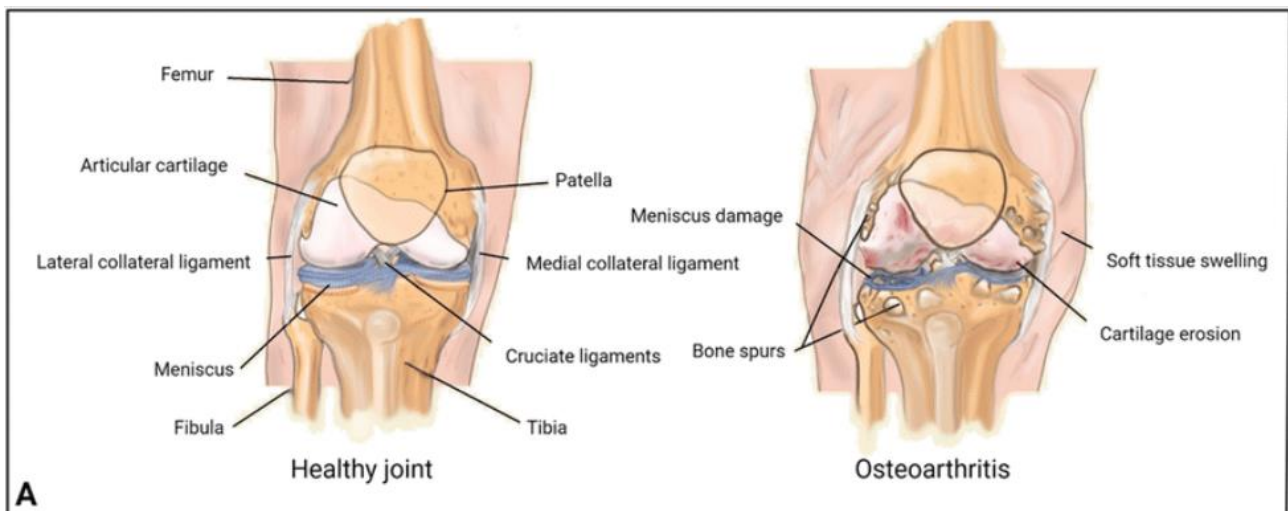


Fig.69: Schematic representation of a knee in healthy condition (on the left) and during osteoarthritis (on the right) [modified from Zhang *et al.*, 2022 (350)].

B. THESIS OBJECTIVES: Exploring the Nervous System and Some Effector Organs in Veterinary Species by Targeting Different Biological Systems

Among the reasons behind the conduction of veterinary-based research there is the undoubted need to better understand the molecular, genetic, phenotypic and pathophysiological background of animal diseases (351), furthermore, veterinary science can also be useful in addressing questions about the evolution of human behaviour and pathologies, overcoming the attempt to biologically pseudo-oligarchise humans among species (352). Finally, and most importantly, the role of anatomy in veterinary research must be maintained, for as the neuropsychiatrist Bernhard von Gudden asserted in the mid-nineteenth century, scientists “faced with an anatomical fact proven beyond doubt, any physiological results that stands in contradiction to it loses all its meaning.... So first anatomy and then physiology; but if first physiology, then not without anatomy” (353) Driven by these three concepts and based on the gaps in the literature, the objectives of my three-year doctoral period, which led to the production of the contents of this work, were to carry out novel investigations on different parts of the central and peripheral nervous system and on some effector organs in different veterinary species, choosing as target molecules those related to CaBPs, the serotonergic, peptidergic and endocannabinoid systems (Fig.70).

The parts of the CNS studied were: the EC of the dolphin (*Tursiops truncatus*), with a focus on CaBPs, chosen mainly for their usefulness in the morphological characterisation of brain regions (4); the AC of the rat (*Rattus norvegicus*), focusing on the distribution of the peptidergic system (VIP) and GABA, chosen mainly because it is the most studied animal model and because the existing literature lacks a systematic description of the distribution of these molecules in all the nuclei constituting the AC; the AC of the sheep (*Ovis aries*), using a novel non-invasive technique to study the AC connections within the brain; finally, the OL of the honeybee (*Apis mellifera*), choosing the serotonergic system (SERT) as a target, with the aim of morphologically describing the distribution of SERT within these structures and correlating it with the aggressive behaviour of the honeybee (58). On the other hand, the parts of the PNS studied were the TG of the horse (*Equus ferus caballus*), targeting different CBr, mainly because of its involvement in the TG-mediated HSK pathology (284,287) and to provide the anatomical basis for the study of novel therapeutic approaches such as cannabinoids; and the ENS of the dolphin (*Tursiops truncatus*), focusing on peptidergic (SP) and nitrergic (nNOS) systems, chosen to highlight the excitatory and inhibitory (176,177,187,188) morphological and quantitative features of the ENS, which were lacking in the literature.

The effector organs studied were: the skin of dog (*Canis familiaris*) affected by AD and synovial membrane of normal horse (*Equus ferus caballus*) and dog (*Canis familiaris*), choosing as target molecules different CBr and different antigen to identify the cytoidentity of cells normally or pathologically distributed in these tissues, with the aim of laying the anatomical foundations for studying novel therapeutic approaches such as the use of cannabinoids molecule in pathologies affecting these organs.

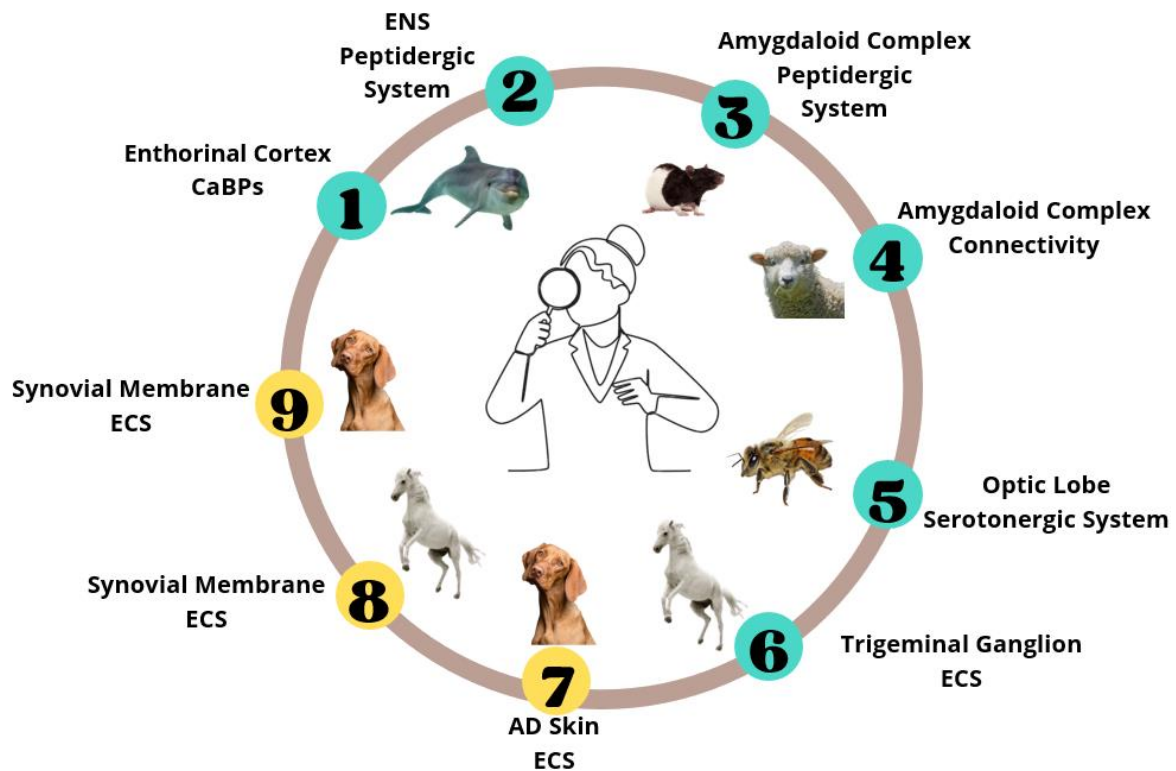


Fig.70: Schematic representation of the topics within this thesis: in azure the studied parts of the nervous system, in yellow the effector organs. In the pictures inside the circle the veterinarian animals under investigations. Abb: CaBPs (Calcium-binding proteins); ENS (Enteric Nervous System); ECS (Endocannabinoid System).

C. PUBLISHED PAPERS

Chapter 1:
**Distribution of calcium-binding proteins immunoreactivity in the bottlenose
dolphin entorhinal cortex**



OPEN ACCESS

EDITED BY

Wen-Jie Song,
Kumamoto University Hospital, Japan

REVIEWED BY

Makoto Takemoto,
Kumamoto University, Japan
Kazuya Saitoh,
Yamagata Prefectural Yonezawa Nutrition
University, Japan

*CORRESPONDENCE

Cristiano Bombardi
✉ cristiano.bombardi@unibo.it

RECEIVED 13 October 2023

ACCEPTED 19 January 2024

PUBLISHED 05 February 2024

CITATION

Graïc J-M, Grandis A, Sacchini S,
Tagliavia C, Salamanca G, Cozzi B and
Bombardi C (2024) Distribution of calcium-
binding proteins immunoreactivity in the
bottlenose dolphin entorhinal cortex.
Front. Neuroanat. 18:1321025.
doi: 10.3389/fnana.2024.1321025

COPYRIGHT

© 2024 Graïc, Grandis, Sacchini, Tagliavia,
Salamanca, Cozzi and Bombardi. This is an
open-access article distributed under the
terms of the [Creative Commons Attribution
License \(CC BY\)](#). The use, distribution or
reproduction in other forums is permitted,
provided the original author(s) and the
copyright owner(s) are credited and that the
original publication in this journal is cited, in
accordance with accepted academic
practice. No use, distribution or reproduction
is permitted which does not comply with
these terms.

Distribution of calcium-binding proteins immunoreactivity in the bottlenose dolphin entorhinal cortex

Jean-Marie Graïc¹, Annamaria Grandis², Simona Sacchini³,
Claudio Tagliavia⁴, Giulia Salamanca², Bruno Cozzi¹ and
Cristiano Bombardi^{2*}

¹Department of Comparative Biomedicine and Food Science, University of Padova, Legnaro, Italy,

²Department of Veterinary Medical Sciences, University of Bologna, Bologna, Italy, ³Department of Morphology, University of Las Palmas de Gran Canaria, Las Palmas de Gran Canaria, Spain,

⁴Department of Veterinary Medicine, University of Teramo, Teramo, Italy

Introduction: The entorhinal cortex has been shown to be involved in high-level cognitive functions in terrestrial mammals. It can be divided into two main areas: the lateral entorhinal area (LEA) and the medial entorhinal area (MEA). Understanding of its structural organization in cetaceans is particularly important given the extensive evidence for their cognitive abilities. The present study describes the cytoarchitectural and immunohistochemical properties of the entorhinal cortex of the bottlenose dolphin (*Tursiops truncatus*, Montagu, 1821), perhaps the most studied cetacean species and a paradigm for dolphins and other small cetaceans.

Methods: Four bottlenose dolphins' entorhinal cortices were processed. To obtain a precise overview of the organization of the entorhinal cortex we used thionin staining to study its laminar and regional organization, and immunoperoxidase technique to investigate the immunohistochemical distribution of three most commonly used calcium-binding proteins (CBPs), calbindin D-28k (CB), calretinin (CR) and parvalbumin (PV). Entorhinal cortex layers thickness were measured, morphological and morphometric analysis for each layer were conducted and statistically compared.

Results: Six layers in both the LEA and MEA were identified. The main difference between the LEA and the MEA is observed in layers II and III: the neurons in layer II of the LEA were denser and larger than the neurons in layer II of MEA. In addition, a relatively cell-free zone between layers II and III in LEA, but not in MEA, was observed. The immunohistochemical distribution of the three CBPs, CB, CR and PV were distinct in each layer. The immunostaining pattern of CR, on one side, and CB/PV, on the other side, appeared to be distributed in a complementary manner. PV and CB immunostaining was particularly evident in layers II and III, whereas CR immunoreactive neurons were distributed throughout all layers, especially in layers V and VI. Immunoreactivity was expressed by neurons belonging to different morphological classes: All CBPs were expressed in non-pyramidal neurons, but CB and CR were also found in pyramidal neurons.

Discussion: The morphological characteristics of pyramidal and non-pyramidal neurons in the dolphin entorhinal cortex are similar to those described in the entorhinal cortex of other species, including primates and rodents. Interestingly, in primates, rodents, and dolphins, most of the CBP-containing neurons are found in the superficial layers, but the large CR-ir neurons are also abundant in the deep layers. Layers II and III of the entorhinal cortex contain neurons that give rise to the perforant pathway, which conveys most of the cortical information to the hippocampal formation. From the hippocampal formation,

reciprocal projections are directed back to the deep layer of the entorhinal cortex, which distributes the information to the neocortex and subcortical area. Our data reveal that in the dolphin entorhinal cortex, the three major CBPs label morphologically heterogeneous groups of neurons that may be involved in the information flow between entorhinal input and output pathways.

KEYWORDS

entorhinal cortex, calretinin, calbindin-D28k, parvalbumin, bottlenose dolphin

1 Introduction

Dolphins have very large brains, making their Encephalization Quotient (EQ) comparable to that of many non-human primates (Jerison, 1973; Morgane et al., 1985; Marino, 2002; Marino et al., 2004, 2007). The increase in brain size is a result of selective pressures imposed by the aquatic environment on motor, sensory and eventually social capabilities (Marino, 2002; Marino et al., 2004, 2007). Although cetacean brain are very large, their entorhinal cortex, a constituent of the periarthricortex, is significantly reduced (Jacobs et al., 1971, 1979; Morgane and Jacobs, 1972; Morgane et al., 1980, 1986; Cozzi et al., 2017). The entorhinal cortex of terrestrial mammals comprises two main cytoarchitectonic subdivision in primates and rodents: the medial entorhinal cortex (MEA) and the lateral entorhinal cortex (LEA). These areas have a fourth layer, the *lamina dissecans*, which is essentially acellular and bears little homology with the layer IV found in the neocortex (Insausti et al., 1995, 1997; Krimer, 1997; Kerr et al., 2007; Insausti and Amaral, 2008; Witter, 2012; Cappaert Van Strien and Witter, 2015; Witter et al., 2017). The evidence from studies in terrestrial mammals, including non-human primates and rodents, shows a general pattern of connectivity and contribution of this cortical region to behavior that can be considered general for all mammals, including cetaceans. In terrestrial mammals the entorhinal cortex is the main entry point for the information processed by the hippocampal formation and provides the main conduit for processed information to be relayed back to the neocortex. In addition, the entorhinal cortex serves as the entry site for the projections directed towards the limbic complex, originating from the amygdala, the neocortex, and the olfactory bulb (Amaral et al., 1987; Carboni et al., 1990; Insausti, 1993; Insausti et al., 1997; Kerr et al., 2007; Insausti and Amaral, 2008, 2012; Witter, 2012; Cappaert Van Strien and Witter, 2015; Maass et al., 2015; Witter et al., 2017). The entorhinal cortex has been shown to be involved in high-level cognitive functions in terrestrial mammals, so understanding of its structural organization in cetaceans is particularly important given the extensive evidence for their cognitive abilities. The entorhinal cortex of the bottlenose dolphin occupies an area within the parahippocampal gyrus (Jacobs et al., 1979; Hof et al., 2005; Hof and Van Der Gucht, 2007). In particular, Jacobs et al. (1979) described a distinct six-layered entorhinal cortex with an extensive *lamina dissecans* and similar patterns to primates (figures 66 to 69), but with less extensive corticopercorant fibers bordering the archicortex [see also Breathnach and Goldby (1954)]. Direct experimental evidence of the connectivity of the dolphin entorhinal cortex is lacking, and thus, the functional significance of the cetacean entorhinal cortex can only be elucidated by comparison with other mammals. The organization of the entorhinal cortex can be studied using a variety of approaches. Most of the cytoarchitectural studies are performed using Nissl staining, which provides information about the organization and layering patterns of the cortex and on the basic morphology of the neurons. However, neurons with comparable

morphology can be characterized by their variable neurochemical profile and thus by different functions. Therefore, it is important to combine morphological and neurochemical studies to obtain a more precise overview of the organization of the entorhinal cortex in a given species. Several neurochemical markers have been used to identify the neurochemical organization of the entorhinal cortex in rodents and primates, and among the most commonly used are the calcium-binding proteins (CaBPs) such as calretinin (CR), calbindin-D28k (CB), and parvalbumin (PV). These studies show that immunoreactivity for these three types of CaBPs is observed in both excitatory (CR and CB) and inhibitory neurons (CR, CB, and PV) (Tuñón et al., 1992; Schmidt et al., 1993; Seress et al., 1994; Wouterlood et al., 1995, 2000; Fujimaru and Kosaka, 1996; Miettinen et al., 1996, 1997; Mikkonen et al., 1997; Berger et al., 1999; Suzuki and Porteros, 2002; Grateron et al., 2003; Kobro-Flatmoen and Witter, 2019). On the contrary, there is a lack of information on the distribution and morphology of CaBPs-immunoreactive (IR) neurons in the cetacean entorhinal cortex. In the present study, we investigated the cytoarchitecture of the entorhinal cortex of the bottlenose dolphin, perhaps the most studied cetacean species and a paradigm for dolphins and other small cetaceans. The distribution of CBP-immunoreactive neurons (CR-ir, CB-ir and PB-ir, respectively) helped us to map and define the organization of the area. The present data on the dolphin entorhinal cortex provide the basis for comparison with that of other mammals.

2 Materials and methods

2.1 Dolphin tissues

Dolphin brains (Table 1) were extracted during routine necropsy performed at the Department of Comparative Biomedicine and Food Science (BCA) of the University of Padova (Italy) on specimens. The brains were consequently fixed in phosphate buffered paraformaldehyde (4%), cut in coronal slices (about 1.5 cm × 2.5 cm) and stored in the *Mediterranean marine mammal tissue bank* (MMMTB, <http://www.marinemammals.eu>), located in BCA. The MMMTB is a CITES recognized (IT020) research center of the University of Padova, sponsored by and collaborating with the Italian Ministry of the Environment. MMMTB collects and stores samples from wild or

TABLE 1 Detail of the sampled bottlenose dolphins.

Specimen	ID	SEX	Origin	Length/Weight	Age
<i>T. truncatus</i>	192	F	Stranded	240 cm/178.5 kg	Adult
	196	M	Stranded	300 cm/219 kg	Adult
	203	M	Stranded	284 cm/288 kg	Adult
	319	M	Stranded	310 cm	Adult

captive marine mammals whose samples or whole carcasses are delivered to BCA for post-mortem diagnostics. Smaller blocks, containing the entorhinal cortex, were cut from the thick formalin-fixed tissue slices, washed in phosphate buffered saline (PBS) (pH 7.4), cryoprotected in 20% glycerol in 0.02 M potassium phosphate buffered saline (PBS) (pH 7.4) at +4°C for 48 h, frozen in dry ice, and stored at −70°C. Fifty- μ m-thick frozen coronal sections (one-in-eight series) throughout the entire rostrocaudal extent of the entorhinal cortex were cut with a sliding microtome. The angle of coronal sectioning performed in this study was perpendicular to the surface of the entorhinal cortex. For immunohistochemical staining, the sections were stored in tissue-collecting solution (30% ethylene glycol, 25% glycerol in 0.05 M sodium phosphate buffer, pH 7.4) at −20°C. Another series of sections to be stained with thionin was stored in 10% formalin.

2.2 Thionin staining

To evaluate the boundaries and the layer-specific neurons of the entorhinal cortex, sections adjacent to immunoperoxidase sections were stained with thionin as follows. Sections were taken out of the 10% formaldehyde solution, mounted on gelatin-coated slides and dried overnight at 37°C. Sections were defatted 1 h in a mixture of chloroform/ethanol 100% (1:1), and then rehydrated through a graded series of ethanol, 2 \times 2 min in 100% ethanol, 2 min in 96% ethanol, 2 min in 70% ethanol, 2 min in 50% ethanol, 2 min in dH₂O, and stained 30 s in a 0.125% thionin (Fisher Scientific) solution, dehydrated and coverslipped with Entellan (Merck, Darmstadt, Germany).

2.3 Immunoperoxidase

Three of the one-in-eight series of free-floating sections were collected from tissue-collecting solution and washed three times (10 min each) in 0.02 M phosphate buffer containing 0.9% sodium chloride (PBS; pH 7.4). To reduce the endogenous peroxidase activity, the sections were incubated in 3% hydrogen peroxide and 10% methanol in PBS for 30 min at room temperature. Nonspecific binding was blocked by incubating sections in a solution (0.5% Triton X-100 in PBS) containing 10% normal horse serum (NHS) for parvalbumin and calbindin immunohistochemistry or normal goat serum (NGS) for calretinin immunohistochemistry for 3 h at room temperature. The primary antibody incubations were done at 4°C for 2 to 3 days in a solution (0.5% Triton X-100 in PBS) containing either 1% NHS and monoclonal mouse anti-parvalbumin (dilution 1:3000, #235, Swant, Bellinzona, Switzerland) or monoclonal mouse anti-calbindin-D28k (dilution 1:3000, #McAB300, Swant), or 1% NGS and polyclonal rabbit anti-calretinin (dilution 1:3000, #7696, Swant, Bellinzona, Switzerland). After three washes (10 min each) in PBS containing either 2% NHS (parvalbumin and calbindin immunohistochemistry) or 2% NGS (calretinin immunohistochemistry), the sections were incubated in the secondary antibody solution (0.3% Triton X-100 in PBS) containing either biotinylated horse anti-mouse immunoglobulin G with 1% NHS (parvalbumin and calbindin; dilution 1:200, #BA-2,000, Vector, Burlingame, CA) or biotinylated goat anti-rabbit immunoglobulin G with 1% NGS (calretinin; dilution 1:200, #BA-1,000, Vector) for 2 h at room temperature. Sections were then washed twice as described above and incubated for 45 min at room temperature in avidin-biotin solution (BioStain SuperABC #11-001, Biomedica, Foster City, CA) in PBS. Thereafter, the sections were washed three times and reacted with 3,3'-diaminobenzidine (0.05%) containing hydrogen peroxide (0.04%)

in KPBS. After three washes, the sections were mounted onto gelatin-coated slides and dried overnight at 37°C.

2.4 Specificity of the antibodies

The amino acid sequence of the proteins investigated in this article of bottlenose dolphin (*Tursiops truncatus*) were compared with those of other mammals (and especially the rat). For this aim we used the Ensemble genomic database 1. The sequence of CB and CR is shared for over 93%, whereas correspondence for Gng2 and PV is over 70%. The specificity of the immuno-histochemical staining was tested in repeated trials as follows: substitution of either the primary antibody, the anti-rabbit or anti-mouse IgG, or the ABC complex by PBS or non-immune serum. Under these conditions the staining was abolished.

2.5 Analysis of sections

Sections stained using thionin and immunoperoxidase were analyzed using an optical microscope (Axiophot, Zeiss, Germany). Brightfield images were recorded with a digital camera (AxioCam ERc5s®, Zeiss, Germany). The distribution of CR, CB, and PV-IR cell bodies in the LEA and MEA were plotted bilaterally in every fifth section throughout the entorhinal cortex with a computer-aided digitizing system (AccuStage 5.1, St. Shoreview, MN). Camera lucida drawings from the adjacent thionin-stained sections were used to define the laminar and regional boundaries of the areas of the entorhinal cortex. The outlines were superimposed on computer-generated plots using Corel Draw X3 (Corel Corporation, Ottawa, Ontario, Canada). AxioVision Rel.4.8 software (Zeiss) was utilized for morphometrical and morphological analysis of the thionin-stained and CR-, CB-, and PV-IR neurons in the LEA and MEA. In particular, for each animal, the perikaryal areas of thionin-stained and IR cell bodies of four non-consecutive sections of each entorhinal area were measured after manual tracing of the cell bodies outline. These morphometrical analyzes were done in each separate layer, with the exception of lamina dissecans, because of its low cellular density. Data were expressed as mean \pm standard deviation (SD). Analysis of variance (ANOVA) was used to analyze whether there was any difference in the perikaryal main area of different IR cell types. The Tukey HSD *post hoc* test was used to make pair-wise comparisons between means. In the thionin-stained sections, cortical layers thicknesses were measured using the AxioVision Rel.4.8 software (Zeiss), using a tool measuring the length perpendicular to a line placed on the pial surface of the cortex. Measurements were made at least 5 times per sample, outside of sulcus bottom or top to avoid distortions. Contrast and brightness were adjusted to reflect the appearance of the labeling seen through the microscope using Adobe Photoshop CS3 Extended 10.0 software (Adobe Systems, San Jose, CA).

3 Results

3.1 Thionin staining: laminar and regional organization of the entorhinal cortex

3.1.1 Laminar organization

The entorhinal cortex was located ventrocaudally to the amygdaloid complex and the hippocampal formation and has been divided into two main areas: lateral entorhinal area (LEA) and medial entorhinal area (MEA). Six layers were identified in the entorhinal

cortex (LEA and MEA): molecular layer (layer I), stellate cell layer (layer II), superficial pyramidal cell layer (Layer III), *lamina dissecans* (layer IV), deep pyramidal cell layer (layer V), and polymorph cell layer (layer VI; [Figure 1](#)).

Layer I was populated by a small number of sparse spheroidal ([Figure 2A](#); $n=67$ in LEA; $n=61$ in MEA), polygonal ([Figure 2B](#); $n=69$ in LEA; $n=64$ in MEA), and fusiform ([Figures 2C,D](#); $n=78$ in LEA; $n=75$ in MEA) neurons of small size. Fusiform neurons were oriented horizontally ([Figure 2C](#)) or vertically ([Figure 2D](#)) with respect to the cortical surface.

Layer II contained darkly stained neurons with a polygonal soma ([Figure 2E](#); $n=170$ in LEA; $n=178$ in MEA). Polygonal neurons were usually aggregated into “islands” ([Figure 2F](#)). Pyramidal neurons with the apical dendrite directed to the cortical surface could be observed ([Figure 2G](#); $n=1,228$ in LEA; $n=1,136$ in MEA). Layer II also showed small spheroidal neurons ([Figure 2H](#); $n=361$ in LEA; $n=354$ in MEA) and medium-sized fusiform cells ([Figure 2I](#); $n=114$ in LEA; $n=111$ in MEA).

Layer III was composed of a wide variety of neurons with a pyramidal ([Figure 3A](#); $n=2,337$ in LEA; $n=2,298$ in MEA), polygonal ([Figure 3B](#); $n=391$ in LEA; $n=389$ in MEA), fusiform ([Figure 3C](#); $n=408$ in LEA; $n=391$ in MEA), or spheroidal cell bodies ([Figure 3D](#); $n=205$ in LEA; $n=197$ in MEA). Pyramidal neurons were the most numerous and appeared densely packed in the inner part of the layer.

Layer IV (*lamina dissecans*) contained rare spheroidal ([Figure 3E](#)), fusiform ([Figure 3F](#)), and polygonal ([Figure 3G](#)) neurons with a small soma. However, darkly stained pyramidal neurons were observed ([Figure 3H](#)).

Layer V showed large and darkly stained pyramidal neurons ([Figure 4A](#); $n=3,528$ in LEA; $n=3,478$ in MEA); interestingly, many inverted pyramidal cells were also observed ([Figure 4B](#); $n=534$ in LEA; $n=528$ in MEA). Lightly stained neurons with a spheroidal ([Figure 4C](#); $n=237$ in LEA; $n=240$ in MEA), fusiform ([Figure 4C](#); $n=461$ in LEA; $n=432$ in MEA) or polygonal ([Figure 4D](#); $n=418$ in LEA; $n=402$ in MEA) morphology could be observed among the pyramidal cells.

Layer VI was composed of a variety of morphological cell types with different sizes and spheroidal ([Figure 4E](#); $n=125$ in LEA; $n=124$ in MEA), polygonal ([Figure 4F](#); $n=361$ in LEA; $n=368$ in MEA), fusiform

([Figure 4G](#); $n=412$ in LEA; $n=406$ in MEA), and pyramidal ([Figure 4H](#); $n=1,469$ in LEA; $n=1,452$ in MEA) morphology.

3.1.2 Regional organization

3.1.2.1 Lateral entorhinal area (LEA)

Layer I was thick. Layer II was narrower, the neurons stained darker than in MEA, and many neurons were densely packed and formed cell islands. Between layers II and III there was a clear zone of sparse cells. Neurons in layer III formed a continuous band. Layer IV (*lamina dissecans*) was clearly visible. Neurons of layer V were dispersed, whereas neurons of layer VI were more densely packed than in layer V ([Figure 1A](#)).

3.1.2.2 Medial entorhinal area (MEA)

Layer I was very thick. Layer II neurons formed a discontinuous band and were larger and stain darker than neurons of layer III. Layer III was much wider than layer II and contained neurons with a small somata. Layer IV (*lamina dissecans*) was not very clearly visible. Layer V contained large neurons, whereas layer VI exhibited smaller and more densely packed neurons than layer V. Layers V and VI were thinner than in LEA ([Figure 1B](#)).

The cortical layer thickness and the morphometric properties of neurons in LEA and MEA are shown in [Figures 5, 6](#).

3.2 Calcium-binding proteins in the entorhinal cortex

Immunoreactivity for the three major calcium-binding proteins (CR, CB, and PV) showed a prominent laminar distribution in the dolphin entorhinal cortex ([Figures 7, 8](#)). Neurons immunostained for CR and, to a lesser extent, CB were prevalent, whereas PV was present in few neurons. The highest concentrations of PV-IR and CB-IR neurons were found in layers II and III, whereas a large number of neurons immunopositive for CR were found in the deep layers. In addition, most of the large CR-IR pyramidal cells were found in the deep layers, whereas most of the PV-IR non-pyramidal neurons were

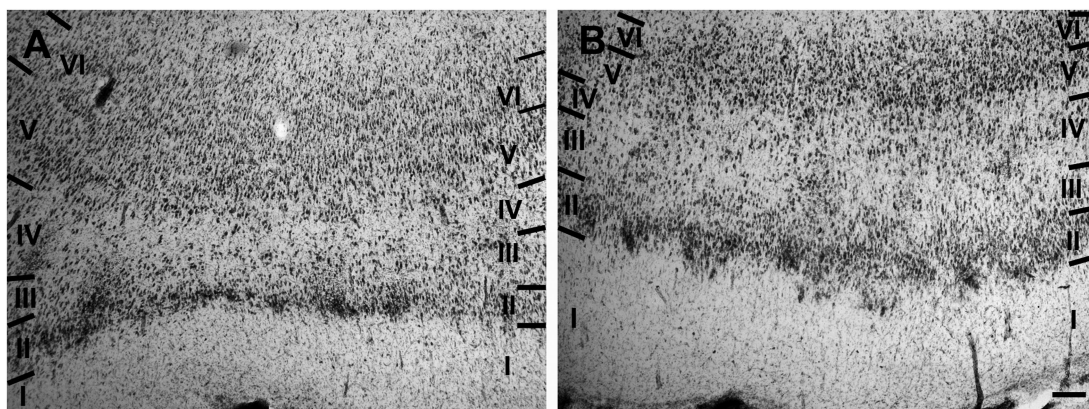


FIGURE 1

Brightfield photomicrographs of thionin-stained coronal sections from lateral entorhinal cortex (LEA) (A) and medial entorhinal cortex (MEA) (B). Scale bar = 200 μ m in B [applied to (A) and (B)].

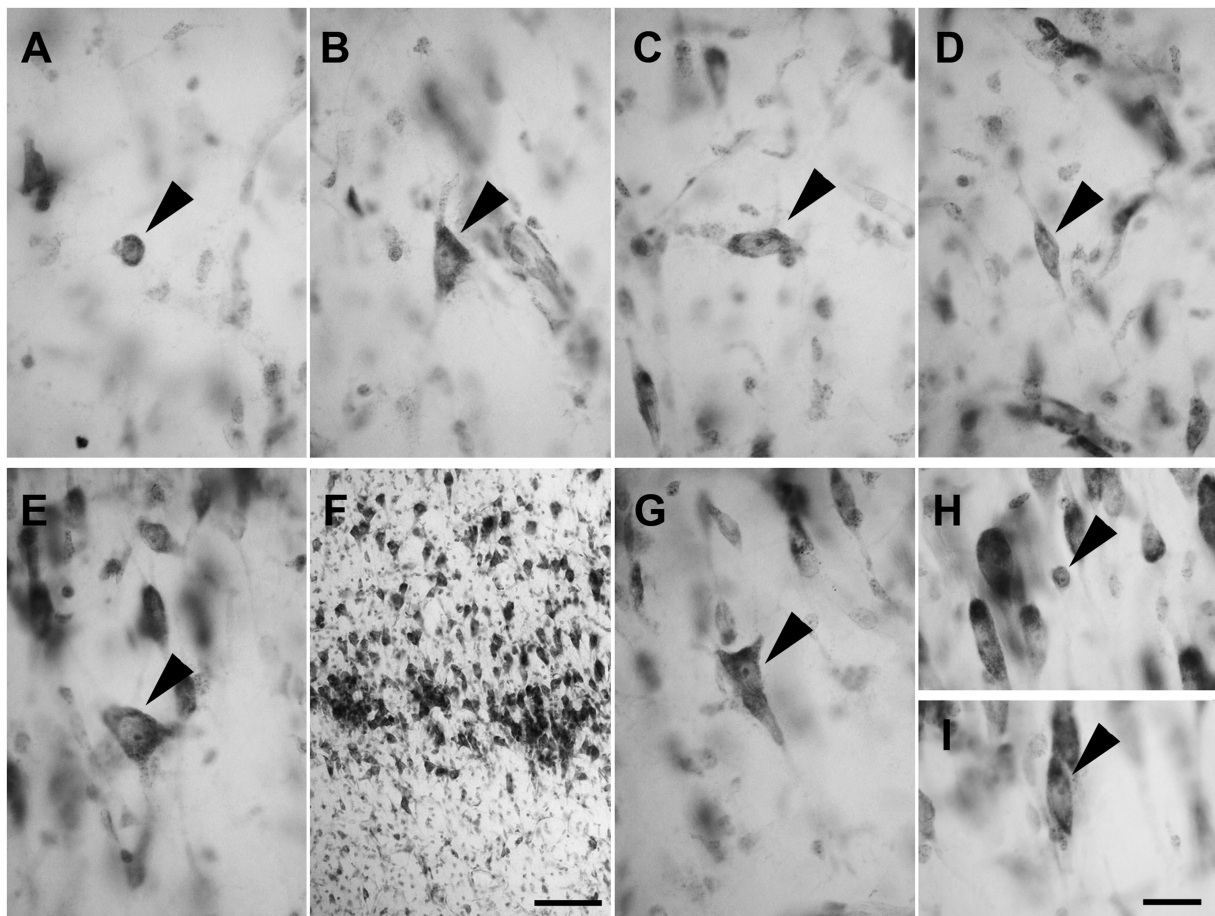


FIGURE 2

Brightfield photomicrographs of thionin-stained coronal sections from layers I (A–D) and II (E–H) of the lateral entorhinal cortex (LEA) and medial entorhinal cortex (MEA). Layer I contains spheroidal [arrowhead in (A), LEA], polygonal [arrowhead in (B), MEA], and fusiform [arrowhead in (C), LEA; (D) MEA] nonpyramidal neurons. Fusiform neurons are oriented horizontally [arrowhead in (C)] or vertically [arrowhead in (D)] with respect to the cortical surface. Layer II shows darkly stained neurons with a polygonal cell body [arrowhead in (E), LEA], usually aggregated into “islands” [arrowhead in (F), LEA]. Layer II shows pyramidal neurons with the apical dendrite directed toward to the cortical surface [arrowhead in (G), MEA], spheroidal neurons [arrowhead in panel (H), LEA], and medium-sized fusiform cells [arrowhead in (I), MEA]. Scale bar = 100 μ m in (F); 20 μ m in (H) [applied to (A–E) and (G–I)].

found in the superficial layers. The distribution of the immunoreactivities did not differ between LEA and MEA.

Neurons containing calcium-binding proteins were morphologically heterogeneous and could be divided into two main categories: pyramidal and non-pyramidal neurons. Non-pyramidal neurons could also subdivided in spheroidal, polygonal and fusiform cells.

3.2.1 Pyramidal neurons

These cells, observed only in CB and CR preparations, had a pyramidal cell body from which the dendrites extended for only a short distance. The largest pyramidal neurons were observed in layers V and VI (Figures 9A,B).

Non-pyramidal spheroidal neurons: These neurons had a small spheroidal cell body that gave rise to a few thin dendrites (Figures 10A–C).

3.2.2 Non-pyramidal polygonal neurons

These cells had a polygonal soma of variable size and giving rise to several dendrites of varying thickness (Figures 11A–C).

3.2.3 Non-pyramidal fusiform neurons

These neurons had two dendrites emerging from opposite poles of fusiform cell bodies. The dendrites often branched near the somata (Figures 12A–C).

The morphometric characteristics of calcium-binding proteins-IR neurons in LEA and MEA are reported in Figure 13. The morphometric features of IR neurons were not statistically different when comparing LEA with MEA. With the exception of CB-IR neurons located in layer V, the mean perikaryal area of the CBPs-IR polygonal neurons was significantly larger than that of spheroidal neurons ($p < 0.001$; Figure 13). Also, the mean perikaryal area of pyramidal neurons immunoreactive for the CR and CB was larger than that of other cell types. In layer II of LEA and MEA, pyramidal neurons IR for the CR are statistically smaller than those IR for CB ($p < 0.001$; Figure 13), whereas the opposite was observed in layers V and VI ($p < 0.001$; Figure 13). Throughout the entorhinal cortex, the perikaryal size of the CR-IR nonpyramidal neurons was statistically smaller than that of

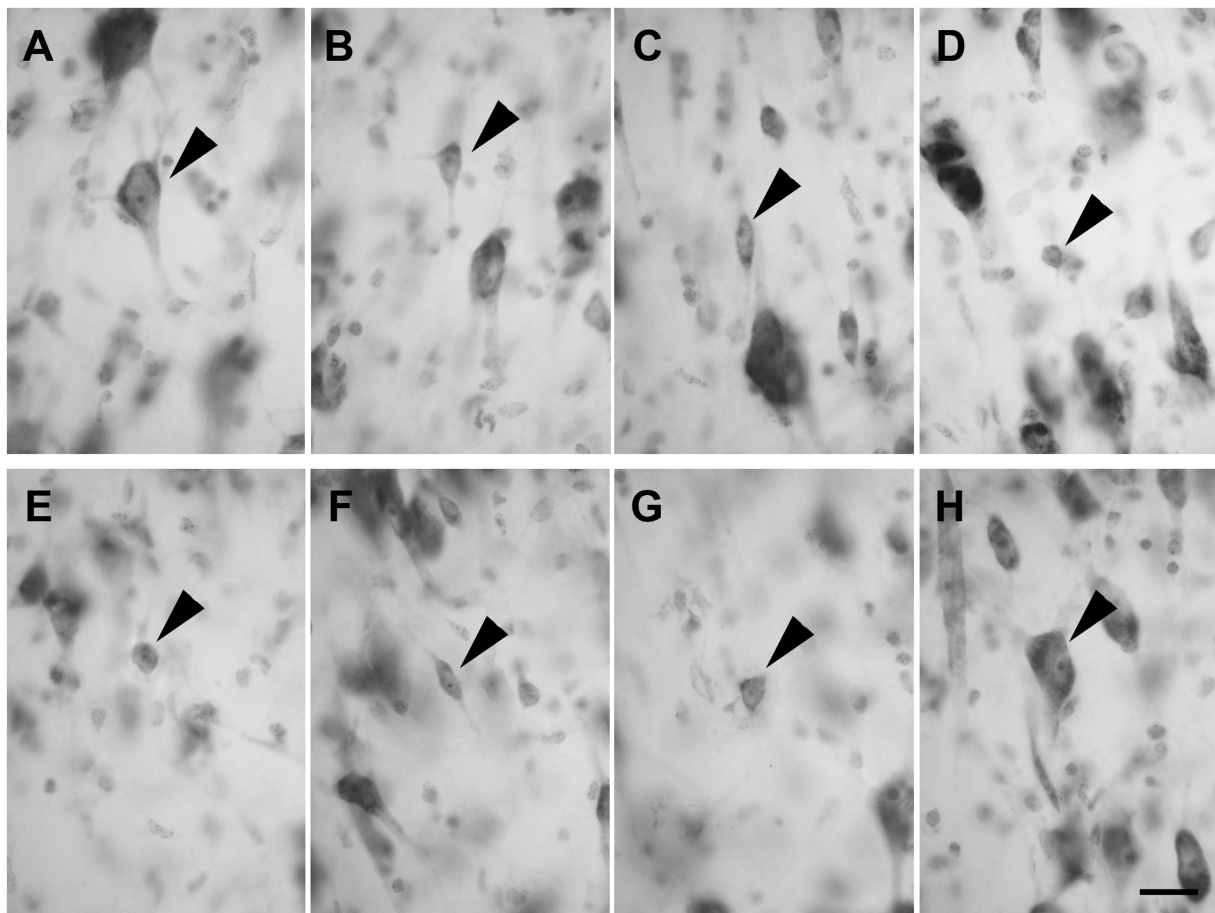


FIGURE 3

Brightfield photomicrographs of thionin-stained coronal sections of layers III (A–D) and IV (E–H) of the lateral entorhinal cortex (LEA) and medial entorhinal cortex (MEA). Layer III is composed of pyramidal neurons [arrowhead in (A), LEA] and non-pyramidal neurons with a polygonal [arrowhead in (B), MEA], fusiform [arrowhead in (C), LEA], or spheroidal somata [arrowhead in (D), MEA]. Layer IV (*lamina dissecans*) contains spheroidal [arrowhead in (E), LEA], fusiform [arrowhead in (F), LEA], polygonal [arrowhead in (G), LEA], and pyramidal neurons [arrowhead in (H), LEA]. Scale bar = 20 μ m in (H) [applied to (A–H)].

nonpyramidal neurons immunoreactive for CB and PV ($p < 0.001$; Figure 13).

3.3 Laminar distribution of calcium-binding proteins immunoreactive neurons in the entorhinal cortex

3.3.1 Layer I

3.3.1.1 CR

Layer I contained some small or medium-sized CR-IR spheroidal ($n = 15$ in LEA; $n = 13$ in MEA), polygonal ($n = 16$ in LEA; $n = 14$ in MEA), and fusiform neurons ($n = 19$ in LEA; $n = 20$ in MEA). Fusiform cells appeared bipolar with horizontally oriented thin dendrites.

3.3.1.2 CB

Scattered spheroidal ($n = 11$ in LEA; $n = 13$ in MEA), polygonal ($n = 9$ in LEA; $n = 12$ in MEA) and fusiform ($n = 9$ in LEA; $n = 10$ in MEA) small or medium-sized CB-IR neurons were observed in layer I, their dendrites appeared mostly confined within the layer.

3.3.1.3 PV

Occasionally PV-IR neurons with spheroidal ($n = 5$ in LEA; $n = 4$ in MEA), polygonal ($n = 6$ in LEA; $n = 4$ in MEA), and fusiform ($n = 5$ in LEA; $n = 5$ in MEA) somata were occasionally observed in layer I.

3.3.2 Layer II

3.3.2.1 CR

Small or medium sized CR-IR nonpyramidal neurons with spheroidal ($n = 112$ in LEA; $n = 117$ in MEA), polygonal ($n = 51$ in LEA; $n = 47$ in MEA) and fusiform ($n = 33$ in LEA; $n = 39$ in MEA) somata were located in layer II. Large CR-IR pyramidal cells were also observed ($n = 68$ in LEA; $n = 65$ in MEA).

3.3.2.2 CB

Neurons immunoreactive for the CB were with a pyramidal ($n = 51$ in LEA; $n = 57$ in MEA) spheroidal ($n = 83$ in LEA; $n = 87$ in MEA), polygonal ($n = 74$ in LEA; $n = 81$ in MEA), and fusiform ($n = 32$ in LEA; $n = 41$ in MEA) somata. Pyramidal neurons were clustered and had an evident apical dendrite directed into layer I.

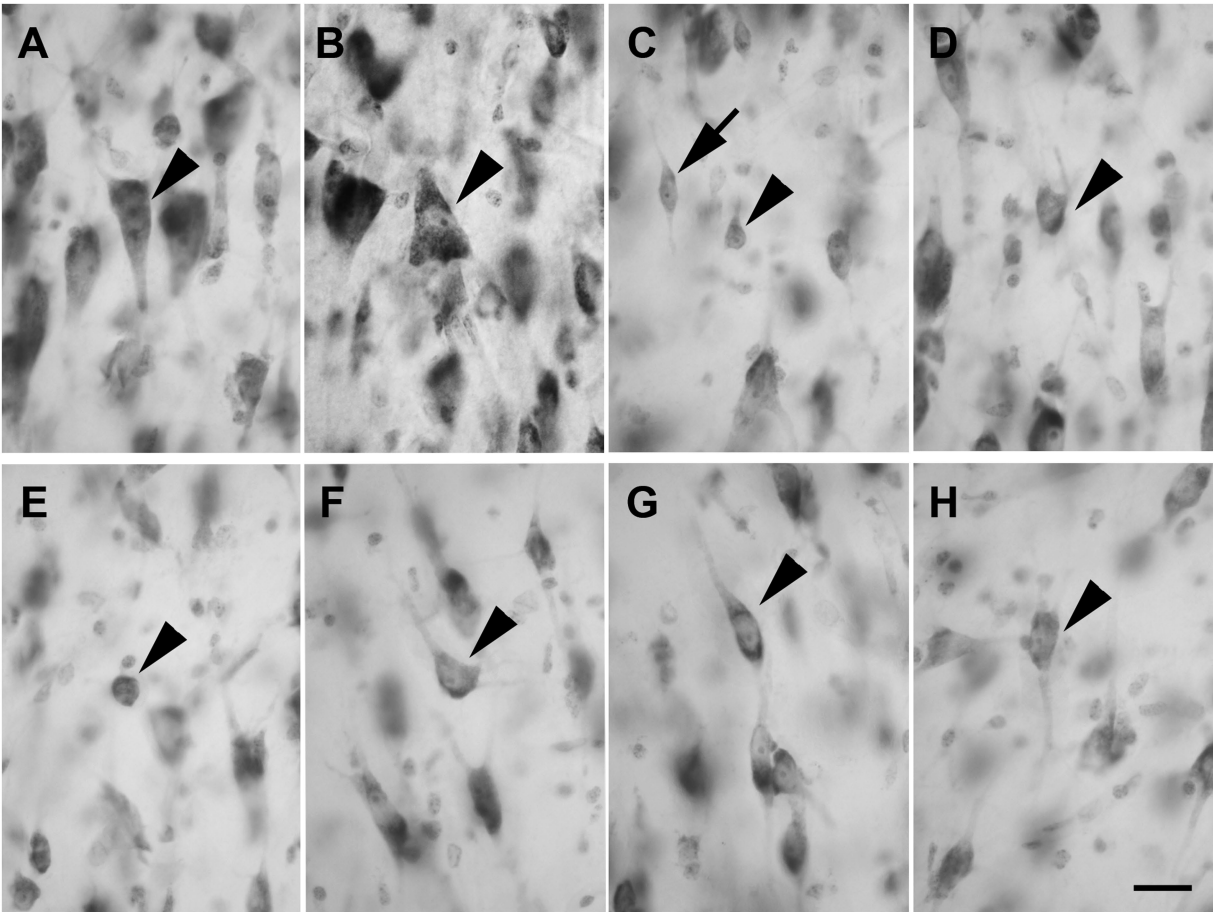


FIGURE 4
Brightfield photomicrographs of thionin-stained coronal sections from layers V (A–D) and VI (E–H) of the lateral entorhinal cortex (LEA) and medial entorhinal cortex (MEA). Layer V shows large pyramidal neurons [arrowhead in (A), LEA]; interestingly, many inverted pyramidal cells are also present [arrowhead in (B), MEA]. Layer V contains non-pyramidal neurons with a spheroidal [arrowhead in (C), LEA], fusiform [arrow in (C), LEA], and polygonal [arrowhead in (D), MEA] cell bodies. Layer VI contains neurons with a spheroidal [arrowhead in (E), LEA], polygonal [arrowhead in (F), MEA], fusiform [arrowhead in (G), LEA], and pyramidal [arrowhead in (H), MEA] morphology. Scale bar = 20 μm in H [applied to (A–H)].

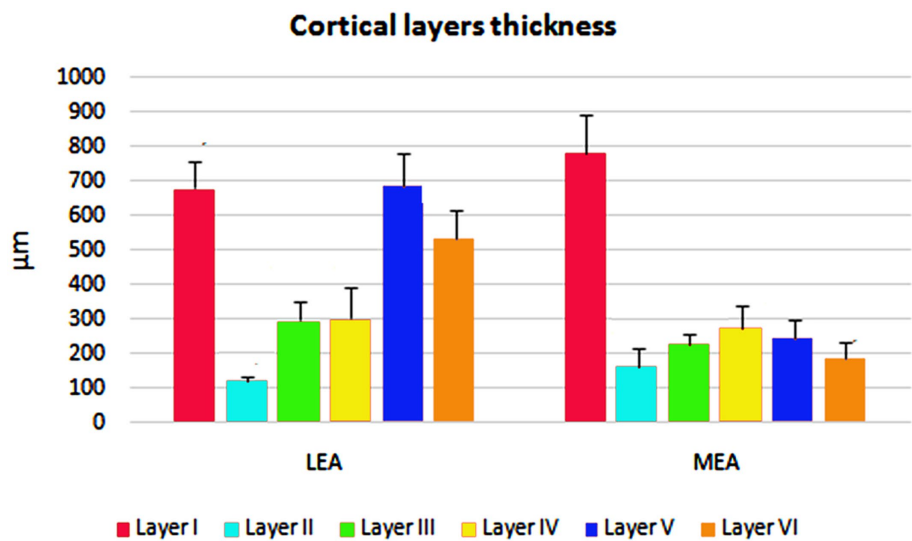


FIGURE 5
Cortical layers thicknesses \pm standard deviation (SD) in lateral entorhinal area (LEA) and medial entorhinal area (MEA) of bottlenose dolphin.

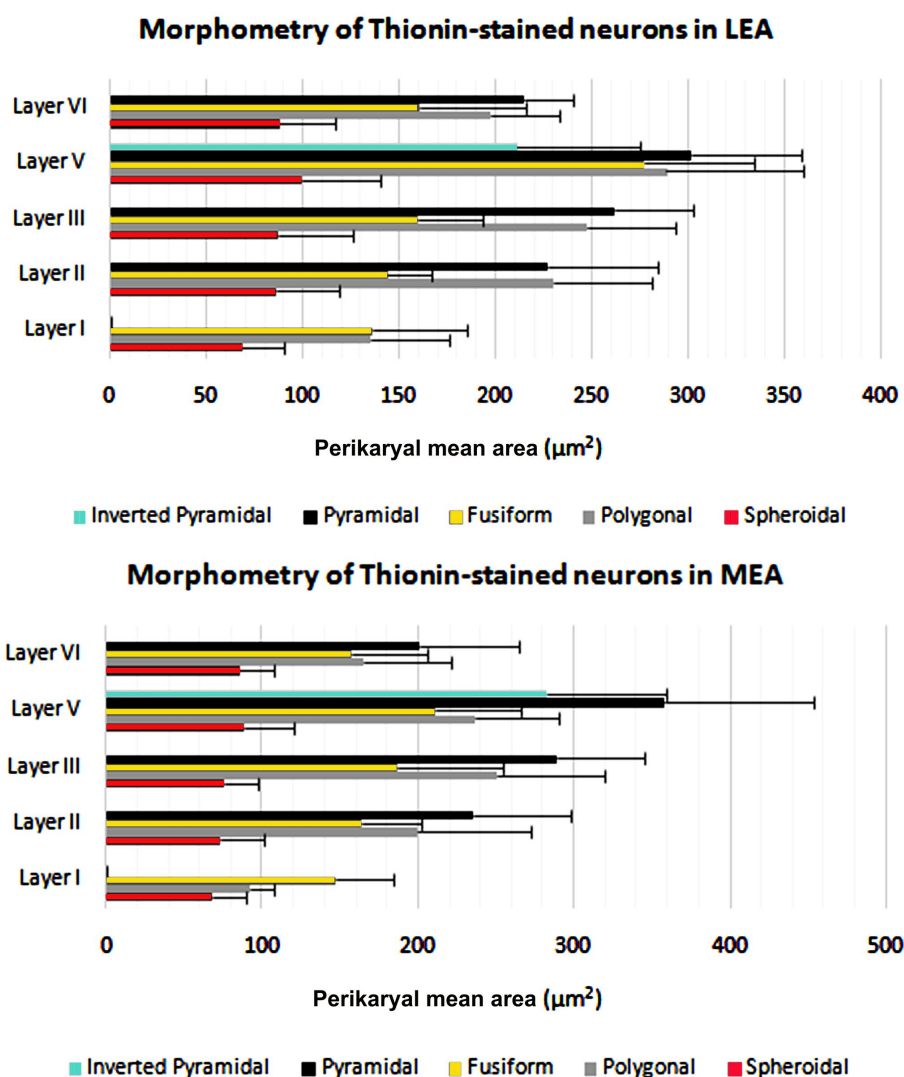


FIGURE 6

Perikaryal mean area \pm standard deviation (SD) of thionin-stained neurons in lateral entorhinal area (LEA) and medial entorhinal area (MEA) of bottlenose dolphin.

3.3.2.3 PV

PV-IR neurons were non-pyramidal cells with a spheroidal ($n=41$ in LEA; $n=47$ in MEA), polygonal ($n=35$ in LEA; $n=37$ in MEA), and fusiform ($n=33$ in LEA; $n=31$ in MEA) morphology. Fusiform neurons showed an evident somata.

3.3.3 Layer III

3.3.3.1 CR

Layer III contained non-pyramidal cells with spheroidal ($n=62$ in LEA; $n=70$ in MEA), polygonal ($n=121$ in LEA; $n=119$ in MEA), and fusiform ($n=130$ in LEA; $n=142$ in MEA) somata of various sizes and medium-sized pyramidal cells ($n=107$ in LEA; $n=106$ in MEA).

3.3.3.2 CB

CB-IR neurons located in layer III were morphologically similar to those observed in CR preparations and showed a spheroidal ($n=121$ in LEA; $n=131$ in MEA), polygonal ($n=54$ in LEA; $n=58$ in

MEA), fusiform ($n=71$ in LEA; $n=76$ in MEA), and pyramidal ($n=44$ in LEA; $n=50$ in MEA) cell bodies.

3.3.3.3 PV

PV-IR neurons in layer III had a polygonal ($n=52$ in LEA; $n=56$ in MEA) and, to a lesser extent, spheroidal ($n=38$ in LEA; $n=39$ in MEA) and fusiform ($n=40$ in LEA; $n=41$ in MEA) morphologies.

3.3.4 Layer IV

Neurons immunoreactive for the three calcium-binding proteins with spheroidal, polygonal, and fusiform cell bodies were seldom observed in layer IV.

3.3.5 Layer V

3.3.5.1 CR

Layer V contained medium-sized non-pyramidal neurons with spheroidal ($n=74$ in LEA; $n=63$ in MEA), polygonal ($n=131$ in LEA; $n=141$ in MEA) or fusiform ($n=150$ in LEA; $n=152$ in MEA) cell

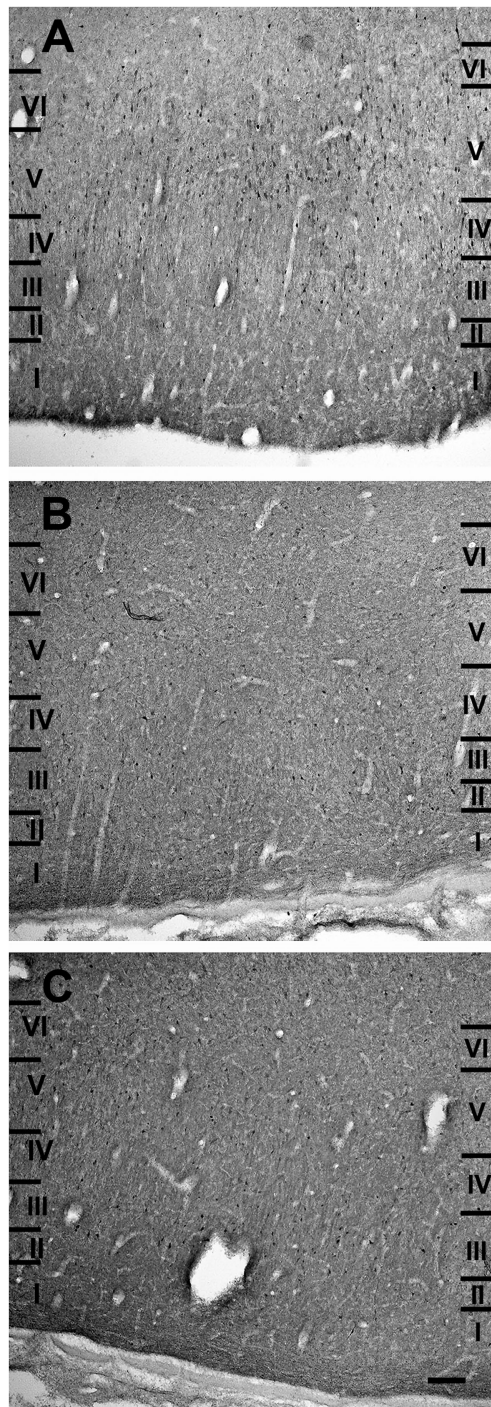


FIGURE 7
Brightfield photomicrographs of immunohistochemically stained sections demonstrating the distribution of calretinin (A), calbindin-D28k (B), and parvalbumin (C) immunoreactivity in the lateral entorhinal cortex. Scale bar = 200 μ m in (C) [applied to (A–C)].

bodies and many pyramidal neurons ($n = 167$ in LEA; $n = 157$ in MEA) with a large somata.

3.3.5.2 CB

Few CB-IR neurons were observed in layer V as compared with layers II and III. These cells could be large pyramidal ($n = 13$ in LEA; $n = 17$ in MEA) and non-pyramidal neurons with spheroidal ($n = 51$ in LEA; $n = 47$ in MEA), polygonal ($n = 63$ in LEA; $n = 68$ in MEA) and

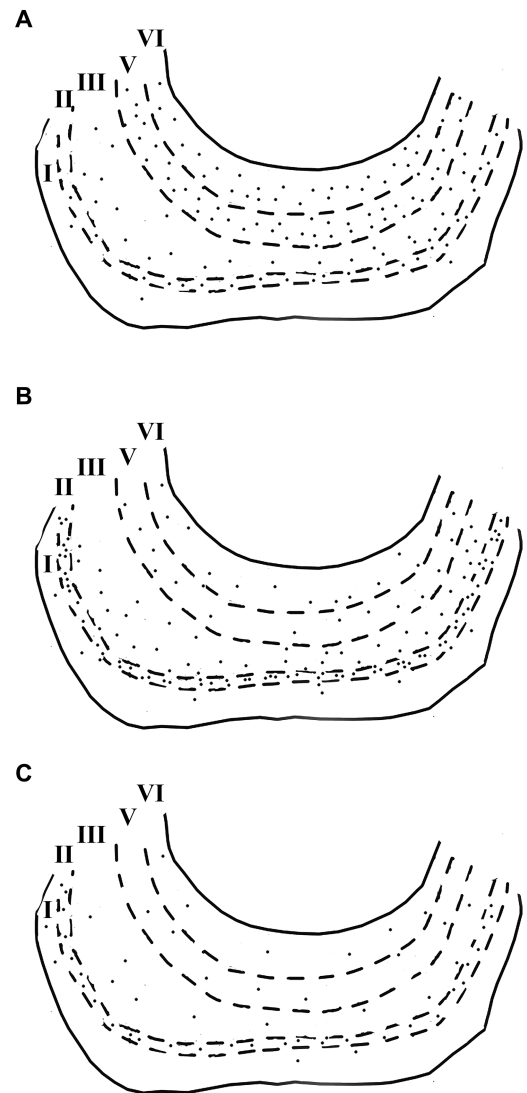


FIGURE 8
Computer-generated plots demonstrating the distribution of neurons immunoreactive for calretinin (A), calbindin-D28k (B), and parvalbumin (C) in the lateral entorhinal cortex. Each dot represents one immunopositive soma. Dashed lines delineate the different layers which are labeled with Roman numerals. Neurons in the putative layer IV were too sparse to be effectively represented here. Scale bar = 500 μ m in (C) [applied to (A–C)].

fusiform ($n = 37$ in LEA; $n = 35$ in MEA) cells bodies. Pyramidal cells are usually smaller than those observed in the CR preparation.

3.3.5.3 PV

The few PV-IR neurons observed in layer V were only medium-sized nonpyramidal cells with a spheroidal ($n = 27$ in LEA; $n = 25$ in MEA), polygonal ($n = 33$ in LEA; $n = 34$ in MEA), and fusiform ($n = 35$ in LEA; $n = 32$ in MEA) cell bodies.

3.3.6 Layer VI

3.3.6.1 CR

Layer VI contained many large CR-IR pyramidal neurons ($n = 62$ in LEA; $n = 70$ in MEA) with an evident apical dendrite. In addition, layer VI contained medium-sized spheroidal ($n = 62$ in LEA;

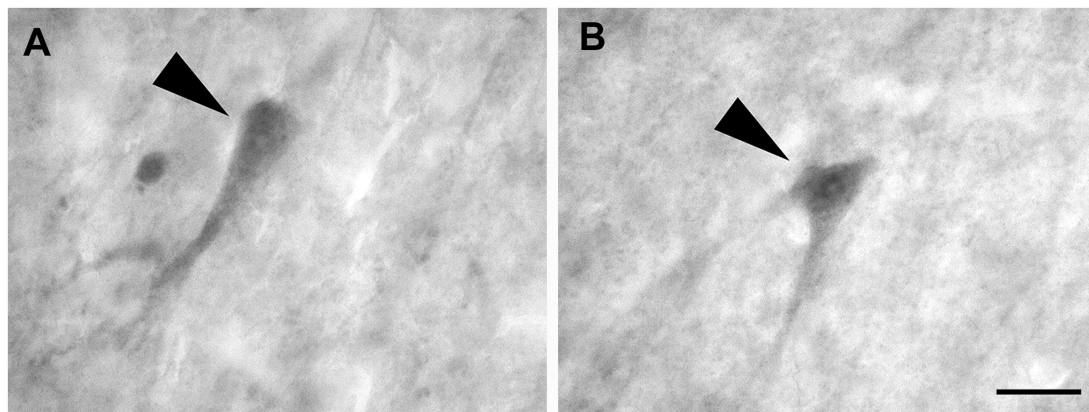


FIGURE 9
Brightfield photomicrographs demonstrating pyramidal neurons (arrowheads) immunoreactive for calretinin (layer V) (A) and calbindin-D28k (layer V) (B). Scale bar = 20 μ m in (B) [applied to (A,B)].

$n=70$ in MEA), polygonal ($n=62$ in LEA; $n=70$ in MEA), and fusiform ($n=62$ in LEA; $n=70$ in MEA) non-pyramidal cells.

3.3.6.2 CB

Layer VI showed the same morphologic types of CB-IR neurons as reported in CR preparation: spheroidal ($n=40$ in LEA; $n=39$ in MEA), polygonal ($n=63$ in LEA; $n=73$ in MEA), fusiform ($n=11$ in LEA; $n=13$ in MEA) and pyramidal ($n=14$ in LEA; $n=17$ in MEA) neurons. However, the pyramidal cells immunoreactive for the CB are smaller than those positive for CR.

3.3.6.3 PV

PV-IR non-pyramidal neurons had a medium sized somata with a spheroidal ($n=23$ in LEA; $n=23$ in MEA) and fusiform ($n=33$ in LEA; $n=34$ in MEA) morphology. Interestingly, large polygonal non-pyramidal cells ($n=31$ in LEA; $n=33$ in MEA) were also observed.

4 Discussion

In recent years, research on the neuroanatomical features of the bottlenose dolphin has increased (Bombardi et al., 2010, 2011, 2013, 2021; Cozzi et al., 2014; Parolisi et al., 2015; Rambaldi et al., 2017; Sacchini et al., 2018, 2022; Graić et al., 2021, 2022; Gerussi et al., 2023). In particular, the precise topographical and functional identification of the dolphin neocortical areas, and their comparison with those of terrestrial mammals, is challenging. Previous studies have mapped the principal motor and sensory areas in common and bottlenose dolphins (Lende and Akdikmen, 1968; Morgane et al., 1980; Ridgway, 1990; Cozzi et al., 2017). A recent study identified the dolphin equivalent of the human prefrontal cortex in the bottlenose dolphin (Gerussi et al., 2023). Overall, however, considered in as a whole, several features of the dolphin brain remain poorly documented compared to other mammals. However, these studies were primarily cytoarchitectural determinations and did not report immunocytochemical characteristics of the neurons in the entorhinal and limbic regions. The entorhinal area is strongly connected with the hippocampal formation in terrestrial mammals, including Artiodactyls (Amaral et al., 1987; Carboni et al., 1990; Insausti, 1993;

Insausti et al., 1997; Kerr et al., 2007; Insausti and Amaral, 2008, 2012; Witter, 2012; Cappaert Van Strien and Witter, 2015; Maass et al., 2015; Witter et al., 2017). The hippocampal formation of dolphins and whales is very small (Morgane et al., 1982; Oelschläger and Buhl, 1985; Oelschläger and Buhl, 1985; Morgane and Jacobs, 1986), leading many authors to propose that the organization of the central part of the limbic system differs significantly from that of terrestrial mammals. Since dolphins lack olfaction [for reference see Cozzi et al. (2017)], the absence of an olfactory bulb raises interest in the entorhinal cortex. In addition, the study of the entorhinal cortex in cetaceans is particularly interesting given the presence of a small hippocampal formation in these animals. In the present study, we report that the dolphin entorhinal cortex, as in terrestrial mammals, is composed of six layers, of which layer IV (*lamina dissecans*) contains rare and irregularly distributed neurons [for details on this entorhinal layer, reference and review see Insausti et al. (2017)]. The classical mammalian entorhinal cortex consists of two divisions: LEA and MEA. This bipartition has been widely used because of LEA and MEA can be easily distinguished by their respective distinct cytoarchitecture. Although several subsequent studies have shown that the entorhinal cortex of primates and rodents can be further partitioned (Insausti et al., 1997; Insausti and Amaral, 2008; Witter, 2012; Cappaert Van Strien and Witter, 2015; Witter et al., 2017; Piguet et al., 2018), here we utilized the traditional subdivision considering that the bottlenose dolphins is a relatively new species to describe. Specifically, our cytoarchitectural analysis shows that the two recognized subdivisions, LEA and MEA, can be easily identified in the bottlenose dolphin, as in terrestrial mammals (Kobro-Flatmoen and Witter, 2019). Layer II is more clearly demarcated in LEA than in MEA; in addition, the boundary between layers II and III is very sharp in LEA. The cell-sparse zone between layers II and III was named *external lamina dissecans* by Jacobs et al. (1979). The neurons in layer II of LEA are clustered in islands and smaller than in the MEA. The layer IV (*lamina dissecans*) of the MEA is less distinct than in the LEA, whereas layers V (thicker in the LEA than in the MEA) and VI (thicker in the LEA than in the MEA) were slightly better differentiated from each other in the MEA than in the LEA. Overall, the general appearance of the dolphin entorhinal cortex is similar to that observed in terrestrial mammals; however, layer VI is characteristically thicker in the dolphin LEA than in other

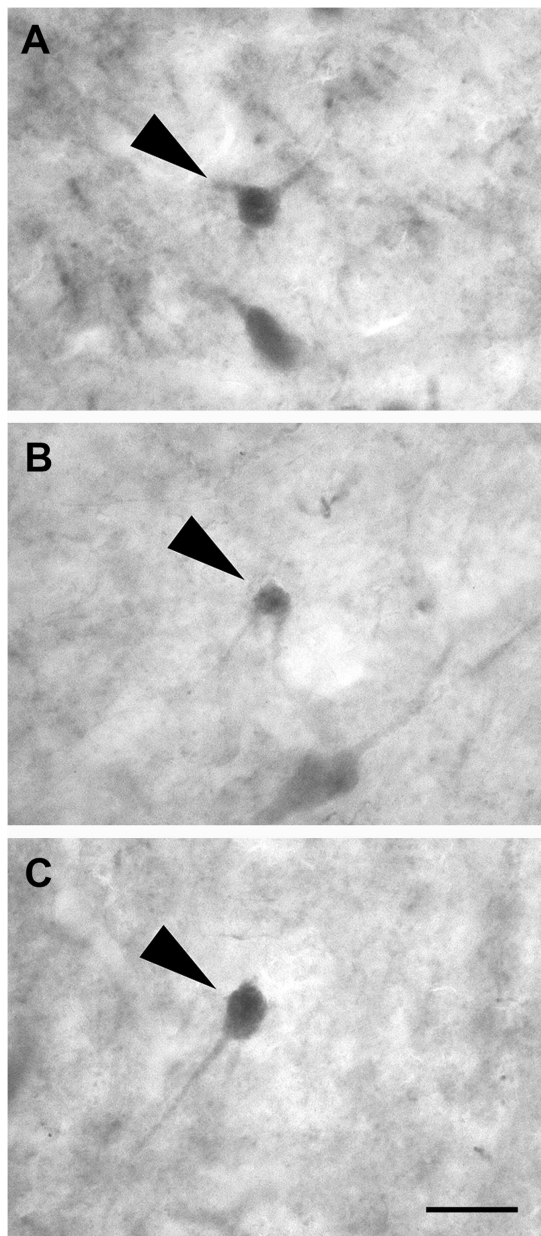


FIGURE 10
Brightfield photomicrographs demonstrating non-pyramidal spheroidal neurons (arrowheads) immunoreactive for calretinin (layer V) (A), calbindin-D28k (layer III) (B), and parvalbumin (layer II) (C). Scale bar = 20 μ m in (C) [applied to (A–C)].

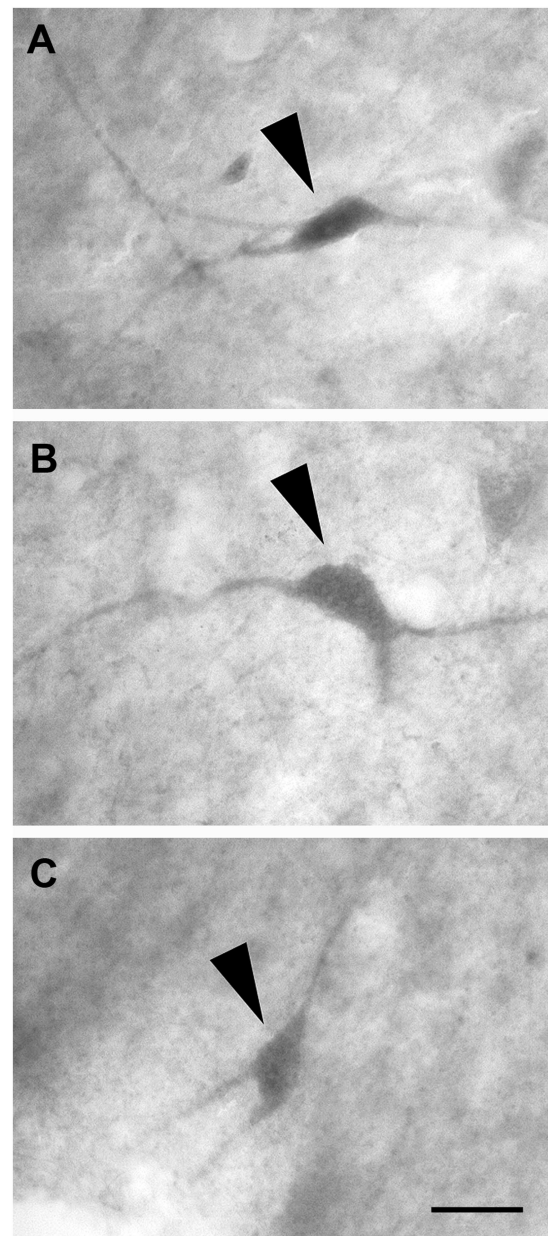


FIGURE 11
Brightfield photomicrographs demonstrating non-pyramidal polygonal neurons (arrowheads) immunoreactive for calretinin (layer V) (A), calbindin-D28k (layer III) (B), and parvalbumin (layer III) (C). Scale bar = 20 μ m in (C) [applied to (A–C)].

mammals (Morgane and Glezer, 1990). We also emphasize the importance of layer II in the thalamo-related circuitry of Artiodactyls (Peruffo et al., 2019), its role as a potential reservoir of immature neurons, and its progressive increase in neuronal density in large-brained species such as the bottlenose dolphin (La Rosa et al., 2020).

We also examined the distribution of CBPs in the entorhinal cortex of the bottlenose dolphin. CBPs, such as CR, CB, and PV have been observed in the entorhinal cortex of different species and found to be localized in morphologically distinct populations of neurons (Tuñón et al., 1992; Schmidt et al., 1993; Seress et al., 1994; Wouterlood et al., 1995, 2000; Fujimaru and Kosaka, 1996; Miettinen et al., 1996,

1997; Mikkonen et al., 1997; Berger et al., 1999; Suzuki and Porteros, 2002; Grateron et al., 2003; Kobre-Flatmoen and Witter, 2019). These proteins are also colocalize with γ -aminobutyric acid (GABA) and can be used as proxy markers of local circuit interneurons (Kobre-Flatmoen and Witter, 2019). CBPs have been studied in the dolphin brain (Glezer et al., 1992, 1993, 1995, 1998; Hof et al., 2000; Cozzi et al., 2014; Graïc et al., 2022), but information on their presence in the entorhinal cortex is limited. In our experimental series, CR-ir and CB-ir neurons were always easily identified. The majority of the CB-ir cells were confined to the superficial layers, whereas the CR-ir neurons were distributed throughout all the cortical columns of the entorhinal

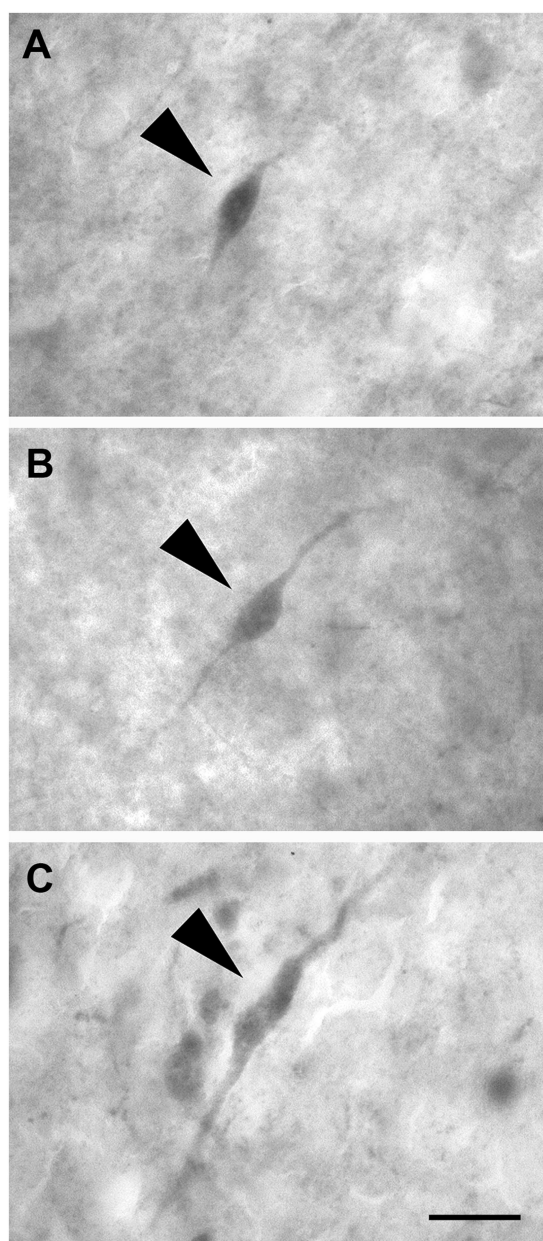


FIGURE 12
Brightfield photomicrographs demonstrating nonpyramidal fusiform neurons (arrowheads) immunoreactive for calretinin (layer III) (A), calbindin-D28k (layer II) (B), and parvalbumin (layer II) (C). Scale bar = 20 μ m in (C) [applied to (A–C)].

cortex. CR-ir and CB-ir neurons were far more present, and consequently distinct, than PV-ir neurons, which were localized mainly in superficial layers II and III. The data that we report here confirm numerous previous experiments using CBPs in different areas of cetacean brain (Hof et al., 1992, 2000; Glezer et al., 1993, 1995; Hof and Sherwood, 2005), as well as evidence showing that PV immunostaining was scarce or utterly absent in the cetacean cortex (Glezer et al., 1998; Cozzi et al., 2014; Graïc et al., 2021).

Immunoreactivity for the CR and the CB neurons was observed in both pyramidal and non-pyramidal neurons, but the PV was only expressed only in non-pyramidal neurons. Pyramidal neurons

expressed both CB and CR in layers II, III, V, and IV. However, there was a population of large pyramidal-shaped CR-ir neurons in layers V and VI that were significantly larger than those observed in the same layers of CB preparations. In addition, we identified three main types of non-pyramidal CBPs-ir neurons: spheroidal, polygonal, and fusiform. Non-pyramidal neurons immunoreactive for CR, CB, and PV are similar, except for fusiform neurons containing CR, which were usually smaller than those immunoreactive for CB and, especially, PV. The presence of CR-ir neurons strongly suggests a GABAergic neuronal population (Glezer et al., 1992). Their presence may also indicate that the absence of a distinct layer IV, as generally expressed in the primate and rodent neocortex, could be replaced here by a *diffuse band* of GABAergic/CR-ir neurons (Graïc et al., 2021), although this specific aspect required further investigation. Overall, our observations, combined with those concerning the laminar distribution, suggest that PV, CB, and CR are primarily localized in non-overlapping neuronal populations in the dolphin entorhinal cortex.

Our immunohistochemical observations are consistent with previous studies in rodents and primates (Tuñón et al., 1992; Schmidt et al., 1993; Seress et al., 1994; Wouterlood et al., 1995, 2000; Fujimaru and Kosaka, 1996; Miettinen et al., 1996, 1997; Mikkonen et al., 1997; Berger et al., 1999; Suzuki and Porteros, 2002; Grateron et al., 2003; Kibro-Flatmoen and Witter, 2019). As in terrestrial mammals, CB and PV are primarily expressed in neurons located in layers II and III, whereas the CR-ir neurons are distributed throughout the layers, and especially in layers V and VI. Studies in terrestrial mammals (Kibro-Flatmoen and Witter, 2019) show that layer I is devoid of PV-ir neurons, but in our study layer I of the dolphin entorhinal cortex contained PV-ir neurons.

In rodents and primates, the distribution of CBPs-ir neurons is highly dependent on the entorhinal subfield analyzed (Tuñón et al., 1992; Schmidt et al., 1993; Seress et al., 1994; Wouterlood et al., 1995, 2000; Fujimaru and Kosaka, 1996; Miettinen et al., 1996, 1997; Mikkonen et al., 1997; Berger et al., 1999; Suzuki and Porteros, 2002; Grateron et al., 2003; Kibro-Flatmoen and Witter, 2019). However, in the present study in the bottlenose dolphin, we noted some differences between the cytoarchitectonic organization of the LEA and MEA (see above), but the distribution of the immunoreactivity for the CR, CB and PV was similar in the two subdivisions of the periarchicortex.

Layers II and III of the entorhinal cortex provide the main cortical input to the hippocampal formation, while layers V and VI receive information from the hippocampal formation and transmit it to the neocortex and other brain structures (Witter and Amaral, 1991; Insausti et al., 1997; van Groen et al., 2003; Kerr et al., 2007; Witter, 2007, 2012; Insausti and Amaral, 2012; Cappaert Van Strien and Witter, 2015; Witter et al., 2017). Our results indicate that calcium-binding protein neurons in the dolphin entorhinal cortex are located in the interface between entorhinal input and output pathways. CB-ir pyramidal neurons in layers II and III may harbor output neurons that project through the perforant pathway to the dentate gyrus and CA1-3 regions of the hippocampus proper. Taken together, our data suggest that pyramidal neurons immunoreactive for the CR in layers V and VI could be projection neurons involved in signal flow between different regions of the hippocampal formation. Non-pyramidal PV-ir neurons, together with those immunoreactive for CB and CR, could act as local interneurons that directly or indirectly regulate the activity

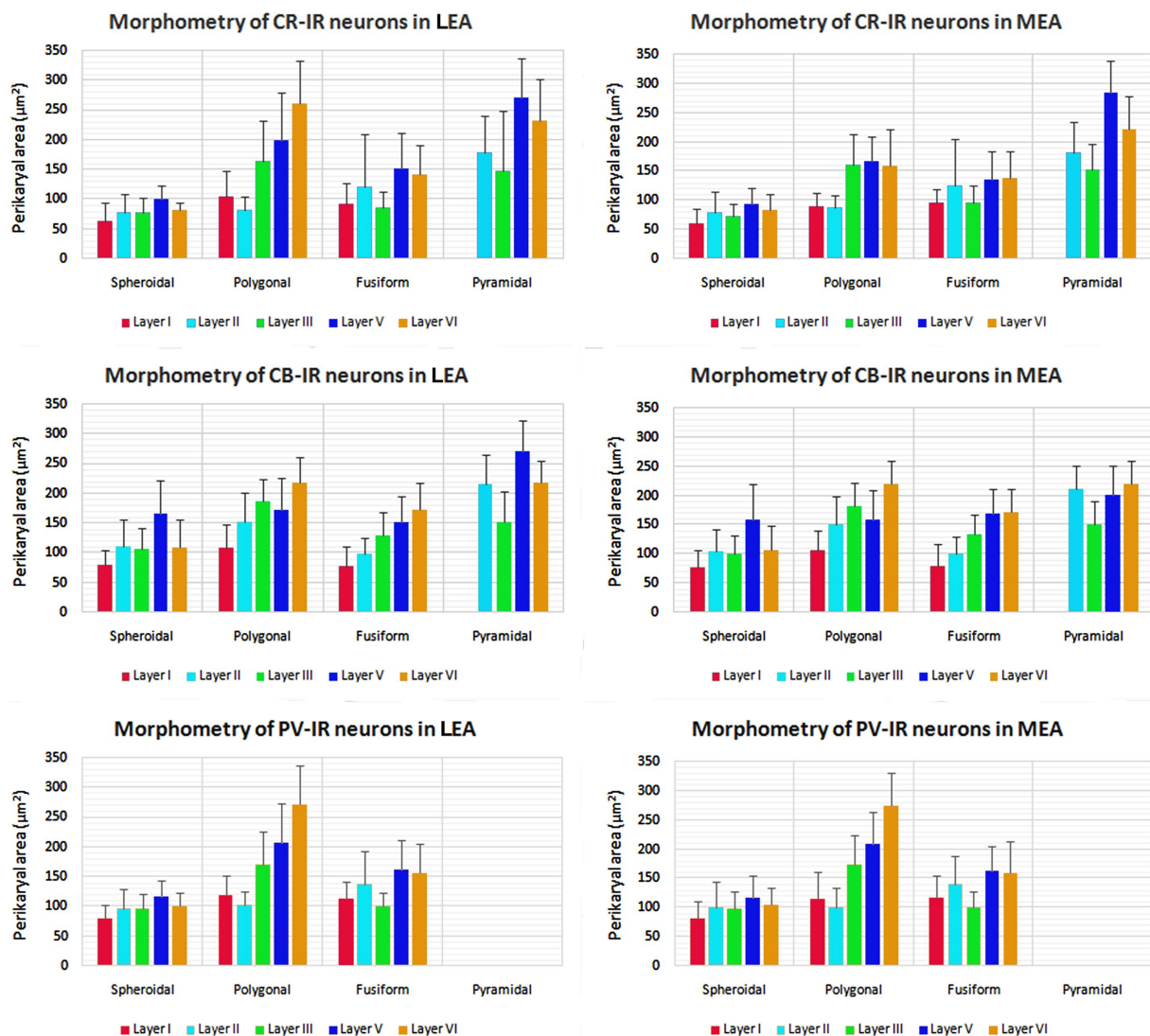


FIGURE 13

Perikaryal mean area \pm standard deviation (SD) of calretinin- (CR), calbindin-D28k (CB), and parvalbumin- (PV) immunoreactive neurons in lateral entorhinal area (LEA) and medial entorhinal area (MEA) of bottlenose dolphin. For the explanations see the text.

of projection cells. Contemplating the entorhinal cortex contextually, since the seminal work from Hafting and colleagues (Hafting et al., 2005) describing a topographical orientation map in the entorhinal cortex of rodents, the entorhinal cortex of cetaceans, a taxa that lives in the ocean with very few external landmarks, could prove to be a very interesting comparative neuroanatomical example. As mentioned in the introduction, dolphins do not possess an olfactory bulb and are indeed deprived of olfaction [but not necessarily of chemoreception; for reference see Cozzi et al. (2017)]. This lack of function may call into question the role of the entorhinal formation and lamina dissecans in cetaceans, as they are usually considered in terrestrial mammals. A working hypothesis is that the entorhinal formation may be the target of projections originating from other sensory areas, possibly related to the establishment of connections to and between the amygdalae. The topography of the sensory areas responsible for echolocation, which map and interpret sound emission and perception into distance and shape, is currently uncertain at best. A recent study (Gerussi et al., 2023) found that the dolphin prefrontal cortex occupies

the cranio-lateral, ectolateral and opercular gyri, with projections involving lateral and ventral parts of the forebrain, hence close to the area presently discussed. A specific study using tractography may help the issue and evaluate the contribution of the entorhinal area to the rest of the cerebral network in dolphins.

Data availability statement

The raw data supporting the conclusions of this article will be made available by the authors, without undue reservation.

Ethics statement

Ethical approval was not required for the study involving humans in accordance with the local legislation and institutional requirements. Written informed consent to participate in this study was not required

from the participants or the participants' legal guardians/next of kin in accordance with the national legislation and the institutional requirements. Ethical approval was not required for the study involving animals in accordance with the local legislation and institutional requirements because Dolphin brains were extracted during routine necropsy performed at the Department of Comparative Biomedicine and Food Science (BCA) of the University of Padova (Italy) on specimens. The brains were consequently fixed in phosphate buffered paraformaldehyde (4%), cut in coronal slices (about 1.5 cm × 2.5 cm) and stored in the Mediterranean marine mammal tissue bank (MMMTB, <http://www.marinemammals.eu>), located in BCA. The MMMTB is a CITES recognized (IT020) research center of the University of Padova, sponsored by and collaborating with the Italian Ministry of the Environment. MMMTB collects and stores samples from wild or captive marine mammals whose samples or whole carcasses are delivered to BCA for post-mortem diagnostics.

Author contributions

J-MG: Conceptualization, Data curation, Investigation, Methodology, Supervision, Writing – original draft, Writing – review & editing. AG: Conceptualization, Data curation, Data curation, Supervision, Validation, Writing – review & editing. SS: Data curation, Supervision, Validation, Writing – review & editing. CT: Data curation, Investigation, Methodology, Software, Writing – review & editing. GS: Data curation, Investigation, Methodology, Software, Writing – review & editing. BC: Conceptualization, Data curation, Formal analysis, Resources, Supervision, Writing – review & editing.

References

- Amaral, D. G., Insausti, R., and Cowan, W. M. (1987). The entorhinal cortex of the monkey: I. Cytoarchitectonic organization. *J. Comp. Neurol.* 264, 326–355. doi: 10.1002/cne.902640305
- Berger, B., De Grissac, N., and Alvarez, C. (1999). Precocious development of parvalbumin-like immunoreactive interneurons in the hippocampal formation and entorhinal cortex of the fetal cynomolgus monkey. *J. Comp. Neurol.* 403, 309–331. doi: 10.1002/(SICI)1096-9861(19990118)403:3<309::AID-CNE3>3.0.CO;2-C
- Bombardi, C., Cozzi, B., Nenzi, A., Mazzariol, S., and Grandis, A. (2011). Distribution of Nitrergic neurons in the dorsal root ganglia of the bottlenose dolphin (*Tursiops truncatus*). *Anat. Rec. Adv. Integr. Anat. Evol. Biol.* 294, 1066–1073. doi: 10.1002/ar.21394
- Bombardi, C., Grandis, A., Gardini, A., and Cozzi, B. (2013). Nitrergic neurons in the spinal cord of the bottlenose dolphin (*Tursiops truncatus*): spinal cord of the bottlenose dolphin. *Anat. Rec.* 296, 1603–1614. doi: 10.1002/ar.22766
- Bombardi, C., Grandis, A., Nenzi, A., Giuriso, M., and Cozzi, B. (2010). Immunohistochemical localization of substance P and cholecystokinin in the dorsal root ganglia and spinal cord of the bottlenose dolphin (*Tursiops truncatus*). *Anat. Rec. Adv. Integr. Anat. Evol. Biol.* 293, 477–484. doi: 10.1002/ar.20975
- Bombardi, C., Rambaldi, A. M., Giallazzo, G., Giancola, F., Gračić, J.-M., Salamanca, G., et al. (2021). Nitrergic and substance P Immunoreactive neurons in the enteric nervous system of the bottlenose dolphin (*Tursiops truncatus*) intestine. *Animals* 11:1057. doi: 10.3390/ani11041057
- Breathnach, A. S., and Goldby, F. (1954). The amygdaloid nuclei, hippocampus and other parts of the rhinencephalon in the porpoise (*Phocaena phocaena*). *J. Anat.* 88, 267–291.
- Cappaert Van Strien, N. M., and Witter, M. P. (2015). “Hippocampal formation” in *The rat nervous system*. ed. G. Paxinos (San Diego, CA: Elsevier Academic Press), 511–574.
- Carboni, A. A., Lavelle, W. G., Barnes, C. L., and Cipolloni, P. B. (1990). Neurons of the lateral entorhinal cortex of the rhesus monkey: a Golgi, histochemical, and immunocytochemical characterization. *J. Comp. Neurol.* 291, 583–608. doi: 10.1002/cne.902910407
- Cozzi, B., Huggenberger, S., and Oelschlager, H. H. A. (2017). *Anatomy of dolphins: Insight into body structure and function*. Boston, MA: Elsevier.
- CB: Conceptualization, Data curation, Investigation, Resources, Supervision, Validation, Writing – original draft, Writing – review & editing.
- Cozzi, B., Roncon, G., Granato, A., Giuriso, M., Castagna, M., Peruffo, A., et al. (2014). The claustrum of the bottlenose dolphin *Tursiops truncatus* (Montagu 1821). *Front. Syst. Neurosci.* 8:42. doi: 10.3389/fnsys.2014.00042
- Fujimaru, Y., and Kosaka, T. (1996). The distribution of two calcium binding proteins, calbindin D-28K and parvalbumin, in the entorhinal cortex of the adult mouse. *Neurosci. Res.* 24, 329–343. doi: 10.1016/0168-0102(95)01008-4
- Gerussi, T., Gračić, J.-M., Peruffo, A., Behrooz, M., Schlaffke, L., Huggenberger, S., et al. (2023). The prefrontal cortex of the bottlenose dolphin (*Tursiops truncatus* Montagu, 1821): a tractography study and comparison with the human. *Brain Struct. Funct.* 228, 1963–1976. doi: 10.1007/s00429-023-02699-8
- Glezer, I. I., Hof, P. R., Istomin, V. V., and Morgane, P. J. (1995). “Comparative immunocytochemistry of calcium-binding protein-positive neurons in visual and auditory systems of cetacean and primate brains” in *Sensory Systems of Aquatic Mammals*. eds. R. A. Kastelein, J. A. Thomas and P. E. Nachtigall (Woerden: De Spil Publishers), 477–513.
- Glezer, I. I., Hof, P. R., Leranath, C., and Morgane, P. J. (1993). Calcium binding protein-containing neuronal populations in mammalian visual cortex: a comparative study in whales, insectivores, bats, rodents, and primates. *Cereb. Cortex* 3, 249–272. doi: 10.1093/cercor/3.3.249
- Glezer, I. I., Hof, P. R., and Morgane, P. J. (1992). Calretinin-immunoreactive neurons in the primary visual cortex of dolphin and human brains. *Brain Res.* 595, 181–188. doi: 10.1016/0006-8993(92)91047-1
- Glezer, I. I., Hof, P. R., and Morgane, P. J. (1998). Comparative analysis of calcium-binding protein-immunoreactive neuronal populations in the auditory and visual systems of the bottlenose dolphin (*Tursiops truncatus*) and the macaque monkey (*Macaca fascicularis*). *J. Chem. Neuroanat.* 15, 203–237. doi: 10.1016/S0891-0618(98)00022-2
- Gračić, J.-M., Peruffo, A., Corain, L., Finos, L., Grisan, E., and Cozzi, B. (2022). The primary visual cortex of Cetartiodactyls: organization, cytoarchitectonics and comparison with perissodactyls and primates. *Brain Struct. Funct.* 227, 1195–1225. doi: 10.1007/s00429-021-02392-8
- Gračić, J., Peruffo, A., Grandis, A., and Cozzi, B. (2021). Topographical and structural characterization of the V1–V2 transition zone in the visual cortex of the long-finned pilot whale *Globicephala melas* (Traill, 1809). *Anat. Rec.* 304, 1105–1118. doi: 10.1002/ar.24558

Funding

The author(s) declare that no financial support was received for the research, authorship, and/or publication of this article.

Conflict of interest

The authors declare that the research was conducted in the absence of any commercial or financial relationships that could be construed as a potential conflict of interest.

The author(s) declared that they were an editorial board member of Frontiers, at the time of submission. This had no impact on the peer review process and the final decision.

Publisher's note

All claims expressed in this article are solely those of the authors and do not necessarily represent those of their affiliated organizations, or those of the publisher, the editors and the reviewers. Any product that may be evaluated in this article, or claim that may be made by its manufacturer, is not guaranteed or endorsed by the publisher.

- Grateron, L., Cebada-Sanchez, S., Marcos, P., Mohedano-Moriano, A., Insausti, A. M., Muñoz, M., et al. (2003). Postnatal development of calcium-binding proteins immunoreactivity (parvalbumin, calbindin, calretinin) in the human entorhinal cortex. *J. Chem. Neuroanat.* 26, 311–316. doi: 10.1016/j.jchemneu.2003.09.005
- Hafting, T., Fyhn, M., Molden, S., Moser, M.-B., and Moser, E. I. (2005). Microstructure of a spatial map in the entorhinal cortex. *Nature* 436, 801–806. doi: 10.1038/nature03721
- Hof, P. R., Chanis, R., and Marino, L. (2005). Cortical complexity in cetacean brains. *Anat. Rec. A Discov. Mol. Cell Evol. Biol.* 287A, 1142–1152. doi: 10.1002/ara.20258
- Hof, P. R., Glezer, I. I., Archin, N., Janssen, W. G., Morgane, P. J., and Morrison, J. H. (1992). The primary auditory cortex in cetacean and human brain: a comparative analysis of neurofilament protein-containing pyramidal neurons. *Neurosci. Lett.* 146, 91–95. doi: 10.1016/0304-3940(92)90180-F
- Hof, P. R., Glezer, I. I., Nimchinsky, E. A., and Erwin, J. M. (2000). Neurochemical and cellular specializations in the mammalian neocortex reflect phylogenetic relationships: evidence from Primates, cetaceans, and artiodactyls. *Brain Behav. Evol.* 55, 300–310. doi: 10.1159/00006665
- Hof, P. R., and Sherwood, C. C. (2005). Morphomolecular neuronal phenotypes in the neocortex reflect phylogenetic relationships among certain mammalian orders. *Anat. Rec. A Discov. Mol. Cell Evol. Biol.* 287A, 1153–1163. doi: 10.1002/ara.20252
- Hof, P. R., and Van Der Gucht, E. (2007). Structure of the cerebral cortex of the humpback whale, *Megaptera novaeangliae* (Cetacea, Mysticeti, Baleenopteridae). *Anat. Rec. Adv. Integr. Anat. Evol. Biol.* 290, 1–31. doi: 10.1002/ar.20407
- Insausti, R. (1993). Comparative anatomy of the entorhinal cortex and hippocampus in mammals. *Hippocampus* 3, 19–26. doi: 10.1002/hipo.1993.4500030705
- Insausti, R., and Amaral, D. G. (2008). Entorhinal cortex of the monkey: IV. Topographical and laminar organization of cortical afferents. *J. Comp. Neurol.* 509, 608–641. doi: 10.1002/cne.21753
- Insausti, R., and Amaral, D. (2012). “Hippocampal formation” in *The human nervous system*. eds. J. Mai and G. Paxinos (London: Academic Press), 896–942.
- Insausti, R., Herrero, M. T., and Witter, M. P. (1997). Entorhinal cortex of the rat: cytoarchitectonic subdivisions and the origin and distribution of cortical efferents. *Hippocampus* 7, 146–183. doi: 10.1002/(sici)1098-1063(1997)7:2<146::aid-hipo4>3.0.co;2-l
- Insausti, R., Muñoz-López, M., Insausti, A. M., and Artacho-Pérula, E. (2017). The human Periallocortex: layer pattern in Presubiculum, Parasubiculum and entorhinal cortex. A review. *Front. Neuroanat.* 11:84. doi: 10.3389/fnana.2017.00084
- Insausti, R., Tuñón, T., Sobreviela, T., Insausti, A. M., and Gonzalo, L. M. (1995). The human entorhinal cortex: a cytoarchitectonic analysis: human entorhinal cortex. *J. Comp. Neurol.* 355, 171–198. doi: 10.1002/cne.903550203
- Jacobs, M. S., McFarland, W. L., and Morgane, P. J. (1979). The anatomy of the brain of the bottlenose dolphin (*Tursiops truncatus*). Rhinic lobe (rhinencephalon): the archicortex. *Brain Res. Bull.* 4, 1–108. doi: 10.1016/0361-9230(79)90299-5
- Jacobs, M. S., Morgane, P. J., and McFarland, W. L. (1971). The anatomy of the brain of the bottlenose dolphin (*Tursiops truncatus*). Rhinic lobe (rhinencephalon). I. The paleocortex. *J. Comp. Neurol.* 141, 205–271. doi: 10.1002/cne.901410205
- Jerison, H. (1973). *Evolution of the brain and intelligence*. New York: Academic Press.
- Kerr, K. M., Agster, K. L., Furtak, S. C., and Burwell, R. D. (2007). Functional neuroanatomy of the parahippocampal region: the lateral and medial entorhinal areas. *Hippocampus* 17, 697–708. doi: 10.1002/hipo.20315
- Kobro-Flatmoen, A., and Witter, M. P. (2019). Neuronal chemo-architecture of the entorhinal cortex: a comparative review. *Eur. J. Neurosci.* 50, 3627–3662. doi: 10.1111/ejn.14511
- Krimer, L. (1997). The entorhinal cortex: an examination of cyto- and myeloarchitectonic organization in humans. *Cereb. Cortex* 7, 722–731. doi: 10.1093/cercor/7.8.722
- La Rosa, C., Cavallo, F., Pecora, A., Chincari, M., Ala, U., Faulkes, C. G., et al. (2020). Phylogenetic variation in cortical layer II immature neuron reservoir of mammals. *eLife* 9:e55456. doi: 10.7554/eLife.55456
- Lende, R. A., and Akdikmen, S. (1968). Motor field in cerebral cortex of the bottlenose dolphin. *J. Neurosurg.* 29, 495–499. doi: 10.3171/jns.1968.29.5.0495
- Maass, A., Berron, D., Libby, L. A., Ranganath, C., and Düzel, E. (2015). Functional subregions of the human entorhinal cortex. *eLife* 4:e06426. doi: 10.7554/eLife.06426
- Marino, L. (2002). Convergence of complex cognitive abilities in cetaceans and Primates. *Brain Behav. Evol.* 59, 21–32. doi: 10.1159/000063731
- Marino, L., Connor, R. C., Fordyce, R. E., Herman, L. M., Hof, P. R., Lefebvre, L., et al. (2007). Cetaceans have complex brains for complex cognition. *PLoS Biol.* 5:e139. doi: 10.1371/journal.pbio.0050139
- Marino, L., McShea, D. W., and Uhen, M. D. (2004). Origin and evolution of large brains in toothed whales. *Anat. Rec.* 281A, 1247–1255. doi: 10.1002/ara.20128
- Miettinen, M., Koivisto, E., Riekkinen, P., and Miettinen, R. (1996). Coexistence of parvalbumin and GABA in nonpyramidal neurons of the rat entorhinal cortex. *Brain Res.* 706, 113–122. doi: 10.1016/0006-8993(95)01203-6
- Miettinen, M., Pitkänen, A., and Miettinen, R. (1997). Distribution of calretinin-immunoreactivity in the rat entorhinal cortex: coexistence with GABA. *J. Comp. Neurol.* 378, 363–378. doi: 10.1002/(SICI)1096-9861(19970217)378:3<363::AID-CNE5>3.0.CO;2-1
- Mikkonen, M., Soininen, H., and Pitkänen, A. (1997). Distribution of parvalbumin-, calretinin-, and calbindin-D28k-immunoreactive neurons and fibers in the human entorhinal cortex. *J. Comp. Neurol.* 388, 64–88. doi: 10.1002/(SICI)1096-9861(19971110)388:1<64::AID-CNE5>3.0.CO;2-M
- Morgane, P. J., and Glezer, I. I. (1990). “Sensory neocortex in dolphin brain” in *Sensory abilities of cetaceans*. eds. J. A. Thomas and R. A. Kastelein (Boston, MA: Springer US), 107–136.
- Morgane, P. J., and Jacobs, M. S. (1972). “Functional anatomy of marine mammals” in *Comparative anatomy of the cetacean nervous system*. eds. P. J. Morgane, I. I. Glezer and M. S. Jacobs (London, UK: Academic Press), 117–244.
- Morgane, P. J., and Jacobs, M. S. (1986). “A morphometric Golgi and cytoarchitectonic study of the hippocampal formation of the bottlenose dolphin, *Tursiops truncatus*,” DijkR. M. van in *The Hippocampus* New York and London: Plenum Press, 369–432.
- Morgane, P. J., Jacobs, M. S., and Galaburda, A. (1985). Conservative features of neocortical evolution in dolphin brain. *Brain Behav. Evol.* 26, 176–184. doi: 10.1159/000118774
- Morgane, P. J., Jacobs, M. S., and Galaburda, A. M. (1986). “Evolutionary morphology of the dolphin brain” in *Dolphin cognition and behavior: A comparative approach*. eds. R. J. Schusterman, J. A. Thomas, F. G. Wood and R. Schusterman (Hillsdale: Lawrence Erlbaum Associates), 5–29.
- Morgane, P. J., Jacobs, M. S., and McFarland, W. L. (1980). The anatomy of the brain of the bottlenose dolphin (*Tursiops truncatus*). Surface configurations of the telencephalon of the bottlenose dolphin with comparative anatomical observations in four other cetacean species. *Brain Res. Bull.* 5, 1–107. doi: 10.1016/0361-9230(80)90272-5
- Morgane, P. J., McFarland, W. L., and Jacobs, M. S. (1982). The limbic lobe of the dolphin brain: a quantitative cytoarchitectonic study. *J. Fur Hirnforsch* 23, 465–552.
- Oelschläger, H. A., and Buhl, E. H. (1985). Development and rudimentation of the peripheral olfactory system in the harbor porpoise *Phocoena phocoena* (Mammalia: Cetacea): olfactory system in the harbor porpoise. *J. Morphol.* 184, 351–360. doi: 10.1002/jmor.1051840309
- Oelschläger, H. A., and Buhl, E. H. (1985). Occurrence of an olfactory-bulb in the early development of the harbor porpoise (*Phocoena phocoena* L.). *Fortschr. Zool.* 30, 695–698.
- Parolisi, R., Peruffo, A., Messina, S., Panin, M., Montelli, S., Giuriso, M., et al. (2015). Forebrain neuroanatomy of the neonatal and juvenile dolphin (*T. Truncatus* and *S. Coerulealba*). *Front. Neuroanat.* 9:140. doi: 10.3389/fnana.2015.00140
- Peruffo, A., Corain, L., Bombardi, C., Centellegh, C., Grisan, E., Graïc, J.-M., et al. (2019). The motor cortex of the sheep: laminar organization, projections and diffusion tensor imaging of the intracranial pyramidal and extrapyramidal tracts. *Brain Struct. Funct.* 224, 1933–1946. doi: 10.1007/s00429-019-01885-x
- Piguet, O., Chareyron, L. J., Banta Lavenex, P., Amaral, D. G., and Lavenex, P. (2018). Stereological analysis of the rhesus monkey entorhinal cortex. *J. Comp. Neurol.* 526, 2115–2132. doi: 10.1002/cne.24496
- Rambaldi, A. M., Cozzi, B., Grandis, A., Canova, M., Mazzoni, M., and Bombardi, C. (2017). Distribution of Calretinin immunoreactivity in the lateral nucleus of the bottlenose dolphin (*Tursiops truncatus*) amygdala: lateral nucleus of dolphin amygdala. *Anat. Rec.* 300, 2008–2016. doi: 10.1002/ar.23634
- Ridgway, S. H. (1990). “The central nervous system of the bottlenose dolphin” in *The bottlenose dolphin*. eds. S. Leatherwood and R. R. Reeves (Cambridge, MA: Academic Press, Inc.), 69–97.
- Sacchini, S., Arbelo, M., Bombardi, C., Fernández, A., Cozzi, B., Bernaldo De Quirós, Y., et al. (2018). Locus coeruleus complex of the family Delphinidae. *Sci. Rep.* 8:5486. doi: 10.1038/s41598-018-23827-z
- Sacchini, S., Herráez, P., Arbelo, M., De Los, E., Monteros, A., Sierra, E., et al. (2022). Methodology and Neuromarkers for cetaceans’ brains. *Vet. Sci.* 9:38. doi: 10.3390/vetsci9020038
- Schmidt, S., Braak, E., and Braak, H. (1993). Parvalbumin-immunoreactive structures of the adult human entorhinal and transentorhinal region. *Hippocampus* 3, 459–470. doi: 10.1002/hipo.450030407
- Seress, L., Léránth, C., and Frotscher, M. (1994). Distribution of calbindin D28k immunoreactive cells and fibers in the monkey hippocampus, subicular complex and entorhinal cortex. A light and electron microscopic study. *J. Hirnforsch.* 35, 473–486.
- Suzuki, W. A., and Porteros, A. (2002). Distribution of calbindin D-28k in the entorhinal, perirhinal, and parahippocampal cortices of the macaque monkey. *J. Comp. Neurol.* 451, 392–412. doi: 10.1002/cne.10370
- Tuñón, T., Insausti, R., Ferrer, I., Sobreviela, T., and Soriano, E. (1992). Parvalbumin and calbindin D-28K in the human entorhinal cortex. An immunohistochemical study. *Brain Res.* 589, 24–32. doi: 10.1016/0006-8993(92)91157-a

- van Groen, T., Miettinen, P., and Kadish, I. (2003). The entorhinal cortex of the mouse: organization of the projection to the hippocampal formation. *Hippocampus* 13, 133–149. doi: 10.1002/hipo.10037
- Witter, M. P. (2007). The perforant path: projections from the entorhinal cortex to the dentate gyrus. *Prog. Brain Res.* 163, 43–61. doi: 10.1016/S0079-6123(07)63003-9
- Witter, M. P. (2012). “Hippocampus” in *The mouse nervous system*. eds. C. Watson, G. Paxinos and L. Puelles (London, UK: Academic Press), 112–139.
- Witter, M. P., and Amaral, D. G. (1991). Entorhinal cortex of the monkey: V. Projections to the dentate gyrus, hippocampus, and subicular complex. *J. Comp. Neurol.* 307, 437–459. doi: 10.1002/cne.903070308
- Witter, M. P., Doan, T. P., Jacobsen, B., Nilssen, E. S., and Ohara, S. (2017). Architecture of the entorhinal cortex a review of entorhinal anatomy in rodents with some comparative notes. *Front. Syst. Neurosci.* 11:46. doi: 10.3389/fnsys.2017.00046
- Wouterlood, F. G., Härtig, W., Brückner, G., and Witter, M. P. (1995). Parvalbumin-immunoreactive neurons in the entorhinal cortex of the rat: localization, morphology, connectivity and ultrastructure. *J. Neurocytol.* 24, 135–153. doi: 10.1007/BF01181556
- Wouterlood, F. G., van Denderen, J. C., van Haften, T., and Witter, M. P. (2000). Calretinin in the entorhinal cortex of the rat: distribution, morphology, ultrastructure of neurons, and co-localization with gamma-aminobutyric acid and parvalbumin. *J. Comp. Neurol.* 425, 177–192. doi: 10.1002/1096-9861(20000918)425:2<177::aid-cne2>3.0.co;2-g

Chapter 2:

**Distribution of vasoactive intestinal peptide (VIP) immunoreactivity in the rat
pallial and subpallial amygdala and colocalization with γ -aminobutyric acid
(GABA)**

RESEARCH ARTICLE

Distribution of vasoactive intestinal peptide (VIP) immunoreactivity in the rat pallial and subpallial amygdala and colocalization with γ -aminobutyric acid (GABA)

G. Salamanca¹ | C. Tagliavia² | A. Grandis¹ | J. M. Graïc³ | B. Cozzi³ | C. Bombardi¹

¹Department of Veterinary Medical Sciences, University of Bologna, Bologna, Italy

²Department of Veterinary Medicine, University of Teramo, Teramo, Italy

³Department of Comparative Biomedicine and Food Science, University of Padova, Legnaro, Italy

Correspondence

C. Bombardi, Department of Veterinary Medical Sciences, University of Bologna, Bologna, Italy.

Email: cristiano.bombardi@unibo.it

Abstract

The amygdaloid complex, also known as the amygdala, is a heterogeneous group of distinct nuclear and cortical pallial and subpallial structures. The amygdala plays an important role in several complex functions including emotional behavior and learning. The expression of calcium-binding proteins and peptides in GABAergic neurons located in the pallial and subpallial amygdala is not uniform and is sometimes restricted to specific groups of cells. Vasoactive intestinal polypeptide (VIP) is present in specific subpopulations of GABAergic cells in the amygdala. VIP immunoreactivity has been observed in somatodendritic and axonal profiles of the rat basolateral and central amygdala. However, a comprehensive analysis of the distribution of VIP immunoreactivity in the various pallial and subpallial structures is currently lacking. The present study used immunohistochemical and morphometric techniques to analyze the distribution and the neuronal localization of VIP immunoreactivity in the rat pallial and subpallial amygdala. In the pallial amygdala, VIP-IR neurons are local inhibitory interneurons that presumably directly and indirectly regulate the activity of excitatory pyramidal neurons. In the subpallial amygdala, VIP immunoreactivity is expressed in several inhibitory cell types, presumably acting as projection or local interneurons. The distribution of VIP immunoreactivity is non-homogeneous throughout the different areas of the amygdaloid complex, suggesting a distinct influence of this neuropeptide on local neuronal circuits and, consequently, on the cognitive, emotional, behavioral and endocrine activities mediated by the amygdala.

KEYWORDS

amygdaloid complex, behavior, GABA, immunohistochemistry, immunoperoxidase

1 | INTRODUCTION

The rat amygdaloid complex (or amygdala) is composed of nuclei and cortical areas defined by specific cytoarchitectural

and immunohistochemical features. Current neurochemical, functional, and developmental data suggest that the amygdala comprises pallial and subpallial structures. The pallial amygdala is composed of cells derived

from the neuroepithelium of the embryonic pallium and ganglionic eminences. Cells of the subpallial amygdala are generated from the telencephalic subpallium (García-López et al., 2007; Martínez-García et al., 2002, 2007; Medina et al., 2004; Puelles et al., 2000; Real et al., 2009; Swanson & Petrovich, 1998; Tole et al., 2005). The pallial amygdala consists of deep and superficial (or cortical) nuclei. The deep pallial nuclei include the basolateral amygdala, the anterior amygdaloid area (dorsal part), and the amygdalohippocampal area (lateral and medial subdivisions). The basolateral amygdala includes the lateral (dorsolateral, medial, and ventrolateral subdivisions), basal (magnocellular, intermediate, and parvicellular subdivisions), and accessory basal (magnocellular and parvicellular subdivisions) nuclei. The superficial pallial nuclei consist of the nucleus of the lateral olfactory tract, the anterior cortical nucleus, the bed nucleus of the accessory olfactory tract, the periamygdaloid cortex (periamygdaloid cortex [PAC], medial [PACm], and sulcal [PACs] subdivisions), and the posterior cortical nucleus. The subpallial amygdala, also known as the extended amygdala (Martínez-García et al., 2008), includes the medial nucleus (rostral, central [dorsal and ventral parts], and caudal subdivisions), the central nucleus (lateral, intermediate, capsular, and medial subdivisions), the bed nucleus of the stria terminalis (medial and lateral subdivisions) (Alheid, 1995; McDonald, 2003), and the intercalated nuclei (García-López et al., 2008; Guirado et al., 2008; Martínez-García et al., 2002, 2007, 2008; Medina et al., 2004; Puelles et al., 2000; Real et al., 2009; Swanson & Petrovich, 1998; Tole et al., 2005). In the present study, the nomenclature of nuclear subdivisions is based on Pitkänen and Kemppainen (2002). The amygdaloid complex is implicated in diverse behavioral functions ranging from the recognition of emotionally significant stimuli to the regulation of declarative memory. In addition, the amygdala is also involved in the regulation of innate processes such as sexual and aggressive behaviors (Aggleton, 2000). Immunohistochemical studies have suggested that the amygdala contains a heterogeneous population of neurons that show cortical-like or striatal-like features. These latter cells can be classified based on their immunoreactivity for calcium-binding protein (calbindin-D28k, parvalbumin, and calretinin) and neuropeptides (somatostatin, neuropeptide Y, and cholecystokinin) (Amaral et al., 1989; Mascagni et al., 2009; McDonald, 1994; McDonald et al., 1995; McDonald & Augustine, 1993; Pitkanen & Amaral, 1994; Pitkänen & Amaral, 1993a, 1993b). In the amygdala there is a subpopulation of inhibitory neurons that contain vasoactive intestinal peptide (VIP). VIP is a 28-amino acid neuropeptide widely distributed in both the central and peripheral nervous systems that exerts its physiological actions through

specific membrane receptors belonging to the superfamily of G protein-coupled receptors (GPCRs) (Fahrenkrug et al., 2000; Harmar et al., 1998; Laburthe et al., 2002). Significant functional and pharmacological evidence indicates that VIP is clearly involved in the regulation of synaptic transmission, acting as a neurotransmitter or neuromodulator (Borghini et al., 1979; Pawelzik et al., 1992; Sun et al., 2003). VIP-IR neurons are widely distributed in the telencephalon, with their highest distribution in the cortex and hippocampal region. Accordingly, VIP signaling pathways are implicated in the regulation of cognitive functions and behavioral activities (Chaudhury et al., 2008; Cottrell et al., 1984; Flood et al., 1990; Itoh et al., 1994) as well as emotional and neuroendocrine activities (Bechtold et al., 2008; Chaudhury et al., 2008; Cozzi, 1999; Gozes, 2008; Loh et al., 2008).

In the neocortex and hippocampal formation, VIP-immunoreactive (IR) neurons control local microcircuits by preferentially targeting other GABAergic interneurons (Freund & Buzsáki, 1996; Lim et al., 2018; Pelkey et al., 2017). Accordingly, these cells can mediate the disinhibition of principal excitatory cells (Rhomberg et al., 2018). In the neocortex, nonpyramidal cells containing calretinin (CR) show a high degree of colocalization with VIP, and CR-IR axon terminals form many symmetric synapses in the rat and human cortex (DeFelipe, 1997). Previous immunohistochemical studies demonstrated the presence of several VIP-immunolabeled neurons in the basolateral and central amygdala. VIP-IR neurons in the rat basolateral amygdala are small bipolar and bitufted GABAergic interneurons that may also contain CCK or CR and innervate both pyramidal and nonpyramidal neurons (Mascagni & McDonald, 2003; McDonald, 1985; Muller et al., 2003). More recently, similar results were obtained in the mouse basolateral amygdala, where VIP-IR neurons were found to be basket cells (Rhomberg et al., 2018). In the central nucleus VIP-IR neurons had a multipolar or bipolar morphology (Cassell & Gray, 1989).

The present study aims at: (i) corroborate these previous results; (ii) identify any morphological types of VIP-IR neurons in the whole amygdaloid complex; and (iii) obtain quantitative data on their intradivisional and laminar distribution. Here, we applied immunohistochemical techniques to analyze morphology, morphometrics, and distribution of neurons in the rat pallial and subpallial amygdala that exhibited VIP immunoreactivity. Consequently, the morphological feature of VIP-IR neurons was correlated to the types of neurons characterized by Golgi stains, as described in the literature. Further, the coexistence of VIP with GABA in the lateral nucleus was studied using also double-labeling immunofluorescence microscopy.

2 | MATERIALS AND METHODS

2.1 | Animals and fixation

Eight male Wistar rats (290–360 g) were used in this study. All animal procedures were conducted in accordance with the guidelines of the European Community Council Directives 219 86/609/EEC. To enhance the concentration of VIP and γ -aminobutyric acid (GABA) in somata, four rats received an injection (15 μ L) of colchicine (1 mg/100 μ L in saline, Sigma Chemical Co., 221 #C-9754, St. Louis, MO) into the left lateral ventricle 48 h before sacrifice. Non-colchicine-injected rats ($n = 4$) were deeply anesthetized with a mixture (4.0 mL/kg) of sodium pentobarbital (48 mg/kg) and chloral hydrate (40 mg/kg; intraperitoneally) and were perfused through the ascending aorta by using a peristaltic pump (flow rate 30–35 mL/min) as follows: 0.9% saline (+4°C) for 2 min, followed by a solution of 4% paraformaldehyde in 0.1 M sodium phosphate buffer, pH 7.4 (flow rate 10 mL/min) for 30 min. Colchicine-injected rats ($n = 4$) were perfused intracardially with 0.9% saline for 2 min, followed by a solution of 4% paraformaldehyde and 0.2% glutaraldehyde in 0.1 M sodium phosphate buffer, pH 7.4 (flow rate 10 mL/min) for 30 min. The brains were removed from the skull and postfixed in the final fixative for 2–4 h. The brains were then cryoprotected in 20% glycerol in 0.02 M potassium phosphate-buffered saline 235 (KPBS) (pH 7.4) at +4°C for 48 h, frozen in dry ice, and stored at –70°C. Brains were cut in the coronal plane at 30- μ m section thickness on a freezing sliding microtome. The sections were stored in a tissue-collecting solution (TCS: 30% ethylene glycol, 25% glycerol in 0.05 sodium phosphate buffer) at –20°C (for immunohistochemical staining) in 10% formalin at room temperature (for thionine staining) until processed.

We underline that colchicine pre-treatment increases the concentration of the VIP and GABA in the neuronal somata. Besides, strong GABA immunoreactivity also requires the addition of glutaraldehyde to the fixative. Consequently, double-immunofluorescence experiments examining the coexistence of VIP with GABA require brains treated with colchicine and fixed with glutaraldehyde. To verify that the glutaraldehyde used to obtain robust GABA immunoreactivity did not significantly affect the VIP immunostaining, the immunoperoxidase experiments were carried out in brains fixed with or without glutaraldehyde. The VIP immunoreactivity did not differ significantly in brains fixed with two different fixatives. As reported in the results, colchicine injections did not increase the numbers of VIP-IR neurons but intensified the cell bodies' immunostaining.

2.2 | Immunoperoxidase staining

This experiment used colchicine and non-colchicine-injected rats (to compare the effect of colchicine and glutaraldehyde on VIP-immunostaining). Sections were stained for VIP using two primary antibodies: a mouse monoclonal antibody (sc-25,347, Santa Cruz Biotechnology, USA) and a rabbit polyclonal antibody (code 20077, Immunostar, USA). The final concentrations of both primary antibodies were established by performing immunoperoxidase using different dilution patterns. The free-floating coronal sections were collected from TCS and washed three times (10 min each time) in 0.02 M KPBS, pH 7.4. To eliminate endogenous peroxidase activity, the sections were treated with 1% H₂O₂ in H₂O for 15–30 min, and then rinsed six times in 0.02 KPBS. To reduce nonspecific binding, the sections were incubated in a solution containing 10% normal horse serum (Colorado Serum Co., Denver, CO, #CS 1324) (for mouse monoclonal antibody) or 10% normal goat serum (Colorado Serum Co., Denver, CO, #CS 2530922) (for rabbit polyclonal antibody) and 0.5% Triton X-100 in 0.02 M KPBS for 2 h at room temperature. Thereafter, the sections were incubated in a solution containing mouse monoclonal antibody anti-VIP (diluted 1:500) or rabbit polyclonal antibody anti-VIP (diluted 1:1000), 0.5% Triton X-100, and 1% normal horse serum (for mouse monoclonal antibody) or 1% normal goat serum (for rabbit polyclonal antibody) for 48 h at 4°C. Following incubation in the primary antiserum, the sections were washed three times for 10 min each in 0.02 M KPBS containing 2% normal horse serum (for mouse monoclonal antibody) or 2% normal goat serum (for rabbit polyclonal antibody). The sections were incubated in a solution containing horse biotinylated anti-mouse (1:200, Vector, Burlingame, CA, BA-2000) (for mouse monoclonal antibody) or goat biotinylated anti-rabbit (1:200, Vector, Burlingame, CA, BA-1000) (for rabbit polyclonal antibody), 1% normal horse (for mouse monoclonal antibody) or 1% normal goat serum (for rabbit polyclonal antibody), and 0.3% Triton X-100 in 0.02 M KPBS, pH 7.4 for 60 min at room temperature. The sections were again washed three times for 10 min each in 0.02 M KPBS containing 2% normal horse serum (for mouse monoclonal antibody) or 2% normal goat serum (for rabbit polyclonal antibody) and transferred to avidin-biotin (ABC) solution for 45 min at room temperature. After the washes in 0.02 M KPBS containing 2% normal horse serum (for mouse monoclonal antibody) or 2% normal goat serum (for rabbit polyclonal antibody), the sections were recycled in the specific secondary antibody solution for 45 min, and then in the ABC solution for 30 min. The sections were washed three times in 0.02 M KPBS, pH 7.4, and immunoperoxidase reaction was developed in a solution containing 3,3'-diaminobenzidine

(DAB; 273 0.05%, Pierce, #34001, Rockford, IL) and H_2O_2 (0.04%) in 0.02 M KPBS. After washing, the sections were mounted onto gelatin-coated slides, dried overnight at 37°C, defatted, and intensified, according to Lewis et al. (1986), with OsO_4 (0.005%, Electron Microscopy Sciences, #19130, Ft. 276 Washington, PA) and thiocarbohydrazide (0.05%, Electron Microscopy Sciences, #21900), and coverslipped with DePeX (BDH Laboratory Supplies Poole, England).

2.3 | Double immunohistochemistry

This experiment used only colchicine-injected rats perfused with 0.2% of glutaraldehyde. The final concentrations of primary antibodies were established by performing double-immunofluorescence using different dilution patterns. Free-floating sections were washed in 0.05 Tris-buffered saline (TBS), pH 7.4 at room temperature (three times, 10 min each). To reduce nonspecific binding, free-floating sections were incubated in 10% normal goat serum (Colorado Serum Co., Denver, CO, #CS 0922) and 0.5% Triton X-100 in 0.05 M TBS for 40 min at room temperature. Thereafter, sections were washed in a solution containing 1% normal goat serum and 0.5% Triton X-100 in 0.05 M TBS. To assess colocalization of the VIP in GABAergic neurons, the sections were incubated for 2 days at 4°C in a mixture of primary antibodies: rabbit polyclonal antibody anti-VIP (diluted 1:500, code 20077, Immunostar, USA) together with mouse monoclonal antibody anti-GABA (diluted 1:500, Sigma #A 0310) which were dissolved in 1% normal goat serum (Colorado Serum Co., Denver, CO, #CS 0922) and 0.5% Triton X-100 in TBS. After washing (1% normal goat serum, 0.5% Triton-X 100 in TBS), the sections were incubated overnight in a secondary antibody solution containing Alexa 488-conjugated goat anti-mouse IgG (1:400, Molecular Probes, #A11029, Leiden, the Netherlands), Alexa 594-conjugated goat anti-rabbit IgG (1:400, Molecular Probes, #A11037, Leiden, the Netherlands), 1% normal goat serum, and 0.5% Triton X-100 in 0.05 M TBS. Sections were then washed with 0.05 M Tris, pH 7.4, and mounted on glass microscope slides (Super Frost Plus, Menzel-Glaser 303 #J1800AMNZ), dried, and coverslipped using Vectashield Mounting Medium (#H-1000, Vector 304 Laboratories, Burlingame, CA).

2.4 | Other staining

To help identify the cytoarchitectural boundaries of different amygdaloid nuclei, one series of sections was stained with thionin as follows. Sections were taken out of the 10% formaldehyde solution, mounted on gelatin-coated slides, and

dried overnight at 37°C. Sections were defatted 1 h in a mixture of chloroform/ethanol 100% (1:1), and then rehydrated through a graded series of ethanol, 2 × 2 min in 100% ethanol, 2 min in 96% ethanol, 2 min in 70% ethanol, 2 min in 50% ethanol, 2 min in dH₂O, and stained 30 s in a 0.125% thionin (Fisher Scientific) solution, dehydrated and coverslipped with DPX (BDH Laboratory Supplies Poole, England).

2.5 | Specificity of antibodies

The mouse monoclonal antibody anti-VIP (sc-25,347, Santa Cruz Biotechnology, USA) is raised against amino acids 1–95 of VIP of human origin. The specificity of this antibody was determined in Western blot analyses and in the positive test control conducted by the manufacturer. The specificity of the rabbit polyclonal antibody anti-VIP (code 20077, Immunostar, USA antibody) was determined previously using preadsorption tests conducted by the manufacturer. We confirmed the specificity of VIP immunostaining by absorption test using 5–10 µg/mL of synthetic peptides (Sigma-Aldrich, V6130). The specificity of mouse monoclonal antibody anti-GABA has been previously characterized (Benson et al., 1992; Storm-Mathisen et al., 1983). For immunoperoxidase experiment, the omission as well as the replacement of the secondary antibodies with inappropriate secondary antibodies resulted in elimination of all immunohistochemical staining. For double immunofluorescence experiment, the controls included omission of one of the two primary antibodies, both primary antibodies, both primary and secondary antibodies, and all combinations of omission of one or both secondary antibodies.

2.6 | Analysis of sections

Sections stained using immunoperoxidase were analyzed using a Leica DMRB microscope. Brightfield images were recorded with a Polaroid DMC digital camera (Polaroid Corporation, Cambridge, MA, USA) and DMC2 software (Polaroid Corporation, Cambridge, MA, USA). To calculate the relative density of VIP-IR cell bodies in the different amygdaloid nuclei and their subdivisions, immunostained neurons were plotted bilaterally in every fifth section throughout the amygdaloid complex with a computer-aided digitizing system (AccuStage 5.1, St. 339 Shoreview, MN). Camera lucida drawings from the adjacent thionin-stained sections were used to define the outline of the nuclei and their subdivisions. Outlines were superimposed on computer generated plots by using Corel Draw X3 (Corel Corporation, Ottawa, Ontario, Canada). Cell counts and the relative density of VIP-IR neurons

(neurons/mm²) were obtained in each section separately. A mean relative density of immunostained neurons was then calculated from all successive sections where the nucleus or subdivision appeared.

AxioVision Rel.4.8 software (Zeiss) was utilized for morphometrical and morphological analysis of the VIP-IR neurons in the following representative pallial amygdalar area: lateral nucleus (dorsolateral, medial and ventrolateral divisions) and posterior cortical nucleus (layers I, II, and III). In particular, for each animal, the perikaryal areas of VIP-IR cell bodies of four non-consecutive sections of each amygdalar area were measured after manual tracing of the cell body outline. Data were expressed as mean \pm standard deviation (SD). In the lateral nucleus (dorsolateral, medial, and ventrolateral divisions) and posterior cortical nucleus (layers I, II, and III), the percentage of different morphological VIP-IR cell types has been reported. In each amygdaloid nucleus/area, the intensity (density) of neuropil staining was evaluated by subjective observations and expressed as very ++++ high, +++ high, ++ moderate, ++, + low, - absent.

Double immunofluorescence sections were analyzed with a Nikon H550L (Nikon Instruments, Tokyo, Japan) equipped with the appropriate filter cubes for immunofluorescence. We used the FITC filter for Alexa 488 (Ex 465–495; DM 505; BA 515–555) and the TRITC filter for Alexa 594 (EX 540/25; DM 565; BA 605–655). For immunofluorescence analysis, the neurons were first located by the presence of a fluorophore, which labeled one antigen, and the filter was then switched to a fluorophore specific for a different wavelength to determine whether or not the neuron was labeled for a second antigen. In this way, the proportions of neurons labeled for pairs of antigens or a single antigen were determined in four rats. Bilateral colocalization studies were assessed at the various rostrocaudal levels of the lateral nucleus. In particular, counts of single- and double-labeled neurons were carried out in five non-consecutive sections obtained from -2.12 to -4.16 bregma levels of each rat brain.

Contrast and brightness were adjusted to reflect the appearance of the labeling seen through the microscope using Adobe Photoshop CS3 Extended 10.0 software (Adobe Systems, San Jose, CA).

3 | RESULTS

3.1 | General characteristics of VIP immunoreactivity

VIP-IR neurons were distributed throughout the rostrocaudal extension of the amygdala (Figure 1a–d). In many amygdaloid nuclei/areas, neuronal labeling was particularly

somatodendritic and the immunoreactivity was cytoplasmic. However, immunolabeled axon-like processes could be seen, especially in the central nucleus. The morphology of VIP-IR neurons is described in detail below. Neuropil labeling density consisted of diffuse staining and neuronal processes (dendrites and axons). The diffuse labeling could not be associated with any specific neuronal elements and the dendrites were devoid of immunopositive spines. Colchicine injections did not increase the number of VIP-IR neurons but did increase cell body immunostaining. Monoclonal and polyclonal antibodies against VIP produced the same immunostaining. The distribution of VIP-IR neurons in different nuclei and regions of the rat amygdala is shown in Figure 2.

3.2 | Pallial amygdala

3.2.1 | Morphology of VIP-IR neurons

On the basis of cell body and dendritic tree characteristics, VIP-IR neurons observed in the pallial amygdala (excluding the anterior amygdaloid area) were classified into four morphological types: multipolar polygonal, multipolar spheroidal, bipolar, and tufted neurons. These cells had a small cell body with a different dendritic pattern.

Multipolar polygonal neurons exhibited a small angular or polygonal (sometimes triangular) cell body and three to five aspiny primary dendrites of variable thickness (Figure 3a).

Multipolar spheroidal neurons had a small roundish or ovoid somata that emitted from three to five thin aspiny primary dendrites of approximately equal thickness (Figure 3b).

Bipolar neurons had a small ovoid or spindle-shaped somata from which emanated two thin aspiny primary dendrites emerged from their opposite poles (Figure 3c).

Tufted neurons had a small-sized ovoid or fusiform cell body with one (single tufted neurons) or, more rarely, two (bitufted neurons) tufts of primary dendrites arising from opposite poles of the somata (Figure 3d).

The relative density and morphometric characteristics of VIP-IR neurons in different amygdaloid nuclei and nuclear subdivisions are summarized in Tables 1 and 2.

3.3 | Deep pallial nuclei

VIP-IR neurons were observed throughout the deep pallial nuclei and were particularly numerous in the amygdalohippocampal area (Table 1). These cells had the characteristic morphological hallmarks of GABAergic

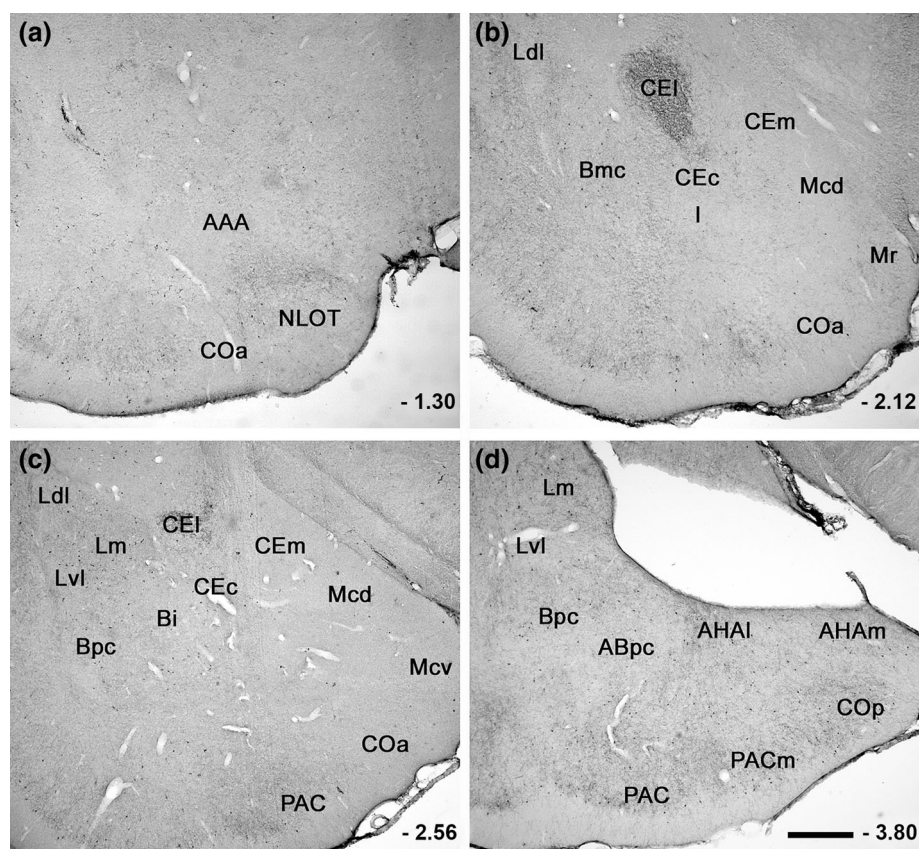


FIGURE 1 Brightfield photomicrographs of four coronal sections showing the distribution of vasoactive intestinal polypeptide (VIP) immunoreactivity in the rat amygdaloid complex. The image in (a) is the most rostral and the image in (d) is the most caudal. The relative density of immunopositive neurons is more evident in the pallial than in the subpallial amygdala. Note, however, a dense plexus of VIP-immunoreactive (IR) axons in the lateral division of the central nucleus. The numbers at the left corner of each panel refer to the rostrocaudal distance from the bregma, according to the atlas of Paxinos and Watson (1998). AAA, anterior amygdaloid area, dorsal part; ABmc, accessory basal nucleus, magnocellular subdivision; ABpc, accessory basal nucleus, parvocellular subdivision; AHAi, amygdalohippocampal area, lateral subdivision; AHAm, amygdalohippocampal area, medial subdivision; Bi, basal nucleus, intermediate subdivision; Bmc, basal nucleus, magnocellular subdivision; Bpc, basal nucleus, parvocellular subdivision; CEC, central nucleus, capsular subdivision; CEi, central nucleus, intermediate subdivision; CEI, central nucleus, lateral subdivision; CEm, central nucleus, medial subdivision; I, intercalated nucleus; COa, cortical anterior nucleus; COp, cortical posterior nucleus; Ldl, lateral nucleus, dorsolateral subdivision; Lm, lateral nucleus, medial subdivision; Lvl, lateral nucleus, ventrolateral subdivision; Mcd, medial nucleus, central subdivision, dorsal part; Mcv, medial nucleus, central subdivision, ventral part; Mr, medial nucleus, rostral subdivision; NLOT, nucleus of the lateral olfactory tract; PAC, periamygdaloid cortex, periamygdaloid cortex subdivision; PACm, periamygdaloid cortex, medial subdivision. Scale bar = 400 μ m in (c) (applies to a–c).

interneurons. The deep nuclei contained a moderate density of VIP-IR fibers. Scattered VIP-IR cells were also found in the anterior cortical nucleus (Table 1).

3.3.1 | Lateral nucleus

The highest number of VIP-IR neurons of the basolateral complex was found in the lateral nucleus (Figures 1b–d and 4a–c; Table 1). The highest relative density of VIP-IR neurons was observed in the ventromedial division, where the majority of immunopositive cells were multipolar angular neurons (Table 1). The lateral nucleus contained

the four morphological cell types (Figure 3a–d). The immunopositive cells belonged especially to multipolar type. Bipolar neurons were in dorsolateral and medial divisions, whereas tufted neurons were observed only in medial division. In the lateral nucleus, 376 VIP-IR neurons were used for morphometric and morphological analysis. The proportions of VIP-IR cell types were: multipolar polygonal 69.1% (260 neurons; mean area $79.5 \pm 17.3 \mu\text{m}^2$; min $51.5 \mu\text{m}^2$; max $130.3 \mu\text{m}^2$), multipolar spheroidal 8.5% (32 neurons; mean area $69.7 \pm 23.8 \mu\text{m}^2$; min $41.2 \mu\text{m}^2$; max $98.7 \mu\text{m}^2$), bipolar 16.5% (62 neurons; mean area $78.7 \pm 23.8 \mu\text{m}^2$; min $47.3 \mu\text{m}^2$; max $106.7 \mu\text{m}^2$), and tufted 5.9% (22 neurons; mean area $83.2 \pm 18.4 \mu\text{m}^2$; min

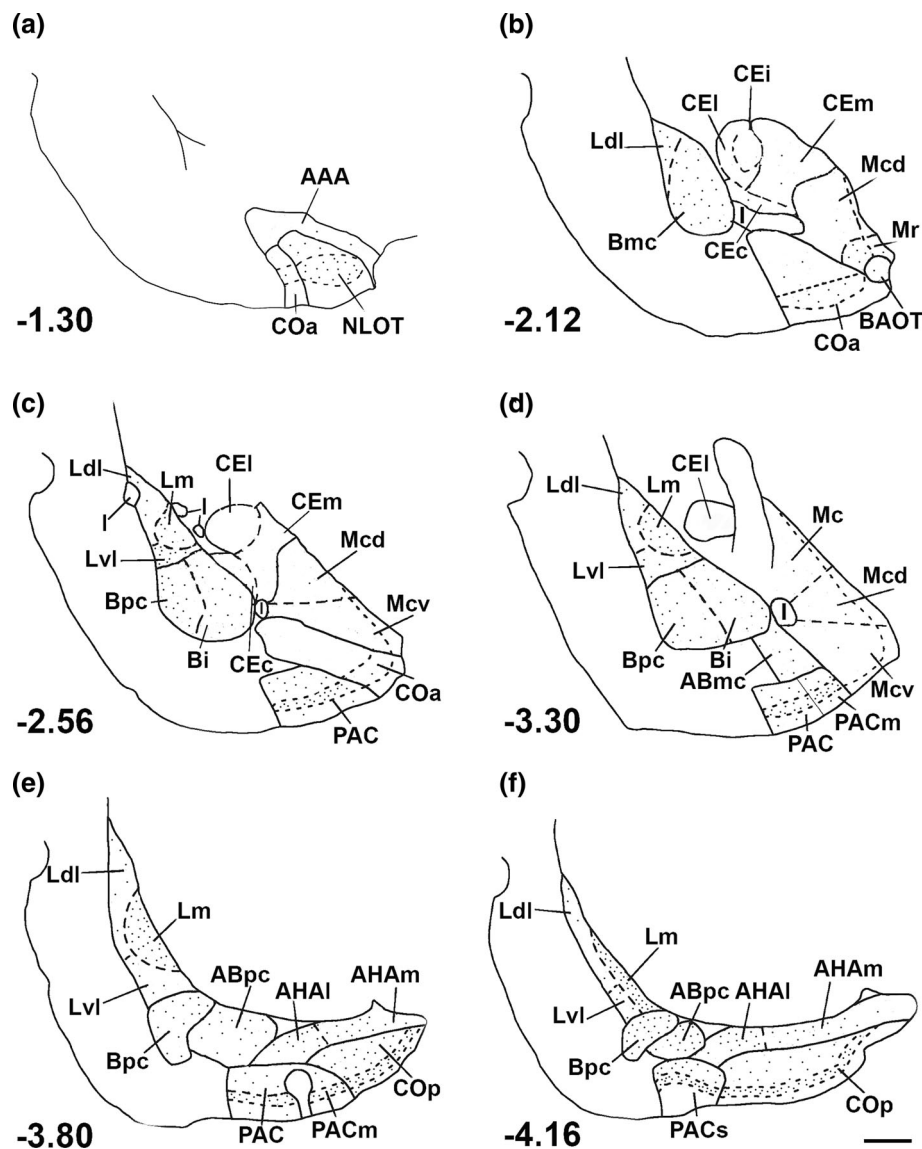


FIGURE 2 (a–f) Computer-generated plots illustrating the distribution of vasoactive intestinal peptide (VIP) immunoreactive neurons in the different nuclei and areas of rat amygdala. Each dot represents one immunostained neuron. Six coronal levels are presented (a is the most rostral and f the most caudal). Numbers at the left lower corner of each panel refer to the rostrocaudal distance from bregma according to the atlas of Paxinos and Watson (1998). AAA, anterior amygdaloid area, dorsal part; ABmc, accessory basal nucleus, magnocellular subdivision; ABpc, accessory basal nucleus, parvocellular subdivision; AHAi, amygdalohippocampal area, lateral subdivision; AHAm, amygdalohippocampal area, medial subdivision; BAOT, bed nucleus of the accessory olfactory tract; Bi, basal nucleus, intermediate subdivision; Bmc, basal nucleus, magnocellular subdivision; Bpc, basal nucleus, parvicellular subdivision; CEC, central nucleus, capsular subdivision; CEi, central nucleus, intermediate subdivision; CEI, central nucleus, lateral subdivision; CEm, central nucleus, medial subdivision; I, intercalated nucleus; COa, cortical anterior nucleus; COp, cortical posterior nucleus; Ldl, lateral nucleus, dorsolateral subdivision; Lm, lateral nucleus, medial subdivision; Lvl, lateral nucleus, ventrolateral subdivision; Mc, medial nucleus, caudal subdivision; Mcd, medial nucleus, central subdivision, dorsal part; Mcv, medial nucleus, central subdivision, ventral part; Mr, medial nucleus, rostral subdivision; NLOT, nucleus of the lateral olfactory tract; PAC, periamygdaloid cortex, periamygdaloid cortex subdivision; PACm, periamygdaloid cortex, medial subdivision; PACs, periamygdaloid complex, sulcal subdivision. Scale bar = 500 μ m in (f) (applies to a–f).

62.1 μ m²; max 96 μ m²). The mean perikaryal area of the VIP-IR neurons in the lateral nucleus was 79.10 \pm 18.4 μ m². Table 2 reports the percentage distribution and morphometric characteristics of the four cell types in the different divisions. The number of VIP-IR neurons

increased caudally. The density of neuropil staining was low in the dorsolateral and ventrolateral divisions. The density of neuropil immunoreactivity increased in the medial division, where immunostained neuronal processes could be observed (Table 1).

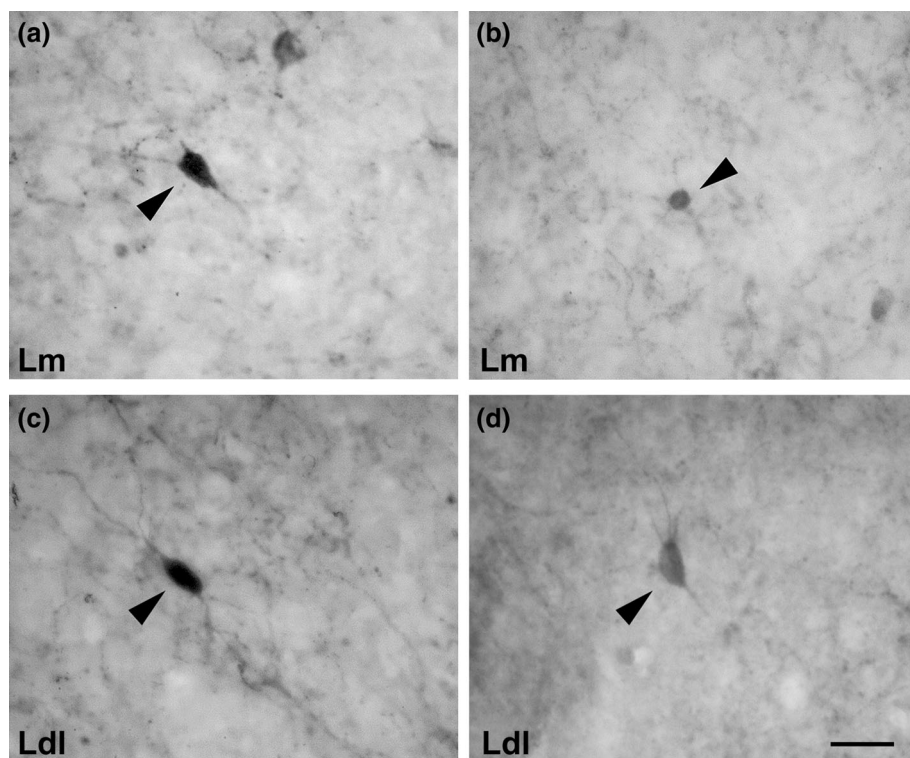


FIGURE 3 Brightfield photomicrographs of different types of vasoactive intestinal polypeptide (VIP)-immunoreactive neurons (arrowhead) in the pallial amygdala (we used the lateral nucleus as an example of the pallial nucleus): (a) multipolar polygonal neuron (medial subdivision, Lm), (b) multipolar spheroidal neuron (medial subdivision, Lm), (c) bipolar neuron (dorsolateral subdivision, Ldl), and (d) tufted (single tufted) neuron (dorsolateral subdivision, Ldl). See text for explanations. Scale bar = 20 μm in (d) (applies to a–d). VIP, vasoactive intestinal polypeptide.

3.3.2 | Basal nucleus

Many VIP-IR neurons were observed in the basal nucleus (Figures 1b–d, 4d–f, and 5a–d; Table 1). VIP-IR neurons were particularly located in the parvicellular division (Table 1). VIP-IR neurons marked in the magnocellular and intermediate division had a multipolar polygonal (Figure 5a–c), multipolar spheroidal, bipolar (Figure 5b), and tufted morphologies. Many (80.1%; 229 neurons) VIP-immunostained neurons in the parvicellular division had a multipolar polygonal morphology (mean area $83 \pm 20.6 \mu\text{m}^2$; min $50.1 \mu\text{m}^2$; max $105 \mu\text{m}^2$) (Figure 5d). However, some (19.9%; 57 neurons) multipolar spheroidal neurons (mean area $58.5 \pm 10.4 \mu\text{m}^2$; min $51.2 \mu\text{m}^2$; max $65.9 \mu\text{m}^2$) were observed in the same division. The density of immunopositive neuropil was high, especially in the parvocellular division, where many IR neuronal processes were observed (Table 1).

3.3.3 | Accessory basal nucleus

VIP-IR neurons observed in the accessory basal nucleus had a multipolar (angular and spheroidal) and bipolar morphology (Figure 6a,b). In the accessory basal nucleus, the number of labeled neurons was higher in the parvicellular division than in the magnocellular division (Figures 1d and 6a,b; Table 1). In the parvicellular division, the majority of cells (81.6%; 196 neurons)

exhibited a multipolar polygonal morphology (mean area $69.7 \pm 15.4 \mu\text{m}^2$; min $47.6 \mu\text{m}^2$; max $98.9 \mu\text{m}^2$). However, multipolar spheroidal (9.2%; 22 neurons; mean area $37.3 \pm 9.1 \mu\text{m}^2$; min $34.1 \mu\text{m}^2$; max $44.4 \mu\text{m}^2$) and bipolar neurons (9.2%; 22 neurons; mean area $68.7 \pm 11.2 \mu\text{m}^2$; min $64.5 \mu\text{m}^2$; max $75.1 \mu\text{m}^2$) were observed. The density of neuropil staining was moderate in both parvicellular and magnocellular divisions (Table 1).

3.3.4 | Amygdalohippocampal area

The amygdalohippocampal area contained many VIP-IR neurons (Figures 1d and 6c). As in the basolateral amygdala, the amygdalohippocampal area contained multipolar polygonal (Figure 6d), multipolar spheroidal, bipolar (Figure 6e), and tufted VIP-IR neurons. The relative density of VIP-IR neurons in the amygdalohippocampal area was very similar to that observed in the basolateral amygdala (Table 1). The density of neuropil labeling, also characterized by numerous immunostained neuronal processes, was high in both divisions (Table 1).

3.3.5 | Anterior amygdaloid area

The anterior amygdaloid area contained VIP-IR neurons with angular or fusiform cell bodies and two to four primary dendrites (Figure 6f). The density of neuropil

TABLE 1 Relative density of VIP-immunoreactive (IR) neurons and neuropil in the different amygdaloid nuclei.

Nucleus or area	Division or layer	VIP neurons (mean/mm ²) ± SD	VIP neuropil
Deep pallial nuclei			
Lateral nucleus		53.5 ± 9.1	+ or + +
	Dorsolateral	36.7 ± 7.2	+
	Medial	55.5 ± 10.5	++
	Ventrolateral	72.3 ± 12.1	+
Basal nucleus		52.3 ± 9.1	+ + or + + +
	Magnocellular	43.7 ± 8.4	++
	Intermediate	48.8 ± 9.6	++
	Parvicellular	57.8 ± 11.1	+++
Accessory basal nucleus		46 ± 8.3	+ +
	Magnocellular	39.7 ± 7.8	++
	Parvicellular	60.1 ± 9.8	++
Amygdalohippocampal area		57.5 ± 10.1	+ + +
	Lateral	49.5 ± 9.3	+++
	Medial	65.5 ± 12.1	+++
Anterior amygdaloid area		6.1 ± 1.2	+ or + +
Superficial pallial nuclei ^a			
NLOT		26.3 ± 4.9	+ or + +
	Layer I: -		+
	Layer II: 82.8%		+ or + +
	Layer III: 17.2%		++
Anterior cortical nucleus		4.8 ± 0.9	+ or + +
	Layer I	Layer I: -	+
	Layer II	Layer II: 83.3%	+ or ++
	Layer III	Layer III: 16.7%	+
BAOT		-	-
Periamygdaloid cortex		42.1 ± 8.3	+ or + + or + + +
		Layer I: 2.9%	+ or ++
		Layer II: 61.5%	+++
		Layer III: 35.6%	+++
	PAC	40.8 ± 8.1	+ or + + or + + +
		Layer I: 4%	+ or ++
		Layer II: 62.7%	+++
		Layer III: 33.3%	+++
	PACm	41.2 ± 8.2	+ or + + or + + +
		Layer I: 3.6%	+ or ++
		Layer II: 63.4%	+++
		Layer III: 33%	+++
	PACs	50 ± 9.1	+ or + + or + + +
		Layer I: -	+ or ++
		Layer II: 58.6%	+++
		Layer III: 41.4%	+++

(Continues)

TABLE 1 (Continued)

Nucleus or area	Division or layer	VIP neurons (mean/mm ²) ± SD	VIP neuropil
Posterior cortical nucleus		54.5 ± 10.5	+ or ++ or +++
	Layer I: 6.8%		+ or ++
	Layer II: 52.3%		+++
	Layer III: 40.9%		+++
Subpallial amygdala			
Medial nucleus		11.3 ± 1.4	+ or ++
	Rostral	28.5 ± 5.4	+ or ++
	Central dorsal	2.7 ± 0.5	+
	Central ventral	3.4 ± 0.6	+
	Caudal	2.9 ± 0.4	+
Central nucleus		17.3 ± 2.9^b	- or + or ++++
	Capsular	27.5 ± 5.3	+
	Lateral	-	++++
	Intermediate	-	- or +
	Medial	7 ± 1.4	+
Intercalated nuclei		-	-

Note: The intensity (density) of neuropil staining is expressed as ++++ very high, +++ high, ++ moderate, + low, - absent. The significance of boldface values refer to the total mean value of each nucleus (mean of the sum of division or layer).

Abbreviations: BAOT, bed nucleus of the accessory olfactory tract; NLOT, nucleus of the lateral olfactory tract; PAC, periamygdaloid cortex, periamygdaloid cortex subdivision; PACm, periamygdaloid cortex, medial subdivision; VIP, vasoactive intestinal polypeptide.

^aIn the superficial pallial amygdala, the table reports the percentage of distribution of VIP-IR neurons in the three layers.

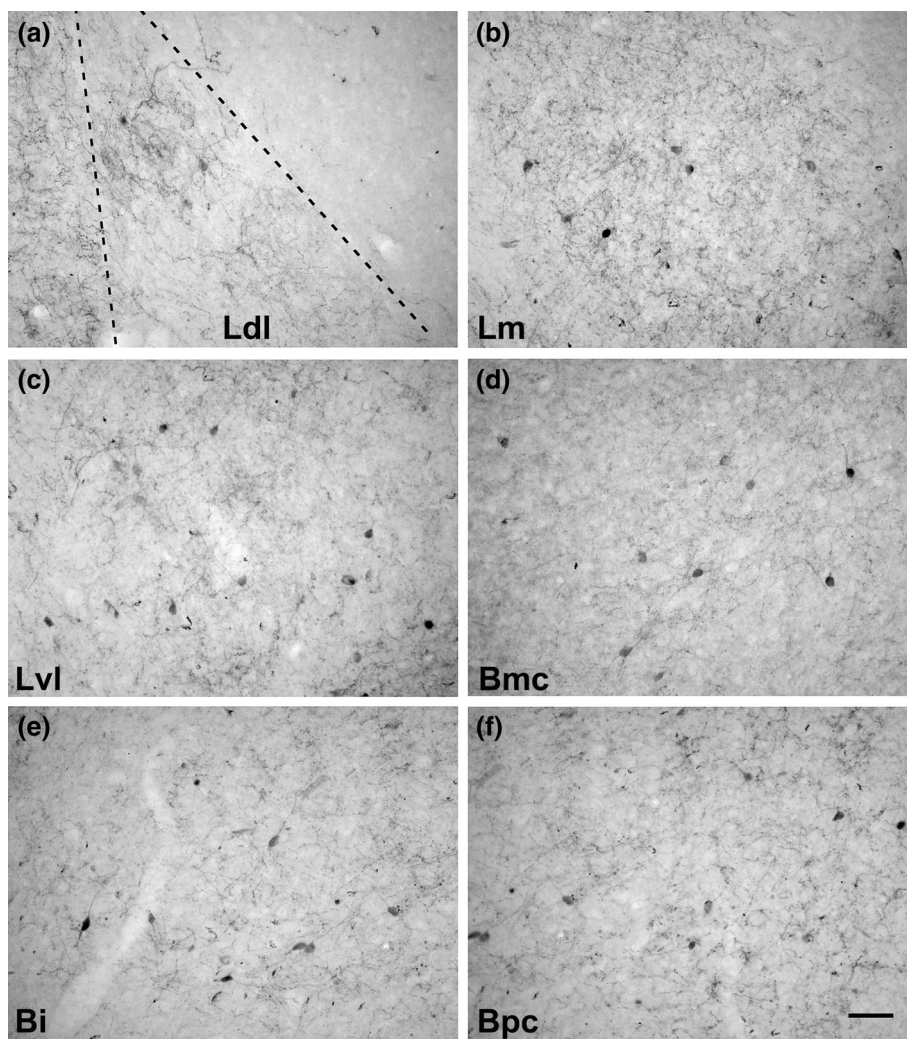
^bIn the central nucleus, the density of the VIP-IR neurons in the lateral division was not determined because of a strong intensity of neuropilar immunostaining.

TABLE 2 Morphometry of VIP-immunoreactive (IR) neurons in the lateral and posterior cortical nuclei.

Nucleus	Division or layer	Cell types and percentage	Mean area (μm ²) ± SD	Min	Max	Total
Lateral						
Nucleus	Dorsolateral	MP: 31 (50%)	97.3 ± 13.9	80.4	114.3	87.2 ± 20.3
		BP: 31 (50%)	77 ± 21.9	47.3	106.7	
	Medial	MP: 170 (69.1%)	79.1 ± 17.5	54.7	130.3	80.2 ± 16.7
		MS: 23 (9.3%)	79.1 ± 17.6	64.8	98.7	
		BP: 31 (12.6%)	79.8 ± 15.7	62.1	92.3	
		TN: 22 (9%)	83.2 ± 18.4	62.1	96	
	Ventrolateral	MP: 59 (86.8%)	74.7 ± 13.7	51.5	90.7	69.9 ± 11.8
		MS: 9 (13.2%)	41.2 ± 8.9	40,3	43.8	
Posterior cortical						
Nucleus	Layer I	MP: 48 (100%)	63.8 ± 10.5	53.4	69.1	63.8 ± 10.5
	Layer II	MP: 184 (50%)	71.2 ± 16.5	43.4	85.4	66.6 ± 14.7
		MS: 110 (29.9%)	64.8 ± 16.7	46.2	78.6	
		TN: 74 (20.1%)	57.8 ± 5.3	53.9	61.8	
	Layer III	MP: 216 (75%)	64.5 ± 11.5	51.2	71.2	63.5 ± 9.6
		BP: 72 (25%)	60.7 ± 10.1	50.1	69.7	

Abbreviations: BP, bipolar neuron; MN, multipolar spheroidal neuron; MP, multipolar polygonal neuron; VIP, vasoactive intestinal polypeptide; TN, tufted neuron.

FIGURE 4 Brightfield photomicrographs of VIP immunohistochemical sections of the lateral (a dorsolateral subdivision, Ldl—bordered by dashed line; b, medial subdivision, Lm; c, ventrolateral subdivision, Lvl) and basal nuclei (d, magnocellular subdivision, Bmc; e, intermediate subdivision, Bi; f, parvocellular subdivision, Bpc). Note the numerous VIP-immunoreactive neurons in the ventrolateral subdivision of the lateral nucleus (c). Scale bar = 40 μ m in (f) (applies to a–f). VIP, vasoactive intestinal polypeptide.



labeling was low (Table 1). In particular, the neuropil staining was lower than in layer III of the NLOT (Figure 1a). Therefore, the boundary between these two areas was easy to identify.

3.4 | Superficial pallial nuclei

In the superficial pallial nuclei, the morphology of the neurons closely resembled that of their counterparts in the deep pallial nuclei. However, bipolar and tufted neurons commonly had both the major somatic axis and the primary dendrites oriented vertically. The superficial nuclei contained moderate numbers of VIP-IR fibers and terminals (Table 1).

3.4.1 | Nucleus of the lateral olfactory tract

In the nucleus of the lateral olfactory tract, VIP-IR neurons were distributed throughout the three layers

(Figures 1a and 7a,b; Table 1). These cells showed a multipolar (polygonal and spheroidal) and bipolar (Figure 7b) morphology. Most VIP-IR neurons were located in layer II and showed a multipolar spheroidal morphology (Table 1). Some multipolar spheroidal neurons were observed in layer III. Neuropil labeling, including neuronal IR processes, was higher in layer III than in layer II (Figures 1a and 7a). The density of neuropil staining was low in layer I (Figure 1a; Table 1).

3.4.2 | Anterior cortical nucleus

Most of the VIP-IR neurons were located in layers II and III (Figures 1a–c and 7c; Table 1). Layer II contained mainly bipolar neurons, whereas layer III exhibited mainly multipolar polygonal (Figure 7d) and spheroidal cells. The density of neuropil labeling was low throughout the nucleus (Table 1). However, some VIP-IR fibers could be seen, especially in layer II.

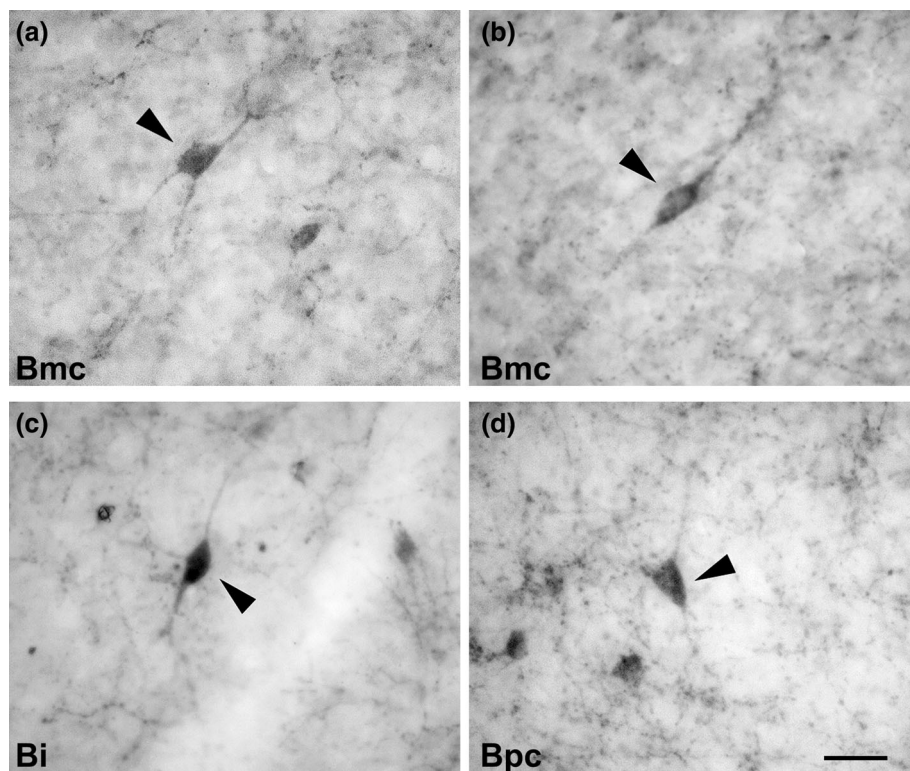


FIGURE 5 High magnification brightfield photomicrographs illustrating the VIP-immunoreactive neurons in the magnocellular (Bmc; a, b), intermediate (Bi; c), and parvocellular subdivision (Bpc; d) of the basal nucleus. In (a, c, and d), an example of multipolar polygonal neurons (arrowheads); in (b), a typical bipolar neuron (arrowhead). Scale bar = 20 μm in (d) (applies to a–d). VIP, vasoactive intestinal polypeptide.

3.4.3 | Bed nucleus of the accessory olfactory tract

VIP-IR neurons with a multipolar angular morphology were occasionally observed. The neuropil density was low to moderate.

3.4.4 | Periamygdaloid complex

Each division of the periamygdaloid complex contained many VIP-IR neurons (Figures 1c,d and 8a; Table 1) with a multipolar polygonal (Figure 8b,c), multipolar spheroidal, bipolar, and tufted morphology. Neuropil labeling was high in layers II and III (Table 1). VIP-IR fibers were more numerous in the periamygdaloid complex than in the anterior cortical nucleus. Layer I showed many dendritic-like structures, but a diffuse neuropil immunostaining was low.

3.4.5 | Posterior cortical nucleus

The posterior cortical nucleus had one of the highest relative densities of VIP-IR neurons observed in the amygdaloid complex (Figures 1d and 8d–f; Table 1). These neurons appeared to be distributed throughout the three layers of the nucleus (Figure 8d; Table 1). The mean perikaryal area of the VIP-IR neurons located in the posterior cortical nucleus was $65.6 \pm 12.7 \mu\text{m}^2$. In the posterior cortical nucleus, 704 VIP-IR neurons were utilized for morphometric and

morphological analysis. The proportions of VIP-IR cell types were: multipolar polygonal 63.7% (448 neurons; mean area $68.1 \pm 13.5 \mu\text{m}^2$; min $43.4 \mu\text{m}^2$; max $85.4 \mu\text{m}^2$) (Figure 8e), multipolar spheroidal 15.6% (110 neurons; mean area $64.7 \pm 16.7 \mu\text{m}^2$; min $46.2 \mu\text{m}^2$; max $78.6 \mu\text{m}^2$), bipolar 10.2% (72 neurons; mean area $57.8 \pm 5.6 \mu\text{m}^2$; min $53.8 \mu\text{m}^2$; max $61.8 \mu\text{m}^2$) (Figure 8f), tufted 10.5% (74 neurons; mean area $60.7 \pm 5.2 \mu\text{m}^2$; min $54.8 \mu\text{m}^2$; max $64.2 \mu\text{m}^2$). Table 2 reports the percentage distribution and morphometric characteristics of the four neuronal types in the different layers. The density of immunopositive neuropil was high, especially in layers II and III, where many IR neuronal processes were observed (Table 1).

3.5 | Subpallial amygdala

The subpallial amygdala neurons typically had an ovoid or fusiform soma and two to five nonspiny primary dendrites. In the subpallial amygdala, VIP-IR neurons were observed primarily in the central and medial nuclei. The relative density of VIP-IR neurons in the subpallial amygdala is reported in Table 1.

3.5.1 | Medial nucleus

The highest relative density of IR cells was observed in the rostral division (Figures 1b,c and 9a; Table 1). Most of the immunopositive neurons had an ovoid somata and

FIGURE 6 Brightfield photomicrographs of VIP immunohistochemical sections of the accessory basal nucleus (a, magnocellular subdivision, ABmc; b, parvocellular subdivision, ABpc), amygdalohippocampal area (c–e, medial subdivision, AHAm), and anterior amygdaloid area (f, AHAm). Note the numerous VIP-immunoreactive neurons in the parvocellular subdivision of the accessory basal nucleus (b) and in the medial subdivision of the amygdalohippocampal area (c). In (d and e), note an example of multipolar polygonal (d) and bipolar neurons (e) (arrowheads) of the medial subdivision of the amygdalohippocampal area. The photomicrograph in (f) illustrates a fusiform neuron (arrowhead) in the anterior amygdaloid area. Scale bar = 40 μ m in (c) (applies to a–c) and 20 μ m in (f) (applies to d–f). VIP, vasoactive intestinal polypeptide.

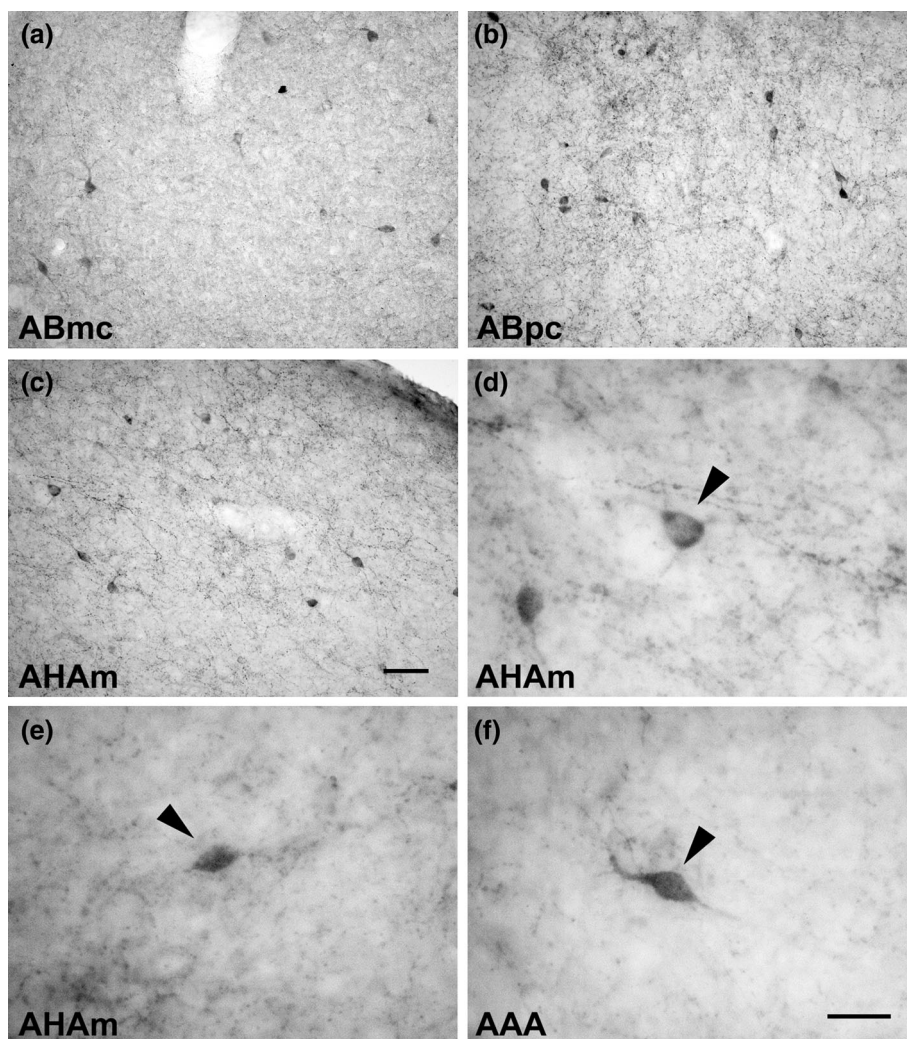
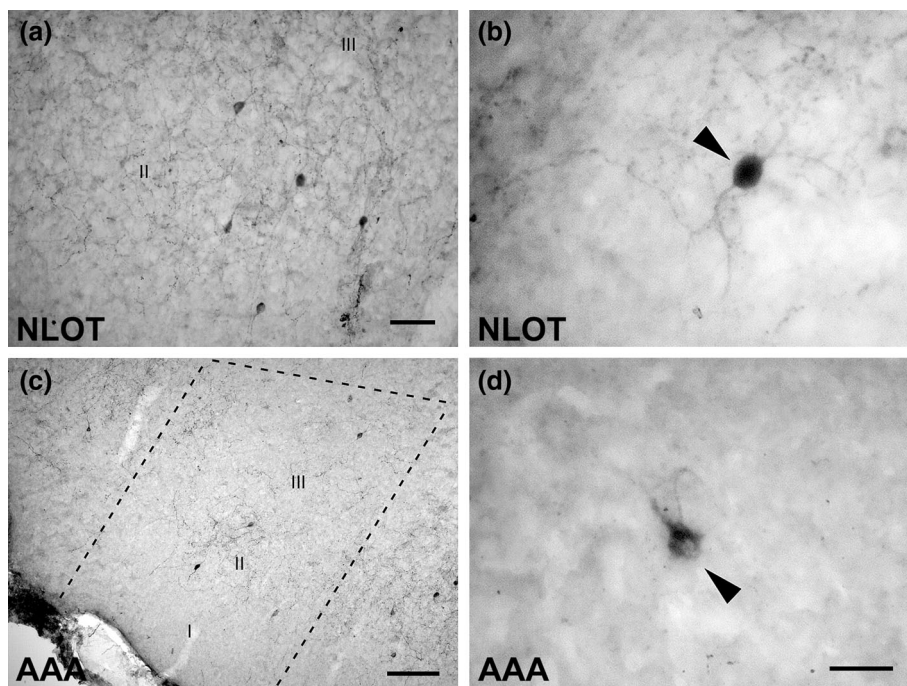


FIGURE 7 Brightfield photomicrographs of VIP immunohistochemical sections of the nucleus of the lateral olfactory tract (a and b, NLOT) and the anterior cortical nucleus (c and d, AAA, bordered by dashed line in c). Note the low level of VIP immunoreactivity in the anterior cortical nucleus (c). As in the deep pallial amygdala, the superficial pallial amygdala also contains VIP-immunoreactive with a bipolar (b, layer II of the NLOT) and multipolar polygonal (d, layer II of the anterior cortical nucleus) morphology (arrowheads). Scale bar = 40 μ m in (a), 100 μ m in (c), and 20 μ m in (d) (applies in b and d). VIP, vasoactive intestinal polypeptide.



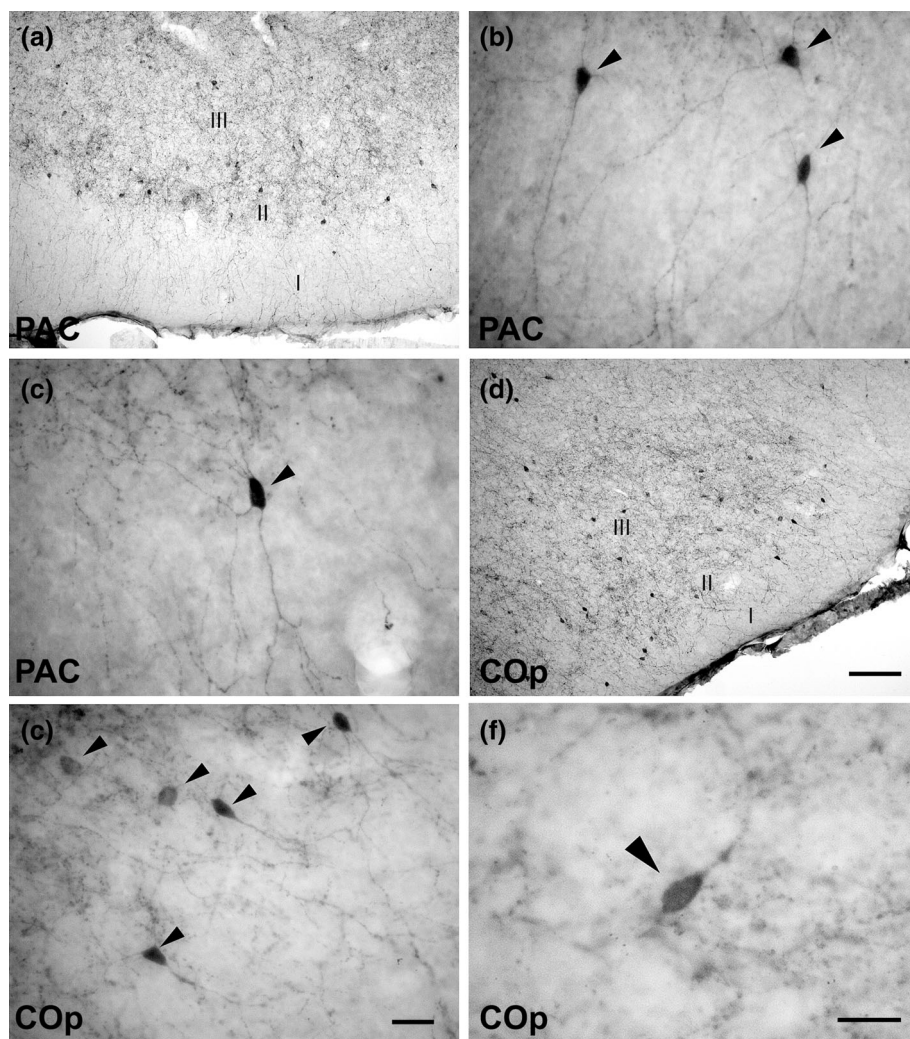


FIGURE 8 Brightfield photomicrographs of VIP immunohistochemical sections of the periamygdaloid cortex (a–c, PAC) and posterior cortical nucleus (d–f, COp). Note the high density of immunoreactive neurons. In these areas, neurons with multipolar polygonal (b, layer I of the PAC subdivision of the PAC; c, layer II of the PAC subdivision of the PAC; e, layer II of the posterior cortical nucleus) and bipolar (e, f, layer II of the posterior cortical nucleus) morphologies can be observed (arrowheads). Scale bar = 100 μ m in (d) (applies to a and d), 20 μ m in (e) (applies in b, c, e), and 20 μ m in (f). VIP, vasoactive intestinal polypeptide.

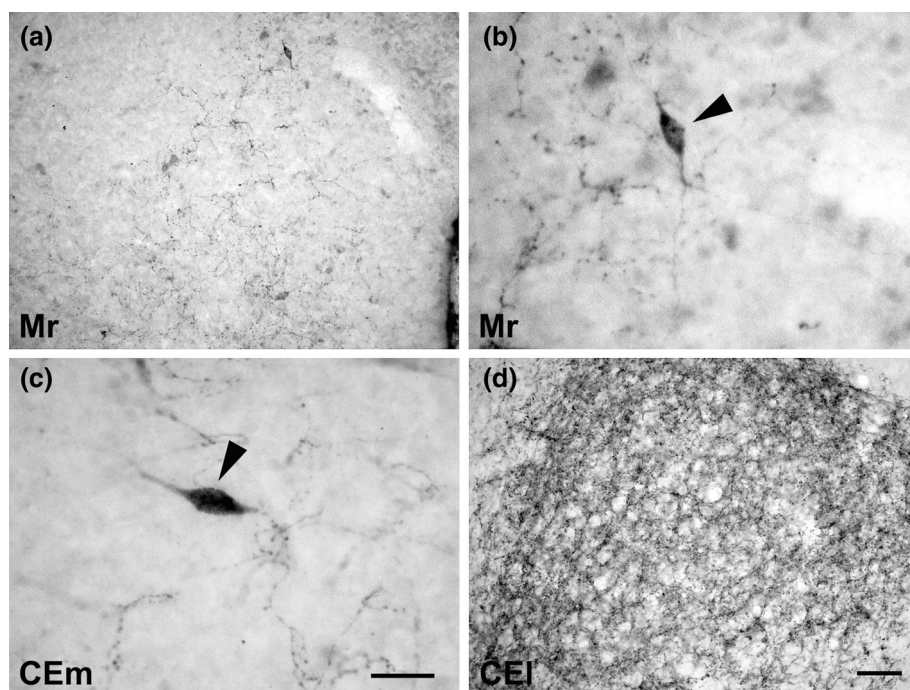


FIGURE 9 Brightfield photomicrographs of VIP immunohistochemical sections of the subpallial amygdala (a–d). In particular, VIP-immunoreactive neurons can be observed in the rostral division of the medial nucleus (a, Mr). In (b), note a neuron with an ovoid soma (arrowhead) located in the rostral subdivision of the medial nucleus (Mr). Note a bipolar neuron (arrowhead) in the medial subdivision of the central nucleus (c, CEm). Interestingly, the lateral subdivision of the central nucleus contains a dense terminal plexus immunoreactive for the VIP (d, CEI). Scale bar = 40 μ m in (d) (applies to a and d) and 20 μ m in (c) (applies to b and c). VIP, vasoactive intestinal polypeptide.

two or three primary dendrites (Figure 9b). The remaining division of the medial nucleus contained a small number of VIP-IR cells (Table 1). The density of neuropil immunostaining was low throughout the nucleus (Table 1). The medial nucleus had only few VIP-IR terminals, especially localized in the rostral division.

3.5.2 | Central nucleus

Small VIP-IR neurons were observed in all subdivisions of the central nucleus (Figure 1b,c). These cells have an ovoid cell body with two to four thick dendrites. In some cases, a characteristic bipolar arrangement of primary dendrites was observed. The central nucleus contained bipolar neurons with fusiform somata and two thick primary dendrites (Figure 9c). Interestingly, a dense terminal plexus IR for the VIP was observed in the lateral division of the central nucleus (Figures 1b,c and 9d; Table 1). Due to the dark staining of the neuropil, it was sometimes difficult to visualize immunostained neurons in the lateral division. The remaining division showed a low neuropil immunostaining and may contain some VIP-IR terminals.

3.5.3 | Intercalated nuclei

VIP-IR neurons were not observed in the intercalated nuclei (Figure 1b).

3.6 | Double immunofluorescence experiments: Colocalization of the VIP with GABA in the lateral nucleus

Double immunofluorescence studies demonstrated that in the lateral nucleus, VIP-IR neurons represent 14.5% of the GABAergic cells (Figure 10a'–c'''; Table 3). All VIP-IR neurons were GABA-positive (Figure 10a'–c'''; Table 3).

4 | DISCUSSION

In the present study, we provide a comprehensive analysis of the distribution and significance of VIP immunoreactivity throughout the rat amygdala. VIP immunoreactivity is associated with somata, primary dendrites and, particularly in the lateral subdivision of the central nucleus, axon terminals. Our study indicates that the distribution of immunoreactivity for VIP differs among areas and cell types, suggesting a distinct influence of this neuropeptide on neuronal amygdaloid circuits.

4.1 | Pallial amygdala

Our investigation confirms the presence of VIP-IR interneurons in the rat pallial amygdala and provides details on their morphological characteristics and quantitative distribution.

FIGURE 10 Colocalization of the vasoactive intestinal peptide with γ -aminobutyric acid (GABA) in the lateral nucleus; dorsolateral division (a'–a''', Ldl), medial division (b'–b''', Lm), and ventrolateral division (c'–c''', Lvl). Double immunofluorescence images showing VIP in red (left column a', b', c'), GABA in green (a'', b'', c''), and colocalization of VIP with GABA in yellow (a''', b''', c'''). Arrowheads indicate double-labeled neurons). In the lateral nucleus, VIP-immunoreactive (IR) neurons represent only 14.5% of GABAergic neurons, whereas all VIP-IR neurons are IR for the GABA. Scale bar = 20 μ m in (c''') (applies to a'–c'''). VIP, vasoactive intestinal polypeptide.

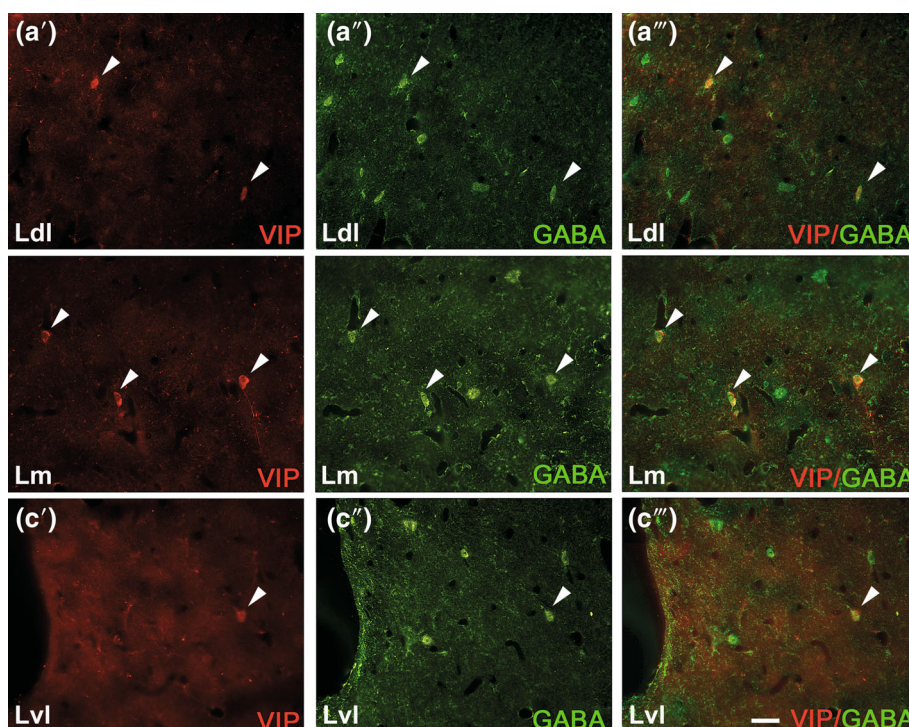


TABLE 3 Colocalization of GABA with VIP in the lateral nucleus of the amygdala.

Nucleus	Subdivisions	GABA-IR single-labeled neurons	VIP-IR single-labeled neurons	GABA/VIP double-labeled neurons	% of GABA-IR double-labeled neurons	% of VIP-IR double-labeled neurons
Lateral Nucleus		1162	0	197	14.5% (197/1359)	100% (197/197)
	Dorsolateral	301	0	59	16.4% (59/360)	100% (59/59)
	Medial	721	0	119	14.2% (119/840)	100% (119/119)
	Ventrolateral	140	0	19	11.9% (19/159)	100% (19/19)

Abbreviations: IR, immunoreactive; VIP, vasoactive intestinal polypeptide.

4.2 | Deep pallial amygdala

Golgi and immunohistochemical studies have demonstrated that the deep pallial amygdala contains two types of neurons, excitatory glutamatergic pyramidal cells and inhibitory nonpyramidal cells that synthesize the neurotransmitter GABA (McDonald, 2020). The principal cell type in the deep pallial amygdala is the pyramidal neuron, also called projective, long-axon neuron (Tombol & Szafranska-Kosmal, 1972), P-cell (Hall, 1972), or Class I neuron (McDonald, 1982a, 1982b). Their size varies depending on the nucleus or the division of the nucleus. In addition to pyramidal cells, there is a heterogeneous population of sparsely spiny or non-spiny nonpyramidal neurons, most of which are local circuit GABAergic neurons (McDonald, 2020). Hall (1972) called these cells the “S” cells because of their resemblance to cortical stellate cells, Tombol and Szafranska-Kosmal (1972) called them Golgi II cells, and McDonald (1982a) called them Class II cells. McDonald (1982b) further classified these cells into three categories based on the shape of their soma and dendritic tree (multipolar, bipolar, and bitufted), and they ranged in size from small to large. Another type of local circuit neuron is the neurogliaform cell (Tombol & Szafranska-Kosmal, 1972) or class III neurons of McDonald (1982b). This latter neural element is a local circuit neuron with a small dendritic field and a highly branched axon that remains within the field (McDonald & Culberson, 1981). GABAergic interneurons are commonly classified by the expression of two types of molecular markers: calcium-binding proteins and neuropeptides, including VIP. Several immunohistochemical studies have demonstrated the colocalization of VIP and calretinin (CR) or cholecystokinin (CCK) in some interneurons of the basolateral amygdala (Mascagni & McDonald, 2003). Accordingly, several CR-containing neurons in the same area are morphologically very similar to VIP-IR interneurons (McDonald, 1994). The morphological and morphometric data obtained in the present study indicate that the VIP-IR neurons observed in the pallial amygdala appear to be a subpopulation of nonpyramidal GABAergic interneurons. Specifically, these neurons

can be classified into four morphological types based on cell body and dendritic tree characteristics: multipolar polygonal, multipolar spheroidal, bipolar, and tufted neurons. Whether morphologically different VIP-IR neurons have different connections, however, remains to be determined.

The present study has also attempted to correlate the morphological features of VIP-IR neurons in the deep nuclei with the cell types characterized by Golgi staining. Accordingly, the perikaryal area and the dendritic branching pattern of VIP-IR neurons in the pallial amygdala suggest that these cells correspond to the multipolar, bipolar, and bitufted small class II neurons seen in Golgi preparations (McDonald, 1982a, 1982b).

Colocalization of VIP with GABA was examined at different levels of the lateral nucleus. Our double immunofluorescence studies have demonstrated that in the lateral nucleus, VIP-IR neurons represent 14.5% of GABA-IR cells. The data we obtained are in agreement with a previous study showed, using a different methodology, that 17.4% of GABAergic neurons contain VIP (McDonald & Pearson, 1989). The colocalization of GABA with the VIP does not vary significantly in the different subdivisions of the lateral nucleus. However, the ventrolateral subdivision showed the lowest percentage of double-labeled cells.

The anterior amygdaloid area is composed mainly of small- to medium-sized ovoid fusiform, or multiangular densely spiny projection neurons. Among them are scattered non-spiny angular or fusiform interneurons with axons that arborize extensively in the vicinity of the cell body (McDonald, 1992). Our results suggest that some of these later cells may contain VIP as a neuropeptide.

Morphological, immunohistochemical, and ultrastructural data suggest that VIP-IR neurons of the basolateral amygdala can not only influence the activity of other GABAergic interneurons but also interact with excitatory pyramidal cells. Previous studies have demonstrated that VIP-IR interneurons in the basolateral amygdala can control local microcircuits by preferentially targeting other GABAergic interneurons, thereby effectively disinhibiting pyramidal neurons (Muller et al., 2003; Rhomberg

et al., 2018; Spanpanato et al., 2011). The synaptic connectivity of VIP-IR interneurons in the rodent basolateral amygdala has been investigated at the ultrastructural level. In particular, VIP-IR interneurons in the rat basolateral amygdala innervate the somata and dendrites of other GABAergic interneurons, especially those IR for CB-D28k (Muller et al., 2003). As in the hippocampus and neocortex (Freund & Buzsáki, 1996), one of the most important functions of VIP-IR interneurons is disinhibition. Since CB-D28K-IR inhibitory interneurons can innervate the perisomatic domain of pyramidal cells, the role of VIP-IR interneurons may be to increase the overall firing rate of pyramidal cells (Collins et al., 2001; Pape et al., 1998; Paré & Gaudreau, 1996). This action, at least in the basolateral complex, could contribute to the generation of the oscillatory pattern of excitatory neurons during periods of synchronous activity (Martina et al., 2001), and facilitate associative plasticity during fear conditioning (Rhombert et al., 2018). The presence of VIP in the deep pallial amygdala supports the role of this neuropeptide in the regulation of cognitive and emotional functions mediated by the amygdala. The present study indicates that in the deep pallial amygdala, VIP-IR interneurons are inhibitory cells that can be divided into four major morphological types. However, the specific functional properties of these morphological cell types remain to be determined.

4.3 | Superficial pallial amygdala

The superficial pallial amygdala is composed of cortical areas that have three distinct layers. Their neurons share morphological similarities with those in the deep pallial amygdala. Layer I is fibrous and virtually devoid of neurons. Spiny pyramidal neurons represent the main cell type found in layers II and III (P-cells of Hall, 1972). However, the majority of the cell population in layer III of the nucleus of the lateral olfactory tract is composed of large, moderately spiny nonpyramidal neurons whose axons give rise to multiple local collaterals. Sparsely spiny or non-spiny neurons, that likely act as local circuit neurons, are distributed among projection neurons. The proportion of inhibitory neurons in the superficial amygdala is similar to the 20% found in the deep pallial amygdala (McDonald, 1983; McDonald & Augustine, 1993). Vaz et al. (2016) reported that in the nucleus of the lateral olfactory tract of the rat, VIP-IR neurons would represent 15% of the inhibitory interneurons. These data are consistent with our unpublished observations. The bed nucleus of the accessory olfactory tract consists mainly of pyramidal neurons (McDonald, 1992). Accordingly, we did not observe any VIP-IR cells in this nucleus. In the superficial pallial amygdala, the VIP-IR neurons were heterogeneous in shape and small in resembling

a subclass of nonpyramidal neurons described using Golgi staining (Alheid, 1995; McDonald, 1983, 1992; Millhouse & Uemura-Sumi, 1985). In addition, double-immunofluorescence experiments showed colocalization of VIP with GABA in these superficial pallial nuclei (personal observation). The exact activity of the neuronal microcircuits of the superficial pallial amygdala is virtually unknown. These superficial pallial nuclei of the amygdala have a cortex-like functional organization. In this sense, we can consider that here inhibitory VIP-IR neurons can modulate the microcircuits through a direct action on both pyramidal and nonpyramidal neurons, as in the neocortex (Lim et al., 2018), hippocampal region (Freund & Buzsáki, 1996; Pelkey et al., 2017), and piriform cortex (Suzuki & Bekkers, 2007). Based on the characteristics of their cell bodies and primary dendrites, VIP-IR neurons of the posterior cortical nucleus can be divided into four major morphological types. Our results indicate that VIP-IR neurons are local circuit neurons, suggesting that VIP may regulate the intranuclear inhibitory circuits in the posterior cortical nucleus. However, the specific target of the different morphological inhibitory interneurons remains to be determined. VIP signaling pathways located in the superficial pallial amygdala may be involved in the regulation of chemosensory behaviors (olfactory and pheromonal activity).

4.4 | Subpallial amygdala

Neurons in the medial nucleus have small- to medium-sized ovoid shaped somata which possess moderately to densely spiny dendrites (McDonald, 1992; Sah et al., 2003). The lateral division of the central nucleus is composed of a homogeneous population of medium-sized ovoid spiny neurons (McDonald, 1982a; Sah et al., 2003). The dendrites of these neurons, that are located in the center of the division, radiate in all directions. The direction of the dendrites of peripheral neurons appears to follow the orientation of the boundaries (McDonald, 1982a; Sah et al., 2003). The subpallial amygdala also contains rare spine-sparse neurons (McDonald, 1982a; Sah et al., 2003). The vast majority of the neurons in the capsular division of the central nucleus are medium-sized spiny cells similar to those in the lateral division, except that their dendrites emerge from opposite poles of the soma (McDonald, 1982a; Sah et al., 2003). The medial division of the central nucleus consists of ovoid, fusiform, and piriform, moderately or sparsely spiny neurons (McDonald, 1982a; Sah et al., 2003). The main neurons in the intercalated nuclei are spinous medium-sized neurons with round to bipolar dendritic trees (Millhouse, 1986; Sah et al., 2003). Among these cells are medium-sized nonspiny neurons that may be involved in local circuits. Rare spiny

or nonspiny (more common) large neurons have also been found (Millhouse, 1986; Sah et al., 2003).

VIP-IR neurons observed in the subpallial amygdala had an ovoid somata with thick primary dendrites. These neurons are mainly located in the rostral division of the medial nucleus (where they show an ovoid morphology) and in the central nucleus (lateral, medial, and capsular divisions). In particular, neurons with a spindle-shaped cell body and a bipolar arrangement of primary dendrites were observed in the central nucleus. A dense plexus of VIP-IR axons is located in the lateral subdivision of the central nucleus. In contrast to the pallial amygdala, the main cell type of the subpallial amygdala is GABAergic (McDonald, 2003; Swanson & Petrovich, 1998). The present study indicates that the few neurons in the subpallial amygdala are IR for the VIP. In addition, double-immunofluorescence experiments revealed colocalization of the VIP with GABA in these subpallial nuclei (personal observation). The morphological features of VIP-IR neurons correspond to those observed in a subclass of Golgi-staining neurons, as shown by previous immunohistochemical studies (Cassell & Gray, 1989). The results of the present study suggest that VIP may modulate the intrinsic and extrinsic GABAergic projection of the subpallial amygdala. Accordingly, VIP signaling pathways have been implicated in the regulation of neuroendocrine and autonomic activities mediated by the amygdala (Bechtold et al., 2008; Chaudhury et al., 2008; Gozes, 2008; Loh et al., 2008).

5 | CONCLUSIONS

All VIP-IR neurons in the pallial and subpallial amygdala are GABAergic cells. However, in the pallial amygdala, these neurons act exclusively as nonpyramidal local interneurons capable of directly and especially indirectly regulating the activity of pyramidal projection neurons. On the other hand, based on the distribution, morphology, and projections of GABAergic neurons, we can hypothesize that VIP-IR neurons of the subpallial amygdala could act as both projection neurons as well as local interneurons (McDonald, 1992; Millhouse, 1986; Sah et al., 2003). Whether morphologically different VIP-IR neurons have different connections, however, remains to be determined. The VIP immunoreactivity is more prominent in the pallial than in the subpallial amygdala.

In conclusion, the present study has provided evidence for the heterogeneous morphologies of VIP-IR neurons in the pallial and subpallial amygdala. Comparison of our data with previous data regarding the morpho-functional activity of the amygdala to our data suggests

that this heterogeneity may reflect a complex role of the VIPergic system in the different subdivisions of the amygdala, including their extrinsic as well as intrinsic connections. Our study indicates that the distribution of VIP immunoreactivity in the amygdala suggests a distinct influence of this neuropeptide on local circuits and out-bound projections.

AUTHOR CONTRIBUTIONS

Cristiano Bombardi: Conceptualization; writing – original draft; methodology; formal analysis; supervision. **G. Salamanca:** Writing – original draft; methodology; formal analysis. **C. Tagliavia:** Formal analysis; writing – original draft. **Annamaria Grandis:** Writing – original draft; methodology. **Jean-Marie Graïc:** Writing – original draft; methodology. **Bruno Cozzi:** Writing – original draft; methodology.

ACKNOWLEDGMENTS

This research was supported by no specific grant from any funding agency in the public, commercial, or not-for-profit sector.

CONFLICT OF INTEREST STATEMENT

The authors declare no conflicts of interest.

ORCID

G. Salamanca  <https://orcid.org/0000-0003-4322-0030>
C. Tagliavia  <https://orcid.org/0000-0002-8628-693X>
A. Grandis  <https://orcid.org/0000-0003-0292-5261>
J. M. Graïc  <https://orcid.org/0000-0002-1974-8356>
B. Cozzi  <https://orcid.org/0000-0002-7531-7040>
C. Bombardi  <https://orcid.org/0000-0002-5685-1977>

REFERENCES

- Aggleton, J. P. (2000). *The amygdala: A functional analysis*. Oxford University Press.
- Alheid, G. F. (1995). Amygdala and extended amygdala. In *The rat nervous system* (pp. 495–578). Academic Press.
- Amaral, D. G., Avendaño, C., & Benoit, R. (1989). Distribution of somatostatin-like immunoreactivity in the monkey amygdala. *Journal of Comparative Neurology*, 284(2), 294–313. <https://doi.org/10.1002/cne.902840211>
- Bechtold, D. A., Brown, T. M., Luckman, S. M., & Piggins, H. D. (2008). Metabolic rhythm abnormalities in mice lacking VIP-VPAC2 signaling. *The American Journal of Physiology-Regulatory, Integrative and Comparative Physiology*, 294(2), R344–R351. <https://doi.org/10.1152/ajpregu.00667.2007>
- Benson, D. L., Isackson, P. J., Gall, C. M., & Jones, E. G. (1992). Contrasting patterns in the localization of glutamic acid decarboxylase and Ca²⁺/calmodulin protein kinase gene expression in the rat central nervous system. *Neuroscience*, 46(4), 825–849. [https://doi.org/10.1016/0306-4522\(92\)90188-8](https://doi.org/10.1016/0306-4522(92)90188-8)
- Borghini, C., Nicosia, S., Giachetti, A., & Said, S. I. (1979). Vasoactive intestinal polypeptide (VIP) stimulates adenylate cyclase in

- selected areas of rat brain. *Life Sciences*, 24(1), 65–70. [https://doi.org/10.1016/0024-3205\(79\)90281-9](https://doi.org/10.1016/0024-3205(79)90281-9)
- Cassell, M. D., & Gray, T. S. (1989). Morphology of peptide-immunoreactive neurons in the rat central nucleus of the amygdala. *Journal of Comparative Neurology*, 281(2), 320–333. <https://doi.org/10.1002/cne.902810212>
- Chaudhury, D., Loh, D. H., Dragich, J. M., Hagopian, A., & Colwell, C. S. (2008). Select cognitive deficits in Vasoactive Intestinal Peptide deficient mice. *BMC Neuroscience*, 9(1), 63. <https://doi.org/10.1186/1471-2202-9-63>
- Collins, D. R., Pelletier, J. G., & Paré, D. (2001). Slow and fast (gamma) neuronal oscillations in the perirhinal cortex and lateral amygdala. *Journal of Neurophysiology*, 85(4), 1661–1672. <https://doi.org/10.1152/jn.2001.85.4.1661>
- Cottrell, G. A., Veldhuis, H. D., Rostene, W. H., & de Kloet, E. R. (1984). Behavioural actions of vasoactive intestinal peptide (VIP). *Neuropeptides*, 4(4), 331–341. [https://doi.org/10.1016/0143-4179\(84\)90008-8](https://doi.org/10.1016/0143-4179(84)90008-8)
- Cozzi, B. (1999). Vipergic innervation of the mammalian pineal gland. *Microscopy Research and Technique*, 46(4–5), 257–264. [https://doi.org/10.1002/\(SICI\)1097-0029\(19990815/01\)46:4<257::AID-JEMT3>3.0.CO;2-W](https://doi.org/10.1002/(SICI)1097-0029(19990815/01)46:4<257::AID-JEMT3>3.0.CO;2-W)
- DeFelipe, J. (1997). Types of neurons, synaptic connections and chemical characteristics of cells immunoreactive for calbindin-D28K, parvalbumin and calretinin in the neocortex. *Journal of Chemical Neuroanatomy*, 14(1), 1–19. [https://doi.org/10.1016/S0891-0618\(97\)10013-8](https://doi.org/10.1016/S0891-0618(97)10013-8)
- Fahrenkrug, J., Hannibal, J., Tams, J., & Georg, B. (2000). Immunohistochemical localization of the VIP1 receptor (VPAC1R) in rat cerebral blood vessels: Relation to PACAP and VIP containing nerves. *Journal of Cerebral Blood Flow & Metabolism*, 20(8), 1205–1214. <https://doi.org/10.1097/00004647-200008000-00006>
- Flood, J. F., Garland, J. S., & Morley, J. E. (1990). Vasoactive intestinal peptide (VIP): An amnesic neuropeptide. *Peptides*, 11(5), 933–938. [https://doi.org/10.1016/0196-9781\(90\)90012-T](https://doi.org/10.1016/0196-9781(90)90012-T)
- Freund, T. F., & Buzsáki, G. (1996). Interneurons of the hippocampus. *Hippocampus*, 6(4), 347–470. [https://doi.org/10.1002/\(SICI\)1098-1063\(1996\)6:4<347::AID-HIPO1>3.0.CO;2-I](https://doi.org/10.1002/(SICI)1098-1063(1996)6:4<347::AID-HIPO1>3.0.CO;2-I)
- García-López, M., Abellán, A., Legaz, I., Rubenstein, J. L. R., Puelles, L., & Medina, L. (2007). Histogenetic compartments of the mouse centromedial and extended amygdala based on gene expression patterns during development. *Journal of Comparative Neurology*, 506(1), 46–74. <https://doi.org/10.1002/cne.21524>
- Gozes, I. (2008). VIP, from gene to behavior and back: Summarizing my 25 years of research. *Journal of Molecular Neuroscience*, 36(1), 115–124. <https://doi.org/10.1007/s12031-008-9105-3>
- Hall, E. (1972). Some aspects of the structural organization of the amygdala. In B. E. Eleftheriou (A. c. Di), *The neurobiology of the amygdala: The proceedings of a symposium on the neurobiology of the amygdala*, Bar Harbor, Maine, June 6–17, 1971 (pp. 95–121). Springer US. https://doi.org/10.1007/978-1-4615-8987-7_5
- Harmar, A. J., Arimura, A., Gozes, I., Journot, L., Laburthe, M., Pisegna, J. R., Rawlings, S. R., Robberecht, P., Said, S. I., Sreedharan, S. P., Wank, S. A., & Waschek, J. A. (1998). International Union of Pharmacology. XVIII. Nomenclature of receptors for vasoactive intestinal peptide and pituitary adenylate cyclase-activating polypeptide. *Pharmacological Reviews*, 50(2), 265–270.
- Itoh, S., Takashima, A., & Morimoto, T. (1994). Impaired spatial learning by vasoactive intestinal peptide in Morris water maze task in the rat. *Canadian Journal of Physiology and Pharmacology*, 72(1), 25–29. <https://doi.org/10.1139/y94-005>
- Laburthe, M., Couvineau, A., & Marie, J.-C. (2002). VPAC receptors for VIP and PACAP. *Receptors and Channels*, 8(3–4), 137–153. <https://doi.org/10.3109/10606820213680>
- Lewis, D. A., Campbell, M. J., & Morrison, J. H. (1986). An immunohistochemical characterization of somatostatin-28 and somatostatin-281-12 in monkey prefrontal cortex. *The Journal of Comparative Neurology*, 248(1), 1–18. <https://doi.org/10.1002/cne.902480102>
- Lim, L., Mi, D., Llorca, A., & Marín, O. (2018). Development and functional diversification of cortical interneurons. *Neuron*, 100(2), 294–313. <https://doi.org/10.1016/j.neuron.2018.10.009>
- Loh, D. H., Abad, C., Colwell, C. S., & Waschek, J. A. (2008). Vasoactive intestinal peptide is critical for circadian regulation of glucocorticoids. *Neuroendocrinology*, 88(4), 246–255. <https://doi.org/10.1159/000140676>
- Martina, M., Royer, S., & Paré, D. (2001). Cell-type-specific GABA responses and chloride homeostasis in the cortex and amygdala. *Journal of Neurophysiology*, 86(6), 2887–2895. <https://doi.org/10.1152/jn.2001.86.6.2887>
- Martínez-García, F., Martínez-Marcos, A., & Lanuza, E. (2002). The pallial amygdala of amniote vertebrates: evolution of the concept, evolution of the structure. *Brain Research Bulletin*, 57(3–4), 463–469. [https://doi.org/10.1016/S0361-9230\(01\)00665-7](https://doi.org/10.1016/S0361-9230(01)00665-7)
- Martínez-García, F., Novejarque, A., & Lanuza, E. (2007). Evolution of the amygdala in vertebrates. In J. H. Kaas (Ed.), *Evolution of Nervous Systems. A Comprehensive Reference* (pp. 255–334). Elsevier Academic Press.
- Mascagni, F., & McDonald, A. J. (2003). Immunohistochemical characterization of cholecystokinin containing neurons in the rat basolateral amygdala. *Brain Research*, 976(2), 171–184.
- Mascagni, F., Muly, E. C., Rainnie, D. G., & McDonald, A. J. (2009). Immunohistochemical characterization of parvalbumin-containing interneurons in the monkey basolateral amygdala. *Neuroscience*, 158(4), 1541–1550. <https://doi.org/10.1016/j.neuroscience.2008.11.017>
- McDonald, A. J. (1982a). Cytoarchitecture of the central amygdaloid nucleus of the rat. *The Journal of Comparative Neurology*, 208(4), 401–418. <https://doi.org/10.1002/cne.902080409>
- McDonald, A. J. (1982b). Neurons of the lateral and basolateral amygdaloid nuclei: A golgi study in the rat. *Journal of Comparative Neurology*, 212(3), 293–312. <https://doi.org/10.1002/cne.902120307>
- McDonald, A. J. (1983). Cytoarchitecture of the nucleus of the lateral olfactory tract: A Golgi study in the rat. *Brain Research Bulletin*, 10(4), 497–503. [https://doi.org/10.1016/0361-9230\(83\)90147-8](https://doi.org/10.1016/0361-9230(83)90147-8)
- McDonald, A. J. (1985). Morphology of peptide-containing neurons in the rat basolateral amygdaloid nucleus. *Brain Research*, 338(1), 186–191. [https://doi.org/10.1016/0006-8993\(85\)90266-5](https://doi.org/10.1016/0006-8993(85)90266-5)
- McDonald, A. J. (1992). Cell types and intrinsic connections of the amygdala. In J. P. Aggleton (Ed.), *The amygdala: Neurobiological aspects of emotion, memory, and mental dysfunction* (pp. 67–96). Wiley-Liss.
- McDonald, A. J. (1994). Calretinin immunoreactive neurons in the basolateral amygdala of the rat and monkey. *Brain Research*, 667(2), 238–242.

- McDonald, A. J. (2003). Is there an amygdala and how far does it extend? *Annals of the New York Academy of Sciences*, 985, 1–21. <https://doi.org/10.1111/j.1749-6632.2003.tb07067.x>
- McDonald, A. J. (2020). Chapter 1—Functional neuroanatomy of the basolateral amygdala: Neurons, neurotransmitters, and circuits. In J. H. Urban & J. A. Rosenkranz (Eds.), *Handbook of behavioral neuroscience* (Vol. 26, pp. 1–38). Elsevier. <https://doi.org/10.1016/B978-0-12-815134-1.00001-5>
- McDonald, A. J., & Augustine, J. R. (1993). Localization of GABA-like immunoreactivity in the monkey amygdala. *Neuroscience*, 52(2), 281–294. [https://doi.org/10.1016/0306-4522\(93\)90156-A](https://doi.org/10.1016/0306-4522(93)90156-A)
- McDonald, A. J., & Culbertson, J. L. (1981). Neurons of the basolateral amygdala: A Golgi study in the opossum (*Didelphis virginiana*). *American Journal of Anatomy*, 162(4), 327–342. <https://doi.org/10.1002/aja.1001620404>
- McDonald, A. J., Mascagni, F., & Augustine, J. R. (1995). Neuropeptide Y and somatostatin-like immunoreactivity in neurons of the monkey amygdala. *Neuroscience*, 66(4), 959–982. [https://doi.org/10.1016/0306-4522\(94\)00629-J](https://doi.org/10.1016/0306-4522(94)00629-J)
- McDonald, A. J., & Pearson, J. C. (1989). Coexistence of GABA and peptide immunoreactivity in non-pyramidal neurons of the basolateral amygdala. *Neuroscience Letters*, 100(1), 53–58. [https://doi.org/10.1016/0304-3940\(89\)90659-9](https://doi.org/10.1016/0304-3940(89)90659-9)
- Medina, L., Legaz, I., González, G., De Castro, F., Rubenstein, J. L. R., & Puelles, L. (2004). Expression of Dbx1, Neurogenin 2, Semaphorin 5A, Cadherin 8, and Emx1 distinguish ventral and lateral pallial histogenetic divisions in the developing mouse claustroramygdaloid complex. *Journal of Comparative Neurology*, 474(4), 504–523. <https://doi.org/10.1002/cne.20141>
- Millhouse, O. E. (1986). The intercalated cells of the amygdala. *Journal of Comparative Neurology*, 247(2), 246–271. <https://doi.org/10.1002/cne.902470209>
- Millhouse, O. E., & Uemura-Sumi, M. (1985). The structure of the nucleus of the lateral olfactory tract. *Journal of Comparative Neurology*, 233(4), 517–552. <https://doi.org/10.1002/cne.902330411>
- Muller, J. F., Mascagni, F., & McDonald, A. J. (2003). Synaptic connections of distinct interneuronal subpopulations in the rat basolateral amygdalar nucleus. *Journal of Comparative Neurology*, 456(3), 217–236. <https://doi.org/10.1002/cne.10435>
- Pape, H.-C., Paré, D., & Driesang, R. B. (1998). Two types of intrinsic oscillations in neurons of the lateral and basolateral nuclei of the amygdala. *Journal of Neurophysiology*, 79(1), 205–216. <https://doi.org/10.1152/jn.1998.79.1.205>
- Paré, D., & Gaudreau, H. (1996). Projection cells and interneurons of the lateral and basolateral amygdala: Distinct firing patterns and differential relation to theta and delta rhythms in conscious cats. *Journal of Neuroscience*, 16(10), 3334–3350. <https://doi.org/10.1523/JNEUROSCI.16-10-03334.1996>
- Pawelzik, H., Dodt, H.-U., & Zieglängsberger, W. (1992). Actions of vasoactive intestinal polypeptide (VIP) on neocortical neurons of the rat in vitro. *Neuroscience Letters*, 147(2), 167–170. [https://doi.org/10.1016/0304-3940\(92\)90586-V](https://doi.org/10.1016/0304-3940(92)90586-V)
- Pelkey, K. A., Chittajallu, R., Craig, M. T., Tricoire, L., Wester, J. C., & McBain, C. J. (2017). Hippocampal GABAergic inhibitory interneurons. *Physiological Reviews*, 97(4), 1619–1747. <https://doi.org/10.1152/physrev.00007.2017>
- Pitkänen, A., & Amaral, D. G. (1993a). Distribution of calbindin-D28k immunoreactivity in the monkey temporal lobe: The amygdaloid complex. *Journal of Comparative Neurology*, 331(2), 199–224. <https://doi.org/10.1002/cne.903310205>
- Pitkänen, A., & Amaral, D. G. (1993b). Distribution of parvalbumin-immunoreactive cells and fibers in the monkey temporal lobe: The amygdaloid complex. *Journal of Comparative Neurology*, 331(1), 14–36. <https://doi.org/10.1002/cne.903310103>
- Pitkanen, A., & Amaral, D. G. (1994). The distribution of GABAergic cells, fibers, and terminals in the monkey amygdaloid complex: An immunohistochemical and in situ hybridization study. *Journal of Neuroscience*, 14(4), 2200–2224. <https://doi.org/10.1523/JNEUROSCI.14-04-02200.1994>
- Pitkänen, A., & Kemppainen, S. (2002 Mar). Comparison of the distribution of calcium-binding proteins and intrinsic connectivity in the lateral nucleus of the rat, monkey, and human amygdala. *Pharmacology Biochemistry and Behavior*, 71(3), 369–377. [https://doi.org/10.1016/S0091-3057\(01\)00690-6](https://doi.org/10.1016/S0091-3057(01)00690-6)
- Puelles, L., Kuwana, E., Puelles, E., Bulfone, A., Shimamura, K., Keleher, J., Smiga, S., & Rubenstein, J. L. R. (2000). Pallial and subpallial derivatives in the embryonic chick and mouse telencephalon, traced by the expression of the genes *Dlx-2*, *Emx-1*, *Nkx-2.1*, *Pax-6*, and *Tbr-1*. *The Journal of Comparative Neurology*, 424(3), 409–438. [https://doi.org/10.1002/1096-9861\(20000828\)424:3<409::aid-cne3>3.0.co;2-7](https://doi.org/10.1002/1096-9861(20000828)424:3<409::aid-cne3>3.0.co;2-7)
- Real, M. A., Heredia, R., del Carmen Labrador, M., Dávila, J. C., & Guirado, S. (2009). Expression of somatostatin and neuropeptide Y in the embryonic, postnatal, and adult mouse amygdalar complex. *Journal of Comparative Neurology*, 513(4), 335–348. <https://doi.org/10.1002/cne.21970>
- Rhomberg, T., Rovira-Esteban, L., Vikór, A., Paradiso, E., Kremser, C., Nagy-Pál, P., Papp, O. I., Tásan, R., Erdélyi, F., Szabó, G., Ferraguti, F., & Hájos, N. (2018). Vasoactive intestinal polypeptide-immunoreactive interneurons within circuits of the mouse basolateral amygdala. *Journal of Neuroscience*, 38(31), 6983–7003. <https://doi.org/10.1523/JNEUROSCI.2063-17.2018>
- Sah, P., Faber, E. S. L., Lopez De Armentia, M., & Power, J. (2003). The amygdaloid complex: Anatomy and physiology. *Physiological Reviews*, 83(3), 803–834. <https://doi.org/10.1152/physrev.00002.2003>
- Spampanato, J., Polepalli, J., & Sah, P. (2011). Interneurons in the basolateral amygdala. *Neuropharmacology*, 60(5), 765–773. <https://doi.org/10.1016/j.neuropharm.2010.11.006>
- Storm-Mathisen, J., Leknes, A. K., Bore, A. T., Vaaland, J. L., Edminson, P., Haug, F.-M. S., & Ottersen, O. P. (1983). First visualization of glutamate and GABA in neurones by immunocytochemistry. *Nature*, 301(5900), 517–520. <https://doi.org/10.1038/301517a0>
- Sun, Q.-Q., Prince, D. A., & Huguenard, J. R. (2003). Vasoactive intestinal polypeptide and pituitary adenylate cyclase-activating polypeptide activate hyperpolarization-activated cationic current and depolarize thalamocortical neurons in vitro. *Journal of Neuroscience*, 23(7), 2751–2758. <https://doi.org/10.1523/JNEUROSCI.23-07-02751.2003>
- Suzuki, N., & Bekkers, J. M. (2007). Inhibitory interneurons in the piriform cortex. *Clinical and Experimental Pharmacology and Physiology*, 34(10), 1064–1069. <https://doi.org/10.1111/j.1440-1681.2007.04723.x>
- Swanson, L. W., & Petrovich, G. D. (1998). What is the amygdala? *Trends in Neurosciences*, 21(8), 323–331. [https://doi.org/10.1016/S0166-2236\(98\)01265-X](https://doi.org/10.1016/S0166-2236(98)01265-X)

- Tole, S., Remedios, R., Saha, B., & Stoykova, A. (2005). Selective requirement of Pax6, But Not Emx2, in the specification and development of several nuclei of the amygdaloid complex. *The Journal of Neuroscience*, 25(10), 2753–2760. <https://doi.org/10.1523/jneurosci.3014-04.2005>
- Tombol, T., & Szafranska-Kosmal, A. (1972). A Golgi study of the amygdaloid complex in the cat. *Acta Neurobiologiae Experimentalis*, 32(4), 835–848.
- Vaz, R. P., Pereira, P. A., & Madeira, M. D. (2016). Age effects on the nucleus of the lateral olfactory tract of the rat. *Journal of Comparative Neurology*, 524(4), 759–771. <https://doi.org/10.1002/cne.23863>

How to cite this article: Salamanca, G., Tagliavia, C., Grandis, A., Graić, J. M., Cozzi, B., & Bombardi, C. (2024). Distribution of vasoactive intestinal peptide (VIP) immunoreactivity in the rat pallial and subpallial amygdala and colocalization with γ -aminobutyric acid (GABA). *The Anatomical Record*, 307(8), 2891–2911. <https://doi.org/10.1002/ar.25390>

Chapter 3:
Connections of the sheep basolateral amygdala: A diffusion tensor imaging study



Connections of the sheep basolateral amygdala: A diffusion tensor imaging study

J.M. Graïc^{a,1}, C. Tagliavia^{b,1}, G. Salamanca^c, T. Gerussi^a, A. Grandis^c, B. Cozzi^a,
C. Bombardi^{c,*}

^a Department of Comparative Biomedicine and Food Science, University of Padova, Legnaro, Italy

^b Department of Veterinary Medicine, University of Teramo, Italy

^c Department of Veterinary Medical Sciences, University of Bologna, Bologna, Italy

ARTICLE INFO

Keywords:

Amygdala
Basolateral complex
Tractography
Sheep
Connections

ABSTRACT

Background: A large amount of anatomic data published over the past decade has provided novel insight into the connections of the basolateral amygdala (BLA) in the rat, cat, and monkey. The mammalian (rat, cat, and monkey) BLA has strong connections with the cortex (especially piriform, and frontal cortices), the hippocampal region (especially perirhinal cortex, entorhinal cortex, and subiculum), the thalamus (in particular, the posterior internuclear nucleus and medial geniculate nucleus) and, to some extent, the hypothalamus. An important question remains as to how well the data obtained in rodents and primates can be extrapolated to ruminants.

New method: To address this issue the connections of the sheep BLA has been determined by Magnetic Resonance Imaging (MRI) and Diffusion Tensor Imaging (DTI, Tractography).

Results: Tractography showed ipsilateral connections between the BLA and several areas.

Comparison with existing method(s): Reviews based mainly on description of the results obtained using antero-grade and retrograde neuronal tracers. In the present research, we prefer to use a non-invasive technique (DTI).

Conclusions: This report shows the existence of specific amygdaloid connections in the sheep.

1. Introduction

The mammalian amygdaloid complex, or amygdala, is a nuclear complex that comprises pallial and subpallial structures (García-López et al., 2008; Guirado et al., 2008; Martínez-García et al., 2002; Martínez-García et al., 2007; Martínez-García et al., 2008; Medina et al., 2004; Puelles et al., 2000; Real et al., 2009; Swanson and Petrovich, 1998; Tole et al., 2005; Bombardi, 2011, 2014). The pallial amygdala is composed of deep and superficial (or cortical) nuclei. The deep pallial nuclei include the basolateral amygdala (BLA), the anterior amygdaloid area, and the amygdalohippocampal area. The superficial pallial nuclei consist of the nucleus of the lateral olfactory tract, the anterior cortical nucleus, the bed nucleus of the accessory olfactory tract, the peri-amygdaloid cortex, and the posterior cortical nucleus. The subpallial amygdala, also called extended amygdala (Martínez-García et al., 2008), includes the medial nucleus, the central nucleus, the bed nucleus of the stria terminalis, and the intercalated nuclei (García-López et al., 2008; Guirado et al., 2008; Martínez-García et al., 2002; Martínez-García et al.,

2007; Martínez-García et al., 2008; Medina et al., 2004; Puelles et al., 2000; Real et al., 2009; Swanson and Petrovich, 1998; Tole et al., 2005). These subdivisions can be identified based on their unique connectivity, immunohistochemical and cytoarchitectural profiles. Interestingly, connectional studies with anterograde and retrograde neuronal tracer have demonstrated that each nucleus is uniquely connected with other brain areas (Pitkänen, 2000). Consistent with anatomic heterogeneity, the amygdala is involved in many different functions, such as neuro-vegetative modulation, emotional control, fear learning, memory processing, decision making, aggression and sexual behavior (Aggleton, 2000; Whalen and Phelps, 2009; Bombardi and Di Giovanni, 2013; Amaral and Adolphs, 2016). The amygdala is also involved in many psychiatric and neurological diseases, such as depression, post-traumatic stress disorders, schizophrenia, autism, Alzheimer's disease, Parkinson's disease, temporal lobe epilepsy and stroke (Aggleton, 2000; Whalen and Phelps, 2009; Amaral and Adolphs, 2016; Andrews et al., 2022; Banwinkler et al., 2022; Luna et al., 2022; Xiao et al., 2022). The BLA including the lateral, basal (or basolateral), and accessory basal

* Corresponding author.

E-mail address: cristiano.bombardi@unibo.it (C. Bombardi).

¹ These authors contributed equally as co-first authors.

(or basomedial) nuclei, forms a major part of the amygdaloid complex and represent the main route by which sensory information from both cortical and subcortical regions enters the amygdala. In particular, the lateral nucleus is retained the main sensory receptive area able to convey sensory information to basal, accessory basal and central nuclei for further processing (Pitkänen, 2000). Many studies of the BLA connections have been reported for rat, cat, and monkey, using classical anterograde and retrograde neuronal tracers (McDonald, 1998, 2020; Pitkänen, 2000; Pitkänen et al., 2000; Whalen and Phelps, 2009; McDonald and Mott, 2017). It must be noted that several studies have validated the use of sheep as interesting alternative mammalian species in comparative neuroscience studies, due to its large and highly convoluted brain (Chiocchetti et al., 2003; Bombardi et al., 2006; Peruffo et al., 2019). The purpose of the present study was to determine the connections of the sheep BLA using validated methods and protocols (Peruffo et al., 2019; Gerussi et al., 2022) for structural imaging analysis by Magnetic Resonance Imaging (MRI) and Diffusion Tensor Imaging (DTI) for tractography. The characterizations of these connections of the sheep may help to further understanding the function of the basolateral amygdala in mammals.

2. Material and methods

The of present study is based on four sheep (*Ovis aries*) brains collected during routine commercial slaughtering processing at the abattoir. The sheep were treated according to the European Community Council directive (86/609/EEC) on animal welfare during the commercial slaughtering process and were constantly monitored under mandatory official veterinary medical care. The definition of “adult” was based on the official documentation available corresponding to each individual ear mark and confirmed by evaluation of body size and examination of teeth wear. All the sheep brains were extracted and fixed by immediate immersion in neutral buffered cold paraformaldehyde (4 %). The time interval between the death of the animal and the extraction of the brain was within 20 min. After at least 1 month of fixation, three sheep brains were transferred to the Department of Neuroscience, Biomedicine and Movement of the University of Verona to perform the MRI using a 4.7 Tesla, 33-cm bore horizontal magnet (Oxford Ltd., Oxford, UK) equipped in a Bruker tomograph (Bruker, Karlsruhe, Germany).

2.1. Diffusion tensor imaging (DTI)

Images were obtained with a single coil. The receiver and transmitter were a birdcage with 7.2 cm of inner diameter. A 2D fast acquisition with relaxation enhancement (RARE) series was used to obtain high resolution T2w structural images. The parameters were: RARE factor 16; field of view (FOV) 6.0×5.0 cm; repetition time (TR) 35,736 ms; matrix size (MTX) 240×200 ; echo time (TE) 78.1 ms; 160 slices of 0.5 mm in thickness; 0.250×0.250 mm resolution; number of averages (NEX) 8. Acquisition time: 1 h and 11 min. DTI images were obtained using an Echo Planar Imaging (EPI) series which settings were: EPI factor 11; FOV 6.0×5.0 cm; TR 20,000 ms; MTX 120×100 ; TE 24.7 ms; 80 slices of 1.00 mm; isotropic in-plane resolution of 0.500 mm; NEX 6. In addition, 5 b0 images and 30 noncollinear directions with a b value of 3000 s/mm² were acquired. Acquisition time: 12 h and 50 min. The BLA identification and selection were performed with the ITK-SNAP 3.8.0 software (www.itksnap.org) following the topographic localization described in the atlas of Ella et al. (2017). Then, the regions were uploaded in DSI Studio (www.dsi-studio.labsolver.org) to identify the tracts. A deterministic fiber tracking algorithm (Yeh et al., 2013) was used with augmented tracking strategies (Yeh, 2020) to improve reproducibility. Seeding was from the whole brain and the BLA regions were ROI. The anisotropy threshold was 0.08. The angular threshold was randomly selected from 15 degrees to 90 degrees. The step size was randomly selected from 0.5 voxel to 1.5 voxels. Tracks with length

shorter than 8 or longer than 100 mm were discarded in order to focus on the main fiber pathways. A total of 500000 seeds were placed. Each BLA region was labeled as an “end region” which allowed to build the tracts that started or arrived from/to the region.

3. Results

A whole tractographic image showing tracts from the BLA is in Fig. 1.

Tractography showed ipsilateral connections between the BLA and several areas. Most important, based on the most numerous, the longest, the most coherent and the clearest in quality, were connections with hippocampus proper, subiculum, and entorhinal cortex. Other, fewer, connections included frontal, and, to some extent, parietal, temporal, and occipital cortices. There were no connections between BLA and presumably primary sensitive cortices located in the occipital and parietal lobes. Evident connections were found to the olfactory system (particularly the pyriform cortex and the olfactory tubercle, via the medial stria), the basal ganglia, the thalamus (mediodorsal thalamic nucleus and midline thalamic nuclei, and medial geniculate nucleus), the hypothalamus (lateral part, via the amygdalofugal pathway), and the brainstem (especially midbrain and pons). Most relevant were ipsilateral connections following the ventral amygdalofugal pathway, the large stria terminalis, the fornix, the internal capsule, and the external capsule. Through these, connections were also made to the septal nuclei (Fig. 1G). The ventral amygdalofugal pathway and the stria terminalis appeared to be primarily subcortical fiber systems, whereas amygdalo-cortical connections were established mostly via the external capsule.

4. Discussion

There is an extensive literature regarding the extrinsic and intrinsic connections of the rat, monkey and, to some extent, cat amygdala. Reviews based mainly on description of the results obtained using anterograde and retrograde neuronal tracers (McDonald, 1998, 2020; Pitkänen, 2000; Pitkänen et al., 2000; Whalen and Phelps, 2009; McDonald and Mott, 2017). In the present research, we studied the connection of the sheep BLA using tractography. DTI is a non-invasive technique which is used to show the connectivity of the brain white matter. Although the FA and other parameters might change in ex-vivo tissues, previous work has shown that this technique gives valuable results on fixed brains, if these have been perfused in-vivo or otherwise fixed through immersion within a few hours after death. In addition, a fixed brain would hypothetically allow an unlimited acquisition time, increased b value, increased number of directions, with relatively no movement artifacts, thus achieving what cannot be done in living tissue (Peruffo et al., 2019; Gerussi et al., 2022).

There is no doubt that diffusion imaging and its associated algorithms have their own limits (Thomas et al., 2014; Schilling et al., 2019, 2020). The present fibers were deterministically generated, and the precision of the tracts is somewhat an illustration, in which no direction can be inferred from the images. Additionally, the hand drawn regions, no matter how precisely following the BLA, are placed near large structures such as the end of the temporal bundle or the external capsule, which as such, can lead to artifacts. We strived to limit those tracts and to be conservative in our analysis. The limited fibers presented here are highly consistent with previous findings using other methods in other species, and therefore constitute a fair approximation of actual pathways. Their value resides in the interpretation made based on known neuroanatomy.

The BLA is divided into the lateral, basal (or basolateral), and accessory basal (or basomedial) nuclei and represents the main route by which sensory information from both cortical and subcortical regions enters the amygdala. In rats, cats, and nonhuman primates the BLA receives different sensory information from frontal cortex and thalamus and in turn, sends projections back to these areas as well as to basal forebrain, hippocampal region, striatum, and hypothalamus (McDonald,

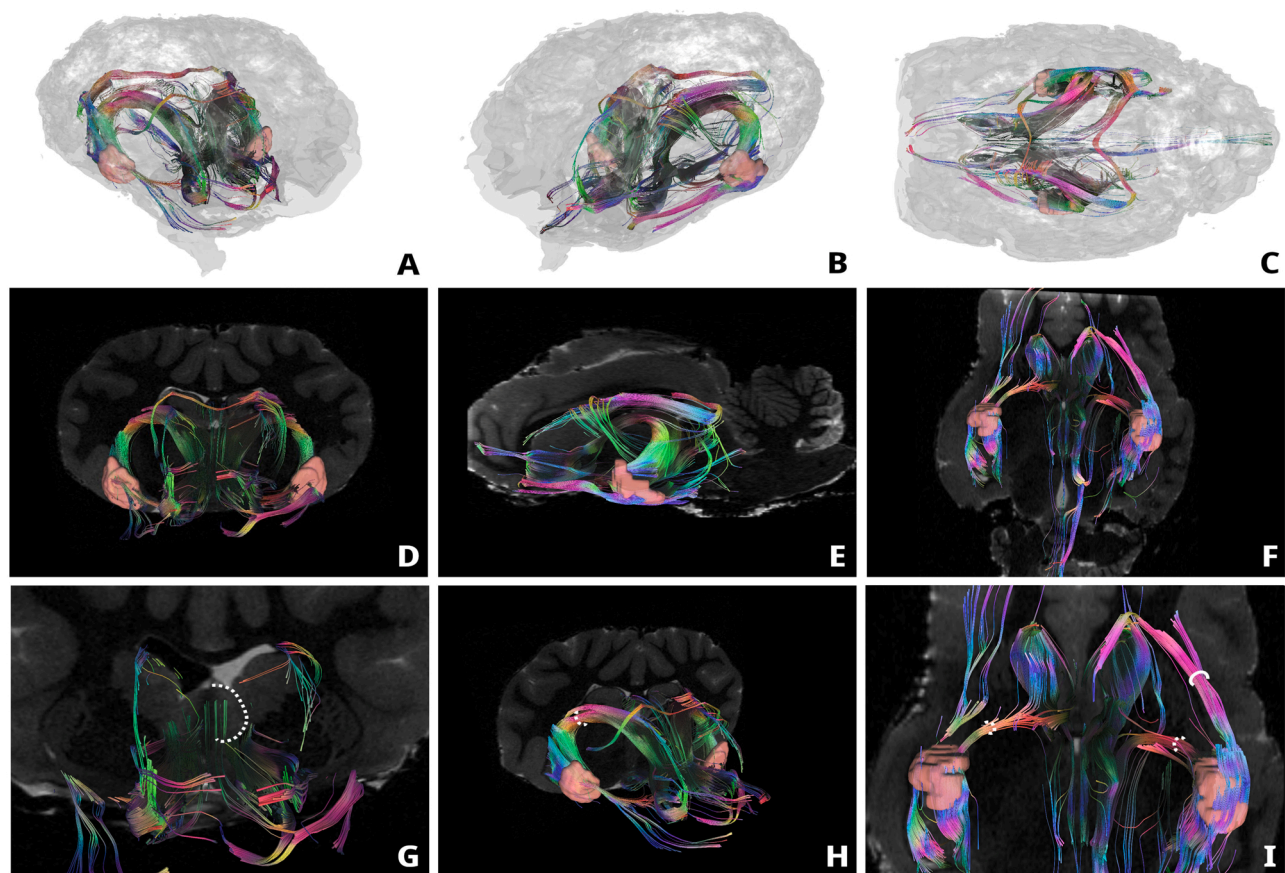


Fig. 1. Tractography of the fibers reaching the amygdala. The pink-red shapes are the delineated amygdala regions considered. A, B and C are 3D illustrations inside the brain surface in gray. D, E and F are coronal, sagittal, and horizontal (ventral) views respectively. G, H, and I are focusing on particular features. In G, the septal nuclei are identified by the dotted line on one half, showing the fibers reaching them. In H, the stria terminalis is encircled by a dotted ring. In I, the amygdalofugal fibers reaching the hypothalamus are identified by a dotted ring; the fibers going to the olfactory tract are identified by a full circle.

1998, 2020; Pitkänen, 2000; Whalen and Phelps, 2009). Each nucleus of the BLA has its own specific connectational pattern and, consequently, main characteristic functional properties. For example, the lateral nucleus, considered the main sensory input station of the BLA, is involved in fear conditioning, and regulates the visceral activity through direct and indirect projection to the central amygdaloid nucleus. The basal nucleus is strongly connected with the prefrontal cortex and cholinergic nuclei, regulating motivational and attentional processes. The accessory basal nucleus appears mainly involved in the processing of the olfactory information together which superficial amygdaloid nuclei (McDonald, 1998, 2020; Pitkänen, 2000).

The mammalian amygdaloid complex has three extrinsic fiber systems: the ventral amygdalofugal pathway, the stria terminalis, and the external capsule. Fibers from ventral amygdalofugal system appear to joint fibers in the stria terminalis throughout their trajectories. The ventral amygdalofugal pathway and the stria terminalis are both primarily subcortical fiber system. The connections between BLA and cortex travel via the external capsule. Our study indicates that also in the sheep the ventral amygdalofugal pathway and the stria terminalis connect the BLA with striatum, thalamus, hypothalamus, and brainstem. In addition, fornix and external capsule connect BLA and hippocampal region. Finally, we observed that the connections of the BLA with the neocortex travel via the external capsule and the subcortical white matter. Taken together our results indicate that the sheep BLA appear to be connected with primary and multimodal cortical areas (including prefrontal cortex), medial temporal lobe memory system, striatum, thalamus and hypothalamus.

4.1. Functional analysis

Our study indicates that the BLA relates to a wide variety of cortical and subcortical areas. In addition, as demonstrated in other species, our results suggest that convergence of information from various functional system occurs within the BLA (Table 1).

Previous studies in rat, cat and monkey have demonstrated that the majority of the olfactory projection to the amygdala is directed to the nucleus of the lateral olfactory tract, the anterior cortical nucleus and

Table 1
Main basolateral amygdalar interconnections in the sheep, as seen in diffusion tensor imaging. The connections are expressed as strong (+++), moderate (++), light (+), absent (-). The same connections have been reported for monkey, cat and rat using neuronal tracers (McDonald, 1998, 2020; Pitkänen, 2000; Pitkänen et al., 2000; Whalen and Phelps, 2009; McDonald and Mott, 2017).

	Sheep	Monkey	Cat	Rat
Pyriform Cortex	+++	-	+++	+++
Frontal cortex	++	+++	+++	+++
Parietal cortex	+	+	+	+
Temporal cortex	+	++	++	++
Occipital cortex	+	++	++	++
Hippocampus proper	+++	+++	+++	+++
Subiculum	+++	+++	+++	+++
Entorhinal cortex	+++	+++	+++	+++
Basal Ganglia	+++	+++	+++	+++
Thalamus	+++	+++	+++	+++
Hypothalamus	+++	+++	+++	+++
Midbrain	++	++	++	++
Pons	++	++	++	++

the periamygdaloid cortex (McDonald, 1998, 2020; Pitkänen, 2000; Whalen and Phelps, 2009). However, as reported in the rat and cat, but not in monkey (McDonald, 1998, 2020; Pitkänen, 2000; Whalen and Phelps, 2009), the connections of the sheep BLA with olfactory areas (primarily piriform cortex) support its role in processing of olfactory information. Input and output of the BLA are not confined to the olfactory system. Accordingly, the BLA also receives input from all the various sensory modalities (McDonald, 1998, 2020; Pitkänen, 2000; Whalen and Phelps, 2009). Hence, the sheep BLA can be retain a subcortical center of coordination for olfactory input with other sensory information.

Interconnections between the amygdala and the hippocampal region in the rat, cat and monkey have been reported in detail many reviews (McDonald, 1998, 2020; Pitkänen, 2000; Pitkänen et al., 2000; Whalen and Phelps, 2009; McDonald and Mott, 2017). Prominent connections of the BLA with the hippocampus proper, subiculum, and entorhinal cortex has been observed also in the sheep where could be critical for contextual aspects of emotional learning and, in addition, may modulate explicit memory processes.

The connections of the BLA with frontal cortex, as observed in rat, cat, and monkey (McDonald, 1998, 2020; Pitkänen, 2000; Whalen and Phelps, 2009) indicates that this amygdaloid area could be crucial for the regulation of motivational behavior. In addition, the extensive direct interconnections between BLA and mediodorsal thalamic nucleus observed in the present study, indicate that the sheep amygdala, as reported in other mammals (McDonald, 1998, 2020; Pitkänen, 2000; Whalen and Phelps, 2009), could also regulate the frontal cortex activity through connections with the thalamus.

As in rat, cat and monkeys (McDonald, 1998, 2020; Pitkänen, 2000; Whalen and Phelps, 2009), also in sheep the connections between BLA and insular cortex could be involved not only in the transmission of somatosensory, taste and visceral information, but also in the conditioned taste aversion, a particular type of aversive learning.

In sheep, as observed in rats, cat and monkeys (McDonald, 1998, 2020; Pitkänen, 2000; Whalen and Phelps, 2009), there do not seem to be connections with the primary acoustic and visual sensory areas (because there are no obvious connections with the corresponding cortices at the temporal and occipital lobes) but with those of a higher order presumably located at the parietal and occipitotemporal level. This data also indicates that the sheep BLA is the sensory gate of the amygdala for highly processed multimodal cortical information.

In the present research, as in other mammals (McDonald, 1998, 2020; Pitkänen, 2000; Whalen and Phelps, 2009), connections between sheep BLA and many subcortical structures has been observed. The connections of the BLA with the basal ganglia (including the *nucleus accumbens*) could be considered the main pathways mediating the integration of reward information with instrumental components of emotional responses. The connections with the midline thalamic nuclei and medial geniculate nuclei, together with those of the sensory cortices, could indicate that the BLA is important for processing sensory and emotional associations. The connection of the BLA with hypothalamus (lateral part), and brainstem (especially midbrain and pons) support the modulatory role of the amygdala on some endocrine and autonomic aspects of sexual and fear behaviors. Finally, fibers running in the commissural formations can provide interamygdaloid connections.

In conclusion, it's believed that the present study has added important neuroanatomical details, thus reducing the knowledge gap, in a species such as the sheep, which is increasingly used as an experimental model (Herrmann et al., 2019; Taha et al., 2022). This report shows the existence of specific amygdaloid connections in the sheep, using diffusion MRI. In previous research the inputs and outputs of the amygdala, including the BLA, has been extensively study in rat, cat, and monkey using classical tract tracing methods. Our results indicate that there are several similarities in the BLA connections comparing sheep with rat, cat, and monkey, which include in all species a strong connection with hippocampus proper, subiculum, and entorhinal cortex. There are also

several interspecies differences in the BLA connections, such as the fact that, unlike the monkey BLA, the BLA of rat, cat, and sheep are directly connected to the olfactory areas (piriform cortex) but appear less connected with the neocortex.

CRediT authorship contribution statement

B. Cozzi, C. Bombardi, and J.M. Graić planned and designed the experiments. C. Tagliavia, T. Gerussi, G. Salamanca, and A. Grandis performed the experiments. J.M. Graić, C. Tagliavia, B. Cozzi and C. Bombardi analyzed experimental results and wrote the manuscript with input from all authors.

Declaration of Competing Interest

- We wish to confirm that there are no known conflicts of interest associated with this publication and there has been no significant financial support for this work that could have influenced its outcome.
- No funding was received for this work.
- We confirm that we have given due consideration to the protection of intellectual property associated with this work and that there are no impediments to publication, including the timing of publication, with respect to intellectual property. In so doing we confirm that we have followed the regulations of our institutions concerning intellectual property.
- We confirm that the manuscript has been read and approved by all named authors.
- We confirm that the order of authors listed in the manuscript has been approved by all named authors.

Data availability

No data was used for the research described in the article.

References

- Aggleton, J.P., 2000. *The amygdala: a functional analysis*, 2nd ed., Oxford Univ. Press, New York.
- Amaral, D.G., Adolphs, R., 2016. *Living without an Amygdala*. The Guilford Press.
- Andrews, D.S., Aksman, L., Kerns, C.M., Lee, J.K., Winder-Patel, B.M., Harvey, D.J., Waizbard-Bartov, E., Heath, B., Solomon, M., Rogers, S.J., Altmann, A., Nordahl, C. W., Amaral, D.G., 2022. Development with different forms of anxiety in autism spectrum disorder. *Biol. Psychiatry Assoc. Amygdala* 91 (977–987). <https://doi.org/10.1016/j.biopsych.2022.01.016>.
- Banwinkler, M., Theis, H., Prange, S., Van Eimeren, T., 2022. Imaging the limbic system in Parkinson's disease—a review of limbic pathology and clinical symptoms. *Brain Sci.* 12, 1248. <https://doi.org/10.3390/brainsci12091248>.
- Bombardi, C., 2011. Distribution of 5-HT_{2A} receptor immunoreactivity in the rat amygdaloid complex and colocalization with γ -aminobutyric acid. *Brain Res.* 1370, 112–128. <https://doi.org/10.1016/j.brainres.2010.11.055>. Epub 2010 Nov 30.
- Bombardi, C., 2014. Neuronal localization of the 5-HT₂ receptor family in the amygdaloid complex. *Front. Pharm.* 5, 68. <https://doi.org/10.3389/fphar.2014.00068> eCollection 2014.
- Bombardi, C., Di Giovanni, G., 2013. Functional anatomy of 5-HT_{2A} receptors in the amygdala and hippocampal complex: relevance to memory functions. *Exp. Brain Res.* 230, 427–439. <https://doi.org/10.1007/s00221-013-3512-6>.
- Bombardi, C., Grandis, A., Chiocchetti, R., Lucchi, M.L., 2006. Distribution of calbindin-D28k, neuronal nitric oxide synthase, and nicotinamide adenine dinucleotide phosphate diaphorase (NADPH-d) in the lateral nucleus of the sheep amygdaloid complex. *Anat. Embryol. (Berl.)* 211, 707–720. <https://doi.org/10.1007/s00429-006-0133-x>. Epub 2006 Oct 18.
- Chiocchetti, R., Clavenzani, P., Barazzoni, A.M., Grandis, A., Bombardi, C., Costerbosa, G.L., Petrosino, G., Avoni, G.B., Bortolami, R., 2003. Viscerotopic representation of the subdiaphragmatic tracts of the digestive apparatus within the vagus complex in the sheep. *Brain Res.* 961, 32–44. [https://doi.org/10.1016/S0006-8993\(02\)03836-2](https://doi.org/10.1016/S0006-8993(02)03836-2).
- Ella, A., Delgadillo, J.A., Chemineau, P., Keller, M., 2017. Computation of a high resolution MRI 3D stereotaxic atlas of the sheep brain. *J. Comp. Neurol.* 525, 676–692. <https://doi.org/10.1002/cne.24079>.
- García-López, M., Abellán, A., Legaz, I., Rubenstein, J.L., Puelles, L., Medina, L., 2008. Histogenetic compartments of the mouse centromedial and extended amygdala

- based on gene expression patterns during development. *J. Comp. Neurol.* 506, 46–74. <https://doi.org/10.1002/cne.21524>.
- Gerussi, T., Graić, J.M., Grandis, A., Peruffo, A., Cozzi, B., 2022. The orbitofrontal cortex of the sheep. Topography, organization, neurochemistry, digital tensor imaging and comparison with the chimpanzee and human. *Brain Struct. Funct.* 227, 1871–1891. <https://doi.org/10.1007/s00429-022-02479-w>.
- Guirado, S., Real, M.A., Dávila, J.C., 2008. Distinct immunohistochemically defined areas in the medial amygdala in the developing and adult mouse. *Brain Res Bull.* 75, 214–217. <https://doi.org/10.1016/j.brainresbull.2007.10.016>.
- Herrmann, A.M., Meckel, S., Gounis, M.J., Kringe, L., Motschall, E., Mülling, C., Boltze, J., 2019. Large animals in neurointerventional research: a systematic review on models, techniques and their application in endovascular procedures for stroke, aneurysms and vascular malformations. *J. Cereb. Blood. Flow. Metab.* 39, 375–394. <https://doi.org/10.1177/0271678x19827446>.
- Luna, L.P., Radua, J., Fortea, L., Sugranyes, G., Fortea, A., Fusar-Poli, P., Smith, L., Firth, J., Shin, J.I., Brunoni, A.R., Husain, M.I., Husian, M.O., Sair, H.I., Mendes, W. O., Uchoa, L.R.A., Berk, M., Maes, M., Daskalakis, Z.J., Frangou, S., Fornaro, M., Vieta, E., Stubbs, B., Solmi, M., Carvalho, A.F., 2022. A systematic review and meta-analysis of structural and functional brain alterations in individuals with genetic and clinical high-risk for psychosis and bipolar disorder. *Prog. Neuropsychopharmacol. Biol. Psychiatry* 13 (117), 110540. <https://doi.org/10.1016/j.pnpbp.2022.110540>.
- Martínez-García, F., Martínez-Marcos, A., Lanuza, E., 2002. The pallial amygdala of amniote vertebrates: evolution of the concept, evolution of the structure. *Brain Res. Bull.* 57, 463–469. [https://doi.org/10.1016/s0361-9230\(01\)00665-7](https://doi.org/10.1016/s0361-9230(01)00665-7).
- Martínez-García, F., Novejarque, A., Lanuza, E., 2007. Evolution of the amygdala in vertebrates. In: Kaas, J.H. (Ed.), *Evolution of Nervous Systems. A Comprehensive Reference*, vol. 2. Elsevier Academic Press, Oxford, pp. 255–334.
- Martínez-García, F., Novejarque, A., Lanuza, E., 2008. Two interconnected functional systems in the amygdala of amniote vertebrates. *Brain Res. Bull.* 75, 206–213. <https://doi.org/10.1016/j.brainresbull.2007.10.019>.
- McDonald, A.J., 1998. Cortical pathways to the mammalian amygdala. *Prog. Neurobiol.* 55, 257–332. [https://doi.org/10.1016/s0301-0082\(98\)00003-3](https://doi.org/10.1016/s0301-0082(98)00003-3).
- McDonald, A.J., 2020. Functional neuroanatomy of the basolateral amygdala: neurons, neurotransmitters, and circuits. *Handb. Behav. Neurosci.* 26, 1–38. <https://doi.org/10.1016/b978-0-12-815134-1.00001-5>.
- McDonald, A.J., Mott, D.D., 2017. Functional neuroanatomy of amygdalohippocampal interconnections and their role in learning and memory. *J. Neurosci. Res.* 95, 797–820. <https://doi.org/10.1002/jnr.23709>.
- Medina, L., Legaz, I., González, G., De Castro, F., Rubenstein, J.L., Puelles, L., 2004. Expression of Dbx1, Neurogenin 2, Semaphorin 5A, Cadherin 8, and Emx1 distinguish ventral and lateral pallial histogenetic divisions in the developing mouse claustroramygdaloid complex. *J. Comp. Neurol.* 474, 504–523. <https://doi.org/10.1002/cne.20141>.
- Peruffo, A., Corain, L., Bombardi, C., Centelleghé, C., Grisan, E., Graić, J.M., Bontempi, P., Grandis, A., Cozzi, B., 2019. The motor cortex of the sheep: laminar organization, projections and diffusion tensor imaging of the intracranial pyramidal and extrapyramidal tracts. *Brain Struct. Funct.* 224, 1933–1946. <https://doi.org/10.1007/s00429-019-01885-x>.
- Pitkänen, A., 2000. Connectivity of the Rat Amygdaloid Complex. In: Aggleton, J.P. (Ed.), *The Amygdala*. Oxford University Press, New York, pp. 31–115.
- Pitkänen, A., Pikkarainen, M., Nurminen, N., Ylinen, A., 2000. Reciprocal connections between the amygdala and the hippocampal formation, perirhinal cortex, and postrhinal cortex in rat. A review. *Ann. N. Y. Acad. Sci.* 911, 369–391. <https://doi.org/10.1111/j.1749-6632.2000.tb06738.x>.
- Puelles, L., Kuwana, E., Puelles, E., Bulfone, A., Shimamura, K., Keleher, J., Smiga, S., Rubenstein, J.L., 2000. Pallial and subpallial derivatives in the embryonic chick and mouse telencephalon, traced by the expression of the genes *Dlx-2*, *Emx-1*, *Nkx-2.1*, *Pax-6*, and *Tbr-1*. *J. Comp. Neurol.* 424, 409–438. [https://doi.org/10.1002/1096-9861\(20000828\)424:3<409::aid-cne3>3.0.co;2-7](https://doi.org/10.1002/1096-9861(20000828)424:3<409::aid-cne3>3.0.co;2-7).
- Real, M.A., Heredia, R., Labrador, Mdel, C., Dávila, J.C., Guirado, S., 2009. Expression of somatostatin and neuropeptide Y in the embryonic, postnatal, and adult mouse amygdalar complex. *J. Comp. Neurol.* 513, 335–348. <https://doi.org/10.1002/cne.21970>.
- Schilling, K.G., Nath, V., Hansen, C., Parvathaneni, P., Blaber, J., Gao, Y., Neher, P., Aydogan, D.B., Shi, Y., Ocampo-Pineda, M., Schiavi, S., Daducci, A., Girard, G., Barakovic, M., Rafael-Patino, J., Romascano, D., Rensonnet, G., Pizzolato, M., Bates, A., Fischl, E., Thiran, J.P., Canales-Rodriguez, E.J., Huang, C., Zhu, H., Zhong, L., Cabeen, R., Toga, A.W., Rheault, F., Theaud, G., Houde, J.C., Sidhu, J., Chamberland, M., Westin, C.F., Dyrby, J., Verma, R., Rathi, Y., Irfanoglu, M.O., Thomas, C., Pierpaoli, C., Descoteaux, M., Anderson, A.W., Landman, B.A., 2019. Limits to anatomical accuracy of diffusion tractography using modern approaches. *Neuroimage* 185, 1–11. <https://doi.org/10.1016/j.neuroimage.2018.10.029>.
- Schilling, K.G., Petit, L., Rheault, F., Remedios, S., Pierpaoli, C., Anderson, A.W., Landman, B.A., Descoteaux, M., 2020. Brain connections derived from diffusion MRI tractography can be highly anatomically accurate—If we know where white matter pathways start, where they end, and where they do not go. *Brain Struct. Funct.* 225, 2387–2402. <https://doi.org/10.1007/s00429-020-02129-z>.
- Swanson, L.W., Petrovich, G.D., 1998. What is the amygdala. *Trends Neurosci.* 21, 323–331. [https://doi.org/10.1016/s0166-2236\(98\)01265-x](https://doi.org/10.1016/s0166-2236(98)01265-x).
- Taha, A., Bobi, J., Dammers, R., Dijkhuizen, R.M., Dreyer, A.Y., van Es, A.C.G.M., Ferrara, F., Gounis, M.J., Nitzsche, B., Platt, S., Stoffel, M.H., Volovici, V., Del Zoppo, G.J., Duncker, D.J., Dippel, D.W.J., Boltze, J., van Beusekom, H.M.M., 2022. Comparison of large animal models for acute ischemic stroke: which model to use. *Stroke* 53, 1411–1422. <https://doi.org/10.1161/STROKEAHA.121.036050>.
- Thomas, C., Ye, F.Q., Irfanoglu, M.O., Modi, P., Saleem, K.S., Leopold, D.A., Pierpaoli, C., 2014. Anatomical accuracy of brain connections derived from diffusion MRI tractography is inherently limited. *Proc. Natl. Acad. Sci.* 111, 16574–16579. <https://doi.org/10.1073/pnas.1405672111>.
- Tole, S., Remedios, R., Saha, B., Stoykova, A., 2005. Selective requirement of Pax6, but not Emx2, in the specification and development of several nuclei of the amygdaloid complex. *J. Neurosci.* 25, 2753–2760. <https://doi.org/10.1523/JNEUROSCI.3014-04.2005>.
- Whalen, P.J., Phelps, E.A., 2009. *The Human Amygdala*, first ed., Guilford Press, New York.
- Xiao, S., Yang, Z., Su, T., Gong, J., Huang, L., Wang, Y., 2022. Functional and structural brain abnormalities in posttraumatic stress disorder: a multimodal meta-analysis of neuroimaging studies. *J. Psychiatr. Res.* 155, 153–162. <https://doi.org/10.1016/j.jpsychires.2022.08.010>.
- Yeh, C., Verstynen, T.D., Wang, Y., Fernandez-Miranda, J.C., Tseng, W.Y., 2013. Deterministic diffusion fiber tracking improved by quantitative anisotropy. *PLoS One* 15 (11), e80713. <https://doi.org/10.1371/journal.pone.0080713>.
- Yeh, F.C., 2020. Shape analysis of the human association pathways. *Neuroimage* 223, 117329. <https://doi.org/10.1016/j.neuroimage.2020.117329>.

Chapter 4:
**Immunohistochemical Distribution of Serotonin Transporter (SERT) in the
Optic Lobe of the Honeybee, *Apis mellifera***

Article

Immunohistochemical Distribution of Serotonin Transporter (SERT) in the Optic Lobe of the Honeybee, *Apis mellifera*

Cristiano Bombardi ^{1,*}, Giulia Salamanca ¹, Claudio Tagliavia ¹, Annamaria Grandis ¹, Fanny Mille ¹, Maria Grazia De Iorio ² and Giulietta Minozzi ^{2,*}

¹ Department of Veterinary Medical Sciences, University of Bologna, Via Tolara di Sopra, 50, Ozzano dell'Emilia, 40064 Bologna, Italy

² Department of Veterinary Medicine and Animal Sciences, University of Milan, 26900 Lodi, Italy

* Correspondence: cristiano.bombardi@unibo.it (C.B.); giulietta.minozzi@unimi.it (G.M.)

Simple Summary: Serotonin is ubiquitously expressed in vertebrates and invertebrates, where it regulates specific behavioural patterns. Though the specific effects of serotonin release in the optic lobe are not entirely known, increasing evidence associates the serotonergic system with optic lobe-mediated behaviours. In this study, the localization of serotonin transporter (SERT) was immunohistochemically analysed in the optic lobes of moderate, docile and aggressive worker honeybees. SERT-immunoreactive fibres were stratified in the optic lobe and distributed in the three visual neuropils: lamina, medulla and lobula. Interestingly, SERT immunoreactivity was inversely related to aggressive behaviour. The present study indicates that low levels of serotonin in the optic lobe are associated with aggressive behaviour.

Abstract: Visual information is processed in the optic lobes, which consist of three retinotopic neuropils. These are the lamina, the medulla and the lobula. Biogenic amines play a crucial role in the control of insect responsiveness, and serotonin is clearly related to aggressiveness in invertebrates. Previous studies suggest that serotonin modulates aggression-related behaviours, possibly via alterations in optic lobe activity. The aim of this investigation was to immunohistochemically localize the distribution of serotonin transporter (SERT) in the optic lobe of moderate, docile and aggressive worker honeybees. SERT-immunoreactive fibres showed a wide distribution in the lamina, medulla and lobula; interestingly, the highest percentage of SERT immunoreactivity was observed across all the visual neuropils of the docile group. Although future research is needed to determine the relationship between the distribution of serotonin fibres in the honeybee brain and aggressive behaviours, our immunohistochemical study provides an anatomical basis supporting the role of serotonin in aggressive behaviour in the honeybee.

Keywords: optic lobe; serotonin; SERT; lamina; medulla; lobula; honeybee



Citation: Bombardi, C.; Salamanca, G.; Tagliavia, C.; Grandis, A.; Mille, F.; De Iorio, M.G.; Minozzi, G. Immunohistochemical Distribution of Serotonin Transporter (SERT) in the Optic Lobe of the Honeybee, *Apis mellifera*. *Animals* **2022**, *12*, 2032. <https://doi.org/10.3390/ani12162032>

Academic Editor: Enrico Alleva

Received: 29 June 2022

Accepted: 8 August 2022

Published: 10 August 2022

Publisher's Note: MDPI stays neutral with regard to jurisdictional claims in published maps and institutional affiliations.



Copyright: © 2022 by the authors. Licensee MDPI, Basel, Switzerland. This article is an open access article distributed under the terms and conditions of the Creative Commons Attribution (CC BY) license (<https://creativecommons.org/licenses/by/4.0/>).

1. Introduction

The capacity of insects to receive sensory input, process information and respond with a specific behaviour is made possible by the brain [1]. The biogenic amine serotonin is widely distributed in the brain of the honeybee, where it modulates a great variety of behavioural processes, such as learning, memory and aggression [2,3]. Accordingly, in honeybees, differences in serotonin activity are related to specific behavioural patterns [4]. The serotonin transporter (SERT) plays a key role in the regulation of serotonin levels in the synapse. In fact, this plasma membrane transporter protein is responsible for the reuptake of serotonin into presynaptic neurons [5]. Interestingly, the serotonergic system, including SERT, is highly conserved between vertebrates and invertebrates [6,7].

The optic lobe, a complex structure located in the protocerebrum of honeybees, consists of three retinotopic neuropils. These are the lamina, the medulla and the lobula. Their

function consists, before the information is integrated in the high-order brain centre, of a consecutive step aimed at visual conversion and segregation [8]. Interestingly, brain activity in the optic lobes precedes behavioural choices, suggesting that attention-like processes are pushed far out into the sensory periphery [9]. Immunohistochemical studies indicate that the honeybee optic lobe receives serotonergic fibres from the cell groups located in the protocerebrum [10]. Serotonin exerts its effects in the optic lobe, acting on 5-HT1A and, to some extent, 5-HT2 receptors [11,12]. Previous studies demonstrated that serotonin is involved in the regulation of honeybee phototactic behaviour, and the 5-HT1A receptor is the main mediator of this effect. In addition, serotonin in the optic lobe can modulate visual responses, such as the motion-sensitive visual antennal reflex and phototactic reflex [11,13]. The aforementioned studies support the idea that the interaction of the optic lobes and the serotonergic system may play a primary role in the management of behaviours.

The goal of the present study was to determine the distribution of serotonin fibres in the optic lobes of different honeybees (docile, moderate and aggressive) using an immunofluorescence method with primary antibody against serotonin transporter (SERT). Although the presence of serotonin immunoreactive fibres has been investigated using primary antibody against serotonin [10,14], different studies reported that antibodies against SERT were preferable to determine serotonergic fibres [15]. Our results provide initial insights into the serotonergic modulation of aggression-related behaviours in honeybee.

2. Materials and Methods

2.1. Animals and Fixation

Thirty worker honeybees (ten bees in the moderate group, ten bees in the docile group and ten bees in the aggressive group) were used in this study.

In detail, the honeybees analysed in this study belonged to a genetic selection program where the docility of 108 colonies was assessed four times a year by an expert beekeeper, following Büchler et al., 2013 and Uzonov et al., 2015 [16,17]. The final phenotype of each colony was obtained from the averages from four tests carried out between March and June. Based on their mean phenotype, the ten best colonies (docility average: 3.43), the ten most aggressive colonies (docility average: 1.8) and ten colonies as a moderate group (docility average: 2.67) were sampled in October 2021. On the same day, one worker bee per colony was taken from the colony and killed by freezing prior to brain analysis.

Docility is composed of two traits: gentleness and calmness. Gentleness, also known as defensive behaviour, measures aggressiveness against humans, while calmness measures the stillness and immobility of worker bees on the comb during the inspection [16]. Both traits were evaluated together and scored on a scale from 1 to 4. A score of 1 referred to the most aggressive behaviour and indicated that the colony is nervous: many bees flew around the comb and tried to sting despite the use of smoke. A score of 2 meant that few bees left the comb and tried to sting, even if smoke was used. A score of 3 indicated that the bees moved on the comb without flying and it was possible to avoid stings with the use of smoke. A score of 4 referred to the calmest behaviour; bees stayed still on the comb, and it was not necessary to use smoke or protective clothes during their handling. Half-points (1.5, 2.5, 3.5) were used to discriminate colonies with intermediate behaviours. Docility is an important trait in beekeeping, as calm and gentle bees are easier to manage and there is less risk for beekeepers of being stung or injuring the queen during the inspection of the apiary. For this reason, docility is one of the most widely selected phenotypes in breeding programs, together with honey production, swarming tendency and varroa resistance [18]. Thanks to breeding selection, docility has significantly increased since 1990 [19].

The animals were deeply anesthetized with ice and perfused with a solution of 4% paraformaldehyde in 0.1 M sodium phosphate buffer, pH 7.4. The brains were dissected, fixed in the same fixative for 3 h and washed (4×15 min) in phosphate-buffered saline (PBS). The brains were then cryoprotected in 30% sucrose solution in PBS, pH 7.4, at +4 °C for 48 h. Tissues were dipped in Tissue Tek® (Sakura Finetek Europe) mounting medium and stored at 4 °C overnight, then frozen in isopentane (Sigma-Aldrich, Co., 270342-1L,

St. Louis, MO, USA) cooled in liquid nitrogen. Serial coronal sections (15 μ m thickness) were cut on a cryostat and mounted on coverslips coated with poly-L-lysine (Thermo Scientific, MA, USA).

2.2. Immunostaining

The final concentrations of primary antibody were established by performing immunofluorescence experiments using different dilution patterns. First of all the cryosections were hydrated and washed in PBS (3 \times 10 min). A solution containing 10% normal goat serum (Colorado Serum Co., Denver, CO, USA, #CS 0922) and 0.3% Triton X-100 in 0.02 M PBS (Sigma-Aldrich, Co., 9036-19-5, St. Louis, MO, USA) was used to block nonspecific binding through incubation of cryosections for 40 min at room temperatures (RT). Subsequently, after three 10-min washes in a solution containing 1% normal goat serum and 0.3% Triton X-100 in 0.02 M PBS, the cryosections were incubated overnight at 4 $^{\circ}$ C in the following primary antisera: rabbit anti-SERT polyclonal antibody (diluted 1:100, code 24330, ImmunoStar, WI, USA) dissolved in 1% normal goat serum (Colorado Serum Co., Denver, CO, USA, #CS 0922) and 0.3% Triton X-100 in 0.02 M PBS. After washing in PBS (3 \times 10 min), the sections were incubated for 2 h at RT with the secondary antibody solution, which contained Alexa 594-conjugated goat anti-rabbit IgG (1:200, #A11012, Molecular Probes, Leiden, the Netherlands) diluted in 1% normal goat serum and 0.3% Triton X-100 in 0.02 M PBS. The sections were then washed with 0.02 M PBS and mounted in buffered glycerol at pH 8.6 with 4',6-diamidino-2-phenylindole (DAPI) (Santa Cruz Biotechnology, Santa Cruz, CA, USA), a cell-permeable DNA-binding dye. The specificity of the rabbit polyclonal antibody directed against insect SERT was determined by the manufacturer. In the present experiments, the pre-adsorption test with SERT peptide control (code 24332, ImmunoStar, WI, USA) abolished the immunostaining (Supplementary File S1). In addition, control sections incubated without the primary antibody resulted in the complete disappearance of stained profiles. The omission, as well as the replacement of the secondary antibody with inappropriate secondary antibody, resulted in the elimination of all immunohistochemical staining.

2.3. Analysis of Sections

Four sections for each animal were examined using a Nikon H550L (Nikon Instruments, Natori, Japan) equipped with the appropriate filter cubes to differentiate the fluorochromes employed. The TRITC filter was employed for Alexa 594 (EX 540/25; DM 565; BA 605–655) and the DAPI/Hoechst/Alexa Fluor 350 filter for DAPI (EX 375/28; DM 415; BA 460/50). Bilateral observations of the optic lobes were carried out, proceeding rostrocaudally. Histological specimens were evaluated blindly. The images were recorded, with identical parameters for the three groups (moderate, docile and aggressive), by a Nikon DS-Qi1Mc digital camera (Nikon Instruments, Japan) and Nikon Elements software, version 4.10. Slight adjustments to the contrast and brightness of the figures were applied using Adobe Photoshop CS3 Extended 10.0 software (Adobe Systems, San Jose, CA, USA). The same adjustments were applied to the figures. The threshold technique in ImageJ (version IJ 1.46r, downloaded from <http://imagej.nih.gov/ij/download.html> accessed on 20 July 2019) was used to analyse the percentage of the image with SERT immunoreactivity. The images were first “thresholded” so that only the pixels above the threshold level were counted as positive labelling elements. The threshold level was set case by case with respect to the background level of the negative control sections. The pixel area occupied by SERT-positive elements above the threshold level was measured and the percentage fractions were calculated. The data were expressed as means \pm standard deviation (SD) with a significance level of $p < 0.05$ and, after being tested for normality with a Shapiro–Wilk test, analysed using a non-parametric Kruskal–Wallis test. Subsequently, the differences between moderate, docile and aggressive groups were evaluated using the Wilcoxon test. The data analysed in this study are available in Supplementary File S1.

3. Results

Distribution of SERT Immunoreactivity in the Optic Lobe

The optic lobe of the honeybees, as is already known, was found to be composed of three visual neuropils: the lamina, medulla and lobula. The lamina was most peripherally located in the optic lobe, just below the retina. The lamina showed two layers: a layer of cell bodies and a fibre layer. The next neuropil sheet, the medulla, was composed of different layers (containing somata and cellular processes), including the outer and inner medulla and the serpentine layer. The third neuropil region, the lobula complex, consisted of a single neuropil. The outer chiasma connected the lamina to the medulla, whereas the inner chiasma connected the medulla to the lobula.

The honeybee optic lobe was innervated with SERT-immunoreactive fibres and demonstrated a specific pattern of innervation in the three visual neuropils: the lamina, medulla and lobula (Figures 1 and 2). In the lamina, serotonergic fibres were located in the cell body layer, where the somata of unipolar and multipolar neurons are located. The lamina exhibited many SERT-immunoreactive fibres in the layer of the fibres, which was a stratum close to the outer chiasma (Figure 2A–C).

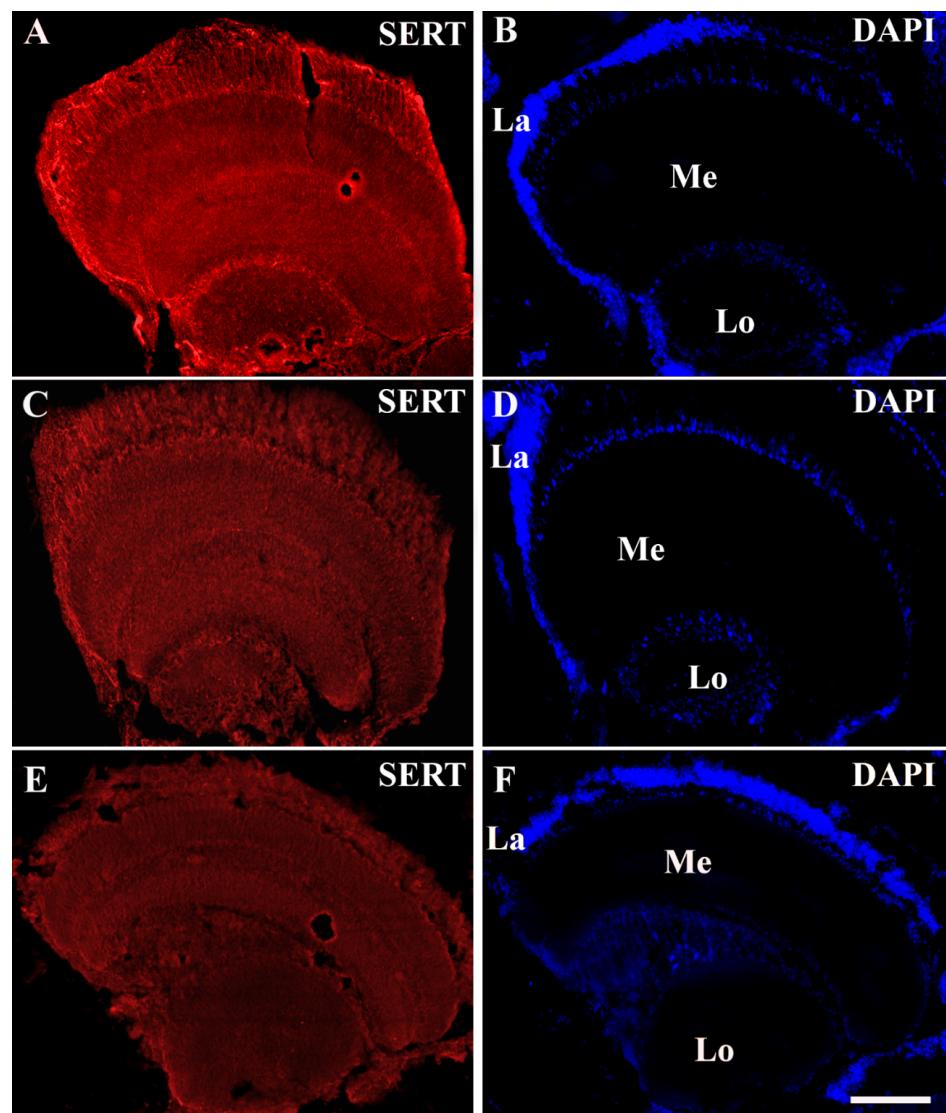


Figure 1. General appearance of serotonin transporter (SERT) immunoreactivity in the optic lobes of the docile (A,B), moderate (C,D) and aggressive (E,F) honeybees. Note that SERT immunoreactable 100 μ m. Abbreviations: La, lamina; Me, medulla; Lo, lobula.

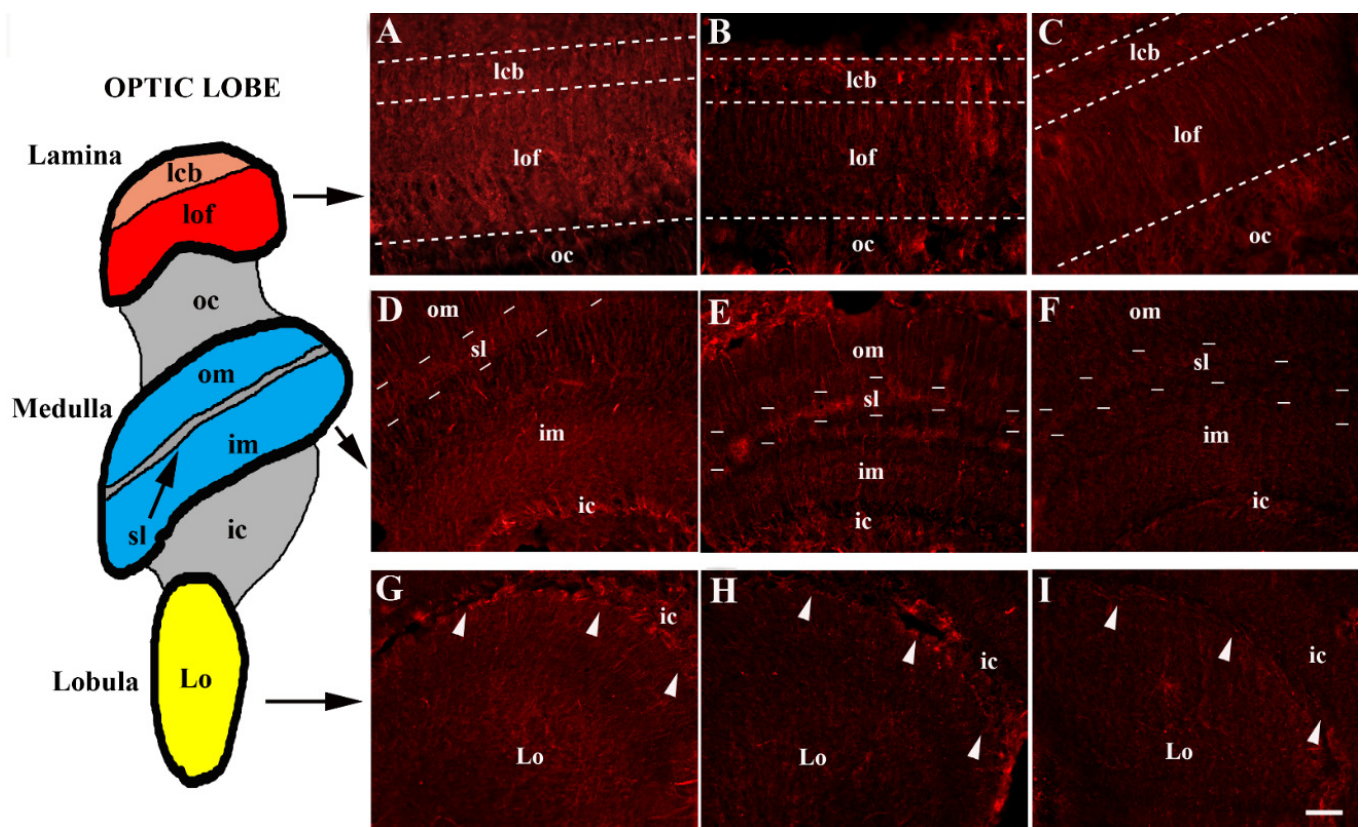


Figure 2. Distribution of serotonin transporter (SERT)-immunoreactive fibres in lamina (A–C), medulla (D–F) and lobula (G–I) of docile (A,D,G), moderate (B,E,H) and aggressive (C,F,I) honeybees. In the lamina, SERT-immunoreactive fibres were located in the cell body layer (lcb). The lamina showed many SERT-immunoreactive fibres in the layer of fibres (lof). The outer medulla (om), the serpentine layer (sl) and the inner medulla (im) contained many SERT-immunoreactive fibres distributed across the different strata of the lobula. Immunoreactive fibres were also located in the outer chiasma (oc) and inner chiasma (ic). Note that, in the lamina, medulla and lobula, the immunoreactivity for the SERT decreased from docile to aggressive honeybees. Arrowheads indicate the border between lobula and inner chiasma. Scale bar: 10 μ m.

In the medulla, serotonergic fibres were present mainly in the serpentine layer and adjacent neuropils of the outer and inner medulla (Figure 2D–F). Immunoreactive fibres were distributed in the different strata of the lobula (Figure 2G–I). Immunoreactive fibres could be observed in the outer and inner chiasmata (Figure 2).

The distribution of SERT immunoreactivity varied in the three visual neuropils (Figures 1–3). In the optic lobe of all the animal groups (moderate, docile, aggressive), the lobula was found to have the lowest percentage covered by SERT immunoreactivity ($p < 0.05$). In moderate honeybees, the percentage of the lamina covered by SERT-immunoreactivity was very similar to that in the medulla, whereas in docile honeybees, the greatest immunoreactivity was calculated in the medulla ($p < 0.05$). In contrast, in the aggressive group, the percentage covered by SERT immunoreactivity was higher in the lamina than in the medulla ($p < 0.05$).

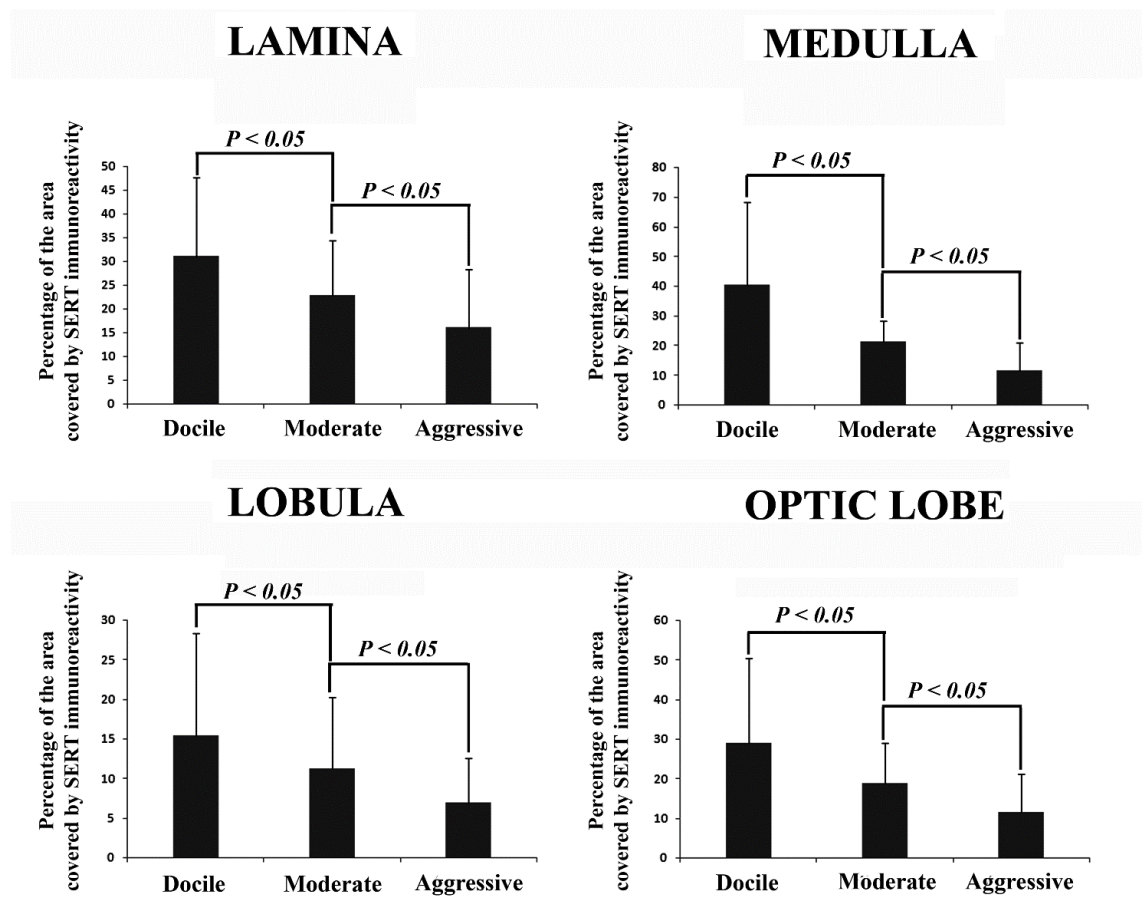


Figure 3. Histograms showing the mean percentages of the image covered by SERT immunoreactivity \pm standard deviation (SD) in the lamina, medulla and lobula and in the optic lobe as a complex for docile, moderate and aggressive honeybees.

A significant variation in SERT immunoreactivity was observed among optic lobes within the different honeybee groups (moderate, docile and aggressive). The lowest SERT immunoreactivity was observed in the aggressive group. In particular, a remarkable decrease in SERT-immunoreactive stain density was seen in all the visual neuropils of the aggressive honeybees (Figures 1–3).

4. Discussion

The optic lobe is a complex extension of the brain and represents the processing centre for visual information. It is made up of several parts, among which are the lamina (distal), the outer chiasma, the medulla, the inner chiasma and the lobula (proximal) [8,9]. In addition, the optic lobe of honeybees also regulates attention-like processes [9]. In the present work, we reported for the first time the distribution of SERT immunoreactivity in the optic lobe of honeybees. Previous studies have demonstrated the presence of serotonergic fibres in the honeybee brain using primary antibodies against serotonin [10,14]. To evaluate the density of serotonergic fibres, we preferred to use primary antibody against SERT. In fact, previous research reported that antibodies against SERT were preferable to determine serotonergic fibres, because, unlike serotonin, SERT is less liable to metabolism and, for this reason, a more stable marker to stain serotonergic fibres [15]. The stratified pattern of distribution of serotonergic fibres in the optic lobe observed in our study was similar to that observed previously using different methods [10]. However, the antibody directed against SERT labelled many fibres located in the outer and inner medulla.

Biogenic amines play a crucial role in the control of insect responsiveness. Serotonin has been repeatedly related to aggressiveness in invertebrates [20], and serotonin is a

component of aggressive behaviours [21,22]; however, the potential role of serotonin in aversive responsiveness has not been addressed until now. The presence of serotonergic fibres in the optic lobe seems to indicate their involvements in visual information processing. Accordingly, serotonin acts as a down-regulator of sting responsiveness and increases non-specific responsiveness [23]. In addition, injection of serotonin into the optic lobe inhibits the response to moving stripe patterns and decreases the amplitude of field potentials [24].

Though the specific effects of serotonin release in the optic lobe are not completely understood, our results link the serotonergic system with optic lobe-mediated behaviours. In particular, we observed that the highest and the lowest SERT immunoreactivity were located in the docile and aggressive groups, respectively. These data suggest that low levels of serotonin in the optic lobe are associated with aggressive behaviour. Interestingly, the distribution of SERT immunoreactivity varied among the three visual neuropils with the behaviour, suggesting a specific local function of serotonin in each visual neuropil.

In the optic lobe, the serotonin release determines particular effects depending on which neuron is engaged, the different kinds of synapses formed and the classes of receptors activated [6,7]. Therefore, in order to provide the basis for subsequent evaluations of the functional role of serotonin in the honeybee optic lobe, an accurate description of serotonin fibres' ultrastructure and receptor distribution is necessary.

5. Conclusions

The description of the serotonergic innervation of the optic lobe provides information for studies that seek to understand the mechanism by which serotonin modulates aggression-related behaviours through its activity in different brain regions. Though more information is needed to evaluate the functional significance of the serotonin innervation of the optic lobe, such as studies involving SERT knock-out animals, the present study demonstrates that serotonin may influence different components of optic lobe function, including aggression-related behaviours.

Supplementary Materials: The following supporting information can be downloaded at: <https://www.mdpi.com/article/10.3390/ani12162032/s1>, Supplementary File S1: Percentage of the image covered by SERT immunoreactivity.

Author Contributions: Conceptualization, G.M. and C.B.; data curation, G.S., C.B., C.T. and A.G.; formal analysis, F.M., C.T. and G.S.; funding acquisition, G.M. and C.B.; sampling, G.M. and M.G.D.I.; methodology, F.M., C.B., C.T. and A.G.; writing—original draft, C.B., G.S. and C.T.; writing—review and editing, C.B., G.S., C.T. and A.G. All authors have read and agreed to the published version of the manuscript.

Funding: This research was funded by the BEENOMIX and BEENOMIX 2.0 projects funded by the Lombardy region (FEASR program), PSR 2014–2020 (grant number 2016/00361532-G42F16000540002) and PSR (grant number 201801057971—G44I19001910002).

Institutional Review Board Statement: Not applicable.

Informed Consent Statement: Not applicable.

Data Availability Statement: Data are available in Supplementary File S1.

Acknowledgments: We thank all beekeepers and bee breeders for providing samples.

Conflicts of Interest: The authors declare no conflict of interest.

References

1. Ito, K.; Shinomiya, K.; Ito, M.; Armstrong, J.D.; Boyan, G.; Hartenstein, V.; Harzsch, S.; Heisenberg, M.; Homberg, U.; Jenett, A.; et al. A systematic nomenclature for the insect brain. *Neuron* **2014**, *81*, 755–765. [CrossRef] [PubMed]
2. Dierick, H.A.; Greenspan, R.J. Serotonin and neuropeptide F have opposite modulatory effects on fly aggression. *Nat. Genet.* **2007**, *39*, 678–682. [CrossRef] [PubMed]
3. Sitaraman, D.; Zars, M.; LaFerriere, H.; Chen, Y.-C.; Sable-Smith, A.; Kitamoto, T.; Rottinghaus, G.E.; Zars, T. Serotonin is necessary for place memory in drosophila. *Proc. Natl. Acad. Sci. USA* **2008**, *105*, 5579–5584. [CrossRef] [PubMed]

4. Scheiner, R.; Baumann, A.; Blenau, W. Aminergic control and modulation of honeybee behaviour. *Curr. Neuropharmacol.* **2006**, *4*, 259–276. [[CrossRef](#)]
5. Martin, C.A.; Krantz, D.E. *Drosophila melanogaster* as a genetic model system to study neurotransmitter transporters. *Neurochem. Int.* **2014**, *73*, 71–88. [[CrossRef](#)]
6. Tierney, A.J. Invertebrate serotonin receptors: A molecular perspective on classification and pharmacology. *J. Exp. Biol.* **2018**, *221*, jeb184838. [[CrossRef](#)]
7. Moutkine, I.; Collins, E.L.; Béchade, C.; Maroteaux, L. Evolutionary considerations on 5-HT₂ receptors. *Pharmacol. Res.* **2019**, *140*, 14–20. [[CrossRef](#)]
8. Brandt, R.; Rohlfing, T.; Rybak, J.; Krofczik, S.; Maye, A.; Westerhoff, M.; Hege, H.-C.; Menzel, R. Three-dimensional average-shape atlas of the honeybee brain and its applications. *J. Comp. Neurol.* **2005**, *492*, 1–19. [[CrossRef](#)]
9. Paulk, A.C.; Stacey, J.A.; Pearson, T.W.J.; Taylor, G.J.; Moore, R.J.D.; Srinivasan, M.V.; van Swinderen, B. Selective attention in the honeybee optic lobes precedes behavioral choices. *Proc. Natl. Acad. Sci. USA* **2014**, *111*, 5006–5011. [[CrossRef](#)]
10. Schürmann, F.W.; Klemm, N. Serotonin-immunoreactive neurons in the brain of the honeybee. *J. Comp. Neurol.* **1984**, *225*, 570–580. [[CrossRef](#)]
11. Thamm, M.; Balfanz, S.; Scheiner, R.; Baumann, A.; Blenau, W. Characterization of the 5-HT_{1A} receptor of the honeybee (*Apis mellifera*) and involvement of serotonin in phototactic behavior. *Cell. Mol. Life Sci.* **2010**, *67*, 2467–2479. [[CrossRef](#)] [[PubMed](#)]
12. Thamm, M.; Rolke, D.; Jordan, N.; Balfanz, S.; Schiffer, C.; Baumann, A.; Blenau, W. Function and distribution of 5-HT₂ receptors in the honeybee (*Apis mellifera*). *PLoS ONE* **2013**, *8*, e82407. [[CrossRef](#)] [[PubMed](#)]
13. Erber, J.; Kloppenburg, P. The modulatory effects of serotonin and octopamine in the visual system of the honey bee (*Apis mellifera* L.). *J. Comp. Physiol. A* **1995**, *176*, 119–129. [[CrossRef](#)]
14. Seidel, C.; Bicker, G. The developmental expression of serotonin-immunoreactivity in the brain of the pupal honeybee. *Tissue Cell* **1996**, *28*, 663–672. [[CrossRef](#)]
15. Nielsen, K.; Brask, D.; Knudsen, G.M.; Aznar, S. Immunodetection of the serotonin transporter protein is a more valid marker for serotonergic fibers than serotonin. *Synapse* **2006**, *59*, 270–276. [[CrossRef](#)] [[PubMed](#)]
16. Buchler, R.; Andonov, S.; Bienefeld, K.; Costa, C.; Hatjina, F.; Kezic, N.; Kryger, P.; Pivak, M.; Uzunov, A.; Wilde, J. Standard methods for rearing and selection of *Apis mellifera* queens. *J. Apic. Res.* **2013**, *52*, 1–30. [[CrossRef](#)]
17. Uzunov, A.; Büchler, R.; Bienefeld, K. *Performance Testing Protocol. A Guide for European Honey Bee Breeders*, 1st ed.; Landesbetrieb Landwirtschaft Hessen: Kirchhain, Germany, 2015.
18. Uzunov, A.; Brascamp, E.W.; Buchler, R. The basic concept of honey bee breeding programs. *Bee World* **2017**, *94*, 84–87. [[CrossRef](#)]
19. Hoppe, A.; Du, M.; Bernstein, R.; Tiesler, F.K.; Kärcher, M.; Bienefeld, K. Substantial genetic progress in the international *Apis mellifera carnica* population since the implementation of genetic evaluation. *Insects* **2020**, *11*, 768. [[CrossRef](#)]
20. Kravitz, E.A.; Huber, R. Aggression in invertebrates. *Curr. Opin. Neurobiol.* **2003**, *13*, 736–743. [[CrossRef](#)]
21. Bubak, A.N.; Watt, M.J.; Yaeger, J.D.W.; Renner, K.J.; Swallow, J.G. The stalk-eyed fly as a model for aggression—Is there a conserved role for 5-HT between vertebrates and invertebrates? *J. Exp. Biol.* **2020**, *223*, jeb132159. [[CrossRef](#)]
22. Poetini, M.R.; Musachio, E.A.S.; Araujo, S.M.; Almeida, F.P.; Dahleh, M.M.M.; Bortolotto, V.C.; Janner, D.E.; Pinheiro, F.C.; Ramborger, B.P.; Roehrs, R.; et al. Iron overload during the embryonic period develops hyperactive like behavior and dysregulation of biogenic amines in *drosophila melanogaster*. *Dev. Biol.* **2021**, *475*, 80–90. [[CrossRef](#)] [[PubMed](#)]
23. Tedjakumala, S.R.; Aimable, M.; Giurfa, M. Pharmacological modulation of aversive responsiveness in honey bees. *Front. Behav. Neurosci.* **2014**, *7*, 221. [[CrossRef](#)] [[PubMed](#)]
24. Birmingham, J.T.; Tauck, D.L. Neuromodulation in invertebrate sensory systems: From biophysics to behavior. *J. Exp. Biol.* **2003**, *206*, 3541–3546. [[CrossRef](#)] [[PubMed](#)]

Chapter 5:
Expression of Cannabinoid Receptors in the Trigeminal Ganglion of the Horse



Article

Expression of Cannabinoid Receptors in the Trigeminal Ganglion of the Horse

Rodrigo Zamith Cunha ¹, Alberto Semprini ¹, Giulia Salamanca ¹, Francesca Gobbo ¹, Maria Morini ¹, Kirstie J. Pickles ², Veronica Roberts ³ and Roberto Chiochetti ^{1,*}

- ¹ Department of Veterinary Medical Sciences, University of Bologna, 37200 Bologna, Italy; rodrigozamithcunha@gmail.com (R.Z.C.); alberto.semprini2@studio.unibo.it (A.S.); giulia.salamanca2@unibo.it (G.S.); francesca.gobbo3@unibo.it (F.G.); maria.morini@unibo.it (M.M.)
² School of Veterinary Medicine and Science, University of Nottingham, Nottingham LE12 5RD, UK; kirstie.pickles@nottingham.ac.uk
³ Bristol Vet School, University of Bristol, Bristol BS40 5DU, UK; veronica.roberts@bristol.ac.uk
* Correspondence: roberto.chiochetti@unibo.it

Abstract: Cannabinoid receptors are expressed in human and animal trigeminal sensory neurons; however, the expression in the equine trigeminal ganglion is unknown. Ten trigeminal ganglia from five horses were collected post-mortem from an abattoir. The expression of cannabinoid receptors type 1 (CB1R) and type 2 (CB2R), and the cannabinoid-related receptors like transient receptor potential vanilloid type 1 (TRPV1), peroxisome proliferator-activated receptor gamma (PPAR γ), and G protein-related receptor 55 (GPR55) in the trigeminal ganglia (TG) of the horse were studied, using immunofluorescence on cryosections and formalin-fixed paraffin-embedded (FFPE) sections. Neurons and glial cells were identified using fluorescent Nissl staining NeuroTrace[®] and an antibody directed against the glial marker glial fibrillary acidic protein (GFAP), respectively. Macrophages were identified by means of an antibody directed against the macrophages/microglia marker ionized calcium-binding adapter molecule 1 (IBA1). The protein expression of CB1R, CB2R, TRPV1, and PPAR γ was found in the majority of TG neurons in both cryosections and FFPE sections. The expression of GPR55 immunoreactivity was mainly detectable in FFPE sections, with expression in the majority of sensory neurons. Some receptors were also observed in glial cells (CB2R, TRPV1, PPAR γ , and GPR55) and inflammatory cells (PPAR γ and GPR55). These results support further investigation of such receptors in disorders of equine trigeminal neuronal excitability.

Keywords: cannabidiol; equine; immunofluorescence; G protein-related receptor 55; peroxisome proliferator-activated receptor gamma; transient receptor potential vanilloid type 1



Citation: Zamith Cunha, R.; Semprini, A.; Salamanca, G.; Gobbo, F.; Morini, M.; Pickles, K.J.; Roberts, V.; Chiochetti, R. Expression of Cannabinoid Receptors in the Trigeminal Ganglion of the Horse. *Int. J. Mol. Sci.* **2023**, *24*, 15949. <https://doi.org/10.3390/ijms242115949>

Academic Editors: Deanne H. Hryciw and Birgit Abler

Received: 10 September 2023
Revised: 17 October 2023
Accepted: 31 October 2023
Published: 3 November 2023



Copyright: © 2023 by the authors. Licensee MDPI, Basel, Switzerland. This article is an open access article distributed under the terms and conditions of the Creative Commons Attribution (CC BY) license (<https://creativecommons.org/licenses/by/4.0/>).

1. Introduction

The most common neuropathic facial pain disorder in horses is trigeminal-mediated (TGM) headshaking, with a reported prevalence of 4% in the United Kingdom equine population [1]. Equine TGM headshaking shares some clinical similarities with human trigeminal neuralgia. However, the underlying pathological mechanisms of TGM headshaking in horses appear to differ from human trigeminal neuralgia, with a functional rather than structural abnormality [2]. Detailed nerve conduction studies of control and headshaking horses identified that the infraorbital branch of the trigeminal nerve in affected horses was sensitised, with a lower threshold for activation than non-affected horses [3].

Research in human trigeminal neuralgia has explored the involvement of the neuromodulatory endocannabinoid system (ECS) [4]. The ECS comprises endocannabinoid molecules involved in signaling processes, along with receptors such as the cannabinoid type 1 (CB1R) and type 2 (CB2R) receptors, and enzymes associated with ligand biosynthesis, activation, and degradation. Cannabinoids derived from *Cannabis sativa*, including cannabidiol (CBD), cannabigerol, cannabichromene, and cannabinol, as well as synthetic

cannabinoids, act on these receptors and other cannabinoid-related receptors such as transient receptor potential (TRP) channels, nuclear peroxisome proliferator-activated receptors (PPARs), and G protein-coupled receptors (GPRs) [5,6].

There is existing evidence suggesting that cannabinoids may effectively alleviate neuropathic pain and hyperalgesia by inhibiting neuronal transmission in pain pathways [7,8]. Although there is a paucity of university-led research on cannabis therapy in equines, in recent years, some interesting studies have shown beneficial therapeutic effects of cannabinoid molecules in horses with allodynia [9], degenerative painful conditions such as osteoarthritis and laminitis [10,11], and also behavioral disturbances [12]. Consequently, considering the pronounced antinociceptive effects of cannabinoids, they could represent a promising therapeutic approach for the clinical management of TGM headshaking, should the appropriate receptors be expressed in the equine trigeminal ganglion. While the localisation of these receptors has been demonstrated in sensory neurons of the equine dorsal root ganglion [13,14], their distribution within the equine trigeminal ganglion is unknown. Therefore, this study aims to immunohistochemically characterise the expression of cannabinoid receptors (CB1R and CB2R) and cannabinoid-related receptors, including TRPV1, PPAR γ , and GPR55, in cryosections and formalin-fixed paraffin-embedded (FFPE) sections of the equine trigeminal ganglion.

2. Results

To the authors' knowledge, the somatotopic organization of the trigeminal nerve and ganglia of the horse has never been investigated; therefore, a portion of the ganglion has been sampled and processed in both cryosections and FFPE. In all sections under examination, there was a voluminous portion of ganglion tissue (with the neuronal component) and a small portion of the adjacent trigeminal nerve (trigeminal root) at the division of the three branches (ophthalmic, maxillary, and mandibular). No differences in immunolabelling were observed across the whole TG examined in all samples.

The immunoreactivity (IR) of all the studied receptors was visible in both the cryosections and the FFPE sections. In cryosections, all the receptors were widely distributed in neurons, with PPAR γ being the most represented receptor in neurons ($95 \pm 8\%$), followed by TRPV1 ($90 \pm 13\%$), CB2R ($87 \pm 18\%$), and CB1R ($80 \pm 12\%$). Since the expression of the GPR55-IR was faint or undetectable in the cryosections of all the subjects analysed, the proportion of TG neurons expressing GPR55-IR was not evaluated; however, the GPR55-IR was more evident in FFPE (see below).

Although the low number of horses from which samples were obtained precludes quantitative evaluation, receptors appeared to have lower expression in older subjects.

Some receptors were also distributed in satellite glial cells (SGCs), vascular cells, and immune/inflammatory cells.

2.1. Immunoreactivity in Neurons—Cryosections

Cannabinoid receptor-1 immunofluorescence was faintly expressed by the cell body cytoplasm of $80 \pm 12\%$ sensory neurons (440/556 cells counted, $n = 5$) and by large nerve fibres (Figure 1a–c). In some neurons, CB1R-IR was also displayed on the cell membrane (Figure 1d–f). Faint CB1R-IR was also expressed by the nucleoli of sensory neurons.

Cannabinoid receptor-2 immunofluorescence was brightly expressed by the cell body cytoplasm of $87 \pm 18\%$ sensory neurons (448/517 cells counted, $n = 5$) and by nerve fibres (Figure 1g–i). Satellite glial cells showed faint CB2R-IR.

Transient receptor potential vanilloid-1 immunofluorescence was brightly expressed by the cell body cytoplasm of $90 \pm 13\%$ neurons (496/553 cells counted, $n = 5$) (Figure 2a–c). The TRPV1 immunolabelling was also visible in the growing tip of the axon (axon hillock) and the nerve fibres surrounding the TG sensory neurons (Figure 2d–f). Satellite glial cells showed faint TRPV1-IR.

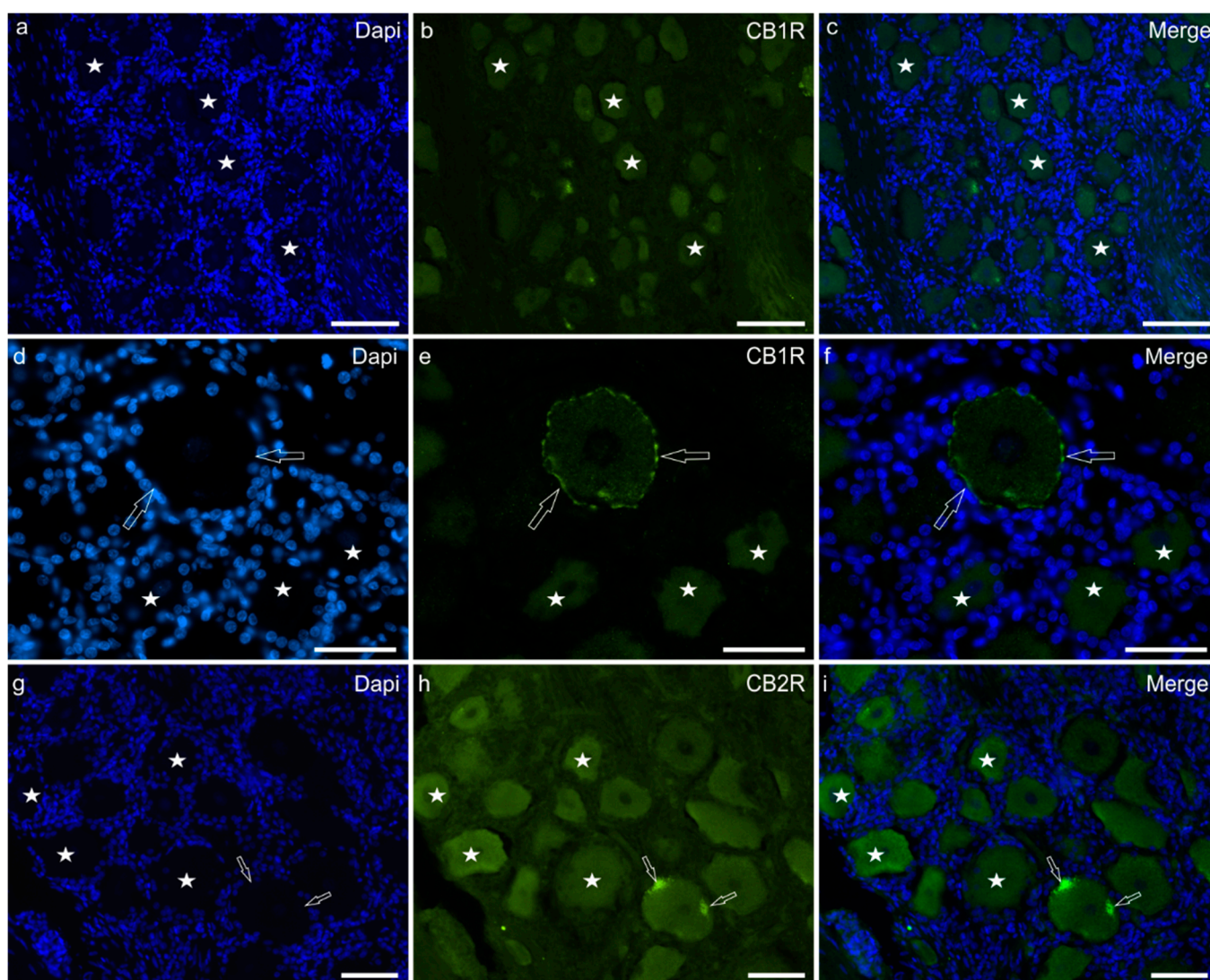


Figure 1. Photomicrographs of equine trigeminal ganglion cryosections showing immunoreactivity for the cannabinoid receptor type 1 (CB1R) (a–f) and type 2 (CB2R) (g–i). (a–f) Stars indicate a few sensory neurons showing faint cytoplasmic CB1R immunoreactivity of the cell body cytoplasm. The open arrows indicate a neuron in which CB1R immunoreactivity was also expressed by the cell membrane. (g–i) Stars indicate neurons expressing moderate CB2R immunoreactivity. Two open arrows indicate autofluorescent pigments which were confined to the edges of the cell. Bar: 50 μ m.

Peroxisome proliferator-activated receptor gamma immunofluorescence was expressed by the nuclei of the great majority ($95 \pm 8\%$) of sensory neurons (509/535 cells counted, $n = 5$) (Figure 2g–i). However, not all the neuronal nuclei showed the same degree of labelling; in fact, in some cells, the nuclei were moderately reactive, while in other neurons, the expression of PPAR γ was bright.

G protein-related receptor-55 immunofluorescence was faint or undetectable within the cell body cytoplasm of the TG neurons. For this reason, the count of GPR55 immunolabelled neurons was not possible.

In cryosections, faint CB2-IR was expressed by the cytoplasm of SGCs. Bright PPAR γ -IR was expressed by the nuclei of SGCs, as also shown by the co-localisation of the anti-PPAR γ and the anti-GFAP antibodies (Figure 3a–d).

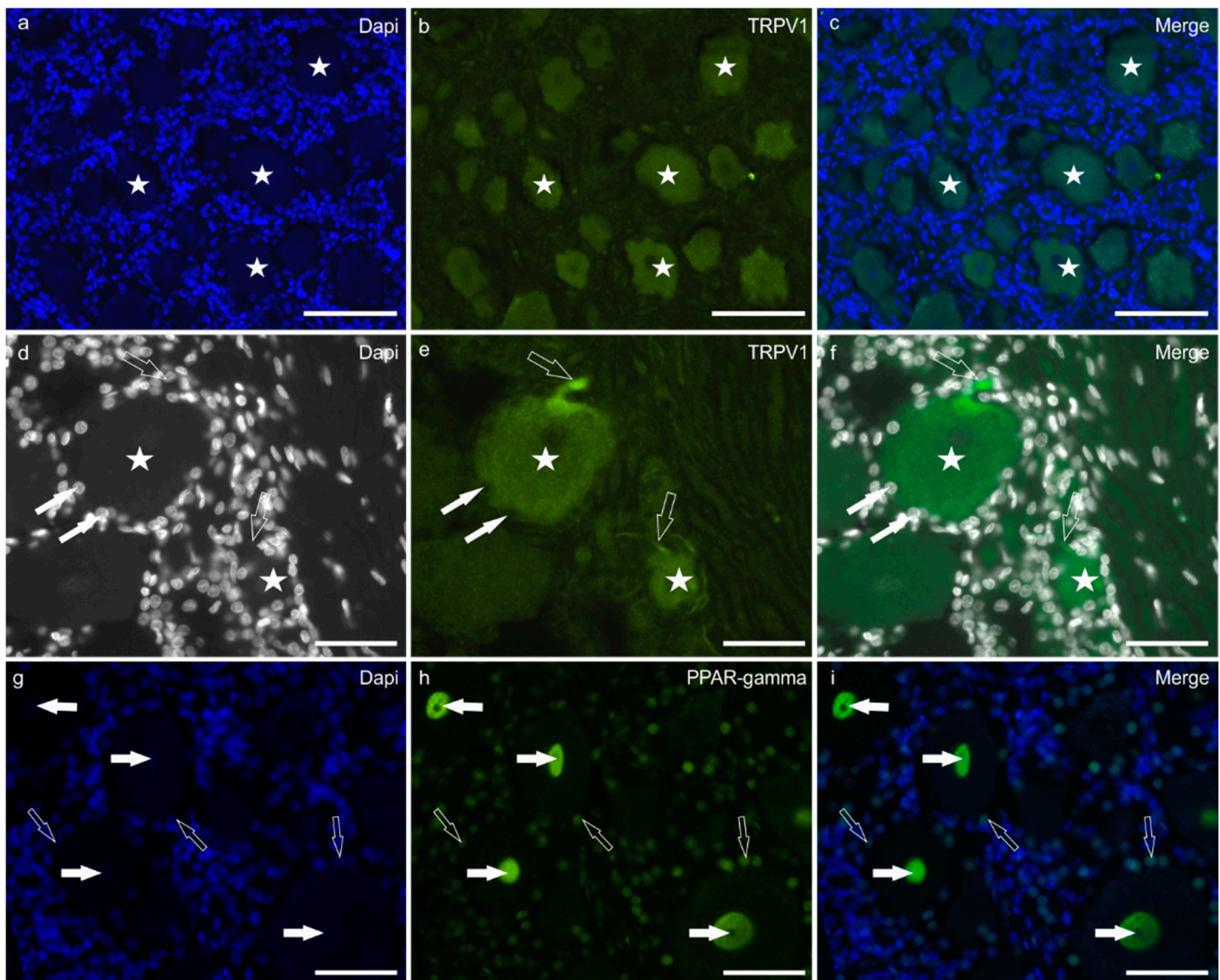


Figure 2. Photomicrographs of equine trigeminal ganglion cryosections showing immunoreactivity for the cannabinoid-related receptor TRPV1 (transient receptor potential vanilloid 1) (a–f), and PPARγ (Peroxisome proliferator-activated receptor gamma) (g–i). (a–f) Stars indicate sensory neurons expressing moderate-to-bright TRPV1 immunoreactivity. The white arrows indicate the Dapi labelled nuclei of satellite glial cells surrounding a large neuron expressing faint TRPV1 immunoreactivity. The open arrows indicate two TRPV1 immunoreactive axon hillocks arising from two sensory neurons. (g–i) The white arrows indicate neuronal nuclei expressing bright PPARγ immunoreactivity. The open arrows indicate the nuclei of satellite glial cells showing moderate PPARγ immunoreactivity. Bar: 50 μm.

Peroxisome proliferator-activated receptor gamma immunofluorescence was also expressed by the nuclei of interneuronal cells, likely macrophages, as shown by the co-localisation of the anti-PPARγ with the anti-IBA1 antibodies (Figure 3e–h).

Numerous inflammatory/immune cells, which were distributed around and between sensory neurons, showed bright GPR55-IR. However, GPR55-IR was not observed in IBA1-IR cells.

2.2. Immunoreactivity in Neurons—FFPE Sections

Cannabinoid receptor 1 immunoreactivity was faintly expressed by the cell body cytoplasm of $63 \pm 11\%$ (288/459 cells counted, $n = 4$) sensory neurons, and by the nucleolus of sensory neurons. No CB1R-IR was expressed by nerve fibres (Figure 4a).

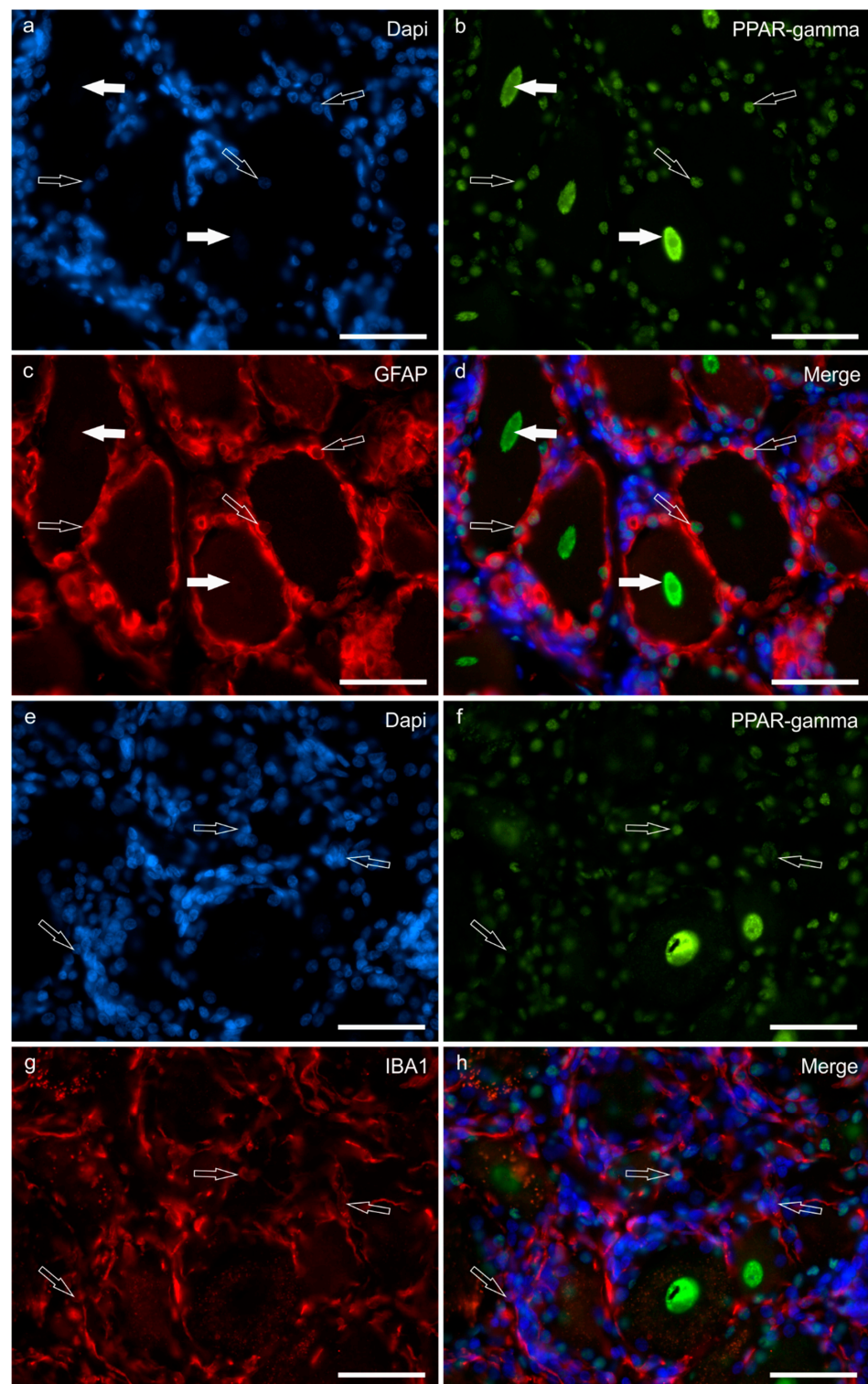


Figure 3. Photomicrographs of equine trigeminal ganglion cryosections showing the co-localisation between the antibody anti-PPAR γ (Peroxisome proliferator-activated receptor gamma) and the satellite glial cells marker GFAP (glial acidic fibrillary protein), (a–d) and between the antibody anti-PPAR γ and the macrophage marker IBA1 (e–h). (a–d) The white arrows indicate two neuronal nuclei showing bright PPAR γ immunoreactivity; the open arrows indicate the dapi labelled nuclei of GFAP immunoreactive satellite glial cells showing moderate PPAR γ immunoreactivity. (e–h) The open arrows indicate the dapi labelled nuclei of IBA1 immunoreactive macrophages which co-expressed PPAR γ immunoreactivity. Bar: 50 μ m.

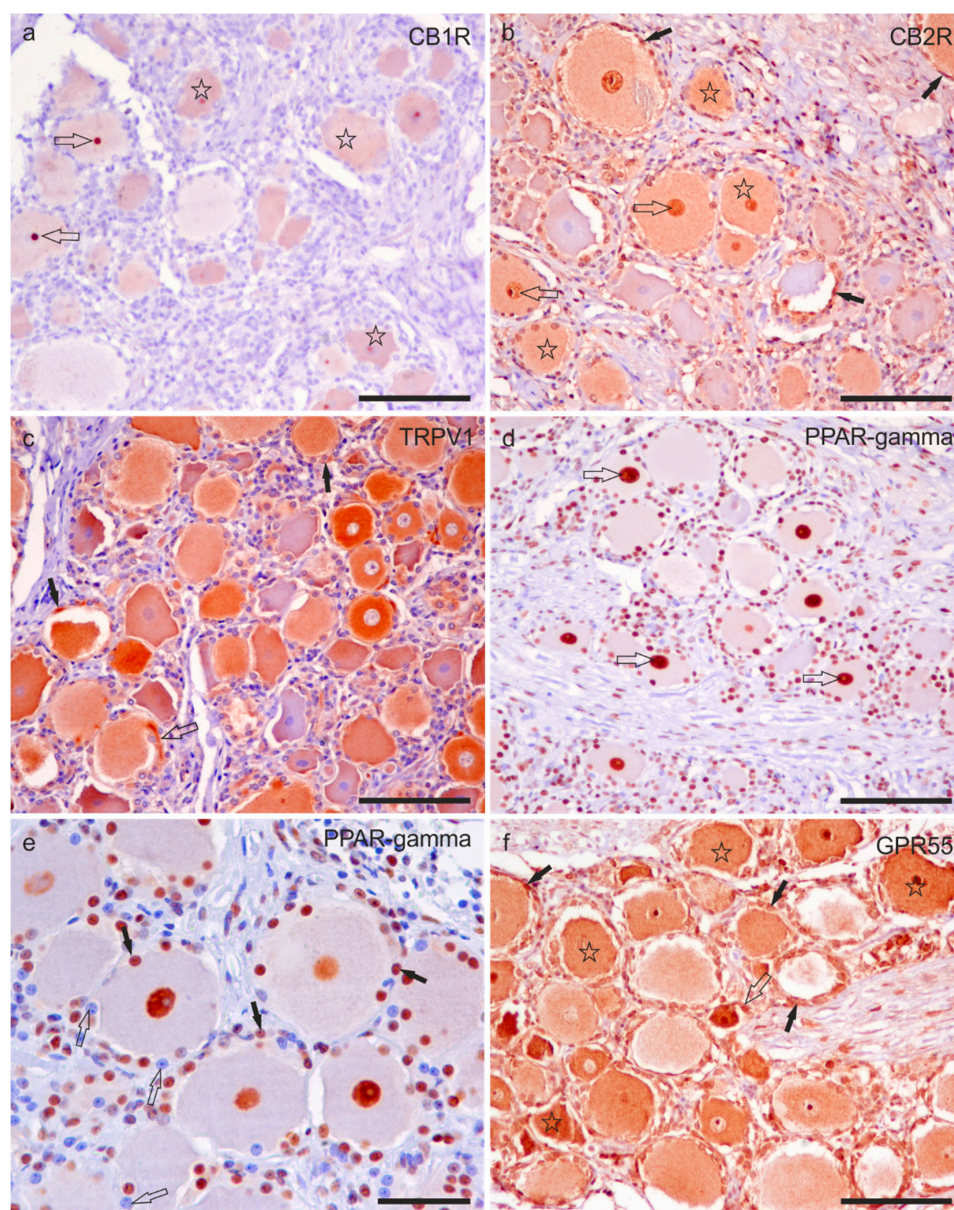


Figure 4. Photomicrographs of formalin-fixed paraffin embedded sections of equine trigeminal ganglion showing immunoreactivity for the cannabinoid receptor type 1 (CB1R) (a) and type 2 (CB2R) (b), transient receptor potential vanilloid 1 (TRPV1) (c), peroxisome proliferator-activated receptor gamma (PPAR γ) (d,e), and G-protein coupled receptor 55 (GPR55) (f). (a) Stars indicate sensory neurons showing faint CB1R immunoreactivity. The open arrows indicate two strongly immunoreactive nucleoli for the CB1R. (b) Stars indicate sensory neurons which showed moderate CB2R immunoreactivity. The open arrows indicate the neuronal nuclei expressing strong CB2R immunoreactivity. Black arrows show satellite glial cells surrounding the sensory neurons, showing faint-to-moderate CB2R immunoreactivity. (c) A large proportion of sensory neurons expressed moderate-to-strong TRPV1 immunoreactivity. Axon hillocks (open arrow) were also positive for TRPV1, as well as satellite glial cells (black arrows). (d) The open arrows indicate the nuclei of the sensory neurons, showing strong PPAR γ immunoreactivity. (e) Not all nuclei of satellite glial cells showed PPAR γ immunoreactivity; some were strongly reactive (black arrows), whereas some appeared negative (open arrows). (f) Stars indicate the cell body cytoplasm of sensory neurons with moderate-to-strong GPR55 immunoreactivity. The open arrows indicate the axon hillock of a small neuron which expressed strong GPR55 immunoreactivity. The black arrows indicate some satellite glial cells which were positive for GPR55. Bars: (a–d,f): 100 μ m; (e): 50 μ m.

Moderate-to-strong CB2R-IR was expressed by the cell body cytoplasm of $72 \pm 12\%$ (288/402 cells counted, $n = 4$) sensory neurons and by the nucleus of sensory neurons, as well as by the nuclei of SGCs (Figure 4b) and Schwann cells.

Moderate-to strong TRPV1-IR was observed in the cell body cytoplasm of $81 \pm 9\%$ (355/435 cells counted, $n = 4$) of sensory neurons and in the nerve fibres (Figure 4c).

Peroxisome proliferator-activated receptor gamma immunoreactivity with strong intensity was expressed by the neuronal nuclei of $87 \pm 6\%$ (284/328 cells counted, $n = 4$) of sensory neurons (Figure 4d,e). It was also expressed by the nuclei of Schwann cells.

G protein-related receptor 55 immunoreactivity was localised in the cell body cytoplasm of $92 \pm 8\%$ (304/328 cells counted, $n = 4$) of sensory neurons and by the nuclei of sensory neurons; the immunolabelling was moderate to strong (Figure 4f).

Satellite glial cells showed cytoplasmic CB2R-, TRPV1- and GPR55-IR, and nuclear PPAR γ -IR (Figure 4b–f). Notably, not all the SGCs showed PPAR γ -IR (Figure 3e).

Small perineuronal and interneuronal immune/inflammatory cells showed a strong cytoplasmic GPR55- and PPAR γ -IR.

Figure 5 shows the graphical representation of the distribution of CB1R, CB2R, TRPV1, GPR55, and PPAR γ in the different cellular elements of the equine TG cells.

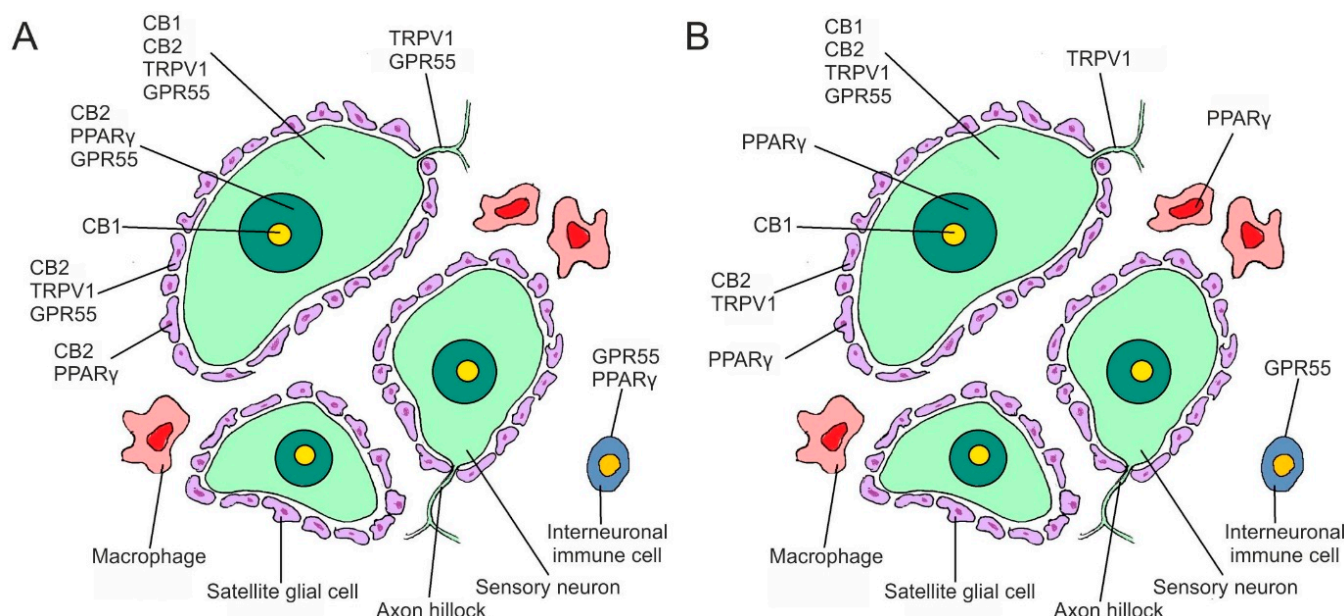


Figure 5. Graphical representation of the distribution of the cannabinoid receptors 1 (CB1R) and 2 (CB2R), and the cannabinoid-related receptors transient receptor potential vanilloid 1 (TRPV1), G protein-coupled receptor 55 (GPR55), and nuclear peroxisome proliferator-activated receptor gamma (PPAR γ), in the different cellular elements of the equine trigeminal ganglion. (A): Expression of immunofluorescence in cryosections; (B): Expression of immunohistochemistry on formalin-fixed paraffin-embedded sections.

Table 1 shows the semiquantitative evaluation of the density of CB1R, CB2R, TRPV1, GPR55, and PPAR-gamma immunoreactivity in different cellular elements of the equine trigeminal ganglia.

Table 1. Semiquantitative evaluation of the density of CB1R, CB2R, TRPV1, GPR55, and PPAR- γ immunoreactivity in different cellular elements of the equine trigeminal ganglia. The immunoreactive cells were graded as: –, negative; +, faint; ++, moderate; +++, bright. Abbreviations: Cryo, cryosections; FFPE, formalin fixed paraffin embedded sections, IF, immunofluorescence; IHC, immunohistochemistry.

Receptors	CB1R	CB2R	TRPV1	GPR55	PPAR- γ
Neurons	+ IF Cryo + IHC iFFPE	++ IF Cryo ++ IHC FFPE	+++ IF Cryo +++ IHC FFPE	+/- IF Cryo ++/+++ IHC FFPE	+++ IF Cryo +++ IHC FFPE
Satellite glial cells	– IF Cryo – IHC FFPE	++ IF Cryo +++ IHC FFPE	– IF Cryo – IHC FFPE	– IF Cryo ++ IHC FFPE	+++ IF Cryo +++ IHC FFPE
Inflammatory or immune cells	– IF Cryo – IHC FFPE	– IF Cryo – IHC FFPE	– IF Cryo – IHC FFPE	– IF Cryo +++ IHC FFPE	+++ IF Cryo +++ IHC FFPE

3. Discussion

Chronic neuropathic pain is characterised by spontaneous pain and hypersensitivity, manifested as hyperalgesia and allodynia, and is often refractory to conventional analgesics and even pharmaceuticals specific for neuropathic pain. Neuropathic pain therefore, most of the time, represents an unmet therapeutic need. Trigeminal-mediated headshaking is likely to be the most common neuropathic facial condition causing pain in horses [1]. It can be a significant source of pain, compromised welfare, and wastage in horses, alongside safety concerns for riders and handlers. Therefore, elucidating better, more rational treatments to alleviate this condition is of paramount importance. The ECS plays a major role in the pain trafficking pathway, at both central and peripheral levels, and modification of this system may open novel therapeutic targets [15,16]. To date, it is known that cannabis-based drugs have important therapeutic potential in people, not only in treating inflammatory diseases (such as osteoarthritis and inflammatory bowel disease), in dermatological diseases such as atopic dermatitis and psoriasis, but also in neurodegenerative diseases such as Alzheimer's, multiple sclerosis and Parkinson's, and neurological pathologies that induce seizures and eating disorders [17–19]. Cannabinoid-based drugs may also be useful in human trigeminal neuralgia [7,20,21]. Recently, Longworth et al. [21] reported that cannabis-based medicines offered therapeutic benefits in 6 out of 8 treatments for people with chronic facial pain, and in all cases, they did not cause undesirable effects.

While there are studies reporting the expression of cannabinoid receptors, endocannabinoids, and their related enzymes in the TG of rodents, and the therapeutic efficacy of CBD in modulating nociceptive transmission and head pain [16,22,23], research on the ECS in the nervous system of horses is in its infancy. Although interesting electrophysiological studies on trigeminal nerve conduction in horses are available [3,24], no functional studies related to the influence of the ECS on the mechanisms of neuropathic pain have been published. In rodents, endocannabinoids may inhibit the trigeminal release of neuropeptides that control nociceptive inputs through a CB1R-dependent mechanism [25]. Since the expression of neuropeptides regulating the nociceptive pathways has been also described in horse sensory neurons [26], it is plausible to hypothesize that the ECS might act with a similar mechanism in this species.

The evidence that cannabinoid receptors (CB1 and CB2) and cannabinoid-related receptors (TRPV1, PPAR γ , and GPR55) are extensively expressed in the majority of equine trigeminal ganglion neurons is indeed an encouraging discovery. In the present study, two different methodological procedures were applied to detect the cannabinoid and cannabinoid-related receptors in the trigeminal ganglia, i.e., immunofluorescence on cryosections and immunohistochemistry on FFPE sections; as these receptors are molecules that could be degraded by the processes used for paraffin embedding. The fact that the antibodies were able to identify neurons in paraffin-fixed tissues is an encouraging finding, which will allow for future comparisons of labelling with TG obtained from horses with

TGM headshaking, where tissues were collected and processed using standard techniques for paraffin embedding.

Immunoreactivity in Trigeminal Neurons

Cannabinoid receptor-1 is widely expressed in the nervous pathways of the nociceptive system of rodents [22,23,27–29], and in other mammals, including dogs [30] and horses [13]. While in rats, CB1R is expressed almost exclusively by myelinated neurons in both the TG [22] and DRG [28], in horses the receptor seems to be localised in neurons of different dimensions.

Cannabinoid receptor-1 can be activated by endogenous and exogenous cannabinoids, and it can modulate the release of nociceptive neurotransmitters. Several studies have shown that CB1 receptor activation by endocannabinoids causes depression of neuronal excitability and neurotransmitter release in presynaptic primary neurons [31,32]. However, there is contradictory evidence showing that endocannabinoids may also contribute to the potentiation of neurotransmission through CB1 receptors, as shown by Zhang et al. [33], who found that the endocannabinoid anandamide (AEA) may cause elevation of the intracellular Ca²⁺ concentration in the small neurons of the rat TG. Another study, which was undertaken to elucidate the effects of certain cannabinoids on nociceptive TG cultured neurons, showed that the predominant effects of AEA on TG nociceptors were excitatory, and in part, also mediated by TRPV1 [34]. Alternatively, Akerman et al. [35] showed that the cannabinoid receptor agonist WIN55,212, which acts on both CB1 and CB2 receptors, was able to significantly inhibit the activation of trigeminal neurons by electrical stimulation of the dura mater by acting and inhibiting neurons with A-fiber and C-fiber inputs. All of these findings highlight the necessity for further study of the ECS as it relates to nociception, with particular attention to the role of CB1R in sensory neurons.

Cannabinoid receptor-2 was initially considered a ‘peripheral cannabinoid receptor’, since it is abundantly expressed in the immune system, including in horses [14]. However, a growing body of evidence indicates that CB2R is not only expressed in brain microglia during neuroinflammation [36], but is also expressed in peripheral sensory neurons, as shown in humans [37], rats [23,30], and horses [13]. Cannabinoid receptor-2 shows vast therapeutic potential. The most promising indications include neuropathic pain, in which CB2R agonists have proven helpful [38,39]. Therefore, the finding that a large proportion of equine TG neurons express CB2R (as seen in the current study) reinforces the evidence that CB2R may play a great role in pain modulation in horses, as also proposed by Sánchez-Aparicio et al. [10].

In both a former study [13] and the current one, CB2R-IR has also been expressed by SGCs; this evidence is consistent with that described in rat sensory neurons [40].

The TRP vanilloid 1 (TRPV1) ion channel is usually expressed by DRG nociceptors of mammals [30,41–43], including horses [14]. In rats, TRPV1 receptors are known to be present in trigeminal neurons with C-fibre inputs [44]. It has been suggested that the role of TRPV1 in neuropathic pain may include sensitisation of intact peripheral terminals, ectopic activity in injured axons (through the activation of axonal TRPV1 receptors), or a contribution to the modulation of transmitter release [45].

It has been shown that TRPV1 antagonists reduced pain sensitivity in models of neuropathic pain [46] and provided pain relief in models of inflammatory pain [47]. In addition, the desensitisation of TRPV1 located in DRG and TG has exhibited analgesic effects, making it a potential therapeutic target for the treatment of neuropathic pain [48].

A recent study has suggested a role for TRPV1 channels in the modulation of synaptic transmission through activation by endocannabinoids, such as anandamide [49]. Additionally, endocannabinoid-like molecules and endovanilloids can desensitise TRPV1, as well as phytocannabinoids such as CBD [50], which shows anti-nociceptive, analgesic, and anti-inflammatory effects [51].

Peroxisome Proliferator Activated Receptor γ , like the other PPAR receptors, acts as a transcription factor, modulating various physiological functions, including lipid

metabolism. It is principally expressed in fatty and vascular tissue [52]; however, it has also been localised in brain tissue, where its activation reduced neurodegeneration [53]. There is some evidence indicating that PPAR γ plays a beneficial role in various neurological diseases and that its activation may represent a potential target for the treatment of numerous acute and chronic neurological diseases [54]. Indeed, the activation of PPAR γ has reduced neuroinflammation in neuropathic pain [55,56]. The role of PPAR γ during inflammatory compression of the trigeminal nerve was investigated by Lyons et al. [57], who demonstrated its important role in pain sensitivity and alleviation of allodynia with PPAR γ agonists. A further study suggests that drugs targeting spinal PPAR γ may yield important therapeutic effects for neuropathic pain [58]. Cannabinoids produce analgesic effects by acting on multiple pain targets in the peripheral and central nervous systems [59]. Cannabidiol, particularly CBD, due to its interaction with PPAR γ , may be useful for treating neuropathic pain [60,61].

In studies performed on equine spinal ganglia, immunoreactivity for the PPAR γ receptor was expressed by sensory neurons, SGC, and other unidentified interneuronal cells [13,14]. The data reported in the current study on horse TG are consistent with those expressed by the spinal ganglia. The localisation of PPAR γ -IR in SGCs of the horse TG may play an important role in ganglion functional homeostasis, as also indicated in mice by Chu et al. [62]. Also, the expression of PPAR γ -IR in the macrophages of the horse TG seems to be an interesting finding, as there are observations suggesting that PPAR γ signaling in macrophages may be a potential therapeutic target for the treatment of acute pain development [63,64].

G protein-coupled receptor 55 (GPR55), which researchers have proposed classifying as a third cannabinoid receptor [65,66], has been identified in the sensory neurons of different species, including dogs, rats [30], and horses [14], and in canine inflammatory cells [67]. While in cryosections, the GPR55 signal was so faint that it prevented cell counting; in FFPE sections, GPR55-IR was strongly expressed (see below).

Unexpectedly, GPR55-IR was not observed in IBA1-IR cells, as previously shown in the horse DRG [14]. This evidence indicates that macrophages (or dendritic or microglia cells) of the equine TG do not express GPR55-IR. However, GPR55-IR has been observed in unidentified inflammatory/immune cells in both cryosections and FFPE sections of the TG, suggesting an active role of the receptor in TG homeostasis and immunity.

In a recent study in mice, GPR55 signaling contributed to the induction of inflammatory responses and chronic pain via the recruitment of neutrophils, monocytes/macrophages, and T-cells, possibly providing a new target for reducing pain [68]. Another study reported that GPR55-KO mice did not develop mechanical pain in chronic pain models developed by peripheral nerve injury and peripheral tissue inflammation [69]. Therefore, molecules that block GPR55 (such as CBD) could potentially help patients with diverse ailments, including chronic pain.

Immunoreactivity in satellite glial cells—localisation of some receptors in SGCs (PPAR γ , CB2R, GPR55) and inflammatory/immune cells (PPAR γ and GPR55) seems to be relevant, because a better understanding of the molecular crosstalk between TG neurons and their surrounding cells may aid in the identification of novel targets for the development of more effective analgesics [70]. In response to injury signals, SGCs and macrophages accumulate around primary sensory neurons, forming a macrophage-SGC-neuron triad, in which macrophages and SGCs work together to enhance and prolong neuropathic pain through ATP and other inflammatory mediators, which promote the development of inflammation-related neuropathic pain [70].

Satellite glial cells that envelop the cell bodies of primary sensory neurons in DRG and TG support normal sensory transmission and nociception by maintaining metabolic and ionic homeostasis [40]. In neuropathic pain and inflammation models, SGCs proliferate and become activated [71,72], resulting in an increased expression of various molecules, such as proinflammatory cytokines [73–75] and neurotrophins [76–78], and changes in functional gap junctions [79,80]. The mechanisms by which peripheral nerve injury causes activation

of SGCs may involve ATP, with ATP released from damaged neurons believed to be one of the critical mediators involved in activating SGCs through the stimulation of purinergic receptors (as reviewed by Ohara et al. [77]). Recent studies have demonstrated that SGCs are able to modulate neuronal excitability, leading to neuropathic pain [76,78].

In the TG, satellite glial cells have been recognised as significant contributors to the regulation of neuronal function in various physiological and pathological conditions, including pulpitis, inflammation of the temporomandibular joint, headaches, and other orofacial neuropathic or inflammatory pain [81,82]. Cannabinoids may have a therapeutic role in neuropathic pain, also reducing the synergy between neurons and SGCs in the nociceptive pathways.

The small sample size, potential regional differences, and lack of close age matching in our cases could represent a significant limitation, as well as the limited number of horses and the uncertainty regarding their health status. Further studies involving a larger number of subjects are required to confirm our results. It cannot be ruled out that some factors, such as the unknown underlying pathological conditions of the horses in the study or the medications they received, could potentially alter the CB1R, CB2R, TRPV1, GPR55, and PPAR γ expression in tissues.

4. Materials and Methods

4.1. Animals

Ten whole trigeminal ganglia (TG) from both sides (right and left) of five healthy horses, which were slaughtered for consumption, were harvested post-mortem from the head. The age of the horses ranged from 10 months to 22 years (6 ± 5 years; mean \pm standard deviation), and their weight ranged from 67 kg to 374 kg (274 ± 121 kg). The breeds included 2 Italian thoroughbred, 2 half-breeds and 1 French saddle horse.

The clinical history of the horses was unknown, but all had been assessed as fit for slaughter for human consumption upon ante-mortem inspection. Heads were routinely removed during carcass preparation and were cut off along the sagittal plane of the head. This cut revealed the trigeminal roots, the attached trigeminal ganglia, and portions of the ophthalmic, maxillary, and mandibular nerves (approximately 1.5 cm in length), which were quickly removed and immersed in the fixative. Dissection was performed within 0.5–1 h of slaughter. The inclusion criteria for the selection of the animals were the normal gross and histological TG appearance.

4.2. Immunofluorescence on Cryosections

Five right TG from the five horses were fixed for 48 h at 4 °C in 4% paraformaldehyde in phosphate buffer (0.1 M, pH 7.2). They were subsequently rinsed in phosphate-buffered saline (PBS; 0.15 M NaCl in 0.01 M sodium phosphate buffer, pH 7.2) and stored at 4 °C in PBS containing 30% sucrose and sodium azide (0.1%). The following day, the tissues were transferred to a mixture of PBS-30% sucrose–azide and Optimal Cutting Temperature (OCT) compound (Sakura Finetek Europe, Alphen aan den Rijn, The Netherlands) at a ratio of 1:1 for an additional 24 h before being embedded in 100% OCT in Cryomold[®] (Sakura Finetek Europe, Alphen aan den Rijn, The Netherlands). The sections were prepared by freezing the tissues in isopentane cooled in liquid nitrogen. Cryosections (14 μ m thick) ($n = 60$) of trigeminal ganglia were cut on a cryostat and mounted on polylysinated slides ($n = 22$).

The cryosections were hydrated in PBS and processed for immunostaining. To block non-specific binding, the sections were incubated in a solution containing 20% normal donkey serum (Colorado Serum Co., Denver, CO, USA), 0.5% Triton X-100 (Sigma Aldrich, Milan, Italy, Europe), and 1% bovine serum albumin in PBS for 1 h at room temperature (RT) (22–25 °C). Serial cryosections of the same TG in all five cases were incubated in a humid chamber overnight at RT with different antibodies directed against CB1R, CB2R, TRPV1, GPR55, and PPAR γ (single immunostaining) or with a cocktail of primary antibodies

(double immunostaining) (Tables 2 and 3), diluted in 1.8% NaCl in 0.01 M PBS containing 0.1% sodium azide.

Table 2. Primary antibodies used in the study.

Primary Antibody	Host	Code	Dilution	Source
CB1R	Rabbit	ab23703	1:100 (IF); 1:400 (IHC)	Abcam
CB2R	Rabbit	PA1-744	1:250 (IF); 1:200 (IHC)	Thermo Fisher
GPR55	Rabbit	NB110-55498	1:200 (IF); 1:200 (IHC)	Novus Biol.
GFAP	Chicken	Ab4674	1:800 (IF)	Abcam
IBA1	Goat	NB100-1028	1:80 (IF)	Novus Biol.
PPAR γ	Rabbit	Ab45036	1:300 (IF); 1:400 (IHC)	Abcam
TRPV1	Rabbit	ACC-030	1:200 (IF); 1:300 (IHC)	Alomone

Table 3. Details of the primary and secondary reagent combination in the double labelling experiments.

Double Labelling Experiment	Secondary Reagent Combination
Rabbit anti-PPAR γ Chicken anti-GFAP	Donkey anti-Rabbit 488 Donkey anti-Chicken TRITC
Rabbit anti-PPAR γ Goat anti-IBA1	Donkey anti-Rabbit 488 Donkey anti-Goat 594
Rabbit anti-GPR55 Chicken anti-GFAP	Donkey anti-Rabbit 488 Donkey anti-Chicken TRITC
Rabbit anti-GPR55 Goat anti-IBA1	Donkey anti-Rabbit 488 Donkey anti-Goat 594

Primary antibody Suppliers: Abcam, Cambridge, UK; Alomone, Jerusalem, Israel; Dako Cytomation, Glostrup, Denmark; Novus Biologicals, Littleton, CO, USA; Santa Cruz Biotechnology, Santa Cruz, CA, USA; Thermo Fisher Scientific, Waltham, MA, USA. Abbreviations: IF, immunofluorescence; IHC, immunohistochemistry.

Secondary antibody Suppliers: Abcam, Cambridge, UK; Dako, Glostrup, Denmark; Jackson Immuno Research Laboratories, Inc Baltimore Pike, PA, USA. Thermo Fisher Scientific, Waltham, MA, USA. Vector Laboratories, Burlingame, CA, USA.

Table 3 summarizes the combination of primary and secondary antibodies used in double labelling experiments.

After washing in PBS (3×10 min), the sections were incubated for 1 h at RT in a humid chamber with the secondary antibodies (Table 4) diluted in PBS.

Table 4. Secondary antibodies used in the study.

Secondary Antibody	Host	Code	Dilution	Source
Anti-chicken TRITC	Donkey	703-025-155	1:200	Jackson
Anti-goat 594	Donkey	ab150132	1:600	Abcam
Anti-rabbit 488	Donkey	A-21206	1:1000	Thermo Fisher
Anti-rabbit biotinylated	Goat	BA-1000	1:200	Vector laboratories

The sections were then washed in PBS (3×10 min) and counterstained with a blue fluorescent Nissl stain solution (NeuroTrace[®], # N-21479, dilution 1:200) (Molecular Probes, Eugene, OR, USA), which was used to label the TG neurons and the satellite glial cells (SGCs) and to determine the percentage of neurons that immunoreacted to each of the markers.

To identify the SGCs, the antibody anti-glial acidic fibrillary protein (GFAP) was also utilised. In addition, since cannabinoid and cannabinoid-related receptors might also be located on inflammatory cells, the anti-ionised calcium binding adapter molecule 1 antibody (IBA1), which recognises the microglia in the central nervous system (CNS) and

the macrophages outside the CNS, was utilised. The cryosections were then washed in PBS (3×10 min) and mounted in buffered glycerol at pH 8.6.

4.3. Immunohistochemistry on FFPE

Five left TG were dissected from five horses (in one case, the sampled tissue was insufficient for further analysis), fixed in 10% (*vol/vol*) phosphate-buffered formalin, and paraffin-embedded according to standard procedures. Subsequently, three-micron-thick consecutive sections were cut and processed for immunohistochemistry ($n = 20$). The sections from each sample were dewaxed and rehydrated. Endogenous peroxidase was blocked by immersion in 3% H_2O_2 in methanol for 30 min at RT. The dilutions of the primary antibodies are reported in Table 2. Antigen retrieval (citrate pH6; 10 min; MW: 750 W) was followed by cooling at RT for 20 min. Blocking of non-specific antigenic sites was achieved by incubating the slides in a solution of 10% normal goat serum in PBS (blocking solution) for 30 min at RT, and incubated overnight in a humid chamber at 4 °C with the primary antibodies diluted in the blocking solution afterwards.

The slides were rinsed in TRIS buffer and then incubated with a secondary anti-rabbit antibody (biotinylated goat anti-rabbit immunoglobulins; Dako, Glostrup, Denmark) diluted to 1:200 in the blocking solution. After two washes in TRIS buffer, immunoreactions were detected with avidin-biotin immunoperoxidase (Vectastain Elite ABC Kit, Vector Laboratories, Burlingame, CA, USA) and visualised with the chromogen 3,3'-diaminobenzidine (0.05% *w/v*, cat# ACB999, Histo-Line Laboratories, Pantigliate, Milan, Italy). The slides were counterstained with Harris haematoxylin (cat# 01HEMH2; Histo-Line Laboratories) and permanently mounted with DPX medium (Fluka, Riedel-de Haen, Germany). Images were acquired with an optical microscope (Eclipse E600; Nikon, Shinjuku, Japan) equipped with the Imaging Source "33" Series USB 3.0 Camera (cat# DFK 33UX264; Bremen, Germany).

4.4. Quantitative Analysis of the Immunoreactivity

The immunoreactivity of the antibodies was evaluated, and its cellular localisation (membranous, cytoplasmic, and/or nuclear) was reported. The intensity of the expression was also evaluated as faint, moderate, and bright (immunofluorescence)/strong (immunohistochemistry) in images acquired using the same exposure times (for immunofluorescence in cryosections), and through microscopy observations (for immunohistochemistry on paraffin-embedded sections).

A minimum of one hundred Nissl-stained neurons were counted for each cannabinoid and cannabinoid-related receptor in cryosections, following the protocol published by Chiochetti et al. [13].

In the FFPE sections, immunopositive neurons were counted in a total of 5 fields at $20\times$ magnification under the optical microscope and compared to the total number of cells present in the same cell compartment.

The relative percentages of immunopositive neurons were expressed as Mean \pm standard deviation (SD).

4.5. Specificity of the Primary Antibodies

The rabbit anti-CB1R [13], -CB2R [83], -TRPV1 [14,30], and -PPAR γ [14] antibodies had previously been tested on horse tissues using Western blot (Wb) analysis. The immunogen used to obtain the anti-GPR55 antibody was a synthetic 20 amino acid peptide from the third cytoplasmic domain of Human GPR55 in amino acids 200–250. The homology between the full amino acid sequences of the horse and human GPR55 was 80%, and the correspondence with the specific sequence of the immunogen was 78% (<https://www.uniprot.org/>, accessed on 7 January 2018). This antibody, which has recently been used in horse sensory neurons [14], had previously been tested on rat and dog dorsal root ganglia (DRG) using immunohistochemistry [30] and on mice tissues using Wb analysis [84]. However, the Wb analysis had not been carried out on horse tissue.

Marker for macrophages—the goat anti-IBA1 antibody, recently used on horse tissue [12,14], was directed against a peptide with the sequence C-TGPPAKKAISELP, from the C Terminus of the porcine IBA1 sequence. Horse and porcine IBA1 molecules share 92.3% identity (<https://www.uniprot.org/>, accessed on 30 June 2019), and it is plausible that the antibody used can also recognise IBA1 in the horse.

4.6. Specificity of the Secondary Antibody

The specificity of the secondary antibodies was tested by applying them to the sections after omitting the primary antibodies. No immunolabelled cells were detected after omitting the primary antibodies.

4.7. Fluorescence Microscopy

The preparations were examined, by the same observer on a Nikon Eclipse Ni microscope (Nikon Instruments Europe BV, Amsterdam, The Netherlands, Europe) equipped with the appropriate filter cubes. The images were recorded with a DS-Qi1Nc digital camera and NIS Elements software BR 4.20.01 (Mountain View, Ottawa, ON, Canada). Slight contrast and brightness adjustments were made using Corel Photo Paint, whereas the figure panels were prepared using Corel Draw (Mountain View).

5. Conclusions

In conclusion, this study provides significant insights into the expression of cannabinoid receptors (CB1 and CB2) and cannabinoid-related receptors (GPR55, PPAR γ , and TRPV1) in the TG neurons and SGCs of horses. To the authors' knowledge, this is the first study to demonstrate this expression. The positive findings demonstrate the presence and potential functional significance of these receptors in the equine TG, highlighting their potential role in the modulation of trigeminal nerve function and neuropathic pain pathways. Considering the pronounced antinociceptive effects of cannabinoids and the expression of their receptors in the TG, these findings hold promise for the therapeutic application of cannabinoids in managing headshaking in horses. By targeting the endocannabinoid system, modulation of the trigeminal neural network and subsequent alleviation of trigeminal-mediated headshaking may be achievable. Investigation of receptor expression in TGM headshaking, and whether it differs from unaffected horses, is warranted and now being undertaken. Such research endeavors could ultimately lead to the development of novel cannabinoid-based therapies for the clinical management of this debilitating condition, thereby enhancing the well-being, performance, and quality of life of these horses and improving safety for riders and handlers.

Author Contributions: Conceptualization, R.C., V.R., R.Z.C. and K.J.P.; Methodology, A.S., R.Z.C., G.S., F.G. and M.M.; Validation, R.C. and M.M.; Formal Analysis, R.C. and F.G.; Investigation, R.C., R.Z.C.; Resources, R.C.; Data Curation, R.C., F.G. and M.M.; Writing—Original Draft Preparation, R.C., R.Z.C. and M.M.; Writing—Review & Editing, V.R. and K.J.P.; Supervision, R.C.; Project Administration, R.C.; Funding Acquisition, R.C. All authors have read and agreed to the published version of the manuscript.

Funding: This study received a grant from Formula Swiss AG, Swiss. The sponsors had no role in the design, execution, interpretation, or writing of the study. The protocol number is 0005122 12-May-2020.

Institutional Review Board Statement: According to Directive 2010/63/EU of the European Parliament and of the Council of 22 September 2010 regarding the protection of animals used for scientific purposes, Italian legislation (D. Lgs. n. 26/2014) does not require any approval by competent authorities or ethics committees as this study did not influence any therapeutic decisions.

Informed Consent Statement: Not applicable.

Data Availability Statement: The data that support the findings of this study are available from the corresponding author upon reasonable request.

Acknowledgments: The availability and collaboration of the health personnel of the “Zerbini Giorgio and Ragazzi Maria Grazia” slaughterhouse (Correggio, Reggio Emilia, Italy) is gratefully acknowledged.

Conflicts of Interest: The authors declare no conflict of interest.

References

- Ross, S.E.; Murray, J.K.; Roberts, V.L.H. Prevalence of Headshaking within the Equine Population in the UK. *Equine Vet. J.* **2018**, *50*, 73–78. [\[CrossRef\]](#) [\[PubMed\]](#)
- Roberts, V.L.; Fewes, D.; McNamara, J.M.; Love, S. Trigeminal Nerve Root Demyelination Not Seen in Six Horses Diagnosed with Trigeminal-Mediated Headshaking. *Front. Vet. Sci.* **2017**, *4*, 72. [\[CrossRef\]](#)
- Aleman, M.; Rhodes, D.; Williams, D.C.; Guedes, A.; Madigan, J.E. Sensory Evoked Potentials of the Trigeminal Nerve for the Diagnosis of Idiopathic Headshaking in a Horse. *J. Vet. Int. Med.* **2014**, *28*, 250–253. [\[CrossRef\]](#)
- Elliott, M.B.; Ward, S.J.; Abood, M.E.; Tuma, R.F.; Jallo, J.I. Understanding the Endocannabinoid System as a Modulator of the Trigeminal Pain Response to Concussion. *Concussion* **2017**, *2*, CNC49. [\[CrossRef\]](#) [\[PubMed\]](#)
- Morales, P.; Hurst, D.P.; Reggio, P.H. Molecular Targets of the Phytocannabinoids: A Complex Picture. In *Phytocannabinoids*; Kinghorn, A.D., Falk, H., Gibbons, S., Kobayashi, J., Eds.; Progress in the Chemistry of Organic Natural Products; Springer International Publishing: Cham, Switzerland, 2017; Volume 103, pp. 103–131, ISBN 978-3-319-45539-6.
- Ligresti, A.; De Petrocellis, L.; Di Marzo, V. From Phytocannabinoids to Cannabinoid Receptors and Endocannabinoids: Pleiotropic Physiological and Pathological Roles Through Complex Pharmacology. *Physiol. Rev.* **2016**, *96*, 1593–1659. [\[CrossRef\]](#) [\[PubMed\]](#)
- Liang, Y.; Huang, C.; Hsu, K. Therapeutic Potential of Cannabinoids in Trigeminal Neuralgia. *Curr. Drug Targets CNS Neurol. Disord.* **2004**, *3*, 507–514. [\[CrossRef\]](#)
- Lee, G.; Grove, B.; Furnish, T.; Wallace, M. Medical Cannabis for Neuropathic Pain. *Curr. Pain. Headache Rep.* **2018**, *22*, 8. [\[CrossRef\]](#)
- Ellis, K.L.; Contino, E.K. Treatment Using Cannabidiol in a Horse with Mechanical Allodynia. *Equine Vet. Educ.* **2021**, *33*, e79–e82. [\[CrossRef\]](#)
- Sánchez-Aparicio, P.; Florán, B.; Rodríguez Velázquez, D.; Ibancovich, J.A.; Varela Guerrero, J.A.; Recillas, S. Cannabinoids CB2 Receptors, One New Promising Drug Target for Chronic and Degenerative Pain Conditions in Equine Veterinary Patients. *J. Equine Vet. Sci.* **2020**, *85*, 102880. [\[CrossRef\]](#)
- Luedke, C.; Wilhelm, T. Cannabinoids in Equine Medicine. In *Cannabis Therapy in Veterinary Medicine: A Complete Guide*; Cital, S., Kramer, K., Hughston, L., Gaynor, J.S., Eds.; Springer International Publishing: Cham, Switzerland, 2021; pp. 295–305. ISBN 978-3-030-68317-7.
- Zamith Cunha, R.; Zannoni, A.; Salamanca, G.; De Silva, M.; Rinnovati, R.; Gramenzi, A.; Forni, M.; Chiocchetti, R. Expression of Cannabinoid (CB1 and CB2) and Cannabinoid-Related Receptors (TRPV1, GPR55, and PPAR α) in the Synovial Membrane of the Horse Metacarpophalangeal Joint. *Front. Vet. Sci.* **2023**, *10*, 1045030. [\[CrossRef\]](#)
- Chiocchetti, R.; Rinnovati, R.; Tagliavia, C.; Stanzani, A.; Galiuzzo, G.; Giancola, F.; Silva, M.D.; Capodanno, Y.; Spadari, A. Localisation of Cannabinoid and Cannabinoid-Related Receptors in the Equine Dorsal Root Ganglia. *Equine Vet. J.* **2021**, *53*, 549–557. [\[CrossRef\]](#) [\[PubMed\]](#)
- Galiuzzo, G.; Tagliavia, C.; Giancola, F.; Rinnovati, R.; Sadeghinezhad, J.; Bombardi, C.; Grandis, A.; Pietra, M.; Chiocchetti, R. Localisation of Cannabinoid and Cannabinoid-Related Receptors in the Horse Ileum. *J. Equine Vet. Sci.* **2021**, *104*, 103688. [\[CrossRef\]](#) [\[PubMed\]](#)
- Tajti, J.; Szok, D.; Csáti, A.; Szabó, Á.; Tanaka, M.; Vécsei, L. Exploring Novel Therapeutic Targets in the Common Pathogenic Factors in Migraine and Neuropathic Pain. *Int. J. Mol. Sci.* **2023**, *24*, 4114. [\[CrossRef\]](#) [\[PubMed\]](#)
- Greco, R.; Demartini, C.; Zanaboni, A.M.; Francavilla, M.; De Icco, R.; Ahmad, L.; Tassorelli, C. The Endocannabinoid System and Related Lipids as Potential Targets for the Treatment of Migraine-related Pain. *Headache* **2022**, *62*, 227–240. [\[CrossRef\]](#) [\[PubMed\]](#)
- Richardson, D.; Pearson, R.G.; Kurian, N.; Latif, M.L.; Garle, M.J.; Barrett, D.A.; Kendall, D.A.; Scammell, B.E.; Reeve, A.J.; Chapman, V. Characterisation of the Cannabinoid Receptor System in Synovial Tissue and Fluid in Patients with Osteoarthritis and Rheumatoid Arthritis. *Arthritis Res. Ther.* **2008**, *10*, R43. [\[CrossRef\]](#)
- O'Brien, M.; McDougall, J.J. Cannabis and Joints: Scientific Evidence for the Alleviation of Osteoarthritis Pain by Cannabinoids. *Curr. Opin. Pharmacol.* **2018**, *40*, 104–109. [\[CrossRef\]](#)
- Lowe, H.; Toyang, N.; Steele, B.; Bryant, J.; Ngwa, W. The Endocannabinoid System: A Potential Target for the Treatment of Various Diseases. *Int. J. Mol. Sci.* **2021**, *22*, 9472. [\[CrossRef\]](#)
- Fiani, B.; Sarhadi, K.J.; Soula, M.; Zafar, A.; Quadri, S.A. Current Application of Cannabidiol (CBD) in the Management and Treatment of Neurological Disorders. *Neurol. Sci.* **2020**, *41*, 3085–3098. [\[CrossRef\]](#)
- Longworth, J.; Szafron, M.; Gruza, A.; Da Silva, K. Cannabis and Cannabinoid Medications for the Treatment of Chronic Orofacial Pain: A Scoping Review. *Dent. Rev.* **2023**, *3*, 100063. [\[CrossRef\]](#)
- Price, T.J.; Helesic, G.; Parghi, D.; Hargreaves, K.M.; Flores, C.M. The Neuronal Distribution of Cannabinoid Receptor Type 1 in the Trigeminal Ganglion of the Rat. *Neuroscience* **2003**, *120*, 155–162. [\[CrossRef\]](#)

23. Christiansen, I.M.; Edvinsson, J.C.A.; Reducha, P.V.; Edvinsson, L.; Haanes, K.A. Dual Action of the Cannabinoid Receptor 1 Ligand Arachidonyl-2'-Chloroethylamide on Calcitonin Gene-Related Peptide Release. *J. Headache Pain.* **2022**, *23*, 30. [\[CrossRef\]](#) [\[PubMed\]](#)
24. Aleman, M.; Williams, D.C.; Brosnan, R.J.; Nieto, J.E.; Pickles, K.J.; Berger, J.; Lecouteur, R.A.; Holliday, T.A.; Madigan, J.E. Sensory Nerve Conduction and Somatosensory Evoked Potentials of the Trigeminal Nerve in Horses with Idiopathic Headshaking. *J. Vet. Intern. Med.* **2013**, *27*, 1571–1580. [\[CrossRef\]](#) [\[PubMed\]](#)
25. Greco, R.; Gasperi, V.; Maccarrone, M.; Tassorelli, C. The Endocannabinoid System and Migraine. *Exp. Neurol.* **2010**, *224*, 85–91. [\[CrossRef\]](#)
26. Russo, D.; Bombardi, C.; Castellani, G.; Chiocchetti, R. Characterization of Spinal Ganglion Neurons in Horse (*Equus caballus*). A Morphometric, Neurochemical and Tracing Study. *Neuroscience* **2011**, *176*, 53–71. [\[CrossRef\]](#) [\[PubMed\]](#)
27. Ahluwalia, J.; Urban, L.; Capogna, M.; Bevan, S.; Nagy, I. Cannabinoid 1 Receptors Are Expressed in Nociceptive Primary Sensory Neurons. *Neuroscience* **2000**, *100*, 685–688. [\[CrossRef\]](#)
28. Bridges, D.; Rice, A.S.C.; Egertová, M.; Elphick, M.R.; Winter, J.; Michael, G.J. Localisation of Cannabinoid Receptor 1 in Rat Dorsal Root Ganglion Using in Situ Hybridisation and Immunohistochemistry. *Neuroscience* **2003**, *119*, 803–812. [\[CrossRef\]](#)
29. Agarwal, N.; Pacher, P.; Tegeder, I.; Amaya, F.; Constantin, C.E.; Brenner, G.J.; Rubino, T.; Michalski, C.W.; Marsicano, G.; Monory, K.; et al. Cannabinoids Mediate Analgesia Largely via Peripheral Type 1 Cannabinoid Receptors in Nociceptors. *Nat. Neuro Sci.* **2007**, *10*, 870–879. [\[CrossRef\]](#)
30. Chiocchetti, R.; Galiazzo, G.; Tagliavia, C.; Stanzani, A.; Giancola, F.; Menchetti, M.; Militerno, G.; Bernardini, C.; Forni, M.; Mandrioli, L. Cellular Distribution of Canonical and Putative Cannabinoid Receptors in Canine Cervical Dorsal Root Ganglia. *Front. Vet. Sci.* **2019**, *6*, 313. [\[CrossRef\]](#)
31. Khasabova, I.A.; Simone, D.A.; Seybold, V.S. Cannabinoids Attenuate Depolarization-Dependent Ca²⁺ Influx in Intermediate-Size Primary Afferent Neurons of Adult Rats. *Neuroscience* **2002**, *115*, 613–625. [\[CrossRef\]](#)
32. Lalonde, M.R.; Jollimore, C.A.B.; Stevens, K.; Barnes, S.; Kelly, M.E.M. Cannabinoid Receptor-Mediated Inhibition of Calcium Signaling in Rat Retinal Ganglion Cells. *Mol. Vis.* **2006**, *12*, 1160–1166.
33. Zhang, Y.; Xie, H.; Lei, G.; Li, F.; Pan, J.; Liu, C.; Liu, Z.; Liu, L.; Cao, X. Regulatory Effects of Anandamide on Intracellular Ca²⁺ Concentration Increase in Trigeminal Ganglion Neurons. *Neural Regen. Res.* **2014**, *9*, 878. [\[CrossRef\]](#)
34. Price, T.J.; Patwardhan, A.; Akopian, A.N.; Hargreaves, K.M.; Flores, C.M. Modulation of Trigeminal Sensory Neuron Activity by the Dual Cannabinoid-Vanilloid Agonists Anandamide, N -Arachidonoyl-Dopamine and Arachidonyl-2-Chloroethylamide: Cannabinoid-Vanilloid Modulation of Trigeminal Neuron Activity. *Br. J. Pharmacol.* **2004**, *141*, 1118–1130. [\[CrossRef\]](#)
35. Akerman, S.; Holland, P.R.; Goadsby, P.J. Cannabinoid (CB1) Receptor Activation Inhibits Trigeminovascular Neurons. *J. Pharmacol. Exp. Ther.* **2007**, *320*, 64–71. [\[CrossRef\]](#)
36. Atwood, B.K.; Mackie, K. CB2: A Cannabinoid Receptor with an Identity Crisis. *Br. J. Pharmacol.* **2010**, *160*, 467–479. [\[CrossRef\]](#)
37. Anand, U.; Otto, W.R.; Sanchez-Herrera, D.; Facer, P.; Yiangou, Y.; Korchev, Y.; Birch, R.; Benham, C.; Bountra, C.; Chessell, I.P.; et al. Cannabinoid Receptor CB2 Localisation and Agonist-Mediated Inhibition of Capsaicin Responses in Human Sensory Neurons. *Pain* **2008**, *138*, 667–680. [\[CrossRef\]](#) [\[PubMed\]](#)
38. Gutierrez, T.; Crystal, J.D.; Zvonok, A.M.; Makriyannis, A.; Hohmann, A.G. Self-Medication of a Cannabinoid CB2 Agonist in an Animal Model of Neuropathic Pain. *Pain* **2011**, *152*, 1976–1987. [\[CrossRef\]](#) [\[PubMed\]](#)
39. Rogers, N. Cannabinoid Receptor with an “identity Crisis” Gets a Second Look. *Nat. Med.* **2015**, *21*, 966–967. [\[CrossRef\]](#)
40. Svízenská, I.H.; Brázda, V.; Klusáková, I.; Dubový, P. Bilateral Changes of Cannabinoid Receptor Type 2 Protein and mRNA in the Dorsal Root Ganglia of a Rat Neuropathic Pain Model. *J. Histochem. Cytochem.* **2013**, *61*, 529–547. [\[CrossRef\]](#)
41. Tominaga, M.; Caterina, M.J.; Malmberg, A.B.; Rosen, T.A.; Gilbert, H.; Skinner, K.; Raumann, B.E.; Basbaum, A.I.; Julius, D. The Cloned Capsaicin Receptor Integrates Multiple Pain-Producing Stimuli. *Neuron* **1998**, *21*, 531–543. [\[CrossRef\]](#) [\[PubMed\]](#)
42. Russo, D.; Clavenzani, P.; Sorteni, C.; Bo Minelli, L.; Botti, M.; Gazza, F.; Panu, R.; Ragionieri, L.; Chiocchetti, R. Neurochemical Features of Boar Lumbosacral Dorsal Root Ganglion Neurons and Characterization of Sensory Neurons Innervating the Urinary Bladder Trigone. *J. Comp. Neurol.* **2013**, *521*, 342–366. [\[CrossRef\]](#)
43. Tanimoto, T.; Takeda, M.; Nasu, M.; Kadoi, J.; Matsumoto, S. Immunohistochemical Co-Expression of Carbonic Anhydrase II with Kv1.4 and TRPV1 in Rat Small-Diameter Trigeminal Ganglion Neurons. *Brain Res.* **2005**, *1044*, 262–265. [\[CrossRef\]](#)
44. Ichikawa, H.; Sugimoto, T. VR1-Immunoreactive Primary Sensory Neurons in the Rat Trigeminal Ganglion. *Brain Res.* **2001**, *890*, 184–188. [\[CrossRef\]](#)
45. Patapoutian, A.; Peier, A.M.; Story, G.M.; Viswanath, V. ThermoTRP Channels and beyond: Mechanisms of Temperature Sensation. *Nat. Rev. Neurosci.* **2003**, *4*, 529–539. [\[CrossRef\]](#) [\[PubMed\]](#)
46. Culshaw, A.J.; Bevan, S.; Christiansen, M.; Copp, P.; Davis, A.; Davis, C.; Dyson, A.; Dziadulewicz, E.K.; Edwards, L.; Eggelte, H.; et al. Identification and Biological Characterization of 6-Aryl-7-Isopropylquinazolinones as Novel TRPV1 Antagonists That Are Effective in Models of Chronic Pain. *J. Med. Chem.* **2006**, *49*, 471–474. [\[CrossRef\]](#) [\[PubMed\]](#)
47. Krause, J.E.; Chenard, B.L.; Cortright, D.N. Transient Receptor Potential Ion Channels as Targets for the Discovery of Pain Therapeutics. *Curr. Opin. Investig. Drugs* **2005**, *6*, 48–57. [\[PubMed\]](#)
48. Marwaha, L.; Bansal, Y.; Singh, R.; Saroj, P.; Sodhi, R.K.; Kuhad, A. Niflumic Acid, a TRPV1 Channel Modulator, Ameliorates Stavudine-Induced Neuropathic Pain. *Inflammopharmacol* **2016**, *24*, 319–334. [\[CrossRef\]](#)

49. Sagar, D.R.; Gaw, A.G.; Okine, B.N.; Woodhams, S.G.; Wong, A.; Kendall, D.A.; Chapman, V. Dynamic Regulation of the Endocannabinoid System: Implications for Analgesia. *Mol. Pain*. **2009**, *5*, 59. [\[CrossRef\]](#) [\[PubMed\]](#)
50. Di Marzo, V.; Piscitelli, F. The Endocannabinoid System and Its Modulation by Phytocannabinoids. *Neurotherapeutics* **2015**, *12*, 692–698. [\[CrossRef\]](#)
51. Mlost, J.; Bryk, M.; Starowicz, K. Cannabidiol for Pain Treatment: Focus on Pharmacology and Mechanism of Action. *Int. J. Mol. Sci.* **2020**, *21*, 8870. [\[CrossRef\]](#) [\[PubMed\]](#)
52. Barak, Y.; Nelson, M.C.; Ong, E.S.; Jones, Y.Z.; Ruiz-Lozano, P.; Chien, K.R.; Koder, A.; Evans, R.M. PPAR γ Is Required for Placental, Cardiac, and Adipose Tissue Development. *Mol. Cell* **1999**, *4*, 585–595. [\[CrossRef\]](#)
53. Tontonoz, P.; Spiegelman, B.M. Fat and Beyond: The Diverse Biology of PPAR γ . *Annu. Rev. Biochem.* **2008**, *77*, 289–312. [\[CrossRef\]](#)
54. Zhao, X.; Ou, Z.; Grotta, J.C.; Waxham, N.; Aronowski, J. Peroxisome-Proliferator-Activated Receptor-Gamma (PPAR γ) Activation Protects Neurons from NMDA Excitotoxicity. *Brain Res.* **2006**, *1073–1074*, 460–469. [\[CrossRef\]](#) [\[PubMed\]](#)
55. Quintanilla, R.A.; Utreras, E.; Cabezas-Opazo, F.A. Role of PPAR γ in the Differentiation and Function of Neurons. *PPAR Res.* **2014**, *2014*, e768594. [\[CrossRef\]](#) [\[PubMed\]](#)
56. Maeda, T.; Kishioka, S. Chapter 13 PPAR and Pain. In *International Review of Neurobiology*; Academic Press: Cambridge, MA, USA, 2009; Volume 85, pp. 165–177.
57. Lyons, D.N.; Zhang, L.; Danaher, R.J.; Miller, C.S.; Westlund, K.N. PPAR γ agonists attenuate trigeminal neuropathic pain. *Clin. J. Pain.* **2017**, *33*, 1071–1080. [\[CrossRef\]](#) [\[PubMed\]](#)
58. Churi, S.B.; Abdel-Aleem, O.S.; Tumber, K.K.; Scuderi-Porter, H.; Taylor, B.K. Intrathecal Rosiglitazone Acts at Peroxisome Proliferator-Activated Receptor-Gamma to Rapidly Inhibit Neuropathic Pain in Rats. *J. Pain.* **2008**, *9*, 639–649. [\[CrossRef\]](#)
59. Vučković, S.; Srebro, D.; Vujović, K.S.; Vučetić, Č.; Prostran, M. Cannabinoids and Pain: New Insights From Old Molecules. *Front. Pharmacol.* **2018**, *9*, 1259. [\[CrossRef\]](#)
60. Aviram, J.; Samuelly-Leichtag, G. Efficacy of Cannabis-Based Medicines for Pain Management: A Systematic Review and Meta-Analysis of Randomized Controlled Trials. *Pain Physician* **2017**, *20*, E755–E796. [\[CrossRef\]](#)
61. Hill, K.P. Medical Marijuana for Treatment of Chronic Pain and Other Medical and Psychiatric Problems: A Clinical Review. *JAMA* **2015**, *313*, 2474. [\[CrossRef\]](#)
62. Chu, Y.; Jia, S.; Xu, K.; Liu, Q.; Mai, L.; Liu, J.; Fan, W.; Huang, F. Single-Cell Transcriptomic Profile of Satellite Glial Cells in Trigeminal Ganglion. *Front. Mol. Neurosci.* **2023**, *16*, 1117065. [\[CrossRef\]](#)
63. Takahashi, Y.; Hasegawa-Moriyama, M.; Sakurai, T.; Inada, E. The Macrophage-Mediated Effects of the Peroxisome Proliferator-Activated Receptor-Gamma Agonist Rosiglitazone Attenuate Tactile Allodynia in the Early Phase of Neuropathic Pain Development. *Anesth. Analg.* **2011**, *113*, 398–404. [\[CrossRef\]](#)
64. Hasegawa-Moriyama, M.; Kurimoto, T.; Nakama, M.; Godai, K.; Kojima, M.; Kuwaki, T.; Kanmura, Y. Peroxisome Proliferator-Activated Receptor-Gamma Agonist Rosiglitazone Attenuates Inflammatory Pain through the Induction of Heme Oxygenase-1 in Macrophages. *Pain* **2013**, *154*, 1402–1412. [\[CrossRef\]](#) [\[PubMed\]](#)
65. Ryberg, E.; Larsson, N.; Sjögren, S.; Hjorth, S.; Hermansson, N.-O.; Leonova, J.; Elebring, T.; Nilsson, K.; Drmota, T.; Greasley, P.J. The Orphan Receptor GPR55 Is a Novel Cannabinoid Receptor. *Br. J. Pharmacol.* **2007**, *152*, 1092–1101. [\[CrossRef\]](#) [\[PubMed\]](#)
66. Console-Bram, L.; Marcu, J.; Abood, M.E. Cannabinoid Receptors: Nomenclature and Pharmacological Principles. *Prog. Neuropsychopharmacol. Biol. Psychiatry* **2012**, *38*, 4–15. [\[CrossRef\]](#)
67. Chiocchetti, R.; De Silva, M.; Aspidi, F.; Cunha, R.Z.; Gobbo, F.; Tagliavia, C.; Sarli, G.; Morini, M. Distribution of Cannabinoid Receptors in Keratinocytes of Healthy Dogs and Dogs with Atopic Dermatitis. *Front. Vet. Sci.* **2022**, *9*, 915896. [\[CrossRef\]](#)
68. Ono, T.; Yamashita, T.; Kano, R.; Inoue, M.; Okada, S.; Kano, K.; Koizumi, S.; Iwabuchi, K.; Hirabayashi, Y.; Matsuo, I.; et al. GPR55 Contributes to Neutrophil Recruitment and Mechanical Pain Induction after Spinal Cord Compression in Mice. *Brain Behav. Immun.* **2023**, *110*, 276–287. [\[CrossRef\]](#) [\[PubMed\]](#)
69. Carey, L.M.; Gutierrez, T.; Deng, L.; Lee, W.-H.; Mackie, K.; Hohmann, A.G. Inflammatory and Neuropathic Nociception Is Preserved in GPR55 Knockout Mice. *Sci. Rep.* **2017**, *7*, 944. [\[CrossRef\]](#) [\[PubMed\]](#)
70. Yang, R.; Du, J.; Li, L.; Xu, X.; Liang, S. Central Role of Purinergic Receptors with Inflammation in Neuropathic Pain-Related Macrophage-SGC-Neuron Triad. *Neuropharmacology* **2023**, *228*, 109445. [\[CrossRef\]](#)
71. Lu, X.; Richardson, P.M. Inflammation near the Nerve Cell Body Enhances Axonal Regeneration. *J. Neurosci.* **1991**, *11*, 972–978. [\[CrossRef\]](#) [\[PubMed\]](#)
72. Liu, F.-Y.; Sun, Y.-N.; Wang, F.-T.; Li, Q.; Su, L.; Zhao, Z.-F.; Meng, X.-L.; Zhao, H.; Wu, X.; Sun, Q.; et al. Activation of Satellite Glial Cells in Lumbar Dorsal Root Ganglia Contributes to Neuropathic Pain after Spinal Nerve Ligation. *Brain Res.* **2012**, *1427*, 65–77. [\[CrossRef\]](#)
73. Dubový, P.; Jančálek, R.; Klusáková, I.; Svíženská, I.; Pejchalová, K. Intra- and Extraneuronal Changes of Immunofluorescence Staining for TNF- and TNFR1 in the Dorsal Root Ganglia of Rat Peripheral Neuropathic Pain Models. *Cell Mol. Neurobiol.* **2006**, *26*, 1203–1215. [\[CrossRef\]](#)
74. Takeda, M.; Tanimoto, T.; Kadoi, J.; Nasu, M.; Takahashi, M.; Kitagawa, J.; Matsumoto, S. Enhanced Excitability of Nociceptive Trigeminal Ganglion Neurons by Satellite Glial Cytokine Following Peripheral Inflammation. *Pain* **2007**, *129*, 155–166. [\[CrossRef\]](#) [\[PubMed\]](#)
75. Dubový, P.; Klusáková, I.; Svíženská, I.; Brázda, V. Satellite Glial Cells Express IL-6 and Corresponding Signal-Transducing Receptors in the Dorsal Root Ganglia of Rat Neuropathic Pain Model. *Neuron Glia Biol.* **2010**, *6*, 73–83. [\[CrossRef\]](#) [\[PubMed\]](#)







76. Hanani, M. Satellite Glial Cells in Sensory Ganglia: From Form to Function. *Brain Res. Rev.* **2005**, *48*, 457–476. [[CrossRef](#)] [[PubMed](#)]
77. Ohara, P.T.; Vit, J.-P.; Bhargava, A.; Romero, M.; Sundberg, C.; Charles, A.C.; Jasmin, L. Gliopathic Pain: When Satellite Glial Cells Go Bad. *Neuroscientist* **2009**, *15*, 450–463. [[CrossRef](#)]
78. Takeda, K.; Muramatsu, M.; Chikuma, T.; Kato, T. Effect of Memantine on the Levels of Neuropeptides and Microglial Cells in the Brain Regions of Rats with Neuropathic Pain. *J. Mol. Neurosci.* **2009**, *39*, 380–390. [[CrossRef](#)]
79. Huang, T.-Y.; Belzer, V.; Hanani, M. Gap Junctions in Dorsal Root Ganglia: Possible Contribution to Visceral Pain. *Eur. J. Pain* **2010**, *14*, 49.e1–49.e11. [[CrossRef](#)]
80. Jasmin, L.; Vit, J.-P.; Bhargava, A.; Ohara, P.T. Can Satellite Glial Cells Be Therapeutic Targets for Pain Control? *Neuron Glia Biol.* **2010**, *6*, 63–71. [[CrossRef](#)]
81. Costa, F.A.L.; Neto, F.L.M. Satellite Glial Cells in Sensory Ganglia: Its Role in Pain. *BJAN* **2015**, *65*, 73–81. [[CrossRef](#)]
82. Ye, Y.; Salvo, E.; Romero-Reyes, M.; Akerman, S.; Shimizu, E.; Kobayashi, Y.; Michot, B.; Gibbs, J. Glia and Orofacial Pain: Progress and Future Directions. *Int. J. Mol. Sci.* **2021**, *22*, 5345. [[CrossRef](#)]
83. Kupczyk, P.; Rykala, M.; Serek, P.; Pawlak, A.; Slowikowski, B.; Holysz, M.; Chodaczek, G.; Madej, J.P.; Ziolkowski, P.; Niedzwiedz, A. The Cannabinoid Receptors System in Horses: Tissue Distribution and Cellular Identification in Skin. *J. Vet. Intern. Med.* **2022**, *36*, 1508–1524. [[CrossRef](#)]
84. Galiazzo, G.; Giancola, F.; Stanzani, A.; Fracassi, F.; Bernardini, C.; Forni, M.; Pietra, M.; Chiocchetti, R. Localization of Cannabinoid Receptors CB1, CB2, GPR55, and PPAR α in the Canine Gastrointestinal Tract. *Histochem. Cell Biol.* **2018**, *150*, 187–205. [[CrossRef](#)] [[PubMed](#)]

Disclaimer/Publisher's Note: The statements, opinions and data contained in all publications are solely those of the individual author(s) and contributor(s) and not of MDPI and/or the editor(s). MDPI and/or the editor(s) disclaim responsibility for any injury to people or property resulting from any ideas, methods, instructions or products referred to in the content.

Chapter 6:
**Nitroergic and Substance P Immunoreactive Neurons in the Enteric Nervous
System of the Bottlenose Dolphin (*Tursiops truncatus*)**

Article

Nitrergic and Substance P Immunoreactive Neurons in the Enteric Nervous System of the Bottlenose Dolphin (*Tursiops truncatus*) Intestine

Cristiano Bombardi ^{1,†} , Anna Maria Rambaldi ^{1,2,†} , Giorgia Galiazzo ¹, Fiorella Giancola ^{1,3}, Jean-Marie Graïc ⁴ , Giulia Salamanca ¹ , Bruno Cozzi ⁴  and Roberto Chiochetti ^{1,*} 

¹ Department of Veterinary Medical Sciences (UNI EN ISO 9001:2008), University of Bologna, 40064 Ozzano dell'Emilia, Bologna, Italy; cristiano.bombardi@unibo.it (C.B.); annamaria.rambaldi@gmail.com (A.M.R.); giorgia.galiazzo2@unibo.it (G.G.); fiorella.giancola2@unibo.it (F.G.); giulia.salamanca@studio.unibo.it (G.S.)

² Unit of Veterinary Histology and Pathology, University Institute of Animal Health and Food Safety (IUSA), Veterinary School, University of Las Palmas de Gran Canaria, 35413 Las Palmas, Spain

³ Department of Translational Medicine, University of Ferrara, 44121 Ferrara, Italy

⁴ Department of Comparative Biomedicine and Food Science, University of Padova, 35020 Legnaro, Padova, Italy; jeanmarie.graic@unipd.it (J.-M.G.); bruno.cozzi@unipd.it (B.C.)

* Correspondence: roberto.chiochetti@unibo.it; Tel.: +39-051-2097946

† Cristiano Bombardi and Anna Maria Rambaldi contributed equally as co-first authors.



Citation: Bombardi, C.; Rambaldi, A.M.; Galiazzo, G.; Giancola, F.; Graïc, J.-M.; Salamanca, G.; Cozzi, B.; Chiochetti, R. Nitrergic and Substance P Immunoreactive Neurons in the Enteric Nervous System of the Bottlenose Dolphin (*Tursiops truncatus*) Intestine. *Animals* **2021**, *11*, 1057. <https://doi.org/10.3390/ani11041057>

Academic Editors: Claudia Gili and Cinzia Centelleghes

Received: 8 March 2021

Accepted: 5 April 2021

Published: 8 April 2021

Publisher's Note: MDPI stays neutral with regard to jurisdictional claims in published maps and institutional affiliations.



Copyright: © 2021 by the authors. Licensee MDPI, Basel, Switzerland. This article is an open access article distributed under the terms and conditions of the Creative Commons Attribution (CC BY) license (<https://creativecommons.org/licenses/by/4.0/>).

Simple Summary: The gastrointestinal tract of the bottlenose dolphin (*Tursiops truncatus*) differs structurally and functionally from that of terrestrial mammals. In particular, the intestine does not show any macroscopic subdivision and lacks a caecum. In addition, the histological aspect of the intestine is relatively constant, without marked differences between the anterior and posterior parts. Although the intestine of these cetaceans presents differences in comparison with terrestrial mammals, little information is currently available on their enteric nervous system. The aim of the present study was to investigate the morphological and quantitative aspects of neurons immunoreactive (IR) for the neuronal nitric oxide synthase (nNOS) and Substance P (SP) in the intestine of bottlenose dolphins (*Tursiops truncatus*). In these dolphin specimens, a smaller number of nNOS-IR neurons in the submucosal plexus and a larger number of SP-IR neurons in the myenteric plexus were observed compared to other mammals. Interestingly, no co-localization between nNOS- and SP-IR neurons was detected in either of the plexuses, suggesting the existence of two completely distinct functional classes of neurons in the intestine of the bottlenose dolphin.

Abstract: Compared with other mammals, the digestive system of cetaceans presents some remarkable anatomical and physiological differences. However, the neurochemical features of the enteric nervous system (ENS) in these animals have only been described in part. The present study gives a description of the nitrergic and selected peptidergic systems in the myenteric plexus (MP) and submucosal plexus (SMP) of the intestine of the bottlenose dolphin (*Tursiops truncatus*). The distribution and morphology of neurons immunoreactive (IR) for the neuronal nitric oxide synthase (nNOS) and Substance P (SP) were immunohistochemically studied in formalin-fixed specimens from the healthy intestine of three animals, and the data were compared with those described in the literature on other mammals (human and non-human). In bottlenose dolphins, the percentages of nitrergic neurons (expressed as median and interquartile range—IQR) were 28% (IQR = 19–29) in the MP and 1% (IQR = 0–2) in the SMP, while the percentages of SP-IR neurons were 31% (IQR = 22–37) in the MP and 41% (IQR = 24–63) in the SMP. Although morphological features of nNOS- and SP-IR neurons were similar to those reported in other mammals, we found some noticeable differences in the percentages of enteric neurons. In fact, we detected a lower proportion of nNOS-IR neurons in the SMP and a higher proportion of SP-IR neurons in the MP compared to other mammals. To the best of the authors' knowledge, this study represents the first description and quantification of nNOS-IR neurons and the first quantification of SP-IR neurons in the intestine of a cetacean species. As nNOS and SP are important mediators of intestinal functions and the nitrergic population is

an important target for many neuroenteropathies, data obtained from a healthy intestine provide a necessary basis to further investigate and understand possible functional differences and motor intestinal dysfunctions/alterations in these special mammals.

Keywords: cetaceans; gut; intestine; immunohistochemistry; nNOS

1. Introduction

Marine Cetartiodactyla underwent extensive morphological and physiological evolutionary adaptations to life in the water [1]. Salinity and wide variations of temperature and pressure are just a few of the environmental characteristics that cetaceans have to deal with. Like other organs and systems of odontocetes, the gastrointestinal (GI) tract differs structurally and functionally from that of terrestrial mammals. The tongue has no taste buds, except in certain species [2], prey is swallowed without being chewed and the larynx, which passes through the pharynx, can be voluntarily displaced to allow the passage of food [2,3]. The stomach of delphinids consists of multiple chambers, including a highly muscular forestomach, necessary to grind and digest the whole prey [4–7]. Unlike terrestrial Cetartiodactyla (including the closely related ruminants and *Hippopotamidae*) which also have multiple-chamber stomachs, the stomach complex of cetaceans does not promote multiple chewing cycles. The intestine itself does not show any macroscopic subdivision into small and large intestine, and the caecum is absent; in addition, the histological aspect is also relatively constant, without marked differences between the anterior and posterior parts [5,6,8]. Cetaceans also lack a gall bladder, an arguable evolutionary consequence of the continuous ingestion of food [6].

Although the digestive system of cetaceans presents such differences, when compared with terrestrial mammals, little information is currently available on their enteric nervous system (ENS) [8–12]. The ENS regulates the great majority of digestive functions and activities such as motility, absorption, secretion and blood flow [13]. In the last decade, advances in our understanding of the brain–gut axis have shown the tremendous influence of the ENS on immune, humoral and metabolic homeostasis (Kulkarni et al., 2018). It consists of a huge integrated network of neurons and fibers arranged in the wall of the digestive system, from the esophagus to the internal anal sphincter, and extending to the pancreas and extrahepatic biliary system [14,15]. In the ENS, neurons, fibers and enteric glial cells are organized into two major ganglionated plexuses, the myenteric (MP) and the submucosal plexus (SMP) [13]. The MP is located between the longitudinal (LML) and circular (CML) muscle layers, and provides motor innervation to the GI smooth muscle cells, while the SMP regulates mainly mucosal and submucosal functions and activities, at least in small laboratory rodents [15]. Enteric neurons can be grouped into different functional classes (intrinsic primary afferent neurons (IPANs), excitatory and inhibitory motor neurons and interneurons), based on their specific neurochemical code (i.e., the cocktail of neurotransmitters that they synthesize). Nitric oxide (NO) is the most important inhibitory neurotransmitter of the GI tract, and in most mammalian species, it is also synthesized by descending interneurons, which do not necessarily have an inhibitory action. Mostly released by MP neurons, NO induces relaxation of the GI musculature and sphincters by acting directly on the intestinal smooth muscle cells or by attenuating the release of the excitatory neurotransmitters, such as acetylcholine and substance P (SP) [16,17]. Nitric oxide is synthesized through the activation of neuronal nitric oxide synthase (nNOS), an enzyme that can be found in MP and SMP neurons and fibers of different species [18–21].

SP belongs to the tachykinin family, a group of neuropeptides involved not only in the regulation of different gastrointestinal functions, such as motility and secretion, but also in inflammation and pain genesis [22–26]. In the gut, SP is found in MP excitatory muscular motor neurons and MP and SMP IPANs, as well as in extrinsic sensory fibers

and enteroendocrine cells [9,15,25]. Frequently detected with acetylcholine in intestinal intramural neurons and fibers, SP is considered a cholinergic co-mediator [15,27]. Since NO and SP play important roles in intestinal motor function, they have been widely regarded as relevant neurotransmitters in the study of GI motility disorders [28–31].

The aim of the present study was to describe and quantify nNOS and SP immunoreactive enteric neurons in the non-pathological gut of bottlenose dolphins. By doing so, we provide a first insight into the complex interaction between two major neurochemical classes of enteric neurons in the intestine of this common marine mammal.

2. Materials and Methods

2.1. Animals

Samples of intestine of three adult bottlenose dolphins were obtained from the Mediterranean marine mammal tissue bank of the Department of Comparative Biomedicine and Food Science of the University of Padova (Italy) (MMMTB, www.marinemammals.eu, accessed on 2 April 2021). The MMMTB (CITES IT020) works under the auspices of the Italian Ministry for the Environment and the University of Padova, and receives tissue specimens from cetaceans stranded along the Italian coast of the Mediterranean, or directly samples tissues from dolphins and whales brought to its facilities for post mortem diagnosis.

According to Directive 2010/63/EU of the European Parliament and of the Council of 22 September 2010 regarding the protection of animals used for scientific purposes, the Italian legislation (D. Lgs. n. 26/2014) does not require any approval by competent authorities or ethics committees because this study did not influence any therapeutic decisions.

2.2. Tissue Collection

Tissues were collected from the antimesenteric side of the intestine in the putative jejunal portion caudal to the duodenal ampulla (marked by the pancreatic and hepatic ducts).

All carcasses were coded for freshness [32]. Once removed, tissue fragments were washed in PBS (0.1 M phosphate buffer saline, pH 7.4), and immersed in 4% buffered formalin for at least 24 h at 4 °C; following fixation, tissue samples were dehydrated and embedded in paraffin. Serial longitudinal and transverse sections (7 µm thick) were collected on poly-L-lysine-coated slides and processed for histological and immunohistochemical labeling.

2.3. Histology

One section for each specimen was stained with hematoxylin and eosin (H&E) to assess tissue condition. Microscopic analysis of the sections showed the absence of pathological alteration in the gut (data not shown), and therefore the tissues from all three animals were included in the present research.

2.4. Double Immunofluorescence

To assess the proportion of subclasses of neurons and evaluate their co-localization, we performed double immunostaining with immunolabeling for either PGP9.5 and nNOS, PGP9.5 and SP or nNOS and SP. Briefly, sections were deparaffinized in xylene, rehydrated through graded ethanol and heated in sodium citrate buffer (pH 6.0) in a microwave (5 min at 700 W) for antigen retrieval. To block non-specific bindings, sections were incubated for 1.5 h at room temperature (RT) in a solution containing 20% normal goat serum (CS9022, Colorado Serum Co., Denver, CO, USA) or 20% normal donkey serum (D9663, Sigma-Aldrich, Saint Louis, MO, USA), and 0.5% Triton X-100 (Merck, Darmstadt, Germany) in PBS. Sections were then incubated overnight in a humid chamber at RT in a cocktail of primary antibodies (Table 1) diluted in 1.8% NaCl in 0.01 M PBS containing 0.1% sodium azide. After rinsing in PBS (3 × 10 min), the sections were incubated for 1.5 h at RT in a solution of secondary antibodies (Table 1) diluted in PBS. Enteric neurons were identified using blue fluorescent Nissl stain solution (NeuroTrace[®], Molecular Probes, Eugene, OR,

USA—NT throughout the text) for 90 min and/or the antibody guinea pig anti-PGP 9.5 (see Table 1 for details). The two neuronal markers identified the same neurons of the MP and SMP (Supplementary Figure S1). After washing, the sections were mounted in buffered glycerol at pH 8.6.

Table 1. Details of antibodies and NeuroTrace[®] used.

Primary Antibodies and NT	Host	Code	Dilution	Source
CHAT	Goat	Ab 144P	1:25	Millipore
cCHAT	Rabbit		1:100	Generous gift of Dr. K. Lips ^a
pCHAT	Rabbit		1:1000	Generous gift of Prof Kimura ^b
HuC/HuD	Mouse	A21271	1:200	Molecular Probes
HuC	Goat	SC-5977	1:100	Santa Cruz Biotechnologies
nNOS	Rabbit	Ab5380	1:300	Millipore
PGP 9.5	Guinea pig	Ab5898	1:100	Millipore
SP	Rat	10-S15A	1:300	Fitzgerald
NT		N21479	1:200	Molecular Probes
Secondary Antibodies		Dilution		Source
Goat anti-rabbit IgG FITC		1:200		Calbiochem
Donkey anti-rat IgG Alexa 594		1:50		Invitrogen
Goat anti-guinea pig TRITC		1:100		Chemicon

Abbreviations: CHAT, choline acetyltransferase; cCHAT, central choline acetyltransferase; pCHAT, peripheral choline acetyltransferase; nNOS, neuronal nitric oxide synthase; NT, blue fluorescent Nissl stain solution; PGP 9.5, protein gene product 9.5; SP, substance P; Suppliers: Calbiochem, Merck Millipore, Merck KGaA, Darmstadt, Germany; Chemicon, Merck Millipore, Merck KGaA, Darmstadt, Germany; Fitzgerald Industries International, Acton, Massachusetts, USA; Invitrogen, Thermo Fisher Scientific, Carlsbad, California, USA; Merck Millipore, Merck KGaA, Darmstadt, Germany; Molecular Probes, Eugene, Oregon, USA; Santa Cruz Biotechnologies, Dallas, Texas, USA;

^a Justus-Liebig-576 University, Giessen, Germany; ^b Shiga University of Medical Science, Otsu, Japan [33].

2.5. Specificity of the Primary Antibodies

The immunogen used to obtain antibody anti-nNOS (Ab5380) was the recombinant human neuronal nitric oxide synthase 1. The homology between the full amino acid sequences of *Tursiops truncatus* (A0A6J3PRR6_TURTR) and Human nNOS (P29475 NOS1_HUMAN) was 94.3%.

The immunogen used to obtain antibody anti-SP (10-S15A) was substance-P-BSA. The sequence of SP is very well conserved among many mammalian species [34], including the *Tursiops truncatus* (A0A2U3V1Z_TURTR), which shows 96.1% homology with the full amino acid sequence of Human SP (P20366 SP_HUMAN) and the 100 % homology with the peptidic sequence used as immunogen (RPKPQQFFGLM).

The homologies of nNOS and SP of *Tursiops truncatus* were verified by the “alignment” tool available on the Uniprot database (www.uniprot.org, accessed on 2 April 2021) and the BLAST tool of the National Center for Biotechnology information (NCBI) (www.ncbi.nlm.nih.gov, accessed on 2 April 2021).

In addition, the anti-SP and anti-nNOS antibodies utilized in the present study have been already successfully employed in the nervous system of the dolphins [35,36].

2.6. Specificity of the Secondary Antibodies

The specificity of the secondary antibodies (Table 1) was tested by the absence of signal after the exclusion of the primary antibodies on bottlenose dolphin intestinal tissues.

2.7. Analysis of Sections

Immunohistochemical preparations were analyzed with a Nikon Eclipse Ni microscope equipped with the appropriate filter cubes. The images were recorded with a DS-Qi1Nc digital camera and NIS Elements software BR 4.20.01 (Nikon Instruments Europe BV, Amsterdam, The Netherlands). The proportions of neurons that were immunoreactive for nNOS or SP were determined by examining fluorescent double-stained preparations. Neurons were first located by PGP9.5 immunostaining and/or by the presence of a fluorophore that labelled NT and then the filter was switched to determine whether or not the

neuron was labelled for a second antigen (nNOS or SP), located with a fluorophore of a different colour.

In this way, proportions of neurons labeled for pairs of antigens were determined. At least 200 NT-labeled neurons were counted for each sample tissue from each animal and the percentage of neurons that were NT labeled and/or PGP 9.5 immunolabeled and that were also immunoreactive for nNOS or SP was calculated and expressed as a relative percentage (median and interquartile range—IQR).

3. Results

3.1. Hematoxylin and Eosin Staining

In the bottlenose dolphin, the MP was organized in large ganglia located between the longitudinal (LML) and circular muscle layer (CML). In longitudinal and transverse sections, ganglia were different sizes and contained up to 43 neurons. The neurons of the SMP were organized in smaller ganglia (up to 18 neurons) distributed at two different levels within the submucosal layer. The inner submucosal plexus (ISMP) was composed of small ganglia located near the *muscularis mucosae*, harboring small cell bodies, whereas the outer submucosal plexus (OSMP), lying close to the CML, was composed of larger neurons. Solitary neurons were also observed, dispersed in the submucosal layer.

3.2. Nitrergic Neurons

The nitrergic subpopulation of enteric neurons presented a homogeneous immunoreactivity of the soma, without nuclear labeling. These neurons showed an irregular outline and short processes, resembling Dogiel type I neurons. In the MP, nNOS immunoreactive (nNOS-IR) neurons represented 28% (IQR = 19–29) of the total neuronal population (404/1478 cells; $n = 3$) (Figure 1A–C). In the SMP, nNOS-IR neurons were observed just occasionally (1% IQR = 0–2), and only in the OSMP, close to the CML (9/1132 cells, $n = 3$) (data not shown).

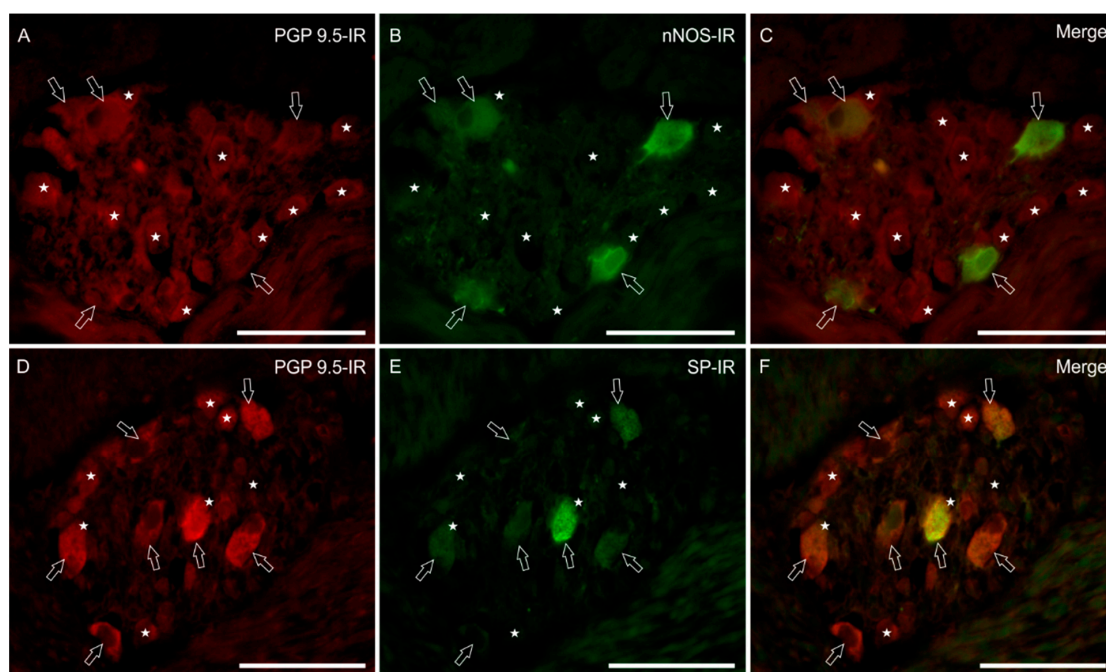


Figure 1. Micrographs showing nNOS (A–C) and SP immunoreactivity (IR) (D–F) in longitudinal sections of the myenteric plexus in bottlenose dolphin intestine. Stars indicate PGP 9.5 immunoreactive myenteric plexus neurons (A,D) which were not immunoreactive for the neuronal nitric oxide synthase (nNOS-IR) and substance P (SP-IR); arrows indicate PGP 9.5 immunoreactive neurons, which were also nNOS-IR (B) and SP-IR (E). (C,F) Merged images. Scale bar: 50 μ m.

3.3. SP-IR Neurons

SP-IR was expressed by 31% (IQR = 22–37) of MP (456/1478 cells, $n = 3$) and 41% (IQR = 24–63) of SMP neurons (412/1132 cells, $n = 3$). The majority of SP-IR myenteric neurons showed a smooth outline of the cell body, a typical feature of Dogiel type II neurons (Figure 1D–F). In the myenteric neuropil, we frequently observed bright SP-IR nerve fibers forming baskets of SP-IR varicosities around nNOS-IR and nNOS-negative neurons (Figure 2G–I). Immunolabeled varicosities and fibers were frequently visible around submucosal blood vessels (data not shown).

3.4. Co-Localizations of nNOS and SP

No co-localization between the two markers was detected, in either of the plexuses (Figure 2A–I).

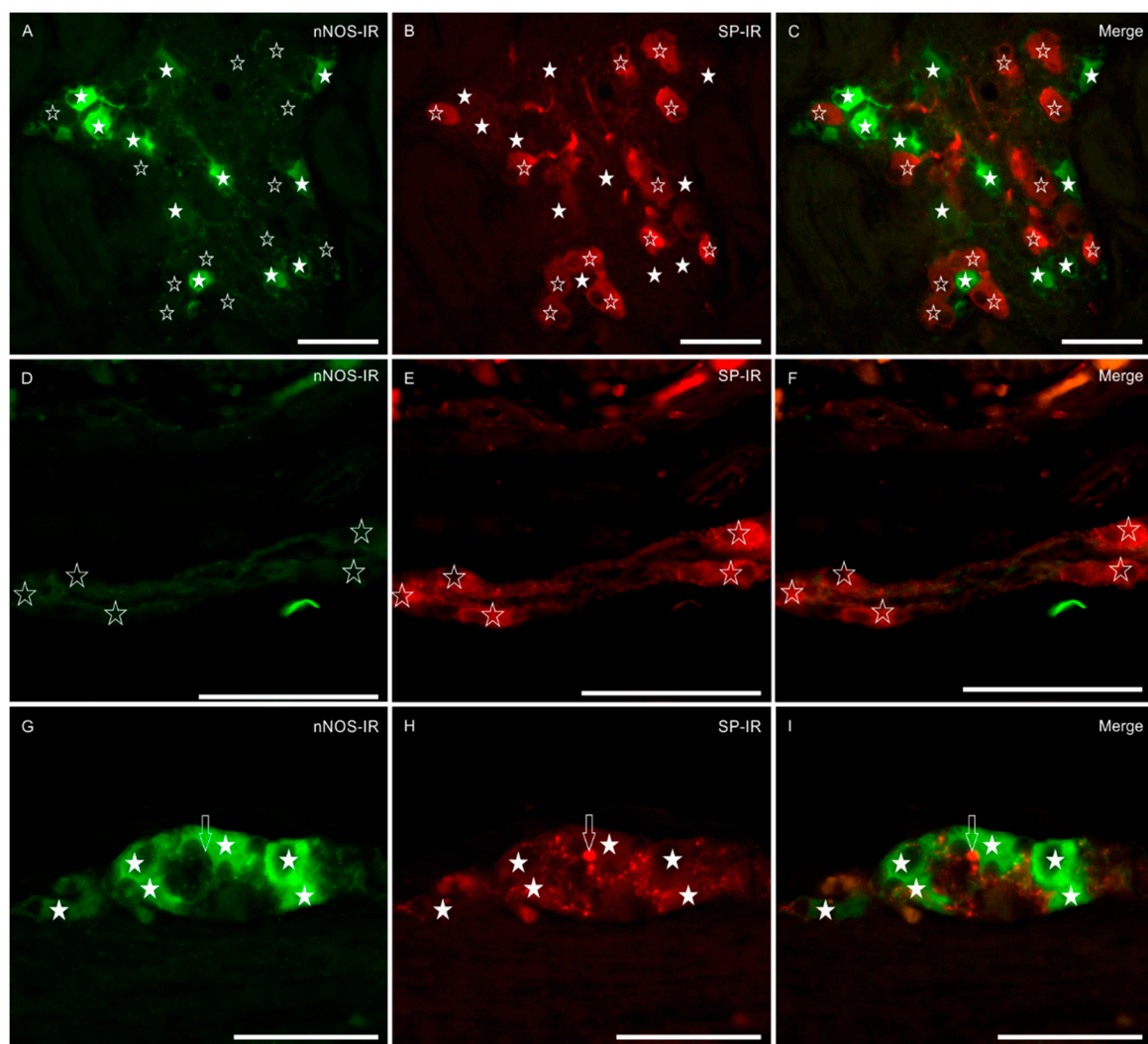


Figure 2. Micrographs of the sections of the myenteric plexus (MP) (A–C) and submucosal plexus (SMP) (D–I) of the bottlenose dolphin intestine. White stars indicate neurons showing neuronal nitric oxide synthase (nNOS) immunoreactivity (nNOS-IR); open stars indicate neurons showing substance P-IR (SP-IR). (A–C) Sections in which it is evident that no MP neurons co-expressed the two neuronal markers. (D–I) The SMP of the dolphin intestine was double layered; in the inner SMP (D–F), neurons preferentially expressed SP-IR (E) and were nNOS negative (D); nitrergic neurons were only observable in the outer SMP (G–I). The arrows indicate SP-IR varicosities encircling nitrergic neurons. (C,F,I) Merged images. Scale bar: 50 μ m.

4. Discussion

One of the unsolved problems with the functional anatomy of the GI tract in dolphins and whales is its subdivision. Since the post-gastric intestine shows no macroscopic change of morphology and diameter, a classification into small and large intestine or any further subdivision is impossible at the moment [2,7]. Waiting for a specific study that may identify the branches of the mesenteric arteries, and thus establish a phylogenetic comparative criterion to adopt for the subdivisions of the cetacean gut, here we describe the whole system without further classification. Our observations on the histological architecture of the ENS in the intestine of the bottlenose dolphin confirm previous findings [5,8–10]. A multi-layered distribution of the submucosal ganglia has already been reported in the intestine of other large mammals [37–49].

Several neurotransmitters, including tachykinins and NO, regulate the contractility of the GI musculature. The balance between excitatory and inhibitory signals to smooth muscle cells generates all the intestinal physiological motor patterns. As NO is the main transmitter involved in inhibitory inputs and SP is considered a co-transmitter in cholinergic neurons, the present study provides the first comprehensive insight into these two functional classes of neurons in the intestine of the bottlenose dolphin. Our data on the nitrergic MP subpopulation (28%) are partially consistent with those obtained in other large terrestrial mammals [50–56] and small terrestrial mammals [15,57,58]. Studies on rats indicate that nitrergic neurons account for 23 to 30% of the entire neuronal population in the ileum [59–63] and for about 34% in the colon [63,64].

The percentage obtained in the MP of bottlenose dolphins diverges from data obtained in the small and large human intestine, where nitrergic neurons represent about 34% and 38%, respectively [65], and from data obtained in the porcine colon, where nitrergic neurons account for about 50% of the enteric neuronal population [66].

In the SMP, nNOS-IR was expressed only by 1% of neurons, exclusively located in the large ganglia close to the CML, whereas they were absent in the ISMP. These percentages are similar to those previously described in the horse ileum [52] and in the small intestine of pigs [55,67–69] where nNOS-IR neurons represented from 1% to 8% of the total SMP neurons. On the other hand, our percentages are quite different from those obtained in the lamb ileum [51] and pig ascending colon [66], where SMP nNOS-IR neurons account for 21% of the former and 45% of the latter.

The great majority of nNOS-IR cells observed in the present research were Dogiel type I shaped. Dogiel type I cells, characterized by an angular outline of the soma and numerous dendritic processes, include interneurons and inhibitory motor neurons [15]. Interestingly, in the bottlenose dolphin intestine, we observed the presence of nitrergic neurons in the OSMP but not in the ISMP. In other species, it is well known that the ISMP and the OSMP present different neurochemical coding and different electrophysiological properties and, therefore, have distinct functions [45,68,70–72]. As OSMP neurons actually show a phenotype more similar to that of the myenteric plexus neurons, it is plausible that they supply an inhibitory innervation of the CML [73,74].

Several pathological conditions of the gastrointestinal tract of humans and other mammals are associated with an impairment of NO neurons [28,31,56,75–82]. Thus, to better understand the implications of nitrergic neurons in gastrointestinal pathologies of dolphins, it is essential to investigate, in particular, the architecture and neurochemistry of the ENS, especially its inhibitory components, in tissues of healthy animals.

To our knowledge, the distribution of SP-IR in the gastrointestinal tract of cetaceans was described only in the striped dolphin (*Stenella coeruleoalba*) by Domeneghini et al. [10], who reported generic values (i.e., low, average or high numbers) of intestinal SP-IR structures. In the bottlenose dolphin intestine, the myenteric SP-IR subpopulation accounts for 31% of the total neuronal population. This value is relatively higher than the percentages reported in the ileum of sheep (13%) [53], horses (14%) [52] and in the small intestine of pigs (from 1% to 9%) [55,69]. The majority of SP-IR neurons observed in the present study resemble Dogiel type II cells. Since SP-IR neurons could possibly be IPANs, interneurons or

excitatory muscular motor neurons [15,83,84], it seems unlikely that almost all MP neurons were Dogiel type II cells, because motor neurons and interneurons usually show Dogiel type I morphology. One explanation might be a reduced immunostaining of SP-IR neurons with the appearance of a smooth outline. However, in contrast to this last hypothesis, there is the clear morphology of nNOS-IR neurons, which showed an unequivocal Dogiel type I morphology.

In the SMP of the bottlenose dolphin, SP-IR neurons represent 41% of the total neuronal population and were largely located in the ISMP. This percentage is similar to that described in the ileum of sheep (38%) [51,53] and in the small intestine of piglets (from 20% to 42%, depending on the tract) [55,69], whereas it differs significantly from data obtained from the horse ileum [52] and from the colon of piglets [85], where SP-IR neurons correspond to 66% and 87% of the total neuronal population, respectively.

As reported in other mammals, like the striped dolphin [10] and the horse [52], we also observed baskets of SP-IR varicosities and fibers around the MP nitrergic and non-nitrergic neurons in the bottlenose dolphin. These fibers, located around somata, might arise from IPANs and interneurons [86] or from peripheral processes of dorsal root ganglion afferent neurons, which participate in the control of gastrointestinal activities [87]. Puzzling and hitherto unconfirmed findings in other marine Cetartiodactyla belonging to the *Ziphiidae* and *Delphinapteridae* families (Pfeiffer, 1993) reported a modified innervation of the myenteric plexus and changes in the *muscularis externa*. Specifically, the musculature of the gut showed the presence of intercalation-like striations, thus hinting at the possibility of a more specific control the movements of the gut, presumably functional in the peculiar modality of suction feeding [2,9]. The presence and distribution of visceral nitrergic and substance P immunoreactive neurons that we report here may further support the existence of such physiological mechanisms; however, voluntary movements would most likely require different neurochemical profiles which would need further investigation.

In contrast to what was described in sheep [53] and similarly to what was described in the small intestine of the mouse [57], no co-localization between nNOS- and SP-IR was detected in either the plexuses, suggesting the existence of two completely distinct functional classes of neurons in the intestine of the bottlenose dolphin. Indeed, also in colon, recent studies have shown distinctly segregated excitatory and inhibitory neurons [88], and their synaptic connections via intrinsic sensory neurons [88].

Limitations of the Study

This study should be considered as an initial preliminary overview and description of nNOS- and SP-IR neurons in the intestine of bottlenose dolphins. Despite many efforts to make the study scientifically accurate, we are aware of the limitations intrinsic to the present research. First of all are the disadvantages of studying free-range animals. In fact, the time between death and sampling is not always as short as it should be, especially regarding tissue in direct contact with the animal's microbiota. To avoid this problem, we chose animals based on the conservation grade that they were assigned, and we selected samples only from the freshest carcasses, with a conservation grade of 1 or 2 [31]. Nevertheless, among the animals chosen, a difference in the quality and preservation of the tissues could have existed, and it could have affected the immunoreactive properties. Furthermore, as there are fewer studies of cetaceans than there are of domestic animals, many antibodies were found to be useless. For instance, after various unsuccessful attempts with antibodies against choline acetyltransferase (CHAT), we were forced to use SP to mark excitatory neurons. In the same way, after many fruitless attempts with the pan-neuronal marker HuC/HuD, we decided to use NT and PGP9.5 in parallel in order to identify neurons in both plexuses. In the abovementioned cases, the lack of immunostaining could reflect conformational differences of the proteins in dolphins or be the consequence of bad tissue preservation. Another limitation was the reduced number of bottlenose dolphin included in the study. For the abovementioned reasons, the results reported here, although of interest, need to be supported by further investigation, with a larger number of cases.

At present, we are unaware of any other quantitative data obtained from other cetaceans with which to compare our data on the bottlenose dolphin. It is important to acknowledge major difference in diet and environment between marine and terrestrial mammals.

5. Conclusions

This is, to the best of the authors' knowledge, the first description and quantification of nNOS-IR neurons, and the first quantification of SP-IR neurons as well, in the intestine of a cetacean species.

Although the general characteristics and morphology of nNOS- and SP-IR neurons are conserved among most mammal species, we found differences in the relative prevalence of neurons expressing either markers, consisting mainly in a very small number of nNOS-IR neurons in the SMP, and a larger number of MP SP-IR neurons. Further investigation is needed to identify neurochemical classes of neurons and fibers in order to give a clearer and more comprehensive picture of the ENS complexity in this species. Providing information on the physiological conditions of a healthy intestine, including its nervous component, is crucial to the understanding of its pathological states.

Supplementary Materials: The following are available online at <https://www.mdpi.com/article/10.3390/ani11041057/s1>, Figure S1: PGP 9.5 immunoreactivity in the myenteric plexus of the bottlenose dolphin intestine.

Author Contributions: A.M.R., C.B. and R.C. co-designed the study. B.C. and J.-M.G. provided the samples. A.M.R., F.G., G.G. and G.S. performed the experiments. C.B. and R.C. supervised the experiments. A.M.R., J.-M.G. and F.G. analyzed the data. A.M.R., B.C. and R.C. wrote the manuscript. All authors contributed to the critical review of the manuscript. All authors have read and agreed to the published version of the manuscript.

Funding: This research received no external funding.

Institutional Review Board Statement: Ethical review and approval were waived for this study, due to the fact that the MMMTB is a CITES registered institution (IT 020) which is authorized to harvest, process and distribute tissues for scientific purposes from stranded marine mammals. No further permits are required for the scientific use of the said tissues under the current Italian and European legislation.

Informed Consent Statement: Not applicable.

Data Availability Statement: The data presented in this study are available on request from the corresponding author.

Conflicts of Interest: The authors have no conflicts of interest.

References

1. Reidenberg, J.S. Anatomical adaptations of aquatic mammals. *Anat. Rec.* **2007**, *290*, 507–513. [\[CrossRef\]](#)
2. Cozzi, B.; Huggenberger, S.; Oelschläger, H. *Anatomy of Dolphins. Insights into Body Structure and Function*; Academic Press: San Diego, CA, USA, 2017; ISBN 978-0-12-407229-9.
3. Reidenberg, J.S.; Laitman, J.T. Position of the larynx in odontoceti (toothed whales). *Anat. Rec.* **1987**, *218*, 98–106. [\[CrossRef\]](#)
4. Harrison, R.J.; Johnson, F.R.; Young, B.A. The oesophagus and stomach of dolphins (*Tursiops*, *Delphinus*, *Stenella*). *J. Zool. Lond.* **1970**, *160*, 377–390. [\[CrossRef\]](#)
5. Gaskin, D.E. Form and function in the digestive tract and associated organs in Cetacea, with a consideration of metabolic rates and specific energy budgets. *Oceanogr. Mar. Biol. Ann. Rev.* **1978**, *16*, 313–345.
6. Mead, J.G. Gastrointestinal tract. In *Encyclopedia of Marine Mammals*, 2nd ed.; Perrin, W., Wursing, B., Thewissen, J., Eds.; Academic Press: New York, NY, USA, 2008; pp. 472–477.
7. Huggenberger, S.; Oelschläger, H.; Cozzi, B. *Atlas of the Anatomy of Dolphins and Whales*; Academic Press: London, UK, 2019; ISBN 978-0-12-802446-1.
8. Russo, F.; Gatta, C.; De Girolamo, P.; Cozzi, B.; Giurisato, M.; Lucini, C.; Varricchio, E. Expression and immunohistochemical detection of leptin-like peptide in the gastrointestinal tract of the South American sea lion (*Otaria flavescens*) and the bottlenose dolphin (*Tursiops truncatus*). *Anat. Rec.* **2012**, *295*, 1482–1493. [\[CrossRef\]](#)

9. Pfeiffer, C.J. Neural and muscular control functions of the gut in odontocetes: Morphologic evidence in beaked whales and beluga whales. *J. Physiol. Paris* **1993**, *87*, 349–354. [[PubMed](#)]
10. Domeneghini, C.; Massoletti, P.; Arrighi, S. Localization of regulatory peptides in the gastrointestinal tract of the striped dolphin, *Stenella coeruleoalba* (Mammalia: Cetacea). An immunohistochemical study. *Eur. J. Histochem.* **1997**, *41*, 285–300.
11. Naka, T.; Katsumata, E.; Sasaki, K.; Minamino, N.; Yoshioka, M.; Takei, Y. Natriuretic peptides in cetacean: Identification, molecular characterization and changes in plasma concentration after landing. *Zool. Sci.* **2007**, *24*, 577–587. [[CrossRef](#)] [[PubMed](#)]
12. Gatta, C.; Russo, F.; Russolillo, M.G.; Varricchio, E.; Paolucci, M.; Castaldo, L.; Lucini, C.; de Girolamo, P.; Cozzi, B.; Maruccio, L. The orexin system in the enteric nervous system of the bottlenose dolphin (*Tursiops truncatus*). *PLoS ONE* **2014**, *9*, e105009. [[CrossRef](#)]
13. Spencer, N.J.; Hu, H. Enteric nervous system: Sensory transduction, neural circuits and gastrointestinal motility. *Nat. Rev. Gastroenterol. Hepatol.* **2020**, *17*, 338–351. [[CrossRef](#)] [[PubMed](#)]
14. Grundy, D.; Schemann, M. Enteric nervous system. *Curr. Opin. Gastroenterol.* **2005**, *21*, 176–182. [[CrossRef](#)]
15. Furness, J.B. *The Enteric Nervous System*; Blackwell: Oxford, UK, 2006.
16. Sanders, K.M.; Ward, S.M. Nitric oxide as a mediator of nonadrenergic noncholinergic neurotransmission. *Am. J. Physiol.* **1992**, *262*, G379–G392. [[CrossRef](#)] [[PubMed](#)]
17. Stark, M.E.; Bauer, A.J.; Sarr, M.G.; Szurszewski, J.H. Nitric oxide mediates inhibitory nerve input in human and canine jejunum. *Gastroenterology* **1993**, *104*, 398–409. [[CrossRef](#)]
18. Costa, M.; Furness, J.B.; Pompolo, S.; Brookes, S.J.; Bornstein, J.C.; Bredt, D.S.; Snyder, S.H. Projections and chemical coding of neurons with immunoreactivity for nitric oxide synthase in the guinea-pig small intestine. *Neurosci. Lett.* **1992**, *148*, 121–125. [[CrossRef](#)]
19. Ekblad, E.; Mulder, H.; Uddman, R.; Sundler, F. NOS-containing neurons in the rat gut and coeliac ganglia. *Neuropharmacology* **1994**, *33*, 1323–1331. [[CrossRef](#)]
20. Timmermans, J.P.; Barbiers, M.; Scheuermann, D.W.; Bogers, J.J.; Adriaensen, D.; Fekete, E.; Mayer, B.; Van Marck, E.A.; De Groodt-Lasseel, M.H. Nitric oxide synthase immunoreactivity in the enteric nervous system of the developing human digestive tract. *Cell Tissue Res.* **1994**, *275*, 235–245. [[CrossRef](#)] [[PubMed](#)]
21. Timmermans, J.P.; Barbiers, M.; Scheuermann, D.W.; Stach, W.; Adriaensen, D.; Mayer, B.; De Groodt-Lasseel, M.H. Distribution pattern, neurochemical features and projections of nitrergic neurons in the pig small intestine. *Ann. Anat.* **1994**, *176*, 515–525. [[CrossRef](#)]
22. Holzer, P.; Holzer-Petsche, U. Tachykinins in the gut. Part I. Expression, release and motor function. *Pharmacol. Ther.* **1997**, *73*, 173–217. [[CrossRef](#)]
23. Holzer, P.; Holzer-Petsche, U. Tachykinins in the gut. Part II. Roles in neural excitation, secretion and inflammation. *Pharmacol. Ther.* **1997**, *73*, 219–263. [[CrossRef](#)]
24. Maggi, C.A.; Catalioto, R.M.; Criscuoli, M.; Cucchi, P.; Giuliani, S.; Lecci, A.; Lippi, A.; Meini, S.; Patacchini, R.; Renzetti, A.R.; et al. Tachykinin receptors and intestinal motility. *Can. J. Physiol. Pharmacol.* **1997**, *75*, 696–703. [[CrossRef](#)]
25. Shimizu, Y.; Matsuyama, H.; Shiina, T.; Takewaki, T.; Furness, J.B. Tachykinins and their functions in the gastrointestinal tract. *Cell. Mol. Life Sci.* **2008**, *65*, 295–311. [[CrossRef](#)] [[PubMed](#)]
26. Steinhoff, M.S.; von Mentzer, B.; Geppetti, P.; Pothoulakis, C.; Bunnett, N.W. Tachykinins and their receptors: Contributions to physiological control and the mechanisms of disease. *Physiol. Rev.* **2014**, *94*, 265–301. [[CrossRef](#)]
27. Brookes, S.J. Classes of enteric nerve cells in the guinea-pig small intestine. *Anat. Rec.* **2001**, *262*, 58–70. [[CrossRef](#)]
28. Sivarao, D.V.; Mashimo, H.; Goyal, R.K. Pyloric sphincter dysfunction in nNOS^{-/-} and W/W^v mutant mice: Animal models of gastroparesis and duodenogastric reflux. *Gastroenterology* **2008**, *135*, 1258–1266. [[CrossRef](#)] [[PubMed](#)]
29. King, S.K.; Sutcliffe, J.R.; Ong, S.Y.; Lee, M.; Koh, T.L.; Wong, S.Q.; Farmer, P.J.; Peck, C.J.; Stanton, M.P.; Keck, J.; et al. Substance P and vasoactive intestinal peptide are reduced in right transverse colon in pediatric slow-transit constipation. *Neurogastroenterol. Motil.* **2010**, *22*, 883–892.e234. [[CrossRef](#)] [[PubMed](#)]
30. Cellini, J.; Pommier, R.; Porter, R.; LePard, K.J. Enhanced nerve-stimulated muscarinic and neurokinin contractions of ileum from streptozotocin guinea-pigs. *Auton. Autacoid. Pharmacol.* **2012**, *32*, 23–39. [[CrossRef](#)]
31. Masaoka, T.; Vanuytsel, T.; Vanormelingen, C.; Kindt, S.; Salim Rasoel, S.; Boesmans, W.; De Hertogh, G.; Farre, R.; Vanden Berghe, P.; Tack, J. A spontaneous animal model of intestinal dysmotility evoked by inflammatory nitrergic dysfunction. *PLoS ONE* **2014**, *9*, e95879. [[CrossRef](#)]
32. Kuiken, T.; García-Hartmann, M. Cetacean Dissection techniques and tissue sampling. In Proceedings of the First ECS Workshop on Cetacean Pathology, Leiden, The Netherlands, 13–14 September 1991.
33. Tooyama, I.; Kimura, H. A protein encoded by an alternative splice variant of choline acetyltransferase mRNA is localized preferentially in peripheral nerve cells and fibers. *J. Chem. Neuroanat.* **2000**, *17*, 217–226. [[CrossRef](#)]
34. Holmgren, S.; Jensen, J. Evolution of vertebrate neuropeptides. *Brain Res. Bull.* **2001**, *55*, 723–735. [[CrossRef](#)]
35. Bombardi, C.; Cozzi, B.; Nenzi, A.; Mazzariol, S.; Grandis, A. Distribution of nitrergic neurons in the dorsal root ganglia of the bottlenose dolphin (*Tursiops truncatus*). *Anat. Rec.* **2011**, *294*, 1066–1073. [[CrossRef](#)] [[PubMed](#)]
36. Ramírez, T.; Sacchini, S.; Paz, Y.; Rosales, R.S.; Cámara, N.; Andrada, M.; Arbelo, M.; Fernández, A. Comparison of Methods for the Histological Evaluation of Odontocete Spiral Ganglion Cells. *Animals* **2020**, *10*, 683. [[CrossRef](#)]
37. Schabadasch, A. Intramurale Nervengeflechte des Darmrohrs. *Z. Zellforsch. Mikr. Anat.* **1930**, *10*, 320–385. [[CrossRef](#)]

38. Gunn, M. Histological and histochemical observations on the myenteric and submucous plexuses of mammals. *J. Anat.* **1968**, *102*, 223–239.
39. Stach, W. The external submucous plexus (Schabadasch) in the small intestine of the swine. I. Form, structure and connections of ganglia and nerve cells. *Z. Mikrosk. Anat. Forsch.* **1977**, *91*, 737–755.
40. Christensen, J.; Rick, G.A. Intrinsic nerves in the mammalian colon: Confirmation of a plexus at the circular muscle-submucosal interface. *J. Auton. Nerv. Syst.* **1987**, *21*, 223–231. [\[CrossRef\]](#)
41. Scheuermann, D.W.; Stach, W.; Timmermans, J.P. Topography, architecture and structure of the plexus submucosus externus (Schabadasch) of the porcine small intestine in scanning electron microscopy. *Acta Anat.* **1987**, *129*, 105–115. [\[CrossRef\]](#) [\[PubMed\]](#)
42. Scheuermann, D.W.; Stach, W.; Timmermans, J.P. Topography, architecture and structure of the plexus submucosus internus (Meissner) of the porcine small intestine in scanning electron microscopy. *Acta Anat.* **1987**, *129*, 96–104. [\[CrossRef\]](#)
43. Timmermans, J.P.; Scheuermann, D.W.; Stach, W.; Adriaensen, D.; De Groodt-Lasseel, M.H. Functional morphology of the enteric nervous system with special reference to large mammals. *Eur. J. Morphol.* **1992**, *30*, 113–122.
44. Timmermans, J.P.; Adriaensen, D.; Cornelissen, W.; Scheuermann, D.W. Structural organization and neuropeptide distribution in the mammalian enteric nervous system, with special attention to those components involved in mucosal reflexes. *Comp. Biochem. Physiol. A Physiol.* **1997**, *118*, 331–340. [\[CrossRef\]](#)
45. Timmermans, J.P.; Hens, J.; Adriaensen, D. Outer submucous plexus: An intrinsic nerve network involved in both secretory and motility processes in the intestine of large mammals and humans. *Anat. Rec.* **2001**, *262*, 71–78. [\[CrossRef\]](#)
46. Pearson, G.T. Structural organization and neuropeptide distributions in the equine enteric nervous system: An immunohistochemical study using whole-mount preparations from the small intestine. *Cell Tissue Res.* **1994**, *276*, 523–534. [\[CrossRef\]](#)
47. Pompolo, S. An immunohistochemical study of neuropeptides and neuron-specific proteins present in the small intestine of the black-capped capuchin (*Cebus appella*). *Neurogastroenterol. Mot.* **1994**, *6*, 223–232. [\[CrossRef\]](#)
48. Balemba, O.B.; Grondahl, M.L.; Mbassa, G.K.; Semuguruka, W.D.; Hay-Smith, A.; Skadhauge, E.; Dantzer, V. The organisation of the enteric nervous system in the submucous and mucous layers of the small intestine of the pig studied by VIP and neurofilament protein immunohistochemistry. *J. Anat.* **1998**, *192*, 257–267. [\[CrossRef\]](#)
49. Balemba, O.B.; Mbassa, G.K.; Semuguruka, W.D.; Assey, R.J.; Kahwa, C.K.; Hay-Schmidt, A.; Dantzer, V. The topography, architecture and structure of the enteric nervous system in the jejunum and ileum of cattle. *J. Anat.* **1999**, *195*, 1–9. [\[CrossRef\]](#) [\[PubMed\]](#)
50. Brehmer, A.; Schrod, F.; Neuhuber, W.; Tooyama, I.; Kimura, H. Co-expression pattern of neuronal nitric oxide synthase and two variants of choline acetyltransferase in myenteric neurons of porcine ileum. *J. Chem. Neuroanat.* **2004**, *27*, 33–41. [\[CrossRef\]](#)
51. Chiocchetti, R.; Grandis, A.; Bombardi, C.; Lucchi, M.L.; Dal Lago, D.T.; Bortolami, R.; Furness, J.B. Extrinsic and intrinsic sources of calcitonin gene-related peptide immunoreactivity in the lamb ileum: A morphometric and neurochemical investigation. *Cell. Tissue Res.* **2006**, *323*, 183–196. [\[CrossRef\]](#)
52. Chiocchetti, R.; Bombardi, C.; Mongardi-Fantaguzzi, C.; Venturelli, E.; Russo, D.; Spadari, A.; Montoneri, C.; Romagnoli, N.; Grandis, A. Intrinsic innervation of the horse ileum. *Res. Vet. Sci.* **2009**, *87*, 177–185. [\[CrossRef\]](#)
53. Mazzuoli, G.; Mazzoni, M.; Albanese, V.; Clavenzani, P.; Lalatta-Costerbosa, G.; Lucchi, M.L.; Furness, J.B.; Chiocchetti, R. Morphology and neurochemistry of descending and ascending myenteric plexus neurons of sheep ileum. *Anat. Rec.* **2007**, *290*, 1480–1491. [\[CrossRef\]](#)
54. Freytag, C.; Seeger, J.; Siegemund, T.; Grosche, J.; Grosche, A.; Freeman, D.E.; Schusser, G.F.; Hartig, W. Immunohistochemical characterization and quantitative analysis of neurons in the myenteric plexus of the equine intestine. *Brain Res.* **2008**, *1244*, 53–64. [\[CrossRef\]](#)
55. Zacharko-Siembida, A.; Valverde Piedra, J.L.; Szymanczyk, S.; Arciszewski, M.B. Immunolocalization of NOS, VIP, galanin and SP in the small intestine of suckling pigs treated with red kidney bean (*Phaseolus vulgaris*) lectin. *Acta Histochem.* **2013**, *115*, 219–225. [\[CrossRef\]](#) [\[PubMed\]](#)
56. Giancola, F.; Fracassi, F.; Gallucci, A.; Sadeghinezhad, J.; Polidoro, G.; Zini, E.; Asti, M.; Chiocchetti, R. Quantification of nitrergic neurons in the myenteric plexus of gastric antrum and ileum of healthy and diabetic dogs. *Auton. Neurosci.* **2016**, *197*, 25–33. [\[CrossRef\]](#)
57. Qu, Z.D.; Thacker, M.; Castelucci, P.; Bagyanszki, M.; Epstein, M.L.; Furness, J.B. Immunohistochemical analysis of neuron types in the mouse small intestine. *Cell Tissue Res.* **2008**, *334*, 147–161. [\[CrossRef\]](#)
58. Lawson, V.A.; Furness, J.B.; Klemm, H.M.; Pontell, L.; Chan, E.; Hill, A.F.; Chiocchetti, R. The brain to gut pathway: A possible route of prion transmission. *Gut* **2010**, *59*, 1643–1651. [\[CrossRef\]](#)
59. Nichols, K.; Staines, W.; Krantis, A. Nitric oxide synthase distribution in the rat intestine: A histochemical analysis. *Gastroenterology* **1993**, *105*, 1651–1661. [\[CrossRef\]](#)
60. Lin, Z.; Liu, Y.; Zheng, Q.; Hu, Q. Increased proportion of nitric oxide synthase immunoreactive neurons in rat ileal myenteric ganglia after severe acute pancreatitis. *BMC Gastroenterol.* **2011**, *11*, 127. [\[CrossRef\]](#) [\[PubMed\]](#)
61. Mann, P.T.; Furness, J.B.; Southwell, B.R. Choline acetyltransferase immunoreactivity of putative intrinsic primary afferent neurons in the rat ileum. *Cell Tissue Res.* **1999**, *297*, 241–248. [\[CrossRef\]](#)
62. Brasileiro, A.D.; Garcia, L.P.; de Carvalho da Silva, S.; Rocha, L.B.; Pedrosa, A.L.; Vieira, A.S.; da Silva, V.J.D.; Rodrigues, A.R.A. Effects of diabetes mellitus on myenteric neuronal density and sodium channel expression in the rat ileum. *Brain Res.* **2019**, *1708*, 1–9. [\[CrossRef\]](#)

63. Chiocchetti, R.; Hitrec, T.; Giancola, F.; Sadeghinezhad, J.; Squarcio, F.; Galiazzo, G.; Piscitiello, E.; De Silva, M.; Cerri, M.; Amici, R.; et al. Phosphorylated Tau protein in the myenteric plexus of the ileum and colon of normothermic rats and during synthetic torpor. *Cell Tissue Res.* **2021**, *29*. [\[CrossRef\]](#)
64. da Silva, M.V.; Marosti, A.R.; Mendes, C.E.; Palombit, K.; Castelucci, P. Differential effects of experimental ulcerative colitis on P2X7 receptor expression in enteric neurons. *Histochem. Cell Biol.* **2015**, *143*, 171–184. [\[CrossRef\]](#) [\[PubMed\]](#)
65. Brehmer, A.; Schrod, F.; Neuhuber, W. Morphology of VIP/nNOS-immunoreactive myenteric neurons in the human gut. *Histochem. Cell. Biol.* **2006**, *125*, 557–565. [\[CrossRef\]](#)
66. Mazzoni, M.; Caremoli, F.; Cabanillas, L.; de Los Santos, J.; Million, M.; Larauche, M.; Clavenzani, P.; De Giorgio, R.; Sternini, C. Quantitative analysis of enteric neurons containing choline acetyltransferase and nitric oxide synthase immunoreactivities in the submucosal and myenteric plexuses of the porcine colon. *Cell Tissue Res.* **2020**, *23*. [\[CrossRef\]](#) [\[PubMed\]](#)
67. Timmermans, J.P.; Scheuermann, D.W.; Stach, W.; Adriaensen, D.; De Groodt-Lasseel, M.H.; Polak, J.M. Neuromedin U-immunoreactivity in the nervous system of the small intestine of the pig and its coexistence with substance P and CGRP. *Cell Tissue Res.* **1989**, *258*, 331–337. [\[CrossRef\]](#) [\[PubMed\]](#)
68. Timmermans, J.P.; Scheuermann, D.W.; Stach, W.; Adriaensen, D.; De Groodt-Lasseel, M.H. Distinct distribution of CGRP-, enkephalin-, galanin-, neuromedin U-, neuropeptide Y-, somatostatin-, substance P-, VIP- and serotonin-containing neurons in the two submucosal ganglionic neural networks of the porcine small intestine. *Cell Tissue Res.* **1990**, *260*, 367–379. [\[CrossRef\]](#)
69. Czajkowska, M.; Calka, J. Neurochemistry of Enteric Neurons Following Prolonged Indomethacin Administration in the Porcine Duodenum. *Front. Pharmacol.* **2020**, *11*, 564457. [\[CrossRef\]](#)
70. Crowe, R.; Kamm, M.A.; Burnstock, G.; Lennard-Jones, J.E. Peptide-containing neurons in different regions of the submucous plexus of human sigmoid colon. *Gastroenterology* **1992**, *102*, 461–467. [\[CrossRef\]](#)
71. Thomsen, L.; Pearson, G.T.; Larsen, E.H.; Skadhauge, E. Electrophysiological properties of neurones in the internal and external submucous plexuses of newborn pig small intestine. *J. Physiol.* **1997**, *498*, 773–785. [\[CrossRef\]](#) [\[PubMed\]](#)
72. Thomsen, L.; Pearson, G.T.; Skadhauge, E. Electrophysiological classification of submucosal plexus neurones in the jejunum of the newborn pig. *Comp. Biochem. Physiol. A Physiol.* **1997**, *118*, 363–366. [\[CrossRef\]](#)
73. Scheuermann, D.W.; Stach, W.; Timmermans, J.P. Morphology and immunocytochemistry of the enteric nervous system in the porcine small intestine. Part II. *Acta Gastroenterol. Belg.* **1988**, *51*, A3.
74. Hens, J.; Schrödl, F.; Brehmer, A.; Adriaensen, D.; Neuhuber, W.; Scheuermann, D.W.; Schemann, M.; Timmermans, J.-P. Mucosal projections of enteric neurons in the porcine small intestine. *J. Comp. Neurol.* **2000**, *421*, 429–436. [\[CrossRef\]](#)
75. Vanderwinden, J.M.; De Laet, M.H.; Schiffmann, S.N.; Mailleux, P.; Lowenstein, C.J.; Snyder, S.H.; Vanderhaeghen, J.J. Nitric oxide synthase distribution in the enteric nervous system of Hirschsprung's disease. *Gastroenterology* **1993**, *105*, 969–973. [\[CrossRef\]](#)
76. Bealer, J.F.; Natuzzi, E.S.; Flake, A.W.; Adzick, N.S.; Harrison, M.R. Effect of nitric oxide on the colonic smooth muscle of patients with Hirschsprung's disease. *J. Pediatr. Surg.* **1994**, *29*, 1025–1029. [\[CrossRef\]](#)
77. Tomita, R.; Munakata, K.; Kurosu, Y.; Tanjoh, K. A role of nitric oxide in Hirschsprung's disease. *J. Pediatr. Surg.* **1995**, *30*, 437–440. [\[CrossRef\]](#)
78. Takahashi, T.; Nakamura, K.; Itoh, H.; Sima, A.A.; Owyang, C. Impaired expression of nitric oxide synthase in the gastric myenteric plexus of spontaneously diabetic rats. *Gastroenterology* **1997**, *113*, 1535–1544. [\[CrossRef\]](#)
79. Ribeiro, U., Jr.; Safatle-Ribeiro, A.V.; Habr-Gama, A.; Gama-Rodrigues, J.J.; Sohn, J.; Reynolds, J.C. Effect of Chagas' disease on nitric oxide-containing neurons in severely affected and unaffected intestine. *Dis. Colon Rectum* **1998**, *41*, 1411–1417. [\[CrossRef\]](#) [\[PubMed\]](#)
80. Spangeus, A.; Suhr, O.; El-Salhy, M. Diabetic state affects the innervation of gut in an animal model of human type 1 diabetes. *Histol. Histopathol.* **2000**, *15*, 739–744.
81. Takahashi, T. Pathophysiological significance of neuronal nitric oxide synthase in the gastrointestinal tract. *J. Gastroenterol.* **2003**, *38*, 421–430. [\[CrossRef\]](#)
82. Rivera, L.R.; Poole, D.P.; Thacker, M.; Furness, J.B. The involvement of nitric oxide synthase neurons in enteric neuropathies. *Neurogastroenterol. Motil.* **2011**, *23*, 980–988. [\[CrossRef\]](#)
83. Sang, Q.; Williamson, S.; Young, H.M. Projections of chemically identified myenteric neurons of the small and large intestine of the mouse. *J. Anat.* **1997**, *190*, 209–222. [\[CrossRef\]](#)
84. Clerc, N.; Furness, J.B.; Li, Z.S.; Bornstein, J.C.; Kunze, W.A. Morphological and immunohistochemical identification of neurons and their targets in the guinea-pig duodenum. *Neuroscience* **1998**, *86*, 679–694. [\[CrossRef\]](#)
85. Petto, C.; Gabel, G.; Pfannkuche, H. Architecture and Chemical Coding of the Inner and Outer Submucous Plexus in the Colon of Piglets. *PLoS ONE* **2015**, *10*, e0133350. [\[CrossRef\]](#) [\[PubMed\]](#)
86. Furness, J.B.; Jones, C.; Nurgali, K.; Clerc, N. Intrinsic primary afferent neurons and nerve circuits within the intestine. *Prog. Neurobiol.* **2004**, *72*, 143–164. [\[CrossRef\]](#) [\[PubMed\]](#)
87. Holzer, P. Role of visceral afferent neurons in mucosal inflammation and defense. *Curr. Opin. Pharmacol.* **2007**, *7*, 563–569. [\[CrossRef\]](#) [\[PubMed\]](#)
88. Smolilo, D.J.; Costa, M.; Hibberd, T.J.; Brookes, S.J.H.; Wattchow, D.A.; Spencer, N.J. Distribution, projections, and association with calbindin baskets of motor neurons, interneurons, and sensory neurons in guinea-pig distal colon. *J. Comp. Neurol.* **2019**, *527*, 1140–1158. [\[CrossRef\]](#) [\[PubMed\]](#)

Chapter 7:

Cannabinoid receptors in the inflammatory cells of canine atopic dermatitis



OPEN ACCESS

EDITED BY

Isaac Karimi,
Razi University, Iran

REVIEWED BY

Shanker Kumar Singh,
U.P. Pandit Deen Dayal Upadhyaya
Veterinary University, India
Vincenzo Miragliotta,
University of Pisa, Italy

*CORRESPONDENCE

Roberto Chiocchetti
roberto.chiocchetti@unibo.it

SPECIALTY SECTION

This article was submitted to
Comparative and Clinical Medicine,
a section of the journal
Frontiers in Veterinary Science

RECEIVED 05 July 2022

ACCEPTED 29 August 2022

PUBLISHED 15 September 2022

CITATION

Chiocchetti R, Salamanca G, De
Silva M, Gobbo F, Aspidi F, Cunha RZ,
Galiazzo G, Tagliavia C, Sarli G and
Morini M (2022) Cannabinoid
receptors in the inflammatory cells of
canine atopic dermatitis.
Front. Vet. Sci. 9:987132.
doi: 10.3389/fvets.2022.987132

COPYRIGHT

© 2022 Chiocchetti, Salamanca, De
Silva, Gobbo, Aspidi, Cunha, Galiazzo,
Tagliavia, Sarli and Morini. This is an
open-access article distributed under
the terms of the [Creative Commons
Attribution License \(CC BY\)](#). The use,
distribution or reproduction in other
forums is permitted, provided the
original author(s) and the copyright
owner(s) are credited and that the
original publication in this journal is
cited, in accordance with accepted
academic practice. No use, distribution
or reproduction is permitted which
does not comply with these terms.

Cannabinoid receptors in the inflammatory cells of canine atopic dermatitis

Roberto Chiocchetti^{1*}, Giulia Salamanca¹,
Margherita De Silva¹, Francesca Gobbo¹, Francesca Aspidi¹,
Rodrigo Zamith Cunha¹, Giorgia Galiazzo¹,
Claudio Tagliavia^{1,2}, Giuseppe Sarli¹ and Maria Morini¹

¹Department of Veterinary Medical Sciences (UNI EN ISO 9001:2008), University of Bologna, Bologna, Italy, ²Faculty of Veterinary Medicine, Università degli Studi di Teramo, Località Piano D'Accio, Teramo, Italy

Background: Atopic dermatitis (AD) is one of the most common cutaneous inflammatory and pruritic diseases in dogs. Considering its multifactorial nature, AD can be a challenging disease to manage, and the therapeutic strategy must often be multimodal. In recent years, research has been moving toward the use of natural products which have beneficial effects on inflammation and itching, and no side effects. Cannabinoid receptors have been demonstrated to be expressed in healthy and diseased skin; therefore, one of the potential alternative therapeutic targets for investigating AD is the endocannabinoid system (ECS).

Objective: To immunohistochemically investigate the expression of the cannabinoid receptor type 2 (CB2R), and the cannabinoid-related receptors G protein-coupled receptor 55 (GPR55), transient receptor potential vanilloid 1 (TRPV1) and ankyrin 1 (TRPA1) in mast cells (MCs), macrophages, dendritic cells (DCs), T cells, and neutrophils of the skin of dogs with AD.

Animals: Samples of skin tissues were collected from eight dogs with AD (AD-dogs).

Materials and methods: The immunofluorescent stained cryosections of the skins of 8 dogs with AD having antibodies against CB2R, GPR55, TRPV1, TRPA1 were semiquantitatively evaluated. The inflammatory cells were identified using antibodies against tryptase (mast cells), ionized calcium binding adaptor molecule 1 (IBA1) (macrophages/DCs), CD3 (T cells), and calprotectin (neutrophils). The proportions of MCs, macrophages/DCs, T cells, and neutrophils expressing CB2R, GPR55, TRPV1 and TRPA1 were evaluated.

Results: The cells of the inflammatory infiltrate showed immunoreactivity (IR) for all or for some of the cannabinoid and cannabinoid-related receptors studied. In particular, MCs and macrophages/DCs showed CB2R-, GPR55-, TRPA1-, and TRPV1-IR; T cells showed CB2R-, GPR55- and TRPA1-IR, and neutrophils expressed GPR55-IR. Co-localization studies indicated that CB2R-IR was co-expressed with TRPV1-, TRPA1-, and GPR55-IR in different cellular elements of the dermis of the AD-dogs.

Conclusions and clinical importance: Cannabinoid receptor 2, and cannabinoid-related receptors GPR55, TRPV1 and TRPA1 were widely expressed in the inflammatory infiltrate of the AD-dogs. Based on the present findings, the ECS could be considered to be a potential therapeutic target for dogs with AD, and may mitigate itch and inflammation.

KEYWORDS

cannabidiol, CB2R, GPR55, immunohistochemistry, TRPA1, TRPV1

Introduction

Atopic dermatitis (AD) is one of the most common cutaneous inflammatory and pruritic diseases in dogs; it affects up to 27% of the canine population (1). Atopic dermatitis is associated with well-defined clinical signs and the overexpression of immunoglobulin IgE directed against environmental allergens, (s.c. extrinsic AD) (2–4) even if cases not due to IgE responses are known (s.c. intrinsic AD or atopic-like) (3). Several factors, in both humans and dogs, appear to contribute to skin inflammation and itching, such as increased exposure to pollutants, changes in dietary habits, stress, genetic factors, and cutaneous infections which predispose to the development of the disease.

The cells of the epidermis (keratinocytes) and the innate immune system play a critical role in AD, as shown not only in humans and rodents (5), but also in dogs (6). It has been shown that the skin of dogs with AD produces potent inflammatory mediators (7) and neurotrophins (8), which may be related to the hyperinnervation of the AD lesions (9). Pruritus, one of the most severe clinical signs of AD, is caused by a complex interface between pruritogenic molecules, keratinocytes, immunocytes, cutaneous nerve fibers, and the peripheral and central nervous systems (10).

Mast cells, strategically located at the sites directly interfacing with the external environment (11, 12), may release a variety of proinflammatory, vasoactive, and nociceptive mediators (13–15). However, in AD, keratinocytes and other inflammatory cell types, such as activated *T*-cells, macrophages, dendritic cells (DCs), Langerhans cells (LCs), basophils, and eosinophils may also display some abnormality (16, 17). In AD-related hypersensitivity a Th2-polarized lymphocyte response is activated by keratinocytes which produce cytokines (Interleukin [IL]-25 and IL-33), and thymic stromal lymphopoietin (TSLP) which leads to Th2 immune deviation (1, 8, 18, 19). Activated Th2 cells release IL-31 which stimulate itching by acting on IL-31 receptor A (IL-31RA) expressed on sensory nerve fibers and various immune cells, such as MCs, macrophages, DCs, eosinophils and basophils (20–26). Macrophages are also stimulated by inflammatory cytokines secreted by keratinocytes, such as granulocyte-macrophage colony-stimulating factor

(GM-CSF), tumor necrosis factor-alpha (TNF- α), IL-6 and IL-2 (17, 27–29).

Over the past few years, research has been moving toward the use of natural products which have beneficial effects on inflammation and itching and, at the same time, do not have the side effects of more established therapies, such as those involving the use of glucocorticoids. One of the alternative potential therapeutic targets to investigate when AD is present is the endocannabinoid system (ECS). The ECS is composed of endogenous ligands (N-arachidonyl ethanolamine [anandamide, AEA] and 2-arachidonoyl glycerol [2-AG]), G-protein-coupled receptors (cannabinoid receptors 1 and 2 [CB1R and CB2R]) and enzymes aimed at degrading and recycling the ligands (30–32). The ECS contributes to the homeostasis of various organs and its dysregulation seems to be associated with several pathological conditions (31, 33–36).

The definition of the ECS has currently been expanded to also include several fatty acid derivatives—the so-called endocannabinoid-like mediators—as well as other cannabinoid-related receptors, such as the G protein-coupled receptors (GPRs), the transient receptor potential (TRP) channels, the nuclear peroxisome proliferator-activated receptors (PPARs), and the serotonin receptors in addition to the classic cannabinoid receptors and endocannabinoids (30, 37–40).

A recent study has demonstrated that cannabidiol (CBD), a non-psychotropic phytocannabinoid showing numerous health-related benefits, including anti-inflammatory and anti-anxiety properties (41, 42), may be useful in dogs with AD (1). Despite these promising clinical studies, there are still few studies dedicated to the histological localization of cannabinoid receptors in the canine inflammatory cells (43, 44). It is evident that knowing the cellular distribution of specific receptors is fundamental to understanding the action of a drug.

The role of the ECS in the keratinocytes of healthy dogs was recently analyzed, and the upregulation of the cannabinoid receptors (CB1R and CB2R) and cannabinoid-related receptors (GPR55, TRPV1, TRPA1; PPAR α , serotonin 1A [5-HT $_{1A}$ R]) was evaluated in dogs with AD (45). In that study, CB2R, GPR55, TRPV1 and TRPA1 immunoreactivity was also observed on different cellular elements of the dermis. Therefore, the aim of the present study was to improve histological knowledge

regarding the expression of cannabinoid and cannabinoid-related receptors in the inflammatory infiltrate of canine atopic dermatitis. In particular, the expression of the CB2R, GPR55, TRPV1, and TRPA1 was immunohistochemically investigated in MCs, macrophages, DCs, T-cells, and neutrophils, and the percentage of immunopositive inflammatory cells present on the total number of the same cell histotype was evaluated.

Materials and methods

Animals

Inclusion criteria

Eight client-owned dogs diagnosed with spontaneous AD, based on predefined diagnostic criteria (45) and on the exclusion of other causes of pruritus (flea bite, allergic dermatitis and adverse food reaction), were enrolled (Table 1). Cutaneous samples were collected from the AD-dogs on which no treatment had been made in the previous 6 months. Written client consent was obtained prior to the enrollment of all cases. The skin samples utilized in the current study derived from the same dogs included in a previous study (45).

Sample collection and processing

In the AD-dogs, a biopsy sample of skin lesions located in the ventral abdominal or axillary areas (Table 1) was collected using a sterile 8 mm biopsy punch. Sampling was carried out under local (2% lidocaine) anesthesia, using the same protocol for all dogs. The tissues from the AD-dogs were processed to obtain cryosections. The samples were fixed overnight in 4% paraformaldehyde in 0.1 M sodium phosphate buffer (pH 7.0) at +4°C. After being washed in phosphate-buffered saline (PBS 0.15 M NaCl in 0.01 M sodium phosphate buffer, pH 7.2), the tissues were immersed in PBS plus sodium azide 0.1% for 48 h (+4°C) and were then preserved in PBS–sodium azide 0.1% plus sucrose 30% (+4°C). All the samples were subsequently frozen in liquid nitrogen, and 14 µm-thick cryosections were obtained. The cryosections were hydrated in PBS and processed for histology and immunostaining.

Histopathology

The sections were hydrated in PBS for 10 mins and processed for histological staining with hematoxylin and eosin (H&E) following standard procedures. The sections were observed under an Eclipse E600 (Nikon, Shinjuku, Japan) optical microscope and evaluated following the criteria of Gross et al. (48). Images were acquired using an optical microscope (Eclipse E600; Nikon, Shinjuku, Japan) equipped with a USB 3.0 camera series “33” Imaging Source (cat. No. DFK 33UX264; Bremen, Germany).

Immunofluorescence

The sections were hydrated in PBS and processed for immunostaining. To block non-specific bindings, the sections were incubated in a solution containing 20% normal donkey serum (Colorado Serum Co., Denver, CO, USA), 0.5% Triton X-100 (Sigma Aldrich, Milan, Italy, Europe) and bovine serum albumin (1%) in PBS for 1 h at room temperature (RT). The sections were incubated in a humid chamber overnight at RT with the antibodies directed against the CB2R and cannabinoid-related receptors (single immunostaining) or with a cocktail of primary antibodies (double immunostaining) (Table 2) diluted in 1.8% NaCl in 0.01 M PBS containing 0.1% sodium azide. After washing in PBS (3 × 10 mins), the sections were incubated for 1 h at RT in a humid chamber with the secondary antibodies (Table 3) diluted in PBS. The cryosections were then washed in PBS (3 × 10 min) and mounted in buffered glycerol at pH 8.6 with 4',6-diamidino-2-phenylindole– DAPI (Santa Cruz Biotechnology, Santa Cruz, CA, USA).

The slides were examined using a Nikon Eclipse Ni microscope equipped with the appropriate filter cubes to differentiate the fluorochrome employed. The images were recorded using a Nikon DS-Qi1Nc digital camera and NIS elements software BR 4.20.01 (Nikon Instruments Europe BV, Amsterdam, Netherlands). The figure panels were prepared using Corel Draw (Corel Photo Paint and Corel Draw, Ottawa, ON, Canada).

Specificity of the primary antibodies

Antibodies anti-cannabinoid receptor 2

The rabbit anti-CB2R antibody (ab45942) utilized in the present study had already been tested with Western blot (Wb) analysis on dog tissues (42) and tested for comparative purposes on rat tissues (49, 50). Another anti-CB2R antibody, raised in mice, was used in the current study to carry out the co-localization studies. Since the specificity of the mouse anti-CB2 antibody (sc-293188) had not already been tested on dog tissues, this antibody was co-localized with the rabbit anti-CB2 antibody in a double-staining protocol. Both the anti-CB2R antibodies were co-localized in keratinocytes and blood vessels (Supplementary Figure 1). In the dermal cells, the immunostaining obtained with the antibody raised in mice (sc-293188) was brighter than that raised in rabbits (ab45942).

Antibodies anti-cannabinoid-related receptors GPR55, TRPA1, and TRPV1

In the present study, the anti-human GPR55 (NB110-55498) antibody was used, the specificity of which was tested on dog tissues using Western blot (Wb) analysis (49).

TABLE 1 The clinical data of the dogs with atopic dermatitis (AD) enrolled in the present study.

Dogs	Breed	Sex	Age	Pruritus visual analog scale (PVAS) ⁽⁴⁶⁾	Canine atopic dermatitis extent and severity index (CADESI-4) ⁽⁴⁷⁾
				Skin area	
AD 1	Jack Russell	F ^S	7 yr	PVAS: 9/10	CADESI-4: 20
				Groin	
AD 2	French Bulldog	F	3 yr	PVAS: 8/10	CADESI-4: 48
				Axilla (right and left)	
AD 3	Cavalier King Charles Spaniel	M	8 yr	PVAS: 8/10	CADESI-4: 30
				Groin	
AD 4	Mixed breed	M	11 yr	PVAS: 6/10	CADESI-4: 20
				Groin	
AD 5	Akita Inu	M	4 yr	PVAS: 8/10	CADESI-4: 55
				Axilla	
AD 6	Golden Retriever	M	8 yr	PVAS: 9/10	CADESI-4: 60
				Groin	
AD 7	American Staffordshire Terrier	M	4 yr	PVAS: 8/10	CADESI-4: 58
				Axilla	
AD 8	French Bulldog	F	3 yr	PVAS: 8/10	CADESI-4: 32
				Groin	

F, female; F^S, spayed female; M, male; M^N, neutered male; NA, not available; yr, years.

The immunogen used to obtain the anti-TRPA1 antibody was the EKQHELIKLIQKME peptide, corresponding to amino acids 1,070–1,085 of rat TRPA1. The homology between the full amino acid sequences of the dog and rat TRPA1 was 82.29%, and correspondence with the specific sequence of the immunogen was 100%; therefore, the anti-TRPA1 antibody should also recognize the same receptor in the dog.

The immunogen of the anti-TRPV1 antibody was the (C)EDAEVFK DSMVPGEK [824–838] peptide of rat TRPV1. The homology between the specific amino acid sequences of the dog and the rat immunogens was 87.51%. The specificity of the rabbit anti-TRPV1 antibody, which has recently been tested on the canine nervous system (49), was tested using a preadsorption test on the canine skin (45).

The homologies of the canine receptors studied in the dogs (CB2R, GPR55, TRPV1, and TRPA1) were verified using the ‘alignment’ tool available on the Uniprot database (www.uniprot.org) and the BLAST tool of the National Center for Biotechnology Information (NCBI) (www.ncbi.nlm.nih.gov).

Anti-mast cells tryptase antibodies

The skin tissues were processed for cryosectioning to avoid any thermal and chemical modifications of the receptors studied and the background and self-marking of the tissues which are unfortunately often observable in paraffin-embedded tissues. Unexpectedly, some difficulties in MC identification were encountered, and it was necessary to test more anti-tryptase antibodies. The only antibody, among those tested, capable of effectively identifying MCs in the cryosections was the rabbit anti-tryptase antibody (PAB070Ca01), raised against the tryptase of dogs (43); its specificity was also tested in the current study by combining immunohistochemical staining in association with toluidine blue as a counterstain (44) (Supplementary Figure 2). In the present study, the rabbit anti-tryptase antibody was used in co-localization with the mouse anti-CB2R antibody.

However, since the antibodies directed against GPR55, TRPV1, and TRPA1 were raised in rabbits, co-localization studies with the rabbit anti-tryptase antibody were not possible. Therefore, the expression of the cannabinoid-related receptors in MCs was evaluated using anti-tryptase antibodies raised in

TABLE 2 Primary antibodies used in the study.

Primary antibody	Host	Code	Dilution	Source
CB2R	Rabbit	ab45942	1:00	Abcam
CB2R	Mouse	sc-293188	1:50	Santa Cruz
CD3	Rat	CD3-12	1:40	Leucocyte's antigen laboratory, UC Davis
GPR55	Rabbit	NB110-55498	1:100	Novus Biol.
IBA1	Goat	NB100-1028	1:80	Novus Biol.
Calprotectin	Mouse	M0747Clone MAC387	1:400	Dako
Tryptase	Rabbit	PAB070Ca01	1:80	Cloude-Clone
Tryptase	Mouse	Clone AA1	1:100	Agilent
Tryptase	Mouse	AM08408PU-NClone 3H2643	1:50	Origene
Tryptase	Mouse	MAB070Ca21Clone C13	1:50	Cloude-Clone
Tryptase	Mouse	sc-33676Clone G3	1:50	Santa Cruz
TRPA1	Rabbit	ab58844	1:200	Abcam
TRPV1	Rabbit	ACC-030	1:200	Alomone

Primary antibody Suppliers: Abcam, Cambridge, UK; Agilent, Santa Clara, CA, USA; Alomone, Jerusalem, Israel; Cloude-Clone Corp., Huston, TX, USA; Dako Cytomation, Golstrup, Denmark; Novus Biologicals, Littleton, CO, USA; Origene Technologies, Rockville, MD, USA.

TABLE 3 Secondary antibodies used in the study.

Secondary antibody	Host	Code	Dilution	Source
Anti-mouse IgG Alexa-488	Donkey	A-21202	1:250	Thermo fisher
Anti-mouse IgG Alexa-594	Donkey	A-21203	1:500	Thermo fisher
Anti-goat 594	Donkey	ab150132	1:600	Abcam
Anti-rabbit 594	Donkey	ab150076	1:1000	Abcam
Anti-rabbit 488	Donkey	A-21206	1:1000	Thermo fisher

Secondary antibody Suppliers: Abcam, Cambridge, UK; Thermo Fisher Scientific, Waltham, MA USA.

mice. Of the four different mouse anti-tryptase antibodies tested (Table 3), only clone 3H2643 was capable of immunolabelling the MCs in the cryosections whereas all the antibodies were capable of identifying the MCs in the paraffin embedded sections (observation of Dr. Gobbo). The co-localization between the dog-specific rabbit anti-tryptase antibody (PAB070Ca01) and the mouse anti-tryptase antibody (clone 3H2643) on the cryosections showed that MCs co-expressed the same tryptase-IR. In addition, only a few other cells (likely basophils) were immunolabelled by the clone 3H2643, and were not recognized by the PAB070Ca01 antibody (data not shown).

Marker for macrophages and dendritic cells

To identify macrophages, the anti-ionized calcium binding adapter molecule 1 (IBA1) antibody was used (43). Since in the dog skin, IBA1-IR is also expressed by DCs (51) and, in the current study, no specific markers to differentiate DCs from macrophages were used, the term “IBA1 immunoreactive cells” will refer to both cellular types (macrophages/DCs). It was also observed that IBA1 immunoreactive DCs were dispersed among the keratinocytes of the basal layer of the epidermis, supporting

the fact that the IBA1 marker is also expressed by dog skin DCs (data not shown). The intraepithelial DCs were more properly defined as Langerhans cells, given their specific site.

Marker for neutrophils

An antibody anti-CAL (clone MAC387), a complex of the mammalian proteins S100A8 and S100A9 (S100A8/A9), was used as a marker for granulocytes/monocytes/macrophages. Since the co-localization between anti-CAL and -IBA1 antibodies did not show any co-localization (Supplementary Figure 3), it is plausible to think that, at least in the skin, the anti-calprotectin (CAL) (MAC387) antibody mainly recognizes neutrophils instead of macrophages (52). The observation of Dapi labeled multilobed nuclei confirmed that the CAL immunoreactive cells were neutrophils. This evidence was supported by the observation of Kerkhoff et al. (53) who showed that S100A8/A9 comprises ~30 to 60% of all cytosolic proteins in neutrophils and only 1–5% of all monocyte cytosolic proteins, and that macrophages express and release significantly less S100A8/A9 than do monocytes. In addition, there was evidence that CAL expression was lost

during the maturation of canine macrophages (54, 55), and that it was more suited to assessing migrating monocytes and early stages of macrophage maturation rather than the resident macrophage population (56).

Marker for T lymphocytes

To identify *T*-cells, the dog-specific anti-cluster of differentiation 3 (CD3) antibody was used (57). A recent study has shown that canine CD3 might also be expressed by Th2 cells (26) which play a pivotal role in AD pathogenesis.

Specificity of the secondary antibodies

The specificity of the secondary antibodies was tested by applying them after omission of the primary antibodies. No stained cells were detected after omitting the primary antibodies.

Semiquantitative and quantitative analysis

The immunoreactivity of the antibodies was evaluated, and its cellular localization (nuclear, membranous, cytoplasmic) was reported. The intensity of the expression was evaluated semiquantitatively in pictures acquired using the same exposure times, as faint, moderate and bright. The proportions of dermal cells which were immunoreactive for the markers of MCs (tryptase), macrophages/DCs (IBA1), *T*-cells (CD3), and neutrophils (CAL), and which were also immunoreactive for one of the cannabinoid receptors studied were determined by examining fluorescently labeled, double-stained preparations. Digital images of areas of the sections with a high density of inflammatory cells, located just below the dermal–epidermal junction, were acquired at $\times 40$ magnification. The cells were first located by the presence of a fluorophore which labeled one antigen; the filter was then switched to determine whether or not the cells were labeled for a second antigen, located with a fluorophore of a different color. In this way, the proportions of inflammatory cells labeled for pairs of antigens were determined. For each staining combination, sections of the skin were used from three to five different AD-dogs. At least 30 cells from each animal were counted for each inflammatory cells marker. The percentage of cells which were immunoreactive for a particular marker (tryptase, IBA1, CD3, and CAL) and which were also immunoreactive for a second marker (CB2, GPR55, TRPV1, TRPA1) was calculated and expressed as mean \pm standard deviation, with n being the number of AD-dogs considered.

Results

Histopathology

All eight samples were histopathologically diagnosed as chronic hyperplastic mixed perivascular dermatitis, consistent with the inflammatory pattern of canine AD. Specifically, the skin showed moderate to severe, focal to diffuse hyperplasia in the superficial (hyperkeratosis) and the suprabasal (acanthosis) layers of the epidermis; in the dermis, superficial perivascular to interstitial mild mixed inflammatory infiltrates (lymphocytes, histiocytes, mast cells, plasma cells and few eosinophils) were detected. In four of the eight cases, a periannal inflammatory infiltrate, predominantly neutrophilic, was also observed (multifocal moderate pyogranulomatous dermatitis, presumably an infection secondary to chronic AD).

Cannabinoid receptors in tryptase immunoreactive mast cells

The mast cells were immunoreactive for all the receptors investigated (CB2R, GPR55, TRPV1, and TRPA1). Approximately a quarter of the MCs expressed moderate CB2-IR in the cell membrane and the cytoplasm ($26 \pm 17\%$, 106/428 cells, $n = 4$) (Figures 1a–d). A large proportion of MCs showed bright cytoplasmic GPR55-IR, albeit with large individual variations ($65 \pm 38\%$, 75/168 cells, $n = 4$) (Figures 1e–h). The mast cells showed moderate cytoplasmic TRPV1-IR ($74 \pm 20\%$, 172/229 cells, $n = 4$) (Figures 2a–d) and TRPA1-IR ($66 \pm 40\%$, 166/302 cells, $n = 5$) (Figures 2e–h).

Cannabinoid receptors in IBA1 immunoreactive macrophages/DCs

Macrophages/DCs were consistently observed in the derma of the AD-dogs, although they had a different distribution and density. Large proportions of IBA1 immunoreactive cells, which were often grouped in close proximity to the blood vessels, showed immunoreactivity for CB2R, GPR55, TRPV1, and TRPA1. In particular, the cell membrane and the cytoplasm of the macrophages/DCs expressed bright CB2R-IR ($91 \pm 16\%$, 294/307 cells, $n = 4$) (Figures 3a–d) and moderate GPR55-IR ($68 \pm 18\%$, 253/390 cells, $n = 3$) (Figures 3e–h). In the subepidermal connective tissue, large IBA1 immunoreactive cells were often intermingled with small GPR55 immunoreactive (and IBA1 negative) cells (likely lymphocytes). The macrophages/DCs also showed cytoplasmic moderate TRPV1-IR ($80 \pm 16\%$, 191/241 cells, $n = 3$) (Figures 4a–d) and faint TRPA1-IR ($81 \pm 14\%$, 224/265 cells, $n = 4$) (Figures 4e–h).

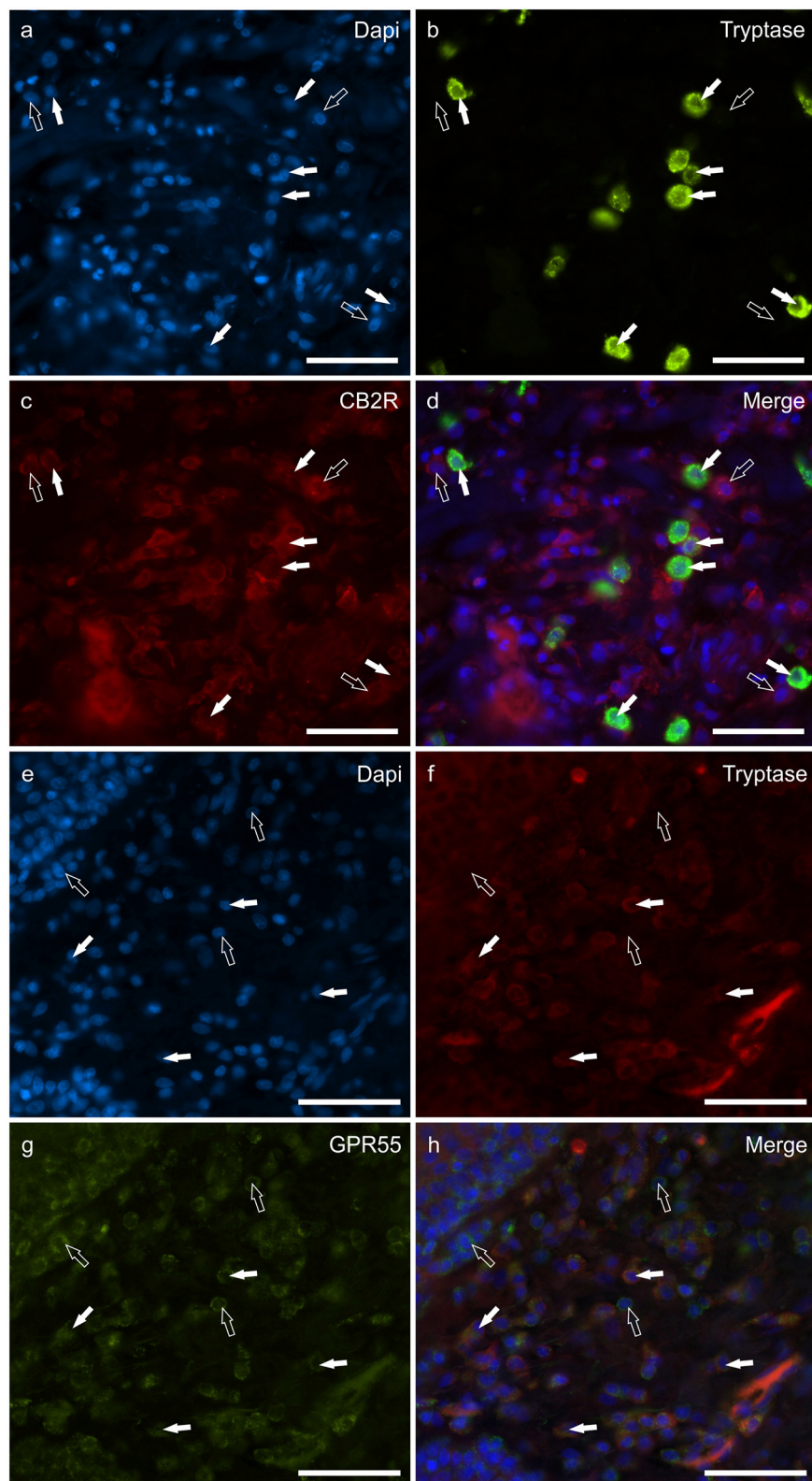


FIGURE 1
Photomicrographs of the cryosections of the skin of dogs with atopic dermatitis (AD) showing tryptase immunoreactive mast cells (MCs) expressing cannabinoid receptor 2 (CB2R) (a–d) and G-protein coupled receptor 55 (GPR55) (e–h) immunoreactivity (IR). The white arrows indicate the Dapi-labeled nuclei of tryptase positive MCs co-expressing CB2R- (c) and GPR55-IR (g). The open arrows indicate some tryptase negative cells of the dermis which expressed CB2R- (c) and GPR55-IR (g). Bar: 50 μm.

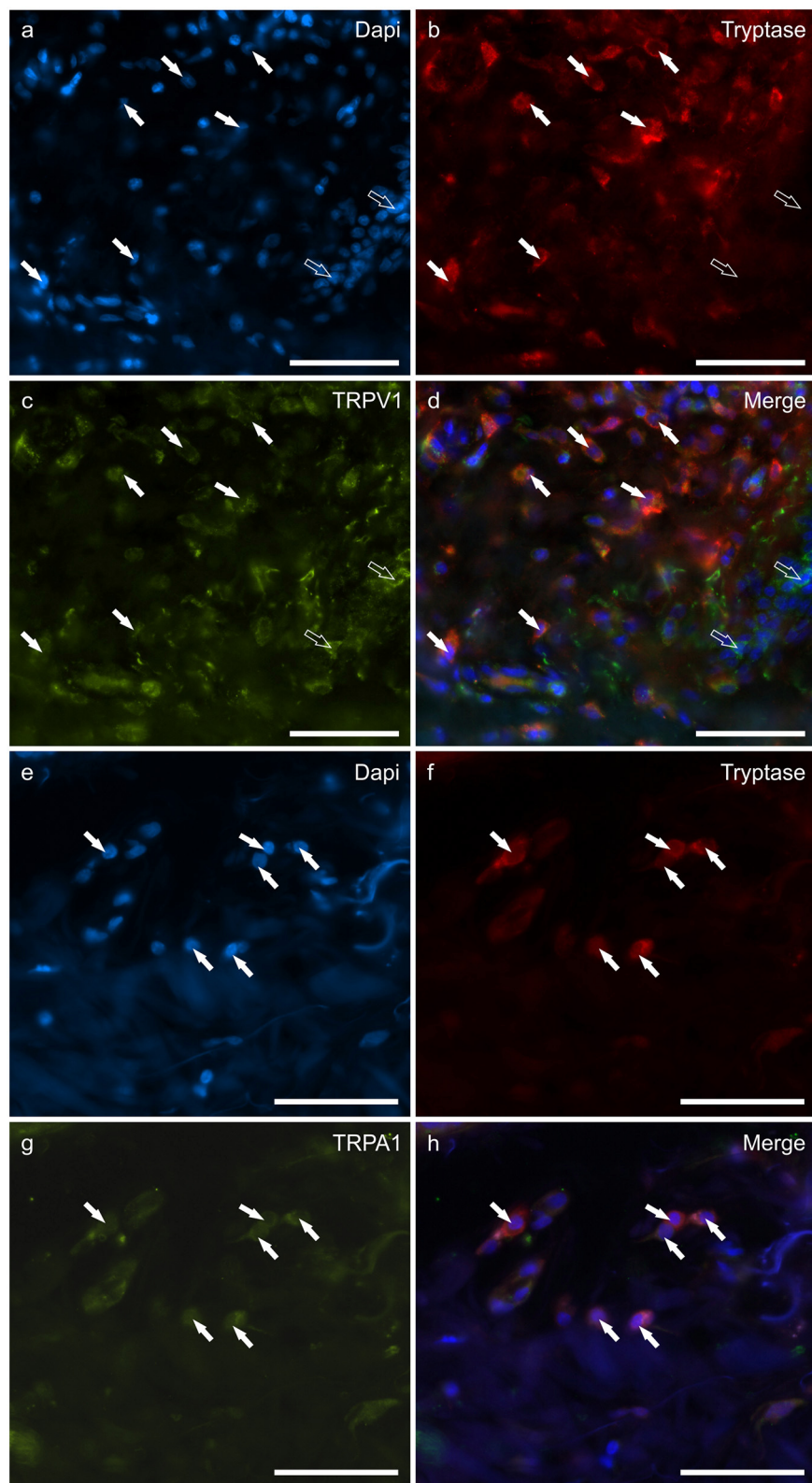


FIGURE 2

Photomicrographs of the cryosections of the skin of dogs with atopic dermatitis (AD) showing tryptase immunoreactive mast cells (MCs) expressing transient receptor potential vanilloid 1 (TRPV1) (a–d) and transient receptor potential ankyrin 1 (TRPA1) (e–h) immunoreactivity (IR). The white arrows indicate the Dapi-labeled nuclei of tryptase positive MCs co-expressing TRPV1- (c) and TRPA1-IR (g). The open arrows indicate some tryptase negative cells of the dermis which expressed TRPV1-IR (c). Bar: 50 μ m.

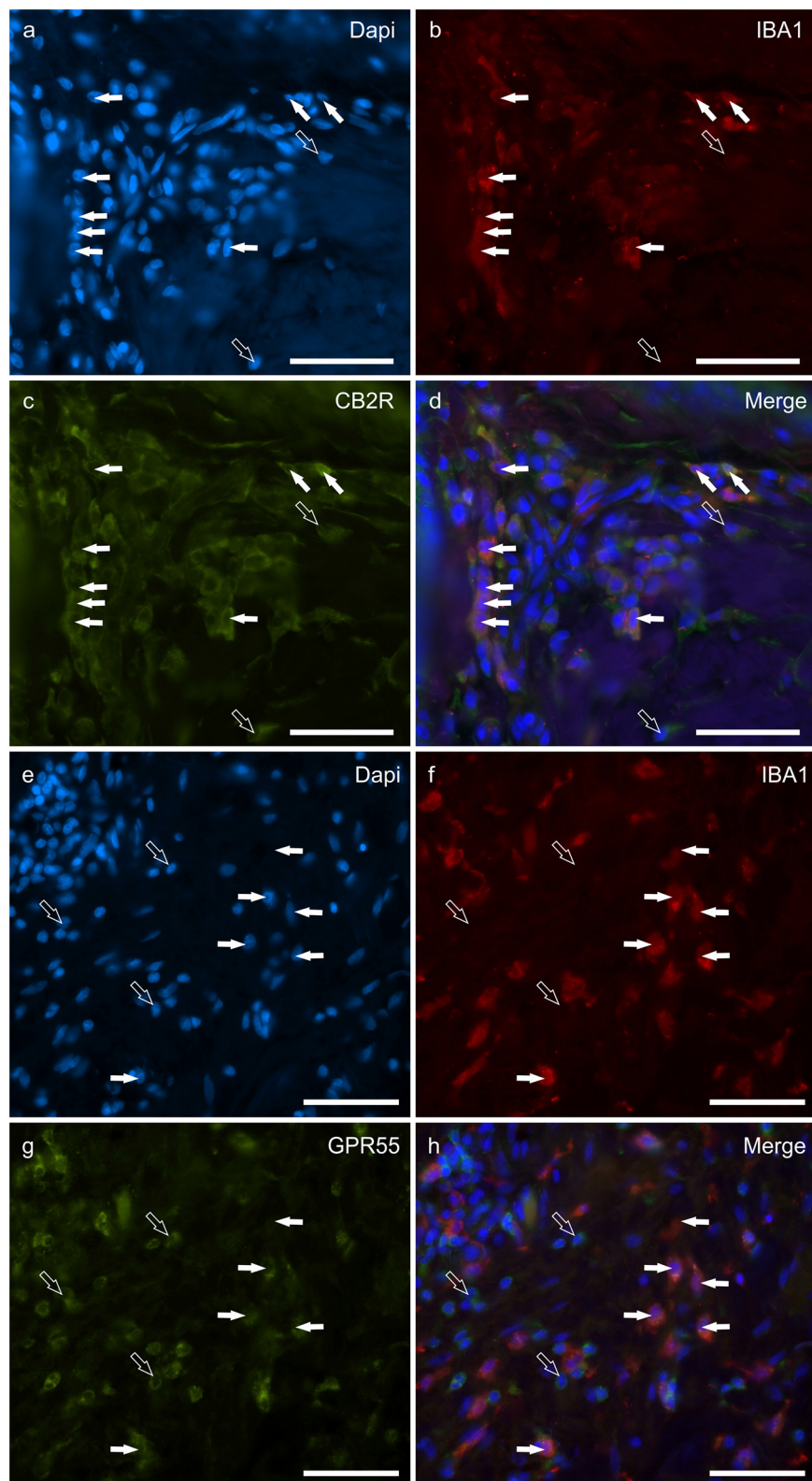


FIGURE 3

Photomicrographs of the cryosections of the skin of dogs with atopic dermatitis (AD) showing IBA1 immunoreactive cells (macrophages and dendritic cells) expressing cannabinoid receptor 2 (CB2R) (a–d) and G-protein coupled receptor 55 (GPR55) (e–h) immunoreactivity (IR). The white arrows indicate the Dapi-labeled nuclei of IBA1 positive cells co-expressing CB2R- (c) and GPR55-IR (g). The open arrows indicate some IBA1 negative cells of the dermis which expressed CB2R- (c) and GPR55-IR (g). Bar: 50 μ m.

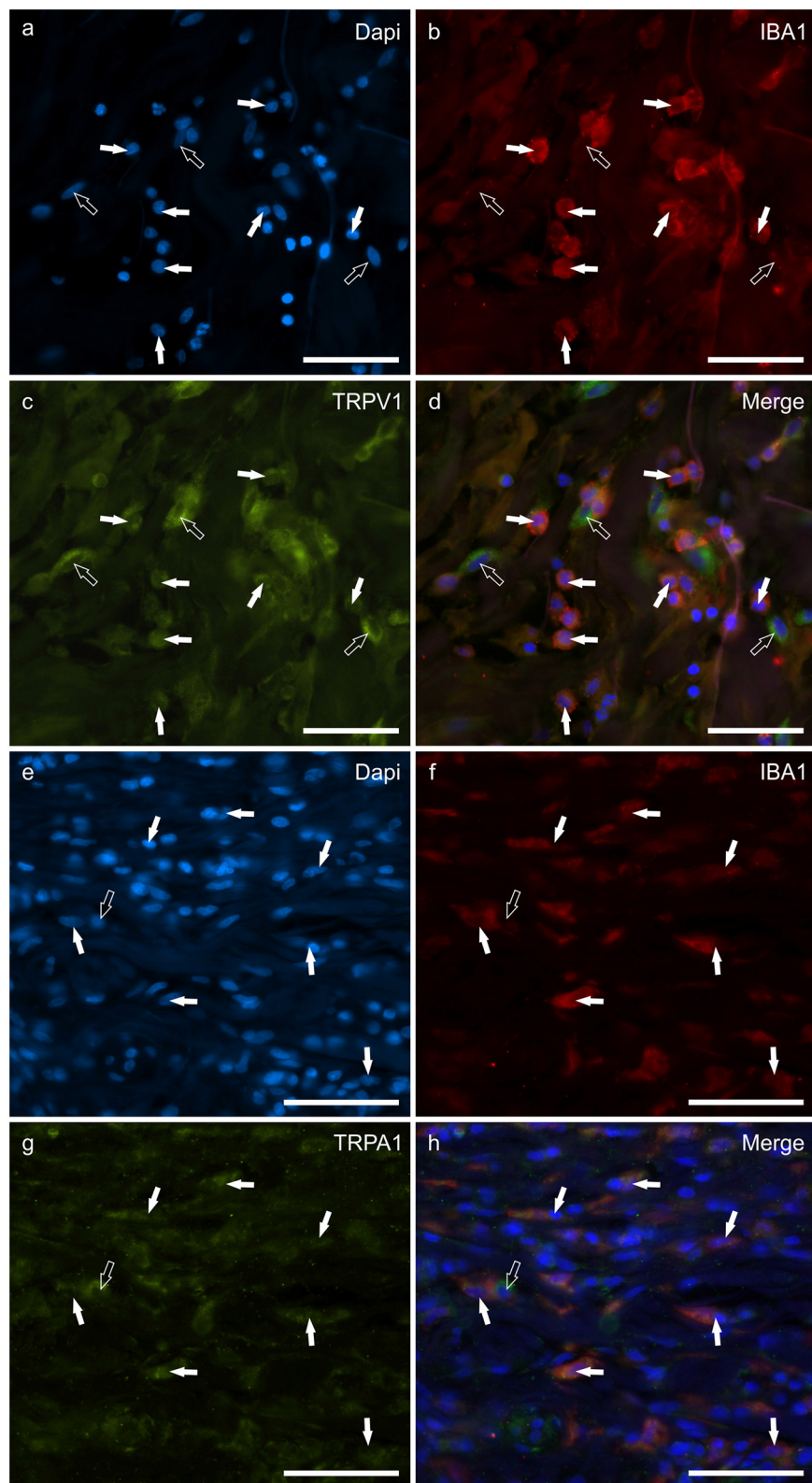


FIGURE 4

Photomicrographs of the cryosections of the skin of a dog with atopic dermatitis (AD) showing IBA1 immunoreactive cells (macrophages and dendritic cells) expressing transient receptor potential vanilloid 1 (TRPV1) (a–d) and ankyrin 1 (TRPA1) immunoreactivity (IR) (e–h). The white arrows indicate the Dapi-labeled nuclei of IBA1 positive cells co-expressing TRPV1-IR (c) and TRPA1-IR (g). The open arrow indicates one IBA1 negative cell which expressed TRPV1-IR (c) and TRPA1-IR (g). Bar: 50 μ m.

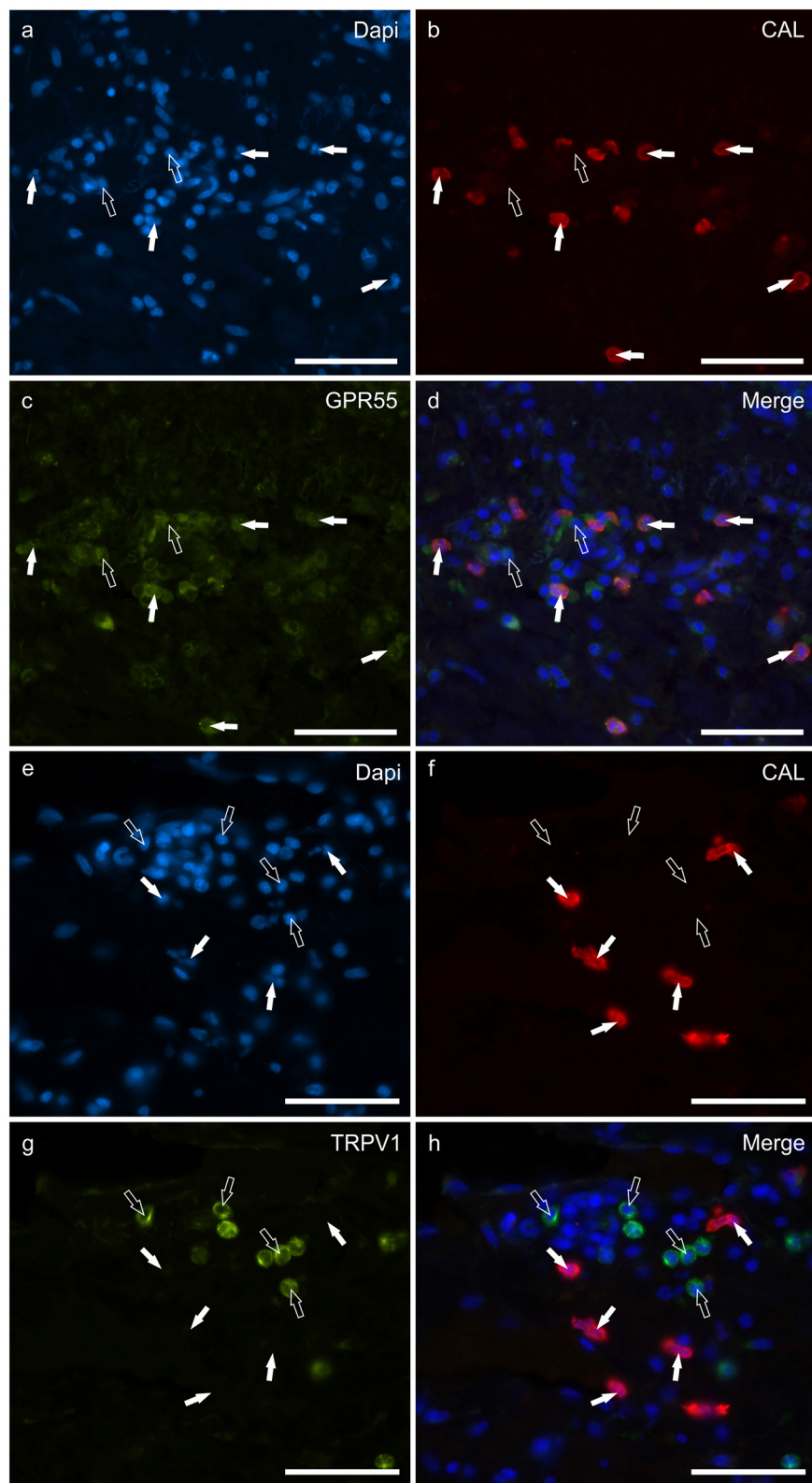


FIGURE 5

Photomicrographs of the cryosections of the skin of dogs with atopic dermatitis (AD) showing Calprotectin (CAL) immunoreactive cells expressing G-protein coupled receptor 55 (GPR55) (**a–d**) and transient receptor potential vanilloid 1 (TRPV1) immunoreactivity (IR) (**e–h**). (**a–d**) The white arrows indicate the Dapi-labeled nuclei of CAL positive cells co-expressing GPR55-IR (**c**). The open arrows indicate some CAL negative cells expressing GPR55-IR (**c**). (**e–h**) The white arrows indicate the Dapi-labeled nuclei of the CAL positive cells which were TRPV1 negative (**g**). The open arrows indicate some TRPV1-IR cells which were CAL negative (**g**). Bar: 50 μ m.

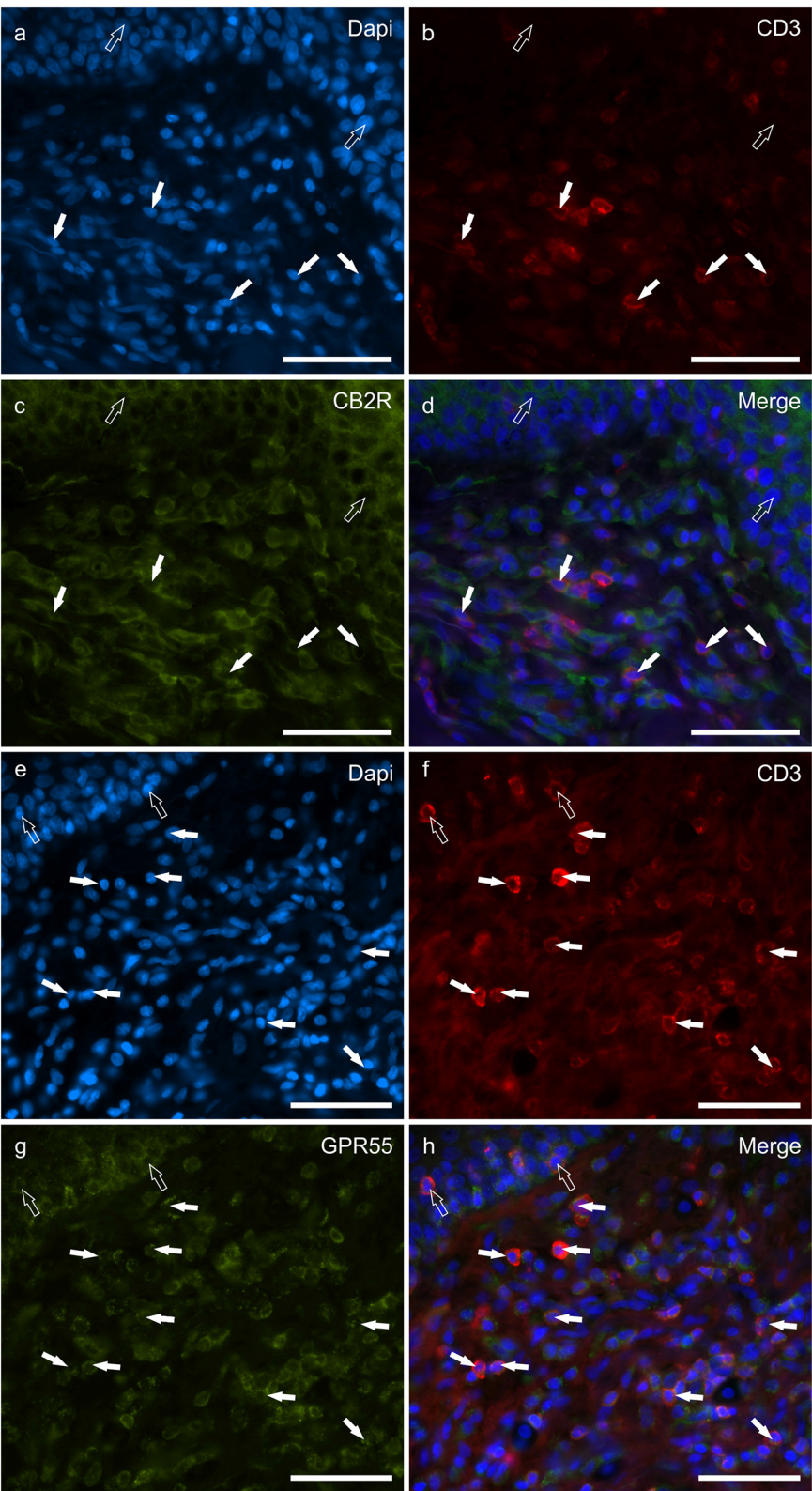


FIGURE 6
Photomicrographs of the cryosections of the skin of dogs with atopic dermatitis (AD) showing CD3 immunoreactive T lymphocytes expressing cannabinoid receptor 2- (CB2R) (**a–d**) and G-protein coupled receptor 55- (GPR55) (**e–h**) immunoreactivity (IR) (**e–h**). (**a–d**) The white arrows indicate the Dapi-labeled nuclei of some CD3 immunoreactive T lymphocytes co-expressing CB2R-IR. The open arrows indicate the nuclei of
(Continued)

FIGURE 6 (Continued)

the keratinocytes expressing CB2R-IR (c). (e–h) The white arrows indicate the dapi-labeled nuclei of some CD3 immunoreactive T lymphocytes co-expressing GPR55-IR (g). The open arrows indicate the nuclei of two intraepithelial T lymphocytes co-expressing CD3- (f) and GPR55-IR (g). Bar: 50 μ m.

Cannabinoid receptors in calprotectin immunoreactive neutrophils

Round, and often irregularly-shaped cells, expressed CAL-IR in the derma of the AD-dogs; the density of the CAL immunoreactive cells was variable depending on the AD-dog skin samples. Small groups of few CAL positive cells were scattered in proximity of the epidermis, or were intravascular. A large proportion ($77 \pm 8\%$, 84/112 cells, $n = 3$) of CAL positive neutrophils showed moderate cytoplasmic GPR55-IR (Figures 5a–d). None of the CAL immunoreactive neutrophils were TRPV1 (0/162 cells, $n = 3$) (Figures 5e–h) or TRPA1 (0/150 cells, $n = 3$) immunoreactive (data not shown). Due to the fact that the anti-CB2 antibody was also raised in mice, co-localization between the anti-CAL and the -CB2R antibodies was not carried out. However, since the co-localization study between the anti-CB2R and the -GPR55 antibodies showed that the inflammatory cells expressed both the markers (Supplementary Figure 4), it is plausible that CAL immunoreactive cells may also express CB2R-IR.

Cannabinoid receptors in CD3 immunoreactive T-cells

T lymphocytes were well represented in the derma of all the AD-dogs considered. The CD3-IR was more expressed in those T-cells scattered within the epithelial cells. However, it was shown that the CD3 immunoreactive cells showed immunoreactivity for CB2R, GPR55, TRPV1 and TRPA1. In particular, the cell membrane and the cytoplasm of the T-cells expressed faint-to-moderate CB2R-IR ($28 \pm 11\%$, 137/278 cells, $n = 5$) (Figures 6a–d) and bright GPR55-IR ($90 \pm 15\%$, 289/352 cells, $n = 4$) (Figures 6e–h). Many other small CD3 negative cells, likely B lymphocytes, expressed GPR55-IR, as recently shown in the dog intestine (43). The cell membrane and the cytoplasm of the T-cells expressed faint TRPV1 ($30 \pm 19\%$, 49/159 cells, $n = 4$) (Figures 7a–d) and moderate TRPA1-IR ($52 \pm 15\%$, 48/112 cells, $n = 4$) (Figures 7e–h).

The semi-quantitative evaluation of the intensity of the immunolabelling of the cannabinoid and cannabinoid-related receptors studied in the skin of the AD-dogs is reported in Table 4. The data related to the distribution of the cannabinoid receptors in MCs, macrophages/DCs, T-cells and neutrophils are graphically represented in Figure 8.

Co-localization studies showed that CB2R-IR was co-expressed by subsets of GPR55- (Supplementary Figure 4), TRPV1- (data not shown) and TRPA1-IR (data not shown) inflammatory cells, supporting the evidence that dermal inflammatory cells may co-express different types of cannabinoid receptors.

Discussion

Mast cell identification

Mast cells, the first-line responders to allergen stimulation (58) and cell injury (59), play a pivotal role in the neuroimmune response of the skin, and their number increases in skin affected by AD (60, 61).

Several methods have been used to identify the MCs; metachromatic stain with toluidine blue (and other cationic stains) represent the first, rapid and inexpensive method for labeling MCs (62). However, as recently shown, metachromatic stains reveal a lower number of MCs when compared with immunostaining for tryptase (63, 64), which represents the most abundant secretory granule-derived serine proteinase contained in MCs. Thus, immunohistochemistry is presently the best technique for revealing the MCs in tissues, also in dogs (43, 63, 65). The mouse anti-tryptase antibody (clone 3H2643) also immunolabelled some other cells which were not identified with the rabbit anti-tryptase antibody. These cells could have been basophils which could express a lesser amount of tryptase in their cytoplasmic granules (66). However, the expression of the cannabinoid receptors on basophils may be relevant due to the role played by basophils in the Th2 immune response (67).

Cannabinoid receptors in mast cells

The expression of cannabinoid and cannabinoid-related receptors has already been shown in the MCs of humans (64, 68–70), rodents (13, 71), dogs (43, 44), and cats (50), and in the MC cell line (72).

In the present study, MCs expressed CB2R, GPR55, TRPV1, and TRPA1. The observation of CB2R-IR in the MCs of canine skin is consistent with that of Galiazzo et al. (43) who described CB2R-IR in the MCs of the dog intestine, and Campora et al. (73), who identified CB2R-IR in cells of dog skin showing an MCs-like morphology. Functional studies regarding the MC cell line (RBL2H3) showed that the CB2R modulates MC

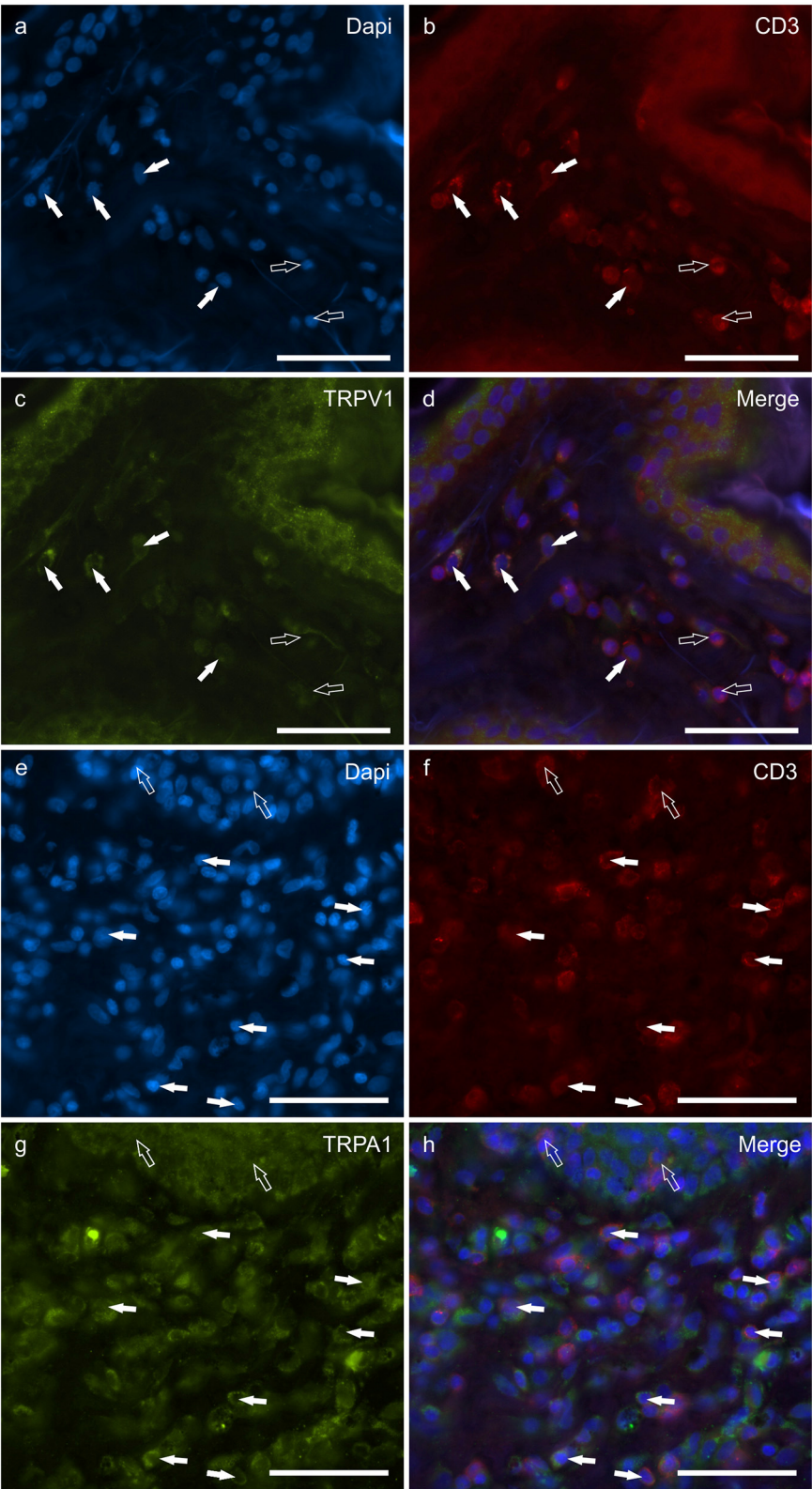


FIGURE 7
Photomicrographs of the cryosections of the skin of dogs with atopic dermatitis (AD) showing CD3 immunoreactive T lymphocytes expressing transient receptor potential vanilloid 1 (TRPV1) **(a–d)** and transient receptor potential ankyrin 1 (TRPA1) **(e–h)** immunoreactivity (IR). **(a–d)** The white arrows indicate the dapi-labeled nuclei of some CD3 immunoreactive T lymphocytes co-expressing TRPV1-IR **(C)**. The open arrows
(Continued)

FIGURE 7 (Continued)

indicate the nuclei of CD3-IR cells which were TRPV1 negative. (e–h) The white arrows indicate the Dapi-labeled nuclei of some CD3 immunoreactive T lymphocytes co-expressing TRPA1-IR (g). The open arrows indicate the nuclei of two intraepithelial CD3 immunoreactive lymphocytes (f). Bar: 50 μ m.

TABLE 4 Semiquantitative evaluation of the density of CB2R, GPR55, TRPV1, and TRPA1 immunoreactivity in different cellular elements of the skin of dogs with atopic dermatitis (AD-dogs).

Receptors	Mast cells (tryptase)	Macrophages and dendritic cells (IBA1)	T-cells (CD3)	Neutrophils (CAL)
CB2R	++	+++	+	NA
GPR55	+++	++	+++	++
TRPV1	++	++	+	–
TRPA1	++	+	++	–

C, cytoplasmic; M, membrane; NA, not applied. Immunoreactive cells were graded as: –, negative; +, faint; ++, moderate; + + +, bright.

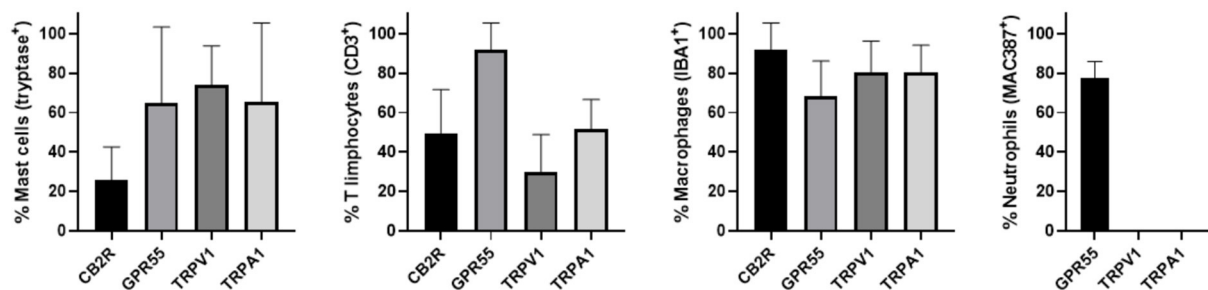


FIGURE 8

Percentage of mast cells, T lymphocytes, macrophages/dendritic cells and neutrophils that expressed CB2R, GPR55, TRPV1 and TRPA1. Mast cells expressing tryptase were immunoreactive for CB2R, GPR55, TRPV1, and TRPA1. T lymphocytes expressing CD3 were immunoreactive for CB2R, GPR55, TRPV1, and TRPA1. Macrophages/dendritic cells expressing IBA1 were immunoreactive for CB2R, GPR55, TRPV1, and TRPA1. Neutrophils expressing MAC387 were immunoreactive only for GPR55. Data are presented as Mean (\pm SD).

degranulation and suppresses their proinflammatory response (74), and that the activation of the CB2R on MCs reduces the release of peripheral mediators of nociceptors, such as the nerve growth factor (NGF), serotonin, histamine, and cytokines (75). An interesting study on mice showed that AEA inhibits MC degranulation by means of a mechanism which includes the participation of the CB2R and GPR55 which act in close cross-talk (76).

The observation of GPR55-IR in the MCs of dog skin, which is consistent with data obtained in the dog intestine (43), is promising evidence since the activation of this receptor seems to have anti-inflammatory effects by inhibiting the MC-mediated release of the NGF, as observed in cultures of human MCs (77). In dogs, it has also been shown that the NGF is one of the mediators of the pruritogenic pathways (8). Sensory nerves within the skin, under stressful conditions, can release neuropeptides, such as substance P (SP), the calcitonin gene-related peptide and the vasoactive intestinal peptide, which may activate a neuroimmune response by acting on the MCs located in close proximity to the sensory nerves (78, 79). On

the other hand, upon activation, MCs may release the NGF and other neurotrophins, and other powerful mediators, such as histamine, tryptase, and cytokines, which can contribute to hyperinnervation and angiogenesis (77), and stimulate the respective receptors on itch-mediating sensory nerves (12, 80). Therefore, modulation of the release of the NGF by GPR55, although not yet demonstrated in dogs, can lead us to speculate that this receptor, in addition to its antinociceptive properties, may also exert an antipruritic effect (81).

The transient receptor potential vanilloid 1 is preferentially expressed in the sensory neurons of the peripheral nervous system in which it is primarily expressed by the nociceptor neurons of the dorsal root ganglia (DRG) (49). However, TRPV1 seems to also be involved in itching conditions, such as AD (82). The expression of TRPV1-IR in the MCs of dogs is consistent with the expression of the same receptor in the MCs of rodents (71) and humans (77, 78). By using a mouse strain (Nc/Nga) commonly utilized as a model for AD studies, it has been shown that the antagonism of TRPV1 attenuates the itching symptoms induced by house-dust mite allergens (83). In addition, it has

been demonstrated that the activation of TRPV1 reduces itching in humans (84) and dogs (85).

The TRPA1 is expressed in neuronal tissues, especially in primary sensory neurons, in which it mediates the peripheral and central processing of pain, itching, and thermal (cold) sensations. Sensory neurons expressing TRPA1-IR usually co-express TRPV1-IR (86). However, TRPA1 is also functionally expressed in skin cells, such as keratinocytes, MCs, macrophages, DCs, melanocytes, and endothelial cells (45, 87–89). The observation of TRPA1-IR in the MCs of the AD-dogs was consistent with the findings of Oh et al. (87) who showed TRPA1 in the MCs of AD lesions of humans and mice. The Authors also showed that IL-13, one of the increasing cytokines in the lesional atopic skin of dogs (90), represents a potent stimulator of TRPA1 expression in MCs and sensory neurons (87). In addition, Kang et al. (91) showed that, in mice, the blockade of TRPA1 inhibits MC degranulation and the production of Th2 cytokine IL-13. More recently, it has been shown that, in a murine model of experimentally induced AD, the genetic deletion of TRPA1 attenuated the pathological findings of AD, including dermal infiltration by MCs and macrophages, Th2 cytokines, and pruritus (92). All these findings robustly emphasize the potential advantage of TRPA1 antagonists as therapy for pathological itching conditions in dogs, although no preclinical or clinical studies have previously been carried out on the skin of this species.

Cannabinoid and cannabinoid-related receptors in macrophages

Macrophages are critically important in the AD pathogenesis, and they are one of the major components of the dermal infiltrate in chronic lesions of human (21, 93) and canine AD (6, 61, 94). Macrophages interact with lymphocytes to start the acquired immune response, acting as antigen presenting cells and releasing cytokines (95). Coordinated interaction between macrophages, and T and B cells is required to obtain a good immune response. It has been shown that MCs may recruit macrophages by means of the release of proinflammatory mediators (96). It is plausible to consider that an alteration to any one or all of these cell types could reduce the effectiveness of the immune system.

Macrophages of the AD-dogs showed CB2R-IR, a finding consistent with a previous study on the human intestine (97) and mouse skin (98). In mice and humans, the CB2R was shown to modulate macrophages in response to chemoattractants (98) and to switch the polarization of M1 macrophages into M2 macrophages (99, 100).

Macrophages of the skin of the AD-dogs showed GPR55-IR, a finding consistent with those obtained in the macrophages of rodents, humans (101, 102) and dogs (43). Macrophages of

the skin of the AD-dogs also expressed TRPV1-IR; this finding supported a recent study which showed the expression of TRPV1 on both the mRNA and the protein levels in canine peripheral blood mononuclear cells and indicated that this ion channel was functional (103). In addition, there is a study on mice supporting the role of the TRPV1 channel in macrophage activation and the effectiveness of a subset of TRPV1 channel antagonists in suppressing inflammatory responses (104).

Large proportions of the dermal macrophages of the AD-dogs showed TRPA1-IR; this evidence was consistent with the data provided in the buccal samples of human patients with oral lichen planus (105) and in skin samples of IL-13-induced chronic AD in mice (87). A recent study involving mice showed that TRPA1 plays a crucial role during AD pathogenesis, and that this receptor could potentially be used as a target for treating chronic skin inflammatory diseases (92); the authors showed that, in addition to lower dermal MC infiltration and proinflammatory cytokines, a lesser infiltration of macrophages was also observed in TRPA1^{-/-} mice (compared to the wild type mice).

Cannabinoid and cannabinoid-related receptors in dendritic cells

Dendritic cells, which are the most potent antigen-presenting cells of the immune system, are important players during AD pathogenesis (29, 106, 107). It was shown that in the skin of AD-dogs there were significantly more DCs as compared to control skin (107, 108).

The dendritic cells of the AD-dogs, although not differentiable from macrophages (since both cell types express IBA1 in dog skin) (51), showed immunoreactivity for all the receptors studied. Although purely speculative (at present, there are no functional data regarding dogs), it can be hypothesized that, even in dogs, DCs might be potential targets for cannabinoid-mediated modulation. The expression of cannabinoid receptors on DCs has already been reported by authors who showed that the ECS could regulate DC growth, maturation, and their antigen presenting and T cell stimulatory capacities (6, 109–111). Studies involving humans have shown that the stimulation of DCs with CB2R agonists reduced their cytokine production (109). In mice it has been shown that AEA may induce DC apoptosis by engaging the CB1R and the CB2R (110), and that CB2R signaling may affect DC migration primarily by means of the inhibition of matrix metalloproteinase 9 expression (112).

This is the first report regarding the expression of GPR55-IR in the DCs of dogs; this finding is consistent with those obtained involving human and mouse DCs (113, 114). At present, the regulatory mechanism of GPR55 within the DC population is poorly understood.

The dendritic cells of the AD-dogs expressed TRPV1-IR, as shown in human DCs (115). The role of this channel in the innate immunity process has been shown in mice, in which capsaicin (TRPV1 agonist) promoted maturation and the migration of skin DCs to draining lymph nodes (116).

The TRPA1 was also largely expressed by the DCs of the AD-dogs. It appears to be the first evidence of immunoreactivity of these receptors on DCs since, in the literature, there is little and controversial evidence regarding the expression of the TRPA1 on human DCs (117, 118).

Cannabinoid receptors in T lymphocytes

Atopic dermatitis-related hypersensitivity is considered to be a Th2-polarized lymphocyte response in which a large number of Th2 genes are upregulated (1, 8, 18, 119). The immune responses of Th2 lymphocytes may drive in the s.c. extrinsic AD (3) allergen-specific IgE production (120, 121), and encourage the development of MCs and eosinophils (122). In addition, the transcriptional effect of Th2 type cytokines seems to reduce the production of filaggrin by keratinocytes, and alter the skin barrier function (123).

The expression of the CB2R-, GPR55-, and TRPA1-IR by T-cells indicates that a therapeutic effect of cannabinoid molecules in dogs with AD may also be at the level of T cell trafficking. There are studies which report that CBD suppresses T cell function and that palmitoylethanolamide (PEA) could directly inhibit T-cell responses by reducing their production of lymphokines (124–126). In the current study, only a very small proportion of T-cells expressed TRPV1-IR.

Cannabinoid receptors in calprotectin immunoreactive neutrophils

Neutrophils, together with eosinophils and B-lymphocytes, represent small subpopulations of skin-infiltrating cells of canine AD (122, 127). However, there are findings obtained in mice showing that neutrophils play a key role in chronic itch and inflammation (128). Neutrophils, which may be recruited in the skin infiltrate of AD-dogs by interleukin-17 (IL-17), produced by CD4+ Th cells, which control neutrophil homeostasis, seem to play an important role in the development of the Th2 response (129). It has been shown that, in canine AD, there is an increase in Th17 lymphocytes (119, 130). However, a recent study has evaluated the mRNA and protein expression of IL-17 and its receptor in the skin of healthy and atopic dogs, and showed that there was no significant difference in the expression of IL-17 and its receptor between healthy and atopic skin (131).

A large percentage of CAL immunoreactive neutrophils co-expressed GPR55-IR; this finding was consistent with the evidence of GPR55 in human neutrophils in which

its activation inhibits their degranulation and the release of reactive oxygen species (132). As shown in human neutrophils (118, 133), also in dogs (current study), no CAL immunoreactive cells expressed TRPA1-IR. Moreover, TRPV1-IR was not expressed by CAL positive neutrophils in the AD-dogs.

The role of endocannabinoids and phytocannabinoids in atopic dermatitis

Considering the general up-regulation of endocannabinoids (134), and cannabinoid and cannabinoid-related receptors in AD lesions of humans (135) and animals (45, 73), it is reasonable to consider the hypothetical role played by endocannabinoid molecules as well as non-psychotropic *Cannabis* derivatives, such as CBD, cannabigerol (CBG) and cannabichromene (CBC), in counteracting the inflammation and itching when AD is present.

In recent years, CBD has garnered significant attention owing to its therapeutic potential in skin disorders (136, 137). The functional activity of CBD on the CB1R is low whereas, on the CB2R, it acts as a weak agonist. Cannabidiol acts as an “indirect” CB1R/CB2R agonist by inhibiting the enzymatic hydrolysis of AEA (138). Cannabichromene may also contribute to the potential therapeutic effectiveness of some *Cannabis* preparations by means of the CB2R-mediated modulation of inflammation (139). The antagonistic effect of CBD on GPR55 seems to prevent inflammation and neuropathic pain by causing the overexpression of endocannabinoids and IL-10 (140). Cannabidiol acts as an agonist and desensitizer of the TRPV1 channel, leading to analgesic and anti-inflammatory effects and to the relief of itching (141). In the same way, CBG activates TRPV1 and inhibits the reuptake of endocannabinoids (142).

In rats, CBD is a potent TRPA1 agonist and desensitizer (40, 141). Other *Cannabis* components, such as THC, CBC and CBG, may activate TRPA1 (142, 143).

The endocannabinoid PEA, which reduces MCs degranulation (13) by means of its interaction with CB2R, also represents a promising molecule to contrast the inflammation and itching in dogs with AD, as has been shown in mice (144). In dogs, it has been shown that the topical application of PEA reduces MC degranulation, and histamine-induced itching and vasodilatation (145). In a rat model of MC cell lines, it has been shown that PEA, which acts as a GPR55 agonist (39), controls the MC degranulation and SP-induced histamine release (146). In addition, PEA, as well as CBD and AEA, acts as a TRPV1 agonist and can desensitize the TRPV1 channel (147, 148).

Considering the endocannabinoid and cannabinoid properties, their mechanisms of action and favorable beneficial results in treating other complex diseases, it is believed that they could exert a positive therapeutic effect on some conditions which are still challenging for veterinarians, such as AD, by

reducing the associated inflammation and itch, as has also been shown by two recent studies (149, 150).

The results of the present study could additionally support the preclinical and clinical trials regarding those molecules which are active on the skin inflammatory infiltrate characteristic of canine AD and which are, therefore, capable of mitigating the symptoms of this dermatologic disease.

Limitation

The mRNA and the molecular expression (Wb) of the CB2R, GPR55, TRPV1 and TRPA1 were not considered. Only the expression of cannabinoid and cannabinoid-related receptors in the inflammatory cells of the skin of AD-dogs having lesions was considered whereas neither the skin of AD-dogs not having lesions, nor the normal skin (control dogs), and nor the skin of dogs with non-allergic dermatosis were evaluated. Although many reports have indicated that cannabinoid and cannabinoid-related receptors are overexpressed during skin inflammation, in the present study, the upregulation (or downregulation) of the immunoreactivity of the receptors studied regarding the inflammatory cells of AD dogs was not evaluated. Therefore, to enhance knowledge regarding the expression and the role of these receptors in canine AD, other routine investigations (molecular and functional) are necessary.

Given the broad expression of the receptors studied in different organs and cell types, which encompasses different biological functions, the development of the *Cannabis*-related drugs should proceed with caution. It must also be taken into account that there can be a great difference between the histological and the functional findings as well as between the results obtained in rodents and those obtained in dogs, or between studies *in vitro* and *in vivo*. Other basic studies are required to support the preclinical and clinical studies regarding the therapeutic use of cannabinoids in dogs. Nevertheless, since the present evidence showed that the receptors identified in MCs, T-cells, macrophages, DCs and neutrophils are crucially involved in the pathogenesis of AD, the pharmacological modulation of these channels could be a valuable complementary strategy for local control of the skin inflammation and pruritus observed in AD.

Conclusion

The evidence regarding the effect of cannabinoid and cannabinoid-related receptors on MCs, macrophages and DCs (CB2R, GPR55, TRPV1, TRPA1), T-cells (CB2R, GPR55, TRPA1), and on neutrophils (GPR55) suggests the possibility that the manipulation of the inflammatory

cell functions with endocannabinoids and cannabinoids could result in a novel approach to the treatment of AD. Phytocannabinoids could potentially modulate inflammatory responses by regulating more than one underlying mechanism (inflammatory cells, keratinocytes, sensory nerves, fibroblasts, etc.).

Data availability statement

The raw data supporting the conclusions of this article will be made available by the authors, without undue reservation.

Ethics statement

All procedures were approved by the National Health Authority (No. 1303/2021) in accordance with DL 26/2014 and European Union Directive 2010/63/EU, under the supervision of the Central Veterinary Service of the University of Bologna. Written informed consent was obtained from the owners for the participation of their animals in this study.

Author contributions

RC, MM, and GS contributed to the study design. FA provided skin biopsies for the cryosections. FG, MD, RC, CT, and GG were carried out the immunohistochemical experiments. RC and FG: acquisition of data. RC and MM: drafting of the manuscript. All authors interpreted the data, contributed to the study execution, and approved the final manuscript.

Funding

This study received a grant from ElleVet Sciences (2021).

Conflict of interest

The authors declare that the research was conducted in the absence of any commercial or financial relationships that could be construed as a potential conflict of interest.

Publisher's note

All claims expressed in this article are solely those of the authors and do not necessarily represent those

of their affiliated organizations, or those of the publisher, the editors and the reviewers. Any product that may be evaluated in this article, or claim that may be made by its manufacturer, is not guaranteed or endorsed by the publisher.

References

- Massimini M, Dalle Vedove E, Bachetti B, Di Pierro F, Ribecco C, D'Addario C, et al. Polyphenols and cannabidiol modulate transcriptional regulation of Th1/Th2 inflammatory genes related to canine atopic dermatitis. *Front Vet Sci.* (2021) 8:606197. doi: 10.3389/fvets.2021.606197
- Halliwell R. Revised nomenclature for veterinary allergy. *Vet Immunol Immunopathol.* (2006) 114:207–8. doi: 10.1016/j.vetimm.2006.08.013
- Tizard I. *Veterinary immunology 10e*. London: Elsevier (2018).
- Santoro D. Therapies in canine atopic dermatitis: an update. *Vet Clin North Am Small Anim Pract.* (2019) 49:9–26. doi: 10.1016/j.cvsm.2018.08.002
- De Benedetto A, Agnihothri R, McGirt LY, Bankova LG, Beck LA. Atopic dermatitis: a disease caused by innate immune defects? *J Invest Dermatol.* (2009) 129:14–30. doi: 10.1038/jid.2008.259
- Pucheu-Haston CM, Santoro D, Bizikova P, Eischen MN, Marsella R, Nuttall T. Review: innate immunity, lipid metabolism and nutrition in canine atopic dermatitis. *Vet Dermatol.* (2015) 26:104–e28. doi: 10.1111/vde.12199
- Schlottter YM, Riemers FM, Rutten VP, Knol EF, Willemsse T. Enzymes involved in the conversion of arachidonic acid to eicosanoids in the skin of atopic dogs. *Exp Dermatol.* (2010) 19:e317–9. doi: 10.1111/j.1600-0625.2009.01037.x
- Olivry T, Mayhew D, Paps JS, Linder KE, Peredo C, Rajpal D, et al. Early activation of Th2/Th22 inflammatory and pruritogenic pathways in acute canine atopic dermatitis skin lesions. *J Invest Dermatol.* (2016) 136:1961–9. doi: 10.1016/j.jid.2016.05.117
- Laprais A, Dunston SM, Torres SME, Favrot C, Olivry T. Evaluation of intraepidermal nerve fibers in the skin of normal and atopic dogs. *Vet Dermatol.* (2017) 28:355–e80. doi: 10.1111/vde.12420
- Mollanazar NK, Smith PK, Yosipovitch G. Mediators of chronic pruritus in atopic dermatitis: getting the itch out? *Clin Rev Allergy Immunol.* (2016) 51:263–92. doi: 10.1007/s12016-015-8488-5
- Church MK, Kolkhir P, Metz M, Maurer M. The role and relevance of mast cells in urticaria. *Immunol Rev.* (2018) 282:232–47. doi: 10.1111/imr.12632
- Siiskonen H, Harvima I. Mast cells and sensory nerves contribute to neurogenic inflammation and pruritus in chronic skin inflammation. *Front Cell Neurosci.* (2019) 13:422. doi: 10.3389/fncel.2019.00422
- Facci L, Dal Toso R, Romanello S, Buriani A, Skaper SD, Leon A. Mast cells express a peripheral cannabinoid receptor with differential sensitivity to anandamide and palmitoylethanolamide. *Proc Natl Acad Sci USA.* (1995) 92:3376–80. doi: 10.1073/pnas.92.8.3376
- De Filippis D, D'Amico A, Iuvone T. Cannabinomimetic control of mast cell mediator release: new perspective in chronic inflammation. *J Neuroendocrinol.* (2008) 1:20–5. doi: 10.1111/j.1365-2826.2008.01674.x
- Amin K. The role of mast cells in allergic inflammation. *Respir Med.* (2012) 106:9–14. doi: 10.1016/j.rmed.2011.09.007
- Esche C, de Benedetto A, Beck LA. Keratinocytes in atopic dermatitis: inflammatory signals. *Curr Allergy Asthma Rep.* (2004) 4:276–84. doi: 10.1007/s11882-004-0071-8
- Asahina R, Maeda S, A. review of the roles of keratinocyte-derived cytokines and chemokines in the pathogenesis of atopic dermatitis in humans and dogs. *Vet Dermatol.* (2017) 28:16–e5. doi: 10.1111/vde.12351
- Brunner PM, Guttman-Yassky E, Leung DYM. The immunology of atopic dermatitis and its reversibility with broad-spectrum and targeted therapies. *J Allergy Clin Immunol.* (2017) 139:S65–76. doi: 10.1016/j.jaci.2017.01.011
- Han H, Roan F, Ziegler SF. The atopic march: current insights into skin barrier dysfunction and epithelial cell-derived cytokines. *Immunol Rev.* (2017) 278:116–30. doi: 10.1111/imr.12546
- Tey HL, Yosipovitch G. Targeted treatment of pruritus: a look into the future. *Br J Dermatol.* (2011) 165:5–17. doi: 10.1111/j.1365-2133.2011.10217.x
- Kasraie S, Niebuhr M, Werfel T. Interleukin (IL)-31 activates signal transducer and activator of transcription (STAT)-1, STAT-5 and extracellular signal-regulated kinase 1/2 and down-regulates IL-12p40 production in activated human macrophages. *Allergy.* (2013) 68:739–47. doi: 10.1111/all.12152
- McCandless EE, Rugg CA, Fici GJ, Messamore JE, Aleo MM, Gonzales AJ. Allergen-induced production of IL-31 by canine Th2 cells and identification of immune, skin, and neuronal target cells. *Vet Immunol Immunopathol.* (2014) 157:42–8. doi: 10.1016/j.vetimm.2013.10.017
- Cevikbas F, Wang X, Akiyama T, Kempkes C, Savinko T, Antal A, et al. A sensory neuron-expressed IL-31 receptor mediates T helper cell-dependent itch: Involvement of TRPV1 and TRPA1. *J Allergy Clin Immunol.* (2014) 133:448–60. doi: 10.1016/j.jaci.2013.10.048
- Nakashima C, Otsuka A, Kabashima K. Interleukin-31 and interleukin-31 receptor: new therapeutic targets for atopic dermatitis. *Exp Dermatol.* (2018) 27:327–31. doi: 10.1111/exd.13533
- Datsi A, Steinhoff M, Ahmad F, Alam M, Buddenkotte J. Interleukin-31: The “itchy” cytokine in inflammation and therapy. *Allergy.* [2021] 76:2982–97. doi: 10.1111/all.14791
- Tamamoto-Mochizuki C, Olivry T. IL-31 and IL-31 receptor expression in acute experimental canine atopic dermatitis skin lesions. *Vet Dermatol.* (2021) 32:631–e169. <https://doi.org/10.1111/vde.13034>
- Enk AH, Katz SI. Early events in the induction phase of contact sensitivity. *J Invest Dermatol.* (1992) 99:39S–41S. doi: 10.1111/1523-1747.ep12668608
- Parameswaran N, Patial S. Tumor necrosis factor- α signaling in macrophages. *Crit Rev Eukaryot Gene Expr.* (2010) 20:87–103. doi: 10.1615/critrevukargeneexpr.v20.i2.10
- Moore PF, A. review of histiocytic diseases of dogs and cats. *Vet Pathol.* (2014) 51:167–84. doi: 10.1177/0300985813510413
- Iannotti FA, Di Marzo V, Petrosino S. Endocannabinoids and endocannabinoid-related mediators: targets, metabolism and role in neurological disorders. *Prog Lipid Res.* (2016) 62:107–128. doi: 10.1016/j.plipres.2016.02.002
- Tóth KF, Adám D, Biró T, Oláh A. Cannabinoid Signaling in the Skin: Therapeutic Potential of the “C(ut)annabinoid” System. *Molecules.* (2019) 24:918. doi: 10.3390/molecules24050918
- Silver RJ. The Endocannabinoid system of animals. *Animals.* (2019) 9:686. doi: 10.3390/ani9090686
- Di Marzo V. Targeting the endocannabinoid system: to enhance or reduce? *Nat Rev Drug Discov.* (2008) 7:438–55. doi: 10.1038/nrd2553
- Kupczyk P, Reich A, Szepietowski JC. Cannabinoid system in the skin—a possible target for future therapies in dermatology. *Exp Dermatol.* (2009) 18:669–79. doi: 10.1111/j.1600-0625.2009.00923.x
- Donvito G, Nass SR, Wilkerson JL, Curry ZA, Schurman LD, Kinsey SG, et al. The endogenous cannabinoid system: a budding source of targets for treating inflammatory and neuropathic pain. *Neuropsychopharmacology.* (2018) 43:52–79. doi: 10.1038/npp.2017.204
- Avila C, Massick S, Kaffenberger BH, Kwatra SG, Bechtel M. Cannabinoids for the treatment of chronic pruritus: a review. *J Am Acad Dermatol.* (2020) 82:1205–12. doi: 10.1016/j.jaad.2020.01.036
- Kreitzer FR, Stella N. The therapeutic potential of novel cannabinoid receptors. *Pharmacol Ther.* (2009) 122:83–96. doi: 10.1016/j.pharmthera.2009.01.005

Supplementary material

The Supplementary Material for this article can be found online at: <https://www.frontiersin.org/articles/10.3389/fvets.2022.987132/full#supplementary-material>

38. Morales P, Hurst DP, Reggio PH. Molecular targets of the phytocannabinoids: a complex picture. *Prog Chem Org Nat Prod.* (2017) 103:103–31. doi: 10.1007/978-3-319-45541-9_4
39. Petrosino S, Di Marzo V. The pharmacology of palmitoylethanolamide and first data on the therapeutic efficacy of some of its new formulations. *Br J Pharmacol.* (2017) 174:1349–65. doi: 10.1111/bph.13580
40. Mlost J, Bryk M, Starowicz K. Cannabidiol for pain treatment: focus on pharmacology and mechanism of action. *Int J Mol Sci.* (2020) 21:8870. doi: 10.3390/ijms21228870
41. Mechoulam R, Peters M, Murillo-Rodriguez E, Hanus LO. Cannabidiol—recent advances. *Chem Biodivers.* (2007) 4:1678–92. doi: 10.1002/cbdv.200790147
42. Pertwee RG. The diverse CB1 and CB2 receptor pharmacology of three plant cannabinoids: delta9-tetrahydrocannabinol, cannabidiol and delta9-tetrahydrocannabinol. *Br J Pharmacol.* (2008) 153:199–215. doi: 10.1038/sj.bjp.0707442
43. Galiasso G, Giancola F, Stanzani A, Fracassi F, Bernardini C, Forni M, et al. Localization of cannabinoid receptors CB1, CB2, GPR55, and PPAR α in the canine gastrointestinal tract. *Histochem Cell Biol.* (2018) 150:187–205. doi: 10.1007/s00418-018-1684-7
44. Gobbo F, Sarli G, De Silva M, Galiasso G, Chiocchetti R, Morini M. A double histochemical/immunohistochemical staining for the identification of canine mast cells in light microscopy. *Vet Sci.* (2021) 8:229. doi: 10.3390/vetsci8100229
45. Chiocchetti R, De Silva M, Aspidi F, Zamith Cunha R, Gobbo F, Tagliavia C, et al. Distribution of cannabinoid receptors in keratinocytes of healthy dogs and dogs with atopic dermatitis. *Front Vet Sci.* (2022) 9:915896. doi: 10.3389/fvets.2022.915896
46. Hill PB, Lau P, Rybníček J. Development of an owner-assessed scale to measure the severity of pruritus in dogs. *Vet Dermatol.* (2007) 18:301–8. doi: 10.1111/j.1365-3164.2007.00616.x
47. Olivry T, Saridomichelakis M, Nuttall T, Bensignor E, Griffin CE, Hill PB; International Committee on Allergic Diseases of Animals (ICADA). Validation of the Canine Atopic Dermatitis Extent and Severity Index (CADESI)-4, a simplified severity scale for assessing skin lesions of atopic dermatitis in dogs. *Vet Dermatol.* (2014) 25:77–85. doi: 10.1111/vde.12107
48. Gross TL, Ihrke PJ, Walder EJ, Affolter VK. *Skin Diseases of the Dog and Cat.* Ames: Blackwell Publishing (2005).
49. Chiocchetti R, Galiasso G, Tagliavia C, Stanzani A, Giancola F, Menchetti M, et al. Cellular distribution of canonical and putative cannabinoid receptors in canine cervical dorsal root ganglia. *Front Vet Sci.* (2019) 6:313. doi: 10.3389/fvets.2019.00313
50. Stanzani A, Galiasso G, Giancola F, Tagliavia C, De Silva M, Pietra M, et al. Localization of cannabinoid and cannabinoid related receptors in the cat gastrointestinal tract. *Histochem Cell Biol.* (2020) 153:339–56. doi: 10.1007/s00418-020-01854-0
51. Pierezan F, Mansell J, Ambrus A, Rodrigues Hoffmann A. Immunohistochemical expression of ionized calcium binding adapter molecule 1 in cutaneous histiocytic proliferative, neoplastic and inflammatory disorders of dogs and cats. *J Comp Pathol.* (2014) 151:347–51. doi: 10.1016/j.jcpa.2014.07.003
52. Villiers E, Baines S, Law AM, Mallovs V. Identification of acute myeloid leukemia in dogs using flow cytometry with myeloperoxidase, MAC387, and a canine neutrophil-specific antibody. *Vet Clin Pathol.* (2006) 35:55–71. doi: 10.1111/j.1939-165x.2006.tb00089.x
53. Kerkhoff C, Voss A, Scholzen TE, Averill MM, Zänker KS, Bornfeldt KE. Novel insights into the role of S100A8/A9 in skin biology. *Exp Dermatol.* (2012) 21:822–6. doi: 10.1111/j.1600-0625.2012.01571.x
54. Mozos E, Pérez J, Day MJ, Lucena R, Ginel PJ. Leishmaniosis and generalized demodicosis in three dogs: a clinicopathological and immunohistochemical study. *J Comp Pathol.* (1999) 120:257–68. doi: 10.1053/jcpa.1998.0273
55. Nolte A, Junginger J, Baum B, Hewicker-Trautwein M. Heterogeneity of macrophages in canine histiocytic ulcerative colitis. *Innate Immun.* (2017) 23:228–39. doi: 10.1177/1753425916686170
56. Dandrieux JR, Martinez Lopez LM, Stent A, Jergens A, Allenspach K, Nowell CJ, et al. Changes in duodenal CD163-positive cells in dogs with chronic enteropathy after successful treatment. *Innate Immun.* (2018) 24:400–10. doi: 10.1177/1753425918799865
57. Levi M, Parenti F, Muscatello LV, Battista S, Santilli R, Perego M, et al. Pathological findings of canine idiopathic pericarditis and pericardial mesotheliomas: correlation with clinical and survival data. *Vet Sci.* (2021) 8:162. doi: 10.3390/vetsci8080162
58. Modena BD, Kristen D, Andrew A. White Emerging concepts: mast cell involvement in allergic diseases. *Translat Res.* (2016) 174:98–121. doi: 10.1016/j.trsl.2016.02.011
59. Enoksson M, Lyberg K, Moller-Westerberg C, Fallon PG, Nilsson G, Lunderius-Andersson C. Mast cells as sensors of cell injury through IL-33 recognition. *J Immunol.* (2011) 186:2523–8. doi: 10.4049/jimmunol.1003383
60. Soter NA. Morphology of atopic eczema. *Allergy.* (1989) 9:16–9. doi: 10.1111/j.1398-9995.1989.tb04310.x
61. Wilkie JS, Yager JA, Eyre P, Parker WM. Morphometric analyses of the skin of dogs with atopic dermatitis and correlations with cutaneous and plasma histamine and total serum IgE. *Vet Pathol.* (1990) 27:179–86. doi: 10.1177/030098589002700305
62. Ribatti D. The staining of mast cells: a historical overview. *Int Arch Allergy Immunol.* (2018) 176:55–60. doi: 10.1159/000487538
63. He SH. Key role of mast cells and their major secretory products in inflammatory bowel disease. *World J Gastroenterol.* (2004) 10:309–18. doi: 10.3748/wjg.v10.i3.309
64. Ständer S, Moormann C, Schumacher M, Buddenkotte J, Artuc M, Shpacovitch V, et al. Expression of vanilloid receptor subtype 1 in cutaneous sensory nerve fibers, mast cells, and epithelial cells of appendage structures. *Exp Dermatol.* (2004) 13:129–39. doi: 10.1111/j.0906-6705.2004.0178.x
65. Atiakshin D, Samoilova V, Buchwalow I, Boecker W, Tiemann M. Characterization of mast cell populations using different methods for their identification. *Histochem Cell Biol.* (2017) 147:683–94. doi: 10.1007/s00418-017-1547-7
66. Jogie-Brahim S, Min HK, Fukuoka Y, Xia HZ, Schwartz LB. Expression of alpha-tryptase and beta-tryptase by human basophils. *J Allergy Clin Immunol.* (2004) 113:1086–92. doi: 10.1016/j.jaci.2004.02.032
67. Yamanishi Y, Miyake K, Iki M, Tsutsui H, Karasuyama H. Recent advances in understanding basophil-mediated Th2 immune responses. *Immunol Rev.* (2017) 278:237–45. doi: 10.1111/immr.12548
68. Lazzeri M, Vannucchi MG, Zardo C, Spinelli M, Beneforti P, Turini D, et al. Immunohistochemical evidence of vanilloid receptor 1 in normal human urinary bladder. *Eur Urol.* (2004) 46:792–8. doi: 10.1016/j.eururo.2004.08.007
69. Ständer S, Schmelz M, Metz D, Luger T, Rukwied R. Distribution of cannabinoid receptor 1 (CB1) and 2 (CB2) on sensory nerve fibers and adnexal structures in human skin. *J Dermatol Sci.* (2005) 38:177–88. doi: 10.1016/j.jdermsci.2005.01.007
70. Rasul A, El-Nour H, Lonne-Rahm SB, Fransson O, Johansson C, Johansson B, et al. Serotonergic markers in atopic dermatitis. *Acta Derm Venereol.* (2016) 96:732–6. doi: 10.2340/00015555-2354
71. Biró T, Maurer M, Modarres S, Lewin NE, Brodie C, Acs G, et al. Characterization of functional vanilloid receptors expressed by mast cells. *Blood.* (1998) 91:1332–40.
72. Samson MT, Small-Howard A, Shimoda LM, Koblan-Huberson M, Stokes AJ, Turner H. Differential roles of CB1 and CB2 cannabinoid receptors in mast cells. *J Immunol.* (2003) 170:4953–62. doi: 10.4049/jimmunol.170.10.4953
73. Campora L, Miragliotta V, Ricci E, Cristino L, Di Marzo V, Albanese F, et al. Cannabinoid receptor type 1 and 2 expression in the skin of healthy dogs and dogs with atopic dermatitis. *Am J Vet Res.* (2012) 73:988–95. doi: 10.2460/ajvr.73.7.988
74. Small-Howard AL, Shimoda LM, Adra CN, Turner H. Anti-inflammatory potential of CB1-mediated AMP elevation in mast cells. *Biochemical Journal.* (2005) 388:465–73. doi: 10.1042/BJ20041682
75. Malan TP, Ibrahim MM, Vanderah TW, Makriyannis A, Porreca F. Inhibition of pain responses by activation of CB(2) cannabinoid receptors. *Chem Phys Lipids.* (2002) 121:191–200. doi: 10.1016/s0009-3084(02)00155-x
76. Cruz SL, Sánchez-Miranda E, Castillo-Arellano JJ, Cervantes-Villagrana RD, Ibarra-Sánchez A, González-Espinosa C. Anandamide inhibits Fc ϵ RI-dependent degranulation and cytokine synthesis in mast cells through CB2 and GPR55 receptor activation. Possible involvement of CB2-GPR55 heteromers. *Int Immunopharmacol.* (2018) 64:298–307. doi: 10.1016/j.intimp.2018.09.006
77. Cantarella G, Scollo M, Lempereur L, Saccani-Jotti G, Basile F, Bernardini R. Endocannabinoids inhibit release of nerve growth factor by inflammation-activated mast cells. *Biochem Pharmacol.* (2011) 82:380–8. doi: 10.1016/j.bcp.2011.05.004
78. Siebenhaar F, Magerl M, Peters EM, Hendrix S, Metz M, Maurer M. Mast cell-driven skin inflammation is impaired in the absence of sensory nerves. *J Allergy Clin Immunol.* (2008) 121:955–61. doi: 10.1016/j.jaci.2007.11.013
79. Serhan N, Basso L, Sibilano R, Petitfils C, Meixiong J, Bonnart C, et al. House dust mites activate nociceptor-mast cell clusters to drive type 2 skin inflammation. *Nat Immunol.* (2019) 20:1435–43. doi: 10.1038/s41590-019-0493-z

80. Rossbach K, Nassenstein C, Gschwandtner M, Schnell D, Sander K, Seifert R, et al. Histamine H1, H3 and H4 receptors are involved in pruritus. *Neuroscience*. (2011) 190:89–102. doi: 10.1016/j.neuroscience.2011.06.002
81. Schlosburg J E, Boger D L, Cravatt B F, Lichtman A H. Endocannabinoid modulation of scratching response in an acute allergic model: a new prospective neural therapeutic target for pruritus. *J Pharmacol Exp Ther*. (2009) 329:314–23. doi: 10.1124/jpet.108.150136
82. Sun S, Dong X, TRP channels and itch. *Semin Immunopathol*. (2016) 38:293–307. doi: 10.1007/s00281-015-0530-4
83. Yun JW, Seo JA, Jang WH, Koh HJ, Bae IH, Park YH, et al. Antipruritic effects of TRPV1 antagonist in murine atopic dermatitis and itching models. *J Invest Dermatol*. (2011) 131:1576–9. doi: 10.1038/jid.2011.87
84. Weisshaar E, Dunker N, Gollnick H. Topical capsaicin therapy in humans with hemodialysis-related pruritus. *Neurosci Lett*. (2003) 345:192–4. doi: 10.1016/s0304-3940(03)00511-1
85. Marsella R, Nicklin CF, Melloy C. The effects of capsaicin topical therapy in dogs with atopic dermatitis: a randomized, double-blinded, placebo-controlled, cross-over clinical trial. *Vet Dermatol*. (2002) 13:131–9. doi: 10.1046/j.1365-3164.2002.00292.x
86. Kobayashi K, Fukuoka T, Obata K, Yamanaka H, Dai Y, Tokunaga A, et al. Distinct expression of TRPM8, TRPA1, and TRPV1 mRNAs in rat primary afferent neurons with delta/c-fibers and colocalization with trk receptors. *J Comp Neurol*. (2005) 493:596–606. doi: 10.1002/cne.20794
87. Oh MH, Oh SY, Lu J, Lou H, Myers AC, Zhu Z, et al. TRPA1-dependent pruritus in IL-13-induced chronic atopic dermatitis. *J Immunol*. (2013) 191:5371–82. doi: 10.4049/jimmunol.1300300
88. Moore C, Gupta R, Jordt SE, Chen Y, Liedtke WB. Regulation of pain and itch by TRP channels. *Neurosci Bull*. (2018) 34:120–42. doi: 10.1007/s12264-017-0200-8
89. Maglie R, Souza Monteiro de Araujo D, Antiga E, Geppetti P, Nassini R, De Logu F. The Role of TRPA1 in skin physiology and pathology. *Int J Mol Sci*. (2021) 22:3065. doi: 10.3390/ijms22063065
90. Marsella R, Olivry T, Maeda S. Cellular and cytokine kinetics after epicutaneous allergen challenge (atopy patch testing) with house dust mites in high-IgE beagles. *Vet Dermatol*. (2006) 17:111–20. doi: 10.1111/j.1365-3164.2006.00508.x
91. Kang J, Ding Y, Li B, Liu H, Yang X, Chen M. TRPA1 mediated aggravation of allergic contact dermatitis induced by DINP and regulated by NF- κ B activation. *Sci Rep*. (2017) 7:43586. doi: 10.1038/srep43586
92. Zeng D, Chen C, Zhou W, Ma X, Pu X, Zeng Y, et al. TRPA1 deficiency alleviates inflammation of atopic dermatitis by reducing macrophage infiltration. *Life Sci*. (2021) 266:118906. doi: 10.1016/j.lfs.2020.118906
93. Leung DY. Atopic dermatitis: the skin as a window into the pathogenesis of chronic allergic diseases. *J Allergy Clin Immunol*. (1995) 96:302–18. doi: 10.1016/s0091-6749(95)70049-8
94. Ricklin Gutzwiller ME, Moulin HR, Zurbriggen A, Roope P, Summerfield A. Comparative analysis of canine monocyte- and bone-marrow-derived dendritic cells. *Vet Res*. (2010) 41:40. doi: 10.1051/vetres/2010012
95. Honda T, Egawa G, Kabashima K. Antigen presentation and adaptive immune responses in skin. *Int Immunol*. (2019) 31:423–9. doi: 10.1093/intimm/dxz005
96. He S, Peng Q, Walls AF. Potent induction of a neutrophil and eosinophil-rich infiltrate in vivo by human mast cell tryptase: selective enhancement of eosinophil recruitment by histamine. *J Immunol*. (1997) 159:6216–25.
97. Wright K, Rooney N, Feeney M, Tate J, Robertson D, Welham M, et al. Differential expression of cannabinoid receptors in the human colon: cannabinoids promote epithelial wound healing. *Gastroenterology*. (2005) 129:437–53. doi: 10.1016/j.gastro.2005.05.026
98. Zheng JL Yu TS, Li XN, Fan YY, Ma WX, Du Y, et al. Cannabinoid receptor type 2 is time-dependently expressed during skin wound healing in mice. *Int J Legal Med*. (2012) 126:807–14. doi: 10.1007/s00414-012-0741-3
99. Du Y, Ren P, Wang Q, Jiang S K, Zhang M, Li JY, et al. Cannabinoid 2 receptor attenuates inflammation during skin wound healing by inhibiting M1 macrophages rather than activating M2 macrophages. *J Inflamm (Lond)*. (2018) 15:25. doi: 10.1186/s12950-018-0201-z
100. Tarique AA, Evron T, Zhang G, Tepper MA, Morshed MM, Andersen ISG, et al. Anti-inflammatory effects of lenabasum, a cannabinoid receptor type 2 agonist, on macrophages from cystic fibrosis. *J Cyst Fibros*. (2020) 19:823–9. doi: 10.1016/j.jcf.2020.03.015
101. Taylor L, Christou I, Kapellos TS, Buchan A, Brodermann MH, Gianella-Borradori M, et al. Primary macrophage chemotaxis induced by cannabinoid receptor 2 agonists occurs independently of the CB2 receptor. *Sci Rep*. (2015) 5:10682. doi: 10.1038/srep10682
102. Lanuti M, Talamonti E, Maccarrone M, Chiurichiu V. Correction: activation of GPR55 receptors exacerbates oxLDL-induced lipid accumulation and inflammatory responses, while reducing cholesterol efflux from human macrophages. *PLoS One*. (2015) 10:e0131850. doi: 10.1371/journal.pone.0131850
103. Bujak JK, Kosmala D, Majchrzak-Kuligowska K, Bednarczyk P. Functional Expression of TRPV1 Ion Channel in the Canine Peripheral Blood Mononuclear Cells. *Int J Mol Sci*. (2021) 22:3177. doi: 10.3390/ijms22063177
104. Ninomiya Y, Tanuma SI, Tsukimoto M. Differences in the effects of four TRPV1 channel antagonists on lipopolysaccharide-induced cytokine production and COX-2 expression in murine macrophages. *Biochem Biophys Res Commun*. (2017) 484:668–74. doi: 10.1016/j.bbrc.2017.01.173
105. Kun J, Perkecz A, Knie L, Sétáló G Jr, Tornóczy T, Pintér E, et al. TRPA1 receptor is upregulated in human oral lichen planus. *Oral Dis*. (2017) 23:189–98. doi: 10.1111/odi.12593
106. Novak N, Bieber T. The role of dendritic cell subtypes in the pathophysiology of atopic dermatitis. *J Am Acad Dermatol*. (2005) 53:171–176. doi: 10.1016/j.jaad.2005.04.060
107. Ricklin ME, Roope P, Summerfield A. Characterization of canine dendritic cells in healthy, atopic, and non-allergic inflamed skin. *J Clin Immunol*. (2010) 30:845–54. doi: 10.1007/s10875-010-9447-9
108. Olivry T, Moore PF, Affolter VK, Naydan DK. Langerhans cell hyperplasia and IgE expression in canine atopic dermatitis. *Arch Dermatol Res*. (1996) 288:579–85. doi: 10.1007/BF02505260
109. Matias I, Pochard P, Orlando P, Salzet M, Pestel J, Di Marzo V. Presence and regulation of the endocannabinoid system in human dendritic cells. *Eur J Biochem*. (2002) 269:3771–8. doi: 10.1046/j.1432-1033.2002.03078.x
110. Do Y, McKallip RJ, Nagarkatti M, Nagarkatti PS. Activation through cannabinoid receptors 1 and 2 on dendritic cells triggers NF-kappaB-dependent apoptosis: novel role for endogenous and exogenous cannabinoids in immunoregulation. *J Immunol*. (2004) 173:2373–82. doi: 10.4049/jimmunol.173.4.2373
111. Svensson M, Chen P, Hammarfjord O. Dendritic cell regulation by cannabinoid-based drugs. *Pharmaceuticals (Basel)*. (2010) 3:2733–50. doi: 10.3390/ph3082733
112. Adhikary S, Kocieda VP, Yen JH, Tuma RF, Ganea D. Signaling through cannabinoid receptor 2 suppresses murine dendritic cell migration by inhibiting matrix metalloproteinase 9 expression. *Blood*. (2012) 120:3741–9. doi: 10.1182/blood-2012-06-435362
113. Castillo-Chabeco B, Figueroa G, Parira T, Napuri J, Agudelo M. Ethanol-induced modulation of GPR55 expression in human monocyte-derived dendritic cells is accompanied by H4K12 acetylation. *Alcohol*. (2018) 71:25–31. doi: 10.1016/j.alcohol.2018.05.008
114. Tanikawa T, Oka S, Nakajima K, Hayashi Y, Nemoto-Sasaki Y, Arata Y, et al. Expression and Distribution of GPR55, a Receptor for Lysophosphatidylinositol, in Mouse Tissues and Cells. *BPB Reports*. (2022) 5:15–20. doi: 10.1248/bpbreports.5.2_16
115. Tóth BI, Benko S, Szöllosi AG, Kovács L, Rajnavölgyi E, Bíró T. Transient receptor potential vanilloid-1 signaling inhibits differentiation and activation of human dendritic cells. *FEBS Lett*. (2009) 583:1619–24. doi: 10.1016/j.febslet.2009.04.031
116. Basu S, Srivastava P. Immunological role of neuronal receptor vanilloid receptor 1 expressed on dendritic cells. *Proc Natl Acad Sci U S A*. (2005) 102:5120–5. doi: 10.1073/pnas.0407780102
117. Szöllosi AG, Oláh A, Tóth IB, Papp F, Czifra G, Panyi G, et al. Transient receptor potential vanilloid-2 mediates the effects of transient heat shock on endocytosis of human monocyte-derived dendritic cells. *FEBS Lett*. (2013) 587:1440–5. doi: 10.1016/j.febslet.2013.03.027
118. Naert R, López-Requena A, Talavera K. TRPA1 Expression and Pathophysiology in Immune Cells. *Int J Mol Sci*. (2021) 22:11460. doi: 10.3390/ijms222111460
119. Marsella R. Advances in our understanding of canine atopic dermatitis. *Vet Dermatol*. (2021) 21:1265. doi: 10.1111/vde.12965
120. Majewska A, Gajewska M, Dembele K, Maciejewski H, Prostek A, Jank M. Lymphocytic, cytokine and transcriptomic profiles in peripheral blood of dogs with atopic dermatitis. *BMC Vet Res*. (2016) 12:174. doi: 10.1186/s12917-016-0805-6
121. Vogelnest L. Canine atopic dermatitis: a common, chronic and challenging dermatosis. *Vet Rec*. (2021) 188:185–7. doi: 10.1002/vetr.273

122. Hill PB, Olivry T. The ACVD task force on canine atopic dermatitis (V): biology and role of inflammatory cells in cutaneous allergic reactions. *Vet Immunol Immunopathol.* (2001) 81:187–98. doi: 10.1016/s0165-2427(01)00310-5
123. Combarros D, Cadiergues MC, Simon M. Update on canine flaggrin: a review. *Vet Q.* (2020) 40:162–8. doi: 10.1080/01652176.2020.1758357
124. Wu HY, Chu RM, Wang CC, Lee CY, Lin SH, Jan TR. Cannabidiol-induced apoptosis in primary lymphocytes is associated with oxidative stress-dependent activation of caspase-8. *Toxicol Appl Pharmacol.* (2008) 226:260–70. doi: 10.1016/j.taap.2007.09.012
125. Kaplan BLF, Springs AEB, Kaminski NE. The profile of immune modulation by cannabidiol (CBD) involves deregulation of nuclear factor of activated T cells (NFAT). *Biochem Pharmacol.* (2008) 76:726–37. doi: 10.1016/j.bcp.2008.06.022
126. Chiurchiù V, van der Stelt M, Centonze D, Maccarrone M. The endocannabinoid system and its therapeutic exploitation in multiple sclerosis: clues for other neuroinflammatory diseases. *Prog Neurobiol.* (2018) 160:82–100. doi: 10.1016/j.pneurobio.2017.10.007
127. Olivry T, Naydan DK, Moore PF. Characterization of the cutaneous inflammatory infiltrate in canine atopic dermatitis. *Am J Dermatopathol.* (1997) 19:477–86. doi: 10.1097/00000372-199710000-00008
128. Walsh CM, Hill RZ, Schwendinger-Schreck J, Deguine J, Brock EC, Kucirek N, et al. Neutrophils promote CXCR3-dependent itch in the development of atopic dermatitis. *Elife.* (2019) 8:e48448. doi: 10.7554/eLife.48448
129. Asahina R, Kamishina H, Kamishina H, Maeda S. Gene transcription of pro-inflammatory cytokines and chemokines induced by IL-17A in canine keratinocytes. *Vet Dermatol.* (2015) 26:426–31. doi: 10.1111/vde.12244
130. Jassies-van der Lee A, Rutten VP, Bruijn J, Willemse T, Broere F. CD4+ and CD8+ skin-associated T lymphocytes in canine atopic dermatitis produce interleukin-13, interleukin-22 and interferon- γ and contain a CD25+ FoxP3+ subset. *Vet Dermatol.* (2014) 25:456–e72. doi: 10.1111/vde.12140
131. Shiomitsu S, Gillen J, Frasca S Jr, Santoro D. Evaluation of the cutaneous expression of IL-17, IL-22, IL-31, and their receptors in canine atopic dermatitis. *Res Vet Sci.* (2021) 136:74–80. doi: 10.1016/j.rvsc.2020.12.015
132. Balenga NA, Aflaki E, Kargl J, Platzer W, Schröder R, Blättermann S, et al. GPR55 regulates cannabinoid 2 receptor-mediated responses in human neutrophils. *Cell Res.* (2011) 21:1452–69. doi: 10.1038/cr.2011.60
133. Foote JR, Behe P, Frampton M, Levine AP, Segal AW. An exploration of charge compensating ion channels across the phagocytic vacuole of neutrophils. *Front Pharmacol.* (2017) 8:94. doi: 10.3389/fphar.2017.00094
134. Abramo F, Campora L, Albanese F, della Valle MF, Cristino L, Petrosino S, et al. Increased levels of palmitoylethanolamide and other bioactive lipid mediators and enhanced local mast cell proliferation in canine atopic dermatitis. *BMC Vet Res.* (2014) 10:21. doi: 10.1186/1746-6148-10-21
135. Martín-Fonchea M, Eiwegger T, Jartti T, Rueda-Zubiaurre A, Tiringier K, Stepanow J, et al. The expression of cannabinoid receptor 1 is significantly increased in atopic patients. *J Allergy Clin Immunol.* (2014) 133:926–9.e2. doi: 10.1016/j.jaci.2013.12.1032
136. Petrosino S, Verde R, Vaia M, Allarà M, Iuvone T, Di Marzo V. Anti-inflammatory properties of cannabidiol, a nonpsychotropic cannabinoid, in experimental allergic contact dermatitis. *J Pharmacol Exp Ther.* (2018) 365:652–63. doi: 10.1124/jpet.117.244368
137. Baswan SM, Klosner AE, Glynn K, Rajgopal A, Malik K, Yim S, et al. Therapeutic potential of cannabidiol (CBD) for skin health and disorders. *Clin Cosmet Investig Dermatol.* (2020) 13:927–42. doi: 10.2147/CCID.S286411
138. Ligresti A, De Petrocellis L, Di Marzo V. From phytocannabinoids to cannabinoid receptors and endocannabinoids: pleiotropic physiological and pathological roles through complex pharmacology. *Physiol Rev.* (2016) 96:1593–659. doi: 10.1152/physrev.00002.2016
139. Udoh M, Santiago M, Devenish S, McGregor IS, Connor M. Cannabichromene is a cannabinoid CB(2) receptor agonist. *Br J Pharmacol.* (2019) 176:4537–47. doi: 10.1111/bph.14815
140. Sunda F, Arowolo A, A. molecular basis for the anti-inflammatory and anti-fibrosis properties of cannabidiol. *FASEB J.* (2020) 34:14083–92. doi: 10.1096/fj.202000975R
141. De Petrocellis L, Ligresti A, Schiano Moriello A, Allarà M, Bisogno T, Petrosino S, et al. Effects of cannabinoids and cannabinoid-enriched Cannabis extracts on TRP channels and endocannabinoid metabolic enzymes. *Br J Pharmacol.* (2011) 163:1479–94. doi: 10.1111/j.1476-5381.2010.01166.x
142. Borrelli F, Pagano E, Romano B, Panzera S, Maiello F, Coppola D, et al. Colon carcinogenesis is inhibited by the TRPM8 antagonist cannabigerol, a Cannabis-derived non-psychotropic cannabinoid. *Carcinogenesis.* (2014) 35:2787–97. doi: 10.1093/carcin/bgu205
143. De Petrocellis L, Vellani V, Schiano-Moriello A, Marini P, Magherini PC, Orlando P, et al. Plant-derived cannabinoids modulate the activity of transient receptor potential channels of ankyrin type-1 and melastatin type-8. *J Pharmacol Exp Ther.* (2008) 325:1007–15. doi: 10.1124/jpet.107.134809
144. Vaia M, Petrosino S, De Filippis D, Negro L, Guarino A, Carnuccio R, et al. Palmitoylethanolamide reduces inflammation and itch in a mouse model of contact allergic dermatitis. *Eur J Pharmacol.* (2016) 791:669–74. doi: 10.1016/j.ejphar.2016.10.005
145. Cerrato S, Brazis P, della Valle MF, Miolo A, Puigdemont A. Effects of palmitoylethanolamide on immunologically induced histamine, PGD2 and TNF α release from canine skin mast cells. *Vet Immunol Immunopathol.* (2010) 133:9–15. doi: 10.1016/j.vetimm.2009.06.011
146. Petrosino S, Schiano Moriello A, Verde R, Allarà M, Imperatore R, Ligresti A, et al. Palmitoylethanolamide counteracts substance P-induced mast cell activation in vitro by stimulating diacylglycerol lipase activity. *J Neuroinflammation.* (2019) 16:274. doi: 10.1186/s12974-019-1671-5
147. Di Marzo V, De Petrocellis L, Fezza F, Ligresti A, Bisogno T. Anandamide receptors. *Prostaglandins Leukot Essent Fatty Acids.* (2002) 66:377–91. doi: 10.1054/plef.2001.0349
148. Ross RA. Anandamide and vanilloid TRPV1 receptors. *Br J Pharmacol.* (2003) 140:790–801. doi: 10.1038/sj.bjp.0705467
149. CannPal Animal Therapeutics Limited. *CBD Substantially Improves Atopic Dermatitis Symptoms in Dogs.* Available online at: <https://www.prnewswire.com/news-releases/cbd-substantially-improves-atopic-dermatitis-symptoms-in-dogs-301095965.html>. (accessed July 21, 2020).
150. ElleVet Sciences. *ElleVet Sciences Announce Results of Atopic Dermatitis Study Using Its CBD+CBDA Oil on Dogs.* Available online at: <https://www.prnewswire.com/news-releases/ellevet-sciences-announces-results-of-atopic-dermatitis-study-using-its-cbdcbda-oil-on-dogs-301189648.html>. (accessed July 9, 2020).

Chapter 8:
Expression of cannabinoid (CB1 and CB2) and cannabinoid-related receptors
(TRPV1, GPR55, and PPAR α) in the synovial membrane of the horse
metacarpophalangeal joint



OPEN ACCESS

EDITED BY

Pablo Martín-Vasallo,
University of La Laguna, Spain

REVIEWED BY

Deanne Helena Hryciw,
Griffith University, Australia
Piotr Kupczyk,
Wrocław Medical University, Poland

*CORRESPONDENCE

Roberto Chiocchetti
✉ roberto.chiocchetti@unibo.it

SPECIALTY SECTION

This article was submitted to
Comparative and Clinical Medicine,
a section of the journal
Frontiers in Veterinary Science

RECEIVED 15 September 2022

ACCEPTED 31 January 2023

PUBLISHED 03 March 2023

CITATION

Zamith Cunha R, Zannoni A, Salamanca G,
De Silva M, Rinnovati R, Gramenzi A, Forni M
and Chiocchetti R (2023) Expression of
cannabinoid (CB1 and CB2) and
cannabinoid-related receptors (TRPV1, GPR55,
and PPAR α) in the synovial membrane of the
horse metacarpophalangeal joint.
Front. Vet. Sci. 10:1045030.
doi: 10.3389/fvets.2023.1045030

COPYRIGHT

© 2023 Zamith Cunha, Zannoni, Salamanca,
De Silva, Rinnovati, Gramenzi, Forni and
Chiocchetti. This is an open-access article
distributed under the terms of the [Creative
Commons Attribution License \(CC BY\)](#). The use,
distribution or reproduction in other forums is
permitted, provided the original author(s) and
the copyright owner(s) are credited and that
the original publication in this journal is cited, in
accordance with accepted academic practice.
No use, distribution or reproduction is
permitted which does not comply with these
terms.

Expression of cannabinoid (CB1 and CB2) and cannabinoid-related receptors (TRPV1, GPR55, and PPAR α) in the synovial membrane of the horse metacarpophalangeal joint

Rodrigo Zamith Cunha¹, Augusta Zannoni¹, Giulia Salamanca¹,
Margherita De Silva¹, Riccardo Rinnovati¹, Alessandro Gramenzi²,
Monica Forni¹ and Roberto Chiocchetti^{1*}

¹Department of Veterinary Medical Sciences (UNI EN ISO 9001:2008), University of Bologna, Bologna, Italy, ²Faculty of Veterinary Medicine, Università degli Studi di Teramo, Teramo, Italy

Background: The metacarpophalangeal joint undergoes enormous loading during locomotion and can therefore often become inflamed, potentially resulting in osteoarthritis (OA). There are studies indicating that the endocannabinoid system (ECS) modulates synovium homeostasis, and could be a promising target for OA therapy. Some cannabinoid receptors, which modulate proliferative and secretory responses in joint inflammation, have been functionally identified in human and animal synovial cells.

Objective: To characterize the cellular distribution of the cannabinoid receptors 1 (CB1R) and 2 (CB2R), and the cannabinoid-related receptors transient receptor potential vanilloid type 1 (TRPV1), G protein-related receptor 55 (GPR55) and peroxisome proliferator-activated receptor alpha (PPAR α) in the synovial membrane of the metacarpophalangeal joint of the horse.

Animals: The dorsal synovial membranes of 14 equine metacarpophalangeal joints were collected post-mortem from an abattoir.

Materials and methods: The dorsal synovial membranes of 14 equine metacarpophalangeal joints were collected post-mortem from an abattoir. The expression of the CB1R, CB2R, TRPV1, GPR55, and PPAR α in synovial tissues was studied using qualitative and quantitative immunofluorescence, and quantitative real-time reverse transcriptase PCR (qRT-PCR). Macrophage-like (MLS) and fibroblast-like (FLS) synoviocytes were identified by means of antibodies directed against IBA1 and vimentin, respectively.

Results: Both the mRNA and protein expression of the CB2R, TRPV1, GPR55, and PPAR α were found in the synoviocytes and blood vessels of the metacarpophalangeal joints. The synoviocytes expressed the mRNA and protein of the CB1R in some of the horses investigated, but not in all.

Conclusions and clinical importance: Given the expression of the CB1R, CB2R, TRPV1, GPR55, and PPAR α in the synovial elements of the metacarpophalangeal

joint, these findings encouraged the development of new studies supporting the use of molecules acting on these receptors to reduce the inflammation during joint inflammation in the horse.

KEYWORDS

cannabidiol, fibroblast-like synoviocytes, G protein-related receptor 55, macrophage-like synoviocytes, peroxisome proliferator-activated receptor alpha, transient receptor potential vanilloid type 1

Introduction

The metacarpophalangeal joint is a high mobility structure which undergoes enormous loading during locomotion and jumping in the horse (1), so much so that it is the most commonly reported joint affected by traumatic and degenerative lesions in equine athletes (2) and results in lameness in thoroughbred racehorses (3, 4). Currently, there is no specific cure for joint disease, and the multimodal pharmacological treatment does not act on the cause of joint inflammation but is aimed at slowing its progression, minimizing/reducing pain, and increasing function and performance (5). In recent decades, some molecules have given encouraging results for the treatment of osteoarthritis, even if it is difficult to draw definitive conclusions (6). Therefore, there is a need for improving the understanding of the pathophysiology and mechanisms of joint pain in order to develop safe and effective drugs to alleviate symptoms in horses with synovitis and osteoarthritis (OA) (7). Joint inflammation can affect cartilage, bone and the synovial membrane within the joint (8). However, regardless of which intra-articular tissue type is first affected, the synovial membrane seems to modulate and reinforce the inflammatory responses of the joints (9, 10). Hence, the synovial membrane is key to enhancing the understanding of the pathophysiological processes within the synovial joint.

The wall of the joint capsule is composed of two distinct layers: the external and thick fibrous layer (*stratum fibrosum*), and the inner and thin synovial membrane (*synovium*). The cells of the intimal lining of the *synovium* secrete the fluid into the joint cavity (synovial fluid), remove debris and are involved in the production of cytokines/molecules which may modulate the joint inflammation (9–13). Two types of synoviocytes lining the luminal side of the joint capsule have been described in depth in humans and animals (14, 15), including horses (11, 13, 16, 17): (1) macrophage-like synoviocytes (MLS), also known as type A synoviocytes, and (2) fibroblast-like synoviocytes (FLS), also known as type B synoviocytes. Embedded in a thin layer of connective tissue rich in fenestrated capillaries, the synoviocytes produce and control the synovial fluid. Fibroblast-like synoviocytes, the dominating cell-type in the synovial intima, produce hyaluronic acid and other lubricating synovial additives of the synovial fluid, and also matrix components (such as collagens, proteoglycans and laminin) and degrading enzymes (such as matrix metalloproteinases [MMPs] and other proteases) (18). In cultured human FLS, it has been shown that these cells organize a basement membrane-like extracellular matrix, capable of supporting monocyte survival and compaction into the lining (19). A more recent study has shown

that fibroblasts might also provide anchorage to the MLS and are also a source of key survival factors of the MLS (20).

Although FLS morphologically differ from the other fibroblasts, these cells may express the typical fibroblast markers vimentin (21) or, uniquely in the horse, the neuronal marker Protein Gene Product 9.5. (16). However, due to the specific functions of the FLS in the synovial lining (22), there are only a few reports of selective markers of FLS, differentiating them from other musculoskeletal fibroblasts (13).

Macrophage-like synoviocytes are macrophages not derived from bone-marrow immune cells (monocytes) but derived from cells which disperse into the tissues during embryonic development and are resident in the joint (23). Macrophage-like synoviocytes may be distributed unevenly adjacent to the joint lumen (11) or, as has recently been described in mice, may congregate to form an internal immunological barrier at the synovial lining which physically seclude the joint (24, 25). General resident macrophage-markers, such as CD11b, CD14, CD68, and CD206, may be expressed by horse MLS (26).

The strong need to develop a treatment for synovial inflammation, cartilage degeneration, and bone deformation has led to research regarding the involvement of the immunomodulatory endocannabinoid system (ECS) in the development of OA (12, 27–32). The involvement of the ECS in immunocytes and macrophages, as well as in regulatory actions on sensory nociceptors to ameliorate pain in OA, has been described (33). The ECS consists of endocannabinoid molecules involved in signaling processes, along with G-protein-coupled receptors (GPCRs) and enzymes associated with ligand biosynthesis, activation and degradation (33). Endocannabinoids and endocannabinoid-like lipid mediators, such as palmitoylethanolamide (PEA) (34), the phytocannabinoids derived from *Cannabis sativa*, such as Δ -9-tetrahydrocannabinol (THC), cannabidiol (CBD), cannabigerol, cannabichromene, and cannabinol (35, 36), and the synthetic cannabinoids all act on canonical cannabinoid-1 (CB1R) and -2 (CB2R) receptors. They also act on cannabinoid-related receptors, such as the transient receptor potential (TRP) channels, the G protein-coupled receptors (GPCRs), the nuclear peroxisome proliferator-activated receptors (PPARs), and the serotonin receptors (12, 35, 37–39).

There are studies showing that the activation of CB1R and CB2R, which are expressed in human, mouse, and horse synoviocytes (28, 40–44), can induce potent anti-inflammatory effects and modulate arthritic disease (31, 43, 45). The TRP vanilloid 1 (TRPV1) ion channel, which is expressed in human and

rat synoviocytes (41, 46), might also be a possible target for treating joint diseases (46).

There are no studies which have reported the expression of G protein-coupled receptor 55 (GPR55) or PPAR α in synoviocytes. However, GPR55 has been localized in human chondrocytes, osteoclasts and osteoblasts (47, 48) and there are studies indicating that PPAR α agonists may exert beneficial effects on OA due to their anti-inflammatory effects (49, 50).

Given the aforementioned data obtained in other species, it is conceivable that the receptors of the endocannabinoid system could be expressed in the horse synovial membrane and represent a pharmacological target for the treatment of joint diseases. Currently, only a few reports have been published regarding the cannabinoid and cannabinoid-related receptors of the horse joint *synovium* (4, 44).

Thus, the current study was designed to identify the mRNA of *Cnr1*, *Cnr2*, *TRPV1*, *GPR55*, and *PPARA* and to immunohistochemically localize these receptors in the synovial membrane of the equine metacarpophalangeal joint.

Materials and methods

Animals

The metacarpophalangeal joints of 14 healthy horses (9 females and 5 males), ranging from 2 to 20 years of age (mean: 12 years; SD \pm 6.5), which were slaughtered for consumption were collected from the thoracic limbs post-mortem. The breeds included 1 Avelignese, 1 Italian thoroughbred, and 12 half-breeds. The distal forelimbs were removed at the carpal joint to obtain the metacarpophalangeal joints.

A complete cell blood count (CBC) and routine serum biochemical analyses were carried out using blood samples taken at the time of exsanguination. The horses, which did not show lameness of either the thoracic or the pelvic limbs, were considered to be healthy on the basis of a summary clinical visit prior to slaughter, normal results of the CBC count and routine serum biochemical analyses. In addition, the presence of OA or other pathological conditions were excluded by post-mortem gross and histological evaluation.

According to Directive 2010/63/EU of the European Parliament and of the Council of 22 September 2010 regarding the protection of animals used for scientific purposes, Italian legislation (D. Lgs. n. 26/2014) does not require any approval by competent authorities or ethics committees as this study did not influence any therapeutic decisions.

RNA isolation and reverse transcription

Total RNA extraction was performed using TRI Reagent (Molecular Research Center Inc., Cincinnati, OH, USA) and a NucleoSpin RNA II kit (Macherey-Nagel GmbH & Co. KG, Dürren, Germany) according to the manufacturer's instructions. Dorsal synovial membranes, collected from eight horses, were homogenized in TRI Reagent (50 mg/ml) with IKA T10 Basic Ultra-Turrax; 200 μ L of chloroform were subsequently added to the

suspension which was then mixed well. After incubation at room temperature (RT) (10 min), the samples were centrifuged (12,000 \times g for 10 min) and the aqueous phase recovered. An equal volume of 70% ethanol was added, and the RNA containing phase was applied to the NucleoSpin RNA Column and cleaned in the further steps of the protocol. Finally, 60 μ L of molecular biology water was applied into the column membrane, centrifuged, and RNA was eluted into a new Eppendorf-type tube. After nanospectrophotometric quantification (DeNovix, DeNovix Inc. Wilmington, DE USA), the total RNA (500 ng) was reverse transcribed to cDNA using 5X iScript RT Supermix (Bio-Rad Laboratories Inc., Hercules, CA, USA) in a final volume of 20 μ L.

Quantitative real-time PCR (RT-PCR) gene expression analysis

To evaluate gene expression profiles, quantitative real-time PCR (qPCR) was carried out in a CFX96 thermal cycler (Bio-Rad Laboratories Inc.) using SYBR green detection (Cat.172-5121, Bio-Rad laboratories Inc) for target genes. Specific primers for the horse were designed (Beacon Designer 2.07, Premier Biosoft International, Palo Alto, CA, USA) using the target genes for *Cnr1* (Cannabinoid receptor 1), *Cnr2* (Cannabinoid receptor 2), *GPR55*, *PPARA*, and *TRPV1* (Table 1). Regarding the reference genes, *GAPDH* (Glyceraldehyde-3-phosphate dehydrogenase), *HPRT* (Hypoxanthine phosphoribosyltransferase 1) and *ACTB* (Actin B) were selected on horse sequences as previously reported (51). All the amplification reactions were carried out in 20 μ L and analyzed in duplicate; the reaction contained 10 μ L of iTaq Universal SYBR Green Supermix (Cat.172-5121, Bio-Rad laboratories Inc.), 0.8 μ L of the forward and reverse primers (5 μ M each) of each target gene, 1.5 μ L cDNA, and 7.7 μ L of water. The real-time procedure included an initial denaturation period of 3 min at 95°C, 40 cycles at 95°C for 15 s, and 60°C for 30 s, followed by a melting step with ramping from 55 to 95°C at a rate of 0.5°C/10 s. To validate the primers chosen, extraction and qPCR from a positive control (equine amygdala) were also performed. The specificity of the amplified PCR products was confirmed by agarose gel electrophoresis and melting curve analysis. The relative expressions of the interest genes (IG) were normalized based on the geometric mean of the three reference genes (RG) (52). The relative mRNA expression of the genes tested was evaluated as using the Δ Ct method with Δ Ct = (Ct geometric mean RG – Ct IG), which directly correlated with the expression level.

Immunofluorescence

Dorsal synovial membrane specimens (\sim 2 cm \times 1 cm) were dissected with a scalpel and fixed for 48 hours at 4°C in 4% paraformaldehyde in phosphate buffer (0.1 M, pH 7.2), subsequently rinsed in phosphate-buffered saline (PBS; 0.15 M NaCl in 0.01 M sodium phosphate buffer, pH 7.2) and stored at 4°C in PBS containing 30% sucrose and sodium azide (0.1%). The following day, the tissues were transferred to a mixture of PBS–30% sucrose–azide and Optimal Cutting Temperature (OCT)

TABLE 1 Primer sequence used for quantitative real time PCR analysis.

Gene		Primer sequence (5' -> 3')	PCR size (bp)	Accession number	References
Cnr1	F	AACCTACCTGATGTTCTGGATTGG	147	NM_001257151.1	Present study
	R	GATGTGTGGATGATGATGCTCTTC			
Cnr2	F	CTCCTGTTTCATTGCCATCCTCTTCTCTG	114	NM_001257179.1	Present study
	R	CTGCCTGTCTTGGTCCTGGTGTTTC			
GPR55	F	CCGCCTTCTCCTCCTTCTCTCAG	118	XM_023642534.1	Present study
	R	TCACTCCTCCACACCCATTCTACCC			
PPARA	F	CATTGGCGAGGACAGTTGCGGAAG	182	NM_001242553.1	Present study
	R	CGATGTTCAATGCTGTGCTGGAAGATTC			
TRPV1	F	ACCTGTGTCGCTTCATGTTTGTCTACC	105	XM_014727972.2	Present study
	R	ATTCAGCCAGCACGGAGTCATTCTTC			

compound (94-4583, Sakura Finetek Europe, Alphen aan den Rijn, The Netherlands) at a ratio of 1:1 for an additional 24 h before being embedded in 100% OCT in Cryomold[®] (94-4566, Sakura Finetek Europe). The samples were prepared by freezing the tissues in isopentane cooled in liquid nitrogen. Cryosections (14 µm thick) of synovial membrane were cut on a cryostat (MC5000, Histo-Line Laboratories, Pantigliate, Italy), and mounted on polylysinated slides (HL26765, Histo-Line Laboratories).

The cryosections were hydrated in PBS and processed for immunostaining. To block non-specific bindings, the sections were incubated in a solution containing 20% normal donkey serum (Colorado Serum Co., Denver, CO, USA), 0.5% Triton X-100 (Sigma Aldrich, Milan, Italy, Europe), and bovine serum albumin—BSA (1%) in PBS for 1 hour at RT (22–25°C). The cryosections were incubated in a humid chamber overnight at RT with the anti-CB1R, -CB2R, -TRPV1, -GPR55, and PPARα antibodies (single immunostaining) or with a cocktail of primary antibodies (double immunostaining) (Table 2) diluted in 1.8% NaCl in 0.01 M PBS containing 0.1% sodium azide. After washing in PBS (3 × 10 min), the sections were incubated for 1 h at RT in a humid chamber with the secondary antibodies (Table 3) diluted in PBS. The cryosections were then washed in PBS (3 × 10 min) and mounted in buffered glycerol at pH 8.6 with 4',6-diamidino-2-phenylindole—DAPI (Santa Cruz Biotechnology, Santa Cruz, CA, USA). To identify macrophages and fibroblasts, the anti-ionized calcium binding adapter molecule 1 (IBA1) (53) and the anti-vimentin (Clone V9) (42) antibodies were used, respectively.

Specificity of the primary antibodies

Antibodies anti-cannabinoid receptors

The rabbit anti-CB1R antibody utilized in the present study had already been tested using Western blot (WB) analysis on horse tissues (54).

The rabbit anti-CB2R antibody (PA1-744) utilized in the present study had already been tested with Western blot (WB) analysis on horse tissues (55). In the current study, another anti-CB2R antibody, raised in mice (sc-293188), was used, the specificity of which has not yet been tested on horse tissues; however, both

TABLE 2 Primary antibodies used in the study.

Primary antibody	Host	Code	Dilution	Source
CB1R	Rabbit	ab23703	1:100	Abcam
CB2R	Mouse	sc-293188	1:50	Santa Cruz
CB2R	Rabbit	PA1-744	1:250	Thermo Fisher
GPR55	Rabbit	NB110-55498	1:200	Novus Biol.
IBA1	Goat	NB100-1028	1:80	Novus Biol.
PPARα	Rabbit	NB600-636	1:200	Novus Biol.
TRPV1	Rabbit	ACC-030	1:200	Alomone
Vimentin	Mouse	IS630 (Clone V9)	1:600	Dako

Primary antibody suppliers: Abcam, Cambridge, UK; Alomone, Jerusalem, Israel; Dako Cytomation, Glostrup, Denmark; Novus Biologicals, Littleton, CO, USA; Santa Cruz Biotechnology, California, USA; Thermo Fisher Scientific, Waltham, MA USA.

TABLE 3 Secondary antibodies used in the study.

Secondary antibody	Host	Code	Dilution	Source
Anti-mouse IgG Alexa-594	Donkey	A-21203	1:500	Thermo Fisher
Anti-goat 594	Donkey	ab150132	1:600	Abcam
Anti-rabbit 488	Donkey	A-21206	1:1000	Thermo FISHER

Secondary antibody suppliers: Abcam, Cambridge, UK; Thermo Fisher Scientific, Waltham, MA USA.

the mouse and rabbit anti-CB2R antibodies were tested using a double-staining protocol and were co-localized in horse tissues (Supplementary Figure 1).

Antibodies anti-cannabinoid-related receptors TRPV1, GPR55, and PPARalpha

The specificity of the anti-TRPV1 antibody had been tested by the research group using Western blot analysis on horse tissue (53). In addition, the specificity of the anti-TRPV1 antibody had previously been tested using WB analysis on rat tissues (56).

The immunogen used to obtain the anti-GPR55 antibody was the synthetic 20 amino acid peptide from the third cytoplasmic domain of Human GPR55 in amino acids 200–250. The homology between the full amino acid sequences of the horse and human GPR55 was 80%, and the correspondence with the specific sequence of the immunogen was 78%. This antibody, which has recently been used in horse sensory neurons (53), had previously been tested on rat and dog dorsal root ganglia (DRG) using immunofluorescence (57) and on mice tissues using WB analysis (58). However, the WB analysis had not been carried out on horse tissue.

The specificity of the primary anti-PPAR α antibody had been tested using WB analysis on horse tissue (54). In addition, the antibody utilized had also recently been tested on rat tissue (57) as the anti-PPAR α antibody reacts with rat tissue, as stated by the antibody supplier. The same anti-PPAR α antibody has recently been used in horse tissues (53, 59).

Marker for macrophages (MLS) and fibroblasts (FLS)

The goat anti-IBA1 antibody, recently used on horse tissue (53), was directed against a peptide having the sequence C-TGPPAKKAISELP, from the C Terminus of the porcine IBA1 sequence. Horse and porcine IBA1 molecules share 92.3% identity (<https://www.uniprot.org/>), and it is plausible that the antibody used can also recognize IBA1 in the horse.

The mouse anti-vimentin antibody (Clone V9) had already been used to label fibroblasts in the horse skin (60).

Specificity of the secondary antibody

The specificity of the secondary antibodies was tested by applying them on the sections after omitting the primary antibodies. No stained cells were detected after omitting the primary antibodies.

Quantitative analysis

Quantitative analysis of the intensity of the expression of cannabinoid and cannabinoid-related receptors in the synovial intimal layer was carried out on 12 horses.

For each animal, and each receptor, two randomly selected images of the synovial membrane (50 μm -thick and 100 μm -wide; 5,000 μm^2 area) were acquired (high magnification, $\times 400$), using the same exposure time for all the images. The 50 μm -thick of synovial membrane encompassed the intimal synoviocytes and a minimal amount of underlying subintimal blood vessels, infiltrating cells and fibroblasts (61). In each image the signal intensity was analyzed using ImageJ software (Image J, version 1.52t, National Institutes of Health, Bethesda, MD, USA) (62) by standardized thresholds for brightness and contrast were determined empirically and applied to all images. The signal intensity was finally obtained using the Color histogram (gMEAN) tool of the software.

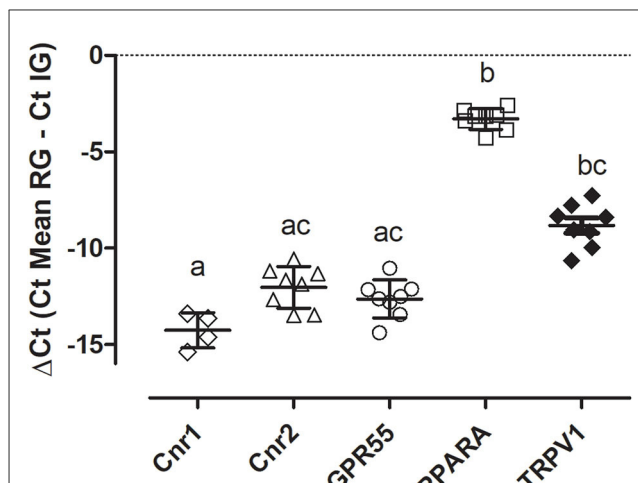


FIGURE 1

Gene expression of *Cnr1*, *Cnr2*, *GPR55*, *PPARA*, and *TRPV1* in equine synovial membranes. The results are presented as $\Delta\text{Ct} = (\text{Ct Mean RG} - \text{Ct IG})$. Symbols indicate individual animals. For each gene, mean \pm SD are indicated by horizontal bars. Different letters indicate statistically significant differences ($p < 0.05$, Kruskal–Wallis test, Dunn's Multiple Comparison *post-hoc* test).

Statistical methods

For each receptor the mean of the two values/case of signal intensity in the 12 horses were evaluated and compared. Statistical analysis was carried out using GraphPad Prism software (version 8.3, La Jolla, CA). The normality distribution of the data was assessed using the Shapiro–Wilk test. Comparisons between groups were performed with one way ANOVA Tukey's multiple comparisons test. A P -value ≤ 0.05 was considered significant.

Fluorescence microscopy

The preparations were examined, by the same observer on a Nikon Eclipse Ni microscope (Nikon Instruments Europe BV, Amsterdam, The Netherlands, Europe) equipped with the appropriate filter cubes. The images were recorded with a DS-Qi1Nc digital camera and NIS Elements software BR 4.20.01 (Mountain View, Ottawa, ON, Canada). Slight contrast and brightness adjustments were made using Corel Photograph Paint whereas the figure panels were prepared using Corel Draw (Mountain View).

Results

qPCR for *Cnr1*, *Cnr2*, *GPR55*, *PPARA* and *TRPV1*

Quantitative PCR data demonstrated that *Cnr2*, *GPR55*, *PPARA*, and *TRPV1* were detected in all the equine synovial samples ($n = 8$) while the transcript for *Cnr1* was detectable in only four synovial samples (50%). As reported in Figure 1, the level

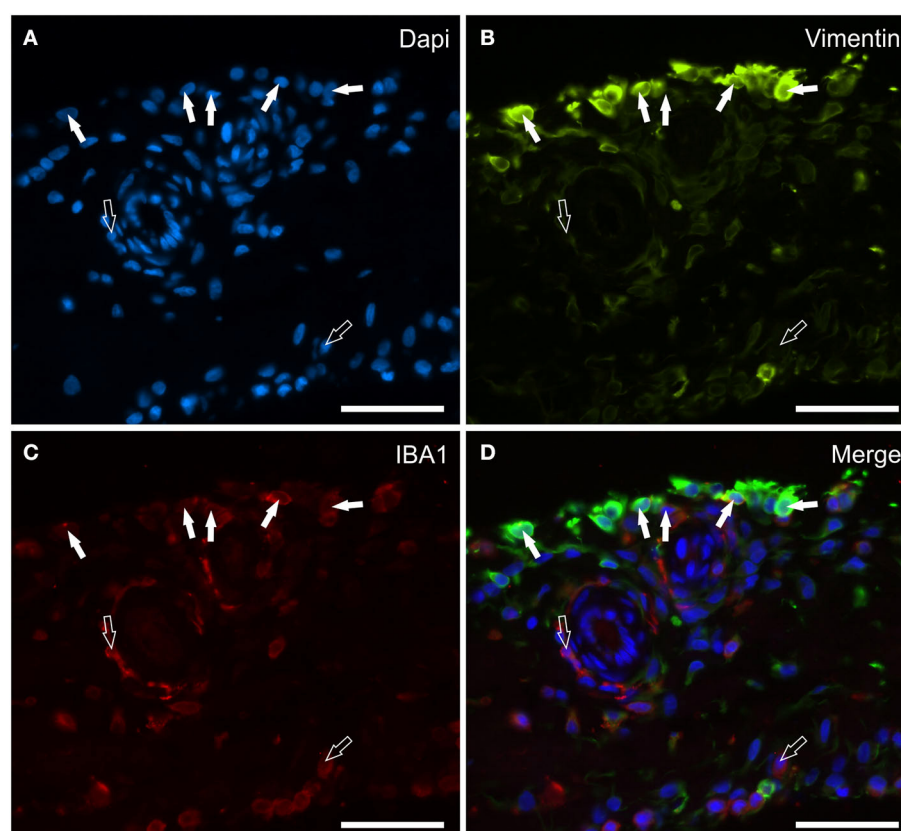


FIGURE 2

Photomicrographs of the cryosections of the synovial membrane of a horse metacarpophalangeal joint showing vimentin (B) and IBA1 (C) immunoreactivity. The white arrows indicate the DAPI (Blue) labeled nuclei (A) of some macrophage-like synoviocytes lining the synovial intima which co-expressed moderate IBA1 (Red) and bright vimentin (Green) immunoreactivity. The open arrows indicate subintimal macrophages, which were IBA1 immunoreactive and vimentin negative. (D) Merged image (Orange). Scale bar = 50 μ m.

of gene expression was different in the synovial samples having a greater expression of *PPARA*.

Immunofluorescence

It is necessary to point out that the identification of the two types of synoviocytes of the equine metacarpophalangeal joints is by no means a simple matter. In fact, there are some articles which testify to the fact that the horse FLS can be very similar to the MLS, from a morphological point of view (11, 16, 17). For this reason, two markers which should be selective for fibroblasts (vimentin) and for macrophages (IBA1) were used.

Vimentin and IBA1 distribution and expression analysis

Vimentin appears to be an excellent marker for identifying the morphology of the cells lining the synovial membrane of the horse joint. Bright vimentin immunoreactivity (vimentin-IR) was mainly expressed by FLS, which were recognizable owing to their long and thin processes extending toward the joint cavity. In

some portions of the synovial intima, these processes exhibited a densely arranged plexus on the surface. Co-localization studies have indicated that a proportion of moderate-to-bright vimentin immunoreactive cells (MLS) also expressed IBA1-IR (Figures 2A–D). In the subintima, the IBA1 immunoreactive macrophages showed faint or moderate vimentin-IR.

CB1R distribution and expression analysis

Faint CB1R-IR was expressed by the cytoplasm of the synoviocytes; however, the CB1R-IR was detectable in only 10/14 (71 %) horses. Co-localization studies have indicated that vimentin immunoreactive FLS (Figures 3A–D) and IBA1 immunoreactive MLS (Figures 3E–H) expressed CB1R-IR. Cannabinoid receptor 1 was not expressed by blood vessels and fibroblasts.

CB2R distribution and expression analysis

Cannabinoid receptor 2 immunoreactivity was expressed by synoviocytes, blood vessels and fibroblasts.

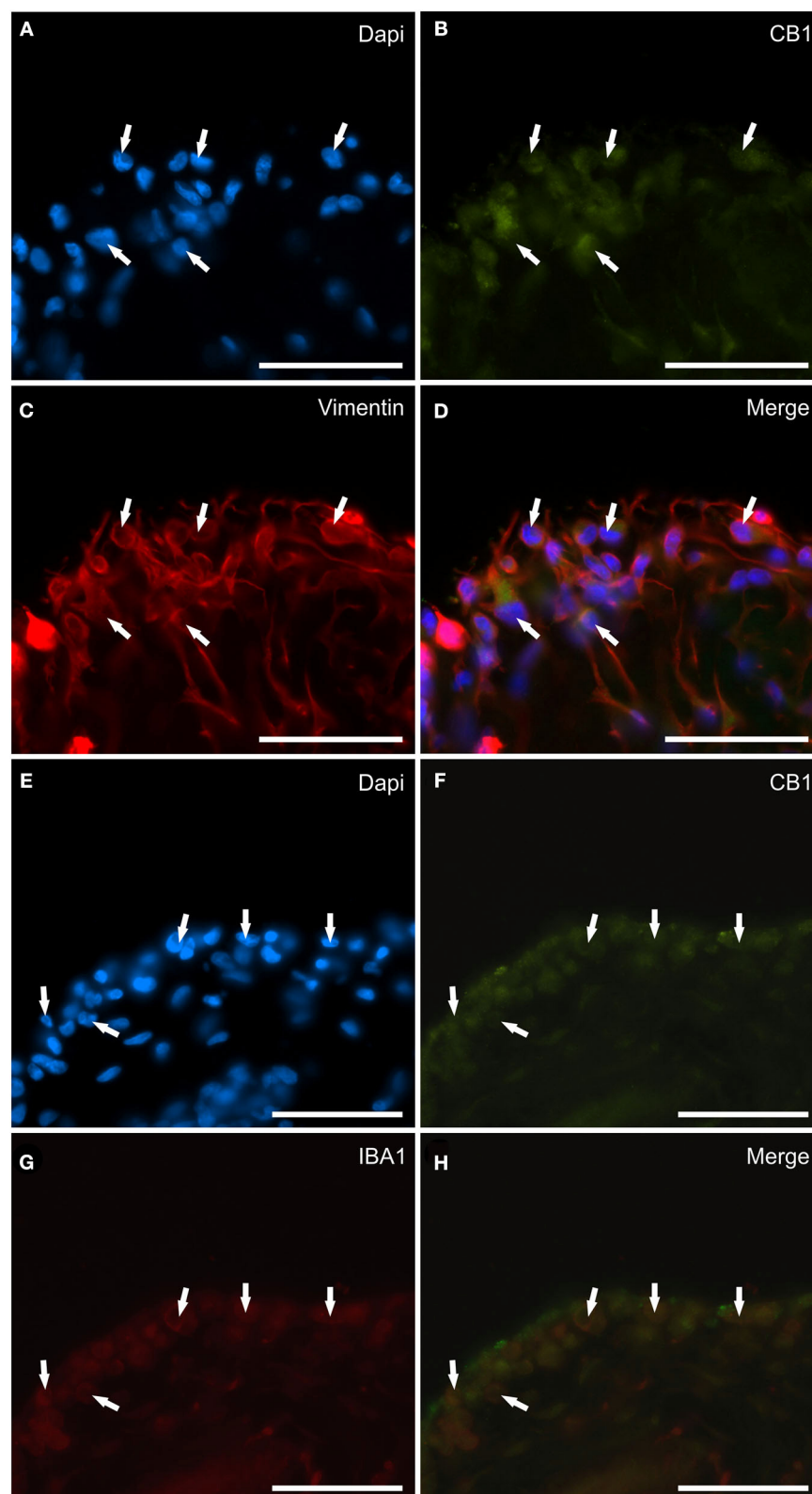


FIGURE 3

Photomicrographs of the cryosections of the synovial membrane of a horse metacarpophalangeal joint showing cannabinoid receptor type 1 (CB1) immunoreactivity in synoviocytes. **(A–D)** The arrows indicate the DAPI (Blue) labeled nuclei **(A)** of cells resembling fibroblast-like synoviocytes co-expressing faint CB1 (Green) receptor immunoreactivity **(B)** and bright vimentin (Red) **(C)** immunoreactivity. **(D)** Merged image (Orange). **(E–H)** The arrows indicate the DAPI (Blue) labeled nuclei **(E)** of round macrophage-like synoviocytes co-expressing faint CB1 (Green) receptor **(F)** and IBA1 (Red) **(G)** immunoreactivity. **(H)** Merged image (Orange). Scale bar = 50 μ m.

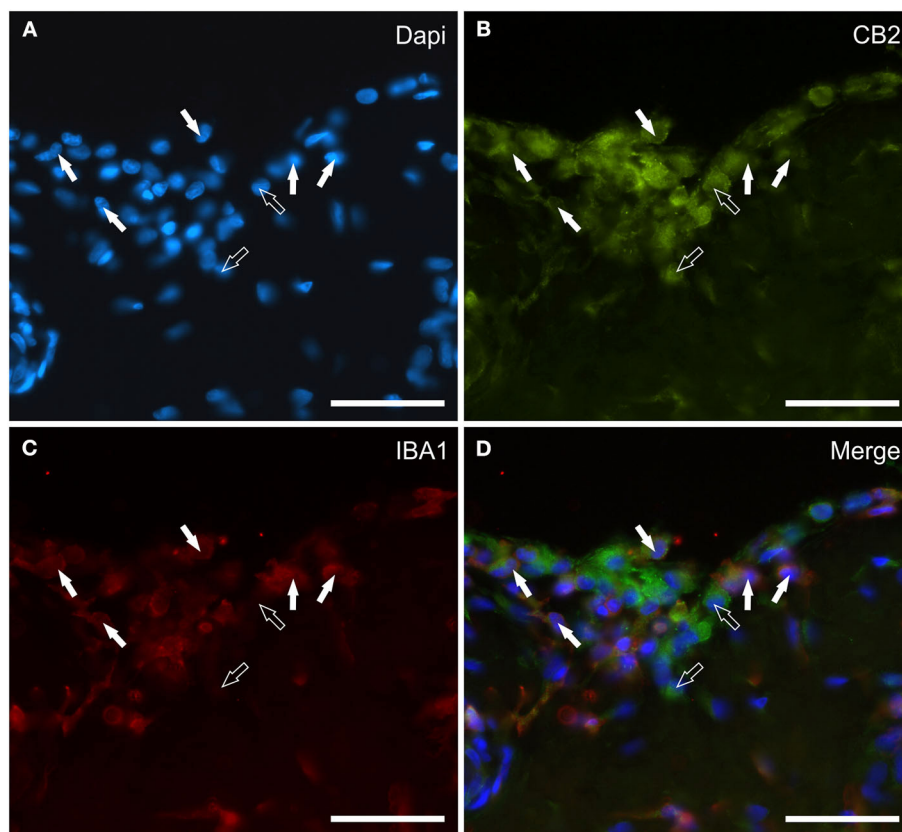


FIGURE 4

Photomicrographs of the cryosections of the synovial membrane of a horse metacarpophalangeal joint showing cannabinoid receptor type 2 (CB2) (B) and IBA1 (C) immunoreactivity. The white arrows indicate the DAPI (Blue) labeled nuclei (A) of some round macrophage-like synoviocytes lining the joint cavity which co-expressed IBA1 (Red) and bright CB2 (Green) receptor immunoreactivity. The open arrows indicate two cells expressing CB2 receptor immunoreactivity (likely fibroblast-like synoviocytes) which were IBA1 negative. (D) Merged image (Orange). Scale bar = 50 μ m.

Bright cytoplasmic CB2R-IR was observed in oval and elongated FLS and in round-shaped IBA1 immunoreactive MLS (Figures 4A–D). Co-localization with the anti-CB1R antibody showed that synoviocytes expressed both receptors in those horses in which CB1R-IR was detectable (Supplementary Figure 2). The vascular endothelial and smooth muscle cells showed bright and moderate CB2R-IR, respectively (Data not shown). Moderate CB2R-IR was also expressed by cells, likely fibroblasts, distributed in the sublining layer.

TRPV1 distribution and expression analysis

Transient receptor potential vanilloid 1 immunoreactivity was expressed by synoviocytes, blood vessels and fibroblasts. Bright TRPV1-IR was mainly expressed by the cell membrane and cytoplasm of FLS and, in particular, also by their long “dendritic” processes which extended irregularly toward the luminal surface of the synovial membrane (Figures 5A–D). Co-localization between TRPV1 and IBA1 showed that TRPV1-IR was also expressed by the cell membrane and cytoplasm of MLS (Figures 5A–D). In some portions of the synovial

intima, oval-shaped synovial cells, expressing moderate-to-bright TRPV1-IR, appeared to be the prevalent cells, and were aligned and organized in such a way as to form an epithelium-like monolayer with the appearance of a barrier, resembling the cellular organization recently described in the rat synovial membrane (24, 25) (Figures 6A–C). In other portions of the membrane, however, the “elongated” FLS seemed to prevail in the most superficial layer (Figures 5A–D). The endothelial cells of the capillaries adjacent to the joint lumen and arteries of the *stratum fibrosum* showed moderate cytoplasmic TRPV1-IR. The vascular smooth muscle cells also showed moderate TRPV1-IR (Figures 6D–F).

GPR55 distribution and expression analysis

G protein-coupled receptor 55 immunoreactivity was expressed by the cytoplasm of synoviocytes and endothelial cells. In particular, faint-to-moderate GPR55-IR was mainly expressed by vimentin immunoreactive FLS showing elongated processes (Figures 7A–D). Only a few IBA1 immunoreactive MLS showed faint-to-moderate GPR55 (Figures 7E–H). Vascular endothelial cells and smooth muscle cells showed moderate

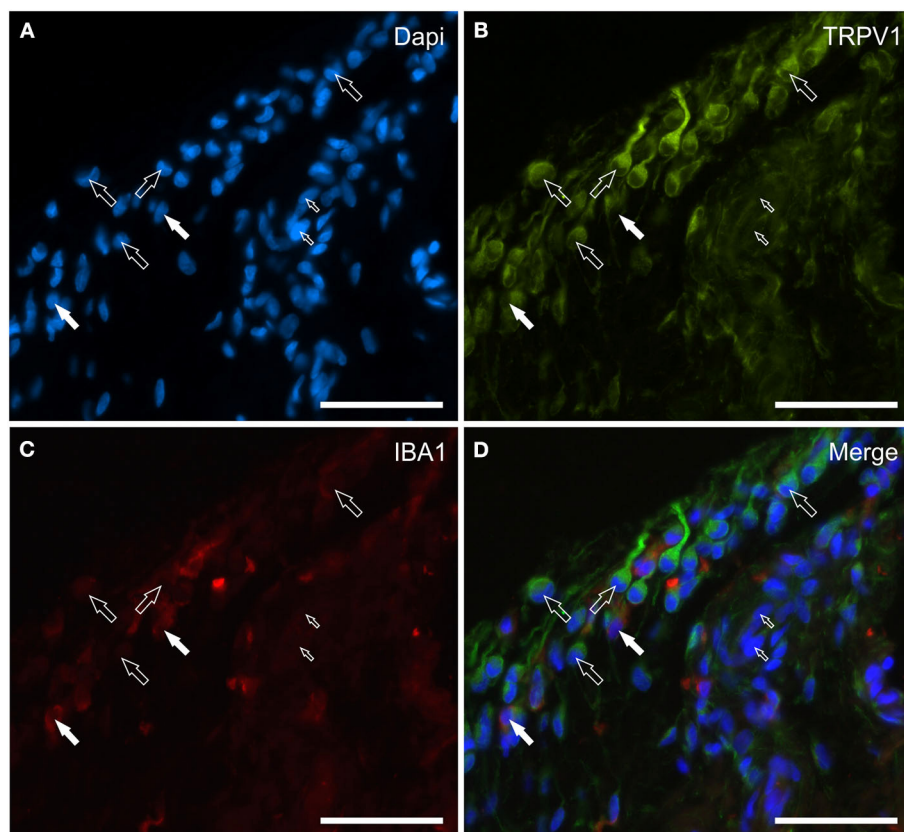


FIGURE 5

Photomicrographs of the cryosections of the synovial membrane of a horse metacarpophalangeal joint showing transient receptor potential vanilloid 1 (TRPV1) (B) and IBA1 (C) immunoreactivity. Both of the two cell types lining the synovial intima, i.e., the fibroblast-like synoviocytes (FLS) and the macrophage-like synoviocytes (MLS), showed bright TRPV1 (Green) immunoreactivity. The TRPV1 immunolabeling was also evident in the elongated cellular process of the FLS extending through the joint cavity. The white arrows indicate the DAPI (Blue) labeled nuclei (A) of two IBA1 (Red) immunoreactive MLS co-expressing bright TRPV1 (B) and moderate IBA1 (C) immunoreactivity. The open arrows indicate some round or elongated FLS which were TRPV1 immunoreactive and IBA1 negative. The small open arrows indicate the DAPI labeled nuclei of the endothelial cells showing moderate TRPV1 immunoreactivity. (D) Merged image (Orange). Scale bar = 50 μ m.

GPR55-IR, respectively (Figures 7A–H). In the subintima, bright GPR55-IR was expressed by unidentified perivascular round-shaped cells (likely lymphocytes) which did not have IBA1-IR (Supplementary Figure 3).

PPAR α distribution and expression analysis

Peroxisome proliferator-activated receptor α immunoreactivity was expressed by synoviocytes, blood vessels and fibroblasts. The pattern of weak-to-moderate PPAR α immunoreactivity was unusual as it appeared to be continuous, granular and indistinct immunolabeling of the cytoplasm of the upper portions/processes of the cellular elements facing the joint lumen (Figures 8A–D). The co-localization with the anti-vimentin antibody showed that the PPAR α immunoreactive synoviocytes were most likely FLS (Figures 8E–H). No IBA1 immunoreactive synovial cells showed PPAR α -IR (data not shown). Endothelial cells, as well as the smooth muscle cells of the blood vessels showed moderate cytoplasmic PPAR α -IR; however, the PPAR α -IR was more appreciable in large vessels (data not shown).

Figure 9 shows the quantification of the intensity of the expression of CB1R, CB2R, GPR55, PPAR α , and TRPV1 in the synovial membrane of the equine metacarpophalangeal joints.

Figure 10 shows the graphical representation of the distribution of the CB1R, CB2R, TRPV1, GPR55, and PPAR α in the different cellular elements of the equine metacarpophalangeal synovial membrane.

Discussion

Arthropathies can be a significant source of pain in horses, and finding new therapeutic treatments to alleviate the pain is of paramount importance (63). It is known that cannabis-based drugs have therapeutic potential in inflammatory diseases, including OA and rheumatoid arthritis (RA), as demonstrated by pre-clinical and clinical studies in animals and humans (28, 64). Interest in this type of molecule in horses has also recently been evidenced by a prospective, randomized, controlled study which attempted to determine the plasma pharmacokinetics, short-term safety, and synovial fluid levels of CBD following oral administration in horses (65).

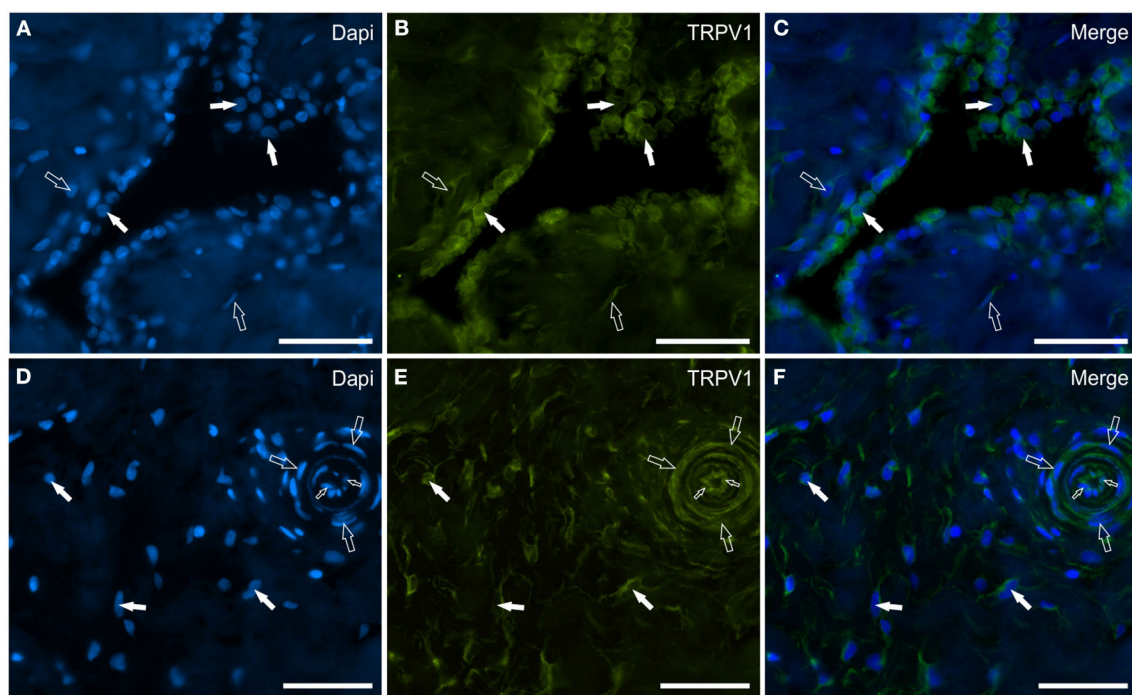


FIGURE 6

Photomicrographs of the cryosections of the synovial membrane of a horse metacarpophalangeal joint showing transient receptor potential vanilloid 1 (TRPV1) (B, E), immunoreactivity in synoviocytes (A–C), and fibroblast and vascular cells (D–F). (A–C) The white arrows indicate the DAPI (Blue) labeled nuclei of some round synoviocytes expressing bright TRPV1 (Green) immunoreactivity. The open arrows indicate subintimal cells (likely fibroblasts) showing faint-to-moderate TRPV1 immunoreactivity. (D–F) The open arrows indicate the DAPI (Blue) labeled nuclei of some cells of the interstitial connective tissues of the synovial membrane (close to the subintima) expressing moderate-to-bright TRPV1 (Green) immunoreactivity. The open arrows and the small open arrows indicate the DAPI labeled nuclei of the vascular smooth muscle cells and endothelial cells, respectively, expressing moderate TRPV1 immunoreactivity. (C, F) Merged images. Scale bar = 50 μ m.

Therefore, the localization of CB1R, CB2R, TRPV1, GPR55, and PPAR α in the synovial FLS and MLS of the metacarpophalangeal joint of the horse is an encouraging finding.

Fibroblast-like synoviocytes are highly specialized mesenchymal cells found in the intimal lining layer of the synovium of diarthrodial joints. In a healthy joint, the FLS form a thin porous barrier at the interface between the sublining and the synovial fluid space (66). Fibroblast-like synoviocytes are pivotal cells in both joint maintenance and integrity, and in the inflammatory response/pathogenesis of arthritis (10, 67). The role of the FLS has also been highlighted in the pathogenesis of RA (15, 29, 68, 69). It has been recognized that, even in horses, FLS participate in the pathogenesis of joint disease by producing proinflammatory cytokines and cartilage-degrading mediators (70, 71). In horses with naturally occurring and experimentally induced OA and septic arthritis, increased levels of inflammatory components, such as leukocytes, interleukin (IL)-1 β , IL-6, tumor necrosis factor α (TNF- α), and matrix metalloproteinases, has been demonstrated (72, 73). In RA, it has been shown that FLS become active upon stimulation by inflammatory cytokines released by macrophage-like synoviocytes (and T-lymphocytes) and secrete matrix metalloproteinases (MMP), causing joint destruction (69).

Macrophages derive from two main cellular lineages; one lineage arises from bone-marrow-derived monocytes and the other is derived from cells which disperse into the

tissues during embryonic development (23). The tissue-resident macrophages have distinctive gene-expression profiles which depend on the particular tissue in which they reside (25).

The three joint macrophage populations, i.e., the lining MLS, the sublining macrophages and the interstitial macrophages, differ in their origins and functions (74). In the healthy synovium, macrophages are predominantly monocyte-independent (20, 24, 74). The proliferation of macrophages harbored in the sublining connective tissue gives rise to both the MLS and the interstitial macrophages (24). In both mice and humans, lining MLS seem to be highly phagocytic and anti-inflammatory (74). In joint inflammation, the *synovium* also contains macrophages originating from recruited monocytes which produce pro-inflammatory cytokines and release molecules with the possibility of attracting lymphocytes which additionally propagate inflammation.

To add to the complexity, macrophages exist as various subsets, some of which are pro-inflammatory (M1) whereas others are anti-inflammatory and favor tissue repair (M2) (75, 76). Undoubtedly, in synovial inflammation and arthritis, monocytes and macrophages play a central role, promoting the onset and the progression of joint inflammation (74). In a recent study regarding the horse synovial membrane, M1 and M2 macrophages were characterized in normal and inflamed joints (26). It appears evident that, given the central role of macrophages in OA, a clinical

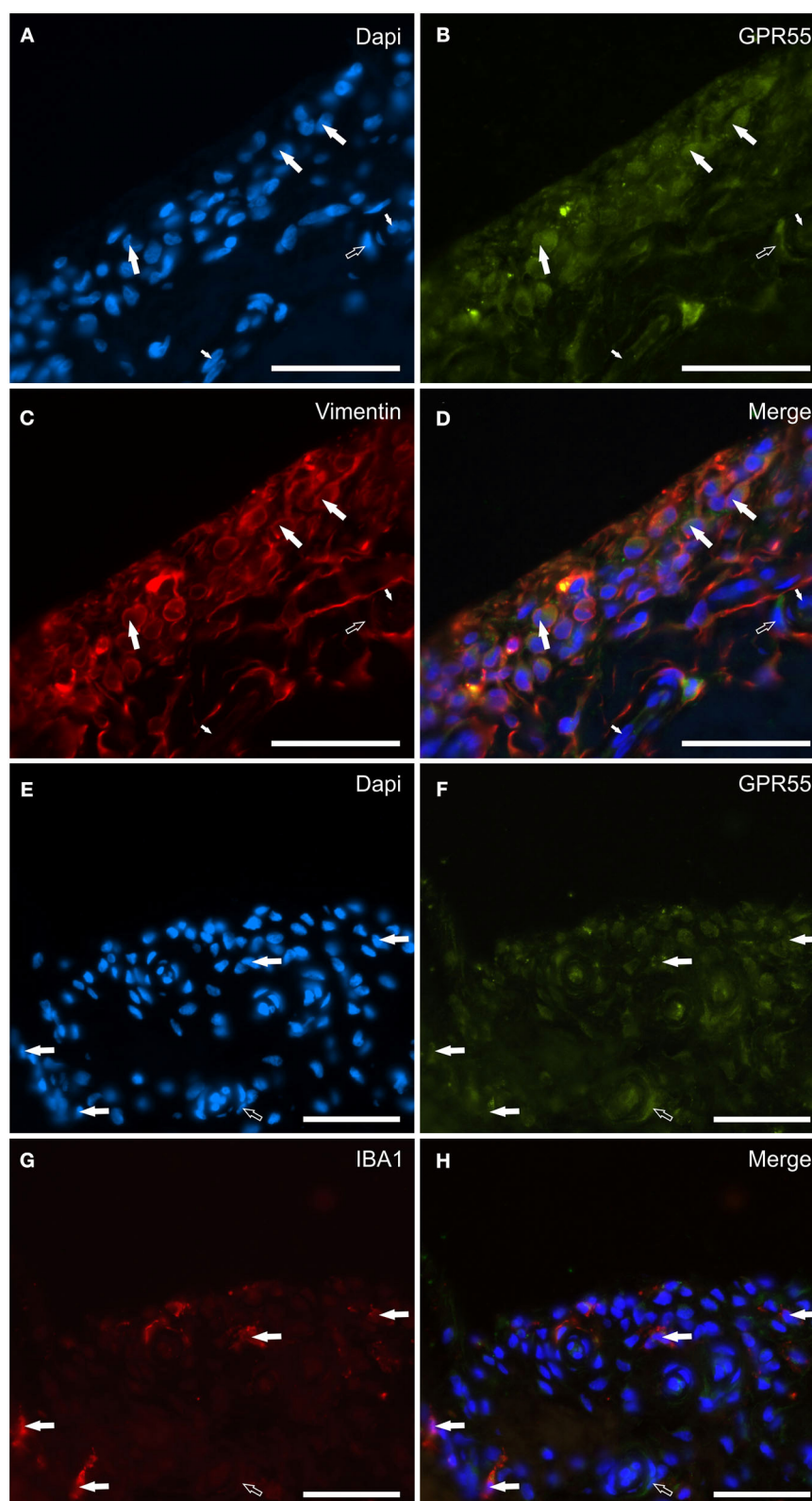


FIGURE 7

Photomicrographs of the cryosections of the synovial membrane of a horse metacarpophalangeal joint showing G protein-related receptor 55 (GPR55) immunoreactivity in synoviocytes and vascular cells. **(A–D)** The white arrows indicate the DAPI (Blue) labeled nuclei **(A)** of elongated cells resembling fibroblast-like synoviocytes co-expressing moderate GPR55 (Green) **(B)** and bright vimentin (Red) **(C)** immunoreactivity. The small white arrows indicate the DAPI labeled nuclei of the endothelial cells of the subintima blood vessels showing moderate GPR55 immunoreactivity which was also expressed by the vascular smooth muscle cells (open arrow). **(E–H)** The white arrows indicate the DAPI (Blue) labeled nuclei of macrophage-like synoviocytes co-expressing faint-to-moderate GPR55 (Green) **(F)** and bright IBA1 (Red) immunoreactivity **(G)**. The open arrow indicates the nuclei of a vascular smooth muscle cell expressing moderate GPR55 immunoreactivity. **(D, H)** Merged images (orange). Scale bar = 50 μ m.

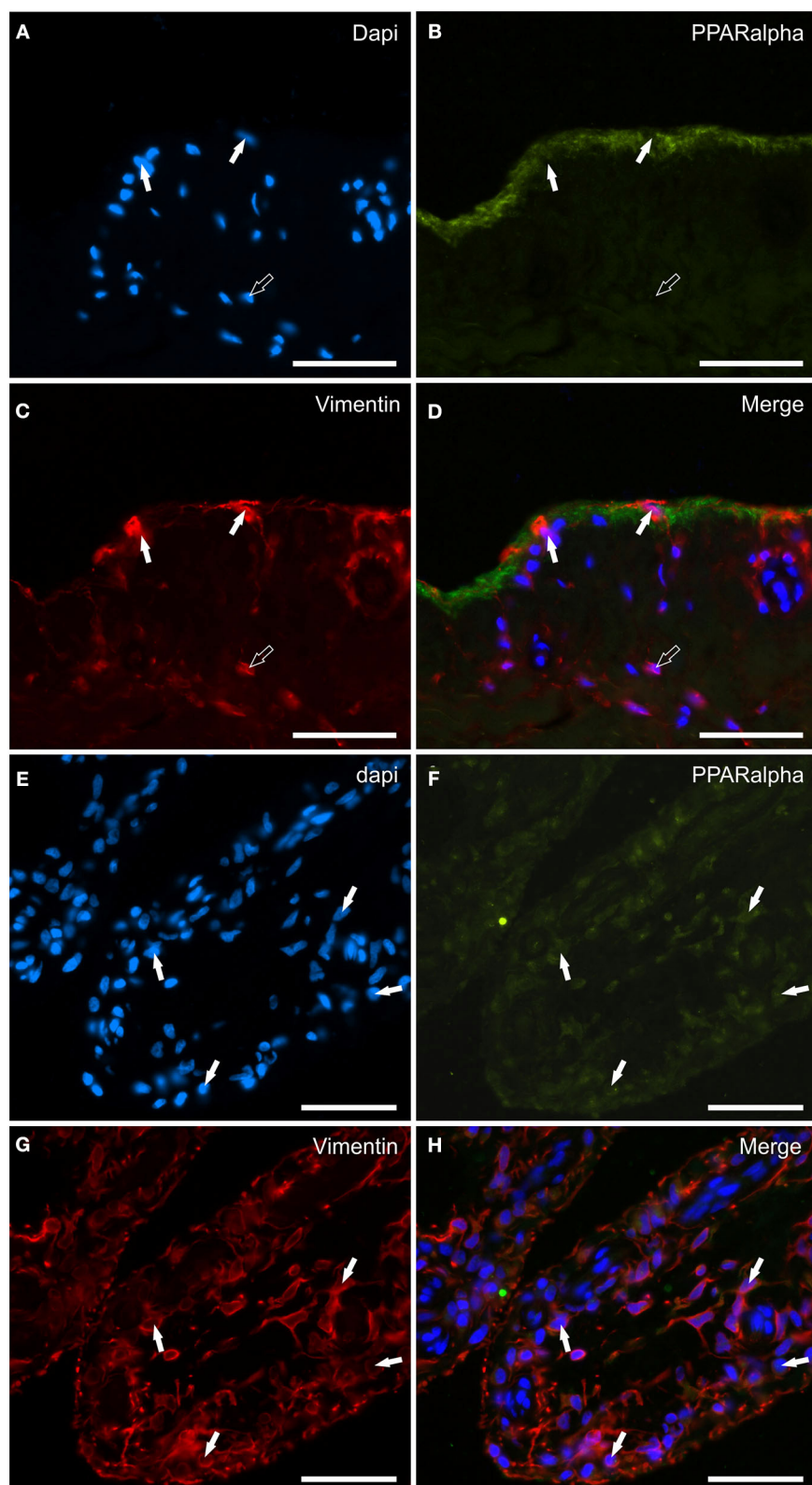


FIGURE 8

Photomicrographs of the cryosections of the synovial membrane of a horse metacarpophalangeal joint showing peroxisome proliferator-activated receptor alpha (PPAR α) immunoreactivity in synoviocytes (A–H). (A–C) The white arrows indicate the DAPI (Blue) labeled nuclei of synoviocytes brightly immunolabelled with the anti-vimentin (Red) antibody which expressed faint-to-moderate PPAR α (Green) immunoreactivity. It is possible to see the indistinct PPAR α immunostaining of the upper portions of the cells lining the joint cavity. (E–H) The figures show the longitudinal sections of two villi of the synovial membrane in which the arrows indicate the DAPI (Blue) labeled nuclei (E) of the cells, likely fibroblast-like synoviocytes and fibroblasts, co-expressing faint-to-moderate PPAR α -(Green) (F) and bright vimentin-(Red) (G) immunoreactivity. (D, H) Merged images (Orange). Scale bar = 50 μ m.

approach targeting activated macrophages at an earlier stage of OA may serve to inhibit or slow the progression of disease (77).

In the current study, all the macrophage populations expressed IBA1-IR; in addition, also MLS, and sublining and interstitial macrophages expressed vimentin-IR with its stronger immunolabeling expressed by the MLS. Vimentin, which is the main intermediate filament protein in mesenchymal cells (such

as epithelial cells and fibroblasts), has already been observed in rat (78) and human FLS (79). However, it has been reported that vimentin could also be expressed in the mononuclear phagocyte system (80); in particular, vimentin manifests enhanced fluorescence in activated macrophages (81). In the current study, only MLS showed bright vimentin-IR, evidence which suggested an activated state of the lining macrophages.

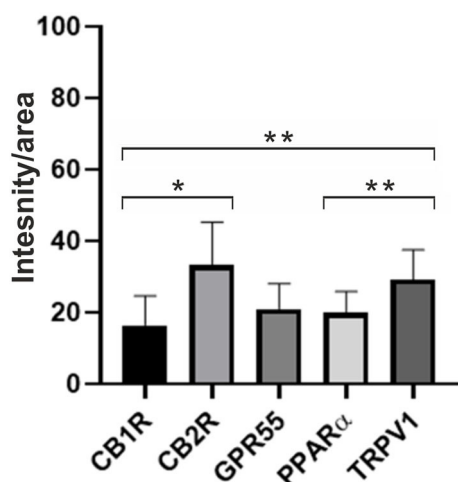


FIGURE 9
Quantification of the intensity of the expression of CB1R, CB2R, GPR55, PPAR α , and TRPV1 in the synovial membrane of metacarpophalangeal joints of 12 horses. Data are represented as Mean \pm SD and were analyzed using One-way ANOVA multiple comparisons test. * $P < 0.05$ and ** $P < 0.01$.

Cnr1, Cnr2, GPR55, TRPV1, and PPARA gene expression in synoviocytes

To date, the gene expression has been reported in the equine synovial membrane only for *TRPV1* (4). The present study confirmed the expression of *TRPV1* and also demonstrated the expression of *Cnr1*, *Cnr2*, *GPR55*, and *PPARA*, according to the Authors' protein data. However, *Cnr1* were not expressed in all the horses.

CB1R, CB2R, GPR55, TRPV1, and PPAR α immunoreactivity in synoviocytes

Cannabinoid receptor 1, which is usually expressed by the neurons, also in horses (54, 82), has been identified in human and mouse synoviocytes (28, 31, 40). Cannabinoid receptor 1 has also been identified in synoviocytes of the horse (44) in which it was co-expressed with CB2R; the Authors were not able to identify the synovial cell types expressing CB1R-IR. Comparing the results of the current study with those described by Miagkoff et al. (43), some differences should be noted. The first difference is related to

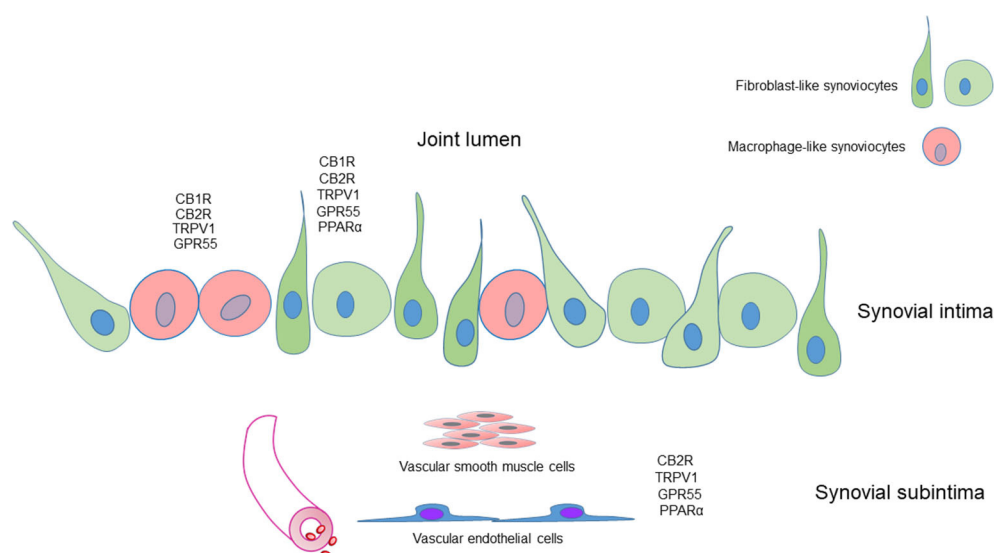


FIGURE 10
Graphical representation of the distribution of the cannabinoid receptors 1 (CB1R) and 2 (CB2R) and the cannabinoid-related receptors transient receptor potential vanilloid 1 (TRPV1), G protein-coupled receptor 55 (GPR55) and nuclear peroxisome proliferator-activated receptor alpha (PPAR α) in the different cellular elements of the synovial membrane of the equine metacarpophalangeal joint. Fibroblast-like synoviocytes (FLS), identified with an anti-vimentin antibody, expressed CB1R, CB2R, TRPV1, GPR55, and PPAR α immunoreactivity. Macrophage-like synoviocytes (MLS), identified with an anti-IBA1 antibody, expressed CB1R, CB2R, TRPV1, and GPR55 immunoreactivity.

the notable expression of CB1R-IR in synoviocytes (greater when compared to CB2R-IR) noted by Miagkoff et al. (44). In the present study, the intensity of CB1R-IR was much lower than that of CB2R-IR; this evidence was also supported by the quantitative data of the mRNA *Cnr1* (although not necessary, a correlation between mRNA and protein expression exists). The difference between the results of the present study and that of Miagkoff et al. (44) did not lie in the use of different anti-cannabinoid receptor antibodies since the same anti-CB1R and -CB2R antibodies were used for both the studies. Instead, a plausible reason for this discrepancy in the results could be the use of sections of paraffin-embedded tissues which may often create a background in immunofluorescence reactions. Unlike what was observed in the Miagkoff et al. study (44), no CB1R-nuclear immunolabeling was observed in the current study. To avoid any tissue background, which might be an interference in the reading of weak receptor immunostaining, cryosections of the synovial membrane were used in the present study.

Cannabinoid receptor 2 is mainly expressed by the immune cells (53), and its activation is usually associated with a decrease in both immune cell function and cytokine release (83). Cannabinoid receptor 2 has been identified in human, mouse, rat, and horse synoviocytes (41–43).

Richardson et al. (28) identified CB2R (RNA and protein) in the FLS of healthy human patients, and patients with OA and AR. It has been shown that, in mouse and human joints, CB2R expression is up-regulated by proinflammatory mediators and injuries, and that its activation plays a key role in regulating inflammatory signaling in macrophages and FLS and suppresses the production of proinflammatory cytokines (42, 45, 84).

In the current study, CB2R-IR was brightly expressed in both FLS and MLS, suggesting a functional role of the endocannabinoid receptor system in horse joints. The evidence that targeting the CB2R in murine MLS and human FLS may be responsible for potent anti-inflammatory effects (45) could allow cautious speculation that the horse intra-articular ECS could be a promising therapeutic target for blocking pathological inflammation.

The TRP vanilloid 1 (TRPV1) ion channel is usually expressed by nociceptors of mammals (57, 85), including horses (53). However, TRPV1 is also expressed in various non-neuronal tissues, such as rat (41) and human (46) synoviocytes. Cells in synovial compartments can be exposed to low pH conditions after inflammation, infection, or injury. An acid sensing receptor (TRPV1) has been identified on synovial cells which are responsive to a low pH (pH 5.5–7.0) (46); TRPV1 is also activated by heat (>43°C) and capsaicin (86). In joint inflammation, the synovial compartments can also be exposed to thermal (>43°C), chemical, and osmotic modifications which can activate the TRPV1 membrane sensors which respond by activating calcium and sodium fluxes.

A number of studies have indicated that the TRPV1, which seems to mediate the calcium dependent proliferative and secretory responses of the synoviocytes in the event of joint inflammation, might be a possible and valuable target for treating joint diseases (46, 87), even in the horse (4). It has been shown that the TRP channels are functionally expressed in human synoviocytes and may play a critical role in adaptive or pathological changes in articular surfaces during arthritic inflammation, in particular in the

response of the synoviocytes to the inflammatory mediator TNF- α (46). This evidence seems to have some therapeutic relevance, given that an *in vitro* study showed that the synovial cells from arthritic animals spontaneously produced large amounts of TNF- α (88).

The finding of TRPV1-IR in the FLS of the horse is consistent with those obtained in humans (46, 89), rats (41), and mice (31). The evidence of TRPV1-IR in MLS (and sublining macrophages) of the horse is also consistent with what has already been observed in human MLS (89). Gene expression and immunohistochemical data strictly correlate and integrate with the recent observations of Braucke et al. (4) who identified and quantified the TRPV1 mRNA and the TRPV1 protein level in the metacarpo/metatarsophalangeal joints of the horse, and observed a higher expression of TRPV1 in samples from joints with pathology.

It has been shown that TRPV1 inhibits M1 macrophage polarization in the synovium and attenuates the progression of OA in a rat model of OA (90). In addition, Engler et al. (91) showed that stimulation of the cultured synovial fibroblasts of OA and RA in human patients with capsaicin (TRPV1 agonist) led to the increased expression of IL-6 mRNA and IL-6 protein, and that IL-6 protein expression could be antagonized with capsazepine (a TRPV1 antagonist). Therefore, TRPV1 may play a role in non-neuronal mechanisms which could modulate nociception in symptomatic OA and RA patients.

Vanilloid receptor 1 (VR1 or TRPV1) is desensitized by endovanilloids, endocannabinoids (anandamide), endocannabinoid-like molecules (92, 93) and phytocannabinoids, such as CBD (38, 94) which shows anti-nociceptive, analgesic, and anti-inflammatory effects (35, 95). The importance of the endocannabinoid signaling acting on TRPV1 has been highlighted by different OA studies in which it has been shown that synovial fibroblasts express several receptors involved in endocannabinoid action, and that endocannabinoid anandamide (AEA) reduces IL-6, IL-8, and TNF- α production by mixed synoviocytes (31).

Studies involving phytocannabinoids showed that CBD, targeting synovial fibroblasts under inflammatory conditions, demonstrated anti-inflammatory effects on arthritis (96). Cannabidiol may exert its anti-inflammatory and protective effects *via* TRPV1 receptors, as shown in the *in vitro* LPS-stimulated murine macrophage cell line (97). In mice, it has been shown that synovial cells treated with CBD produced significantly less TNF α in culture and that CBD suppressed clinical signs of the disease without obvious side effects during chronic treatment (27). Since CBD binds to several other receptors (TRPA1, GPR55, PPAR gamma, serotonin receptors, etc.), its mode of action remains elusive. However, CBD reduces IL-6/IL-8/MMP-3 production of RA synovial fibroblasts (96).

Not only phytocannabinoids but also the synthetic cannabinoid WIN55,212-2 mesylate (WIN) demonstrated strong anti-inflammatory effects in monocytes and synovial fibroblasts *via* a TRPV1 (and TRPA1) dependent pathway (12).

G protein-coupled receptor 55 (GPR55), which is considered to be the third cannabinoid receptor, has been identified in the sensory neurons of different species, including dogs, rats (57) and horses (53), and in canine inflammatory cells (58). In addition, GPR55 has also been localized in human chondrocytes (48), osteoclasts and osteoblasts (47), and seems to be associated with

bone remodeling and vascular homeostasis (98). To the best of the Authors' knowledge, no data are available regarding the expression of GPR55 in synoviocytes and subintimal synovial cells. The expression of GPR55-IR has recently been shown in the macrophages harbored within the horse dorsal root ganglia (53). A study on rodents has shown that the peripheral activation of GPR55 can reduce mechanosensitivity in the event of joint inflammation (99). However, it is not clear whether this effect was exerted only at the level of the peripheral and central nervous system or also locally, at the level of the synovial cells.

In the present study, GPR55-IR has been demonstrated in both FLS, MLS, subintimal macrophages, and unidentified inflammatory/immunitary cells, suggesting an active role of the receptor in synovial membrane homeostasis and immunity. Cannabidiol, which acts as a GPR55 antagonist, should be able to reduce the migration of macrophages, as shown in mice (100).

Peroxisome proliferator-activated receptor alpha seems to have a role in sensory modulation due to its expression in the sensory neurons of animals, including horses (54).

Peroxisome proliferator-activated receptor alpha can be expressed by different cells of innate immunity, including monocytes and macrophages (101). A number of studies have documented the anti-inflammatory consequences of PPAR α activation in human and murine macrophages (102, 103). Ligands of PPAR- α have been shown to regulate inflammatory responses (104) so much so that, in PPAR- α deficient mice, abnormally prolonged responses to different inflammatory stimuli have been noted (105). The endogenous and exogenous PPAR-alpha ligands reduce the degree of macrophage inflammation caused by LPS/IFN-gamma stimulation (106).

There are studies indicating that PPAR α agonists may exert beneficial effects on OA due to their anti-inflammatory effects (49). Fenofibrate, a PPAR-alpha ligand, has been shown to inhibit the development of arthritis in a rat model of human RA by reducing cytokine production (IL-6, IL-8 and granulocyte monocyte colony-stimulating factor) from FLS (107).

There is extensive documentation regarding the anti-inflammatory, analgesic, immunomodulatory and neuroprotective effects of the endocannabinoid-like lipid mediator PEA, also for joint health and pain modulation (108, 109). Palmitoylethanolamide exerts its analgesic and anti-inflammatory effects primarily by activating the PPAR- α ; however, binding to PPAR- α , PEA triggers TRPV1 channel activation, providing another mode of action in which PEA interacts with the endocannabinoid and endovanilloid systems (110).

CB1R, CB2R, GPR55, TRPV1, and PPAR α immunoreactivity in synovial blood vessels

Endothelial cells and smooth muscle cells were positive for analyzed markers. However, since among cells surrounding endothelial cells there are not only smooth muscle cells but also pericytes as well as adventitial cells (111, 112) and no specific markers for these cellular cytotypes have been used, it cannot be excluded that cannabinoid and cannabinoid-related receptors may also be expressed by other vascular cells.

The principal functions of the endothelium are to promote smooth muscle cell relaxation and arterial dilation, control vascular permeability, exert an antithrombotic effect, and regulate angiogenesis (113).

The angiogenesis may exacerbate OA pain, and the upregulated angiogenic factors and the molecules produced by vascular cells may also stimulate nerve growth (7, 114). In addition to the role they play regarding pain, neuropeptides released by stimulated nerve endings are involved in vasodilation, inflammation (by producing proinflammatory cytokines and by activating inflammatory infiltrating cells), and synoviocyte proliferation and activation (115, 116). During joint diseases, the proliferation of endothelial cells and their morphological differentiation to form tubes accompanies extracellular matrix degradation which facilitates the tissutal invasion of inflammatory cells and is perpetuated by various mediators (2, 116–118). Therefore, angiogenesis and matrix degradation may be interesting/key targets to counteract the progression and chronicity of joint inflammation and degeneration.

Cannabinoids are hypotensive and vasodilator molecules which can exert their effects by acting on the vascular smooth muscle cells and/or endothelial cells (119).

Cannabinoid receptor 1 has been observed in both vascular cellular elements (120) in which it exerts vasodilatory effects. However, in the present study, any CB1R-IR was observed in the capillaries or larger blood vessels of the horse *synovium*; this finding was also in contrast to the data published by Miagkoff et al. (44).

In the present study, the expression of CB2R-IR by vascular endothelial and smooth muscle cells was described. The Expression of CB2R-IR has previously been observed in the vascular endothelial cells of humans and animals (57, 121, 122), including horses (44).

The expression of CB2R-IR in blood vessels may functionally be in relation to the data observed in normal joint of rats in which it has been shown that the CB2R agonist JWH133 caused hyperemia *via* a CB2R and TRPV1 mechanism, and that, during acute and chronic inflammation, this vasodilatory response was significantly attenuated (122). Rajesh et al. (123), by investigating the effect of CB2R receptor agonists on TNF α -induced proliferation, migration and signal transduction in the smooth muscle cells of human coronary arteries, observed that CB2R agonists decreased vascular smooth muscle proliferation and migration. Although for the most part, hypothetically and totally not demonstrated, the Authors cannot exclude that CB2R agonists might also reduce the angiogenesis and inflammation in an inflamed horse joint.

In the current study, TRPV1-IR was observed in both the endothelial and smooth muscle cells of the synovial blood vessels, a finding consistent with that obtained in humans and other animals (124–127).

The notable anti-angiogenic activities of cannabinoid compounds, which have mainly been tested in tumor experiments, are carried out directly, inhibiting vascular endothelial cell migration and survival, and decreasing the expression of proangiogenic factors (35, 128). It has been shown that CBD may inhibit angiogenesis by the down-modulation of several angiogenesis-related molecules (117). Cannabinoids may act on different receptors to obtain their effect; however, the expression of

TRPV1-IR in the endothelial cells of the horse synovial membrane is relevant as it is known that TRPV1 promotes endothelial cell proliferation and network-formation by means of the cellular uptake of the endocannabinoid anandamide (127). Therefore, CBD, which stimulates and desensitizes TRPV1, may potentially contrast angiogenesis in horse joint inflammation.

The endothelium exerts a profound relaxing effect on the underlying smooth muscle cells; nitric oxide (NO) is a well-characterized vasoactive substance produced by the endothelium which diffuses to and relaxes the smooth muscle, causing arterial dilation (129). It has been shown that CBD causes vasorelaxation of the human mesenteric arteries *via* activation of the CB1 and TRPV1 channels, and it is endothelium- and nitric oxide-dependent (129).

G protein-coupled receptor 55 was observed in the blood vessels of the horse joint, a finding which is consistent with that of Xu et al. (130) who identified GPR55 in the endothelium of human and mouse aortas, and of Daly et al. (131) who located GPR55 in the endothelium of mouse blood vessels. The first evidence of the functional role of GPR55 was obtained in the vascular system in which it was shown to regulate systemic vascular resistance and angiogenesis (98, 132). Scientific evidence indicates that the agonists of GPR55 can elicit either vasoconstriction or vasorelaxation (133). Recent studies involving humans have indicated that L- α -lysophosphatidylinositol, a GPR55 agonist, induced endothelium-dependent vasorelaxation in the pulmonary arteries (134) and mediated ovarian carcinoma cell-induced angiogenesis (135). Due to the antagonist effect of CBD on GPR55, it is reasonable to consider, although in a purely speculative way, that CBD might reduce angiogenesis and vasorelaxation of the blood vessels of the horse joint *via* GPR55.

Also the expression of PPAR α -IR was observed in the endothelial cells of the horse joint, as has already been described in the blood vessels of the cervical DRG (53). The anti-proliferative and anti-angiogenic properties of PPAR α in endothelial cells have been demonstrated in a variety of *in vitro* and *in vivo* models (104). Taken together, these findings lead us to hypothesize that the analgesic and anti-inflammatory properties of this receptor, as previously described in other species, are also present in the horse (38, 136).

The present study demonstrated that, in the equine synovial membrane in healthy joints, the mRNA of *Cnr1*, *Cnr2*, *TRPV1*, *GPR55*, and *PPARA* was present, according to the protein results. Moreover, the mRNA results of *TRPV1* were consistent with a previous study regarding equine articular tissue (4). To the best of the Authors' knowledge, no data have been reported on equine articular tissue regarding the expression of the other receptors described in this paper.

Limitation

There are some limitations which should be taken into consideration when interpreting the results of this study. It cannot be ruled out that some factors could potentially alter the CB1R, CB2R, TRPV1, GPR55, and PPAR α expression in tissues, such as the unknown underlying pathological conditions of the horses in the study or the medications received. In

addition, the limited number of horses considered in the current study, the reduced representation of male to female horses, as well as adult and young horses, represent another limitation of the study.

Conclusion

The present study was the first study to demonstrate the mRNA presence and the protein cellular distribution of the cannabinoid receptors (CB1 and CB2) and three cannabinoid-related receptors (TRPV1, GPR55, and PPAR α) in the horse synovial tissues of the metacarpophalangeal joint of the horse. Cannabinoid receptor 1 was identified in FLS and MLS, although it was not expressed in all the horses. Cannabinoid receptor 2, TRPV1 and GPR55 were identified in FLS, MLS, and blood vessels, while PPAR α -IR was identified in FLS and blood vessels. Due to their cellular localization, these receptors may be the target of many drugs (endocannabinoids and endocannabinoid-related molecules, non-psychoactive phytocannabinoids, synthetic cannabinoids and several agonist and antagonist drugs) which could potentially be utilized to improve inflammation and pain in horses with joint diseases. These results should hopefully encourage the development of new molecular and preclinical studies supporting the use of molecules already tested and used in humans and animals which could potentially reduce the joint inflammation in horses with joint diseases. Comparison of the data of the current study with the data obtained from the synovial tissues of horses with metacarpophalangeal joint disease could be of interest to verify whether mRNA of *Cnr1*, *Cnr2*, *TRPV1*, *GPR55*, and *PPARA*, and the immunoreactivity for the same receptors are up- or down-regulated during joint disease.

Data availability statement

The raw data supporting the conclusions of this article will be made available by the authors, without undue reservation.

Ethics statement

Ethical review and approval was not required for the animal study because the metacarpophalangeal joints of horses slaughtered for consumption were collected post-mortem. According to Directive 2010/63/EU of the European Parliament and of the Council of 22 September 2010 regarding the protection of animals used for scientific purposes, the Italian legislation (D. Lgs. no. 26/2014) does not require any approval by competent authorities or ethics committees because this study did not influence any therapeutic decisions.

Author contributions

RC, RZC, RR, and AG contributed to the study design. The mRNA analysis was carried out by AZ

and MF. The immunohistochemical experiments were carried out by RZC, MDS, and GS. Acquisition of data and drafting of the manuscript was done by RC. All authors interpreted the data. All authors contributed to the study execution and approved the final manuscript.

Funding

This study received a grant from NBF Lanes, Milan, Italy.

Acknowledgments

The excellent technical assistance of Dr. Francesca Gobbo is gratefully acknowledged. The availability and collaboration of the health personnel of the Zerbini Giorgio and Ragazzi Maria Grazia slaughterhouse (Correggio, Reggio Emilia, Italy) is gratefully acknowledged.

References

- Lapjitz C, Charoenchakran P, Petchkaew P, Sukpipattanamongkol S, Yodsheewan R, Theerapan W, et al. Diagnostic imaging and cytological analysis aid the clinical investigation of long digital extensor tendon subtendinous bursitis in a horse. *J Equine Vet Sci.* (2021) 101:103449. doi: 10.1016/j.jevs.2021.103449
- Kawcak CE, McIlwraith CW, Norrdin RW, Park RD, Steyn PS. Clinical effects of exercise on subchondral bone of carpal and metacarpophalangeal joints in horses. *Am J Vet Res.* (2000) 61:1252–8. doi: 10.2460/ajvr.2000.61.1252
- Neundorff HR, Lowerison BM, Cruz MA, Thomason JJ, McEwen JB, Hurtig BM. Determination of the prevalence and severity of metacarpophalangeal joint osteoarthritis in Thoroughbred racehorses via quantitative macroscopic evaluation. *Am J Vet Res.* (2010) 71:1284–93. doi: 10.2460/ajvr.71.11.1284
- vom Braucke AFG, Lysemose Frederiksen N, Berg LC, Aarsvold S, Müller FC, Ploug Boesen M, et al. Identification and quantification of transient receptor potential vanilloid 1 (TRPV1) in equine articular tissue. *Animals.* (2020) 10:506. doi: 10.3390/ani10030506
- Contino EK. Management and rehabilitation of joint disease in sport horses. *Vet Clin Equine Pract.* (2018) 34:345–58. doi: 10.1016/j.cveq.2018.04.007
- Spadari A, Rinnovati R, Babbini S, Romagnoli N. Clinical evaluation of intra-articular administration of stanozolol to manage lameness associated with acute and chronic osteoarthritis in horses. *J Equine Vet Sci.* (2015) 35:105–10. doi: 10.1016/j.jevs.2014.12.003
- Pujol R, Girard CA, Richard H, Hassanpour I, Binette MP, Beauchamp G, et al. Synovial nerve fiber density decreases with naturally-occurring osteoarthritis in horses. *Osteoarthr Cartil.* (2018) 26:1379–88. doi: 10.1016/j.joca.2018.06.006
- Goodrich LR, Nixon AJ. Medical treatment of osteoarthritis in the horse – a review. *Vet J.* (2006) 171:51–69. doi: 10.1016/j.tvjl.2004.07.008
- Bondeson J, Wainwright SD, Lauder S, Amos N, Hughes CE. The role of synovial macrophages and macrophage-produced cytokines in driving aggrecanases, matrix metalloproteinases, and other destructive and inflammatory responses in osteoarthritis. *Arthritis Res Ther.* (2006) 8:R187. doi: 10.1186/ar2099
- Kyung Chang S, Gu Z, Brenner MB. Fibroblast-like synoviocytes in inflammatory arthritis pathology: the emerging role of cadherin-11. *Immunol Rev.* (2010) 233:256–66. doi: 10.1111/j.0105-2896.2009.00854.x
- Iwanaga T, Shikichi M, Kitamura H, Yanase H, Nozawa-Inoue K. Morphology and functional roles of synoviocytes in the joint. *Arch Histol Cytol.* (2000) 63:17–31. doi: 10.1679/aohc.63.17
- Lowin T, Pongratz G, Straub RH. The synthetic cannabinoid WIN55,212-2 mesylate decreases the production of inflammatory mediators in rheumatoid arthritis synovial fibroblasts by activating CB2, TRPV1, TRPA1 and yet unidentified receptor targets. *J Inflamm.* (2016) 13:15. doi: 10.1186/s12950-016-0114-7
- Thomsen LN, Thomsen PD, Downing A, Talbot R, Berg LC. FOXO1, PDK, PYCARD and SAMD9L are differentially expressed by fibroblast-like cells in equine synovial membrane compared to joint capsule. *BMC Vet Res.* (2017) 13:106. doi: 10.1186/s12917-017-1003-x
- Graabæk PM. Ultrastructural evidence for two distinct types of synoviocytes in rat synovial membrane. *J Ultrastruct Res.* (1982) 78:321–39. doi: 10.1016/S0022-5320(82)80006-3
- Nygaard G, Firestein GS. Restoring synovial homeostasis in rheumatoid arthritis by targeting fibroblast-like synoviocytes. *Nat Rev Rheumatol.* (2020) 16:316–33. doi: 10.1038/s41584-020-0413-5
- Kitamura HP, Yanase H, Kitamura H, Iwanaga T. Unique localization of protein gene product 9.5 in type B synoviocytes in the joints of the horse. *J Histochem Cytochem.* (1999) 47:343–51. doi: 10.1177/002215549904700308
- Shikichi M, Kitamura HP, Yanase H, Konno A, Takahashi-Iwanaga H, Iwanaga T. Three-dimensional ultrastructure of synoviocytes in the horse joint as revealed by the scanning electron microscope. *Arch Histol Cytol.* (1999) 62:219–29. doi: 10.1679/aohc.62.219
- Levick JR, McDonald JN. Fluid movement across synovium in healthy joints: role of synovial fluid macromolecules. *Ann Rheum Dis.* (1995) 54:417–23. doi: 10.1136/ard.54.5.417
- Karpus ON, Kiener HP, Niederreiter B, Yilmaz-Elis A, van der Kaa J, Ramaglia V, et al. CD55 deposited on synovial collagen fibers protects from immune complex-mediated arthritis. *Arthritis Res Ther.* (2015) 17:6. doi: 10.1186/s13075-015-0518-4
- Haubruck P, Pinto MM, Moradi B, Little CB, Gentek R. Monocytes, macrophages, and their potential niches in synovial joints – therapeutic targets in post-traumatic osteoarthritis? *Front Immunol.* (2021) 12:763702. doi: 10.3389/fimmu.2021.763702
- Müller-Ladner U, Ospelt C, Gay S, Distler O, Pap T. Cells of the synovium in rheumatoid arthritis. Synovial fibroblasts. *Arthritis Res Ther.* (2007) 9:223. doi: 10.1186/ar2337
- Kiener HP, Watts GFM, Cui Y, Wright J, Thornhill TS, Sköld M, et al. Synovial fibroblasts self-direct multicellular lining architecture and synthetic function in three-dimensional organ culture. *Arthritis Rheum.* (2010) 62:742–52. doi: 10.1002/art.27285
- Davies LC, Jenkins SJ, Allen JE, Taylor PR. Tissue-resident macrophages. *Nat Immunol.* (2013) 14:986–95. doi: 10.1038/ni.2705
- Culemann S, Grüneboom A, Nicolás-Ávila JA, Weidner D, Lämmle KF, Rothe T, et al. Locally renewing resident synovial macrophages provide a protective barrier for the joint. *Nature.* (2019) 572:670–5. doi: 10.1038/s41586-019-1471-1
- Buckley CD. Macrophages form a protective cellular barrier in joints. *Nature.* (2019) 572:590–2. doi: 10.1038/d41586-019-02340-x

Conflict of interest

The authors declare that the research was conducted in the absence of any commercial or financial relationships that could be construed as a potential conflict of interest.

Publisher's note

All claims expressed in this article are solely those of the authors and do not necessarily represent those of their affiliated organizations, or those of the publisher, the editors and the reviewers. Any product that may be evaluated in this article, or claim that may be made by its manufacturer, is not guaranteed or endorsed by the publisher.

Supplementary material

The Supplementary Material for this article can be found online at: <https://www.frontiersin.org/articles/10.3389/fvets.2023.1045030/full#supplementary-material>

26. Menarim BC, Gillis KH, Oliver A, Mason C, Werre SR, Luo X, et al. Inflamed synovial fluid induces a homeostatic response in bone marrow mononuclear cells *in vitro*: implications for joint therapy. *FASEB J.* (2020) 34:4430–44. doi: 10.1096/fj.201902698R
27. Malfait AM, Gallily R, Sumariwalla PF, Malik AS, Andreaskos E, Mechoulam R, et al. The nonpsychoactive cannabis constituent cannabidiol is an oral anti-arthritis therapeutic in murine collagen-induced arthritis. *Proc Natl Acad Sci USA.* (2000) 97:9561–6. doi: 10.1073/pnas.160105897
28. Richardson D, Pearson RG, Kurian N, Latif ML, Garle MJ, Barrett DA, et al. Characterisation of the cannabinoid receptor system in synovial tissue and fluid in patients with osteoarthritis and rheumatoid arthritis. *Arthritis Res Ther.* (2008) 10:R43. doi: 10.1186/ar2401
29. Gui H, Tong Q, Qu W, Mao CM, Dai SM. The endocannabinoid system and its therapeutic implications in rheumatoid arthritis. *Int Immunopharmacol.* (2015) 26:86–91. doi: 10.1016/j.intimp.2015.03.006
30. Gui H, Liu X, Liu LR, Su DF, Dai SM. Activation of cannabinoid receptor 2 attenuates synovitis and joint destruction in collagen-induced arthritis. *Immunobiology.* (2015) 220:817–22. doi: 10.1016/j.imbio.2014.12.012
31. Lowin T, Apitz M, Anders S, Straub RH. Anti-inflammatory effects of N-acyl ethanolamines in rheumatoid arthritis synovial cells are mediated by TRPV1 and TRPA1 in a COX-2 dependent manner. *Arthritis Res Ther.* (2015) 17:321. doi: 10.1186/s13075-015-0845-5
32. Malek N, Starowicz K. Joint problems arising from lack of repair mechanisms: can cannabinoids help?: cannabinoids for OA treatment. *Br J Pharmacol.* (2019) 176:1412–20. doi: 10.1111/bph.14204
33. Kaur I, Behl T, Bungau S, Zengin G, Kumar A, El-Esawi MA, et al. The endocannabinoid signaling pathway as an emerging target in pharmacotherapy, earmarking mitigation of destructive events in rheumatoid arthritis. *Life Sci.* (2020) 257:118109. doi: 10.1016/j.lfs.2020.118109
34. Clayton P, Hill M, Bogoda N, Subah S, Venkatesh R. Palmitoylethanolamide: a natural compound for health management. *Int J Mol Sci.* (2021) 22:5305. doi: 10.3390/ijms22105305
35. Ligresti A, De Petrocellis L, Di Marzo V. From phytocannabinoids to cannabinoid receptors and endocannabinoids: pleiotropic physiological and pathological roles through complex pharmacology. *Physiol Rev.* (2016) 96:1593–659. doi: 10.1152/physrev.00002.2016
36. Maroon J, Bost J. Review of the neurological benefits of phytocannabinoids. *Surg Neurol Int.* (2018) 9:91. doi: 10.4103/sni.sni_45_18
37. Kreitzer FR, Stella N. The therapeutic potential of novel cannabinoid receptors. *Pharmacol Ther.* (2009) 122:83–96. doi: 10.1016/j.pharmthera.2009.01.005
38. Morales P, Hurst DP, Reggio PH. Molecular targets of the phytocannabinoids: a complex picture. In: Kinghorn AD, Falk H, Gibbons S, Kobayashi J, editors. *Phytocannabinoids (Progress in the Chemistry of Organic Natural Products)*. Cham: Springer International Publishing (2017). Vol. 103. p. 103–31.
39. Mlost J, Bryk M, Starowicz K. Cannabidiol for pain treatment: focus on pharmacology and mechanism of action. *IJMS.* (2020) 21:8870. doi: 10.3390/ijms21228870
40. Selvi E, Lorenzini S, Garcia-Gonzalez E, Maggio R, Lazzerini PE, Capocchi PL, et al. Inhibitory effect of synthetic cannabinoids on cytokine production in rheumatoid fibroblast-like synoviocytes. *Clin Exp Rheumatol.* (2008) 26:574–81.
41. Schuelert N, Zhang C, Mogg AJ, Broad LM, Hepburn DL, Nisenbaum ES, et al. Paradoxical effects of the cannabinoid CB2 receptor agonist GW405833 on rat osteoarthritic knee joint pain. *Osteoarthritis Cartil.* (2010) 18:1536–43. doi: 10.1016/j.joca.2010.09.005
42. Fukuda S, Kohsaka H, Takayasu A, Yokoyama W, Miyabe C, Miyabe Y, et al. Cannabinoid receptor 2 as a potential therapeutic target in rheumatoid arthritis. *BMC Musculoskelet Disord.* (2014) 15:275. doi: 10.1186/1471-2474-15-275
43. Gui H, Liu X, Wang ZW, He DY, Su DF, Dai SM. Expression of cannabinoid receptor 2 and its inhibitory effects on synovial fibroblasts in rheumatoid arthritis. *Rheumatology.* (2014) 53:802–9. doi: 10.1093/rheumatology/ket447
44. Miagkoff L, Girard CA, St-Jean G, Richard H, Beauchamp G, Laverty S. Cannabinoid receptors are expressed in equine synovium and upregulated with synovitis. *Equine Vet J.* (2022) 2022:evj.13860. doi: 10.1111/evj.13860
45. Rzezycki P, Rasner C, Lammlin L, Junginger L, Goldman S, Bergman R, et al. Cannabinoid receptor type 2 is upregulated in synovium following joint injury and mediates anti-inflammatory effects in synovial fibroblasts and macrophages. *Osteoarthritis Cartil.* (2021) 29:1720–31. doi: 10.1016/j.joca.2021.09.003
46. Kochukov MY, McNearney TA, Fu Y, Westlund KN. Thermosensitive TRP ion channels mediate cytosolic calcium response in human synoviocytes. *Am J Physiol Cell Physiol.* (2006) 291:C424–32. doi: 10.1152/ajpcell.00553.2005
47. Whyte LS, Ryberg E, Sims NA, Ridge SA, Mackie K, Greasley PJ, et al. The putative cannabinoid receptor GPR55 affects osteoclast function *in vitro* and bone mass *in vivo*. *Proc Natl Acad Sci USA.* (2009) 106:16511–6. doi: 10.1073/pnas.0902743106
48. Andersson J, Sophocleous A, Zhou Y, Rischitor G, Ralston S, Salter D. Expression of cannabinoid receptors by human articular chondrocytes. *Bone.* (2011) 48:S141. doi: 10.1016/j.bone.2011.03.293
49. van Eekeren ICM, Clockaerts S, Bastiaansen-Jenniskens YM, Lubberts E, Verhaar JAN, van Osch GJVM, et al. Fibrates as therapy for osteoarthritis and rheumatoid arthritis? A systematic review. *Ther Adv Musculoskel.* (2013) 5:33–44. doi: 10.1177/1759720X12468659
50. Huang D, Zhao Q, Liu H, Guo Y, Xu H. PPAR- α agonist WY-14643 inhibits LPS-induced inflammation in synovial fibroblasts via NF- κ B pathway. *J Mol Neurosci.* (2016) 59:544–53. doi: 10.1007/s12031-016-0775-y
51. Zannoni A, Bombardi C, Dondi F, Morini M, Forni M, Chiochetti R, et al. Proteinase-activated receptor 2 expression in the intestinal tract of the horse. *Res Vet Sci.* (2014) 96:464–71. doi: 10.1016/j.rvsc.2014.03.006
52. Vandesompele J, De Preter K, Pattyn F, Poppe B, Van Roy N, De Paepe A, et al. Accurate normalization of real-time quantitative RT-PCR data by geometric averaging of multiple internal control genes. *Genome Biol.* (2002) 3:research0034.1. doi: 10.1186/gb-2002-3-7-research0034
53. Gializzo G, De Silva M, Giancola F, Rinnovati R, Peli A, Chiochetti R. Cellular distribution of cannabinoid-related receptors TRPV1, PPAR- γ , GPR55 and GPR3 in the equine cervical dorsal root ganglia. *Equine Vet J.* (2022) 54:788–98. doi: 10.1111/evj.13499
54. Chiochetti R, Rinnovati R, Tagliavia C, Stanzani A, Gializzo G, Giancola F, et al. Localisation of cannabinoid and cannabinoid-related receptors in the equine dorsal root ganglia. *Equine Vet J.* (2021) 53:549–57. doi: 10.1111/evj.13305
55. Kupczyk P, Rykala M, Serek P, Pawlak A, Slowikowski B, Holysz M, et al. The cannabinoid receptors system in horses: tissue distribution and cellular identification in skin. *Vet Intern Med.* (2022) 36:1508–24. doi: 10.1111/jvim.16467
56. Wang S, Kobayashi K, Kogure Y, Yamanaka H, Yamamoto S, Yagi H, et al. Negative regulation of TRPA1 by AMPK in primary sensory neurons as a potential mechanism of painful diabetic neuropathy. *Diabetes.* (2018) 67:98–109. doi: 10.2337/db17-0503
57. Chiochetti R, Gializzo G, Tagliavia C, Stanzani A, Giancola F, Menchetti M, et al. Cellular distribution of canonical and putative cannabinoid receptors in canine cervical dorsal root ganglia. *Front Vet Sci.* (2019) 6:313. doi: 10.3389/fvets.2019.00313
58. Gializzo G, Giancola F, Stanzani A, Fracassi F, Bernardini C, Forni M, et al. Localization of cannabinoid receptors CB1, CB2, GPR55, and PPAR α in the canine gastrointestinal tract. *Histochem Cell Biol.* (2018) 150:187–205. doi: 10.1007/s00418-018-1684-7
59. Jørgensen E, Pirone A, Jacobsen S, Miragliotta V. Epithelial-to-mesenchymal transition and keratinocyte differentiation in equine experimental body and limb wounds healing by second intention. *Vet Dermatol.* (2019) 30:417. doi: 10.1111/vde.12774
60. Cerrato S, Ramíó-Lluch L, Brazis P, Rabanal RM, Fondevila D, Puigdemont A. Development and characterization of an equine skin-equivalent model. *Vet Dermatol.* (2014) 25:475–77. doi: 10.1111/vde.12134
61. Smith DM. The normal synovium. *TORJ.* (2011) 5:100–6. doi: 10.2174/1874312901105010100
62. Kupczyk P, Simiczyjew A, Marczuk J, Dratkiewicz E, Beberok A, Rok J, et al. PAR1 as a marker of an aggressive clinical phenotype in cutaneous melanoma—a clinical and an *in vitro* study. *Cells.* (2021) 10:286. doi: 10.3390/cells10020286
63. Kleine SA, Budsberg SC. Synovial membrane receptors as therapeutic targets: a review of receptor localization, structure, and function: synovial membrane receptors as therapeutic targets. *J Orthop Res.* (2017) 35:1589–605. doi: 10.1002/jor.23568
64. O'Brien M, McDougall JJ. Cannabis and joints: scientific evidence for the alleviation of osteoarthritis pain by cannabinoids. *Curr Opin Pharmacol.* (2018) 40:104–9. doi: 10.1016/j.coph.2018.03.012
65. Yocom AF, O'Fallon ES, Gustafson DL, Contino EK. Pharmacokinetics, safety, and synovial fluid concentrations of single- and multiple-dose oral administration of 1 and 3 mg/kg cannabidiol in horses. *J Equine Vet Sci.* (2022) 113:103933. doi: 10.1016/j.jevs.2022.103933
66. Valencia X, Higgins JMG, Kiener HP, Lee DM, Podrebarac TA, Dascher CC, et al. Cadherin-11 provides specific cellular adhesion between fibroblast-like synoviocytes. *J Exp Med.* (2004) 200:1673–9. doi: 10.1084/jem.20041545
67. Müller-Ladner U, Gay RE, Gay S. Activation of synoviocytes. *Curr Opin Rheumatol.* (2000) 12:186–94. doi: 10.1097/00002281-200005000-00005
68. Bartok B, Firestein GS. Fibroblast-like synoviocytes: key effector cells in rheumatoid arthritis. *Immunol Rev.* (2010) 233:233–55. doi: 10.1111/j.0105-2896.2009.00859.x
69. Bottini N, Firestein GS. Duality of fibroblast-like synoviocytes in RA: passive responders and imprinted aggressors. *Nat Rev Rheumatol.* (2013) 9:24–33. doi: 10.1038/nrrheum.2012.190
70. Briston L, Dudhia J, Lees P. Age-related differences in prostaglandin E2 synthesis by equine cartilage explants and synoviocytes. *J Vet Pharmacol Ther.* (2010) 33:268–76. doi: 10.1111/j.1365-2885.2009.01131.x

71. Benito MJ, Veale DJ, FitzGerald O, Berg WB van den, Bresnihan B. Synovial tissue inflammation in early and late osteoarthritis. *Ann Rheum Dis.* (2005) 64:1263–7. doi: 10.1136/ard.2004.025270
72. Ross TN, Kisiday JD, Hess T, McIlwraith CW. Evaluation of the inflammatory response in experimentally induced synovitis in the horse: a comparison of recombinant equine interleukin 1 beta and lipopolysaccharide. *Osteoarthritis Cartil.* (2012) 20:1583–90. doi: 10.1016/j.joca.2012.08.008
73. Andreassen SM, Berg LC, Nielsen SS, Kristensen AT, Jacobsen S. mRNA expression of genes involved in inflammation and haemostasis in equine fibroblast-like synoviocytes following exposure to lipopolysaccharide, fibrinogen and thrombin. *BMC Vet Res.* (2015) 11:141. doi: 10.1186/s12917-015-0448-z
74. Culemann S, Grüneboom A, Krönke G. Origin and function of synovial macrophage subsets during inflammatory joint disease. *Adv Immunol.* (2019) 143:75–98. doi: 10.1016/bs.ai.2019.08.006
75. Murray PJ, Allen JE, Biswas SK, Fisher EA, Gilroy DW, Goerdt S, et al. Macrophage activation and polarization: nomenclature and experimental guidelines. *Immunity.* (2014) 41:14–20. doi: 10.1016/j.immuni.2014.06.008
76. Udalova IA, Mantovani A, Feldmann M. Macrophage heterogeneity in the context of rheumatoid arthritis. *Nat Rev Rheumatol.* (2016) 12:472–85. doi: 10.1038/nrrheum.2016.91
77. Murray PJ, Wynn TA. Protective and pathogenic functions of macrophage subsets. *Nat Rev Immunol.* (2011) 11:723–37. doi: 10.1038/nri3073
78. Yocum DE, Lafyatis R, Remmers EF, Schumacher HR, Wilder RL. Hyperplastic synoviocytes from rats with streptococcal cell wall-induced arthritis exhibit a transformed phenotype that is thymic-dependent and retinoid inhibitable. *Am J Pathol.* (1988) 132:38–48.
79. Xue C, Takahashi M, Hasunuma T, Aono H, Yamamoto K, Yoshino S, et al. Characterisation of fibroblast-like cells in pannus lesions of patients with rheumatoid arthritis sharing properties of fibroblasts and chondrocytes. *Ann Rheum Dis.* (1997) 56:262–7. doi: 10.1136/ard.56.4.262
80. Steinert PM, Roop DR. Molecular and cellular biology of intermediate filaments. *Annu Rev Biochem.* (1988) 57:593–625. doi: 10.1146/annurev.bi.57.070188.003113
81. Cain H, Kraus B. Cytoskeleton in Cells of the mononuclear phagocyte system. *Virchows Archiv B Cell Pathol.* (1981) 36:159–76. doi: 10.1007/BF02912064
82. Galiazzo G, Tagliavia C, Giancola F, Rinnovati R, Sadeghinezhad J, Bombardi C, et al. Localisation of cannabinoid and cannabinoid-related receptors in the horse ileum. *J Equine Vet Sci.* (2021) 104:103688. doi: 10.1016/j.jevs.2021.103688
83. Croxford JL, Yamamura T. Cannabinoids and the immune system: potential for the treatment of inflammatory diseases? *J Neuroimmunol.* (2005) 166:3–18. doi: 10.1016/j.jneuroim.2005.04.023
84. Fechtner S, Singh AK, Ahmed S. Role of cannabinoid receptor 2 in mediating interleukin-1 β -induced inflammation in rheumatoid arthritis synovial fibroblasts. *Clin Exp Rheumatol.* (2019) 37:1026–35.
85. Tominaga M, Caterina MJ, Malmberg AB, Rosen TA, Gilbert H, Skinner K, et al. The cloned capsaicin receptor integrates multiple pain-producing stimuli. *Neuron.* (1998) 21:531–43. doi: 10.1016/S0896-6273(00)80564-4
86. Caterina MJ, Schumacher MA, Tominaga M, Rosen TA, Levine JD, Julius D. The capsaicin receptor: a heat-activated ion channel in the pain pathway. *Nature.* (1997) 389:816–24. doi: 10.1038/39807
87. Kelly S. TRPV1 antagonists in the treatment of osteoarthritis pain. *Int J Clin Rheumatol.* (2015) 10:161–75. doi: 10.2217/ijr.15.14
88. Malfait AM, Butler DM, Presky DH, Maini RN, Brennan FM, Feldmann M. Blockade of IL-12 during the induction of collagen-induced arthritis (CIA) markedly attenuates the severity of the arthritis. *Clin Exp Immunol.* (1998) 111:377–83. doi: 10.1046/j.1365-2249.1998.00485.x
89. Kelly S, Chapman RJ, Woodhams S, Sagar DR, Turner J, Burston JJ, et al. Increased function of pronociceptive TRPV1 at the level of the joint in a rat model of osteoarthritis pain. *Ann Rheum Dis.* (2015) 74:252–9. doi: 10.1136/annrheumdis-2013-203413
90. Lv Z, Xu X, Sun Z, Yang YX, Guo H, Li J, et al. TRPV1 alleviates osteoarthritis by inhibiting M1 macrophage polarization via Ca²⁺/CaMKII/Nrf2 signaling pathway. *Cell Death Dis.* (2021) 12:504. doi: 10.1038/s41419-021-03792-8
91. Engler A, Aeschlimann A, Simmen BR, Michel BA, Gay RE, Gay S, et al. Expression of transient receptor potential vanilloid 1 (TRPV1) in synovial fibroblasts from patients with osteoarthritis and rheumatoid arthritis. *Biochem Biophys Res Commun.* (2007) 359:884–8. doi: 10.1016/j.bbrc.2007.05.178
92. Zygmunt PM, Petersson J, Andersson DA, Chuang H, Sörgård M, Di Marzo V, et al. Vanilloid receptors on sensory nerves mediate the vasodilator action of anandamide. *Nature.* (1999) 400:452–7. doi: 10.1038/22761
93. Patapoutian A, Peier AM, Story GM, Viswanath V. ThermoTRP channels and beyond: mechanisms of temperature sensation. *Nat Rev Neurosci.* (2003) 4:529–39. doi: 10.1038/nrn1141
94. Anand U, Jones B, Korchev Y, Bloom SR, Pacchetti B, Anand P, et al. CBD effects on TRPV1 signaling pathways in cultured DRG neurons. *J Pain Res.* (2020) 13:2269–78. doi: 10.2147/JPR.S258433
95. Costa B, Trovato AE, Comelli F, Giagnoni G, Colleoni M. The non-psychoactive cannabis constituent cannabidiol is an orally effective therapeutic agent in rat chronic inflammatory and neuropathic pain. *Eur J Pharmacol.* (2007) 556:75–83. doi: 10.1016/j.ejphar.2006.11.006
96. Lowin T, Tingting R, Zurmahr J, Classen T, Schneider M, Pongratz G. Cannabidiol (CBD): a killer for inflammatory rheumatoid arthritis synovial fibroblasts. *Cell Death Dis.* (2020) 11:714. doi: 10.1038/s41419-020-02892-1
97. Rajan TS, Giacompo S, Iori R, De Nicola GR, Grassi G, Pollastro F, et al. Anti-inflammatory and antioxidant effects of a combination of cannabidiol and moringin in LPS-stimulated macrophages. *FitoTerapia.* (2016) 112:104–15. doi: 10.1016/j.fitote.2016.05.008
98. Lanuti M, Talamonti E, Maccarrone M, Chiurchiù V. Activation of GPR55 receptors exacerbates oxLDL-induced lipid accumulation and inflammatory responses, while reducing cholesterol efflux from human macrophages. *PLoS ONE.* (2015) 10:e0126839. doi: 10.1371/journal.pone.0126839
99. Schuelert N, McDougall JJ. The abnormal cannabidiol analogue O-1602 reduces nociception in a rat model of acute arthritis via the putative cannabinoid receptor GPR55. *Neurosci Lett.* (2011) 500:72–6. doi: 10.1016/j.neulet.2011.06.004
100. Sacerdote P, Martucci C, Vaccani A, Bariselli F, Panerai AE, Colombo A, et al. The nonpsychoactive component of marijuana cannabidiol modulates chemotaxis and IL-10 and IL-12 production of murine macrophages both *in vivo* and *in vitro*. *J Neuroimmunol.* (2005) 159:97–105. doi: 10.1016/j.jneuroim.2004.10.003
101. Chinetti G, Fruchart JC, Staels B. Peroxisome proliferator-activated receptors: new targets for the pharmacological modulation of macrophage gene expression and function. *Curr Opin Lipidol.* (2003) 14:459–68. doi: 10.1097/00041433-200310000-00006
102. Shu H, Wong B, Zhou G, Li Y, Berger J, Woods JW, et al. Activation of PPAR α or γ reduces secretion of matrix metalloproteinase 9 but not interleukin 8 from human monocytic THP-1 cells. *Biochem Biophys Res Commun.* (2000) 267:345–9. doi: 10.1006/bbrc.1999.1968
103. Pontis S, Ribeiro A, Sasso O, Piomelli D. Macrophage-derived lipid agonists of PPAR- α as intrinsic controllers of inflammation. *Crit Rev Biochem Mol Biol.* (2016) 51:7–14. doi: 10.3109/10409238.2015.1092944
104. Grabacka M, Pierzchalska M, Plonka PM, Pierzchalski P. The role of PPAR alpha in the modulation of innate immunity. *IJMS.* (2021) 22:10545. doi: 10.3390/ijms221910545
105. Devchand PR, Keller H, Peters JM, Vazquez M, Gonzalez FJ, Wahli W. The PPAR α -leukotriene B₄ pathway to inflammation control. *Nature.* (1996) 384:39–43. doi: 10.1038/384039a0
106. Crisafulli C, Cuzzocrea S. The role of endogenous and exogenous ligands for the peroxisome proliferator-activated receptor alpha (PPAR- α) in the regulation of inflammation in macrophages. *Shock.* (2009) 32:62–73. doi: 10.1097/SHK.0b013e31818bbad6
107. Okamoto H, Iwamoto T, Kotake S, Momohara S, Yamanaka H, Kamatani N. Inhibition of NF- κ B signaling by fenofibrate, a peroxisome proliferator-activated receptor- α ligand, presents a therapeutic strategy for rheumatoid arthritis. *Clin Exp Rheumatol.* (2005) 23:323–30.
108. Marini I, Bartolucci ML, Bortolotti F, Gatto MR, Bonetti GA. Palmitoylethanolamide versus a nonsteroidal anti-inflammatory drug in the treatment of temporomandibular joint inflammatory pain. *J Orofac Pain.* (2012) 26:99–104.
109. Jung JJ, Lee HS, Jeon YE, Kim SM, Hong SH, Moon JM, et al. Anti-inflammatory activity of palmitoylethanolamide ameliorates osteoarthritis induced by monosodium iodoacetate in Sprague–Dawley rats. *Inflammopharmacol.* (2021) 29:1475–86. doi: 10.1007/s10787-021-00870-3
110. Ambrosino P, Soldovieri MV, De Maria M, Russo C, Tagliatalela M. Functional and biochemical interaction between PPAR α receptors and TRPV1 channels: potential role in PPAR α agonists-mediated analgesia. *Pharmacol Res.* (2014) 87:113–22. doi: 10.1016/j.phrs.2014.06.015
111. Esteves CL, Sheldrake TA, Mesquita SP, Pesántez JJ, Menghini T, Dawson L, et al. Isolation and characterization of equine native MSC populations. *Stem Cell Res Ther.* (2017) 8:80. doi: 10.1186/s13287-017-0525-2
112. Esteves CL, Sheldrake TA, Dawson L, Menghini T, Rink BE, Amilon K, et al. Equine mesenchymal stromal cells retain a pericyte-like phenotype. *Stem Cells Dev.* (2017) 26:964–72. doi: 10.1089/scd.2017.0017
113. Earley S, Brayden JE. Transient receptor potential channels in the vasculature. *Physiol Rev.* (2015) 95:645–90. doi: 10.1152/physrev.00026.2014
114. Mapp PI, Walsh DA. Mechanisms and targets of angiogenesis and nerve growth in osteoarthritis. *Nat Rev Rheumatol.* (2012) 8:390–8. doi: 10.1038/nrrheum.2012.80
115. Takeshita M, Nakamura J, Ohtori S, Inoue G, Orita S, Miyagi M, et al. Sensory innervation and inflammatory cytokines in hypertrophic synovia associated with pain transmission in osteoarthritis of the hip: a case-control study. *Rheumatology.* (2012) 51:1790–5. doi: 10.1093/rheumatology/kes173
116. Henrotin Y, Pesses L, Lambert C. Targeting the synovial angiogenesis as a novel treatment approach to osteoarthritis. *Ther Adv Musculoskel.* (2014) 6:20–34. doi: 10.1177/1759720X13514669

117. Solinas M, Massi P, Cantelmo A, Cattaneo M, Cammarota R, Bartolini D, et al. Cannabidiol inhibits angiogenesis by multiple mechanisms: cannabidiol and angiogenesis. *Br J Pharmacol.* (2012) 167:1218–31. doi: 10.1111/j.1476-5381.2012.02050.x
118. Balogh E, Binińska M, Fearon U, Veale DJ, Szekanecz Z. Angiogenesis in inflammatory arthritis. *Isr Med Assoc J.* (2019) 21:345–52.
119. Ashton JC, Friberg D, Darlington CL, Smith PF. Expression of the cannabinoid CB2 receptor in the rat cerebellum: an immunohistochemical study. *Neurosci Lett.* (2006) 396:113–6. doi: 10.1016/j.neulet.2005.11.038
120. Bártkai S, Járjai Z, Wagner JA, Goparaju SK, Varga Ká, Liu J, et al. Endocannabinoids acting at vascular CB1 receptors mediate the vasodilated state in advanced liver cirrhosis. *Nat Med.* (2001) 7:827–32. doi: 10.1038/89953
121. Sato J, Segami N, Yoshitake Y, Kaneyama K, Abe A, Yoshimura H, et al. Expression of capsaicin receptor TRPV-1 in synovial tissues of patients with symptomatic internal derangement of the temporomandibular joint and joint pain. *Oral Surg Oral Med Oral Pathol Oral Radiol Endodontol.* (2005) 100:674–81. doi: 10.1016/j.tripleo.2005.03.008
122. McDougall JJ, Yu V, Thomson J. *In vivo* effects of CB₂ receptor-selective cannabinoids on the vasculature of normal and arthritic rat knee joints: CB₂ effects on joint blood flow. *Br J Pharmacol.* (2008) 153:358–66. doi: 10.1038/sj.bjp.0707565
123. Rajesh M, Mukhopadhyay P, Haskó G, Huffman JW, Mackie K, Pacher P. CB₂ cannabinoid receptor agonists attenuate TNF- α -induced human vascular smooth muscle cell proliferation and migration: CB₂ receptor and smooth muscle proliferation. *Br J Pharmacol.* (2008) 153:347–57. doi: 10.1038/sj.bjp.0707569
124. Yang D, Luo Z, Ma S, Wong WT, Ma L, Zhong J, et al. Activation of TRPV1 by dietary capsaicin improves endothelium-dependent vasorelaxation and prevents hypertension. *Cell Metab.* (2010) 12:130–41. doi: 10.1016/j.cmet.2010.05.015
125. Toschi A, Galiasso G, Piva A, Tagliavia C, Mazzuoli-Weber G, Chiocchetti R, et al. Cannabinoid and cannabinoid-related receptors in the myenteric plexus of the porcine ileum. *Animals.* (2021) 11:263. doi: 10.3390/ani11020263
126. Tóth A, Czíkora Á, Pásztor ET, Dienes B, Bai P, Csernoch L, et al. Vanilloid receptor-1 (TRPV1) expression and function in the vasculature of the rat. *J Histochem Cytochem.* (2014) 62:129–44. doi: 10.1369/0022155413513589
127. Hofmann NA, Barth S, Waldeck-Weiermair M, Klec C, Strunk D, Malli R, et al. TRPV1 mediates cellular uptake of anandamide and thus promotes endothelial cell proliferation and network-formation. *Biol Open.* (2014) 3:1164–72. doi: 10.1242/bio.20149571
128. Blázquez C, Casanova ML, Planas A, Gómez del Pulgar T, Villanueva C, Fernández-Aceñero MJ, et al. Inhibition of tumor angiogenesis by cannabinoids. *FASEB J.* (2003) 17:1–16. doi: 10.1096/fj.02-0795fje
129. Stanley CP, Hind WH, Tufarelli C, O'Sullivan SE. Cannabidiol causes endothelium-dependent vasorelaxation of human mesenteric arteries via CB₁ activation. *Cardiovasc Res.* (2015) 107:568–78. doi: 10.1093/cvr/cvv179
130. Xu K, Shao Y, Saaoud F, Gillespie A, Drummer C, Liu L, et al. Novel knowledge-based transcriptomic profiling of lipid lysophosphatidylinositol-induced endothelial cell activation. *Front Cardiovasc Med.* (2021) 8:773473. doi: 10.3389/fcvm.2021.773473
131. Daly C, Ross R, Whyte J, Henstridge C, Irving A, McGrath J. Fluorescent ligand binding reveals heterogeneous distribution of adrenoceptors and 'cannabinoid-like' receptors in small arteries. *Br J Pharmacol.* (2010) 159:787–96. doi: 10.1111/j.1476-5381.2009.00608.x
132. Zhang X, Maor Y, Wang JF, Kunos G, Groopman JE. Endocannabinoid-like N-arachidonoyl serine is a novel pro-angiogenic mediator. *Br J Pharmacol.* (2010) 160:1583–94. doi: 10.1111/j.1476-5381.2010.00841.x
133. Wróbel A, Szopa A, Serefko A, Poleszak E. A novel alternative in the treatment of detrusor overactivity? *In vivo* activity of O-1602, the newly synthesized agonist of GPR55 and GPR18 cannabinoid receptors. *Molecules.* (2020) 25:1384. doi: 10.3390/molecules25061384
134. Karpińska O, Baranowska-Kuczeko M, Malinowska B, Kloza M, Kusaczuk M, Gegotek A, et al. Mechanisms of l- α -lysophosphatidylinositol-induced relaxation in human pulmonary arteries. *Life Sci.* (2018) 192:38–45. doi: 10.1016/j.lfs.2017.11.020
135. Hofmann NA, Yang J, Trauger SA, Nakayama H, Huang L, Strunk D, et al. The GPR 55 agonist, L - α -lysophosphatidylinositol, mediates ovarian carcinoma cell-induced angiogenesis. *Br J Pharmacol.* (2015) 172:4107–18. doi: 10.1111/bph.13196
136. O'Sullivan SE. Cannabinoids go nuclear: evidence for activation of peroxisome proliferator-activated receptors. *Br J Pharmacol.* (2007) 152:576–82. doi: 10.1038/sj.bjp.0707423

Chapter 9:
Endocannabinoid System Receptors at the Hip and Stifle Joints of Middle-Aged
Dogs: A Novel Target for the Therapeutic Use of Cannabis sativa Extract in
Canine Arthropathies

Article

Endocannabinoid System Receptors at the Hip and Stifle Joints of Middle-Aged Dogs: A Novel Target for the Therapeutic Use of *Cannabis sativa* Extract in Canine Arthropathies

Rodrigo Zamith Cunha ^{1,2} , Giulia Salamanca ¹ , Fanny Mille ¹, Cecilia Delprete ³, Cecilia Franciosi ³, Giuliano Piva ⁴, Alessandro Gramenzi ² and Roberto Chiochetti ^{1,*} 

- ¹ Department of Veterinary Medical Sciences, University of Bologna, 40126 Bologna, Italy; rodrigo.zamithcunha2@unibo.it (R.Z.C.); giulia.salamanca2@unibo.it (G.S.); fanny.mille@studio.unibo.it (F.M.)
² Department of Veterinary Medicine, University of Teramo, 64100 Teramo, Italy; agramenzi@unite.it
³ Laboratory of Cellular Physiology, Department of Pharmacy and Biotechnology (FaBiT), University of Bologna, 40126 Bologna, Italy; cecilia.delprete2@unibo.it (C.D.); cecilia.franciosi2@studio.unibo.it (C.F.)
⁴ Veterinary Clinic Dr. Giuliano Piva, 41049 Sassuolo, Italy; giulianopivavet@gmail.com
* Correspondence: roberto.chiochetti@unibo.it

Simple Summary: The endocannabinoid system (ECS) plays a crucial role in various processes in animals, including pain, inflammation, and immune function. In this study, the presence and distribution of specific ECS receptors (CB1R, CB2R, and GPR55) in the joints of middle-aged dogs was investigated. By analysing the synovial tissues from the hip and the stifle joints, it was found that both CB2R and GPR55 were more prominently expressed by the synoviocytes as compared to CB1R. In addition, immune cells, such as macrophages and neutrophils, also exhibited some of these receptors. This intriguing finding suggested that the receptors in the ECS, particularly CB2R and GPR55, could be promising targets for therapeutic interventions, such as using *Cannabis sativa* extract, to address arthropathies in dogs.



Citation: Zamith Cunha, R.; Salamanca, G.; Mille, F.; Delprete, C.; Franciosi, C.; Piva, G.; Gramenzi, A.; Chiochetti, R. Endocannabinoid System Receptors at the Hip and Stifle Joints of Middle-Aged Dogs: A Novel Target for the Therapeutic Use of *Cannabis sativa* Extract in Canine Arthropathies. *Animals* **2023**, *13*, 2833. <https://doi.org/10.3390/ani13182833>

Academic Editor: Elbert Lambooj

Received: 30 June 2023

Revised: 24 July 2023

Accepted: 3 September 2023

Published: 6 September 2023



Copyright: © 2023 by the authors. Licensee MDPI, Basel, Switzerland. This article is an open access article distributed under the terms and conditions of the Creative Commons Attribution (CC BY) license (<https://creativecommons.org/licenses/by/4.0/>).

Abstract: The endocannabinoid system (ECS) has emerged as a potential therapeutic target in veterinary medicine due to its involvement in a wide range of physiological processes including pain, inflammation, immune function, and neurological function. Modulation of the ECS receptors has been shown to have anti-inflammatory, analgesic, and immunomodulatory effects in various animal models of disease, including dogs with osteoarthritis. The goal of this study was to identify and compare the cellular expression and distribution of cannabinoid receptor type 1 (CB1R) and type 2 (CB2R) and the cannabinoid-related G protein-coupled receptor 55 (GPR55) on the synovial cells of hip and stifle joints of seven dogs of different breeds without overt signs of osteoarthritis (OA). The synovial membranes of seven hips and seven stifle joints were harvested post mortem. The expression of the CB1R, CB2R, and GPR55 present in the synovial tissues was investigated using qualitative and quantitative immunofluorescence and Western blot (Wb) analysis. Synoviocytes of the stifle and hip joints expressed CB1R, CB2R, and GPR55 immunoreactivity (IR); no significant differences were observed for each different joint. Cannabinoid receptor 2- and GPR55-IR were also expressed by macrophages, neutrophils, and vascular cells. The ECS receptors were widely expressed by the synovial elements of dogs without overt signs of OA. It suggests that the ECS could be a target for the therapeutic use of *Cannabis sativa* extract in canine arthropathies.

Keywords: cannabinoids; cannabinoid receptor type 1; cannabinoid receptor type 2; G protein-coupled receptor 55

1. Introduction

In recent years, the endocannabinoid system (ECS) has materialised as a possible therapeutic target in veterinary medicine owing to its complicity in a plethora of phys-

iological processes including pain, inflammation, immune function, neurological function, and body homeostasis [1,2]. The ECS consists of the endogenous cannabinoids N-arachidonyl ethanolamine (anandamide; AEA) and 2-arachidonylglycerol (2-AG), receptors, and enzymes which regulate the synthesis and degradation of endocannabinoids. Cannabinoid receptors, namely, cannabinoid receptor 1 (CB1R) and cannabinoid receptor 2 (CB2R), are widely distributed throughout the body, including the central nervous system, immune cells, and other peripheral tissues [3–5]. In addition, cannabinoids (exogenous and endogenous) and other *Cannabis sativa* compounds (terpenes and flavonoids) interact with a diversity of other receptors such as the G protein-coupled receptor 55 (GPR55), G protein-coupled receptor 119 (GPR119), transient receptor potential vanilloid 1 (TRPV1), transient potential receptor vanilloid 4 (TRPV4), and peroxisome proliferator receptor alpha (PPAR α) and gamma (PPAR γ) [6–8].

The endogenous ligands of CB1R and CB2R are AEA and 2-AG, respectively, two endocannabinoids which are produced by the cells “on demand” and play a role in a wide range of physiological and pathophysiological processes [9].

Endocannabinoids and phytocannabinoids, binding to the cannabinoid receptors of the membranes of the neurons, can modulate and inhibit the hyperactivity of primary afferent fibres and decrease the release of neurotransmitters [10].

Both AEA and 2-AG were found in the synovial fluid of osteoarthritic joints of dogs and their contralateral nonaffected joints; as a matter of fact, an increase in 2-AG levels was noted in the stifle joints of arthritic knees when compared to the contralateral joints [11]; the higher concentrations of 2AG in the affected joints may indicate that it plays a role in the pathophysiological process of joint diseases.

Recent studies have shown that the activation of CB1R by minor phytocannabinoids exerts anti-arthritis activity in murine models, highlighting its potential for the treatment of chronic inflammatory diseases such as rheumatoid arthritis (RA) [12]. Similarly, CB2R pharmacological activation in a mouse model of osteoarthritis (OA) showed a protective effect, indicating the potential role of CB2R in the pathogenesis of the disease [13].

G protein-coupled receptor 55, which is currently thought of as the third cannabinoid receptor (CB3R) [14], is a member of the endocannabinoid receptor family; in fact, one of its endogenous ligands is the endocannabinoid neurotransmitter lysophosphatidylinositol [15]. G protein-coupled receptor 55 is implicated in various physiological processes, including bone metabolism and inflammation [16], the regulation of osteoclast and osteoblast functions [17], and the reduction of pain in joint inflammation, indicating a potential therapeutic role for GPR55 in the treatment of joint diseases such as osteoarthritis and RA [18,19]. While the exact role of GPR55 in joint health is still being elucidated, current evidence suggests that it is a promising target for the development of novel therapeutics for joint disorders.

Modulation of the ECS receptors has been shown to have anti-inflammatory, analgesic, and immunomodulatory effects in various animal models of disease, including dogs with OA [20–23]. As such, targeting the ECS might represent a promising approach for the development of safe and effective therapies for a range of veterinary conditions. The ECS plays a crucial role in maintaining joint health and bone metabolism by modulating the activity of immune cells and reducing inflammation in both tissues, with evidence suggesting that it can regulate bone formation and resorption [24,25]. The mRNA and the immunoreactivity for the CB1R, CB2R, and GPR55 have already been described in the synovial membrane of the metacarpophalangeal joints of horses [1].

Understanding and correctly managing musculoskeletal diseases and arthropathies in veterinary patients is of great importance, since articulations can be affected by a diversity of pathologies such as arthritis, osteoarthritis (OA), septic arthritis, synovitis, capsulitis, and ligament rupture [26]. Studies have shown that approximately 20% of dogs will develop some form of joint disease during their lifetime, with an increasing incidence in older dogs; it has been found that in dogs older than 7 years, about 80% of them showed radiographic evidence of osteoarthritis (OA) in at least one joint [27–31]. In addition, a study on a population of dogs aged 10 years or older found that more than 40% of them

had radiographic evidence of hip dysplasia, a common joint disease in dogs [32,33]. Canine hip OA shares anatomical/pathological characteristics with developmental dysplasia of the hip in humans, and therefore, canines have been proposed as the best spontaneous animal model for joint problems [34,35].

These findings emphasised the elevated prevalence of joint diseases in dogs, especially in older dogs [36], and highlighted the importance not only of an early diagnosis, but also effective management in order to improve their quality of life. It is vital to understand the underlying mechanisms of homeostasis of an organism if one wants to develop new drugs and properly use substances already available to manage and treat joint disorders and support healthy joints, thereby delaying the development of arthropathies. Knowledge of the species-specific distribution of the ECS receptors, known by its regulatory function of tissue homeostasis, represents the basic pillar for later clinical trials and novel therapies for each veterinary category of patients.

While there are few and contradictory publications regarding the therapeutic use of cannabinoid molecules [11,21,22] in osteoarthritic dogs, to the best of the authors' knowledge, no literature is available regarding the expression and cellular distribution of cannabinoid receptors at the levels of the joints of canines.

The author's hypothesis is that, similar to other mammalian species, middle-aged dogs will present different cellular distribution of the cannabinoid receptors in the synovial membrane and its adjacent structures, depending on the role each receptor plays in maintaining organic homeostasis. Therefore, the objective of the present study was to identify the expression and distribution of the CB1R, CB2R, and GPR55 at the synovial cells of the hip and stifle joints of dogs without overt signs of OA using qualitative and quantitative immunofluorescence and qualitative Western Blot (Wb) analysis.

2. Materials and Methods

2.1. Animals

The inclusion criteria for the selection of the animals were: animals from 2–15 years of age, male or female of any breed, and no clinical history of joint-related lameness or OA related to the hip and stifle joints. Synovial membrane tissues from the hip and stifle joints were collected post mortem from 7 dogs (3 males and 4 females, from 2 to 15 years of age (10 ± 4 years; average \pm St. Dev.). A dog died from postoperative complications and 6 were euthanised for humane reasons due to different diseases (not involving OA); the patient which suffered from osteosarcoma had pain related to the cancer; the tissues were collected after owner consent was obtained (Table 1).

Table 1. Animals.

Dogs	Breed	Sex	Age (Years)	Cause of Death
#1	Golden retriever	Male, not neutered	9	Euthanasia/osteosarcoma left tibia
#2	Mixed breed	Male, not neutered	15	Euthanasia/mastocytoma
#3	Golden retriever	Female, spayed	9	Euthanasia/leukaemia
#4	English setter	Female, spayed	12	Euthanasia/mastocytoma
#5	Mixed breed	Female, spayed	2	Emergency/amputation of the right hind leg
#6	Mixed breed	Female, spayed	8	Euthanasia
#7	Pit bull terrier	Male, neutered	14	Euthanasia

2.2. Tissue Collection

The synovial membranes of the hip and the stifle joints were analysed for the presence of OA. Macroscopically, the synovial fluid appeared normal in all the patients, and no signs of ischemia, cartilage disease, or bone disease were observed. Samples (~ 1 cm \times 0.5 cm) of the lateral portion of the synovial membrane and synovial capsule from the hip and the stifle joints were harvested using a scalpel post mortem within 1 h of death.

Regarding the immunofluorescence, the tissues were gently pinned on balsa wood with entomological pins (with the synovial membrane face-up), fixed for 24 h at 4 °C in 4% paraformaldehyde in phosphate buffer (0.1 M, pH 7.2), and were subsequently processed to obtain cryosections (14 µm thick) which were later processed for immunofluorescence, as previously described [1]. For the Wb analysis, the tissues were placed in sterilised Eppendorf tubes which were immersed in liquid nitrogen and then stored at −80 °C.

2.3. Immunofluorescence

Hydration of the cryosections in phosphate-buffered saline (PBS) was carried out for immunostaining. The sections were incubated in a solution of 20% normal donkey serum (Colorado Serum Co., Denver, CO, USA), 0.5% Triton X-100 (Sigma-Aldrich, Milan, Italy, Europe), and bovine serum albumin (1%) in PBS for 1 h at room temperature (RT) to block nonspecific binding. The cryosections were incubated overnight in a humid chamber at RT with a mixture of primary antibodies (Table 2) diluted in 1.8% NaCl in 0.01 M PBS of 0.1% sodium azide. Following a wash in PBS (3 × 10 min), the sections were incubated for 1 h at RT in a humid chamber which contained the secondary antibodies (Table 3) diluted in PBS. The cryosections were again washed in PBS (3 × 10 min) and were subsequently mounted in buffered glycerol at pH 8.6 with the fluorescent stain 4',6-diamidino-2-phenylindole—DAPI (Santa Cruz Biotechnology, Santa Cruz, CA, USA), which strongly binds to the adenine–thymine-rich regions of DNA.

Table 2. Primary antibodies used in the study.

Primary Antibody	Host	Code	Dilution	Source
CB1R	Rabbit	Orb10430	1:200	Byorbit
CB2R	Mouse	sc-293188	1:50	Santa Cruz
CB2R	Rabbit	PA1-744	1:250	Thermo Fisher
Calprotectin	Mouse	M0747 Clone MAC387	1:400	Dako
CD31	Mouse	M0823 Clone JC70A	1:30	Dako
GPR55	Rabbit	NB110-55498	1:200	Novus Biol.
IBA1	Goat	NB100-1028	1:80	Novus Biol.
Vimentin	Mouse	IS630 Clone V9	1:600	Dako

Primary antibody suppliers: Alomone, Jerusalem, Israel; Dako Cytomation, Glostrup, Denmark; Biorbyt Ltd., Cambridge, UK; Novus Biologicals, Littleton, CO, USA; Santa Cruz Biotechnology, Dallas, TX, USA; Thermo Fisher Scientific, Waltham, MA, USA.

Table 3. Secondary antibodies used in the study.

Secondary Antibody	Host	Code	Dilution	Source
Anti-goat 594	Donkey	ab150132	1:500	Abcam
Anti-mouse 594	Donkey	A-21203	1:500	Thermo Fisher
Anti-rabbit 488	Donkey	A-21206	1:1000	Thermo Fisher
Anti-rat 594	Donkey	A-21209	1:500	Thermo Fisher

Secondary antibody suppliers: Abcam, Cambridge, UK; Thermo Fisher Scientific, Waltham, MA, USA.

As the receptors studied could have been expressed by different cellular types of the synovial membrane (synoviocytes and immune/inflammatory cells), different primary antibodies were applied in order to identify the intimal fibroblast-like (FLSs) and macrophage-like (MLSs) synoviocytes, subintimal macrophages and neutrophils, and vascular endothelial cells.

To identify the FLS and MLS, the antibodies directed against the fibroblast marker Vimentin and the macrophage/dendritic cell marker ionized calcium binding adapter molecule 1 (IBA1) were used, respectively.

To identify neutrophils, the antibody against calprotectin (MAC387) was used [37,38]. The endothelial cells were identified using the anti-endothelial marker CD31 antibody [39].

2.4. Specificity of the Primary Antibodies

The provider of the anti-CB1R antibody, raised in rabbit against the human CB1R, predicted cross-reactivity with the mouse, rat, and dog antigens. The sequence of canine CB1 protein is homologous (98.3%) to the sequence of human CB1 protein (<https://www.uniprot.org/>, accessed on 30 June 2018) [40]. In addition, the same antibody has been tested by Wb analysis on dog intestinal tissues [4].

In total, 2 anti-CB2 receptor antibodies directed against human CB2R were used in this study. The sequence of canine CB2R is the same (98.3%) as that of the sequence of the human CB2 protein (<https://www.uniprot.org/>). Dog tissues had already been utilised to test the specificity of the mouse anti-CB2 antibody (sc-293188) [37]. Dog tissues had not been used to test the specificity of the rabbit anti-CB2R antibody (PA1-744) using Wb analysis; however, in the current study, a double-staining method was used to colocalise the rabbit anti-CB2R antibody with the mouse anti-CB2R antibody.

The antibody anti-GPR55 receptor was raised against a 17 amino acid synthetic peptide of human GPR55 receptor. The sequence of canine GPR55 protein is homologous (83.5%) to the sequence of human GPR55 protein (<https://www.uniprot.org/>). The antibody provider indicated more (94%) cross-reactivity of this antibody with the canine GPR55 protein. In addition, dog nervous tissues were utilised to test the specificity of this antibody using Wb analysis [39].

In the present study, the specificities of the anti-CB1R, CB2R, and GPR55 antibodies were also tested on canine synovial tissues using Wb analysis (see below).

The anti-IBA1 antibody, which should recognise microglia in the central nervous system and macrophages/dendritic cells in the peripheral tissues [41], was raised in goats and is used against porcine IBA1. The dog IBA1 molecule has a 91.2% identity with the porcine molecule (<https://www.uniprot.org/>).

To identify the neutrophils, an antibody anti-calretinin (clone MAC387) was used [37]. It has recently been shown that this antibody does not recognise macrophages in canine tissues; however, it recognises neutrophils rather exclusively [37,38].

The antibody directed against the endothelial marker CD31 had already been used in dog tissues [39]. The antibody against vimentin had already been tested on canine tissues using Wb analysis [42].

2.5. Specificity of the Secondary Antibodies

The specificity of the secondary antibodies was tested by applying them after omission of the primary antibodies. No stained cells or protein bands were detected after omitting the primary antibodies.

2.6. Quantitative Analysis

Quantitative analysis of the intensity of the expression of CB1R, CB2R, and GPR55 in the synovial intimal layer was carried out on 7 dogs. For each animal, and each receptor, 3 randomly selected images of the synovial membrane (50 μm -thick and 100 μm wide; 5000 μm^2 area) were acquired at high magnification ($\times 40$) using the same exposure time for all the images. ImageJ software (Image J, version 1.52t, National Institutes of Health, Bethesda, MD, USA) was used to analyse the signal intensity of each image; standardised thresholds were calculated empirically for brightness and contrast and were then applied to all images. The Color Histogram (gMEAN or rMEAN) tool of the software ImageJ (Image J, version 1.52t, National Institutes of Health, Bethesda, MD, USA) was then used to obtain the signal intensity.

Quantitative analysis of the number of cell layers of the synovial membrane and the cell density was carried out on 3 randomly selected areas (50 μm -thick and 100 μm wide; 5000 μm^2 area); they were acquired at high magnification ($\times 40$) on 3 randomly selected images of the synovial membrane of the hip and of the stifle joint for each animal using a DAPI signal to stain the cell nuclei.

2.7. Statistical Methods

For each receptor, the mean of the 3 values/case of signal intensity in the 7 dogs was evaluated and compared. Statistical analysis was carried out using GraphPad Prism software (version 8.3, La Jolla, CA, USA). The normality distribution of the data was assessed using the Shapiro–Wilk test.

Comparisons between groups (receptors) within the same joint were carried out using the one-way ANOVA Tukey's multiple comparisons test. A p -value ≤ 0.05 was considered significant.

Comparisons between groups (receptors) within the same joint and the 2 different joints were carried out using two-way ANOVA Tukey's multiple comparisons test. A p -value ≤ 0.05 was considered significant.

Comparisons between the mean of each receptor at the 2 different joints were carried out using the Wilcoxon test and the paired t -test. A p -value ≤ 0.05 was considered significant.

Comparisons between the numbers of cell layers of the different joints were carried out using the Wilcoxon Test (nonparametric) and the paired t -test (parametric). A p -value ≤ 0.05 was considered significant.

Comparisons between the cell density of the different joints were carried out using the Wilcoxon Test (nonparametric) and the Paired t -test (parametric). A p -value ≤ 0.05 was considered significant.

Correlations between the number of layers of the synovial membrane and the density of the cells in the hip joint and stifle joint were carried out using the Pearson correlation test. A p -value ≤ 0.05 was considered significant.

2.8. Fluorescence Microscopy

The preparations were examined using a Nikon Eclipse Ni microscope equipped with the appropriate filter cubes to differentiate the fluorochromes utilised for differentiating between Alexa 488 and Alexa 594 fluorescence. The filter was set at 10 for the Alexa 488 (450–490 nm excitation filter and 515–565 nm emission filter) and the filter was set at 00 for Alexa 594 (530–585 nm excitation filter and 615 nm emission filter).

A Nikon DS-Qi1Nc digital camera and NIS Elements software Version 4.20.01 BR (Nikon Instruments Europe BV, Amsterdam, The Netherlands) were used to record the images. The same fluorochrome label was used for the 3 receptors, allowing for quantification. Corel Photo Paint was used to slightly adjust the contrast and brightness, whereas Corel Draw (Corel Photo Paint and Corel Draw, Ottawa, ON, Canada) was used to prepare the figure panels.

2.9. Western Blot

Tissue samples (hip and stifle synovial membranes) were collected from 3 dogs, frozen in liquid nitrogen, and stored at -80°C until sample processing. An amount of 50 mg of tissue was fractionated into small pieces and homogenised in 500 μL of RIPA buffer (50 mM TRIS-HCl, pH 7.4, 100 mM NaCl, 1 mM PMSF, 1 mM EDTA, 5 mM Iodacetamide 1% Triton X-100, 0.5% sodium dodecylsulphate) supplemented with a protease inhibitor cocktail (Sigma-Aldrich, Co, St. Louis, MO, USA). The extract was sonicated for 10 min at 20 s intervals every 2 min and pelleted for 20 min at 14,000 rpm. Total protein content was determined by Bradford method. Proteins (10 μg) were separated by 10–12% SDS–polyacrylamide gel and transferred to a PVDF membrane. After transfer, the membrane was blocked by 5% milk powder in PBST (PBS 0.01 M, pH 7.4) with 0.05% Tween 20 (Sigma-Aldrich, St. Louis, MO, USA) for 1 h at room temperature (RT). The membranes were incubated with primary antibodies (rabbit anti-CB1R, Orb10430; mouse anti-CB2R, Santa Cruz #sc293188; rabbit anti-GPR55, NB11055498) overnight at 4°C , diluted 1:1000 in PBST 0.1% containing 1% milk. The following day, the membranes were rinsed 3 times with PBST, each for 15 min, and IgG horseradish peroxidase-conjugated secondary antibodies anti-rabbit (1:5000, Santa Cruz) and anti-mouse (1:5000, Sigma) were employed for incubation in 1% milk powder in PBST for 2 h at RT. After washout of secondary-HRP binding

antibody, membrane was incubated with chemiluminescence substrate and developed with the enhancing chemiluminescence detection system (Santa Cruz Biotechnology or Cyanagen–Westar ηC ultra 2.0). Blots were visualised with the ChemiDoc™ (Bio-Rad) imaging system.

3. Results

3.1. Western Blot Analysis

To determine whether the canine synovial membrane expresses proteins for CB1R, CB2R, and GPR55, Western blot analysis was performed. The present results showed that the anti-CB1R antibody revealed a band of 70 kDa, while the anti-CB2R antibody revealed a band of 55 kDa (Figure 1). The authors have recently demonstrated that anti-CB1R and anti-CB2R in the canine small intestine recognised slightly different bands; however, it should be emphasised that the present results in the canine synovial membrane were aligned with previous reports regarding the detection of CB1R (molecular weight between 35 and ~70 kDa) and CB2R (molecular weight of ~35 and ~60 kDa) using Western blot analysis [43–46]. The anti-GPR55 antibody recognised a major band around 35 kDa and its dimer at 70 kDa, as previously described [4,39], in the canine gastrointestinal tract (Figure 1, right panel). Negative controls, in which the primary antibodies were not involved in the incubation with the membrane, did not show bands (left panel).

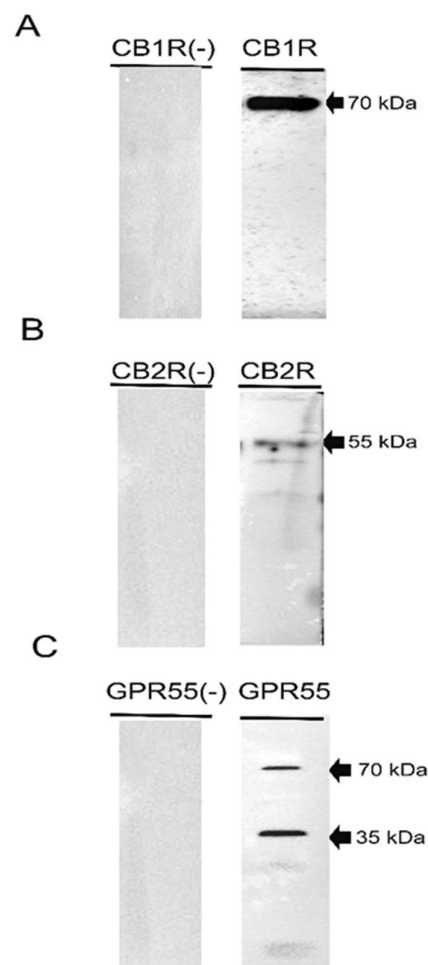


Figure 1. Representative image of Western blot analysis showing the specificity of the primary antibodies utilised (right panel): rabbit anti-cannabinoid receptor 1 (A), mouse anti-cannabinoid receptor 2 (B), and rabbit anti-G protein-coupled receptor 55 (GPR55) (C). Negative controls, in which the primary antibodies were not involved in the incubation with the membrane, did not show bands (left panel).

The expression of CB1R, CB2R, and GPR55 in the canine synovial membrane was also confirmed on the protein level.

3.2. Immunofluorescence

Vimentin and IBA1 Immunoreactivity

A subset of cells lining the synovial membrane, i.e., FLSs, displayed prominent cytoplasmic vimentin immunoreactivity (vimentin-IR) in the hip and stifle joints (Figure 2a–c). In both joints, the FLSs were characterised by fusiform rounded nuclei and elongated, slender cytoplasmic processes. However, in the stifle, these cytoplasmic processes extended vertically toward the joint cavity within the different layers of the FLSs whereas, in the hip, the processes primarily extended horizontally.

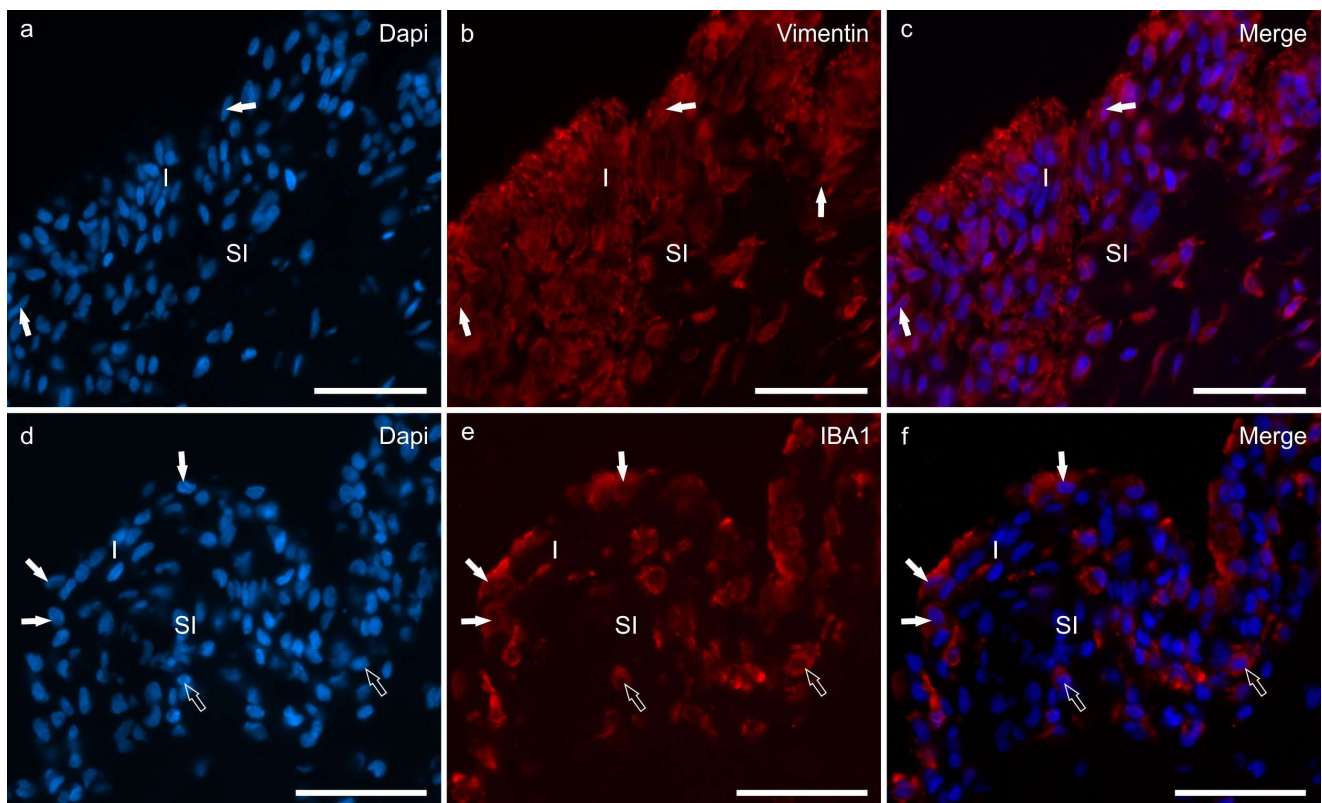


Figure 2. Photomicrographs of cryosections of the synovial membrane of the stifle joints of dogs showing immunoreactivity for the fibroblast marker vimentin (b) and the macrophage marker IBA1 (e). (a–c) The synovial membrane of the stifle joint showed different layers of synoviocytes (arrows) which expressed moderate-to-bright vimentin immunoreactivity (b). (d–f) Three macrophage-like synoviocytes lining the joint cavity, expressing bright IBA1 immunoreactivity, are indicated by the white arrows (e). The subintimal macrophages (open arrows) also expressed IBA1 immunoreactivity. Abbreviations: I, intima; SI, subintima. Bar: 50 μ m.

Macrophage-like synoviocytes and subintimal macrophages expressed IBA1-IR; MLSs showed rounded nuclei and abundant cytoplasm (Figure 2d–f).

3.3. CB1R Immunoreactivity

Faint CB1R-IR was detected by the cytoplasm of the hip and stifle FLSs and MLSs. The CB1R-IR was detectable in seven of seven dogs (100%) and at both joints of the same dog (Figure 3a–f). Colocalisation studies showed that synoviocytes at both joints coexpressed CB1R and CB2R (Figure 3g–i). In some sections in which a small fragment of articular cartilage was present, it was possible to observe that the chondrocytes expressed moderate CB1R-IR.

Cannabinoid receptor 1 immunoreactivity was not expressed by the neutrophils or the endothelial cells either in the hip or in the stifle joints.

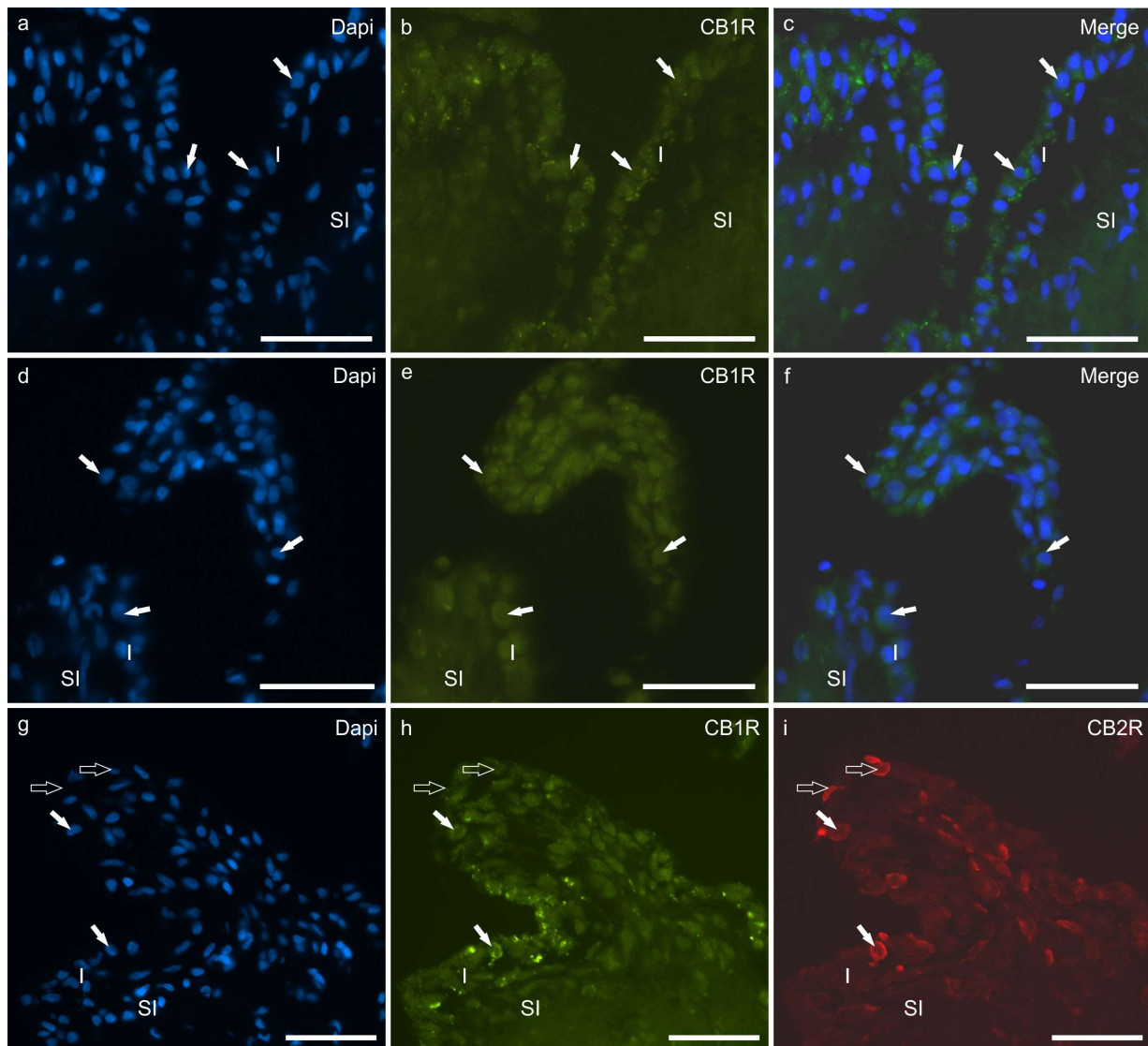


Figure 3. (a–f) Photomicrographs of cryosections of the synovial membrane of the hip (a–c) and stifle (d–f) joints of dogs showing immunoreactivity for the cannabinoid receptor type 1 (CB1R). The arrows indicate some synoviocytes showing faint CB1R immunoreactivity. (g–i) Photomicrographs of cryosections of the synovial membrane of the stifle joint of dog showing colocalisation between two antibodies directed against the cannabinoid receptor type 1 (CB1R) (h) and the cannabinoid receptor type 2 (CB2R) (i). The white arrows indicate two synoviocytes coexpressing CB1R and CB2R immunoreactivity. The open arrows indicate two synoviocytes which were immunoreactive only for the CB2R. Abbreviations: I, intima; SI, subintima. Bar: 50 µm.

3.4. CB2R Immunoreactivity

A double-staining method was used to colocalise the rabbit anti-CB2R antibody with the mouse anti-CB2R antibody; both anti-CB2R antibodies were colocalised in the same synoviocytes and blood vessel cells (Figure 4a–d).

Moderate-to-bright CB2R-IR was detected by the cytoplasm of the hip and the stifle synoviocytes in seven of seven dogs (100%) by using both the anti-CB2R antibodies (from mouse and rabbit) (Figure 4a–e). Colocalisation studies showed that CB2R-IR was expressed by vimentin immunoreactive FLSs and IBA1 immunoreactive MLSs in both joints (Figure 4e–l).

Cannabinoid 2 receptor immunoreactivity was moderately expressed by MAC387-positive neutrophils (Figure 4m–p), CD31-positive endothelial cells (Figure 4m–p), and unidentified immune/inflammatory cells.

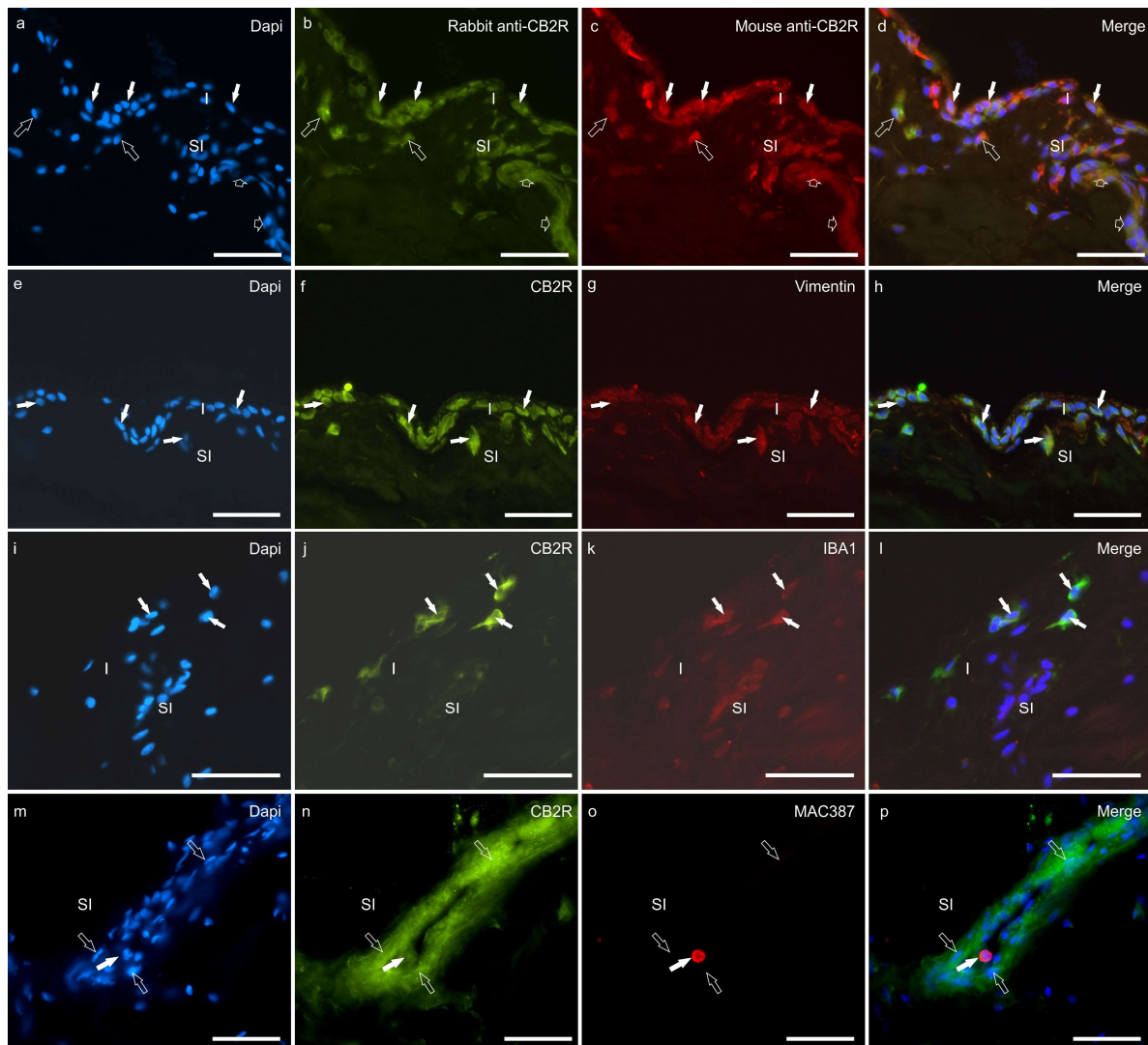


Figure 4. (a–d) Photomicrographs of cryosections of the hip synovial membrane of a dog showing colocalisation between two different antibodies directed against cannabinoid receptor 2 (CB2R). The white arrows indicate synoviocytes identified with the mouse anti-CB2R (b) and the rabbit anti-CB2R (c). The open arrows indicate two subintimal cells (likely inflammatory/immune cells) identified with both the anti-CB2R antibodies. The small open arrows indicate a subintimal capillary showing CB2R immunoreactivity. (e–h) Photomicrographs of cryosections of the synovial membrane of the hip (e–h) and stifle (i–l) joints of dogs showing immunoreactivity for the fibroblast marker vimentin (e–h) and the macrophage marker IBA1 (i–l). (e–h) The arrows indicate synoviocytes which showed bright cannabinoid receptor type 2 (CB2R) (f) immunoreactivity and moderate vimentin immunoreactivity (g). (i–l) The arrows indicate three macrophage-like synoviocytes which coexpressed bright CB2R immunoreactivity (j) and moderate IBA1 immunoreactivity (k). (m–p) Photomicrographs of cryosections of the synovial membrane of the stifle joint of a dog showing immunoreactivity for the cannabinoid receptor type 2 (CB2R) (n) and the neutrophils marker MAC387 (o). The open arrows indicate some endothelial cells of a subintimal blood vessel expressing bright CB2R immunoreactivity. The white arrow indicates one neutrophil inside the blood vessel coexpressing bright MAC387 and moderate CB2R immunoreactivity. Abbreviations: I, intima; SI, subintima. Bar: 50 μ m.

3.5. GPR55 Immunoreactivity

Moderate-to-bright GPR55-IR was expressed by the cytoplasm of the hip and the stifle synoviocytes in seven of seven dogs (100%). Colocalisation studies showed that the vimentin immunoreactive FLSs and the IBA1 immunoreactive MLSs expressed GPR55-IR at both joints (Figure 5a–l).

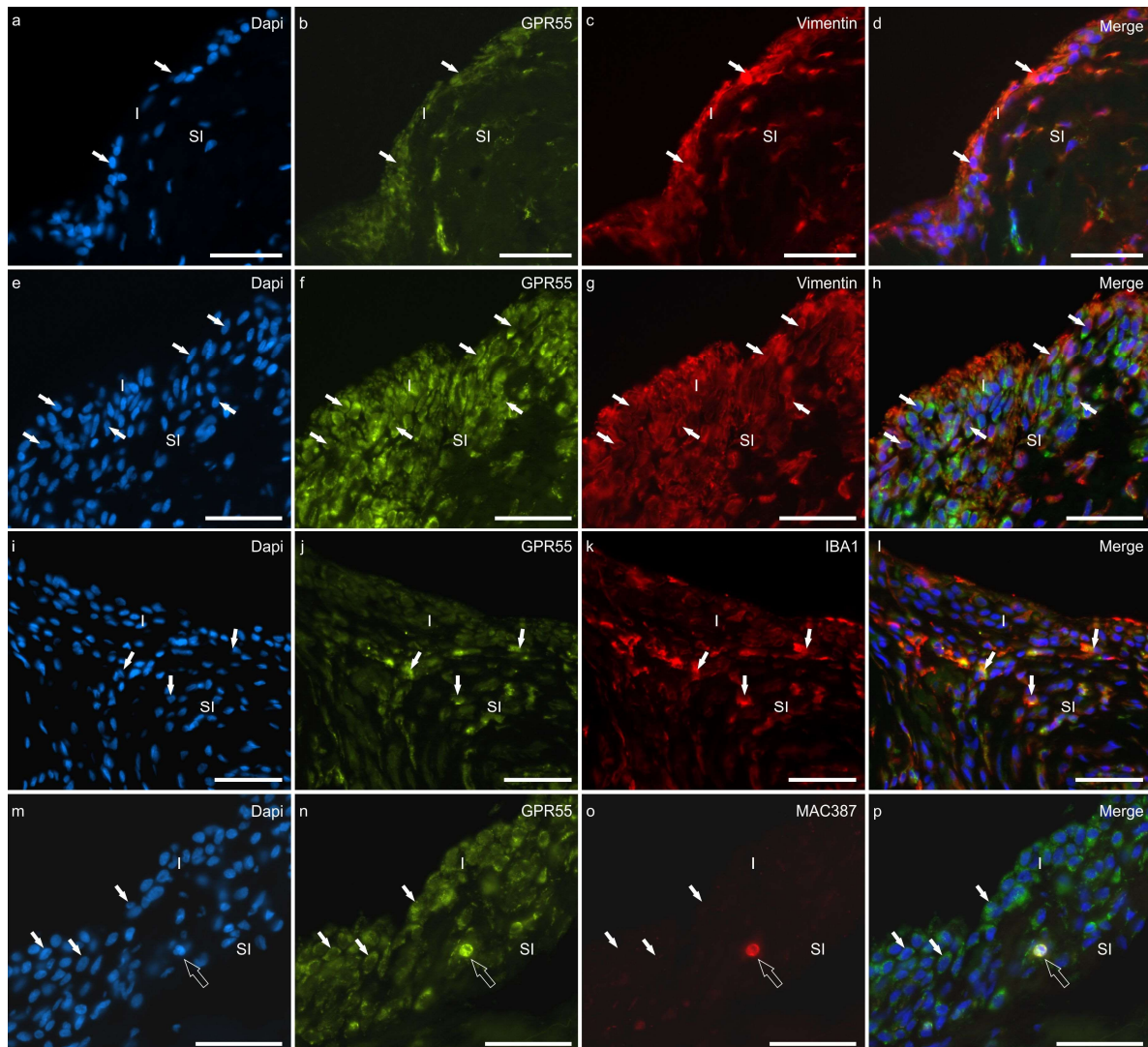


Figure 5. Photomicrographs of cryosections of the synovial membrane of the hip (a–d) and stifle (e–p) joints of dogs showing colocalisations of the antibody anti-G protein-coupled receptor 55 (GPR55) with the antibodies directed against the fibroblast marker vimentin (a–h), the macrophage marker IBA1 (i–l), and the neutrophils marker MAC387 (m–p). (a–h) the arrows indicate some synoviocytes (fibroblast-like synoviocytes) which were immunoreactive for GPR55 and vimentin. The different thicknesses of the epithelium lining the joint cavity of the hip (a–d) and stifle (e–h) joints (stifle > hip) should be noted. (i–l) The arrows indicate some macrophage-like synoviocytes which coexpressed GPR55 and IBA1 immunoreactivity. Given that the cut of the synovial membrane does not appear perfectly orthogonal, it cannot, however, be excluded that some IBA1 immunoreactive R cells are subintimal macrophages. (m–p) The white arrows indicate some synoviocytes expressing GPR55 immunoreactivity. The open arrow indicates one subintimal neutrophil, with a dapi-labelled polilobated nuclei, coexpressing GPR55 and MAC387 immunoreactivity. Abbreviations: I, intima; SI, subintima. Bar: 50 μ m.

G-coupled protein receptor 55 was also brightly expressed by MAC387-positive neutrophils (Figure 5m–p), CD31-positive endothelial cells (Figure S1), unidentified immune/inflammatory cells, and chondroblasts.

There were no differences regarding the cellular distribution of the CB1R, CB2R, and GPR55 immunofluorescence at the stifle and hip joint elements.

3.6. Quantitative and Comparative Analysis of CB1R, CB2R, and GPR55 Immunoreactivity by the Synoviocytes

Quantitative analysis showed that there was less expression of CB1R, in comparison with CB2R ($\sim p$ values of 0.0014 and 0.0020 for the stifle joints and the hips, respectively) and GPR55-IR ($\sim p$ values of 0.00002 and 0.0001 for the stifle joints and the hips, respectively), in both the hip and the stifle joints of dogs without overt signs of OA.

Quantitative analysis also showed that the expression of CB2R-IR was statistically greater when compared with that of CB1R-IR ($\sim p$ values of 0.0014 and 0.0020 for the stifle joints and the hips, respectively), but not statistically different when compared with that of GPR55-IR ($\sim p$ values of 0.5655 and 0.2444 for the stifle joints and the hips, respectively).

Analogously, the analysis of the expression of GPR55-IR showed that it was statistically greater when compared with CB1R ($\sim p$ values of 0.0002 and 0.0001 for the stifle joints and the hips, respectively), but not statistically different when compared with CB2R ($\sim p$ values of 0.5655 and 0.2444 for the stifle joints and the hips, respectively) (Figure 6).

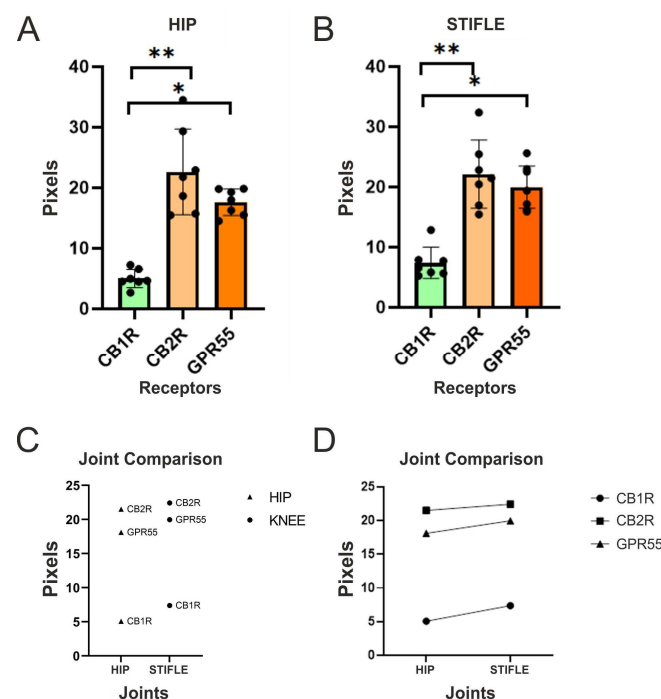


Figure 6. (A,B) Quantitative analysis of the hip (A) and stifle joint (B) using one-way ANOVA showed that the expression of CB2R-IR (**) was statistically different when compared with that of CB1R-IR, but not when compared with that of GPR55-IR. Analogously, the analysis of the expression of GPR55-IR showed that it is statistically different when compared with CB1R (*), but not with CB2R, at both joint sites. (C) To additionally examine the differences between the receptors, a Tukey's multiple comparisons test was carried out. The results showed that the mean difference in expression between CB1R and CB2R was significant (mean diff = -16.19 , $p < 0.0001$). Similarly, the mean difference between CB1R and the GPR55 was also significant (mean diff = -12.58 , $p < 0.0001$). However, there was no significant difference in expression between CB2R and GPR55 (mean diff = 3.603 , $p = 0.1413$, at both joints). (D) The statistical analysis carried out showed that there was no significant difference between the receptor expression of the different joints. In both the hip and the stifle joints, the receptors followed the same pattern of cellular distribution and expression (scatter dot plot with mean and SD).

The cellular expression of CB1R, CB2R, and GPR55 in the synoviocytes of the hip and the stifle joints of dogs was additionally analysed using other statistical tests which indicated that there was no significant difference in the cellular expression of CB1R, CB2R, and GPR55 between the stifle and hip joints of dogs (Figure 7).

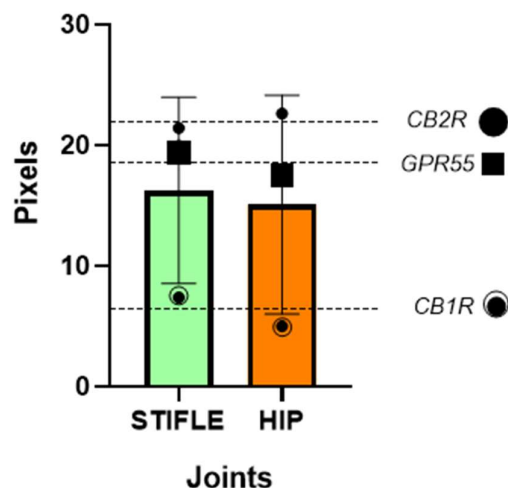


Figure 7. The Wilcoxon signed-rank test was carried out to assess the differences in expression between the mean of hip and stifle joints mean of each receptor. The Wilcoxon test results showed that the differences between joint were not statistically significant, with p -values of 0.2500 for both receptors (scatter dot plot with mean and SD).

The expression levels of CB1R, CB2R, and GPR55 in the synoviocytes of the stifle and the hip joints in dogs were analysed using two-way ANOVA. The significance level (alpha) was set at 0.05. The ANOVA results indicated that neither the interaction between the row factor (dogs) and the column factor (joints), nor the individual factors, had a significant effect on the expression levels of the receptors and was not statistically significant ($p = 0.9015$), suggesting that the differences in expression across the dogs were not influenced by the joint type.

In summary, the two-way ANOVA results suggested that there were no significant differences in the expression levels of CB1R, CB2R, and GPR55 between the stifle and the hip joints of dogs. The lack of significant interactions and individual effects of dogs and joints indicated that the variation in receptor expression was not dependent on these factors. However, it is important to note that the difference in mean expression between the hip and the stifle joints was small and not statistically significant.

4. Discussion

The discoveries regarding the ECS receptors evidenced their important regulatory role in organic homeostasis and their involvement in several pathophysiological processes; the clinical and scientific demand is currently growing with respect to how best to use them as a therapeutic target. For this, one needs to first identify the presence or not of the ECS components in the organ of the pathology of interest.

Currently, the definition of the ECS is expanding to include other cannabinoid-related receptors [47,48]. This is the case, for example, for the GPR55, TRPV1, and nuclear PPAR α , all of which are currently considered to be possible cannabinoid receptors [4].

Cannabinoid receptors are widely expressed through different cellular types of the organism; their distribution will be different depending on the organ and cell-type of interest [9]. Within the canine species, the expression of the CB1R, CB2R, and GPR55 was shown at the central nervous system (CNS) and the peripheral nervous system (PNS) [39,49,50], at the skin [37], and at the gastrointestinal tract [4]. Furthermore, the authors' group recently showed the expression of cannabinoid and cannabinoid-related receptors at the synovio-

cytes (FLSs and MLSs) of horses [1], in which the mRNA and the immunoreactivity of CB1R was found in the synoviocytes of some but not all the subjects. The findings of the present study showed an important species-related particularity. In the equine species, only 71% of the equines expressed the CB1R by the synovial cells [1]; on the contrary, in the canine species, 100% of the dogs expressed the CB1R by the synoviocytes.

Although the exact factors which will regulate the ECS tone expression of the receptors related to species are still unknown, knowing the difference will reflect directly on the therapeutic choice for each veterinary patient. Moreover, the immunohistochemical expression of CB1R has been shown at the synovial membrane of all cats both with healthy joints and with degenerative joint disease [51]—and its upregulation was directly correlated to the degree of severity of the disease. Comparatively, the expression of CB1R is upregulated at the joint level in horses with synovitis [52,53]. Pointing to the role of CB1R in keeping a healthy joint environment, as well as its involvement within the pathogenesis of joint inflammation and its potential as a therapeutic target, new information regarding the moderate expression of CB1R by the synoviocytes and chondroblasts of dogs suggests a potential role in modulating pain and inflammation in joint tissue within canine species.

Although the use of the most known agonist molecule of the CB1R (Δ^9 -Tetrahydrocannabinol—THC) is still controversial, science can no longer deny the evidence of its use as a therapy for many pathologies. In a recently published study, Lowin et al. [54] were able to show the biphasic effects of THC on synovial fibroblasts from human patients with rheumatoid arthritis (synovial fibroblasts of rheumatoid arthritis—RASf) and peripheral blood mononuclear cells (PBMC) from healthy donors; THC provides proinflammatory and anti-inflammatory effects on the RASf and the PBMC. The effectiveness of THC in treating inflammation pertaining to rheumatoid arthritis may vary depending on the activating stimulus and the THC concentration. Therefore, it is important to titrate THC dosage to determine the therapeutic window.

Other minor phytocannabinoids also seem to exert therapeutic effects by means of CB1R modulation. Palomares et al. [12] showed that Δ^9 -Tetrahydrocannabinolic acid (Δ^9 -THCA-A), the precursor of Δ^9 -THC, can act as an orthosteric CB1R agonist; in vivo, Δ^9 -THCA-A reduced arthritis in collagen-induced arthritic mice, preventing the infiltration of inflammatory cells, synovium hyperplasia, and cartilage damage. Furthermore, Δ^9 -THCA-A inhibited the expression of inflammatory and catabolic genes on stifle joints; Δ^9 -THCA-A exerts anti-arthritis activity through the CB1R pathways, highlighting its potential in the treatment of chronic inflammatory diseases such as RA.

In the current study, the FLSs showed moderate/bright CB1R immunostaining, and only a few MLSs showed weak CB1R-IR. The authors' hypothesis was that the CB1R pathway was directly involved in maintaining the structural integrity and physical barrier of the synovial membrane as well as regulating the synthesis of the synovial fluid. Therefore, one can reduce the inflammatory and degenerative synovium response by means of CB1R modulation [12,54]. The acquisition of this piece of information will directly determine the clinician's therapeutic choice and positively change the case outcome. Molecule agonists of the CB1R would provide benefits for patients suffering from inflammatory joint disease directly at the pathological site, slowing the disease evolution and supporting the maintenance of a healthy synovial environment. However, more in vitro species-specific studies and clinical trials are needed.

Cannabinoid receptor 2 has already been identified in the synovium cells of mice [55], rats, humans [56,57], and horses [1]. In the present study, the FLSs, the MLSs, and the macrophage/dendritic cell antigen-presenters exhibited an elevated expression of CB2R. Furthermore, it was found that the FLSs coexpressed CB1R and CB2R, while the dendritic cells expressing CB1R also expressed CB2R. This indicates that synovial cells expressing CB1R also expressed CB2R, whereas not all the CB2R-expressing synovial cells expressed the CB1R. Notably, this difference in expression was more pronounced among the MLSs, which reinforced the role of the CB2R, rather than the CB1R, in regulating immune response.

Inflammatory processes within the stifle joint can alter the composition of the cruciate ligaments [58], and patients with a cruciate ligament rupture will have a higher density of macrophages and MLSs at the joint infiltrate and synovium [59]. By means of the CB2R pathways, one can regulate macrophage signalling and proinflammatory cytokine release; thus, as a result of the strong immunolabeling of MLSs and dendritic cells for the CB2R at the synovium of dogs, one could postulate that modulating its activity could benefit patients suffering from inflammatory degenerative joint diseases, specifically immune mediated diseases. In addition to cannabinoids, other compounds of the cannabis plant can interact with the CB2R, such as terpenes and β -Caryophyllene [60].

G protein-coupled receptor 55 is a relatively new and poorly understood cannabinoid receptor. It has been identified in a variety of cell types including sensory neurons, inflammatory cells, and bone cells [17]. Recent studies have shown that GPR55 is expressed in the synovial cells of horses [1], T cells and neutrophils of dogs [37], and chondrocytes of humans [61] and may play a role in regulating inflammation and immune response in joint tissue. In vitro studies have shown that activation of GPR55 in synoviocytes can increase the production of proinflammatory cytokines, such as Interleukin-6 (IL-6) and IL-8, which are associated with the pathogenesis of RA [54].

Neutrophils are important immune cells which infiltrate the synovium during inflammation [62]. Healthy joints are not expected to have an elevated presence of neutrophils; in the current study, very few neutrophils, scattered in the subintima of the synovial membranes, expressed cytoplasmatic GPR55-IR. Neutrophils in the synovial fluid of human patients with RA have been shown to express GPR55; its activation can induce neutrophil chemotaxis which can contribute to joint inflammation and damage in RA [63].

In the present study, FLSs, MLSs, and neutrophils (and chondrocytes) demonstrated GPR55-IR; these findings suggested that GPR55 may play a role in regulating synovial inflammation and joint destruction in inflammatory degenerative joint disease. Cannabidiol, being a GPR55 antagonist, may play a role in reducing the secretion of proinflammatory cytokines and in immune and inflammatory cell migration.

Minor cannabinoids, such as cannabigerol (CBG), Δ^9 -Tetrahydrocannabivarin (THCV), and cannabidivarin (CBDV), have been found to interact with GPR55 [64]. Δ^9 -Tetrahydrocannabivarin, a partial agonist of GPR55, is capable of inhibiting the activity of the full agonist lysophosphatidylinositol (LPI); CBG has also been shown to weakly inhibit the LPI response in GPR55 assays [65]. Another study found that CBD and other GPR55 antagonists can inhibit bone resorption in vivo; additionally, GPR55 ligands affect osteoclast formation in vitro, suggesting a potential therapeutic role for CBD and minor cannabinoids in bone disorders [17,66].

Chondroblasts are cells which produce and maintain the extracellular matrix of cartilage. G protein-coupled receptor 55 expression has been detected in human chondrocytes [67], and studies have shown that the activation of GPR55 in chondrocytes can induce the production of matrix metalloproteinases (MMPs), which are enzymes that degrade the extracellular matrix and contribute to cartilage destruction in arthritis [17]. Therefore, targeting GPR55 in chondrocytes may represent a potential therapeutic approach for slowing down cartilage destruction in dogs with arthritis, thus enhancing the welfare of older dogs, those most affected by spontaneous OA, using a molecular antagonist such as CBD.

Although there was no macroscopic or microscopic evidence of OA development or a history of lameness in the animals included in the small sample size of the present study, it is crucial to note that the median age of the animals was 10 years. This represented an important number of canine patients which could potentially be undergoing early development of OA or be suffering from subclinical OA, as age-related involution in dogs involves the loss of muscle mass and changes in the connective tissue and articular cartilage [36,68]. By discovering the cellular expression pattern of the ECS receptors in the joints of animals in this age group, one could speculate that it could be used as a target to treat and prevent the development of arthropathies in patients with elevated risk for the development of the disease.

The fact that no significant difference was found in the cellular distribution and expression of CB1R, CB2R, and GPR55 between hip and stifle joints without overt signs of OA is important in understanding the patterns of the ECS in these joints and in the organism. Understanding the patterns of the ECS in joints of mostly aged dogs provides a foundation for exploring its potential therapeutic applications in arthropathy treatment. Modulating the ECS using cannabinoid-based therapies or other approaches may offer promising avenues to alleviate pain and reduce inflammation in affected joints.

By recognising the similarities in the expression of CB1R, CB2R, and GPR55 in both the hip and the stifle joints of individuals without overt signs of OA, researchers and veterinarians can focus on developing targeted interventions which harness the ECS to restore joint health. Furthermore, the virtually slight (not statistically significant) difference in the mean expression of each receptor between the hip and the stifle joints was due to the different structure of each joint, as the stifle synovial membrane was shown to be composed of more cell layers than that of the hip joint; therefore, there are more cells to be analysed in the same area.

The results of the CB1R, CB2R, and GPR55 codistribution and coexpression within different cell types at different joint environments suggested that these receptors played a role in regulating inflammation and immune response in joint tissue and points to the complexity of the ECS. Additional research is warranted to fully elucidate the specific roles and interactions of the ECS receptors in joint health and disease, enabling the development of more effective and tailored treatment strategies for arthropathies in dogs.

5. Conclusions

The discovery of cannabinoid receptors (CB1R, CB2R, GPR55) in the synovial tissue of middle-aged dogs provides compelling molecular evidence supporting the use of cannabinoids for treating and delaying joint diseases. This breakthrough suggests the potential for developing the therapeutic agonists/antagonists targeting these receptors. Understanding the cellular expression of CB1R, CB2R, and GPR55 allows us to comprehend the role of the ECS in modulating inflammation, pain, and immune responses in canine synovia. This knowledge opens avenues for novel interventions utilising the ECS to maintain and enhance joint health and well-being in dogs.

Supplementary Materials: The following supporting information can be downloaded at: <https://www.mdpi.com/article/10.3390/ani13182833/s1>, Figure S1. Colocalisation between the anti-GPR55 and anti-CD31 antibodies in the synovial membrane of the stifle joint of a dog.

Author Contributions: R.Z.C., R.C., A.G. and G.P. contributed to the study design. Acquisition of data: R.C. and R.Z.C. R.Z.C., F.M. and G.S. carried out the immunohistochemical experiments. C.D. and C.F. carried out the Western blot experiments. All authors interpreted the data. Drafting of the manuscript: R.Z.C. and R.C. All authors have read and agreed to the published version of the manuscript.

Funding: This study received funding from NBF Lanes, Milan.

Institutional Review Board Statement: Ethical review and approval were not required as, according to Directive 2010/63/EU of the European Parliament and of the Council of 22 September 2010 regarding the protection of animals used for scientific purposes, Italian legislation (D. Lgs. n. 26/2014) did not require any approval by competent authorities or ethics committees as this study did not influence any therapeutic decisions.

Informed Consent Statement: Informed consent was obtained from the owners of all the dogs included in the study.

Data Availability Statement: The data presented in this study are available on request from the corresponding author.

Acknowledgments: The excellent technical assistance of Sara Del Magno and Veronica Cola is gratefully acknowledged.

Conflicts of Interest: The authors declare no conflict of interest.

References

1. Zamith Cunha, R.; Zannoni, A.; Salamanca, G.; De Silva, M.; Rinnovati, R.; Gramenzi, A.; Forni, M.; Chiocchetti, R. Expression of Cannabinoid (CB1 and CB2) and Cannabinoid-Related Receptors (TRPV1, GPR55, and PPAR α) in the Synovial Membrane of the Horse Metacarpophalangeal Joint. *Front. Vet. Sci.* **2023**, *10*, 1045030. [\[CrossRef\]](#) [\[PubMed\]](#)
2. Osafo, N.; Yeboah, O.K.; Antwi, A.O. Endocannabinoid System and Its Modulation of Brain, Gut, Joint and Skin Inflammation. *Mol. Biol. Rep.* **2021**, *48*, 3665–3680. [\[CrossRef\]](#) [\[PubMed\]](#)
3. Barrie, N.; Kuruppu, V.; Manolios, E.; Ali, M.; Moghaddam, M.; Manolios, N. Endocannabinoids in Arthritis: Current Views and Perspective. *Int. J. Rheum. Dis.* **2017**, *20*, 789–797. [\[CrossRef\]](#) [\[PubMed\]](#)
4. Galiazzo, G.; Giancola, F.; Stanzani, A.; Fracassi, F.; Bernardini, C.; Forni, M.; Pietra, M.; Chiocchetti, R. Localization of Cannabinoid Receptors CB1, CB2, GPR55, and PPAR α in the Canine Gastrointestinal Tract. *Histochem. Cell Biol.* **2018**, *150*, 187–205. [\[CrossRef\]](#)
5. Tam, J. The Emerging Role of the Endocannabinoid System in the Pathogenesis and Treatment of Kidney Diseases. *J. Basic Clin. Physiol. Pharmacol.* **2016**, *27*, 267–276. [\[CrossRef\]](#)
6. De Petrocellis, L.; Orlando, P.; Moriello, A.S.; Aviello, G.; Stott, C.; Izzo, A.A.; Di Marzo, V. Cannabinoid Actions at TRPV Channels: Effects on TRPV3 and TRPV4 and Their Potential Relevance to Gastrointestinal Inflammation. *Acta Physiol.* **2012**, *204*, 255–266. [\[CrossRef\]](#)
7. Hu, F.; Hui, Z.; Wei, W.; Yang, J.; Chen, Z.; Guo, B.; Xing, F.; Zhang, X.; Pan, L.; Xu, J. Hypotonic Stress Promotes ATP Release, Reactive Oxygen Species Production and Cell Proliferation via TRPV4 Activation in Rheumatoid Arthritis Rat Synovial Fibroblasts. *Biochem. Biophys. Res. Commun.* **2017**, *486*, 108–115. [\[CrossRef\]](#)
8. Muller, C.; Morales, P.; Reggio, P.H. Cannabinoid Ligands Targeting TRP Channels. *Front. Mol. Neurosci.* **2019**, *11*, 487. [\[CrossRef\]](#)
9. Pertwee, R.G.; Howlett, A.C.; Abood, M.E.; Alexander, S.P.H.; Marzo, V.D.; Elphick, M.R.; Greasley, P.J.; Hansen, H.S.; Kunos, G.; Mackie, K.; et al. International Union of Basic and Clinical Pharmacology. LXXIX. Cannabinoid Receptors and Their Ligands: Beyond CB1 and CB2. *Pharmacol. Rev.* **2010**, *62*, 588–631. [\[CrossRef\]](#)
10. Rea, K.; Roche, M.; Finn, D.P. Supraspinal Modulation of Pain by Cannabinoids: The Role of GABA and Glutamate: GABA and Glutamate in Cannabinoid-Mediated Analgesia. *Br. J. Pharmacol.* **2007**, *152*, 633–648. [\[CrossRef\]](#)
11. Valastro, C.; Campanile, D.; Marinaro, M.; Franchini, D.; Piscitelli, F.; Verde, R.; Di Marzo, V.; Di Bello, A. Characterization of Endocannabinoids and Related Acylethanolamides in the Synovial Fluid of Dogs with Osteoarthritis: A Pilot Study. *BMC Vet. Res.* **2017**, *13*, 309. [\[CrossRef\]](#)
12. Palomares, B.; Garrido-Rodriguez, M.; Gonzalo-Consuegra, C.; Gómez-Cañas, M.; Saen-on, S.; Soliva, R.; Collado, J.A.; Fernández-Ruiz, J.; Morello, G.; Calzado, M.A.; et al. Δ^9 -Tetrahydrocannabinolic Acid Alleviates Collagen-Induced Arthritis: Role of PPAR γ and CB1 Receptors. *Br. J. Pharmacol.* **2020**, *177*, 4034–4054. [\[CrossRef\]](#) [\[PubMed\]](#)
13. Sophocleous, A.; Börjesson, A.E.; Salter, D.M.; Ralston, S.H. The Type 2 Cannabinoid Receptor Regulates Susceptibility to Osteoarthritis in Mice. *Osteoarthr. Cartil.* **2015**, *23*, 1586–1594. [\[CrossRef\]](#) [\[PubMed\]](#)
14. Ryberg, E.; Larsson, N.; Sjögren, S.; Hjorth, S.; Hermansson, N.-O.; Leonova, J.; Elebring, T.; Nilsson, K.; Drmota, T.; Greasley, P.J. The Orphan Receptor GPR55 Is a Novel Cannabinoid Receptor. *Br. J. Pharmacol.* **2007**, *152*, 1092–1101. [\[CrossRef\]](#)
15. Oka, S.; Nakajima, K.; Yamashita, A.; Kishimoto, S.; Sugiura, T. Identification of GPR55 as a Lysophosphatidylinositol Receptor. *Biochem. Biophys. Res. Commun.* **2007**, *362*, 928–934. [\[CrossRef\]](#)
16. Gomes, T.M.; Dias da Silva, D.; Carmo, H.; Carvalho, F.; Silva, J.P. Epigenetics and the Endocannabinoid System Signaling: An Intricate Interplay Modulating Neurodevelopment. *Pharmacol. Res.* **2020**, *162*, 105237. [\[CrossRef\]](#)
17. Whyte, L.S.; Ryberg, E.; Sims, N.A.; Ridge, S.A.; Mackie, K.; Greasley, P.J.; Ross, R.A.; Rogers, M.J. The Putative Cannabinoid Receptor GPR55 Affects Osteoclast Function in Vitro and Bone Mass in Vivo. *Proc. Natl. Acad. Sci. USA* **2009**, *106*, 16511–16516. [\[CrossRef\]](#) [\[PubMed\]](#)
18. Lauckner, J.E.; Jensen, J.B.; Chen, H.-Y.; Lu, H.-C.; Hille, B.; Mackie, K. GPR55 Is a Cannabinoid Receptor That Increases Intracellular Calcium and Inhibits M Current. *Proc. Natl. Acad. Sci. USA* **2008**, *105*, 2699–2704. [\[CrossRef\]](#)
19. Staton, P.C.; Hatcher, J.P.; Walker, D.J.; Morrison, A.D.; Shapland, E.M.; Hughes, J.P.; Chong, E.; Mander, P.K.; Green, P.J.; Billinton, A.; et al. The Putative Cannabinoid Receptor GPR55 Plays a Role in Mechanical Hyperalgesia Associated with Inflammatory and Neuropathic Pain. *Pain* **2008**, *139*, 225–236. [\[CrossRef\]](#)
20. Elmes, S.J.R.; Winyard, L.A.; Medhurst, S.J.; Clayton, N.M.; Wilson, A.W.; Kendall, D.A.; Chapman, V. Activation of CB1 and CB2 Receptors Attenuates the Induction and Maintenance of Inflammatory Pain in the Rat. *Pain* **2005**, *118*, 327–335. [\[CrossRef\]](#)
21. Gamble, L.-J.; Boesch, J.M.; Frye, C.W.; Schwark, W.S.; Mann, S.; Wolfe, L.; Brown, H.; Berthelsen, E.S.; Wakshlag, J.J. Pharmacokinetics, Safety, and Clinical Efficacy of Cannabidiol Treatment in Osteoarthritic Dogs. *Front. Vet. Sci.* **2018**, *5*, 165. [\[CrossRef\]](#) [\[PubMed\]](#)
22. Mejia, S.; Duerr, F.M.; Griffenhagen, G.; McGrath, S. Evaluation of the Effect of Cannabidiol on Naturally Occurring Osteoarthritis-Associated Pain: A Pilot Study in Dogs. *J. Am. Anim. Hosp. Assoc.* **2021**, *57*, 81–90. [\[CrossRef\]](#)
23. Smith, F.L.; Fujimori, K.; Lowe, J.; Welch, S.P. Characterization of Δ^9 -Tetrahydrocannabinol and Anandamide Antinociception in Nonarthritic and Arthritic Rats. *Pharmacol. Biochem. Behav.* **1998**, *60*, 183–191. [\[CrossRef\]](#) [\[PubMed\]](#)

24. Bryk, M.; Starowicz, K. Cannabinoid-Based Therapy as a Future for Joint Degeneration. Focus on the Role of CB2 Receptor in the Arthritis Progression and Pain: An Updated Review. *Pharmacol. Rep.* **2021**, *73*, 681–699. [[CrossRef](#)] [[PubMed](#)]
25. Xin, Y.; Tang, A.; Pan, S.; Zhang, J. Components of the Endocannabinoid System and Effects of Cannabinoids Against Bone Diseases: A Mini-Review. *Front. Pharmacol.* **2022**, *12*, 793750. [[CrossRef](#)]
26. Lewis, R.; Gómez Álvarez, C.B.; Rayman, M.; Lanham-New, S.; Woolf, A.; Mobasheri, A. Strategies for Optimising Musculoskeletal Health in the 21st Century. *BMC Musculoskelet Disord.* **2019**, *20*, 164. [[CrossRef](#)]
27. Nganvongpanit, K.; Itthiarbha, A.; Ong-Chai, S.; Kongtawelert, P. Evaluation of Serum Chondroitin Sulfate and Hyaluronan: Biomarkers for Osteoarthritis in Canine Hip Dysplasia. *J. Vet. Sci.* **2008**, *9*, 317. [[CrossRef](#)]
28. Anderson, K.L.; O'Neill, D.G.; Brodbelt, D.C.; Church, D.B.; Meeson, R.L.; Sargan, D.; Summers, J.F.; Zulch, H.; Collins, L.M. Prevalence, Duration and Risk Factors for Appendicular Osteoarthritis in a UK Dog Population under Primary Veterinary Care. *Sci. Rep.* **2018**, *8*, 5641. [[CrossRef](#)]
29. Guercio, A.; Di Marco, P.; Casella, S.; Cannella, V.; Russotto, L.; Purpari, G.; Di Bella, S.; Piccione, G. Production of Canine Mesenchymal Stem Cells from Adipose Tissue and Their Application in Dogs with Chronic Osteoarthritis of the Humeroradial Joints. *Cell. Biol. Int.* **2012**, *36*, 189–194. [[CrossRef](#)]
30. Muir, P. *Advances in the Canine Cranial Cruciate Ligament*; John Wiley & Sons: Hoboken, NJ, USA, 2018; ISBN 978-1-119-26171-1.
31. Anderson, K.L.; Zulch, H.; O'Neill, D.G.; Meeson, R.L.; Collins, L.M. Risk Factors for Canine Osteoarthritis and Its Predisposing Arthropathies: A Systematic Review. *Front. Vet. Sci.* **2020**, *7*, 220. [[CrossRef](#)]
32. Genevois, J.-P.; Remy, D.; Viguier, E.; Carozzo, C.; Collard, F.; Cachon, T.; Maitre, P.; Fau, D. Prevalence of Hip Dysplasia According to Official Radiographic Screening, among 31 Breeds of Dogs in France. *Vet. Comp. Orthop. Traumatol.* **2008**, *21*, 21–24. [[CrossRef](#)] [[PubMed](#)]
33. Kirkby, K.A.; Lewis, D.D. Canine Hip Dysplasia: Reviewing the Evidence for Nonsurgical Management. *Vet. Surg.* **2012**, *41*. [[CrossRef](#)] [[PubMed](#)]
34. Myers, S.L. Synovial fluid markers in osteoarthritis. *Rheum. Dis. Clin. North Am.* **1999**, *25*, 433–449. [[CrossRef](#)] [[PubMed](#)]
35. Olsson, D.C.; Teixeira, B.L.; Jeremias, T.D.S.; Réus, J.C.; De Luca Canto, G.; Porporatti, A.L.; Trentin, A.G. Administration of Mesenchymal Stem Cells from Adipose Tissue at the Hip Joint of Dogs with Osteoarthritis: A Systematic Review. *Res. Vet. Sci.* **2021**, *135*, 495–503. [[CrossRef](#)] [[PubMed](#)]
36. Fujita, Y.; Hara, Y.; Nezu, Y.; Yamaguchi, S.; Schulz, K.S.; Tagawa, M. Direct and Indirect Markers of Cartilage Metabolism in Synovial Fluid Obtained from Dogs with Hip Dysplasia and Correlation with Clinical and Radiographic Variables. *Am. J. Vet. Res.* **2005**, *66*, 2028–2033. [[CrossRef](#)]
37. Chiocchetti, R.; De Silva, M.; Aspidi, F.; Cunha, R.Z.; Gobbo, F.; Tagliavia, C.; Sarli, G.; Morini, M. Distribution of Cannabinoid Receptors in Keratinocytes of Healthy Dogs and Dogs With Atopic Dermatitis. *Front. Vet. Sci.* **2022**, *9*, 915896. [[CrossRef](#)]
38. Lazzarini, G.; Abramo, F.; Albanese, F.; Pirone, A.; Miragliotta, V. Combined Immunohistochemical Protocols to Differentiate Macrophages within the Mononuclear-Phagocyte System. *Ann. Anat. Anat. Anz.* **2023**, *249*, 152107. [[CrossRef](#)]
39. Chiocchetti, R.; Galiazzo, G.; Tagliavia, C.; Stanzani, A.; Giancola, F.; Menchetti, M.; Militerno, G.; Bernardini, C.; Forni, M.; Mandrioli, L. Cellular Distribution of Canonical and Putative Cannabinoid Receptors in Canine Cervical Dorsal Root Ganglia. *Front. Vet. Sci.* **2019**, *6*, 313. [[CrossRef](#)]
40. Anday, J.K.; Mercier, R.W. Gene Ancestry of the Cannabinoid Receptor Family. *Pharmacol. Res.* **2005**, *52*, 463–466. [[CrossRef](#)]
41. Pierezan, F.; Mansell, J.; Ambrus, A.; Hoffmann, A.R. Immunohistochemical Expression of Ionized Calcium Binding Adapter Molecule 1 in Cutaneous Histiocytic Proliferative, Neoplastic and Inflammatory Disorders of Dogs and Cats. *J. Comp. Pathol.* **2014**, *151*, 347–351. [[CrossRef](#)]
42. Wensman, H.; Flama, V.; Pejler, G.; Hellmén, E. Plasticity of Cloned Canine Mammary Spindle Cell Tumor, Osteosarcoma and Carcinoma Cells. *Vet. Pathol.* **2008**, *45*, 803–815. [[CrossRef](#)] [[PubMed](#)]
43. Rodrigues, R.S.; Ribeiro, F.F.; Ferreira, F.; Vaz, S.H.; Sebastião, A.M.; Xapelli, S. Interaction between Cannabinoid Type 1 and Type 2 Receptors in the Modulation of Subventricular Zone and Dentate Gyrus Neurogenesis. *Front. Pharmacol.* **2017**, *8*, 516. [[CrossRef](#)] [[PubMed](#)]
44. Poddighe, L.; Carta, G.; Serra, M.P.; Melis, T.; Boi, M.; Lisai, S.; Murru, E.; Muredda, L.; Collu, M.; Banni, S.; et al. Acute Administration of Beta-Caryophyllene Prevents Endocannabinoid System Activation during Transient Common Carotid Artery Occlusion and Reperfusion. *Lipids Health Dis.* **2018**, *17*, 23. [[CrossRef](#)]
45. Pietrovito, L.; Iozzo, M.; Bacci, M.; Giannoni, E.; Chiarugi, P. Treatment with Cannabinoids as a Promising Approach for Impairing Fibroblast Activation and Prostate Cancer Progression. *IJMS* **2020**, *21*, 787. [[CrossRef](#)] [[PubMed](#)]
46. Costa, L.; Moreia-Pinto, B.; Felgueira, E.; Ribeiro, A.; Rebelo, I.; Fonseca, B.M. The Major Endocannabinoid Anandamide (AEA) Induces Apoptosis of Human Granulosa Cells. *Prostaglandins Leukot. Essent. Fat. Acids* **2021**, *171*, 102311. [[CrossRef](#)]
47. Kreitzer, F.R.; Stella, N. The Therapeutic Potential of Novel Cannabinoid Receptors. *Pharmacol. Ther.* **2009**, *122*, 83–96. [[CrossRef](#)]
48. Iannotti, F.A.; Di Marzo, V.; Petrosino, S. Endocannabinoids and Endocannabinoid-Related Mediators: Targets, Metabolism and Role in Neurological Disorders. *Prog. Lipid Res.* **2016**, *62*, 107–128. [[CrossRef](#)]
49. Pirone, A.; Cantile, C.; Miragliotta, V.; Lenzi, C.; Giannessi, E.; Cozzi, B. Immunohistochemical Distribution of the Cannabinoid Receptor 1 and Fatty Acid Amide Hydrolase in the Dog Claustrum. *J. Chem. Neuroanat.* **2016**, *74*, 21–27. [[CrossRef](#)]
50. Kostic, D.; Nowakowska, M.; Freundt Revilla, J.; Attig, F.; Rohn, K.; Gualtieri, F.; Baumgärtner, W.; Potschka, H.; Tipold, A. Hippocampal Expression of the Cannabinoid Receptor Type 1 in Canine Epilepsy. *Sci. Rep.* **2023**, *13*, 3138. [[CrossRef](#)]

51. Ruel, H.L.M.; Monteiro, B.P.; Blais, E.; Richard, H.; St-Jean, G.; Laverty, S.; Steagall, P.V. Immunohistochemical Localization of Cannabinoid Receptor Type I in the Feline Synovial Membrane with and without Degenerative Lesions. In Proceedings of the Association of Veterinary Anaesthetists (AVA) Spring Meeting (2022): Spring Meeting, Nafplio, Greece, 19–20 May 2022.
52. Miagkoff, L.; Girard, C.; Richard, H.; Laverty, S. Cannabinoid Receptors Expression Positively Correlated with Synovitis in Horses with Spontaneous Osteoarthritis. *Osteoarthr. Cartil.* **2021**, *29*, S426–S427. [\[CrossRef\]](#)
53. Miagkoff, L.; Girard, C.A.; St-Jean, G.; Richard, H.; Beauchamp, G.; Laverty, S. Cannabinoid Receptors Are Expressed in Equine Synovium and Upregulated with Synovitis. *Equine Vet. J.* **2023**, *55*, 681–695. [\[CrossRef\]](#)
54. Lowin, T.; Kok, C.; Smutny, S.; Pongratz, G. Impact of Δ^9 -Tetrahydrocannabinol on Rheumatoid Arthritis Synovial Fibroblasts Alone and in Co-Culture with Peripheral Blood Mononuclear Cells. *Biomedicines* **2022**, *10*, 1118. [\[CrossRef\]](#) [\[PubMed\]](#)
55. Schuelert, N.; Zhang, C.; Mogg, A.J.; Broad, L.M.; Hepburn, D.L.; Nisenbaum, E.S.; Johnson, M.P.; McDougall, J.J. Paradoxical Effects of the Cannabinoid CB2 Receptor Agonist GW405833 on Rat Osteoarthritic Knee Joint Pain. *Osteoarthr. Cartil.* **2010**, *18*, 1536–1543. [\[CrossRef\]](#) [\[PubMed\]](#)
56. Fukuda, S.; Kohsaka, H.; Takayasu, A.; Yokoyama, W.; Miyabe, C.; Miyabe, Y.; Harigai, M.; Miyasaka, N.; Nanki, T. Cannabinoid Receptor 2 as a Potential Therapeutic Target in Rheumatoid Arthritis. *BMC Musculoskelet Disord.* **2014**, *15*, 275. [\[CrossRef\]](#) [\[PubMed\]](#)
57. Gui, H.; Liu, X.; Wang, Z.-W.; He, D.-Y.; Su, D.-F.; Dai, S.-M. Expression of Cannabinoid Receptor 2 and Its Inhibitory Effects on Synovial Fibroblasts in Rheumatoid Arthritis. *Rheumatology* **2014**, *53*, 802–809. [\[CrossRef\]](#) [\[PubMed\]](#)
58. Doom, M.; de Bruin, T.; de Rooster, H.; van Bree, H.; Cox, E. Immunopathological Mechanisms in Dogs with Rupture of the Cranial Cruciate Ligament. *Vet. Immunol. Immunopathol.* **2008**, *125*, 143–161. [\[CrossRef\]](#)
59. Klocke, N.W.; Snyder, P.W.; Widmer, W.R.; Zhong, W.; McCabe, G.P.; Breur, G.J. Detection of Synovial Macrophages in the Joint Capsule of Dogs with Naturally Occurring Rupture of the Cranial Cruciate Ligament. *Am. J. Vet. Res.* **2005**, *66*, 493–499. [\[CrossRef\]](#)
60. Baradaran Rahimi, V.; Askari, V.R. A Mechanistic Review on Immunomodulatory Effects of Selective Type Two Cannabinoid Receptor β -Caryophyllene. *BioFactors* **2022**, *48*, 857–882. [\[CrossRef\]](#)
61. Henstridge, C.M.; Balenga, N.A.B.; Kargl, J.; Andradas, C.; Brown, A.J.; Irving, A.; Sanchez, C.; Waldhoer, M. Minireview: Recent Developments in the Physiology and Pathology of the Lysophosphatidylinositol-Sensitive Receptor GPR55. *Mol. Endocrinol.* **2011**, *25*, 1835–1848. [\[CrossRef\]](#)
62. Woodell-May, J.E.; Sommerfeld, S.D. Role of Inflammation and the Immune System in the Progression of Osteoarthritis. *J. Orthop. Res.* **2020**, *38*, 253–257. [\[CrossRef\]](#)
63. Chiurchiù, V.; Lanuti, M.; De Bardi, M.; Battistini, L.; Maccarrone, M. The Differential Characterization of GPR55 Receptor in Human Peripheral Blood Reveals a Distinctive Expression in Monocytes and NK Cells and a Proinflammatory Role in These Innate Cells. *Int. Immunol.* **2015**, *27*, 153–160. [\[CrossRef\]](#) [\[PubMed\]](#)
64. Morales, P.; Hurst, D.P.; Reggio, P.H. Molecular Targets of the Phytocannabinoids: A Complex Picture. In *Phytocannabinoids*; Kinghorn, A.D., Falk, H., Gibbons, S., Kobayashi, J., Eds.; Progress in the Chemistry of Organic Natural Products; Springer International Publishing: Cham, Switzerland, 2017; Volume 103, pp. 103–131. ISBN 978-3-319-45539-6.
65. Anavi-Goffer, S.; Baillie, G.; Irving, A.J.; Gertsch, J.; Greig, I.R.; Pertwee, R.G.; Ross, R.A. Modulation of L- α -Lysophosphatidylinositol/GPR55 Mitogen-Activated Protein Kinase (MAPK) Signaling by Cannabinoids. *J. Biol. Chem.* **2012**, *287*, 91–104. [\[CrossRef\]](#) [\[PubMed\]](#)
66. Mosca, M.G.; Mangini, M.; Cioffi, S.; Barba, P.; Mariggiò, S. Peptide Targeting of Lysophosphatidylinositol-Sensing GPR55 for Osteoclastogenesis Tuning. *Cell Commun. Signal.* **2021**, *19*, 48. [\[CrossRef\]](#) [\[PubMed\]](#)
67. Andersson, J.; Sophocleous, A.; Zhou, Y.; Rischitor, G.; Ralston, S.; Salter, D. Expression of Cannabinoid Receptors by Human Articular Chondrocytes. *Bone* **2011**, *48*, S141. [\[CrossRef\]](#)
68. Lorke, M.; Willen, M.; Lucas, K.; Beyerbach, M.; Wefstaedt, P.; Murua Escobar, H.; Nolte, I. Comparative Kinematic Gait Analysis in Young and Old Beagle Dogs. *J. Vet. Sci.* **2017**, *18*, 521. [\[CrossRef\]](#)

Disclaimer/Publisher's Note: The statements, opinions and data contained in all publications are solely those of the individual author(s) and contributor(s) and not of MDPI and/or the editor(s). MDPI and/or the editor(s) disclaim responsibility for any injury to people or property resulting from any ideas, methods, instructions or products referred to in the content.

D. DISCUSSION AND CONCLUSIONS

Veterinary anatomy plays a very important role as a basic science, necessary to lay the foundations for the pathophysiological aspects of animal organism and its behaviour, which can also be used as a comparison for aspects relating to humans. This is the context of my thesis, which consists of nine research studies aimed at enriching the anatomical knowledge of areas of the nervous system and certain effector organs of different species of veterinary interest.

We studied the EC and the ENS in the dolphin, a species very particular in veterinary medicine for its social and cognitive abilities (215). Despite the relatively high level of development of the central nervous system in cetaceans (215), several features of the dolphin brain remain poorly documented compared to other mammals, such as the immunocytochemical characteristics of neurons in the EC and their cytoarchitecture. This area is of interest due to its close relationship with the limbic system and, in particular, with the hippocampal formation, which is relatively small in cetaceans compared to other mammals. Furthermore, the absence of olfaction and olfactory bulbs in cetaceans lends an air of mystery to the EC, as this region is typically associated with olfactory functions in other mammals (215). Our work (Section C, Chapter 1), which used the thionine staining to study the general cytoarchitecture of the EC and immunoperoxidase against the CaBPs (PV, CB and CR) to investigate the immunocytochemical characteristics of neurons in EC, found that this structure in dolphins consists of six layers and it can be divided into two parts: LEA and MEA, a result consistent with findings in other mammals (217); layer VI is characteristically thicker in the dolphin LEA than in other mammals (354). CaBPs were found to be distributed in both pyramidal and non-pyramidal neurons, but the PV was only expressed in non-pyramidal neurons. All CaBPs immunoreactive (IR) neurons were primarily localised in non-overlapping neuronal populations in the dolphin EC, results consistent with other mammals such as rodents and primates. As in terrestrial mammals, CB and PV were expressed primarily in neurons located in layers II and III, whereas CR-IR neurons are distributed throughout layers, particularly in layers V and VI. Studies in terrestrial mammals show that layer I is devoid of PV-IR neurons (217), but in our study layer I of the dolphin EC contained PV-IR neurons. Our results suggest that CaBPs neurons in the dolphin EC are located at the interface between entorhinal input and output pathways, as layers II and III of the entorhinal cortex provide the main cortical input to the hippocampal formation, while layers V and VI receive information from the hippocampal formation and transmit it to the neocortex and other brain structures (212).

In our study on the dolphin ENS (Section C, Chapter 6), we used immunofluorescence to detect SP and nNOS in the neuronal population of the two ENS plexus (SMP and MP), as these markers

are known to identify excitatory and inhibitory neurons respectively (176,177,187,188). This approach provided the first comprehensive insight into the distribution, morphology and quantification of these two functional classes of neurons in the bottlenose dolphin gut. We observed differences in the relative prevalence of neurons expressing both markers, finding a notably small number of nNOS-IR neurons in the SMP and a larger number SP-IR neurons in the MP, although general characteristics and morphology are conserved across most mammalian species. In contrast to what has been described in sheep, and similarly to mouse small intestine (184,355), no co-localisation between nNOS and SP immunoreactivity was detected in either plexus, suggesting the existence of two completely different functional classes of neurons in the bottlenose dolphin gut.

Another brain region studied was the AC of the rat (Section C, Chapter 2) and the sheep (Section C, Chapter 3), two diametrically opposed species, as the rat is one of the most widely used laboratory animals (356) and the sheep is beginning to be used increasingly as an experimental model (357,358). The AC is a brain region of great interest because of its involvement in high cognitive functions and emotional processes (228), but a comprehensive analysis of the distribution and significance of VIP immunoreactivity throughout the rat AC and a description of the connections occurring within the sheep AC were lacking. Using immunoperoxidase and the non-invasive technique of diffusion tensor imaging, we found that in the rat VIP immunoreactivity is associated with somata, primary dendrites and, particularly in the lateral subdivision of the central nucleus, axon terminals. Moreover, the distribution differs between areas and cell types, suggesting a distinct influence of this neuropeptide on neuronal amygdaloid circuits. In sheep, AC was shown to be connected to the striatum, thalamus, hypothalamus and brainstem via the ventral amygdalofugal pathway and the *stria terminalis*. In addition, the fornix and external capsule connected the AC with the hippocampal region. Finally, we showed that the connections to the neocortex were via the external capsule and subcortical white matter. Taken together, our results indicate that the sheep AC appears to be connected to primary and multimodal cortical areas (including the prefrontal cortex), the medial temporal lobe memory system, the striatum, the thalamus and the hypothalamus, data that are consistent with other studies conducted mainly in rat, cat and monkey using invasive tracing techniques. Unlike the monkey, the sheep AC is directly connected to olfactory areas such as the piriform cortex, but appears to be less connected to the neocortex (232,258–260), highlighting possible functional differences in the AC between species.

Another region of the CNS studied was the OL, the centre for processing visual information (280) in the honeybee (Section C, Chapter 4) an unconventional veterinary species important for agricultural pollination across the world (359). In particular, we used immunofluorescence against the SERT to study the distribution and quantification among the three neuropils that constitute the

OL: lamina, medulla and lobula (275) in three groups of bees divided according to their behaviour in: docile, moderate and aggressive. We found that the highest and lowest SERT immunoreactivity were in the docile and aggressive groups respectively, suggesting that low 5HT levels in the OL are associated with aggressive behaviour. Interestingly, the distribution of SERT immunoreactivity between the three visual neuropils varied with behaviour, suggesting a specific local function of 5HT in each visual neuropil.

A considerable part of this thesis focused on the investigation of the ECS through the detection of its CBr (CB₁, CB₂, TRPA1, TRPV1, PPAR α , PPAR γ , GPR55) mainly using immunofluorescence in different regions and species: the TG of horse (Section C, Chapter 5), the skin of dog affected by AD (Section C, Chapter 7) and the synovial membrane of the horse metacarpophalangeal joint (Section C, Chapter 8) and of the dog hip and stifle joints (Section C, Chapter 9). The aim was to provide a rationale and foundation for improving cannabinoid-based therapies in pathologies such as TG-mediated HSK in horses, AD in dogs and OA in both dogs and horses. All the studies confirm the presence of different types of CB receptors in the different types of cells that form the tissues in question. CB₁, CB₂, TRPV1, GPR55, and PPAR α were found differently in MLS and FLS in horse metacarpophalangeal joint, with CB₁ identified in FLS and MLS, although it was not expressed in all the horses. CB₂, TRPV1 and GPR55 were identified in FLS, MLS, and blood vessels, while PPAR α was identified in FLS and blood vessels. CB₁, CB₂, and GPR55 were found in MLS and FLS in dog hip and stifle joints with both CB₂ and GPR55 being more prominently expressed by the synoviocytes compared to CB₁. The IR of CB₁, CB₂, TRPV1, and PPAR γ was found in most of TG neurons. The expression of GPR55 immunoreactivity was mainly detectable in formalin-fixed paraffin-embedded sections, with expression in the majority of sensory neurons. Some receptors were also observed in glial cells (CB₂R, TRPV1, PPAR γ , and GPR55) and inflammatory cells (PPAR γ and GPR55). Finally, in the skin of AD dogs the cells of the inflammatory infiltrate showed immunoreactivity for all or for some of the CBr studied. In particular, MCs and macrophages/DCs showed CB₂, GPR55, TRPA1, and TRPV1 immunoreactivity; T cells showed CB₂, GPR55 and TRPA1 immunoreactivity, and neutrophils expressed GPR55 immunoreactivity. Co-localisation studies showed that CB₂ immunoreactivity was co-expressed with TRPV1, TRPA1, and GPR55 immunoreactivity in different cellular elements of the dermis of the AD-dogs. Taken together, these findings encouraged the development of new studies to support the use of molecules acting on these receptors to reduce inflammation in joint pathologies such as OA in dogs and horses, in disorders such as TG-mediated HSK in horses, and in dogs with AD where they may alleviate pruritus and inflammation.

To the best of the author's knowledge, none of these studies has been published before, so this work provides the first anatomical basis for: the cytoarchitecture and cytoidentity of the dolphin EC; the functional description of the neuronal population in the dolphin ENS; the characteristics of VIP and the connectivity of the rat and sheep AC; the functional significance of the serotonergic system in the honeybee OL; and the use of molecules targeting the ECS in different animal species and tissues.

LIST OF ABBREVIATIONS

Abbreviation	Definition
2-AG	2-arachidonoyl-glycerol
2-AGE	2-arachidonoyl glycerol ether
5-HIAA	5-hydroxyindoleacetic acid
5-HT	5-hydroxytryptamine
5HT _r	5-hydroxytryptamine receptors
5HTT	5-hydroxytryptamine transporter
AC	Amygdaloid complex
AD	Atopic dermatitis
AEA	arachidonylethanolamide
ARA-S	N-arachidonoyl serine
Ca ²⁺	Calcium ion
CaBPs	Calcium-binding proteins
CB	Calbindin D-28k
CB ₁	Cannabinoid receptor type 1
CB ₂	Cannabinoid receptor type 2
CBD	Cannabidiol
CBG	Cannabigerol
CBr	Cannabinoid receptors
CCK	Cholecystokinin
CNS	Central Nervous System
CR	Calretinin
DAGL α	diacylglycerol lipase alfa
DAGL β	diacylglycerol lipase beta
DCs	dendritic cells
DRG	dorsal root ganglion
EC	Entorhinal Cortex
eCBs	endocannabinoids
ECS	Endocannabinoid System
EMT	Endocannabinoid Membrane Transporter
ENS	Enteric Nervous system
FAAH	Fatty Acid Amide Hydrolase
FLS	Fibroblast-Like Synoviocytes
GABA	Gamma-Aminobutyric Acid
GI	gastrointestinal
GPCr	G protein-coupled receptors
GPR119	G protein-coupled receptor 119
GPR18	G protein-coupled receptor 18
GPR55	G protein-coupled receptor 55
HSK	Head shaking
Ig	Immunoglobulin
IPANs	Intrinsic primary afferent neurons
IR	Immunoreactive
KO	Knock-out
LEA/LEC	Lateral Entorhinal Area/Cortex

MAGL	Monoacylglycerol lipase
MAO	Monoamine oxidase
MCs	Mast cells
MEA/MEC	Medial Entorhinal Area/Cortex
MLS	Macrophage-like synoviocytes
MP	Myenteric Plexus
NADA	N-arachidonoyl dopamine
NAPE-PLD	N-arachidonoyl phosphatidyl ethanol-preferring phospholipase D
nNOS	Neuronal Nitric Oxide Synthase
NSAIDs	Non-steroidal anti-inflammatory drugs
O-AEA	Virodhamine
OEA	N-oleoylethanolamide
OL	Optic Lobe
PEA	N-palmitoylethanolamine
PLC	Phospholipase C
PNS	Peripheral Nervous System
PPAR α	Peroxisome proliferator activated receptor alfa
PPAR γ	Peroxisome proliferator activated receptor beta
PV	Parvalbumin
SERT	Serotonin transporter
SMP	Submucosal plexus
SOG	Suboesophageal ganglion
SP	Substance P
TG	Trigeminal ganglion
THC	Tetrahydrocannabinol
TRP	Transient Receptor Potential Cation Channel
TRPA1	Transient Receptor Potential Cation Channel Ankyrin
TRPM8	Transient Receptor Potential Cation Channel M8
TRPV1	Transient Receptor Potential Cation Channel Vanilloid 1
VIP	Vasoactive Intestinal Peptide

REFERENCES

1. Baimbridge KG, Celio MR, Rogers JH. Calcium-binding proteins in the nervous system. *Trends in Neurosciences*. 1992 Aug 1;15(8):303–8.
2. Mady LJ, Haleem F, Christakos S. Calcium-Buffering Proteins: Calbindin. In: Lennarz WJ, Lane MD, editors. *Encyclopedia of Biological Chemistry (Second Edition)*. Waltham: Academic Press; 2013. p. 284–9. Available from: <https://www.sciencedirect.com/science/article/pii/B9780123786302002280>
3. Camp AJ, Wijesinghe R. Calretinin: Modulator of neuronal excitability. *The International Journal of Biochemistry & Cell Biology*. 2009 Nov 1;41(11):2118–21.
4. Elías J, Yáñez M, Pereira TMC, Gil-Longo J, MacDougall DA, Campos-Toimil M. An Update to Calcium Binding Proteins. *Adv Exp Med Biol*. 2020;1131:183–213.
5. Miettinen M, Pitkänen A, Miettinen R. Distribution of calretinin-immunoreactivity in the rat entorhinal cortex: Coexistence with GABA. *Journal of Comparative Neurology*. 1997;378(3):363–78.
6. Mikkonen M, Soininen H, Pitkänen A. Distribution of parvalbumin-, calretinin-, and calbindin-D28k-immunoreactive neurons and fibers in the human entorhinal cortex. *Journal of Comparative Neurology*. 1997;388(1):64–88.
7. Grisar T, Lakaye B, de Nijs L, LoTurco J, Daga A, Delgado-Escueta AV. Myoclonin1/EFHC1 in cell division, neuroblast migration, synapse/dendrite formation in juvenile myoclonic epilepsy. In: Noebels JL, Avoli M, Rogawski MA, Olsen RW, Delgado-Escueta AV, editors. *Jasper's Basic Mechanisms of the Epilepsies*. 4th ed. Bethesda (MD): National Center for Biotechnology Information (US); 2012. Available from: <http://www.ncbi.nlm.nih.gov/books/NBK98188/>
8. Permyakov EA, Uversky VN. What Is Parvalbumin for? *Biomolecules*. 2022 May;12(5):656.
9. Permiakov EA, Permiakov EA. *Parvalbumin*. Nova Publishers; 2007. 212 p.
10. Celio MR. Parvalbumin. In: Celio MR, editor. *Guidebook to the Calcium-binding Proteins*. Oxford University Press; 1996. Available from: <https://doi.org/10.1093/oso/9780198599517.003.0016>
11. Arif SH. A Ca²⁺-binding protein with numerous roles and uses: parvalbumin in molecular biology and physiology. *BioEssays*. 2009;31(4):410–21.
12. Godoy LD, Prizon T, Rossignoli MT, Leite JP, Liberato JL. Parvalbumin Role in Epilepsy and Psychiatric Comorbidities: From Mechanism to Intervention. *Front Integr Neurosci*. 2022. Available from: <https://www.frontiersin.org/journals/integrative-neuroscience/articles/10.3389/fnint.2022.765324/full>
13. Distribution of calbindin-D28k immunoreactivity in the monkey temporal lobe: The amygdaloid complex - Pitkänen - 1993 - *Journal of Comparative Neurology* - Wiley Online Library. Available from: <https://onlinelibrary.wiley.com/doi/abs/10.1002/cne.903310205>

14. Suzuki WA, Porteros A. Distribution of calbindin D-28k in the entorhinal, perirhinal, and parahippocampal cortices of the macaque monkey. *Journal of Comparative Neurology*. 2002;451(4):392–412.
15. del Río MR, DeFelipe J. Colocalization of calbindin D-28k, calretinin, and GABA immunoreactivities in neurons of the human temporal cortex. *Journal of Comparative Neurology*. 1996;369(3):472–82.
16. Celio MR. Calbindin D-28k. In: Celio MR, editor. *Guidebook to the Calcium-binding Proteins*. Oxford University Press; 1996. Available from: <https://doi.org/10.1093/oso/9780198599517.003.0003>
17. Rogers JH. Calretinin: a gene for a novel calcium-binding protein expressed principally in neurons. *Journal of Cell Biology*. 1987 Sep 1;105(3):1343–53.
18. Doglioni C, Dei AP, Laurino L, Iuzzolino P, Chiarelli C, Celio MR, et al. Calretinin: A Novel Immunocytochemical Marker for Mesothelioma. *The American Journal of Surgical Pathology*. 1996 Sep;20(9):1037.
19. Lugli A, Forster Y, Haas P, Nocito A, Bucher C, Bissig H, et al. Calretinin expression in human normal and neoplastic tissues: a tissue microarray analysis on 5233 tissue samples. *Human Pathology*. 2003 Oct 1;34(10):994–1000.
20. Schwaller B. The continuing disappearance of “pure” Ca²⁺ buffers. *Cell Mol Life Sci*. 2009 Jan 1;66(2):275–300.
21. Rogers J, Khan M, Ellis J. Calretinin and Other CaBPs in the Nervous System. In: Pochet R, Lawson DEM, Heizmann CW, editors. *Calcium Binding Proteins in Normal and Transformed Cells*. Boston, MA: Springer US; 1990. p. 195–203. Available from: https://doi.org/10.1007/978-1-4684-5754-4_32
22. Celio MR. Calbindin D-28k and parvalbumin in the rat nervous system. *Neuroscience*. 1990 Jan 1;35(2):375–475.
23. Braun K. Calcium-binding proteins in avian and mammalian central nervous system: localization, development and possible functions. *Prog Histochem Cytochem*. 1990;21(1):1–64.
24. Résibois A, Blachier F, Rogers JH, Lawson DE, Pochet R. Comparison between rat brain calbindin- and calretinin-immuno-reactivities. *Adv Exp Med Biol*. 1990;269:211–4.
25. Pasteels B, Rogers J, Blachier F, Pochet R. Calbindin and calretinin localization in retina from different species. *Visual Neuroscience*. 1990 Jul;5(1):1–16.
26. Kalinichenko SG, Pushchin II. Calcium-binding proteins in the cerebellar cortex of the bottlenose dolphin and harbour porpoise. *J Chem Neuroanat*. 2008 Jul;35(4):364–70.
27. Hof PR, Glezer II, Condé F, Flagg RA, Rubin MB, Nimchinsky EA, et al. Cellular distribution of the calcium-binding proteins parvalbumin, calbindin, and calretinin in the neocortex of mammals: phylogenetic and developmental patterns. *Journal of Chemical Neuroanatomy*. 1999 Feb 1;16(2):77–116.
28. Bombardi C, Grandis A, Chiochetti R, Lucchi ML. Distribution of calbindin-D28k, neuronal nitric oxide synthase, and nicotinamide adenine dinucleotide phosphate diaphorase

- (NADPH-d) in the lateral nucleus of the sheep amygdaloid complex. *Anat Embryol (Berl)*. 2006 Nov;211(6):707–20.
29. Hof PR, Glezer II, Nimchinsky EA, Erwin JM. Neurochemical and Cellular Specializations in the Mammalian Neocortex Reflect Phylogenetic Relationships: Evidence from Primates, Cetaceans, and Artiodactyls. *Brain Behavior and Evolution*. 2000 Sep 11;55(6):300–10.
 30. Glezer II, Hof PR, Leranth C, Morgane PJ. Calcium-binding Protein-containing Neuronal Populations in Mammalian Visual Cortex: A Comparative Study in Whales, Insectivores, Bats, Rodents, and Primates. *Cerebral Cortex*. 1993 May 1;3(3):249–72.
 31. Glezer II, Hof PR, Morgane PJ. Comparative analysis of calcium-binding protein-immunoreactive neuronal populations in the auditory and visual systems of the bottlenose dolphin (*Tursiops truncatus*) and the macaque monkey (*Macaca fascicularis*). *Journal of Chemical Neuroanatomy*. 1998 Oct 1;15(4):203–37.
 32. Dell LA, Karlsson KÆ, Patzke N, Spocter MA, Siegel JM, Manger PR. Organization of the sleep-related neural systems in the brain of the minke whale (*Balaenoptera acutorostrata*). *Journal of Comparative Neurology*. 2016;524(10):2018–35.
 33. Sacchini S, Bombardi C, Arbelo M, Herráez P. The amygdaloid body of the family Delphinidae: a morphological study of its central nucleus through calbindin-D28k. *Front Neuroanat*. 2024 May 30. Available from: <https://www.frontiersin.org/journals/neuroanatomy/articles/10.3389/fnana.2024.1382036/full>
 34. Törk I. Anatomy of the Serotonergic System. *Annals of the New York Academy of Sciences*. 1990;600(1):9–34.
 35. Mann JJ. Role of the Serotonergic System in the Pathogenesis of Major Depression and Suicidal Behavior. *Neuropsychopharmacol*. 1999 Aug;21(1):99–105.
 36. Mohammad-Zadeh LF, Moses L, Gwaltney-Brant SM. Serotonin: a review. *Journal of Veterinary Pharmacology and Therapeutics*. 2008;31(3):187–99.
 37. Naeem M, Chadeayne AR, Golen JA, Manke DR. Crystal structure of serotonin. *Acta Crystallogr E Crystallogr Commun*. 2022 Mar 10;78(Pt 4):365–8.
 38. Aghajanian GK, Marek GJ. Serotonin and Hallucinogens. *Neuropsychopharmacol*. 1999 Aug;21(1):16–23.
 39. Jonnakuty C, Gragnoli C. What do we know about serotonin? *Journal of Cellular Physiology*. 2008;217(2):301–6.
 40. McCorvy JD, Roth BL. Structure and function of serotonin G protein-coupled receptors. *Pharmacology & Therapeutics*. 2015 Jun 1;150:129–42.
 41. Berger M, Gray JA, Roth BL. The Expanded Biology of Serotonin. *Annual Review of Medicine*. 2009 Feb 18;60(Volume 60, 2009):355–66.
 42. Twarog BM, Page IH. Serotonin Content of Some Mammalian Tissues and Urine and a Method for Its Determination. *American Journal of Physiology-Legacy Content*. 1953 Sep 30;175(1):157–61.

43. Hornung JP. The human raphe nuclei and the serotonergic system. *Journal of Chemical Neuroanatomy*. 2003 Dec 1;26(4):331–43.
44. Jacobs BL, Azmitia EC. Structure and function of the brain serotonin system. *Physiological Reviews*. 1992 Jan;72(1):165–229.
45. Hornung JP. CHAPTER 1.3 - The Neuroanatomy of the Serotonergic System. In: Müller CP, Jacobs BL, editors. *Handbook of Behavioral Neuroscience* [Internet]. Elsevier; 2010. p. 51–64. (*Handbook of the Behavioral Neurobiology of Serotonin*; vol. 21). Available from: <https://www.sciencedirect.com/science/article/pii/S1569733910700710>
46. Graeff FG. SEROTONERGIC SYSTEMS. *Psychiatric Clinics of North America*. 1997 Dec 1;20(4):723–39.
47. Hay-Schmidt A. The evolution of the serotonergic nervous system. *Proc Biol Sci*. 2000 Jun 7;267(1448):1071–9.
48. Seidel C, Bicker G. The developmental expression of serotonin-immunoreactivity in the brain of the pupal honeybee. *Tissue and Cell*. 1996 Dec 1;28(6):663–72.
49. Schürmann FW, Klemm N. Serotonin-immunoreactive neurons in the brain of the honeybee. *Journal of Comparative Neurology*. 1984;225(4):570–80.
50. Bicker G. Biogenic amines in the brain of the honeybee: Cellular distribution, development, and behavioral functions. *Microscopy Research and Technique*. 1999;44(2–3):166–78.
51. De Neve JE. Functional polymorphism (5-HTTLPR) in the serotonin transporter gene is associated with subjective well-being: evidence from a US nationally representative sample. *J Hum Genet*. 2011 Jun;56(6):456–9.
52. Nielsen K, Brask D, Knudsen GM, Aznar S. Immunodetection of the serotonin transporter protein is a more valid marker for serotonergic fibers than serotonin. *Synapse*. 2006;59(5):270–6.
53. Moutkine I, Collins EL, Béchade C, Maroteaux L. Evolutionary considerations on 5-HT₂ receptors. *Pharmacological Research*. 2019 Feb 1;140:14–20.
54. Tierney AJ. Invertebrate serotonin receptors: a molecular perspective on classification and pharmacology. *Journal of Experimental Biology*. 2018 Oct 4;221(19):jeb184838.
55. Chiocchetti R, Galiazzo G, Giancola F, Tagliavia C, Bernardini C, Forni M, et al. Localization of the Serotonin Transporter in the Dog Intestine and Comparison to the Rat and Human Intestines. *Front Vet Sci*. 2022 Jan 5. Available from: <https://www.frontiersin.org/journals/veterinary-science/articles/10.3389/fvets.2021.802479/full>
56. Kroeze WK, Kristiansen K, Roth BL. Molecular biology of serotonin receptors structure and function at the molecular level. *Curr Top Med Chem*. 2002 Jun;2(6):507–28.
57. Scheiner R, Baumann A, Blenau W. Aminergic Control and Modulation of Honeybee Behaviour. *Current Neuropharmacology*. 2006 Oct 1;4(4):259–76.
58. Popova NK. From genes to aggressive behavior: the role of serotonergic system. *BioEssays*. 2006;28(5):495–503.

59. Zou S, Kumar U. Cannabinoid Receptors and the Endocannabinoid System: Signaling and Function in the Central Nervous System. *International Journal of Molecular Sciences*. 2018 Mar;19(3):833.
60. Crocq MA. History of cannabis and the endocannabinoid system. *Dialogues in Clinical Neuroscience*. 2020 Sep 30;22(3):223–8.
61. Devane WA, Dysarz FA, Johnson MR, Melvin LS, Howlett AC. Determination and characterization of a cannabinoid receptor in rat brain. *Mol Pharmacol*. 1988 Nov;34(5):605–13.
62. Devane WA, Hanus L, Breuer A, Pertwee RG, Stevenson LA, Griffin G, et al. Isolation and structure of a brain constituent that binds to the cannabinoid receptor. *Science*. 1992 Dec 18;258(5090):1946–9.
63. Kilaru A, Chapman KD. The endocannabinoid system. *Essays in Biochemistry*. 2020 Jul 10;64(3):485–99.
64. Mangal N, Erridge S, Habib N, Sadanandam A, Reebye V, Sodergren MH. Cannabinoids in the landscape of cancer. *J Cancer Res Clin Oncol*. 2021 Sep 1;147(9):2507–34.
65. Busquets-García A, Bolaños JP, Marsicano G. Metabolic Messengers: endocannabinoids. *Nat Metab*. 2022 Jul;4(7):848–55.
66. Maccarrone M, Bab I, Bíró T, Cabral GA, Dey SK, Di Marzo V, et al. Endocannabinoid signaling at the periphery: 50 years after THC. *Trends in Pharmacological Sciences*. 2015 May 1;36(5):277–96.
67. Lu HC, Mackie K. An Introduction to the Endogenous Cannabinoid System. *Biological Psychiatry*. 2016 Apr 1;79(7):516–25.
68. Khoury M, Cohen I, Bar-Sela G. “The Two Sides of the Same Coin”—Medical Cannabis, Cannabinoids and Immunity: Pros and Cons Explained. *Pharmaceutics*. 2022 Feb;14(2):389.
69. Navarrete F, García-Gutiérrez MS, Jurado-Barba R, Rubio G, Gasparyan A, Austrich-Olivares A, et al. Endocannabinoid System Components as Potential Biomarkers in Psychiatry. *Front Psychiatry* [Internet]. 2020 Apr 27. Available from: <https://www.frontiersin.org/journals/psychiatry/articles/10.3389/fpsy.2020.00315/full>
70. Lu HC, Mackie K. Review of the Endocannabinoid System. *Biological Psychiatry: Cognitive Neuroscience and Neuroimaging*. 2021 Jun 1;6(6):607–15.
71. Reddy V, Grogan D, Ahluwalia M, Salles ÉL, Ahluwalia P, Khodadadi H, et al. Targeting the endocannabinoid system: a predictive, preventive, and personalized medicine-directed approach to the management of brain pathologies. *EPMA Journal*. 2020 Jun 1;11(2):217–50.
72. Landa L, Sulcova A, Gbelec P. The use of cannabinoids in animals and therapeutic implications for veterinary medicine: a review. *Veterinární medicína*. 2016;61(3).
73. Cristino L, Bisogno T, Di Marzo V. Cannabinoids and the expanded endocannabinoid system in neurological disorders. *Nat Rev Neurol*. 2020 Jan;16(1):9–29.

74. Pertwee RG, Howlett AC, Abood ME, Alexander SPH, Marzo VD, Elphick MR, et al. International Union of Basic and Clinical Pharmacology. LXXIX. Cannabinoid Receptors and Their Ligands: Beyond CB1 and CB2. *Pharmacol Rev.* 2010 Dec 1;62(4):588–631.
75. Ligresti A, De Petrocellis L, Di Marzo V. From Phytocannabinoids to Cannabinoid Receptors and Endocannabinoids: Pleiotropic Physiological and Pathological Roles Through Complex Pharmacology. *Physiol Rev.* 2016 Oct;96(4):1593–659.
76. Galiazzo G, Tagliavia C, Giancola F, Rinnovati R, Sadeghinezhad J, Bombardi C, et al. Localisation of Cannabinoid and Cannabinoid-Related Receptors in the Horse Ileum. *J Equine Vet Sci.* 2021 Sep;104:103688.
77. Galiazzo G, Giancola F, Stanzani A, Fracassi F, Bernardini C, Forni M, et al. Localization of cannabinoid receptors CB1, CB2, GPR55, and PPAR α in the canine gastrointestinal tract. *Histochem Cell Biol.* 2018 Aug;150(2):187–205.
78. Stanzani A, Galiazzo G, Giancola F, Tagliavia C, De Silva M, Pietra M, et al. Localization of cannabinoid and cannabinoid related receptors in the cat gastrointestinal tract. *Histochem Cell Biol.* 2020 May;153(5):339–56.
79. Chiocchetti R, De Silva M, Aspidi F, Cunha RZ, Gobbo F, Tagliavia C, et al. Distribution of Cannabinoid Receptors in Keratinocytes of Healthy Dogs and Dogs With Atopic Dermatitis. *Front Vet Sci.* 2022 Jul 8;9:915896.
80. Zamith Cunha R, Grilli E, Piva A, Delprete C, Franciosi C, Caprini M, et al. The Expression of Cannabinoid and Cannabinoid-Related Receptors on the Gustatory Cells of the Piglet Tongue. *Molecules.* 2024 Jan;29(19):4613.
81. Price TJ, Helesic G, Parghi D, Hargreaves KM, Flores CM. The neuronal distribution of cannabinoid receptor type 1 in the trigeminal ganglion of the rat. *Neuroscience.* 2003 Aug;120(1):155–62.
82. Greco R, Gasperi V, Maccarrone M, Tassorelli C. The endocannabinoid system and migraine. *Experimental Neurology.* 2010 Jul 1;224(1):85–91.
83. Selvi E, Lorenzini S, Garcia-Gonzalez E, Maggio R, Lazzerini PE, Capecchi PL, et al. Inhibitory effect of synthetic cannabinoids on cytokine production in rheumatoid fibroblast-like synoviocytes. *Clin Exp Rheumatol.* 2008 Aug;26(4):574–81.
84. Miagkoff L, Girard CA, St-Jean G, Richard H, Beauchamp G, Laverty S. Cannabinoid receptors are expressed in equine synovium and upregulated with synovitis. *Equine Veterinary Journal.* 2023;55(4):681–95.
85. Richardson D, Pearson RG, Kurian N, Latif ML, Garle MJ, Barrett DA, et al. Characterisation of the cannabinoid receptor system in synovial tissue and fluid in patients with osteoarthritis and rheumatoid arthritis. *Arthritis Res Ther.* 2008;10(2):R43.
86. Kaur I, Behl T, Bungau S, Zengin G, Kumar A, El-Esawi MA, et al. The endocannabinoid signaling pathway as an emerging target in pharmacotherapy, earmarking mitigation of destructive events in rheumatoid arthritis. *Life Sciences.* 2020 Sep 15;257:118109.
87. Mechoulam R, Parker LA. The Endocannabinoid System and the Brain. *Annual Review of Psychology.* 2013 Jan 3;64(Volume 64, 2013):21–47.

88. Chen D jie, Gao M, Gao F fei, Su Q xi, Wu J. Brain cannabinoid receptor 2: expression, function and modulation. *Acta Pharmacol Sin.* 2017 Mar;38(3):312–6.
89. An D, Peigneur S, Hendrickx LA, Tytgat J. Targeting Cannabinoid Receptors: Current Status and Prospects of Natural Products. *International Journal of Molecular Sciences.* 2020 Jan;21(14):5064.
90. Ständer S, Schmelz M, Metze D, Luger T, Rukwied R. Distribution of cannabinoid receptor 1 (CB1) and 2 (CB2) on sensory nerve fibers and adnexal structures in human skin. *J Dermatol Sci.* 2005 Jun;38(3):177–88.
91. Hussain MT, Greaves DR, Iqbal AJ. The Impact of Cannabinoid Receptor 2 Deficiency on Neutrophil Recruitment and Inflammation. *DNA and Cell Biology.* 2019 Oct;38(10):1025–9.
92. Simard M, Rakotoarivelo V, Di Marzo V, Flamand N. Expression and Functions of the CB2 Receptor in Human Leukocytes. *Front Pharmacol.* 2022 Feb 22. Available from: <https://www.frontiersin.org/journals/pharmacology/articles/10.3389/fphar.2022.826400/full>
93. Malan TP, Ibrahim MM, Vanderah TW, Makriyannis A, Porreca F. Inhibition of pain responses by activation of CB(2) cannabinoid receptors. *Chem Phys Lipids.* 2002 Dec 31;121(1–2):191–200.
94. Zheng JL, Yu TS, Li XN, Fan YY, Ma WX, Du Y, et al. Cannabinoid receptor type 2 is time-dependently expressed during skin wound healing in mice. *Int J Legal Med.* 2012 Sep;126(5):807–14.
95. Matias I, Pochard P, Orlando P, Salzet M, Pestel J, Di Marzo V. Presence and regulation of the endocannabinoid system in human dendritic cells. *Eur J Biochem.* 2002 Aug;269(15):3771–8.
96. Lucaciu O, Aghiorghiesei O, Petrescu NB, Mirica IC, Benea HRC, Apostu D. In quest of a new therapeutic approach in COVID-19: the endocannabinoid system. *Drug Metab Rev.* 2021 Nov;53(4):478–90.
97. Christiansen IM, Edvinsson JCA, Reducha PV, Edvinsson L, Haanes KA. Dual action of the cannabinoid receptor 1 ligand arachidonyl-2'-chloroethylamide on calcitonin gene-related peptide release. *J Headache Pain.* 2022 Dec;23(1):30.
98. Anand U, Otto WR, Sanchez-Herrera D, Facer P, Yiangou Y, Korchev Y, et al. Cannabinoid receptor CB2 localisation and agonist-mediated inhibition of capsaicin responses in human sensory neurons. *Pain.* 2008 Sep 15;138(3):667–80.
99. Chiocchetti R, Galiazzo G, Tagliavia C, Stanzani A, Giancola F, Menchetti M, et al. Cellular Distribution of Canonical and Putative Cannabinoid Receptors in Canine Cervical Dorsal Root Ganglia. *Front Vet Sci.* 2019 Sep 19;6:313.
100. Chiocchetti R, Rinnovati R, Tagliavia C, Stanzani A, Galiazzo G, Giancola F, et al. Localisation of cannabinoid and cannabinoid-related receptors in the equine dorsal root ganglia. *Equine Vet J.* 2020 Jun 11;
101. Sánchez-Aparicio P, Florán B, Rodríguez Velázquez D, Ibancovich JA, Varela Guerrero JA, Recillas S. Cannabinoids CB2 Receptors, One New Promising Drug Target for Chronic and

Degenerative Pain Conditions in Equine Veterinary Patients. *Journal of Equine Veterinary Science*. 2020 Feb;85:102880.

102. Gutierrez T, Crystal JD, Zvonok AM, Makriyannis A, Hohmann AG. Self-medication of a cannabinoid CB2 agonist in an animal model of neuropathic pain. *Pain*. 2011 Sep;152(9):1976–87.
103. Rogers N. Cannabinoid receptor with an ‘identity crisis’ gets a second look. *Nat Med*. 2015 Sep;21(9):966–7.
104. Schuelert N, Zhang C, Mogg AJ, Broad LM, Hepburn DL, Nisenbaum ES, et al. Paradoxical effects of the cannabinoid CB2 receptor agonist GW405833 on rat osteoarthritic knee joint pain. *Osteoarthritis and Cartilage*. 2010 Nov 1;18(11):1536–43.
105. Gui H, Liu X, Wang ZW, He DY, Su DF, Dai SM. Expression of cannabinoid receptor 2 and its inhibitory effects on synovial fibroblasts in rheumatoid arthritis. *Rheumatology*. 2014 May 1;53(5):802–9.
106. Fukuda S, Kohsaka H, Takayasu A, Yokoyama W, Miyabe C, Miyabe Y, et al. Cannabinoid receptor 2 as a potential therapeutic target in rheumatoid arthritis. *BMC Musculoskelet Disord*. 2014 Aug 12;15(1):275.
107. Sophocleous A, Börjesson AE, Salter DM, Ralston SH. The type 2 cannabinoid receptor regulates susceptibility to osteoarthritis in mice. *Osteoarthritis and Cartilage*. 2015 Sep 1;23(9):1586–94.
108. Rzeczycki P, Rasner C, Lammlin L, Junginger L, Goldman S, Bergman R, et al. Cannabinoid receptor type 2 is upregulated in synovium following joint injury and mediates anti-inflammatory effects in synovial fibroblasts and macrophages. *Osteoarthritis and Cartilage*. 2021 Dec 1;29(12):1720–31.
109. Morales P, Hurst DP, Reggio PH. Molecular Targets of the Phytocannabinoids: A Complex Picture. In: Kinghorn AD, Falk H, Gibbons S, Kobayashi J, editors. *Phytocannabinoids*. Cham: Springer International Publishing; 2017. p. 103–31. (Progress in the Chemistry of Organic Natural Products; vol. 103). Available from: http://link.springer.com/10.1007/978-3-319-45541-9_4
110. Caterina MJ. TRP Channel Cannabinoid Receptors in Skin Sensation, Homeostasis, and Inflammation. *ACS Chem Neurosci*. 2014 Jun 10;5(11):1107–16.
111. Premkumar LS, Sikand P. TRPV1: A Target for Next Generation Analgesics. *Curr Neuropharmacol*. 2008 Jun;6(2):151–63.
112. Nilius B, Appendino G, Owsianik G. The transient receptor potential channel TRPA1: from gene to pathophysiology. *Pflugers Arch - Eur J Physiol*. 2012 Nov 1;464(5):425–58.
113. Kim YS, Son JY, Kim TH, Paik SK, Dai Y, Noguchi K, et al. Expression of transient receptor potential ankyrin 1 (TRPA1) in the rat trigeminal sensory afferents and spinal dorsal horn. *Journal of Comparative Neurology*. 2010;518(5):687–98.
114. Galiazzo G, De Silva M, Giancola F, Rinnovati R, Peli A, Chiocchetti R. Cellular distribution of cannabinoid-related receptors TRPV1, PPAR-gamma, GPR55 and GPR3 in the equine cervical dorsal root ganglia. *Equine Veterinary Journal*. 2022;54(4):788–98.

115. Oh MH, OH SY, Lu J, Lou H, Myers A, Zhu Z, et al. TRPA1-Dependent Pruritus in IL-13-Induced Chronic Atopic Dermatitis. *J Immunol*. 2013 Dec 1;191(11):5371–82.
116. Bíró T, Maurer M, Modarres S, Lewin NE, Brodie C, Ács G, et al. Characterization of Functional Vanilloid Receptors Expressed by Mast Cells. *Blood*. 1998 Feb 15;91(4):1332–40.
117. Kang J, Ding Y, Li B, Liu H, Yang X, Chen M. TRPA1 mediated aggravation of allergic contact dermatitis induced by DINP and regulated by NF- κ B activation. *Sci Rep*. 2017 Feb 27;7:43586.
118. Yun JW, Seo JA, Jang WH, Koh HJ, Bae IH, Park YH, et al. Antipruritic Effects of TRPV1 Antagonist in Murine Atopic Dermatitis and Itching Models. *Journal of Investigative Dermatology*. 2011 Jul 1;131(7):1576–9.
119. Kun J, Perkecz A, Knie L, Sétáló Jr G, Tornóczy T, Pintér E, et al. TRPA1 receptor is upregulated in human oral lichen planus. *Oral Diseases*. 2017;23(2):189–98.
120. Bujak JK, Kosmala D, Majchrzak-Kuligowska K, Bednarczyk P. Functional Expression of TRPV1 Ion Channel in the Canine Peripheral Blood Mononuclear Cells. *Int J Mol Sci*. 2021 Mar 20;22(6):3177.
121. Ninomiya Y, Tanuma SI, Tsukimoto M. Differences in the effects of four TRPV1 channel antagonists on lipopolysaccharide-induced cytokine production and COX-2 expression in murine macrophages. *Biochem Biophys Res Commun*. 2017 Mar 11;484(3):668–74.
122. Zeng D, Chen C, Zhou W, Ma X, Pu X, Zeng Y, et al. TRPA1 deficiency alleviates inflammation of atopic dermatitis by reducing macrophage infiltration. *Life Sci*. 2021 Feb 1;266:118906.
123. Basu S, Srivastava P. Immunological role of neuronal receptor vanilloid receptor 1 expressed on dendritic cells. *Proc Natl Acad Sci U S A*. 2005 Apr 5;102(14):5120–5.
124. Naert R, López-Requena A, Talavera K. TRPA1 Expression and Pathophysiology in Immune Cells. *International Journal of Molecular Sciences*. 2021 Jan;22(21):11460.
125. Bertin S, Aoki-Nonaka Y, de Jong PR, Nohara LL, Xu H, Stanwood SR, et al. The ion channel TRPV1 regulates the activation and proinflammatory properties of CD4⁺ T cells. *Nat Immunol*. 2014 Nov;15(11):1055–63.
126. Sahoo SS, Majhi RK, Tiwari A, Acharya T, Kumar PS, Saha S, et al. Transient receptor potential ankyrin1 channel is endogenously expressed in T cells and is involved in immune functions. *Bioscience Reports*. 2019 Sep 20;39(9):BSR20191437.
127. Szabó K, Kemény Á, Balázs N, Khanfar E, Sándor Z, Boldizsár F, et al. Presence of TRPA1 Modifies CD4⁺/CD8⁺ T Lymphocyte Ratio and Activation. *Pharmaceuticals*. 2022 Jan;15(1):57.
128. Heiner I, Eisfeld J, Halaszovich CR, Wehage E, Jüngling E, Zitt C, et al. Expression profile of the transient receptor potential (TRP) family in neutrophil granulocytes: evidence for currents through long TRP channel 2 induced by ADP-ribose and NAD. *Biochem J*. 2003 May 1;371(3):1045–53.

129. Andersen G, Kahlenberg K, Krautwurst D, Somoza V. [6]-Gingerol Facilitates CXCL8 Secretion and ROS Production in Primary Human Neutrophils by Targeting the TRPV1 Channel. *Molecular Nutrition & Food Research*. 2023;67(4):2200434.
130. Ichikawa H, Sugimoto T. VR1-immunoreactive primary sensory neurons in the rat trigeminal ganglion. *Brain Res*. 2001 Jan 26;890(1):184–8.
131. Marwaha L, Bansal Y, Singh R, Saroj P, Sodhi RK, Kuhad A. Niflumic acid, a TRPV1 channel modulator, ameliorates stavudine-induced neuropathic pain. *Inflammopharmacol*. 2016 Dec;24(6):319–34.
132. Kochukov MY, McNearney TA, Fu Y, Westlund KN. Thermosensitive TRP ion channels mediate cytosolic calcium response in human synoviocytes. *Am J Physiol Cell Physiol*. 2006 Sep;291(3):C424–432.
133. Kelly S, Chapman RJ, Woodhams S, Sagar DR, Turner J, Burston JJ, et al. Increased function of pronociceptive TRPV1 at the level of the joint in a rat model of osteoarthritis pain. *Ann Rheum Dis*. 2015 Jan;74(1):252–9.
134. Lowin T, Apitz M, Anders S, Straub RH. Anti-inflammatory effects of N-acylethanolamines in rheumatoid arthritis synovial cells are mediated by TRPV1 and TRPA1 in a COX-2 dependent manner. *Arthritis Res Ther*. 2015 Nov 14;17:321.
135. Braucke AFGV, Frederiksen NL, Berg LC, Aarsvold S, Müller FC, Boesen MP, et al. Identification and Quantification of Transient Receptor Potential Vanilloid 1 (TRPV1) in Equine Articular Tissue. *Animals (Basel)*. 2020 Mar 18;10(3):506.
136. Lv Z, Xu X, Sun Z, Yang YX, Guo H, Li J, et al. TRPV1 alleviates osteoarthritis by inhibiting M1 macrophage polarization via Ca²⁺/CaMKII/Nrf2 signaling pathway. *Cell Death Dis*. 2021 May 18;12(6):504.
137. Engler A, Aeschlimann A, Simmen BR, Michel BA, Gay RE, Gay S, et al. Expression of transient receptor potential vanilloid 1 (TRPV1) in synovial fibroblasts from patients with osteoarthritis and rheumatoid arthritis. *Biochemical and Biophysical Research Communications*. 2007 Aug;359(4):884–8.
138. Mackie K, Stella N. Cannabinoid receptors and endocannabinoids: Evidence for new players. *AAPS J*. 2006 Jun 1;8(2):34.
139. He Y, Shen H, Bi GH, Zhang HY, Soler-Cedeño O, Alton H, et al. GPR55 is expressed in glutamate neurons and functionally modulates drug taking and seeking in rats and mice. *Transl Psychiatry*. 2024 Feb 19;14(1):1–12.
140. Staton PC, Hatcher JP, Walker DJ, Morrison AD, Shapland EM, Hughes JP, et al. The putative cannabinoid receptor GPR55 plays a role in mechanical hyperalgesia associated with inflammatory and neuropathic pain. *PAIN*. 2008 Sep 30;139(1):225–36.
141. Carey LM, Gutierrez T, Deng L, Lee WH, Mackie K, Hohmann AG. Inflammatory and Neuropathic Nociception is Preserved in GPR55 Knockout Mice. *Sci Rep*. 2017 Apr 20;7:944.
142. Stančić A, Jandl K, Hasenöhr C, Reichmann F, Marsche G, Schuligoi R, et al. The GPR55 antagonist CID16020046 protects against intestinal inflammation. *Neurogastroenterology & Motility*. 2015;27(10):1432–45.

143. Cantarella G, Scollo M, Lempereur L, Saccani-Jotti G, Basile F, Bernardini R. Endocannabinoids inhibit release of nerve growth factor by inflammation-activated mast cells. *Biochemical Pharmacology*. 2011 Aug 15;82(4):380–8.
144. Taylor L, Christou I, Kapellos TS, Buchan A, Brodermann MH, Gianella-Borradori M, et al. Primary Macrophage Chemotaxis Induced by Cannabinoid Receptor 2 Agonists Occurs Independently of the CB2 Receptor. *Sci Rep*. 2015 Jun 2;5:10682.
145. Lanuti M, Talamonti E, Maccarrone M, Chiurchiù V. Correction: activation of GPR55 receptors exacerbates oxLDL-induced lipid accumulation and inflammatory responses, while reducing cholesterol efflux from human macrophages. *PLoS One*. 2015;10(6):e0131850.
146. Chiurchiù V, Lanuti M, De Bardi M, Battistini L, Maccarrone M. The differential characterization of GPR55 receptor in human peripheral blood reveals a distinctive expression in monocytes and NK cells and a proinflammatory role in these innate cells. *International Immunology*. 2015 Mar 1;27(3):153–60.
147. Castillo-Chabeco B, Figueroa G, Parira T, Napuri J, Agudelo M. Ethanol-induced modulation of GPR55 expression in human monocyte-derived dendritic cells is accompanied by H4K12 acetylation. *Alcohol*. 2018 Sep 1;71:25–31.
148. Tanikawa T, Oka S, Nakajima K, Hayashi Y, Nemoto-Sasaki Y, Arata Y, et al. Expression and Distribution of GPR55, a Receptor for Lysophosphatidylinositol, in Mouse Tissues and Cells. *BPB Reports*. 2022;5(2):16–20.
149. Sumida H, Lu E, Chen H, Yang Q, Mackie K, Cyster JG. GPR55 regulates intraepithelial lymphocyte migration dynamics and susceptibility to intestinal damage. *Science Immunology*. 2017 Dec 8;2(18):eaao1135.
150. Balenga NAB, Aflaki E, Kargl J, Platzer W, Schröder R, Blättermann S, et al. GPR55 regulates cannabinoid 2 receptor-mediated responses in human neutrophils. *Cell Res*. 2011 Oct;21(10):1452–69.
151. Whyte LS, Ryberg E, Sims NA, Ridge SA, Mackie K, Greasley PJ, et al. The putative cannabinoid receptor GPR55 affects osteoclast function in vitro and bone mass in vivo. *Proc Natl Acad Sci USA*. 2009 Sep 22;106(38):16511–6.
152. Dunn SL, Wilkinson JM, Crawford A, Bunning RAD, Le Maitre CL. Expression of Cannabinoid Receptors in Human Osteoarthritic Cartilage: Implications for Future Therapies. *Cannabis Cannabinoid Res*. 2016 Jan 1;1(1):3–15.
153. Henstridge CM, Balenga NAB, Kargl J, Andradas C, Brown AJ, Irving A, et al. Minireview: Recent Developments in the Physiology and Pathology of the Lysophosphatidylinositol-Sensitive Receptor GPR55. *Molecular Endocrinology*. 2011 Nov 1;25(11):1835–48.
154. Sharir H, Abood ME. Pharmacological characterization of GPR55, a putative cannabinoid receptor. *Pharmacology & Therapeutics*. 2010 Jun 1;126(3):301–13.
155. Schuelert N, McDougall JJ. The abnormal cannabidiol analogue O-1602 reduces nociception in a rat model of acute arthritis via the putative cannabinoid receptor GPR55. *Neurosci Lett*. 2011 Aug 1;500(1):72–6.

156. Tontonoz P, Spiegelman BM. Fat and Beyond: The Diverse Biology of PPAR γ . *Annual Review of Biochemistry*. 2008;77(1):289–312.
157. Chiocchetti R, Rinnovati R, Tagliavia C, Stanzani A, Galiazzo G, Giancola F, et al. Localisation of cannabinoid and cannabinoid-related receptors in the equine dorsal root ganglia. *Equine Vet J*. 2021 May;53(3):549–57.
158. Chu Y, Jia S, Xu K, Liu Q, Mai L, Liu J, et al. Single-cell transcriptomic profile of satellite glial cells in trigeminal ganglion. *Frontiers in Molecular Neuroscience*. 2023. Available from: <https://www.frontiersin.org/articles/10.3389/fnmol.2023.1117065>
159. Lyons DN, Zhang L, Danaher RJ, Miller CS, Westlund KN. PPAR γ Agonists Attenuate Trigeminal Neuropathic Pain. *The Clinical Journal of Pain*. 2017 Dec;33(12):1071.
160. van Eekeren ICM, Clockaerts S, Bastiaansen-Jenniskens YM, Lubberts E, Verhaar JAN, van Osch GJVM, et al. Fibrates as therapy for osteoarthritis and rheumatoid arthritis? A systematic review. *Ther Adv Musculoskelet Dis*. 2013 Feb;5(1):33–44.
161. Okamoto H, Iwamoto T, Kotake S, Momohara S, Yamanaka H, Kamatani N. Inhibition of NF-kappaB signaling by fenofibrate, a peroxisome proliferator-activated receptor-alpha ligand, presents a therapeutic strategy for rheumatoid arthritis. *Clin Exp Rheumatol*. 2005;23(3):323–30.
162. Jung JI, Lee HS, Jeon YE, Kim SM, Hong SH, Moon JM, et al. Anti-inflammatory activity of palmitoylethanolamide ameliorates osteoarthritis induced by monosodium iodoacetate in Sprague–Dawley rats. *Inflammopharmacology*. 2021;29(5):1475–86.
163. Schotman P, Schrama LH, Edwards PM. Peptidergic Systems. In: Lajtha A, editor. *Neurochemical Systems*. Boston, MA: Springer US; 1985. p. 243–79. Available from: https://doi.org/10.1007/978-1-4684-7018-5_11
164. De Haes W, Van Sinay E, Detienne G, Temmerman L, Schoofs L, Boonen K. Functional neuropeptidomics in invertebrates. *Biochimica et Biophysica Acta (BBA) - Proteins and Proteomics*. 2015 Jul 1;1854(7):812–26.
165. Jékely G, Melzer S, Beets I, Kadow ICG, Koene J, Haddad S, et al. The long and the short of it – a perspective on peptidergic regulation of circuits and behaviour. *Journal of Experimental Biology*. 2018 Feb 8;221(3):jeb166710.
166. Hökfelt T, Broberger C, Xu ZQD, Sergeev V, Ubink R, Diez M. Neuropeptides — an overview. *Neuropharmacology*. 2000 Jul 1;39(8):1337–56.
167. Grimmelikhuijzen CJP, Hauser F. Mini-review: The evolution of neuropeptide signaling. *Regulatory Peptides*. 2012 Aug 10;177:S6–9.
168. Eiden LE, Hernández VS, Jiang SZ, Zhang L. Neuropeptides and small-molecule amine transmitters: cooperative signaling in the nervous system. *Cell Mol Life Sci*. 2022 Aug 23;79(9):492.
169. Sharma D, Kumar K, Bisht GS. A Mini-Review on Potential of Neuropeptides as Future Therapeutics. *Int J Pept Res Ther*. 2022 Jan 3;28(1):39.
170. Waite GN, Geib RW, King MW. Neuropeptides as biological system integrators – mini review. *Biomed Sci Instrum*. 2014;50:1–11.

171. Dudás B, Merchenthaler I. Chapter 4 - Morphology and distribution of hypothalamic peptidergic systems. In: Swaab DF, Kreier F, Lucassen PJ, Salehi A, Buijs RM, editors. *Handbook of Clinical Neurology*. Elsevier; 2021. p. 67–85. (The Human Hypothalamus: Anterior Region; vol. 179). Available from: <https://www.sciencedirect.com/science/article/pii/B9780128199756000029>
172. Steinhoff MS, von Mentzer B, Geppetti P, Pothoulakis C, Bunnett NW. Tachykinins and Their Receptors: Contributions to Physiological Control and the Mechanisms of Disease. *Physiol Rev*. 2014 Jan;94(1):265–301.
173. Mashaghi A, Marmalidou A, Tehrani M, Grace PM, Pothoulakis C, Dana R. Neuropeptide substance P and the immune response. *Cell Mol Life Sci*. 2016 Nov 1;73(22):4249–64.
174. Graefe SB, Rahimi N, Mohiuddin SS. Biochemistry, Substance P. In: StatPearls [Internet] [Internet]. StatPearls Publishing; 2023. Available from: <https://www.ncbi.nlm.nih.gov/books/NBK554583/>
175. Vilisaar J, Arsenescu RI. Roles of Substance P in Gastrointestinal Functions and Neuroimmune Interactions. In: Constantinescu C, Arsenescu R, Arsenescu V, editors. *Neuro-Immuno-Gastroenterology*. Cham: Springer International Publishing; 2016. p. 53–73. Available from: https://doi.org/10.1007/978-3-319-28609-9_4
176. Shimizu Y, Matsuyama H, Shiina T, Takewaki T, Furness JB. Tachykinins and their functions in the gastrointestinal tract. *Cell Mol Life Sci*. 2007 Oct 20;65(2):295–311.
177. Furness JB. *The Enteric Nervous System*. John Wiley & Sons; 2008. 291 p.
178. Brookes SJH. Classes of enteric nerve cells in the guinea-pig small intestine. *The Anatomical Record*. 2001;262(1):58–70.
179. Holzer P, Holzer-Petsche U. Tachykinins in the gut. Part I. Expression, release and motor function. *Pharmacology & Therapeutics*. 1997 Jan 1;73(3):173–217.
180. Holzer P, Holzer-Petsche U. Tachykinins in the gut. Part II. Roles in neural excitation, secretion and inflammation. *Pharmacol Ther*. 1997;73(3):219–63.
181. Petto C, Gäbel G, Pfannkuche H. Architecture and Chemical Coding of the Inner and Outer Submucous Plexus in the Colon of Piglets. *PLoS One*. 2015;10(7):e0133350.
182. Czajkowska M, Całka J. Neurochemistry of Enteric Neurons Following Prolonged Indomethacin Administration in the Porcine Duodenum. *Front Pharmacol*. 2020 Sep 8. Available from: <https://www.frontiersin.org/journals/pharmacology/articles/10.3389/fphar.2020.564457/full>
183. Chiocchetti R, Bombardi C, Mongardi-Fantaguzzi C, Venturelli E, Russo D, Spadari A, et al. Intrinsic innervation of the horse ileum. *Research in Veterinary Science*. 2009 Oct 1;87(2):177–85.
184. Mazzuoli G, Mazzoni M, Albanese V, Clavenzani P, Lalatta-Costerbosa G, Lucchi ML, et al. Morphology and Neurochemistry of Descending and Ascending Myenteric Plexus Neurons of Sheep Ileum. *The Anatomical Record*. 2007;290(12):1480–91.

185. Polidoro G, Giancola F, Fracassi F, Pietra M, Bettini G, Asti M, et al. Substance P and the neurokinin-1 receptor expression in dog ileum with and without inflammation. *Research in Veterinary Science*. 2017 Oct 1;114:297–307.
186. Domeneghini C, Massoletti P, Arrighi S. Localization of regulatory peptides in the gastrointestinal tract of the striped dolphin, *Stenella coeruleoalba* (Mammalia: Cetacea). An immunohistochemical study. *Eur J Histochem*. 1997 Jan 1;41(4):285–300.
187. Stark ME, Bauer AJ, Sarr MG, Szurszewski JH. Nitric oxide mediates inhibitory nerve input in human and canine jejunum. *Gastroenterology*. 1993 Feb;104(2):398–409.
188. Timmermans JP, Barbiers M, Scheuermann DW, Bogers JJ, Adriaensen D, Fekete E, et al. Nitric oxide synthase immunoreactivity in the enteric nervous system of the developing human digestive tract. *Cell Tissue Res*. 1994 Feb;275(2):235–45.
189. Deng G, Jin L. The effects of vasoactive intestinal peptide in neurodegenerative disorders. *Neurological Research*. 2017 Jan 2;39(1):65–72.
190. Said SI, Mutt V. Polypeptide with Broad Biological Activity: Isolation from Small Intestine. *Science*. 1970 Sep 18;169(3951):1217–8.
191. Stanley AG. Chapter 32 - Other Peptide and Related Systems including Substance P, Calcitonin Gene-Related Peptide, and Serotonin. In: Lip GYH, Hall JE, editors. *Comprehensive Hypertension*. Philadelphia: Mosby; 2007. p. 363–75. Available from: <https://www.sciencedirect.com/science/article/pii/B9780323039611500350>
192. Nguyen TD. Vasoactive Intestinal Peptide (VIP). In: Johnson LR, editor. *Encyclopedia of Gastroenterology*. New York: Elsevier; 2004. p. 604–10. Available from: <https://www.sciencedirect.com/science/article/pii/B0123868602007139>
193. Thorndyke MC, Riddell JH, Thwaites DT, Dimaline R. Vasoactive Intestinal Polypeptide and its Relatives: Biochemistry, Distribution, and Functions. *The Biological Bulletin*. 1989 Oct;177(2):183–6.
194. Fahrenkrug J, Hannibal J, Tams J, Georg B. Immunohistochemical Localization of the VIP1 Receptor (VPAC1R) in Rat Cerebral Blood Vessels: Relation to PACAP and VIP Containing Nerves. *J Cereb Blood Flow Metab*. 2000 Aug 1;20(8):1205–14.
195. Sun QQ, Prince DA, Huguenard JR. Vasoactive intestinal polypeptide and pituitary adenylyl cyclase-activating polypeptide activate hyperpolarization-activated cationic current and depolarize thalamocortical neurons in vitro. *J Neurosci*. 2003 Apr 1;23(7):2751–8.
196. Rhomberg T, Rovira-Esteban L, Vikór A, Paradiso E, Kremser C, Nagy-Pál P, et al. Vasoactive Intestinal Polypeptide-Immunoreactive Interneurons within Circuits of the Mouse Basolateral Amygdala. *J Neurosci*. 2018 Aug 1;38(31):6983–7003.
197. Pelkey KA, Chittajallu R, Craig MT, Tricoire L, Wester JC, McBain CJ. Hippocampal GABAergic Inhibitory Interneurons. *Physiological Reviews*. 2017 Oct;97(4):1619–747.
198. Gonkowski S. Vasoactive Intestinal Polypeptide in the Carotid Body—A History of Forty Years of Research. A Mini Review. *International Journal of Molecular Sciences*. 2020 Jan;21(13):4692.

199. Chaudhury D, Loh DH, Dragich JM, Hagopian A, Colwell CS. Select cognitive deficits in Vasoactive Intestinal Peptide deficient mice. *BMC Neuroscience*. 2008 Jul 10;9(1):63.
200. Cottrell GA, Veldhuis HD, Rostene WH, de Kloet ER. Behavioral actions of vasoactive intestinal peptide (VIP). *Neuropeptides*. 1984 Jun;4(4):331–41.
201. Bechtold DA, Brown TM, Luckman SM, Piggins HD. Metabolic rhythm abnormalities in mice lacking VIP-VPAC2 signaling. *American Journal of Physiology-Regulatory, Integrative and Comparative Physiology*. 2008 Feb;294(2):R344–51.
202. Gozes I. VIP, From Gene to Behavior and Back: Summarizing my 25 Years of Research. *J Mol Neurosci*. 2008 Nov 1;36(1):115–24.
203. Dh L, C A, Cs C, Ja W. Vasoactive intestinal peptide is critical for circadian regulation of glucocorticoids. *Neuroendocrinology*. 2008;88(4). Available from: <https://pubmed.ncbi.nlm.nih.gov/18562786/>
204. Mascagni F, McDonald AJ. Immunohistochemical characterization of cholecystokinin containing neurons in the rat basolateral amygdala. *Brain research*. 2003;976(2):171–84.
205. McDonald AJ. Morphology of peptide-containing neurons in the rat basolateral amygdaloid nucleus. *Brain Research*. 1985 Jul 8;338(1):186–91.
206. Muller JF, Mascagni F, McDonald AJ. Synaptic connections of distinct interneuronal subpopulations in the rat basolateral amygdalar nucleus. *J Comp Neurol*. 2003 Feb 10;456(3):217–36.
207. Cassell MD, Gray TS. Morphology of peptide-immunoreactive neurons in the rat central nucleus of the amygdala. *Journal of Comparative Neurology*. 1989;281(2):320–33.
208. Shin MS. Vasoactive intestinal peptide in the amygdala inhibits tail flick reflexes in rats. *Brain Res*. 2005 Apr 8;1040(1–2):197–201.
209. Simon RA, Barazani N, Jones MP, Bednarska O, Icenhour A, Engström M, et al. Vasoactive intestinal polypeptide plasma levels associated with affective symptoms and brain structure and function in healthy females. *Sci Rep*. 2021 Jan 14;11(1):1406.
210. Simón-Arceo K, Ramírez-Salado I, Calvo JM. Long-Lasting Enhancement of Rapid Eye Movement Sleep and Pontogeniculooccipital Waves by Vasoactive Intestinal Peptide Microinjection into the Amygdala Temporal Lobe. *Sleep*. 2003 May 1;26(3):259–64.
211. Suzuki WL, Amaral DG. Perirhinal and parahippocampal cortices of the macaque monkey: Cortical afferents. *Journal of Comparative Neurology*. 1994;350(4):497–533.
212. Witter MP, Doan TP, Jacobsen B, Nilssen ES, Ohara S. Architecture of the Entorhinal Cortex A Review of Entorhinal Anatomy in Rodents with Some Comparative Notes. *Front Syst Neurosci*. 2017 Jun 28;11. Available from: <https://www.frontiersin.org/journals/systems-neuroscience/articles/10.3389/fnsys.2017.00046/full>
213. Raslau FD, Mark IT, Klein AP, Ulmer JL, Mathews V, Mark LP. Memory Part 2: The Role of the Medial Temporal Lobe. *AJNR Am J Neuroradiol*. 2015 May;36(5):846–9.

214. Marino L, Connor RC, Fordyce RE, Herman LM, Hof PR, Lefebvre L, et al. Cetaceans Have Complex Brains for Complex Cognition. *PLOS Biology*. 2007 May 15;5(5):e139.
215. Cozzi B, Huggenberger S, Oelschläger HA. *Anatomy of Dolphins: Insights into Body Structure and Function*. Academic Press; 2016. 458 p.
216. Jacobs MS, Morgane PJ, McFarland WL. The anatomy of the brain of the bottlenose dolphin (*Tursiops truncatus*). Rhinic lobe (rhinencephalon). I. The paleocortex. *Journal of Comparative Neurology*. 1971;141(2):205–71.
217. Kobro-Flatmoen A, Witter MP. Neuronal chemo-architecture of the entorhinal cortex: A comparative review. *European Journal of Neuroscience*. 2019;50(10):3627–62.
218. Jacobs MS, McFarland WL, Morgane PJ. The anatomy of the brain of the bottlenose dolphin (*Tursiops truncatus*). Rhinic lobe (Rhinencephalon): The archicortex. *Brain Res Bull*. 1979;4 Suppl 1:1–108.
219. Kerr KM, Agster KL, Furtak SC, Burwell RD. Functional neuroanatomy of the parahippocampal region: The lateral and medial entorhinal areas. *Hippocampus*. 2007;17(9):697–708.
220. Sah P, Faber ESL, Lopez De Armentia M, Power J. The Amygdaloid Complex: Anatomy and Physiology. *Physiological Reviews*. 2003 Jul 1;83(3):803–34.
221. Swanson LW, Petrovich GD. What is the amygdala? *Trends in Neurosciences*. 1998 Aug 1;21(8):323–31.
222. Šimić G, Tkalčić M, Vukić V, Mulc D, Španić E, Šagud M, et al. Understanding Emotions: Origins and Roles of the Amygdala. *Biomolecules*. 2021 Jun;11(6):823.
223. Weiss A, Di Carlo DT, Di Russo P, Weiss F, Castagna M, Cosottini M, et al. Microsurgical anatomy of the amygdaloid body and its connections. *Brain Struct Funct*. 2021 Apr 1;226(3):861–74.
224. McDONALD AJ. Is There an Amygdala and How Far Does It Extend? *Annals of the New York Academy of Sciences*. 2003;985(1):1–21.
225. Meyer A. Karl Friedrich Burdach and his place in the history of neuroanatomy. *J Neurol Neurosurg Psychiatry*. 1970 Oct;33(5):553–61.
226. Pabba M. Evolutionary development of the amygdaloid complex. *Front Neuroanat*. 2013 Aug 28;7. Available from: <https://www.ncbi.nlm.nih.gov/pmc/articles/PMC3755265/>
227. Burdach KF. *Von Baue und Leben des Gehirns* (Leipzig 1822). 1822;
228. LeDoux J. The amygdala. *Current Biology*. 2007 Oct 23;17(20):R868–74.
229. Nikolenko VN, Oganessian MV, Rizaeva NA, Kudryashova VA, Nikitina AT, Pavliv MP, et al. Amygdala: Neuroanatomical and Morphophysiological Features in Terms of Neurological and Neurodegenerative Diseases. *Brain Sciences*. 2020 Aug;10(8):502.
230. Aggleton JP, Mishkin M. The amygdala: Sensory gateway to the emotions. In: *Biological foundations of emotion*. Elsevier; 1986. p. 281–99.

231. Hariri AR, Whalen PJ. The amygdala: inside and out. *F1000 Biol Rep*. 2011 Jan 14;3. Available from: <https://www.ncbi.nlm.nih.gov/pmc/articles/PMC3042316/>
232. McDonald AJ. Cortical pathways to the mammalian amygdala. *Progress in Neurobiology*. 1998;55(3):257–332.
233. Bubbs E, Kinnavane L, Aggleton J. Hippocampal–diencephalic–cingulate networks for memory and emotion: An anatomical guide. *Brain and Neuroscience Advances*. 2017 Aug 4;1:239821281772344.
234. Maclean PD. Some psychiatric implications of physiological studies on frontotemporal portion of limbic system (visceral brain). *Electroencephalography & Clinical Neurophysiology*. 1952;4:407–18.
235. Adolphs R. The biology of fear. *Current biology*. 2013;23(2):R79–93.
236. LeDoux JE. Emotion Circuits in the Brain. *Annu Rev Neurosci*. 2000 Mar;23(1):155–84.
237. Gouveia FV, Hamani C, Fonoff ET, Brentani H, Alho EJJ, de Moraes RMCB, et al. Amygdala and Hypothalamus: Historical Overview With Focus on Aggression. *Neurosurgery*. 2019 Jul 1;85(1):11–30.
238. Kaas JH. *Evolutionary neuroscience*. Academic Press; 2020.
239. Davis M, Shi C. The amygdala. *Current Biology*. 2000 Feb 15;10(4):R131.
240. Davis M, Whalen PJ. The amygdala: vigilance and emotion. *Molecular Psychiatry*. 2001 Jan;6(1):13–34.
241. AbuHasan Q, Reddy V, Siddiqui W. *Neuroanatomy, Amygdala*. In: StatPearls. Treasure Island (FL): StatPearls Publishing; 2021. Available from: <http://www.ncbi.nlm.nih.gov/books/NBK537102/>
242. Récamier-Carballo S, Estrada-Camarena E, López-Rubalcava C. Maternal separation induces long-term effects on monoamines and brain-derived neurotrophic factor levels on the frontal cortex, amygdala, and hippocampus: differential effects after a stress challenge. *Behavioural Pharmacology*. 2017 Oct 1;28(7):545–57.
243. Baron-Cohen S, Ring HA, Bullmore ET, Wheelwright S, Ashwin E, Williams SCR. The amygdala theory of autism. *Neuroscience & Biobehavioral Reviews*. 2000 May 1;24(3):355–64.
244. Benarroch EE. The amygdala: Functional organization and involvement in neurologic disorders. *Neurology*. 2015 Jan 20;84(3):313–24.
245. Neugebauer V. Amygdala Pain Mechanisms. In: Schaible HG, editor. *Pain Control*. Berlin, Heidelberg: Springer Berlin Heidelberg; 2015. p. 261–84. (Handbook of Experimental Pharmacology; vol. 227). Available from: http://link.springer.com/10.1007/978-3-662-46450-2_13
246. Pitkänen A, Kempainen S. Comparison of the distribution of calcium-binding proteins and intrinsic connectivity in the lateral nucleus of the rat, monkey, and human amygdala. *Pharmacology Biochemistry and Behavior*. 2002 Mar 1;71(3):369–77.

247. García-López M, Abellán A, Legaz I, Rubenstein JLR, Puelles L, Medina L. Histogenetic compartments of the mouse centromedial and extended amygdala based on gene expression patterns during development. *Journal of Comparative Neurology*. 2008;506(1):46–74.
248. Alheid GF. Amygdala and extended amygdala. *The rat nervous system*. 1995;495–578.
249. Martínez-García F, Novejarque A, Lanuza E. Evolution of the Amygdala in Vertebrates. In: *Evolution of Nervous Systems*. Elsevier; 2007. p. 255–334. Available from: <https://linkinghub.elsevier.com/retrieve/pii/B0123708788001397>
250. Martínez-García F, Novejarque A, Lanuza E. Two interconnected functional systems in the amygdala of amniote vertebrates. *Brain Research Bulletin*. 2008 Mar 18;75(2):206–13.
251. F MG, A MM, E L. The pallial amygdala of amniote vertebrates: evolution of the concept, evolution of the structure. *Brain research bulletin*. 2002 Mar;57(3–4). Available from: <https://pubmed.ncbi.nlm.nih.gov/11923011/>
252. Medina L, Legaz I, González G, De Castro F, Rubenstein JLR, Puelles L. Expression of Dbx1, Neurogenin 2, Semaphorin 5A, Cadherin 8, and Emx1 distinguish ventral and lateral pallial histogenetic divisions in the developing mouse claustroramygdaloid complex. *Journal of Comparative Neurology*. 2004;474(4):504–23.
253. Puelles L, Kuwana E, Puelles E, Bulfone A, Shimamura K, Keleher J, et al. Pallial and subpallial derivatives in the embryonic chick and mouse telencephalon, traced by the expression of the genes *Dlx-2*, *Emx-1*, *Nkx-2.1*, *Pax-6*, and *Tbr-1*. *Journal of Comparative Neurology*. 2000;424(3):409–38.
254. Real MA, Heredia R, del Carmen Labrador M, Dávila JC, Guirado S. Expression of somatostatin and neuropeptide Y in the embryonic, postnatal, and adult mouse amygdalar complex. *Journal of Comparative Neurology*. 2009;513(4):335–48.
255. Tole S, Remedios R, Saha B, Stoykova A. Selective Requirement of Pax6, But Not Emx2, in the Specification and Development of Several Nuclei of the Amygdaloid Complex. *J Neurosci*. 2005 Mar 9;25(10):2753–60.
256. George I, Alawa J, Akpulu P, Alawa C. Comparative neuroanatomical study of the amygdala and fear conditioning in Nigerian breeds of Artiodactyla: Sheep (Uda) and goats (Red Sokoto). *The Anatomical Record*. 2021;304(4):692–703.
257. McDonald AJ, Mott DD. Functional neuroanatomy of amygdalohippocampal interconnections and their role in learning and memory. *Journal of Neuroscience Research*. 2017;95(3):797–820.
258. McDonald AJ. Functional neuroanatomy of the basolateral amygdala: Neurons, neurotransmitters, and circuits. *Handb Behav Neurosci*. 2020;26:1–38.
259. Pitkänen A, Jolkkonen E, Kempainen S. Anatomic heterogeneity of the rat amygdaloid complex. *Folia Morphologica*. 2000;59(1):1–24.
260. Whalen PJ, Phelps EA. *The Human Amygdala*. Guilford Press; 2009. 465 p.

261. Pitkänen A, Savander V, LeDoux JE. Organization of intra-amygdaloid circuitries in the rat: an emerging framework for understanding functions of the amygdala. *Trends in Neurosciences*. 1997 Nov 1;20(11):517–23.
262. Paré D, Smith Y, Paré JF. Intra-amygdaloid projections of the basolateral and basomedial nuclei in the cat: Phaseolus vulgaris-leucoagglutinin anterograde tracing at the light and electron microscopic level. *Neuroscience*. 1995 Nov 1;69(2):567–83.
263. Martínez-Lorenzana G, Jiménez JR, Condés-Lara M. Interamygdaloid connection of basolateral nucleus through the anterior commissure in the rat. *Neuroscience Letters*. 2004 Aug 12;366(2):154–7.
264. Meurisse M, Chaillou E, Lévy F. Afferent and efferent connections of the cortical and medial nuclei of the amygdala in sheep. *Journal of Chemical Neuroanatomy*. 2009 Mar 1;37(2):87–97.
265. Contessi A, Celli G. *Le api: biologia, allevamento, prodotti*. Edagricole; 1990.
266. Snodgrass RE. *Anatomy of the Honey Bee*. Cornell University Press; 1956. 356 p.
267. Nervous system | Honey bee. Available from: <https://honeybee.drawwing.org/book/nervous-system>
268. ZBrushCentral. 2019. Honey bee (*Apis mellifera*) nervous system scientific illustration. Available from: <http://www.zbrushcentral.com/t/honey-bee-apis-mellifera-nervous-system-scientific-illustration/212333>
269. Ribi W, Senden TJ, Sakellariou A, Limaye A, Zhang S. Imaging honey bee brain anatomy with micro-X-ray-computed tomography. *Journal of Neuroscience Methods*. 2008 Jun 15;171(1):93–7.
270. Menzel R. The honeybee as a model for understanding the basis of cognition. *Nat Rev Neurosci*. 2012 Nov;13(11):758–68.
271. Smarandache-Wellmann CR. Arthropod neurons and nervous system. *Current Biology*. 2016 Oct 24;26(20):R960–5.
272. Urbach R, Technau GM. 1.21 - Segmental Organization of Cephalic Ganglia in Arthropods. In: Kaas JH, editor. *Evolution of Nervous Systems*. Oxford: Academic Press; 2007. p. 337–48. Available from: <https://www.sciencedirect.com/science/article/pii/B0123708788001580>
273. Søvik E, Perry CJ, Barron AB. Chapter Six - Insect Reward Systems: Comparing Flies and Bees. In: Zayed A, Kent CF, editors. *Advances in Insect Physiology*. Academic Press; 2015. p. 189–226. (Genomics, Physiology and Behaviour of Social Insects; vol. 48). Available from: <https://www.sciencedirect.com/science/article/pii/S0065280614000071>
274. Lösel PD, Monchanin C, Lebrun R, Jayme A, Relle J, Devaud JM, et al. Natural variability in bee brain size and symmetry revealed by micro-CT imaging and deep learning. *bioRxiv*; 2022. Available from: <https://www.biorxiv.org/content/10.1101/2022.10.12.511944v1>
275. Brandt R, Rohlfing T, Rybak J, Kroficzek S, Maye A, Westerhoff M, et al. Three-dimensional average-shape atlas of the honeybee brain and its applications. *Journal of Comparative Neurology*. 2005;492(1):1–19.

276. Honkanen A, Hensgen R, Kannan K, Adden A, Warrant E, Weislo W, et al. Parallel motion vision pathways in the brain of a tropical bee. *J Comp Physiol A*. 2023 Jul 1;209(4):563–91.
277. Shinomiya K, Horne JA, McLin S, Wiederman M, Nern A, Plaza SM, et al. The Organization of the Second Optic Chiasm of the *Drosophila* Optic Lobe. *Front Neural Circuits*. 2019 Oct 11;13. Available from: <https://www.frontiersin.org/journals/neural-circuits/articles/10.3389/fncir.2019.00065/full>
278. Özel MN, Simon F, Jafari S, Holguera I, Chen YC, Benhra N, et al. Neuronal diversity and convergence in a visual system developmental atlas. *Nature*. 2021 Jan;589(7840):88–95.
279. Paulk AC, Gronenberg W. Higher order visual input to the mushroom bodies in the bee, *Bombus impatiens*. *Arthropod Structure & Development*. 2008 Nov 1;37(6):443–58.
280. Paulk AC, Stacey JA, Pearson TWJ, Taylor GJ, Moore RJD, Srinivasan MV, et al. Selective attention in the honeybee optic lobes precedes behavioral choices. *Proceedings of the National Academy of Sciences*. 2014 Apr;111(13):5006–11.
281. Calábria LK, Teixeira RR, Coelho Gonçalves SM, Passos Lima AB, Santos AADD, Martins AR, et al. Comparative analysis of two immunohistochemical methods for antigen retrieval in the optical lobe of the honeybee *Apis mellifera*: Myosin-v assay. *Biological Research*. 2010;43(1):7–12.
282. Zhang X, Bai Y, Hou J, Chen W, Cheng K, Zi L, et al. Anatomical measurements of trigeminal ganglion: a cadaver study. *Anat Sci Int*. 2024 Jan 1;99(1):98–105.
283. Barone R, Simoens P. *Anatomia comparata dei mammiferi domestici*. Vol. Volume 7- Neurologia: Sistema nervoso periferico, ghiandole endocrine, estesiologia. 2012.
284. Pickles K, Madigan J, Aleman M. Idiopathic headshaking: Is it still idiopathic? *The Veterinary Journal*. 2014 Jul;201(1):21–30.
285. Becker R, Haenssger K, Precht C, Khoma OZ, Hlushchuk R, Koch C, et al. An anatomical study of the subarachnoid space surrounding the trigeminal ganglion in horses—in preparation for a controlled glycerol rhizotomy in equids. *Front Vet Sci*. 2024 Jul 18;11. Available from: <https://www.frontiersin.org/journals/veterinary-science/articles/10.3389/fvets.2024.1424890/full>
286. Ross SE, Murray JK, Roberts VLH. Prevalence of headshaking within the equine population in the UK. *Equine Vet J*. 2018 Jan;50(1):73–8.
287. Aleman M, Williams DC, Brosnan RJ, Nieto JE, Pickles KJ, Berger J, et al. Sensory nerve conduction and somatosensory evoked potentials of the trigeminal nerve in horses with idiopathic headshaking. *J Vet Intern Med*. 2013;27(6):1571–80.
288. Pickles K. Trigeminal-mediated headshaking: A diagnostic challenge. *Equine Veterinary Education*. 2023;35(4):195–6.
289. Roberts V. Trigeminal-mediated headshaking in horses: prevalence, impact, and management strategies. *VMRR*. 2019 Jan 9;10:1–8.
290. Liang Y, Huang C, Hsu K. Therapeutic Potential of Cannabinoids in Trigeminal Neuralgia. *CDTCNSND*. 2004 Dec 1;3(6):507–14.

291. Lee G, Grovey B, Furnish T, Wallace M. Medical Cannabis for Neuropathic Pain. *Curr Pain Headache Rep.* 2018 Feb 1;22(1):8.
292. Reidenberg JS, Laitman JT. Position of the larynx in odontoceti (toothed whales). *The Anatomical Record.* 1987;218(1):98–106.
293. <https://www.centroricercacetacei.org/it/respirazione-per-via-orale-in-tursiops-truncatus>.
294. Mead JG. G - Gastrointestinal Tract. In: Perrin WF, Würsig B, Thewissen JGM, editors. *Encyclopedia of Marine Mammals (Second Edition)*. London: Academic Press; 2009. p. 472–7. Available from: <https://www.sciencedirect.com/science/article/pii/B9780123735539001139>
295. Russo F, Gatta C, De Girolamo P, Cozzi B, Giurisato M, Lucini C, et al. Expression and Immunohistochemical Detection of Leptin-Like Peptide in the Gastrointestinal Tract of the South American Sea Lion (*Otaria flavescens*) and the Bottlenose Dolphin (*Tursiops truncatus*). *The Anatomical Record.* 2012;295(9):1482–93.
296. Gatta C, Russo F, Russolillo MG, Varricchio E, Paolucci M, Castaldo L, et al. The Orexin System in the Enteric Nervous System of the Bottlenose Dolphin (*Tursiops truncatus*). *PLOS ONE.* 2014 Aug 21;9(8):e105009.
297. Furness JB, Stebbing MJ. The first brain: Species comparisons and evolutionary implications for the enteric and central nervous systems. *Neurogastroenterology & Motility.* 2018;30(2):e13234.
298. Sharkey KA, Mawe GM. The enteric nervous system. *Physiological Reviews.* 2023 Apr;103(2):1487–564.
299. Wood JD. Enteric Nervous System: Physiology. In: Squire LR, editor. *Encyclopedia of Neuroscience*. Oxford: Academic Press; 2009. p. 1103–13. Available from: <https://www.sciencedirect.com/science/article/pii/B9780080450469006641>
300. Spencer NJ, Hu H. Enteric nervous system: sensory transduction, neural circuits and gastrointestinal motility. *Nat Rev Gastroenterol Hepatol.* 2020 Jun;17(6):338–51.
301. GrepMed. 2021. Layers of the Intestinal Wall - Anatomy • Serosa: ... Available from: <https://grepmed.com/images/13666/intestinal-wall-layers-anatomy-intestine>
302. Kulkarni S, Ganz J, Bayrer J, Becker L, Bogunovic M, Rao M. Advances in Enteric Neurobiology: The “Brain” in the Gut in Health and Disease. *J Neurosci.* 2018 Oct 31;38(44):9346–54.
303. Kim JY, Dao H. Physiology, Integument. In: StatPearls. Treasure Island (FL): StatPearls Publishing; 2024. Available from: <http://www.ncbi.nlm.nih.gov/books/NBK554386/>
304. Pavletic MM. Anatomy and circulation of the canine skin. *Microsurgery.* 1991;12(2):103–12.
305. Nguyen AV, Soulika AM. The Dynamics of the Skin’s Immune System. *International Journal of Molecular Sciences.* 2019 Jan;20(8):1811.

306. Dermitzakis I, Chatzi D, Kyriakoudi SA, Evangelidis N, Vakirlis E, Meditskou S, et al. Skin Development and Disease: A Molecular Perspective. *Current Issues in Molecular Biology*. 2024 Aug;46(8):8239–67.
307. Gould J. Superpowered skin. *Nature*. 2018 Nov 21;563(7732):S84–5.
308. Ah E. The skin as sensor and effector organ orchestrating cutaneous and systemic disease. *Journal of dermatological science*. 2017 Sep;87(3). Available from: <https://pubmed.ncbi.nlm.nih.gov/28838617/>
309. Kolarsick PAJ, Kolarsick MA, Goodwin C. Anatomy and Physiology of the Skin. *Journal of the Dermatology Nurses' Association*. 2011 Aug;3(4):203.
310. Gross TL, Ihrke PJ, Walder EJ, Affolter VK. *Skin Diseases of the Dog and Cat: Clinical and Histopathologic Diagnosis*. Wiley; 2005. 945 p.
311. Massimini M, Dalle Vedove E, Bachetti B, Di Pierro F, Ribecco C, D'Addario C, et al. Polyphenols and Cannabidiol Modulate Transcriptional Regulation of Th1/Th2 Inflammatory Genes Related to Canine Atopic Dermatitis. *Front Vet Sci*. 2021 Mar 5;8. Available from: <https://www.frontiersin.org/journals/veterinary-science/articles/10.3389/fvets.2021.606197/full>
312. Santoro D. Therapies in Canine Atopic Dermatitis: An Update. *Vet Clin North Am Small Anim Pract*. 2019 Jan;49(1):9–26.
313. Amin K. The role of mast cells in allergic inflammation. *Respiratory Medicine*. 2012 Jan 1;106(1):9–14.
314. Asahina R, Maeda S. A review of the roles of keratinocyte-derived cytokines and chemokines in the pathogenesis of atopic dermatitis in humans and dogs. In: *Advances in Veterinary Dermatology*. John Wiley & Sons, Ltd; 2017. p. 15–25. Available from: <https://onlinelibrary.wiley.com/doi/abs/10.1002/9781119278368.ch2.1>
315. Esche C, de Benedetto A, Beck LA. Keratinocytes in Atopic dermatitis: Inflammatory signals. *Curr Allergy Asthma Rep*. 2004 Jul 1;4(4):276–84.
316. Schlotter YM, Riemers FM, Rutten VPMG, Knol EF, Willemse T. Enzymes involved in the conversion of arachidonic acid to eicosanoids in the skin of atopic dogs. *Exp Dermatol*. 2010 Aug;19(8):e317-319.
317. Olivry T, Mayhew D, Paps JS, Linder KE, Peredo C, Rajpal D, et al. Early Activation of Th2/Th22 Inflammatory and Pruritogenic Pathways in Acute Canine Atopic Dermatitis Skin Lesions. *J Invest Dermatol*. 2016 Oct;136(10):1961–9.
318. Laprais A, Dunston SM, Torres SMF, Favrot C, Olivry T. Evaluation of intraepidermal nerve fibres in the skin of normal and atopic dogs. *Vet Dermatol*. 2017 Aug;28(4):e355-e80.
319. Mollanazar NK, Smith PK, Yosipovitch G. Mediators of Chronic Pruritus in Atopic Dermatitis: Getting the Itch Out? *Clin Rev Allergy Immunol*. 2016 Dec;51(3):263–92.
320. Petrosino S, Moriello AS, Cerrato S, Fusco M, Puigdemont A, Petrocellis L de, et al. The anti-inflammatory mediator palmitoylethanolamide enhances the levels of 2-arachidonoyl-glycerol and potentiates its actions at TRPV1 cation channels. *British Journal of Pharmacology*. 2016;173(7):1154–62.

321. Baswan SM, Klosner AE, Glynn K, Rajgopal A, Malik K, Yim S, et al. Therapeutic Potential of Cannabidiol (CBD) for Skin Health and Disorders. *Clin Cosmet Investig Dermatol*. 2020;13:927–42.
322. Sciences E. ElleVet Sciences Announces Results of Atopic Dermatitis Study Using Its CBD+CBDA Oil On Dogs. Available from: <https://www.prnewswire.com/news-releases/ellevet-sciences-announces-results-of-atopic-dermatitis-study-using-its-cbdcbda-oil-on-dogs-301189648.html>
323. Limited CAT. CBD Substantially Improves Atopic Dermatitis Symptoms in Dogs. Available from: <https://www.prnewswire.com/news-releases/cbd-substantially-improves-atopic-dermatitis-symptoms-in-dogs-301095965.html>
324. Drake RL, Vogl AW, Mitchell AWM. Gray's Anatomy for Students E-Book: Gray's Anatomy for Students E-Book. Elsevier Health Sciences; 2019. 1299 p.
325. Barbe M, Driban J, Barr A, Popoff S, Safadi F. Structure and Function of Joints. In: Bone Pathology. 2009. p. 51–60.
326. Iwanaga T, Shikichi M, Kitamura H, Yanase H, Nozawa-Inoue K. Morphology and functional roles of synoviocytes in the joint. *Arch Histol Cytol*. 2000 Mar;63(1):17–31.
327. Thomsen LN, Thomsen PD, Downing A, Talbot R, Berg LC. FOXO1, PDK, PYCARD and SAMD9L are differentially expressed by fibroblast-like cells in equine synovial membrane compared to joint capsule. *BMC Vet Res*. 2017 Apr 14;13(1):106.
328. Graabaek PM. Ultrastructural evidence for two distinct types of synoviocytes in rat synovial membrane. *J Ultrastruct Res*. 1982 Mar;78(3):321–39.
329. Nygaard G, Firestein GS. Restoring synovial homeostasis in rheumatoid arthritis by targeting fibroblast-like synoviocytes. *Nat Rev Rheumatol*. 2020 Jun;16(6):316–33.
330. Kitamura HP, Yanase H, Kitamura H, Iwanaga T. Unique localization of protein gene product 9.5 in type B synoviocytes in the joints of the horse. *J Histochem Cytochem*. 1999 Mar;47(3):343–52.
331. Shikichi M, Kitamura HP, Yanase H, Konno A, Takahashi-Iwanaga H, Iwanaga T. Three-dimensional ultrastructure of synoviocytes in the horse joint as revealed by the scanning electron microscope. *Arch Histol Cytol*. 1999 Aug;62(3):219–29.
332. Levick JR, McDonald JN. Fluid movement across synovium in healthy joints: role of synovial fluid macromolecules. *Ann Rheum Dis*. 1995 May;54(5):417–23.
333. Jang S, Kwon EJ, Lee JJ. Rheumatoid Arthritis: Pathogenic Roles of Diverse Immune Cells. *International Journal of Molecular Sciences*. 2022 Jan 14;23(2):905.
334. Biddle K, Sofat N. Understanding the Mechanisms of Pain in Rheumatoid Arthritis. Hamdy A. Mohammed R, editor. *Rheumatoid Arthritis - Other Perspectives towards a Better Practice*. 2020 Nov 19; Available from: <https://www.intechopen.com/books/rheumatoid-arthritis-other-perspectives-towards-a-better-practice/understanding-the-mechanisms-of-pain-in-rheumatoid-arthritis>

335. Ireland JL, Wylie CE, Collins SN, Verheyen KLP, Newton JR. Preventive health care and owner-reported disease prevalence of horses and ponies in Great Britain. *Research in Veterinary Science*. 2013 Oct 1;95(2):418–24.
336. Neundorff RH, Lowerison MB, Cruz AM, Thomason JJ, McEwen BJ, Hurtig MB. Determination of the prevalence and severity of metacarpophalangeal joint osteoarthritis in Thoroughbred racehorses via quantitative macroscopic evaluation. *Am J Vet Res*. 2010 Nov;71(11):1284–93.
337. Contino EK. Management and Rehabilitation of Joint Disease in Sport Horses. *Vet Clin North Am Equine Pract*. 2018 Aug;34(2):345–58.
338. Lowin T, Pongratz G, Straub RH. The synthetic cannabinoid WIN55,212-2 mesylate decreases the production of inflammatory mediators in rheumatoid arthritis synovial fibroblasts by activating CB2, TRPV1, TRPA1 and yet unidentified receptor targets. *J Inflamm (Lond)*. 2016;13:15.
339. Malfait AM, Gallily R, Sumariwalla PF, Malik AS, Andreaskos E, Mechoulam R, et al. The nonpsychoactive cannabis constituent cannabidiol is an oral anti-arthritic therapeutic in murine collagen-induced arthritis. *Proc Natl Acad Sci U S A*. 2000 Aug 15;97(17):9561–6.
340. Gui H, Tong Q, Qu W, Mao CM, Dai SM. The endocannabinoid system and its therapeutic implications in rheumatoid arthritis. *Int Immunopharmacol*. 2015 May;26(1):86–91.
341. Gui H, Liu X, Liu LR, Su DF, Dai SM. Activation of cannabinoid receptor 2 attenuates synovitis and joint distruction in collagen-induced arthritis. *Immunobiology*. 2015 Jun;220(6):817–22.
342. Malek N, Starowicz K. Joint problems arising from lack of repair mechanisms: can cannabinoids help? *Br J Pharmacol*. 2019 May;176(10):1412–20.
343. Xin Y, Tang A, Pan S, Zhang J. Components of the Endocannabinoid System and Effects of Cannabinoids Against Bone Diseases: A Mini-Review. *Front Pharmacol*. 2022 Jan 19;12. Available from: <https://www.frontiersin.org/journals/pharmacology/articles/10.3389/fphar.2021.793750/full>
344. Bryk M, Starowicz K. Cannabinoid-based therapy as a future for joint degeneration. Focus on the role of CB2 receptor in the arthritis progression and pain: an updated review. *Pharmacol Rep*. 2021 Jun 1;73(3):681–99.
345. Bland SD. Canine osteoarthritis and treatments: a review. *Veterinary Science Development*. 2015 Jul 17;5(2). Available from: <https://www.pagepress.org/journals/vsd/article/view/5931>
346. Valastro C, Campanile D, Marinaro M, Franchini D, Piscitelli F, Verde R, et al. Characterization of endocannabinoids and related acylethanolamides in the synovial fluid of dogs with osteoarthritis: a pilot study. *BMC Vet Res*. 2017 Nov 6;13(1):309.
347. Gamble LJ, Boesch JM, Frye CW, Schwark WS, Mann S, Wolfe L, et al. Pharmacokinetics, Safety, and Clinical Efficacy of Cannabidiol Treatment in Osteoarthritic Dogs. *Front Vet Sci*. 2018 Jul 23;5:165.

348. Mejia S, Duerr FM, Griffenhagen G, McGrath S. Evaluation of the Effect of Cannabidiol on Naturally Occurring Osteoarthritis-Associated Pain: A Pilot Study in Dogs. *Journal of the American Animal Hospital Association*. 2021 Jan 15;57(2):81–90.
349. Vinall M. Osteoarthritis in Dogs. *MD Conference Express*. 2014 Sep 1;14(25):15–15.
350. Zhang P, Li K, Kamali A, Ziadlou R, Ahmad P, Wang X, et al. Small molecules of herbal origin for osteoarthritis treatment: in vitro and in vivo evidence. *Arthritis Research & Therapy*. 2022 May 11;24(1):105.
351. Hammad S, Othman A, Abdel-Wareth AAA, Ahmed H, Abdel-Daim MM, Gherbawy YA. From basic research to applied veterinary sciences: current status, challenges and perspectives. *Arch Toxicol*. 2018 Jun 1;92(6):2141–3.
352. La Rosa C, Bonfanti L. Brain Plasticity in Mammals: An Example for the Role of Comparative Medicine in the Neurosciences. *Front Vet Sci*. 2018 Nov 1;5. Available from: <https://www.frontiersin.org/journals/veterinary-science/articles/10.3389/fvets.2018.00274/full>
353. Zaborszky L, Zilles K. Prologue. *Brain Struct Funct*. 2007 Jul 1;212(1):1–2.
354. Morgane PJ, Glezer II. Sensory Neocortex in Dolphin Brain. In: Thomas JA, Kastelein RA, editors. *Sensory Abilities of Cetaceans: Laboratory and Field Evidence*. Boston, MA: Springer US; 1990. p. 107–36. Available from: https://doi.org/10.1007/978-1-4899-0858-2_7
355. Qu ZD, Thacker M, Castelucci P, Bagyánszki M, Epstein ML, Furness JB. Immunohistochemical analysis of neuron types in the mouse small intestine. *Cell Tissue Res*. 2008 Nov 1;334(2):147–61.
356. Bryda EC. The Mighty Mouse: The Impact of Rodents on Advances in Biomedical Research. *Missouri Medicine*. 2013 Jun;110(3):207.
357. Herrmann AM, Meckel S, Gounis MJ, Kringe L, Motschall E, Mülling C, et al. Large animals in neurointerventional research: A systematic review on models, techniques and their application in endovascular procedures for stroke, aneurysms and vascular malformations. *J Cereb Blood Flow Metab*. 2019 Mar 1;39(3):375–94.
358. Taha A, Bobi J, Dammers R, Dijkhuizen RM, Dreyer AY, van Es ACGM, et al. Comparison of Large Animal Models for Acute Ischemic Stroke: Which Model to Use? *Stroke*. 2022 Apr;53(4):1411–22.
359. López-Urbe MM, Simone-Finstrom M. Special Issue: Honey Bee Research in the US: Current State and Solutions to Beekeeping Problems. *Insects*. 2019 Jan;10(1):22.